

THE UNIVERSITY of ADELAIDE

Studies on the nature of crude oil strandings collected from the South Australian coastline

Alexander James Corrick

B.Sc. Hons. (Geology), University of Adelaide
B.Sc. (Geology, Geophysics, Spatial Information), University of Adelaide

This thesis is submitted in fulfilment of the requirements for the degree of

Doctor of Philosophy

Department of Earth Sciences

School of Physical Sciences

University of Adelaide

May 2020

The Great Australian Bight Research Program is a collaboration between BP, CSIRO, the South Australian Research and Development Institute (SARDI), the University of Adelaide, and Flinders University. The program aims to provide a whole-of-system understanding of the environmental and social values of the region; providing an information source for all to use.













TABLE OF CONTENTS

Abstract vi
Thesis declaration vii
Acknowledgements viii

Chapter 1: Introduction and thesis outline 11

1. Project background 13
1.1. The global context of crude oil in marine and coastal environments 13
1.2. The occurrence of crude oil on the South Australian coastline 14
1.2.1. Asphaltites 14
1.2.2. Waxy bitumens 17
1.2.3. Previous coastal surveys 18
2. Research aims and thesis outline 20
References 22

Chapter 2: Remotely constraining the temporal evolution of offshore oil systems 29

Statement of authorship 30
Abstract 33
1. Introduction 33
2. Results 36
2.1. Asphaltite Re-Os data 36
2.2. Extent of alteration in the marine environment 37
2.3. Comparison with the OAE2 osmium isotope record 39
3. Discussion 41
4. Conclusions 44
5. Materials and methods 45
5.1. Re-Os isotope data 45
5.2. Re-Os data deviation assessment 45
5.3. Calculation of OAE2 osmium composition during the asphaltite generation window 46
5.4. Whole-oil gas chromatography-mass spectrometry 46
5.5. Isolation of saturated, aromatic and asphaltene fractions 47
5.6. Selected ion monitoring gas chromatography-mass spectrometry (SIM GC-MS) 47
Acknowledgements 48
References 49

Chapter 3: A second type of highly asphaltic crude oil seepage stranded on the South Australian coastline 55

Statement of authorship 56
Abstract 59
1. Introduction 59
2. Materials and methods 61
2.1. Sample suite 61
2.2. Bulk bitumen analyses 63
2.2.1. Whole-oil gas chromatography-mass spectrometry 63
2.2.2. Elemental analysis (EA) 63
2.2.3. Elemental analysis-isotope ratio mass spectrometry (EA-IRMS) 63
2.2.4. Re-Os isotopic composition 64
2.3. Analysis of saturated, aromatic and polar fractions 64
2.3.1. Oil fractionation 64
2.3.2. Separation of *n*-alkanes and branched/cyclic alkanes 64
2.3.3. Selected ion monitoring gas chromatography-mass spectrometry (SIM GC-MS) 64
2.3.4. Gas chromatography tandem mass spectrometry (GC-MS-MS) with cold electron ionisation 65
2.3.5. Carbon compound-specific isotope analysis (CSIA) 65
2.3.6. GC-MS analyses of aromatic and polar fractions 66
2.4. Asphaltene separation 66
3. Results and discussion 66
3.1. Comparison of source-specific saturated hydrocarbons 66
3.2. Comparison of stable isotopic composition 71
3.3. Comparison of thermal maturity parameters 73
3.4. Comparison of Re-Os systematics 75
4. Do both oils originate from the same source rock? 77
4.1. The case for two separate source rocks 77
4.2. The case for a single source rock 78
4.3. Potential mechanisms of heavy petroleum formation 81
4.4. Constraining the location of the asphaltic tar petroleum system 84
5. Conclusions 85
Acknowledgements 86
References 87

Chapter 4: The identification and provenance of crude oils stranded on the South Australian coastline 97

Statement of authorship 98
Abstract 101
1. Introduction 101
2. Materials and methods 104
2.1. Sample suite 104
2.2. Oil classification rationale 104
2.3. Whole-oil gas chromatography-mass spectrometry 105
2.4. Isolation of saturated hydrocarbon fractions 105
2.5. Separation of branched/cyclic saturated hydrocarbons by molecular sieve 106
2.6. Selected ion monitoring gas chromatography-mass spectrometry (SIM GC-MS) 106
3. Classification from visual assessment 106
3.1. Asphaltites 107
3.2. Waxy bitumens 107
3.3. Tars 108
4. Classification using bulk geochemistry 108
4.1. Asphaltic oils 111
4.2. Waxy oils 112
5. Geochemical alteration due to weathering 114
5.1. Assessing weathering in whole-oil GC-MS 114
5.2. Assessing weathering of source-specific biomarkers in SIM GC-MS 115
6. Classification using source-specific geochemistry and assessing potential parent petroleum systems 118
6.1. Asphaltic oils 123
6.1.1. Asphaltite 123
6.1.2. Asphaltic tar 125
6.2. Waxy oils 127
6.2.1. Waxy oils of lacustrine/brackish shale source affinity (types I, IIIA–C, IIIF and IVC) 128
6.2.2. Waxy oils of fluvio-deltaic source affinity (types IIID, IVB and Sandy River tars) 132
6.2.3. Waxy oils of marine shale source affinity (types IIIE and IVA) 135
6.2.4. Waxy oils of marine carbonate source affinity (types IVD and IVE) 138
6.2.5. Waxy oil of mixed lacustrine/marine carbonate source affinity (type II) 141
6.3. Classification and provenance summary 143
6.4. Oceanic transportation of SE Asian crude oils to the Australian coastline 144
6.5. Could any of these oils represent anthropogenic discharges or spills? 146
7. Conclusions 147
Acknowledgements 148
References 149

Chapter 5: The hydrocarbon loading of the South Australian coastline 159

Statement of authorship 160
Abstract 163
1. Introduction 163
1.1. The occurrence of crude oil on the South Australian coastline 164
1.2. The 1990–1991 hydrocarbon loading baseline 170
1.3. Present investigation 171
2. Materials and methods 171
2.1. Coastal surveying 171
2.2. Sample classification by whole-oil GC-MS 172
2.3. Quantification of hydrocarbon loading 176
3. Results 176
3.1. November 2014 hydrocarbon loading 177
3.2. September 2015 hydrocarbon loading 179
3.3. October 2016 hydrocarbon loading 181
3.4. 2014–2016 total summary 184
4. Discussion 186
4.1. Comparison to the 1990–1991 hydrocarbon loading baseline 186
4.2. Linking changes in geochemistry with hydrocarbon loading 187
4.3. Considerations regarding the hydrocarbon loading baseline 190
4.3.1. Seasonal variability 190
4.3.2. Abnormal weather conditions 190
4.3.3. Alteration by local beach activities 190
4.3.4. Potential for extrapolation between survey areas 191
4.3.5. A hydrocarbon loading baseline is not comparable to oil spill forecasting 191
5. Conclusions 193
Acknowledgements 194
References 195

Chapter 6: Conclusions and future research directions 201

1. Conclusions 203
2. Future research directions 204
2.1. The application of Re-Os geochronology to crude oil seepage 204
2.2. The Re-Os generation age of the asphaltites 204
2.3. Linking the asphaltic oils to the Bight Basin 205
2.4. Assessing if thermochemical sulphate reduction occurred in the Bight Basin 206
2.5. Assessment of unanalysed coastal bitumens 206
2.6. Further comparisons to produced oils and seafloor seeps in Southeast Asia 208
2.7. Maintaining and expanding the hydrocarbon loading baseline 208
References 209

Supplementary information 213

Chapter 2: Remotely constraining the temporal evolution of offshore oil systems 214
1. Supplementary data tables 214

Chapter 3: A second type of highly asphaltic crude oil seepage stranded on the South Australian coastline 231
1. Supplementary figures 231
2. Compound identification lists 233
3. Supplementary data tables 235

Chapter 4: The identification and provenance of crude oils stranded on the South Australian coastline 238
1. Survey details 238
2. Chromatogram peak assignments 239
    2.1. Whole-oil GC-MS total ion chromatograms 239
    2.2. Saturated fraction SIM GC-MS *m/z* 191 (terpanes and hopanes) 239
    2.3. Saturated fraction SIM GC-MS *m/z* 217, 218, 259 (steranes and diasteranes) 240
    2.4. Bicadinanes (minor fragment ions in saturated fraction SIM GC-MS *m/z* 191, 217, 218 and 259) 240
    3. Sample collection and classification details 241
    4. Supplementary geochemical data 255
    4.1. Biomarker degradation in type I waxy bitumen 255
4.2. Asphaltites 256
4.3. Asphaltic tars 261
4.4. Waxy oils of lacustrine source affinity (types I, IIIA–C, IIIF and IVC) 263
4.5. Waxy oils of fluvio-deltaic source affinity (types IIID, IVB and Sandy River tars) 275
4.6. Waxy oils of marine shale source affinity (types IIIE and IVA) 280
4.7. Waxy oils of marine carbonate source affinity (types IVD and IVE) 285
4.8. Waxy oil of mixed lacustrine/marine carbonate source affinity (type II) 288

Chapter 5: The hydrocarbon loading of the South Australian coastline 290
1. Supplementary data tables 290

Published manuscripts 307

Remotely constraining the temporal evolution of offshore oil systems 309

A second type of highly asphaltic crude oil seepage stranded on the South Australian coastline 319

ABSTRACT

The stranding of semi-solid to solid crude oil on the South Australian coastline has been known since the late 1800s. Previous studies have reported two main varieties, referred to as asphaltite and waxy bitumen. The former represents a single oil family thought to originate from the nearby Bight Basin, while the latter comprises multiple families, geochemically related to petroleum systems in the Indonesian Archipelago and transported to the Australian coastline by regional ocean currents.

Annual surveys of thirty beaches across Australia's southern margin were conducted in 2014–2016 to collect examples of these stranded oils as part of the Great Australian Bight Research Program. This thesis, comprising four individual research articles, employs the geochemistry and spatial distribution of these oils to further our understanding of potential petroleum systems within the Bight Basin and construct an environmental baseline of the natural or "background" hydrocarbon contamination of the South Australian coastline.

The first article documents the successful application of rhenium-osmium (Re-Os) radiometric dating to oil seepage, constraining the timing of asphaltite generation and comparing these results to what is known of the geology of the offshore Bight Basin. It demonstrates that the Re-Os geochronometer has the potential to be used as an exploration tool by dating oils of unknown origin encountered in coastal environments.

The second article reports a series of highly asphaltic tar strandings recovered from the coastline in 2016 and compares them to the well-studied asphaltites. Similarities in their respective source-specific biomarker signatures suggest that they may share a common origin within the Bight Basin. However, notable points of variation preclude their direct correlation. The observed differences could be attributed to alteration of the asphaltic tar by thermochemical sulphate reduction, or their derivation from similar but separate source rocks.

The third article summarises the key features which may be used to identify the 16 different oil families encountered over the course of the project and discusses their likely provenance. The results of this study demonstrate that the South Australian coastline collects a far greater variety of geochemically distinct crude oils than previously reported. With the exception of the aforementioned asphaltic tars, all of the newly identified oils likely originate from petroleum systems in Southeast Asia.

The fourth article quantifies the hydrocarbon loading of the coastline, demonstrating which areas are most prone to accumulating these documented oils. Despite the greater variety of oil families identified during this study, the overall abundance of waxy bitumen on the coastline has significantly declined since 1990–1991. Furthermore, modern examples of the most abundant type of waxy bitumen are more weathered than historical examples, suggesting a lack of fresh oil input to the marine environment. Given the prolonged history of oil production across the Indonesian Archipelago, it's likely the decline in waxy bitumen loading may be due to reduced reservoir pressures, causing the cessation of formerly active seeps. This decline is likely to continue until the remnants of this waxy oil are no longer recognised on the coastline.

THESIS DECLARATION

I certify that this work contains no material which has been accepted for the award of any other degree or diploma in my name in any university or other tertiary institution and, to the best of my knowledge and belief, contains no material previously published or written by another person, except where due reference has been made in the text. In addition, I certify that no part of this work will, in the future, be used in a submission in my name for any other degree or diploma in any university or other tertiary institution without the prior approval of the University of Adelaide and where applicable, any partner institution responsible for the joint award of this degree.

The author acknowledges that copyright of the published works contained within this thesis (as listed below) resides with the copyright holder(s) of those works.

I give permission for the digital version of my thesis to be made available on the web, via the University's digital research repository, the Library Search and also through web search engines, unless permission has been granted by the University to restrict access for a period of time.

I acknowledge the support I have received for my research through the provision of an Australian Government Research Training Program Scholarship.

Corrick, A.J., Selby, D., McKirdy, D.M., Hall, P.A., Gong, S., Trefry, C., Ross, A.S., 2019. **Remotely constraining the temporal evolution of offshore oil systems**. Scientific Reports vol. 9, article 1327, pp. 1–10. doi: 10.1038/s41598-018-37884-x.
© The Authors 2019, Creative Commons Attribution 4.0 International Licence.

Corrick, A.J., Hall, P.A., Gong, S., McKirdy, D.M., Selby, D., Trefry, C., Ross, A.S., 2020. **A second type of highly asphaltic crude oil seepage stranded on the South Australian coastline**. Marine and Petroleum Geology vol. 112, article 104062. doi:10.1016/j.marpetgeo.2019.104062
Crown Copyright © 2019 Published by Elsevier Ltd. All rights reserved.

Alexander J. Corrick

ACKNOWLEDGEMENTS

Firstly, I'd like to thank my primary supervisor David McKirdy, for his constant support, guidance and encouragement throughout the highs and lows of this project. It would also be remiss of me not to acknowledge his unparalleled editing abilities, which have immeasurably improved my scientific writing.

I also have to dedicate a significant amount of space on this page to the truly monumental efforts of my co-supervisor Tony Hall. He recommended me for this project (twice), revived malfunctioning mass spectrometers at some of the most inconvenient times imaginable and processed a mountain of raw biomarker data files in record time so we could meet our internal reporting deadlines despite some serious setbacks. I never would have come close to finishing this without his help from start to finish and it's a fact I won't soon forget.

Thanks to my external co-supervisor Andrew Ross from CSIRO for his efforts keeping me on track with all things related to the Great Australian Bight Research Program, and still making time for my random phone calls while juggling an impossible number of other projects.

Thanks to Prof. David Selby for his help with all things related to rhenium and osmium, and for having the fastest email response time of anyone I've ever worked with despite our 10+ hour time zone difference. Travelling to the UK to work in the laboratories at Durham University was one of the notable highlights of this project.

Thanks to Se Gong for her help in collecting vast amounts of data from some very problematic samples and for always helping me with any geochemistry questions I had.

I also need to give a huge thank you to the rotating cast of characters who came on the annual coastal surveys, including: Christine Trefry, Chris Dyt, Zachary Angelini, Se Gong, Cameron White, Stacey Maslin, Stefane Armand, April Pickard, Richard Kempton, David McKirdy, Andrew Ross, Les Tucker and Sue Margot. I doubt any of them can still set foot on the beach without subconsciously scanning the sand for oil, and I thank them for their sacrifice.

Special thanks must go to Christine Trefry for handling all of the logistics of conducting such large field seasons, surveying more beaches than anyone else in the survey team and keeping CSIRO's database of all the collected samples updated despite my endless changes to the sample classifications. Also, to Chris Dyt for surveying by day and keeping the field team fed by night for the majority of the surveys, and to Zachary Angelini for bringing his unrelenting optimism to counterbalance my (alleged) pessimism when surveying the fifth completely empty beach in a row. I'd also like to thank Stuart Valladares and Tony Hill for donating their personally collected coastal bitumens to our collection for this project.

Finally, thanks to Lachy, Rob and Katie for the procrastination coffee breaks (probably too many in the early days), and to all of my friends and family for checking in on me to make sure I actually got out of the lab once in a while.

CHAPTER 1

Introduction and
thesis outline

1. PROJECT BACKGROUND

1.1. The global context of crude oil in marine and coastal environments

Semi-solid to solid pieces of crude oil, often referred to as tar balls, have been reported either in local waters or stranded on various coastlines worldwide, including Australia (McKirdy and Horvath, 1976; Alexander et al., 1994; Edwards et al., 2016), Oman (Burns et al., 1982), Iran (Shirneshan et al., 2016), India (Dwivedi and Parulekar, 1974; Oostdam, 1984; Suneel et al., 2016), Israel (Golik, 1982), the United States of America (Curtis and Saner, 1974; Henry et al., 1993; Lorenson et al., 2009), Japan (Ohya et al., 1973), Sumatra (Oostdam, 1984), Trinidad and Tobago (Georges and Oostdam, 1983) and the Sargasso Sea (Peters and Siuda, 2014). In the many these reports, particularly those from the 1970s to 1990s, the observed tar balls originated from oil spills associated with tanker shipping activities, with few examples considered the result of natural offshore oil seepage. However, the amount of oil released into the marine environment due to human activities has declined over the past 30 years, due in part to an increase in environmentally conscientious shipping practices (Fig. 1). Presently, natural seeps are estimated to contribute ~600,000 metric tonnes of oil to the ocean each year, representing ~45% of the global input, with the remaining sources attributed to petroleum extraction, transportation and consumption (NAS, 2003; Kvenvolden and Cooper, 2003).

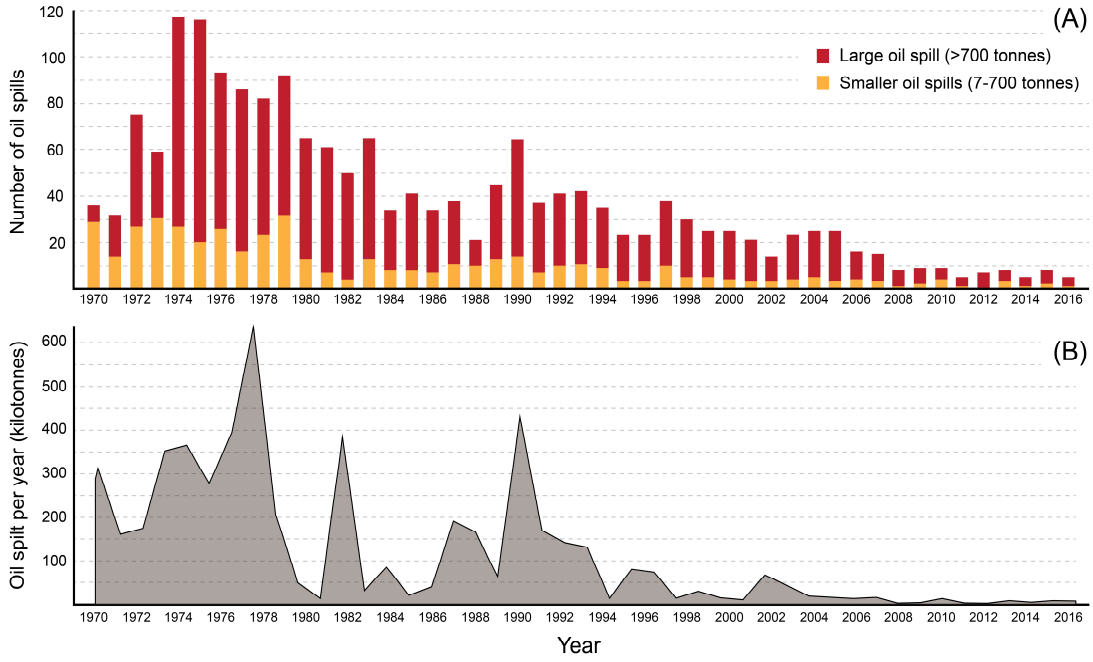


Figure 1: Record of tanker-related oil spills from 1970–2016. (A) Number of tanker-related oil spills per year. (B) Quantity of oil spilled from tankers per year. Adapted from Roser (2020).

Given the significant amount of petroleum released from seafloor seeps, when oil is encountered in coastal environments, particularly in areas not known to be affected by recent spills, it is important to consider whether the oil in question originated from natural or anthropogenic processes. Where oil from offshore seepage is recovered from a given coastline, its analysis may be used to improve our understanding of the parent petroleum system (e.g. Edwards et al., 1998) and to define the natural or "background" level of petroleum contamination in the region for future comparison in the event of an oil spill (Kvenvolden and Cooper, 2003).

1.2. The occurrence of crude oil on the South Australian coastline

Semi-solid to solid pieces of crude oil, referred to locally as "coastal bitumen", have been reported along Australia's southern margin coastline since the mid-late 1800s (Trewartha, 1850; Tolmer, 1882; Howchin, 1903, 1919; Ward, 1913, 1944; Sprigg and Woolley, 1963). These early reports pre-dated both the shipping of petroleum by tanker and offshore oil exploration in Australian waters, suggesting that the stranded bitumen originated from natural seepage, rather than anthropogenic sources.

Geochemical assessment of these bitumens began in the 1970s, using examples collected from the coastlines of the Northern Territory and South Australia (McKirdy and Horvath, 1976). Subsequent studies then included further assessment of coastal bitumens collected from the coastlines of Western Australia (Currie et al., 1992; Alexander et al., 1994), the Northern Territory (Summons et al., 1993), South Australia, Victoria (Padley, 1995; Edwards et al., 2016, 2018) and Tasmania (Volkman et al., 1992). Presently, South Australian coastal bitumens are considered to comprise two key varieties: asphaltite, formerly referred to as "asphaltum", and waxy bitumen, also known as tar balls (Edwards et al., 2016).

1.2.1. Asphaltites

Asphaltites have been found primarily along the coastlines of South Australia, western Victoria and Tasmania, although in rare instances, highly weathered examples have also been reported as far away as Macquarie Island and the southwestern coast of New Zealand (Volkman et al., 1992; Dowling et al., 1995; Padley, 1995; Edwards et al., 1998, 2016; Hall et al., 2014). This particular type of bitumen is visually distinct, due to the unusually large size of the specimens (up to 7 kg; Edwards et al., 1998), their deep shrinkage cracks and tendency to break apart with

a diagnostic conchoidal fracture (Fig. 2). Visually, these bitumen appear somewhat analogous to the asphalt flows originating from natural seeps in the Gulf of Mexico, which similarly crack and eventually fragment due to shrinkage associated with the loss of volatile components (Brüning et al., 2010).

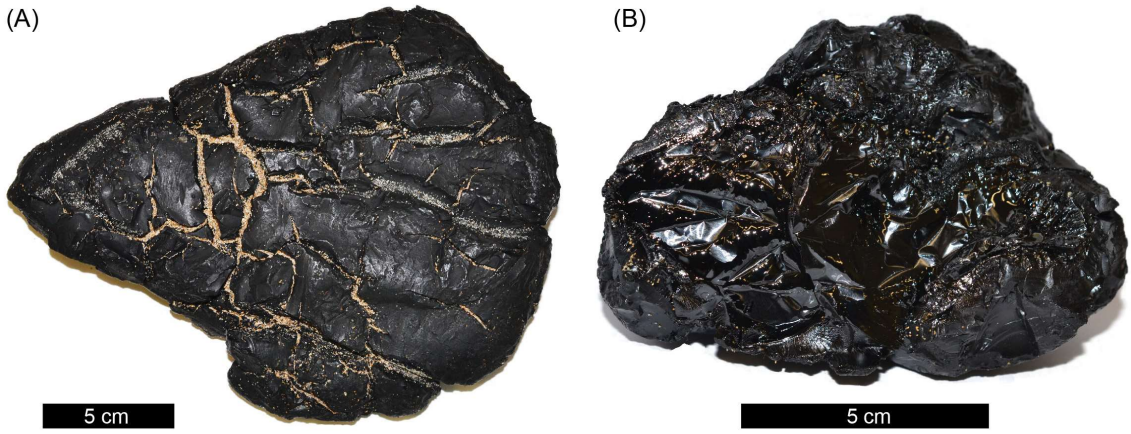


Figure 2: Representative examples of asphaltite collected as part of this study. (A) Asphaltite sample W13/007507 with prominent shrinkage cracks. (B) Asphaltite sample W13/007742, which has been broken open to show a characteristic conchoidal fracture.

Assessment of their source-specific biomarker parameters indicates that the asphaltites originate from a Mesozoic marine shale deposited under sub-oxic to euxinic conditions (Edwards et al., 1998; Hall et al., 2014; Scarlett et al., 2019). Asphaltites collected pre-1900 have a uniform geochemistry consistent with that of modern examples, supporting the interpretation that these bitumens represent a single oil family which originates from natural seepage (Volkman et al., 1992; Edwards et al., 1998). Current interpretations of the source rock are divided between several Mesozoic ocean anoxic events (OAE), including the Cenomanian-Turonian OAE2 (Totterdell et al., 2008; Boreham, 2009; Hall et al., 2014), the Albian OAE1d (Boult et al., 2005; Hall et al., 2014), and the Aptian OAE1a/Albian OAE1b events (Scarlett et al., 2019). Comparison of their source-specific composition to ~4000 oils using the GeoMark^{TM} global petroleum database found no direct analogues, suggesting that their parent petroleum system has not yet been found (Summons et al., 2001). However, the presence of abundant water-soluble aromatic compounds such as methylnaphthalenes in previously analysed examples suggests that these bitumens have undergone minimal water-washing, despite their exposure to the marine environment (Volkman et al., 1992). This supports their local origin, allowing for minimal oceanic transportation prior to stranding on the coastline. However, despite their large size and apparent close proximity to their point of origin, asphaltites are

exceedingly rare on the coastline, accounting for only ~2% of all coastal bitumens collected during the last coastal surveys conducted in the early 1990s (Padley, 1995; Edwards et al., 2016). This may be due to a low rate of seepage and/or the fact that the asphaltites have quasi-neutral buoyancy in seawater (API gravity 4–18°: Edwards et al., 1998), which would limit their ability to ascend to the uppermost level of the water column where surface currents and wave action may carry flotsam onto the coastline.

Presently the asphaltites are thought to originate from low intensity seepage from the Jurassic-Cretaceous Bight Basin (Boreham et al., 2001; Totterdell et al., 2008; Boreham, 2009; Hall et al., 2014). This predominantly offshore basin lies along Australia's southern margin and is currently considered one of the world's most prospective frontier basins (Upton, 2014; Wood Mackenzie, 2015). While a total of ten exploration wells have previously been drilled (Fig. 3), to-date no effective petroleum systems have been found. Evidence supporting the existence of one or more active petroleum systems within the basin includes the presence of asphaltites found on the nearby South Australian coastline; minor oil shows observed in the Greenly-1 well in the Duntroon Sub-basin (Smith and Donaldson, 1995); the dredging of immature Late Cenomanian-Early Turonian organic-rich shales attributed to OAE2 that may have a mature equivalent laterally within the basin (Totterdell et al., 2008; Boreham, 2009); and oils and gas-condensates trapped within fluid inclusions collected from the previous exploration wells that suggest multiple phases of hydrocarbon migration have occurred within the basin (Kempton et al., 2020).

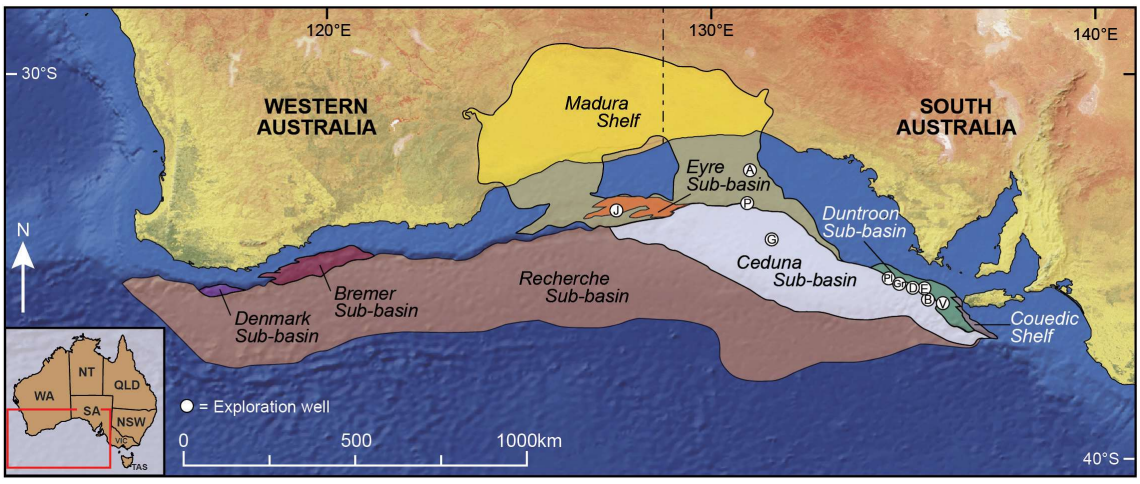


Figure 3: Location of the Bight Basin, sub-basins and previously drilled exploration wells. J = Jerboa-1, A = Apollo-1, P = Potoroo-1, G = Gnarlyknots 1/1A, Pl = Platypus-1, Gr = Greenly-1, D = Duntroon-1, E = Echinda-1, B = Borda-1, V = Vivonne-1.

1.2.2. Waxy bitumens

Waxy bitumens (Fig. 4) are more widely distributed across the Australian coastline, with studies documenting their occurrence on the coastlines of the Northern Territory (McKirdy and Horvath, 1976; Summons et al., 1993), Western Australia (Currie et al., 1992; Alexander et al., 1994), South Australia (McKirdy and Horvath, 1976; Padley, 1995; Edwards et al., 2016, 2018) and western Victoria (Padley, 1995; Edwards et al., 2016). Although visually indistinguishable, geochemical analysis reveals the waxy bitumens actually belong to multiple oil families. Each subsequent study has defined their own distinguishing criteria and more oil families have been identified as the number of samples analysed has increased (Summons et al., 1993; Alexander et al., 1994; Edwards et al., 2018). The most recent previous study investigating the different types of waxy bitumen recognised on the South Australian coastline was that of Padley (1995), based on bitumens collected during surveys conducted in 1990–1991 (see Section 1.2.3.). However, the results of this work have only recently been published (Edwards et al., 2016, 2018).

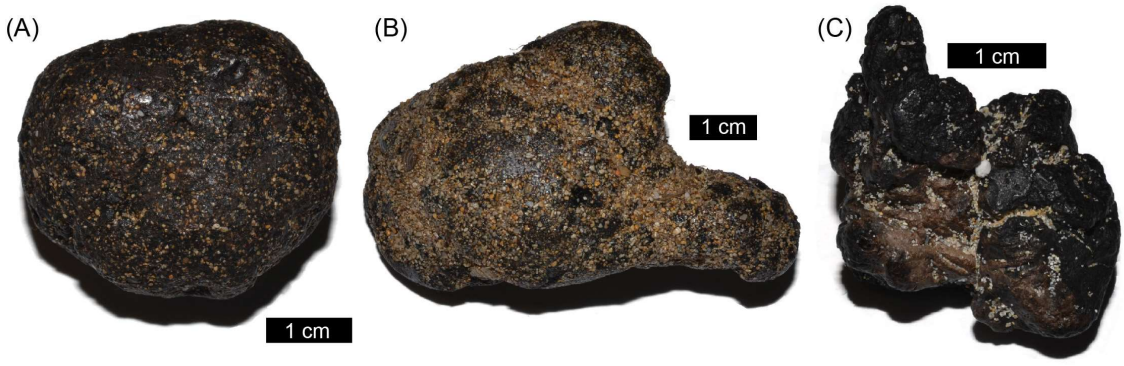


Figure 4: Representative examples of waxy bitumen collected as part of this study. (A) Rounded waxy bitumen sample W13/007680. (B) Sub-rounded waxy bitumen sample W13/007697. (C) Waxy bitumen sample W13/007625, which exhibits partial surficial browning due to oxidation associated with weathering.

The majority of the identified waxy bitumen oil families contain some combination of Cenozoic freshwater and/or terrestrial biomarkers, such as botryococcane, oleanane and bicadinanes (McKirdy et al., 1986; Summons et al., 1993; Alexander et al., 1994; Edwards et al., 2018). The presence of these markers in particularly high abundance is not consistent with oils produced from Australian sedimentary basins, but is characteristic of numerous petroleum systems in the Indonesian Archipelago (ten Haven and Schiefelbein, 1995; Schiefelbein et al., 1997). These waxy bitumens are delivered from Southeast Asia to various parts of the Australian coastline by a combination of regional ocean currents (Padley et al., 1993; Alexander et al., 1994;

Edwards et al., 2016, 2018), most notably the North Pacific thermocline and the Leeuwin Current (Fig. 5). Whilst these oils demonstrate strong source-specific similarities to petroleum systems in Southeast Asia, as yet no perfect correlations have been established. There are at least two possible reasons for this. First, numerous oils in different basins across the region originated from source rocks containing the same organic facies. Second, numerous points of geochemical variation arise when waxy bitumens from offshore seeps are compared directly to produced oils, which are predominantly extracted from onshore wells (Edwards et al., 2018).

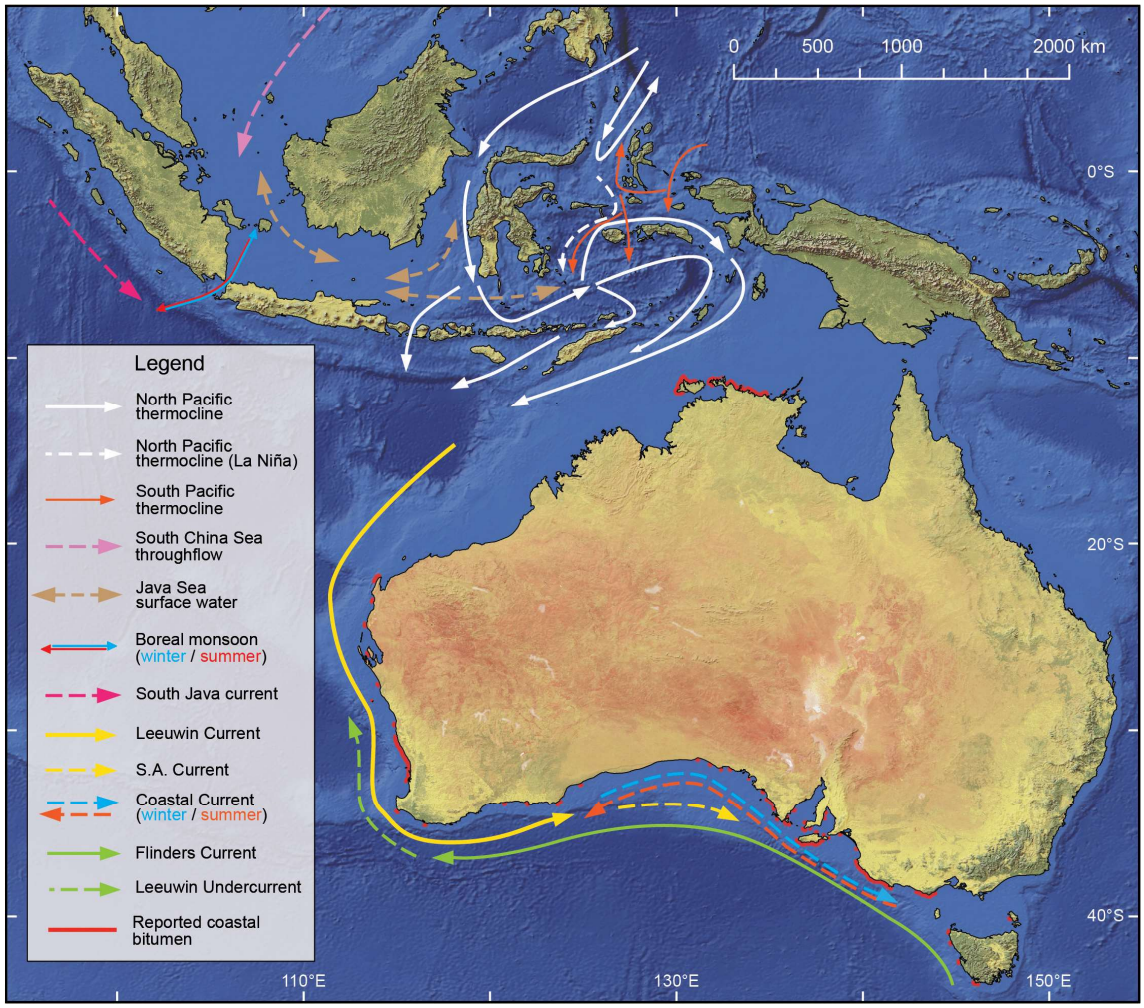


Figure 5: Generalised pathways of selected ocean currents between Southeast Asia and Australia. Distribution of reported coastal bitumen modified after Edwards et al. (2016) to include the results of this study. Simplified ocean currents after Lukas et al. (1996); Cirano and Middleton (2004); Gordon (2005); Middleton and Bye (2007); Gordon et al. (2012) and Susanto et al. (2016). For a more complex representation of the various inputs to the Leeuwin Current (including the Eastern Gyral and Subtropical Indian currents, not shown here) see Domingues et al. (2007).

1.2.3. Previous coastal surveys

Although accumulation of both asphaltite and waxy bitumen on ocean beaches is well-known, there are few detailed records of their distribution along the South Australian coastline. The first systematic surveys to retrieve and analyse coastal bitumens were conducted in 1983 by the South Australian Department of Mines and Energy (SADME). These surveys collected more than 200 waxy bitumen specimens from South Australia and western Victoria (of which 45 were analysed), in addition to two asphaltites. The details and results of these surveys are compiled in the associated open-file reports and subsequent publications (McKirdy, 1984a, 1984b; McKirdy et al., 1986, 1994). A follow-up study was conducted in 1990–1991 and while coastal bitumens were collected from a wide geographic area, systematic surveying was limited to six beaches on the south-eastern portion of mainland South Australia (Fig. 6). At each of these sites all visible pieces of solid bitumen were retrieved from a measured 200–300 m length of beach (Padley, 1995) and each location was re-surveyed every 2–4 months. The results of these surveys demonstrated a strong seasonal influence on the occurrence of waxy bitumen on the coastline, with most samples being collected during the September/October period (Padley, 1995; Edwards et al., 2016).

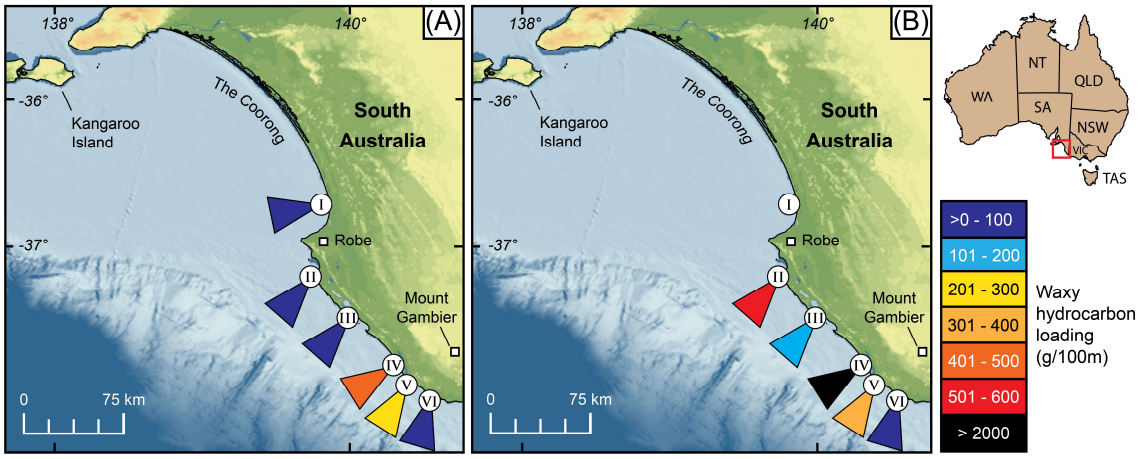


Figure 6: Beaches systematically surveyed during 1990–1991. (A) Results from September 1990 survey. (B) Results from September 1991 survey. I = The Granites, II = Long Gulley, Little Dip Conservation Park. III = Three Mile Rocks, Beachport Conservation Park. IV = Number 1 and 2 Rocks, V = Admella Dunes, VI = Nene Valley. Adapted from the results of Edwards et al. (2016).

These surveys also identified several anthropogenic oil slicks, which occurred as thin (≤5 mm) sheets of oil, or discrete globules of oil ~10–20 mm in diameter. However, the occurrence of these oil spills on the coastline was short-lived. When the affected areas were revisited two to four months after the initial stranding, the only evidence of the original spillage included rare

examples of solidified oil spots on rocks and hard discs of oil-cemented sand (Padley, 1995; Edwards et al., 2016).

As the first studies to record the length of beach surveyed, the number of bitumens collected and their total weight, the results of these 1990–1991 surveys were recently used to retroactively define the historical environmental baseline for the occurrence of stranded crude oil on the Australian coastline (Edwards et al., 2016). As no asphaltites were found at these six sites, there is presently no reliable baseline for the occurrence of these rare bitumens. Furthermore, this historical baseline is geographically restricted to the south-eastern portion of mainland South Australia. Aside from these measured surveys, all previous collections of oil strandings lacked a record of the length of coastline surveyed at each site. Therefore, the amount of oil historically reported from each location is difficult to ascertain and compare. This issue can now be easily addressed through the use of handheld global positioning systems (GPS), and hence modern surveys can be significantly more detailed and reproducible.

2. RESEARCH AIMS AND THESIS OUTLINE

Given the recent resurgence of interest in offshore oil exploration of the Bight Basin, this thesis is intended to provide an updated record of the occurrence of crude oil strandings on the South Australian coastline, prior to any significant exploratory drilling or oil production in the region. The key aims of this project are twofold:

1) to further our present understanding of potential petroleum system(s) that may reside within the Bight Basin; and

2) to revise the existing environmental baseline of the hydrocarbon loading of the South Australian coastline, providing an updated assessment of the spatial distribution, abundance, geochemistry and likely provenance of the different types of crude oils which may found on South Australian beaches.

To address these research objectives, a total of 30 ocean beaches across Australia's southern margin were systematically surveyed for coastal bitumen in November 2014, September 2015 and October 2016 as part of the Great Australian Bight Research Program (Baghurst et al., 2017; Ross et al., 2017; Begg, 2018; Smith et al., 2018). This thesis comprises four studies based on the oils recovered from these surveys, supplemented with additional samples donated

from private collections accrued within the study period. Two of these studies have been published in peer-reviewed scientific journals, while the remaining two are written in manuscript-format for future publication. As each of these chapters is intended to function as an independent study outside of this thesis, there is some unavoidable repetition of relevant background information in the respective introductory sections.

Chapter 2 was published in the journal *Scientific Reports* and presents the first successful application of the Re-Os geochronometer to petroleum seepage. The study determines the timing of petroleum generation for the asphaltites' parent petroleum system, compares this age to basin models for an OAE2 source rock in the Bight Basin, and assesses the utility of osmium isotopes in oil-source rock correlations.

Chapter 3 was published in the journal *Marine and Petroleum* Geology. It reports the discovery of a new type of highly asphaltic tar on the South Australian coastline which bears remarkable geochemical resemblance to the asphaltites. The strong similarities between these two oil types suggest the asphaltic tars may also originate from the Bight Basin. However, their direct correlation is complicated by several key differences in geochemistry which may represent primary variations in the respective source rock(s), or alteration associated with thermochemical sulphate reduction.

Chapter 4 is written for publication *Marine Pollution Bulletin* and summarises the different types of oil identified from the entire 2014–2016 sample suite. It outlines the distinguishing features of these oils in terms of their visual and physical attributes, in addition to their bulk and source-specific geochemistry. A total of 16 distinct oils were identified on the basis of their source-specific biomarker assemblages, many of which have not previously been documented on the South Australian coastline.

Chapter 5 is written for publication in *Marine Pollution Bulletin* and assesses the spatial distribution and abundance of the oil strandings collected during the 2014–2016 surveys. These results establish a modern environmental baseline for hydrocarbon loading of the South Australian coastline for both the waxy and asphaltic oils. Comparison with the results of previous surveys conducted in 1990–1991 reveals that the overall abundance of waxy oil strandings derived from Indonesian petroleum systems has markedly decreased, suggesting that the parent seeps may no longer be active.

Chapter 6 provides brief concluding remarks and recommendations for future research.

Supplementary Information for chapters 2–5 is compiled in order at the end of this thesis.

REFERENCES

Alexander, R., Currie, T.J., Kagi, R.I., 1994. The origins of coastal bitumens from Western Australia. Australian Petroleum Exploration Association Journal 34(1), 787–798.

Baghurst, B., Lukatelich, R., Smith, D., Begg, G., Lewis, R., Smith, R., 2017. Findings from the Great Australian Bight Research Program – an integrated study of environmental, economic and social values. The Australian Petroleum, Production and Exploration Association Journal 57, 388–392.

Begg, G.A., 2018. The Great Australian Bight Research Program. Deep-Sea Research Part II: Topical Studies in Oceanography.

Boreham, C., 2009. Organic geochemistry – source rock characterisation, in: Totterdell, J., Mitchell, C. (Eds.), Bight Basin Geological Sampling and Seepage Survey: RV Southern Surveyor SS01/2007. Geoscience Australia Record 2009/24. Geoscience Australia, pp. 36–60.

Boreham, C.J., Krassay, A.A., Totterdell, J.M., 2001. Geochemical comparisons between asphaltites on the southern Australian margin and Cretaceous source rock analogues, in: Hill, K.C., Bernecker, T. (Eds.), Eastern Australasian Basins Symposium, A Refocused Energy Perspective for the Future. Petroleum Exploration Society of Australia Special Publication, pp. 531–541.

Boult, P.J., McKirdy, D., Blevin, J., Heggeland, R., Lang, S., Vinall, D., 2005. The oil-prone Morum Sub-basin petroleum system, Otway Basin, South Australia. MESA Journal 38, 28–33.

Brüning, M., Sahling, H., MacDonald, I.R., Ding, F., Bohrmann, G., 2010. Origin, distribution, and alteration of asphalts at Chapopote Knoll, Southern Gulf of Mexico. Marine and Petroleum Geology 27, 1093–1106.

Burns, K.A., Villeneuve, J.P., Anderlin, V.C., Fowler, S.W., 1982. Survey of tar, hydrocarbon and metal pollution in the coastal waters of Oman. Marine Pollution Bulletin 13, 240–247.

Cirano, M., Middleton, J.F., 2004. Aspects of the Mean Wintertime Circulation along Australia's Southern Shelves: Numerical Studies. Journal of Physical Oceanography 34, 668–684.

Currie, T.J., Alexander, R., Kagi, R.I., 1992. Coastal bitumens from Western Australia - long distance transport by ocean currents. Organic Geochemistry 18, 595–601.

Curtis, M., Saner, A., 1974. Tar ball loadings on Golden Beach, Florida. US Department of Commerce, Washington, DC (National Bureau of Standards special publication) 79–81.

Domingues, C.M., Maltrud, M.E., Wijffels, S.E., Church, J.A., Tomczak, M., 2007. Simulated Lagrangian pathways between the Leeuwin Current System and the upper-ocean circulation of the southeast Indian Ocean. Deep Sea Research Part II: Topical Studies in Oceanography 54, 797–817.

Dowling, L.M., Boreham, C.J., Hope, J.M., Murray, A.P., Summons, R.E., 1995. Carbon isotopic composition of hydrocarbons in ocean-transported bitumens from the coastline of Australia. Organic Geochemistry 23, 729–737.

Dwivedi, S.N., Parulekar, A.H., 1974. Oil pollution along the Indian coastline, in: Marine Pollution Monitoring (Petroleum) Symposium and Workshop, National Bureau of Standards, Maryland. pp. 101–105.

Edwards, D., McKirdy, D.M., Summons, R.E., 1998. Enigmatic asphaltites from the southern Australian margin: molecular and carbon isotopic composition. Petroleum Exploration Society of Australia Journal 26, 397–420.

Edwards, D.S., McKirdy, D.M., Rowland, S.J., Heath, D.J., Gray, P.S., 2018. Waxy bitumen stranding in southern Australia: A geochemical study of multiple oil families and their likely origins. Organic Geochemistry 118, 132–151.

Edwards, D.S., Vinall, D.R., Corrick, A.J., McKirdy, D.M., 2016. Natural bitumen stranding on the ocean beaches of Southern Australia: a historical and geospatial review. Transactions of the Royal Society of South Australia 140, 152–185.

Georges, C., Oostdam, B.L., 1983. The characteristics and dynamics of tar pollution on the beaches of Trinidad and Tobago. Marine Pollution Bulletin 14, 170–178.

Golik, A., 1982. The distribution and behaviour of tar balls along the Israeli coast. Estuarine, Coastal and Shelf Science 15, 267–276.

Gordon, A.L., 2005. Oceanography of the Indonesian Seas and their throughflow. Oceanography 18, 14–27.

Gordon, A.L., Huber, B.A., Metzger, E.J., Susanto, R.D., Hurlburt, H.E., Adi, T.R., 2012. South China Sea throughflow impact on the Indonesian throughflow. Geophysical Research Letters 39(11).

Hall, P.A., McKirdy, D.M., Grice, K., Edwards, D.S., 2014. Australasian asphaltite strandings: Their origin reviewed in light of the effects of weathering and biodegradation on their biomarker and isotopic profiles. Marine and Petroleum Geology 57, 572–593.

Henry, C.B., Roberts, P.O., Overton, E.B., 1993. Characterization of chronic sources and impacts of tar along the Louisiana Coast. U.S. Department of the Interior, Minerals Management Service, Gulf of Mexico OCS Regional Office, New Orleans, La. OCS Study MMS 93-0046

Howchin, W., 1903. Further notes on the geology of Kangaroo Island. Transactions of the Royal Society of South Australia1 27, 75–90.

Howchin, W., 1919. Geological memoranda (first contributions). Transactions of the Royal Society of South Australia 43, 45–48.

Kempton, R.H., Bourdet, J., Gong, S., Ross, A.S., 2020. Revealing oil migration in the frontier Bight Basin, Australia. Marine and Petroleum Geology 113, 104124.

Kvenvolden, K.A., Cooper, C.K., 2003. Natural seepage of crude oil into the marine environment. Geo-Marine Letters 23, 140–146.

Lorenson, T.D., Hostettler, F.D., Rosenbauer, R.J., Peters, K.E., Dougherty, J.A., Kvenvolden, K.A., Gutmacher, C.E., Wong, F.L., Normark, W.R., 2009. Natural Offshore Oil Seepage and Related Tarball Accumulation on the California Coastline; Santa Barbara Channel and the Southern Santa Maria Basin; source identification and inventory, U.S. Geological Survey Open-File Report 2009-1225 and MMS report 2009-030.

Lukas, R., Yamagata, T., McCreary, J.P., 1996. Pacific low-latitude western boundary currents and the Indonesian throughflow. Journal of Geophysical Research 101, 12209–12216.

McKirdy, D., Summons, R., Padley, D., Serafini, K., Boreham, C., Struckmeyer, H., 1994. Molecular fossils in coastal bitumens from southern Australia: signatures of precursor biota and source rock environments. Organic Geochemistry 21, 265–286.

McKirdy, D.M., 1984a. Coastal bitumens and potential source rocks in the western Otway Basin, South Australia and Victoria. AMDEL Report F 5840/84 for Australian Aquitaine Petroleum Pty Ltd. and Ultramar Australia Inc., South Australian Department of Mines and Energy Open File Envelope No. 5876, pp. 3–365.

McKirdy, D.M., 1984b. Coastal bitumens and potential source rocks, Duntroon Basin, South Australia. AMDEL Report F 5769/84 for Getty Oil Development Company Ltd., South Australian Department of Mines and Energy Open File Envelope No. 5876, pp. 366–402.

McKirdy, D.M., Cox, R.E., Volkman, J.K., Howell, V.J., 1986. Botryococcane in a new class of Australian non-marine crude oils. Nature 320, 57–59.

McKirdy, D.M., Horvath, Z., 1976. Geochemistry and significance of coastal bitumen from Southern and Northern Australia. Australian Petroleum Exploration Association Journal 123–135.

Middleton, J.F., Bye, J.A.T., 2007. A review of the shelf-slope circulation along Australia's southern shelves: Cape Leeuwin to Portland. Progress in Oceanography 75, 1–41.

NAS, 2003. Oil in the Sea III: Inputs, Fates and Effects. The National Academies Press, Washington DC. doi:10.17226/10388

Ohya, M., Otsuki, T., Saito, M., 1973. Oil pollution in the Izu Islands waters. Journal of Oceanography 29, 121–129.

Oostdam, B.L., 1984. Tar pollution of beaches in the Indian Ocean, the South China Sea and the South Pacific Ocean. Marine Pollution Bulletin 15, 267–270.

Padley, D., 1995. Petroleum geochemistry of the Otway Basin and the significance of coastal bitumen strandings on adjacent southern Australian beaches (PhD thesis). University of Adelaide.

Padley, D., McKirdy, D.M., Murray, A., Summons, R.E., 1993. Oil strandings on the beaches of Southern Australia: Origins from natural seepage and shipping, in: Øygard, K. (Ed.), Poster Sessions from the 16th International Meeting On Organic Geochemistry, Stavanger 1993. Falch Hurtigtrykk, pp. 660–663.

Peters, A.J., Siuda, A.N.S., 2014. A Review of Observations of Floating Tar in the Sargasso Sea. Oceanography 27, 217–221.

Roser, M., 2020. Oils Spills. Our World in Data. URL: https://ourworldindata.org/oil-spills

Ross, A., Corrick, A., Trefry, C., Gong, S., McKirdy, D., Hall, T., Dyt, C., Angelini, Z., Kempton, R., Pickard, A., White, C., Maslin, S., Griffin, D., Middleton, J., Luick, J., Armand, S., Vergara, T., Schinteie, R., 2017. Asphaltite and tarball surveys. Final Report GABRP Project 5.2. Research Report Series Number 25a.

Scarlett, A.G., Holman, A.I., Georgiev, S. V., Stein, H.J., Summons, R.E., Grice, K., 2019. Multi-spectroscopic and elemental characterization of southern Australian asphaltites. Organic Geochemistry 133, 77–91.

Schiefelbein, C.F., Zumberge, J.E., Brown, S.W., 1997. Petroleum Systems in the Far East, in: Proceedings of an International Conference on Petroleum Systems of SE Asia and Australiasia Conference, May 1997. Indonesian Petroleum Association, pp. 101–113.

Shirneshan, G., Bakhtiari, A.R., Memariani, M., 2016. Identification of sources of tar balls deposited along the Southwest Caspian Coast, Iran using fingerprinting techniques. Science of the Total Environment 568, 979–989.

Smith, D.C., Begg, G.A., Lukatelich, R., Anson, T., Baghurst, B., Ham, J., Lapidge, S., Lewis, R., Ormandy, P., Smith, R., Ward, T., 2018. A whole of systems approach to improved understanding of the environmental, economic and social values of a frontier marine oil and gas field: Establishment, success factors and lessons learnt. Deep-Sea Research Part II: Topical Studies in Oceanography 157–158, 3–10.

Smith, M.A., Donaldson, I.F., 1995. The hydrocarbon potential of the Duntroon Basin. The Australian Petroleum Production and Exploration Association Journal. 35(1), 203–219.

Sprigg, R.C., Woolley, J.B., 1963. Coastal bitumen in southern Australia with special reference to observations at Geltwood Beach, south-east South Australia. Transactions of the Royal Society of South Australia 86, 67–103.

Summons, R.E., Bradshaw, J., Brooks, D.M., Goody, A.K., Murray, A.P., Foster, C.B., 1993. Hydrocarbon composition and origins of coastal bitumens from the Northern Territory, Australia. PESA Journal 21, 31–42.

Summons, R.E., Logan, G.A., Edwards, D.S., Boreham, C.J., Bradshaw, M.T., Blevin, J.E., Totterdell, J.M., Zumberge, J.E., 2001. Geochemical analogs for australian coastal asphaltites

- search for the source rock. In: Abstracts, AAPG Annual Convention, Denver, Colorado. American Association of Petroleum Geologists Bulletin 85 (Suppl.).

Suneel, V., Ciappa, A., Vethamony, P., 2016. Backtrack modeling to locate the origin of tar balls depositing along the west coast of India. Science of The Total Environment 569–570, 31–39.

Susanto, R.D., Wei, Z., Adi, T.R., Zheng, Q., Fang, G., Fan, B., Supangat, A., Agustiadi, T., Li, S., Trenggono, M., Setiawan, A., 2016. Oceanography Surrounding Krakatau Volcano in the Sunda Strait, Indonesia. Oceanography 29, 264–272.

ten Haven, H.L., Schiefelbein, C., 1995. The Petroleum Systems of Indonesia, in: Proceedings Indonesian Petroleum Association: Twenty Fourth Annual Convention Proceedings. pp. 443–459.

Tolmer, A., 1882. Reminiscences of an adventurous and chequered career at home and at the antipodes. Sampson Low, Marston, Searle & Rivington, London.

Totterdell, J.M., Struckmeyer, H.I.M., Boreham, C.J., Mitchell, C.H., Monteil, E., Bradshaw, B.E., 2008. Mid-Late Cretaceous organic-rich rocks from the eastern Bight Basin : implications for prospectivity, in: Blevin, J.E., Bradshaw, B.E., Uruski, E. (Eds.), PESA Eastern Australasian Basins Symposium III Special Publication. pp. 137–158.

Trewartha, J., 1850. South Australian Government Gazette, 25 April, p. 282.

Upton, D., 2014. The Great Australian Bight: an emerging global hotspot. GeoExPro 11, 20–24.

Volkman, J.K., O'Leary, T., Summons, R.E., Bendall, M.R., 1992. Biomarker composition of some asphaltic coastal bitumens from Tasmania, Australia. Organic Geochemistry 18, 669–682.

Ward, L.K., 1913. The possibilities of the discovery of petroleum on Kangaroo Island and the western coast of Eyre's Peninsula. Bulletin of the Geological Survey of South Australia 2, 1–27.

Ward, L.K., 1944. The search for oil In South Australia. Bulletin of the Geological Survey of South Australia 22, 11–13.

Wood Mackenzie, 2015. Australia Great Australian Bight exploration basin, asset report.

CHAPTER 2

Remotely constraining the temporal evolution of offshore oil systems

Statement of Authorship

Title of Paper	Remotely constraining the temporal evolution of offshore oil systems	
Publication Status	☑ Published ☐ Accepted for Publication	☐ Submitted for Publication ☐ Unpublished and Unsubmitted w ork w ritten in manuscript style
Publication Details	Published in Scientific Reports. https://www.nature.com/articles/s41598-018-37884-x DOI: 10.1038/s41598-018-37884-x	

Principal Author

Name of Principal Author (Candidate)	Alexander J. Corrick		
Contribution to the Paper	Project design, fieldwork, sample preparation, geochemical data collection, processing and interpretation, wrote the manuscript and drafted all figures.		
Overall percentage (%)	75		
Certification:	This paper reports on original research I conducted during the period of my Higher Degree by Research candidature and is not subject to any obligations or contractual agreements with a third party that would constrain its inclusion in this thesis. I am the primary author of this paper.		
Signature		Date	4/10/2019

Co-Author Contributions

By signing the Statement of Authorship, each author certifies that:

i. the candidate's stated contribution to the publication is accurate (as detailed above);
ii. permission is granted for the candidate in include the publication in the thesis; and
iii. the sum of all co-author contributions is equal to 100% less the candidate's stated contribution.

Name of Co-Author	David Selby		
Contribution to the Paper	Project design, assistance with sample preparation, data collection and interpretation. Provided input to the final manuscript.		
Signature		Date	7/10/2019

Name of Co-Author	David M. McKirdy		
Contribution to the Paper	Project design, fieldwork and assistance with data interpretation. Provided input to the final manuscript.		
Signature		Date	4/10/2019

Name of Co-Author	Philip A. Hall		
Contribution to the Paper	Project design, assistance with geochemical data collection, processing and interpretation. Provided input to the final manuscript.		
Signature		Date	15/10/2019

Name of Co-Author	Se Gong		
Contribution to the Paper	Fieldwork, assistance with sample preparation, geochemical data collection and interpretation. Provided input to the final manuscript.		
Signature		Date	4/10/2019

Name of Co-Author	Christine Trefry		
Contribution to the Paper	Fieldwork, database management. Provided input to the final manuscript.		
Signature		Date	22/10/2019

Name of Co-Author	Andrew S. Ross		
Contribution to the Paper	Project design, fieldwork, assistance with data interpretation. Provided input to the final manuscript.		
Signature		Date	21/10/2019

Journal Format: ***Scientific Reports***
Status: Published (https://www.nature.com/articles/s41598-018-37884-x)
DOI: 10.1038/s41598-018-37884-x

Remotely constraining the temporal evolution of offshore oil systems

Alexander J. Corrick[1*], David Selby[2,3], David M. McKirdy[1], Phillip A. Hall[1], Se Gong[4], Christine Trefry[5] and Andrew S. Ross[5]

[1] Department of Earth Sciences, School of Physical Sciences, University of Adelaide, SA 5005, Australia

[2] Department of Earth Sciences, Durham University, Durham, DH1 3LE, UK

[3] State Key Laboratory of Geological Processes and Mineral Resources, School of Earth Resources, China University of Geosciences, Wuhan, 430074, Hubei, China

[4] Energy, CSIRO, North Ryde, NSW 2113, Australia

[5] Energy, CSIRO, Kensington, WA 6151, Australia

*** Corresponding author**

ABSTRACT

An understanding of the temporal evolution of a petroleum system is fundamental to interpreting where hydrocarbons may be trapped in the subsurface. However, traditional exploration methods provide few absolute constraints on the timing of petroleum generation. Here we show that $^{187}Re/^{187}Os$ geochronology may be applied to natural crude oil seepage to determine when petroleum generation occurred in offshore sedimentary basins. Using asphaltites collected from the South Australian coastline, our determined Re-Os age (68 ± 15 million years ago) is consistent with their derivation from a Late Cretaceous source rock in the nearby Bight Basin, an interpretation similarly favoured by source-specific biomarker constraints. Furthermore, the calculated initial $^{187}Os/^{188}Os$ composition of the asphaltites, a value inherited from the source rock at the time of oil generation, suggests that the source rock represents the later stage of Oceanic Anoxic Event 2. Our results demonstrate a new approach to identifying the origin of crude oils encountered in coastal environments by providing direct constraints on the timing of petroleum generation and potential source rock intervals in poorly characterised offshore sedimentary basins prior to exploratory drilling.

1. INTRODUCTION

Natural seepage is a major contributor of oil to the marine environment, estimated at ~600,000 tonnes per year[1]. When entrained in prevailing ocean currents, this seepage may strand along the coastline as liquid oil, viscous tar or semi-solid bitumen[2,3,4]. The distance crude oils are transported by ocean currents may be short if the seepage site is near the coastline[5]. However, there is evidence of significantly longer transport, where bitumens are found on distant foreign coastlines[3]. The geochemistry of these crude oils can be used to characterise and identify their respective parent petroleum systems and potentially distinguish them from anthropogenic inputs of oil such as tanker spillage[6].

The traditional approach to geochemically characterising and correlating crude oils utilises carbon isotopes and biomarkers to ascertain the depositional environment and organic facies of their source rocks[7]. Although specific biomarkers may broadly constrain the depositional age of a source rock and provide an estimate of its thermal maturity, none of these analytical tools yields an absolute age. Understanding the timing of oil generation from the source rock is vital to assessing the potential migration pathways and structural traps which form viable

hydrocarbon reservoirs. Consequently, petroleum exploration relies heavily on a theoretical timing of hydrocarbon generation determined from basin modelling[8]. These models are generally based on assumptions about the source rocks that may be active in the basin, which in turn introduces a component of uncertainty that may affect exploration prospects.

A major recent advance in petroleum geochemistry has been the ability to directly determine the timing of hydrocarbon generation from the source rock using the decay of ^{187}Re to ^{187}Os within the produced oil[9,10,11,12,13,14]. Studies using naturally formed oils and those produced via artificial maturation of source rocks in a laboratory setting have also demonstrated that the initial $^{187}Os/^{188}Os$ composition of an oil (Os_i) is inherited directly from the source rock at the time of generation[13,14,15]. Therefore, comparison of this Os_i value of an oil to the $^{187}Os/^{188}Os$ composition of a proposed source rock at the time of generation (Os_g) may be used to aid oil-to-source correlations, should data on the source rock be available[11,14,16]. However, previous applications of Re-Os dating using oils and bitumens have been restricted to samples collected *in-situ*, rather than examples released from the subsurface into the marine environment through natural seepage. The successful application of Re-Os geochronology to seep emissions will permit the timing of oil generation to be constrained prior to exploratory drilling.

Australia's southern margin collects bitumens emitted from a variety of different petroleum systems[2,3,17,18]. One of the rarest, but most distinctive, types encountered is known as asphaltite[2,17]. These bitumens are easily identified by their striking appearance defined by deep shrinkage cracks, conchoidal fracture and jet-black colour (Fig. 1). A combination of highly reproducible source-specific biomarkers and other hydrocarbons constrains the origin of these asphaltites to a single oil family expelled early in the oil generation window from a Mesozoic marine shale deposited under anoxic/sulfidic conditions[2,17]. Their biomarker composition is unique, and yet to be linked to any produced oil worldwide[19]. This suggests that the asphaltites are not the result of anthropogenic spillage, but rather the product of seafloor seepage from an unidentified petroleum system. Despite their prior extended immersion in seawater, recently stranded asphaltite specimens also preserve high abundances of slightly water-soluble aromatic hydrocarbons such as methylnaphthalenes and phenanthrene, indicating that the parent petroleum system is proximal to their region of stranding[2,17]. Presently, the origin of these asphaltite strandings is attributed to a source rock deposited during the Late Cretaceous global oceanic anoxic event (OAE2) at the Cenomanian-Turonian boundary (93.9 Ma) within the nearby Bight Basin[17,20]. This predominantly offshore Jurassic-Cretaceous rift basin formed

during the separation of Australia and Antarctica[21,22] and remains relatively unexplored. However, it is proposed to contain marine-derived source rocks deposited during the latest Cenomanian to earliest Turonian[20].

Here we present Re-Os data from asphaltites collected from the South Australian coastline (n = 11; Fig. 2; Table S1) during annual beach surveys in 2014–2016, as part of the Great Australian Bight Research Program[18,23]. We show that the timing of oil generation in an offshore sedimentary basin may be constrained directly using hydrocarbon seepage. This information may then be used to inform, refine or support petroleum systems models for assessing offshore exploration prospects. We then use the calculated asphaltite Os_i value to assess if their origin is consistent with an OAE2 source rock. Our findings demonstrate that the Re-Os isotope systematics of hydrocarbon seepage can provide important information constraining the evolution of offshore oil systems prior to costly exploratory drilling.



Figure 1: Large asphaltite exhibiting deep shrinkage cracks following devolatilization of low-molecular-weight hydrocarbons. Sample W13/007507, collected from Waitpinga Beach, South Australia in 2014.

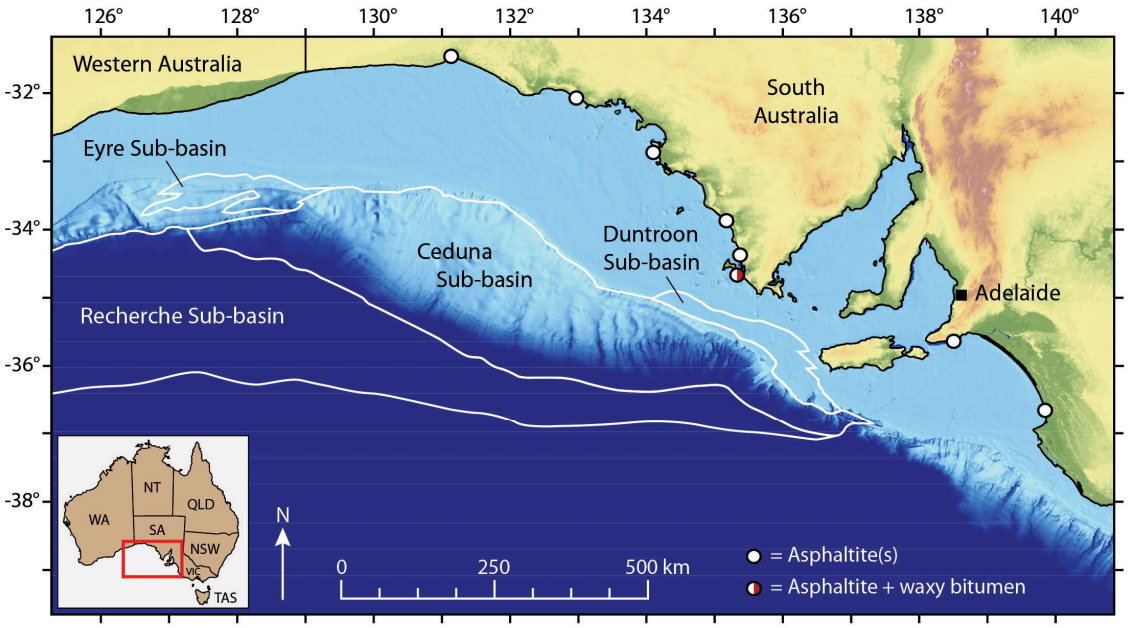


Figure 2: Stranding locations of analysed samples and the offshore Jurassic-Cretaceous sub-basins of the Bight Basin. See Table S1 for further sample collection information.

2. RESULTS

2.1. Asphaltite Re-Os data

The asphaltites contain between 2.59 and 4.02 parts per billion (ppb) Re and 24.6 to 43.1 parts per trillion (ppt) Os. The $^{187}Re/^{188}Os$ ratios are high (400.5–547.8) and positively correlate with the $^{187}Os/^{188}Os$ ratios (1.122–1.303). Regression of all the asphaltite Re-Os data from sample interiors, exteriors and replicate analyses (n = 16; Table S2) yields a Model 3 age (for which the scatter in the data exceeds that expected from analytical precision)[24] of 74 ± 26 Ma, with an Os_i of 0.63 ± 0.22 and a degree of fit (mean square of weighted deviates; MSWD) value of 2.6 (Fig. 3A). The low precision of this age (35%) can be attributed to specific data points which deviate from the best-fit regression line (i.e. the isochron). A refined Re-Os age may therefore be determined by limiting the regression to the data points with low deviation from the predicted $^{187}Os/^{188}Os$ value determined from the entire dataset[25]. A revised regression restricted to samples with less than 2% deviation from the regression line (n = 9; Table S3) yields a Model 1 age (for which the scatter in data is consistent with the uncertainties attributable to analytical precision)[24] of 68 ± 15 Ma, an Os_i of 0.66 ± 0.12 and a MSWD of 0.95 (Fig. 3B). Of the seven data points excluded, five were replicate analyses of counterparts that deviated <2% from the initial regression and were still included. The remaining two excluded data points were obtained from specimens with no replicate analyses but returned $^{187}Os/^{188}Os$ values comparable to the

other excluded data points. Samples with $^{187}Os/^{188}Os$ values that differ from the majority of the dataset could be interpreted as having originated from a second source rock. However, this is not the case here because the biomarker geochemistry of all samples analysed is highly consistent (Table S4).

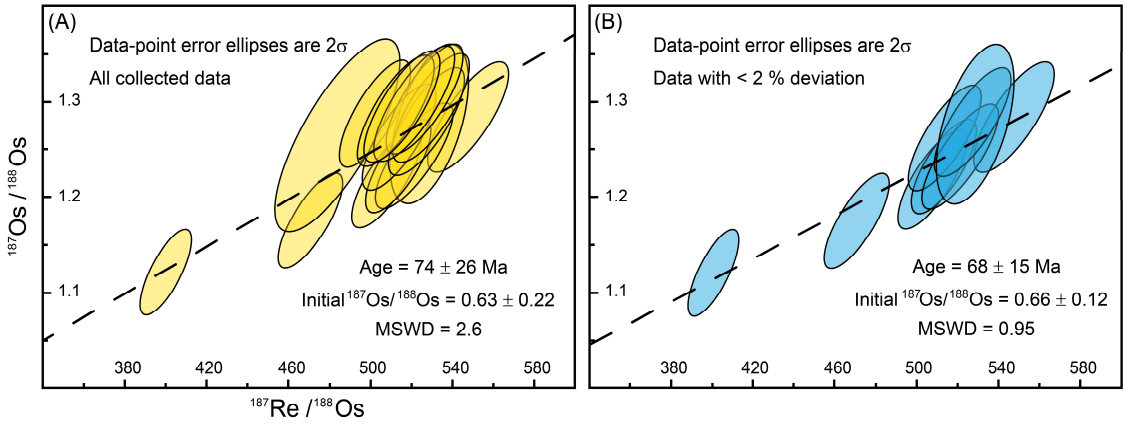


Figure 3: Re-Os isochron diagrams for South Australian asphaltites. (A) Regression of all Re-Os data (n = 16) from asphaltite interiors, weathered exteriors and replicate analyses yields an age of 74 ± 26 Ma. (B) Regression of asphaltite data with <2% deviation from the regression of all data points (n = 9; Table S3) yields an age of 68 ± 15 Ma.

2.2. Extent of alteration in the marine environment

The majority of the Re and Os in a crude oil is located in its asphaltene fraction, which is highly resistant to the effects of biodegradation[16]. However, to test if exposure to seawater influenced the Re-Os systematics of the asphaltites, the extent of degradation (Fig. 4) in each specimen was assessed based on the alteration and removal of key compounds by evaporation, water washing and biodegradation (Table S5). This assessment revealed that variation in $^{187}Re/^{188}Os$ and $^{187}Os/^{188}Os$ ratios in the sample suite is not systematic with increasing alteration. Furthermore, comparison of the weathered exteriors (top 2 mm) of four asphaltites with their respective interiors all returned ratios within the range of analytical uncertainty (Table S2). Finally, the Re-Os characteristics of the asphaltites were compared to those of a waxy bitumen specimen (W13/007697) recovered from the same coastline and known to originate from one of several distant Cenozoic lacustrine petroleum systems in the Indonesian archipelago[3]. The waxy bitumen contained very low abundances of Re and Os (0.02 ppb and 1.34 ppt, respectively), with a $^{187}Re/^{188}Os$ ratio of 84.4 and $^{187}Os/^{188}Os$ ratio of 0.486. As only a single waxy bitumen specimen was analysed for comparison, no isochron could be constructed to calculate a generation age for its parent crude oil. Nevertheless, the fact that the asphaltites and waxy bitumen, two distinctly different oil types, have clearly different Re-Os abundances and

ratios (Table S2) is significant because it suggests they have retained the signatures of their parent oils, despite their exposure to the same marine environment.

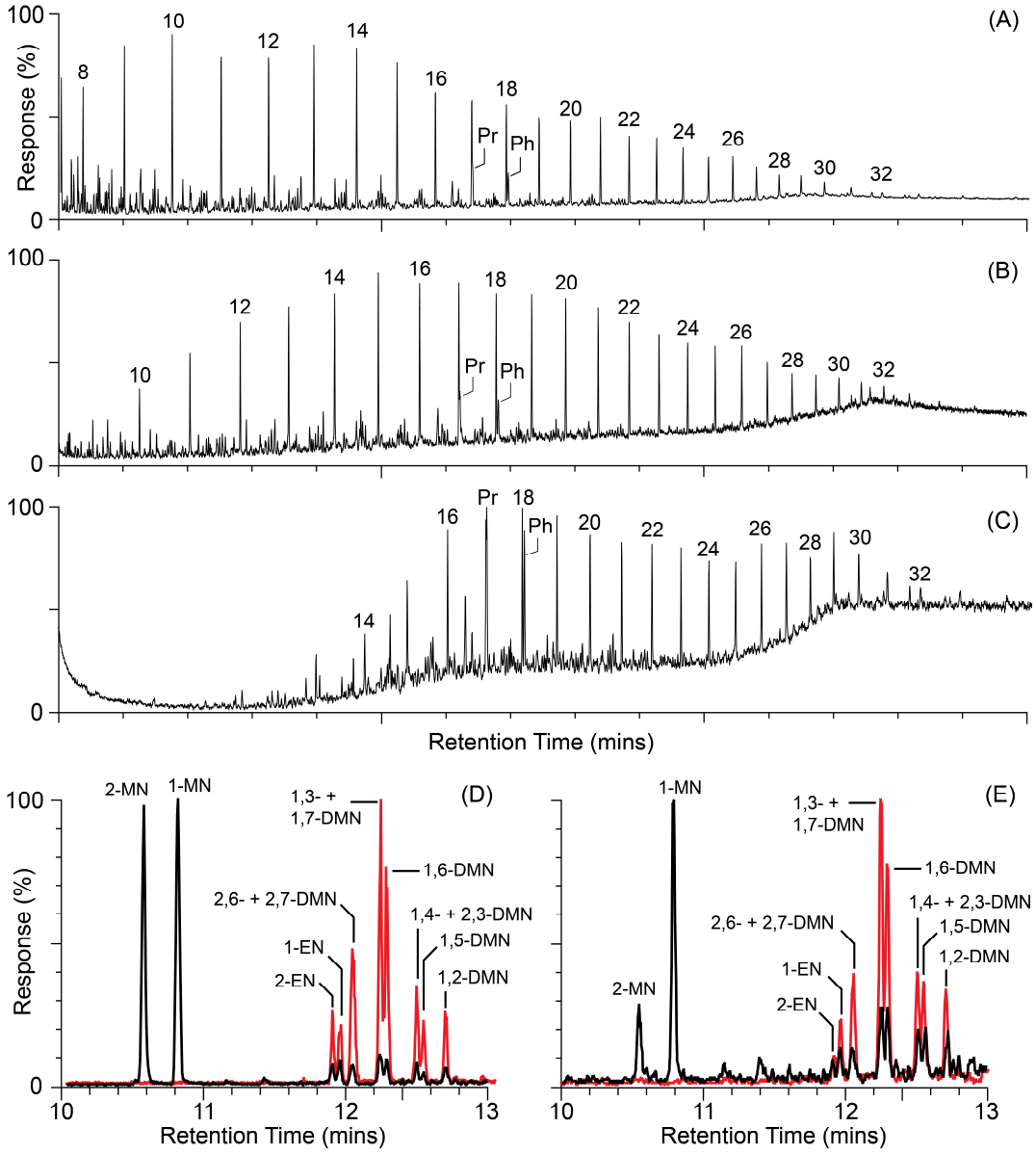


Figure 4: GC-MS chromatograms illustrating the variation in degradation across the suite of analysed asphaltites. (A) Whole-oil total ion chromatogram (TIC) of a minimally degraded asphaltite (W13/007976). (B) Whole-oil TIC of a moderately degraded asphaltite (W13/007507) showing depletion of low-molecular-weight *n*-alkanes. (C) Whole-oil TIC of a highly degraded asphaltite (W13/007668) showing loss of gasoline and kerosene-range alkanes. (D) Selected ion monitoring (SIM) chromatograms (black = *m/z* 142, red = *m/z* 156) of the aromatic fraction of a fresh asphaltite (W13/007976), preserving abundant methylnaphthalenes, ethylnaphthalenes and dimethylnaphthalenes. (E) SIM chromatograms of the aromatic fraction of a highly degraded asphaltite (W13/007668), displaying prominent loss of 2-MN, 2-EN and 1,5-DMN due to weathering. Key: peak numbers in whole-oil TIC chromatograms correspond to *n*-alkane carbon chain length; Pr = pristane; Ph = phytane; MN = methylnaphthalene; EN = ethylnaphthalene; DMN = dimethylnaphthalene. Geochemical data and assigned level of degradation for each sample is listed in Table S4. The criteria used to define each level of alteration are listed in Table S5.

2.3. Comparison with the OAE2 osmium isotope record

Following the generation and expulsion of hydrocarbons, the different abundances of ^{187}Re in the source rock and its expelled oil will cause their $^{187}Os/^{188}Os$ compositions to gradually diverge as ^{187}Re continues to decay to ^{187}Os. Therefore, in order to use osmium isotopes to assess the correlation of an oil and a potential source rock, the $^{187}Os/^{188}Os$ values at the time of oil generation must be known (i.e. it is the Os_i and Os_g values that must be compared), as this is the point when the osmium composition of the source rock was imparted directly to the oil. Unfortunately, there is no established osmium isotope record across the Cenomanian-Turonian boundary in the Bight Basin from which to determine an Os_g value for direct correlation. However, OAE2 is associated with an $^{187}Os/^{188}Os$ anomaly expressed in widely separated palaeogeographic settings[26,27,28] (Fig. 5). Therefore, to assess if the asphaltite Os_i value (0.66 ± 0.12) is consistent with that of an OAE2 source rock, we calculated the $^{187}Os/^{188}Os$ composition for each of these published records across the asphaltite generation window of 68 ± 15 Ma (Fig. 6; Table S6). These Os_g profiles preserve an abrupt shift towards non-radiogenic values (~0.2) at the onset of OAE2. The anomalously non-radiogenic conditions are maintained across the A-B stage (94.38–94.23 Ma), prior to a progressive return to radiogenic values within the B-C stage (94.23–93.95 Ma). Despite local variability, the asphaltite Os_i value most commonly intersects these OAE2 records during this B-C stage.

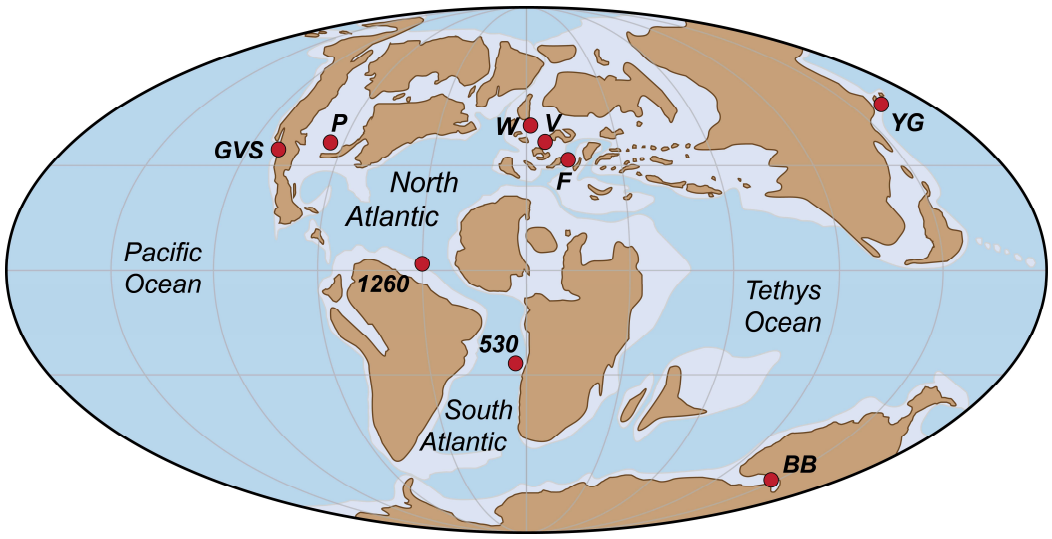


Figure 5: Palaeogeographic map identifying locations of Os isotope records across OAE2 and the location of the Bight Basin. GVS = Great Valley Sequence, P = Portland #1 (GSSP), W = Wunstorf, V = Vocontian Basin, F = Furlo, 1260 = ODP Site 1260, 530 = DSDP Site 530, YG = Yezo Group, BB = Bight Basin. Modified after reference[28].

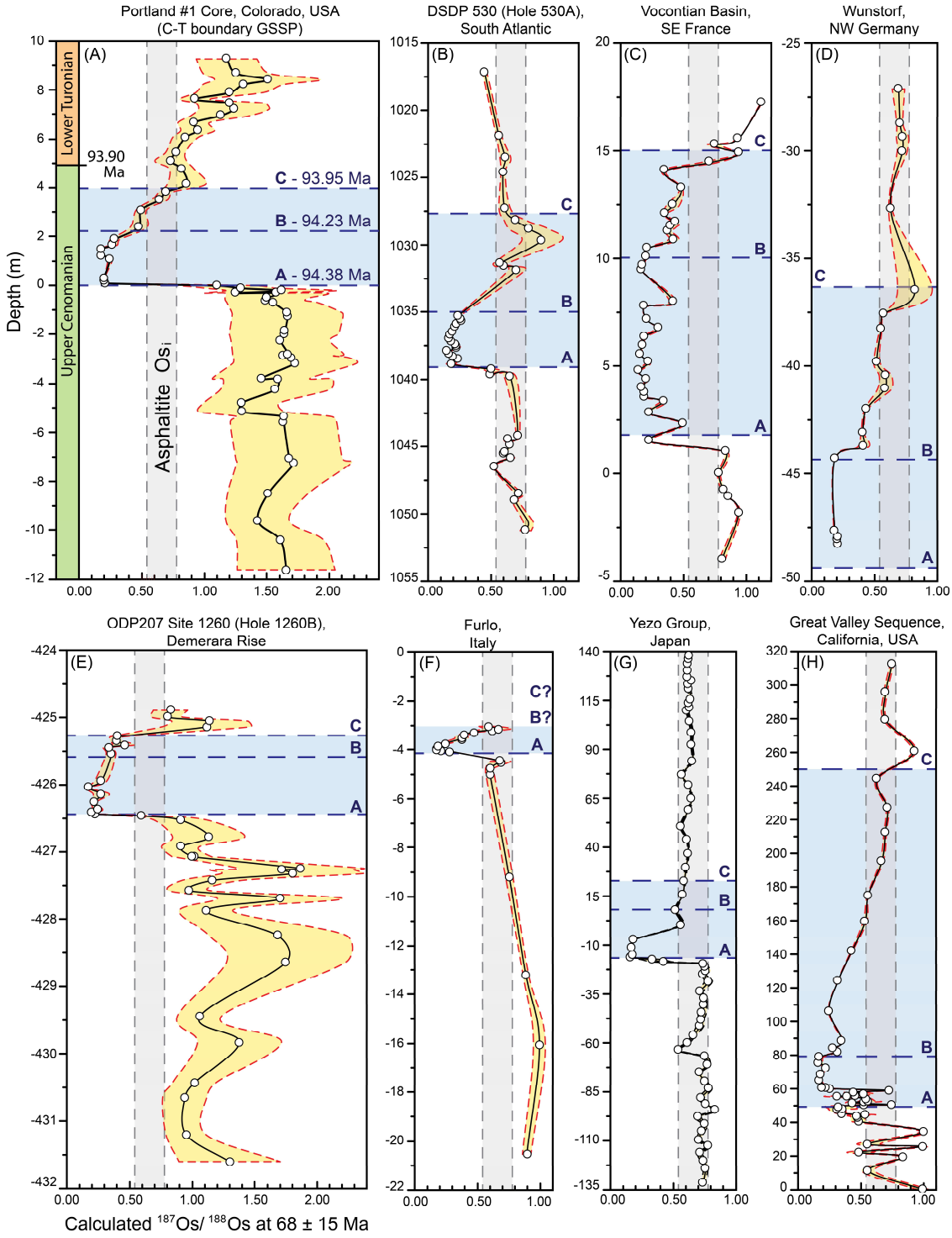


Figure 6: Variation of the calculated $^{187}Os/^{188}Os$ compositions at 68 ± 15 Ma with depth for OAE2 sections during the asphaltite generation window. The asphaltite Os_i value (0.66 ± 0.12) is shown in grey. Data points and black trendline correspond to the calculated Os_g at 68 Ma, while variation in this value due to the uncertainty associated with the generation age is shown in yellow. Areas where asphaltite Os_i value = OAE2 section Os_g value support potential oil-source correlation. Re-Os data from OAE2 sections after references[26,27,28]. Location of datums A, B and C labelled in blue within each section are defined by references[27,28,37,38,39,40,41]. The ages of these datums in the Portland #1 core were determined by references[27,42] and are supported by comparable ages in the Yezo Group[28]. All compiled Re-Os data from these records is listed in Table S6.

3. DISCUSSION

To produce a reliable age using Re-Os data three conditions must be met: (1) there must have been no addition or removal of Re or Os, i.e. the samples must remain within a closed system; (2) sufficient variation must exist in the parent/daughter ratios ($^{187}Re/^{188}Os$) to produce an isochron; and (3) the samples analysed must contain the same or near-identical initial $^{187}Os/^{188}Os$ composition[29].

A major concern when assessing material released from hydrocarbon seeps is the continued integrity of its Re-Os system despite exposure to formation waters and the marine environment. Studies of weakly to heavily biodegraded crude oils have repeatedly shown that their Re-Os system is not significantly affected by microbial alteration[10,11,13,14]. However, laboratory experiments have demonstrated rapid transfer of Re and Os to liquid oils from an enriched aqueous solution[30]. The authors of this study note that the concentrations of Re and Os used in their experiments were not intended to accurately mimic the natural environment, and that experiments attempting to do so are unlikely to yield meaningful results due to current technical limitations associated with extremely low Re and Os abundances[31]. However, their results demonstrate that Re and Os from formation waters could potentially be imparted to oil in a natural setting. This presents an alternative mechanism for resetting the Re-Os geochronometer and therefore, what the resulting age constrains. If interaction with formation waters occurred in a geologically short timeframe after generation then Re-Os geochronology may still approximate a generation age, although it would actually represent the timing of formation water interaction. Additionally, if the formation waters comprised contemporaneous seawater from when the source rocks were deposited, the resulting $^{187}Os/^{188}Os$ composition of the oil would still correlate to the average source rock value. However, if interaction with formation waters occurred much later, the resetting of the geochronometer would constrain the timing of this later alteration. Additionally, if the formation waters comprised migrated groundwater containing Os inherited from sources other than seawater from the time of source rock deposition, then oil-source correlation using the oil's Os_i value would be compromised. Understanding the role played by formation waters in the Re-Os systematics of crude oils in a natural setting is clearly a crucial topic which warrants further investigation. However, it is not practical to assess this competing hypothesis here, as the parent petroleum system of the asphaltites remains undiscovered and is thought to reside within a relatively unexplored basin. Therefore, reliably constraining the impact of groundwater-oil interactions in the subsurface for this system is not currently possible.

Similarly, if the asphaltites sequestered Re and Os from seawater during their time exposed to the marine environment, the required closed system may be compromised, progressively altering the $^{187}Os/^{188}Os$ composition of the bitumen towards the present marine value of ~1.06[32]. Such alteration would be expected to increase with continued exposure to seawater. In the case of the asphaltites, their degree of alteration due to both water washing and biodegradation permits an assessment of which specimens have spent the most time in contact with seawater (Fig. 4; Tables S4 and S5). Increasingly degraded asphaltites and interior/exterior comparisons show no systematic trends in their $^{187}Re/^{188}Os$ and $^{187}Os/^{188}Os$ ratios which could reasonably be attributed to weathering. Furthermore, comparison with a second variety of coastal bitumen from a different petroleum system (waxy bitumen sample W13/007697) demonstrates that the oils retain unique values. Therefore, any alteration of the asphaltites due to their contact with seawater, which contains only trace concentrations of Re and Os, does not appear to have caused a quantifiable disruption of their Re-Os system.

Although our asphaltite sample suite displays sufficient variation in $^{187}Re/^{188}Os$ to produce a meaningful isochron (Fig. 3), the mechanism behind this variation is not fully understood. As discussed above, variation may be driven by interaction with formation waters[30], or because the asphaltites analysed in this study were collected over the course of three years, and likely represent products of continuous, low intensity seepage. Therefore, the variation could also be attributable to the prolonged duration (>1 Myr) of bitumen generation and expulsion when the chronometer is initially reset[12].

The MSWD of the revised regression (Fig. 3B) is low (<1), owing to the tight clustering of the analysed samples. Although an improvement from the regression of all asphaltite Re-Os data, the revised regression also yields a date that is still relatively imprecise (68 ± 15 Ma, 22%). Such a spread in a Re-Os generation age is not abnormal[11,13,14], and likely the result of prolonged generation over millions of years, combined with variation in the initial $^{187}Os/^{188}Os$ composition of the source unit[11,12,14]. Potential mixing of variable $^{187}Os/^{188}Os$ values across a source rock may be particularly applicable to oils and bitumen derived from OAE2 deposits, given the extent of variability at metre to centimetre scale across the interval (Fig. 6). Progressive generation across the OAE2 interval, potentially augmented by hydrocarbons expelled from thermally mature, pre- or post-OAE2 organic matter, would likely create a spread in the Os_i values of the resulting oil, thereby reducing the precision of the final Re-Os age.

Assessment of Cretaceous potential source rocks in the Bight Basin using a two-dimensional basin model suggests that a Cenomanian-Turonian source interval would have generated and expelled hydrocarbons from the mid-Campanian (~74 Ma) to the present[20]. A previous one-dimensional model also supports generation starting from approximately the mid-Campanian[33]. The age determined by the Re-Os systematics of the asphaltites is consistent with these models, supporting the interpretation that this age represents the timing of generation and that the parent petroleum system incorporates an OAE2 source rock.

Previous studies conclude that the Os_i value of an oil is inherited directly from its source rock and may therefore aid oil-source correlations[9,10,11,13,14,15]. The comparison of the asphaltite Os_i with the Os_g profiles of other, well-studied examples of OAE2 may provide preliminary interpretations regarding the nature of the asphaltite source, as the event preserves globally reproducible trends (Fig. 6). In no case do the asphaltites appear likely to be derived exclusively from organic matter deposited during the onset of OAE2, as the Os_i (0.66 ± 0.12) is notably more radiogenic than the calculated Os_g of the A-B interval (~0.2; Fig. 6). However, in most examples, the asphaltite Os_i range is consistent with the Os_g values in the latter section of OAE2 (interval B-C), as well as those of the pre- and post-OAE2 intervals in certain regions (Fig. 6).

Although the asphaltites are thought to originate from an OAE2 source rock[17,20], no exploratory or stratigraphic drilling within the Bight Basin has reached the Cenomanian-Turonian boundary to provide confirmation. A recent attempt to assess the potential for preservation of an OAE2 interval within the Bight Basin by the International Ocean Discovery Program (IODP) Expedition 369 was unable to reach to the necessary depth, due to a hole deviation of ~26° from vertical during coring operations[34]. The fact that organic-rich lithofacies associated with OAE2 are yet to identified and sampled does not preclude the possibility that other source rocks which may have been deposited in the offshore Bight Basin due to local anoxic conditions arising from its palaeogeographic location within a narrow re-entrant of the Tethys Ocean (Fig. 5). This scenario would similarly satisfy the requirements defined by their geochemistry[2,17]. Multiple alternative marine intervals with high source potential are also inferred from the late Aptian to Santonian in the Bight Basin based on the tectonostratigraphic framework defined by data from wells drilled in the proximal regions of the basin[21,33]. However, the existence of these putative basinward source intervals is similarly yet to be confirmed.

While the OAE2 interval is characterised by an abrupt non-radiogenic shift in $^{187}Os/^{188}Os$ values (Fig. 6), the global record also demonstrates regional variability driven by differential inputs of osmium from local continental weathering and submarine volcanism[27,28]. The extent to which such inputs may have impacted the $^{187}Os/^{188}Os$ ratio across the Cenomanian-Turonian boundary interval in the Bight Basin remains unknown until a local record becomes available. Meanwhile, the lack of relevant analytical data on potential source rocks in the distal reaches of the basin precludes definitive asphaltite-source rock correlation. Such gaps in the knowledge of frontier basins are common. The uncertainties inherent in our initial interpretation of the Os isotope signatures of these Australian asphaltites will be reduced as understanding of the geology and geochemistry of the Bight Basin improves with further exploration.

4. CONCLUSIONS

Through the application of Re-Os radiometric dating to heavy asphaltic crude oil released from natural seafloor seepage we have demonstrated that the technique may be applied to constrain the timing of hydrocarbon generation and potential source intervals within offshore sedimentary basins. The Re-Os systematics of crude oils stranding in coastal environments may therefore have widespread application to the identification of their respective offshore hydrocarbon systems. The ability to inform or validate the timing of generation determined from basin models provides a new approach to reducing the uncertainty and risk associated with petroleum exploration in frontier basins, particularly in deepwater settings where the cost of exploratory drilling is extremely high. Our findings also highlight the potential use of Os isotopes in correlating oils to their parent source rocks at high resolution, particularly those deposited during OAE2 which exhibit highly anomalous $^{187}Os/^{188}Os$ values. However, such correlations may be affected by inherent local variability in the marine osmium isotope record and hence wherever possible should use data from the proposed source rock in the basin of origin, rather than the global record.

5. MATERIALS AND METHODS

5.1. Re-Os isotope data

All Re-Os sample preparation and isotopic analyses were conducted at the Laboratory for Source Rock Geochronology and Geochemistry and Arthur Holmes Laboratory at Durham University (UK). Samples were prepared for Re-Os analysis using published methods[16]. Approximately 200 mg of whole oil sample from each asphaltite was dissolved in a minimum volume of chloroform ($CHCl_3$) and loaded into a Carius tube, with the solvent subsequently evaporated at 65 °C. All samples were then spiked with a mixed tracer solution containing a known amount of ^{185}Re and ^{190}Os. The tracer solution was homogenised with the sample in the Carius tube using inverse *aqua regia* (3 mL of ~12 N HCl, 6 mL of 16 N HNO_3) and heated at 220 °C for 48 hours. Osmium was subsequently extracted and purified using $CHCl_3$ solvent extraction and microdistillation. The Re-bearing *aqua regia* was dried on a hot plate at 80 °C overnight and then purified by NaOH-acetone solvent extraction and anion chromatography.

The purified Re and Os were loaded onto Ni and Pt wire filaments, respectively, and analysed by Negative Thermal Ionization Mass Spectrometry (NTIMS) on a Thermo Scientific TRITON mass spectrometer. The total procedural blanks were 2.4 ± 1.0 pg/g for Re and 0.15 ± 0.05 pg/g for Os, with a $^{187}Os/^{188}Os$ of 0.25 ± 0.05 (n = 4). The uncertainty for all Re-Os data was determined using full error propagation of uncertainties. The Re-Os data were regressed using *Isoplot V4.15*[24] and a ^{187}Re decay constant of 1.666×10^{-11} a^{-1} [35].

5.2. Re-Os data deviation assessment

Data points responsible for introducing significant uncertainty in the regression of all the available data (Fig. 3A) were identified by determining the percentage of deviation between the observed $^{187}Os/^{188}Os$ composition in each sample compared to the predicted value defined by the regression described by Equation (1). The calculated value for each sample was obtained using the isochron equation listed as Equation (2), where λ is the decay constant for ^{187}Re and t is the age in years, using values defined by the regression of all of data points (i.e. where $t = 68$ Myr and $^{187}Os/^{188}Os_{initial} = 0.63$). Samples with a deviation of >2% from the initial regression were excluded for the revised regression (Fig. 3B).

$$\text{Deviation (\%)} = ({}^{187}Os/{}^{188}Os_{measured} - {}^{187}Os/{}^{188}Os_{calculated\ from\ data\ best\text{-}fit\ initial}) \times 100 \quad (1)$$

$${}^{187}Os/{}^{188}Os = {}^{187}Os/{}^{188}Os_{initial} + {}^{187}Re/{}^{188}Os \times (e^{\lambda t} - 1) \quad (2)$$

5.3. Calculation of OAE2 osmium composition during the asphaltite generation window

The $^{187}Os/^{188}Os$ composition of each OAE2 section during the asphaltite generation window of 68 ± 15 Ma was calculated using Equation (2) and the composition of each individual data point is listed in Table S6.

5.4. Whole-oil gas chromatography-mass spectrometry

All sample preparation and analyses were conducted in the Biogeochemistry Laboratory at the University of Adelaide. A sub-sample (≤200 mg) was removed from each bitumen specimen and dissolved in 10 mL of dichloromethane/methanol (93:7, v:v). An aliquot of this solution was used for whole-oil GC-MS. Analyses of the samples collected in 2014 and 2015 were performed on an Agilent 6890 gas chromatograph interfaced with a 5973 N MSD (electron energy 70 eV) and tuned using automatic setup parameters for each sequence. Chromatography was carried out on an Agilent HP-5MS fused silica column (30 m × 0.25 mm i.d. × 0.25 μm film thickness), using either a split (50 mL/min) or splitless injection mode, the latter employed if split injection data showed low responses. The oven was held at an initial temperature of 50 °C for 1 min, followed by heating at 8 °C/min to 300 °C. The carrier gas was helium at a flow rate of 1 mL/minute. GC-MS analyses of the samples collected in 2016 were performed on an Agilent 7890B gas chromatograph interfaced with a 5977B MSD (electron energy 70 eV) and tuned using automatic setup parameters for each sequence. Chromatography was undertaken on a J&W DB-5MS fused silica column (30 m × 0.25 mm i.d. × 0.25 μm film thickness), using the same operating conditions as employed for the 2014 and 2015 samples. In both cases, whole-oil GC-MS was conducted in the scan mode (scan interval 45–500 AMU at approx. 3 scans/sec). All data were processed using *MSD ChemStation* (Agilent Technologies, Inc.).

5.5. Isolation of saturated, aromatic and asphaltene fractions

The saturated and aromatic hydrocarbon fractions were separated from 20 mg aliquots of whole bitumen using silica gel liquid chromatography[36]. The recovered saturated hydrocarbons were stored in 2 mL chromatography vials and the aromatics in 2 mL amber glass vials to ensure minimal degradation by ultraviolet light. The asphaltene fraction of each sample was separated by adding an excess of *n*-pentane to bulk bitumen sub-samples (0.3–0.7 g) dissolved in a mixture of dichloromethane and methanol (93:7). The dissolved maltene fraction was then removed using a Pasteur pipette, allowing the precipitated asphaltene fraction to be dried and weighed.

5.6. Selected ion monitoring gas chromatography-mass spectrometry (SIM GC-MS)

GC-MS analysis of the saturated hydrocarbon fractions for sterane and hopane degradation assessment was performed on an Agilent 7890 A gas chromatograph interfaced with a 5975 C MSD (electron energy 70 eV) tuned using automatic setup parameters on the day of the analysis. Chromatography was carried out on a J&W DB-5MS fused silica column (60 m × 0.25 mm i.d. × 0.25 µm film thickness). A 1 µL aliquot of the saturates fraction was injected into the split/splitless injector at 300 °C operating in splitless mode. After being held at an initial temperature of 40 °C for 2 minutes, the oven was heated at 20 °C/minute to 200 °C and then ramped to 310 °C at 2 °C/minute. The carrier gas was helium at a flow rate of 1.5 mL/min.

GC-MS analyses of the aromatic fractions to determine alteration to water-soluble compounds was performed on a Perkin Elmer SQ8T/680 Clarus gas chromatograph. Chromatography was carried out on a Perkin Elmer PE-5MS fused silica column (30 m × 0.25 mm i.d. × 0.25 µm film thickness). A 1 µL aliquot of the aromatics fraction was injected into the split/splitless injector at 300 °C operating in splitless mode. The oven temperature was held at 50 °C for 1 min., followed by heating at 8 °C/min to 300 °C. Helium was the carrier gas at a flow rate of 1 ml/min. Data were acquired in the scan mode (Scan 45:500AMU at approx. 3 scans/sec).

ACKNOWLEDGEMENTS

We thank C. Dyt, Z. Angelini, R. Kempton, C. White, A. Pickard, S. Maslin, S. Armand, L. Tucker and S. Margot for assistance in completing the 2014–2016 beach surveys. We also thank S. Valladares for the donation of asphaltites from his private collection for this research and A. Hofmann and G. Nowell for assistance with the Re-Os determinations. A.J.C. acknowledges the support of a University of Adelaide postgraduate scholarship. D.S. acknowledges the Total Endowment Fund and the CUG Wuhan Dida Scholarship. This research was funded by the Bernold M. “Bruno” Hanson Memorial Environmental Grant awarded by the AAPG Grants-In-Aid Program and the D R Stranks Travelling Fellowship awarded by the University of Adelaide to A.J.C. Fieldwork and further travel financial support was provided by the Great Australian Bight Research Program. The Great Australian Bight Research Program is a collaboration between BP, CSIRO, the South Australian Research and Development Institute (SARDI), the University of Adelaide, and Flinders University. The program aims to provide a whole-of- system understanding of the environmental and social values of the region; providing an information source for all to use.

SUPPLEMENTARY INFORMATION AND PUBLISHED MANUSCRIPT

The supplementary information for this chapter may be found in pages 214–230.

The published version of this chapter may be found in pages 309–318.

REFERENCES

1. National Research Council. *Oil in the Sea III: Inputs, Fates and Effects*. (The National Academies Press, Washington DC, 2003). doi:10.17226/10388

2. Edwards, D., McKirdy, D. M. & Summons, R. E. Enigmatic asphaltites from the southern Australian margin: molecular and carbon isotopic composition. *Pet. Explor. Soc. Aust. J.* **26,** 397–420 (1998).

3. Edwards, D. S., McKirdy, D. M., Rowland, S. J., Heath, D. J. & Gray, P. S. Waxy bitumen stranding in southern Australia: A geochemical study of multiple oil families and their likely origins. *Org. Geochem.* **118,** 132–151 (2018).

4. Warnock, A. M., Hagen, S. C. & Passeri, D. L. Marine Tar Residues: a Review. *Water, Air, Soil Pollut.* **226,** 24 (2015).

5. Lorenson, T. D. *et al. Natural Offshore Oil Seepage and Related Tarball Accumulation on the California Coastline; Santa Barbara Channel and the Southern Santa Maria Basin; source identification and inventory*. *U.S. Geological Survey Open-File Report 2009-1225 and MMS report 2009-030* (2009).

6. Kvenvolden, K. A. & Cooper, C. K. Natural seepage of crude oil into the marine environment. *Geo-Marine Lett.* **23,** 140–146 (2003).

7. Peters, K. E., Walters, C. C. & Moldowan, J. M. *The Biomarker Guide Volume 2: Biomarkers and Isotopes in Petroleum Exploration and Earth History*. (Cambridge University Press, 2005).

8. Olaru, R. *et al.* 3D Basin modelling of Oligocene - Miocene Maikop source rocks offshore Romania and in and in the Western Black Sea. *J. Pet. Geol.* **41,** 351–365 (2018).

9. Selby, D. & Creaser, R. A. Direct radiometric dating of hydrocarbon deposits using rhenium-osmium isotopes. *Science* **308,** 1293–5 (2005).

10. Selby, D., Creaser, R., Dewing, K. & Fowler, M. Evaluation of bitumen as a Re–Os geochronometer for hydrocarbon maturation and migration: A test case from the Polaris MVT deposit, Canada. *Earth Planet. Sci. Lett.* **235,** 1–15 (2005).

11. Finlay, A. J., Selby, D. & Osborne, M. J. Re-Os geochronology and fingerprinting of United Kingdom Atlantic margin oil: Temporal implications for regional petroleum systems. *Geology* **39,** 475–478 (2011).

12. Lillis, P. G. & Selby, D. Evaluation of the rhenium–osmium geochronometer in the Phosphoria petroleum system, Bighorn Basin of Wyoming and Montana, USA. *Geochim. Cosmochim. Acta* **118,** 312–330 (2013).

13. Cumming, V. M., Selby, D., Lillis, P. G. & Lewan, M. D. Re–Os geochronology and Os isotope fingerprinting of petroleum sourced from a Type I lacustrine kerogen: Insights from the natural Green River petroleum system in the Uinta Basin and hydrous pyrolysis experiments. *Geochim. Cosmochim. Acta* **138,** 32–56 (2014).

14. Liu, J., Selby, D., Obermajer, M. & Mort, A. Re-Os geochronology and oil-source correlation of Duvernay Petroleum System, Western Canada Sedimentary Basin: Implications for the application of the Re-Os geochronometer to petroleum systems. *Am. Assoc. Pet. Geol. Bull.* **102,** 1627–1656 (2017).

15. Rooney, A. D., Selby, D., Lewan, M. D., Lillis, P. G. & Houzay, J.-P. Evaluating Re–Os systematics in organic-rich sedimentary rocks in response to petroleum generation using hydrous pyrolysis experiments. *Geochim. Cosmochim. Acta* **77,** 275–291 (2012).

16. Selby, D., Creaser, R. A. & Fowler, M. G. Re–Os elemental and isotopic systematics in crude oils. *Geochim. Cosmochim. Acta* **71,** 378–386 (2007).

17. Hall, P. A., McKirdy, D. M., Grice, K. & Edwards, D. S. Australasian asphaltite strandings: Their origin reviewed in light of the effects of weathering and biodegradation on their biomarker and isotopic profiles. *Mar. Pet. Geol.* **57,** 572–593 (2014).

18. Ross, A. *et al. Asphaltite and tarball surveys. Final Report GABRP Project 5.2. Research Report Series Number 25a*. (2017).

19. Summons, R. E. *et al.* Geochemical Analogs for Australian Coastal Asphaltites - Search for the Source Rock. in *AAPG Annual Convention, Denver, Colorado* (AAPG Search and Discovery Article #90906, 2001).

20. Totterdell, J. M. *et al.* Mid-Late Cretaceous organic-rich rocks from the eastern Bight Basin : implications for prospectivity. in *PESA Eastern Australasian Basins Symposium III Special Publication* (eds. Blevin, J. E., Bradshaw, B. E. & Uruski, E.) 137–158 (2008).

21. Totterdell, J. M. *et al.* A new sequence framework for the Great Australian Bight: Starting with a clean slate. *APPEA J.* **40,** 95–118 (2000).

22. Totterdell, J. M. & Bradshaw, B. E. The structural framework and tectonic evolution of the Bight Basin. in *PESA Eastern Australasian Basins Symposium II* (eds. Boult, P. J., Johns, D. R. & Lang, S. C.) 41–61 (Petroleum Exploration Society of Australia (PESA), 2004).

23. Baghurst, B. *et al.* Findings from the Great Australian Bight Research Program – an integrated study of environmental, economic and social values. *APPEA J.* **57,** 388–392 (2017).

24. Ludwig, K. *User's manual for Isoplot version 3.75-4.15: a geochronological toolkit for Microsoft Excel*. (Berkley Geochronological Center Special Publication No. 5, 2012).

25. Selby, D. & Creaser, R. A. Re–Os geochronology of organic rich sediments: an evaluation of organic matter analysis methods. *Chem. Geol.* **200,** 225–240 (2003).

26. Turgeon, S. C. & Creaser, R. A. Cretaceous oceanic anoxic event 2 triggered by a massive magmatic episode. *Nature* **454,** 323–326 (2008).

27. Du Vivier, A. D. C. *et al.* Marine $^{187}Os/^{188}Os$ isotope stratigraphy reveals the interaction of volcanism and ocean circulation during Oceanic Anoxic Event 2. *Earth Planet. Sci. Lett.* **389,** 23–33 (2014).

28. Du Vivier, A. D. C., Selby, D., Condon, D. J., Takashima, R. & Nishi, H. Pacific 187Os/188Os isotope chemistry and U–Pb geochronology: Synchroneity of global Os isotope change across OAE 2. *Earth Planet. Sci. Lett.* **428,** 204–216 (2015).

29. Cohen, A. S., Coe, A. L., Bartlett, J. M. & Hawkesworth, C. J. Precise Re–Os ages of organic-rich mudrocks and the Os isotope composition of Jurassic seawater. *Earth Planet. Sci. Lett.* **167,** 159–173 (1999).

30. Mahdaoui, F., Michels, R., Reisberg, L., Pujol, M. & Poirier, Y. Behavior of Re and Os during contact between an aqueous solution and oil: Consequences for the application of the Re–Os geochronometer to petroleum. *Geochim. Cosmochim. Acta* **158,** 1–21 (2015).

31. Reisberg, L., Michels, R. & Mahdaoui, F. Reply to the comment by Wu et al. (2016) on "Behavior of Re and Os during contact between an aqueous solution and oil: Consequences for the application of the Re–Os geochronometer to petroleum" [Geochim. Cosmochim. Acta 158 (2015) 1–21]. *Geochim. Cosmochim. Acta* **186,** 348–350 (2016).

32. Peucker-Ehrenbrink, B. & Ravizza, G. The marine osmium isotope record. *Terra Nov.* **12,** 205–219 (2000).

33. Struckmeyer, H. I. M. *et al.* in *Eastern Australian Basin Symposium, A Refocused Energy Perspective for the Future. Petroleum Exploration Society of Australia, Special Publication* (eds. Hill, K. C. & Bernecker, T.) 543–552 (2001).

34. Huber, B. T., Hobbs, R. W., Bogus, K. A. & Scientists, E. 369. *Expedition 369 Preliminary Report: Australia Cretaceous Climate and Tectonics*. (2018). doi:10.14379/iodp.pr.369.2018

35. Smoliar, M. I., Walker, R. J. & Morgan, J. W. Re-Os Ages of Group IIA, IIIA, IVA, and IVB Iron Meteorites. *Science (80-.).* **271,** 1099–1102 (1996).

36. Bastow, T. P., van Aarssen, B. G. K. & Lang, D. Rapid small-scale separation of saturate, aromatic and polar components in petroleum. *Org. Geochem.* **38,** 1235–1250 (2007).

37. Sageman, B. B., Meyers, S. R. & Arthur, M. A. Orbital time scale and new C-isotope record for Cenomanian-Turonian boundary stratotype. *Geology* **34,** 125–128 (2006).

38. Jenkyns, H. C., Matthews, A., Tsikos, H. & Erel, Y. Nitrate reduction, sulfate reduction, and sedimentary iron isotope evolution during the Cenomanian-Turonian oceanic anoxic event. *Paleoceanography* **22,** 1–17 (2007).

39. Forster, A., Schouten, S., Moriya, K., Wilson, P. A. & Sinninghe Damsté, J. S. Tropical warming and intermittent cooling during the Cenomanian/Turonian oceanic anoxic event 2: Sea surface temperature records from the equatorial Atlantic. *Paleoceanography* **22,** 1–14 (2007).

40. Forster, A. *et al.* The Cenomanian/Turonian oceanic anoxic event in the South Atlantic: New insights from a geochemical study of DSDP Site 530A. *Palaeogeogr. Palaeoclimatol. Palaeoecol.* **267,** 256–283 (2008).

41. Jarvis, I., Lignum, J. S., Gröcke, D. R., Jenkyns, H. C. & Pearce, M. A. Black shale deposition, atmospheric CO2 drawdown, and cooling during the Cenomanian-Turonian Oceanic Anoxic Event. *Paleoceanography* **26,** 1–17 (2011).

42. Meyers, S. R. *et al.* Intercalibration of radioisotopic and astrochronologic time scales for the Cenomanian-Turonian boundary interval, western interior Basin, USA. *Geology* **40,** 7–10 (2012).

CHAPTER 3

A second type of highly asphaltic crude oil seepage stranded on the South Australian coastline

Statement of Authorship

Title of Paper	A second type of highly asphaltic crude oil seepage stranded on the South Australian coastline	
Publication Status	☑ Published ☐ Accepted for Publication	☐ Submitted for Publication ☐ Unpublished and Unsubmitted w ork w ritten in manuscript style
Publication Details	Published in Marine and Petroleum Geology. https://www.sciencedirect.com/science/article/pii/S026481721930491X DOI: 10.1016/J.MARPETGEO.2019.104062	

Principal Author

Name of Principal Author (Candidate)	Alexander J. Corrick		
Contribution to the Paper	Project design, fieldwork, sample preparation, geochemical data collection, processing and interpretation, wrote the manuscript and drafted all figures.		
Overall percentage (%)	80		
Certification:	This paper reports on original research I conducted during the period of my Higher Degree by Research candidature and is not subject to any obligations or contractual agreements with a third party that would constrain its inclusion in this thesis. I am the primary author of this paper.		
Signature		Date	4/10/2019

Co-Author Contributions

By signing the Statement of Authorship, each author certifies that:

i. the candidate's stated contribution to the publication is accurate (as detailed above);
ii. permission is granted for the candidate in include the publication in the thesis; and
iii. the sum of all co-author contributions is equal to 100% less the candidate's stated contribution.

Name of Co-Author	Philip A. Hall		
Contribution to the Paper	Assisted with geochemical data collection, processing and interpretation. Provided input to the final manuscript.		
Signature		Date	15/10/2019

Name of Co-Author	Se Gong		
Contribution to the Paper	Fieldwork, assistance with sample preparation, geochemical data collection and interpretation. Provided input to the final manuscript.		
Signature		Date	4/10/2019

Name of Co-Author	David M. McKirdy		
Contribution to the Paper	Project design, fieldwork and assistance with data interpretation. Provided input to the final manuscript.		
Signature		Date	4/10/2019

Name of Co-Author	David Selby		
Contribution to the Paper	Assistance with sample preparation, data collection and interpretation. Provided input to the final manuscript.		
Signature		Date	7/10/2019

Name of Co-Author	Christine Trefry		
Contribution to the Paper	Fieldwork, database management. Provided input to the final manuscript.		
Signature		Date	22/10/2019

Name of Co-Author	Andrew S. Ross		
Contribution to the Paper	Project design, fieldwork, assistance with data interpretation. Provided input to the final manuscript.		
Signature		Date	21/10/2019

Journal Format: ***Marine and Petroleum Geology***
Status: Published (https://www.sciencedirect.com/science/article/pii/S026481721930491X)
DOI: 10.1016/J.MARPETGEO.2019.104062

A second type of highly asphaltic crude oil seepage stranded on the South Australian coastline

Alexander J. Corrick[1*], Phillip A. Hall[1], Se Gong[2], David M. McKirdy[1], David Selby[3,4], Christine Trefry[5] and Andrew S. Ross[5]

[1] Department of Earth Sciences, School of Physical Sciences, University of Adelaide, SA 5005, Australia

[2] Energy, CSIRO, North Ryde, NSW 2113, Australia

[3]Department of Earth Sciences, Durham University, Durham, DH1 3LE, UK

[4] State Key Laboratory of Geological Processes and Mineral Resources, School of Earth Resources, China University of Geosciences, Wuhan, 430074, Hubei, China

[5] Energy, CSIRO, Kensington, WA 6151, Australia

*** Corresponding author**: *alexander.corrick@adelaide.edu.au*

HIGHLIGHTS

1) Report a new type of oil found on South Australian coastline termed asphaltic tar

2) Asphaltic tars share several source characteristics with well-studied asphaltites

3) Clear correlation to asphaltites is complicated by differences in thermal maturity

4) Asphaltic tars may have been altered by thermochemical sulphate reduction

KEYWORDS

Bight Basin; asphaltite; asphaltic tar; oil-oil correlation; CSIA; sulphur isotopes; Re-Os; thermochemical sulphate reduction

ABSTRACT

Strandings of semi-solid to solid asphaltic bitumen along the coastline of South Australia have been reported as far back as the late 1800s. Hitherto only a single variety, now referred to as asphaltite, has been attributed to seepage from the nearby Bight Basin. The geochemistry of the asphaltites suggest they were derived from a marine source rock deposited under anoxic or euxinic conditions, most likely a Cretaceous ocean anoxic event, and were generated within the early/main oil window. Here we identify a new type of semi-solid asphaltic bitumen collected following a severe storm event in 2016. Termed asphaltic tars, these viscous oils bear a strong geochemical resemblance to the asphaltites. Both oil types have high asphaltene contents, identical *n*-alkane carbon isotopic profiles and near identical source-specific sterane distributions. However, several notable geochemical variations can distinguish these new strandings from the asphaltites. The most notable of these differences include heavier bulk sulphur isotopic composition, extremely high abundances of Re and Os with distinct $^{187}Re/^{188}Os$ and $^{187}Os/^{188}Os$ values and thermal maturity parameters consistent with generation in the late oil window. The differences in sulphur isotopic composition and Re-Os systematics could be considered evidence that despite their other source-specific similarities, the asphaltic tars originated from a different source rock. However, alteration of these two parameters can occur due to thermochemical sulphate reduction. Conclusive identification of this alteration process typically relies on further diagnostic parameters which are unfortunately not available in the case of coastal oil strandings. This introduces uncertainty to the correlation of these two types of asphaltic oil. In either scenario, the similarities between these two types of oil suggest their source rock(s) contained highly comparable organic matter inputs. We therefore attribute the origin of these new asphaltic tar strandings to natural seepage from the offshore Bight Basin.

1. INTRODUCTION

Ocean beaches along Australia's southern margin are known to collect bitumen emitted from seafloor seeps associated with a variety of different petroleum systems (e.g. McKirdy et al., 1986, 1994; Padley, 1995; Edwards et al., 1998, 2016, 2018). Reports of asphaltene-rich coastal bitumen strandings (asphaltum, now referred to as asphaltite) in the region date back to the early 1800s and continue to the present (Trewartha, 1850; Tolmer, 1882; Sprigg and Woolley, 1963; Volkman et al., 1992; Edwards et al., 1998; Hall et al., 2014; Ross et al., 2017). Historical reports of these asphaltite strandings predate anthropogenic inputs of hydrocarbons to the region, suggesting that they are the product of natural offshore seepage. Although asphaltite is

the least common variety of coastal bitumen recognised along the Australian coastline, it contributes the largest specimens, with individual pieces weighing up to 7 kg (Edwards et al., 1998, 2016).

Source and maturity-specific biomarkers indicate that these asphaltites are derived from a Mesozoic marine shale, deposited under sub-oxic to euxinic conditions, which expelled petroleum within the early oil window (Edwards et al., 1998; Hall et al., 2014; Scarlett et al., 2019). The source rock is presently thought to have been deposited during an oceanic anoxic event (OAE). However, interpretations vary from the Cenomanian-Turonian OAE2 (Totterdell et al., 2008; Boreham, 2009; Hall et al., 2014; Corrick et al., 2019), the Albian OAE1d (Boult et al., 2005; Hall et al., 2014), the Aptian OAE1a and Albian OAE1b events (Scarlett et al., 2019). Inspection of the GeoMark^{TM} global petroleum database suggests that the asphaltites are not products of any documented petroleum system (Summons et al., 2001). Unlike the majority of the tar balls found along the South Australian coastline (viz. 'waxy bitumens') which have been geochemically linked to Cenozoic petroleum systems in southeast Asia (Padley, 1995; Edwards et al., 2016, 2018), the asphaltites are currently thought to originate from an undiscovered petroleum system in the offshore Bight Basin (Fig. 1A) located on Australia's southern margin (Boreham et al., 2001; Totterdell et al., 2008; Hall et al., 2014). This interpretation is supported by analysis of organic-rich samples with similar geochemistry dredged from the basin (Totterdell et al., 2008; Boreham, 2009) and rhenium-osmium (Re-Os) geochronology of the asphaltites (Corrick et al., 2019), which demonstrated their timing of generation is consistent with existing petroleum systems models for the basin (Struckmeyer et al., 2001; Totterdell et al., 2008). Previous studies have also proposed seepage from other nearby basins, such as the Otway Basin (Boult et al., 2005; Hall et al., 2014). However, recent modelling of the metaocean conditions of the Great Australian Bight suggests that offshore seepage from the Otway Basin is unlikely to migrate west, a requirement given the observed spatial distribution of asphaltite strandings along the coastline (Ross et al., 2017). Seepage from the Ceduna or Duntroon sub-basins of the Bight Basin, however, is consistent with the documented regions of asphaltite stranding (Ross et al., 2017).

The Bight Basin comprises an approximately 15 km-thick succession of Late Jurassic to Cretaceous sediments (Fig. S1) deposited in response to the separation of Australia and Antarctica during the break-up of the supercontinent Gondwana (Fraser and Tilbury, 1979; Totterdell et al., 2000; Totterdell and Bradshaw, 2004). These Mesozoic deposits are

unconformably overlain by Palaeogene sediments with no source potential (Totterdell et al., 2008). Proposed petroleum systems in the basin are primarily associated with thick mid- to late Cretaceous deltaic and marine sediments, namely the Blue Whale, White Pointer, Tiger and Hammerhead supersequences (Blevin et al., 2000; Struckmeyer et al., 2001; Totterdell et al., 2000, 2008). However, no working petroleum systems have yet been proven within the basin.

Aside from the asphaltite strandings, no other seeped hydrocarbons that have been found on the South Australian coastline are considered products of the Bight Basin. In this study we report a new variety of asphaltene-rich crude oil stranded on the southeastern coastline of South Australia in October 2016. Referred to herein as asphaltic tar, these new strandings display strong geochemical similarities to the asphaltites, suggesting that the two oil types may originate from lateral equivalents of the same source rock.

2. MATERIALS AND METHODS

2.1. Sample Suite

The stranding locations of the specimens analysed in this study are shown in Figure 1A and their collection details are summarised in Table S1. Details of the four representative waxy bitumen samples also included in this study to illustrate their contrasting *n*-alkane δ13C profiles may be found in Ross et al. (2017). The asphaltites are visually distinctive, jet black, semi-solid to solid bitumens with a petroliferous odour and commonly exhibit deep shrinkage cracks (Fig. 1B). Fresh specimens with a soft and slightly pliable interior are rare, as most asphaltites collected on the coastline have become brittle, breaking apart with a diagnostic conchoidal fracture. The asphaltic tars are similarly jet black in colour but emit a stronger petroliferous odour and have remained viscous and sticky with a surficial sand coating (Fig. 1C).

The specimens compared in this study were recovered during three systematic annual surveys of 30 ocean beaches spanning the South Australian coastline in the period 2014 to 2016, as part of the Great Australian Bight Research Program (Ross et al., 2017). The sample suite was further supplemented with additional samples donated from private collections. Representative asphaltites were selected from each of the three surveys while ensuring a spatial distribution that encompassed the entire survey area (Fig. 1A). Asphaltic tar samples were only encountered in the final survey conducted in October of 2016, at the Number 1 and 2 Rocks beach in the Canunda National Park, located on the Bonney Coast approximately 40 km west of Mount

Gambier. This survey occurred 24 days after a one-in-fifty-year storm event that affected much of the South Australian coastline (Bureau of Meteorology, 2016; Burns et al., 2017) and found the spatial distribution of coastal bitumen deviated significantly from the previous two surveys (Ross et al., 2017).

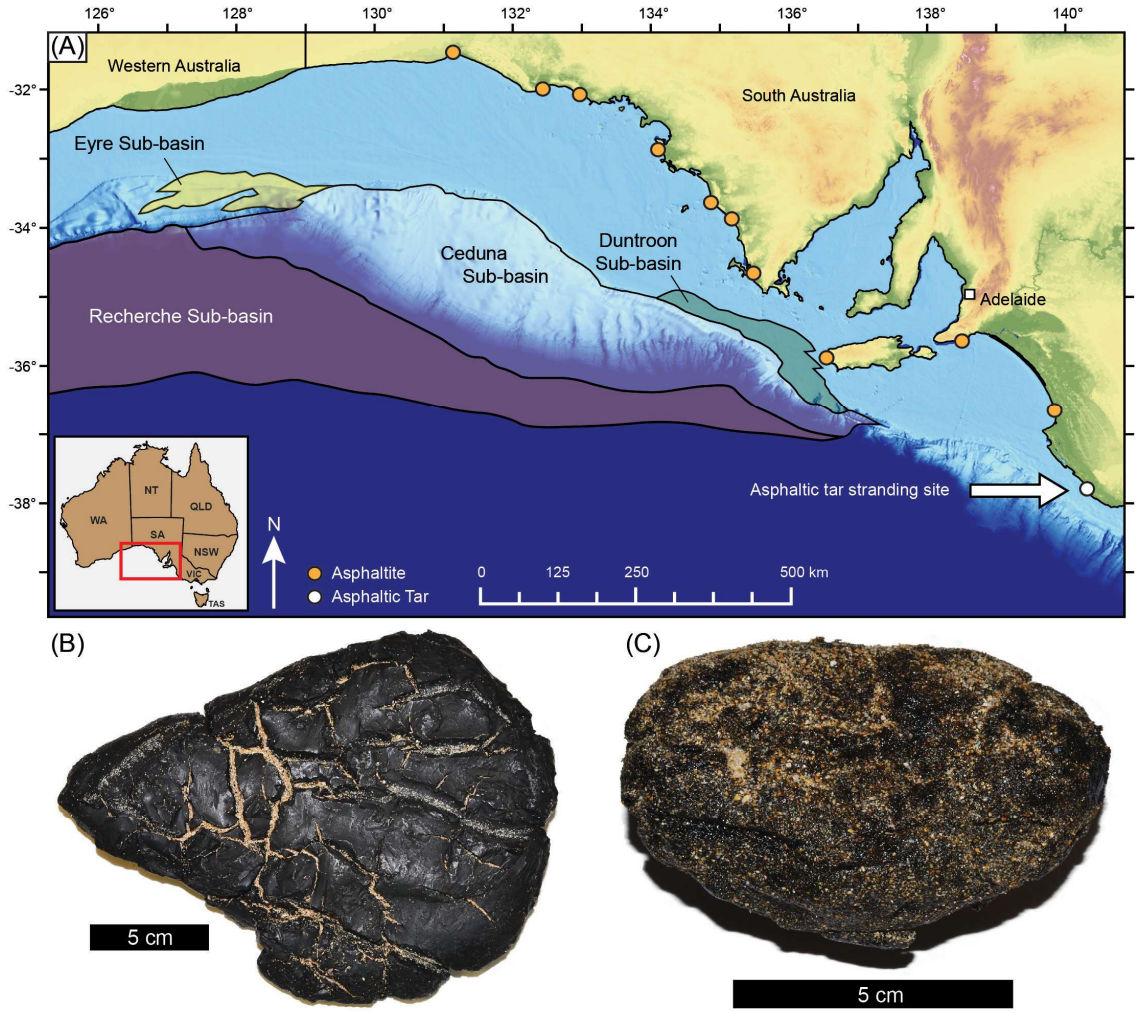


Figure 1: (A) Locations of analysed asphaltite and asphaltic tar samples and the Jurassic-Cretaceous sub-basins of the offshore Bight Basin. (B) Photograph of asphaltite sample W13/007507 collected from Waitpinga Beach in 2014, exhibiting characteristic shrinkage cracks. (C) Photograph of asphaltic tar sample /001059 collected from Number 1 and 2 Rocks in 2016.

2.2. Bulk bitumen analyses

2.2.1. Whole-oil gas chromatography-mass spectrometry

A sub-sample (≤200 mg) was removed from each bitumen specimen and dissolved in 10 mL of dichloromethane/methanol (93:7, v:v). An aliquot of this solution was used for whole-oil GC-MS. Analyses of the samples collected in 2014 and 2015 were performed on an Agilent 6890 gas chromatograph interfaced with a 5973N MSD (electron energy 70 eV) and tuned using automatic setup parameters for each sequence. Chromatography was carried out on an Agilent HP-5MS fused silica column (30m×0.25mm i.d. ×0.25 μm film thickness), using either a split (50 mL/min) or splitless injection mode, the latter employed if split injection data showed low responses. The oven was programmed at an initial temperature of 50 °C for 1 min, followed by heating at 8 °C/min to 300 °C. The carrier gas was helium at a flow rate of 1 mL/min. GC-MS analyses of the samples collected in 2016 were performed on an Agilent 7890B gas chromatograph interfaced with a 5977B MSD (electron energy 70 eV) and tuned using automatic setup parameters for each sequence. Chromatography was carried out on a J&W DB-5MS fused silica column (30m×0.25mm i.d.×0.25 μm film thickness), using the same operating conditions as employed for the 2014 and 2015 samples. In both cases, whole-oil GC-MS was conducted in scan mode (scan interval 45–500 AMU at approx. 3 scans/sec).

2.2.2. Elemental analysis (EA)

The sulphur content (weight %) of each sample was determined using a Perkin Elmer 2400 series II CHNS/O Elemental Analyzer in CHNS configuration. The combined combustion/reduction tube was packed with Perkin Elmer EA6000 and Perkin Elmer 'Hi-Purity' Copper (reaction temperature of 975°C). Results were calibrated against a Perkin Elmer Organic Analytical Standard (cystine, 3–4 mg) with a known abundance of sulphur (26.69 ± 0.3%). The maximum uncertainty in sulphur content values was ±0.5%.

2.2.3. Elemental analysis – isotope ratio mass spectrometry (EA-IRMS)

Sulphur isotope data ($\delta^{34}S$) were collected using a Eurovector EuroEA Elemental Analyzer modified with a Valco valve to allow separation of combustion SO_2 from CO_2 and N_2. Results from interior subsamples of each bitumen specimen were calibrated to two in-house standards (S2 and S3) of silver sulphide (Ag_2S) with $\delta^{34}S$ values of +22.7‰ and -32.3‰, respectively. Due to the range in sulphur content between the asphaltites and asphaltic tars, results were

calibrated against multiple weights of each standard (in the range 2–4 mg). The maximum uncertainty in $\delta^{34}S$ values was ±0.38‰.

2.2.4. Re-Os isotopic composition

Re-Os analysis of three asphaltic tars was conducted using the same analytical approach as that taken for the asphaltites by Corrick et al. (2019), based on the methods of Selby et al. (2007). The precision for all Re-Os data was determined using full error propagation of all sources of uncertainty.

2.3. Analysis of saturated, aromatic and polar fractions

2.3.1. Oil fractionation

The saturated, aromatic and polar fractions were separated from 20 mg aliquots of whole bitumen using the procedure of Bastow et al. (2007). The recovered saturated hydrocarbons and polar fractions were stored in 2 mL chromatography vials, while the aromatics fraction was stored in 2 mL amber glass vials to ensure minimal degradation by ultraviolet light.

2.3.2. Separation of *n*-alkanes and branched/cyclic alkanes

Saturates fractions were dissolved in cyclohexane and transferred on to 5Å molecular sieve (activated at 450°C) before heating in an oven at 80°C overnight to ensure complete *n*-alkane absorption. The resulting branched/cyclic alkane fraction was used for biomarker analyses (see Sections 2.3.3 and 2.3.4). For selected samples, the separated *n*-alkanes were then retrieved for compound-specific isotope analysis by digesting the molecular sieve in approximately 8 mL of 40% hydrofluoric acid in a polytetrafluoroethylene test tube and extracting the released *n*-alkanes using *n*-pentane. The resulting *n*-alkane fractions were concentrated under a stream of nitrogen prior to further analysis.

2.3.3. Selected ion monitoring gas chromatography-mass spectrometry (SIM GC-MS)

GC-MS analysis of the branched/cyclic alkanes was performed on an Agilent 7890A gas chromatograph interfaced with a 5975C MSD (electron energy 70 eV) tuned using automatic setup parameters on the day of the analysis. Chromatography was carried out on a J&W DB-5MS fused silica column (60 m x 0.25 mm i.d. x 0.25 µm film thickness). A 1 µL aliquot of the branched/cyclic saturate fraction dissolved in petroleum ether was injected into the

split/splitless injector at 300°C operating in split mode (20 mL/min). After being held at an initial temperature of 40°C for 2 min., the oven was heated at 20°C/min to 200°C and then ramped to 310°C at 2°C/min. The carrier gas was helium at a flow rate of 1.5 mL/min.

2.3.4. Gas chromatography tandem mass spectrometry (GC-MS-MS) with cold electron ionisation

GC-MS-MS analysis of the branched/cyclic alkanes was performed on a Perkin Elmer 680 Clarus gas chromatograph interfaced with a Perkin Elmer iQT Quadrupole Time of Flight (QToF) mass spectrometer fitted with a Cold-EI source and tuned using automatic setup parameters for each sequence. Chromatography was carried out on a J&W DB-5MS fused silica column (60 m x 0.25 mm i.d. x 0.25 µm film thickness). A 1 µL aliquot of saturates fraction dissolved in cyclohexane was injected at 300°C into the injector operating in splitless mode. The oven was held at an initial temperature of 50°C for 1 min., followed by heating at 12°C/min to 180°C and then at 4°C/min to 310°C. Helium was the carrier gas at a flow rate of 2 mL/min.

2.3.5. Carbon compound-specific isotope analysis (CSIA)

The carbon isotopic composition ($\delta^{13}C$) of individual *n*-alkanes from representative asphaltite, asphaltic tar and waxy bitumen samples was measured by gas chromatography-combustion-isotope ratio mass spectrometry using a 6890N GC connected to a GC-C/TC III combustion device coupled via open split to a Thermo MAT 253 mass spectrometer. The *n*-alkane fractions (1 µL) were injected into the inlet system in splitless mode (1 min). The injector was held at a temperature of 290°C. The *n*-alkanes were separated on a fused silica capillary column (SGE BP-5, 30 m x 0.25 mm ID, 0.25 mm film thickness). The GC oven was held at 50°C for 2 minutes, then heated at 25°C/min to 120°C, followed by a second heating ramp of 5°C/min to 310 °C, and finally held isothermal for 8 minutes. The analytes of the GC effluent stream were oxidised to CO_2 in the combustion furnace at 950°C on a CuO/NiO/Pt catalyst. The produced CO_2 was transferred on-line to the mass spectrometer to determine its $\delta^{13}C$ value. All results were calibrated to replicate measurements of individual *n*-alkanes from internal reference standards (IU A6 and B3). The maximum error in analytical precision was ±0.26‰.

2.3.6. GC-MS analyses of aromatic and polar fractions

Analyses of the aromatic and polar fractions were performed on a Perkin Elmer SQ8T/680 Clarus GC-MS fitted with a Perkin Elmer PE-5MS fused silica column (30 m x 0.25 mm i.d. x 0.25µm film thickness). A 1 µL aliquot was injected at 300°C into the injector operating in splitless mode. The oven was held at an initial temperature of 50°C for 1 min., followed by heating at 8°C/min to 300°C. Helium was the carrier gas at a flow rate of 1 ml/min. Data acquisition was conducted in scan mode (Scan 45:500AMU at approx. 3 scans/sec).

2.4. Asphaltene separation

The asphaltene content of each specimen was determined by dissolving a bulk sub-sample (0.3–0.7 g) in a minimum volume of dichloromethane/methanol (93:7). The asphaltene fraction was then precipitated by adding an excess of *n*-pentane. After the asphaltene precipitate settled from suspension, the maltene supernatant was removed using a Pasteur pipette and further *n*-pentane added. This process was repeated several times, until the maltene fraction had been entirely removed. The remaining asphaltene fraction was then rinsed with a final wash of *n*-pentane, dried and weighed.

3. RESULTS AND DISCUSSION

3.1. Comparison of source-specific saturated hydrocarbons

Source-specific biomarker parameters of the asphaltites and asphaltic tars are listed in Table 1. The freshest asphaltite specimen (W13/007976) preserves *n*-alkanes as light as C_8 (note that lighter gasoline-range *n*-alkanes would lie outside the detection range), with a slightly bimodal front-end distribution displaying maxima at C_{10} and C_{13}, thereafter decreasing in abundance towards C_{35} (Fig. 2A). Relative to this specimen, other asphaltites in the sample suite have less low-molecular-weight *n*-alkanes. This mild weathering results in a unimodal *n*-alkane distribution in the range C_{10}–C_{35}, with a maximum between C_{15} and C_{17} (Fig. 2B). Although the majority of samples selected for comparison were not significantly weathered asphaltites, two mildly degraded specimens (W13/007493 and W13/007668) are also included in the sample suite for reference. These samples contain less *n*-alkanes, demonstrated by elevated Pr/C_{17} ratios compared to the other specimens. The asphaltic tar specimens preserve *n*-alkanes from C_9 to C_{35} with a maximum at C_{17} (Fig. 2C). Having been recovered from a single stranding location during one survey and being of highly uniform composition, the asphaltic tars are likely

fragments of a single larger piece of tar separated by wave action during or shortly prior to stranding.

The C_{27} : C_{28} : C_{29} and C_{27} Dia/(Dia+Reg) sterane ratios of both families are highly consistent (Fig. 3; Table 1). Some minor grouping of the two oils is based on the relative proportions of the C_{27} and C_{28} ααα 20*R* steranes. The asphaltic tars typically contain a slightly lower proportion of C_{27} steranes and slightly elevated C_{28} steranes. However, there remains some overlap between the two oil types based on variability in these values in specific samples. The C_{31} (22R)/C_{30} αβ hopane ratios of the asphaltites and asphaltic tars are effectively identical, with respective values of 0.30–0.35 and 0.31–0.34, consistent with a marine source (Peters et al., 2005). This is supported in both oil families by the presence of diagnostic marine biomarkers such as dinosterane, a 4-methylsterane derived from marine dinoflagellates (Summons et al., 1987) and 24-*n*-propylcholestanes derived from marine chrysophyte algae (Moldowan et al., 1990). Furthermore, the complete lack of freshwater algal markers such as botryococcane (e.g. Moldowan and Seifert, 1980; McKirdy et al., 1986), and of angiosperm markers such as oleanane or bicadinanes (e.g. Edwards et al., 2018) together with a low abundance of tetracyclic polyprenoids (Holba et al., 2000) suggests negligible inputs from terrestrial or freshwater biota. Hence, the parent oils of both types of asphaltic bitumen originated from source rocks which contain only marine organic matter, consistent with the previously inferred source affinity of the asphaltites (Edwards et al., 1998; Hall et al., 2014).

The pristane/phytane ratio (Pr/Ph), a commonly used indicator of source redox conditions (Powell and McKirdy, 1973), varies between 1.1 and 1.4 in the asphaltite sample suite, suggesting that their source rock was deposited under sub-oxic conditions. However, their high C_{35} homohopane index values (7–9) and high sulphur content (≈ 4 wt. %) are consistent with more reducing conditions. The Pr/Ph ratios of the asphaltic tars are consistently lower, suggesting anoxia (<1; Table 1). This evidence of anoxia is further supported by a higher abundance of C_{35} homohopanes, expressed by high values of the C_{35} homohopane index (10–12) and C_{35}/C_{34} hopane ratio (1.00–1.05). Despite the evidence of a more oxygen-depleted (anoxic) setting (cf. the conflicting sub-oxic to anoxic parameters of the asphaltites), the sulphur content of the asphaltic tars varies between 2.5 and 3.5%, which is generally lower than that of the asphaltites (viz. 3.6–4.4% in the analysed suite).

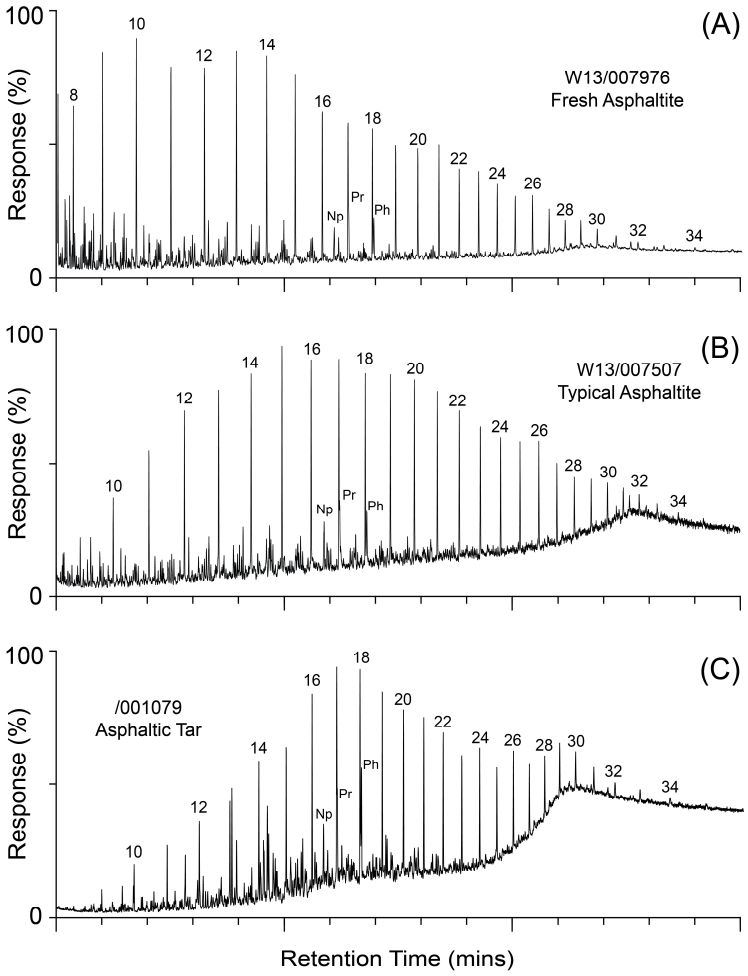


Figure 2: Whole-oil GC-MS total ion chromatograms for: (A) The freshest identified asphaltite specimen W13/007976; (B) A typical, lightly weathered asphaltite specimen W13/007507; and (C) An asphaltic tar specimen /001079; Np = norpristane, Pr = pristane, Ph = phytane, peak numbers correspond to *n*-alkane chain length.

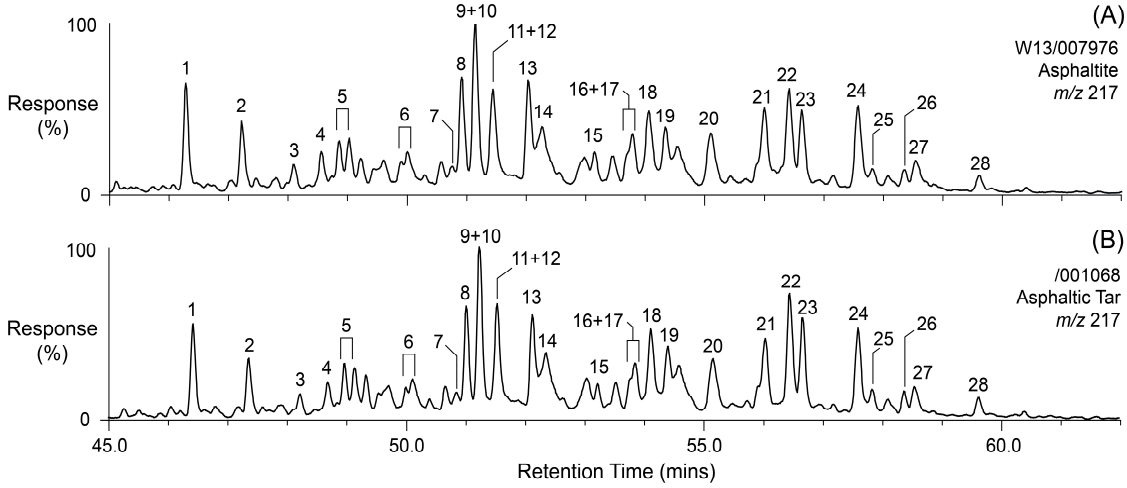


Figure 3: Partial *m/z* 217 chromatograms of representative asphaltite and asphaltic tar specimens demonstrating the similarity of their sterane and diasterane distributions. For a full list of peak assignments see Supplementary Information.

Table 1: Asphaltene content and selected biomarker parameters of asphaltite and asphaltic tar specimens. See Supplementary Information for explanation of compound abbreviations.

Samples	Asphaltene %	Sulphur %	$\delta^{34}S$ (‰)	Pr / Ph	Pr/C_{17}	27 : 28 : 29 ααα 20*R* steranes (*m/z* 217)	27 : 28 : 29 αββ (20*R*+*S*) steranes (*m/z* 218)	C_{27} Dia / (Dia+Reg) steranes (*m/z* 217)	C_{35} homohopane index (%)	C_{29} / C_{30} αβ hopane (*m/z* 191)	C_{31} (22*R*) / C_{30} αβ hopane (*m/z* 191)	C_{35} (22*S*) / C_{34} (22*S*) hopane (*m/z* 191)	Ts / (Ts+Tm)
Asphaltites													
W13/007472	59	4.0	-5.79	1.3	0.5	40 : 23 : 36	37 : 25 : 37	0.41	9.3	0.64	0.34	0.95	0.40
W13/007475	58	4.1	-6.58	1.3	0.5	38 : 23 : 39	38 : 26 : 37	0.45	7.8	0.65	0.33	0.90	0.41
W13/007476	53	4.3	-5.34	1.3	0.5	43 : 20 : 38	38 : 25 : 37	0.42	7.6	0.60	0.35	0.90	0.41
W13/007488	56	4.4	-5.30	1.2	0.5	43 : 20 : 37	38 : 25 : 37	0.43	8.6	0.64	0.33	0.92	0.39
W13/007493	52	4.1	-5.97	1.4	0.7	44 : 19 : 36	37 : 25 : 38	0.34*	8.3	0.69*	0.31	0.91	0.35
W13/007507	54	3.9	-5.66	1.2	0.5	40 : 27 : 33	39 : 25 : 36	0.43	7.4	0.65	0.32	0.79	0.40
W13/007516	55	4.0	-6.15	1.3	0.5	44 : 19 : 37	38 : 25 : 37	0.42	8.0	0.66	0.33	0.91	0.38
W13/007668	59	4.1	-7.18	1.1	1.3	37 : 27 : 36	37 : 26 : 37	0.45	7.7	0.67	0.30	0.90	0.38
W13/007671	54	3.8	-7.59	1.1	0.5	37 : 23 : 39	37 : 25 : 38	0.42	7.9	0.65	0.32	0.90	0.41
W13/007672	54	3.8	-7.34	1.2	0.4	43 : 20 : 37	39 : 25 : 36	0.43	8.4	0.65	0.33	0.94	0.38
W13/007845	51	3.7	-8.82	1.2	0.5	39 : 27 : 34	39 : 26 : 35	0.46	7.2	0.64	0.30	0.82	0.37
W13/007976	51	3.6	-7.80	1.2	0.4	38 : 26 : 36	38 : 25 : 37	0.45	7.6	0.62	0.30	0.82	0.41
Asphaltic Tars													
/001056	35	2.8	+2.61	0.7	0.6	35 : 29 : 36	36 : 26 : 38	0.43	11.0	0.82	0.32	1.02	0.22
/001063	22	3.2	+2.88	0.7	0.5	35 : 29 : 36	36 : 26 : 38	0.43	10.4	0.80	0.32	1.00	0.22
/001067	35	2.7	+4.84	0.7	0.6	34 : 29 : 37	35 : 25 : 40	0.43	11.3	0.78	0.33	1.03	0.22
/001068	25	3.2	+4.50	0.8	0.6	35 : 29 : 36	36 : 25 : 39	0.44	10.6	0.75	0.31	1.01	0.22
/001076	25	2.5	+4.27	0.7	0.5	37 : 26 : 37	36 : 23 : 42	0.43	11.0	0.79	0.34	1.05	0.27
/001079	27	3.0	+4.30	0.7	0.6	33 : 29 : 38	35 : 25 : 41	0.43	11.8	0.73	0.33	1.02	0.19
/001081	26	3.5	+4.85	0.7	0.5	32 : 29 : 38	35 : 25 : 40	0.44	11.8	0.76	0.33	1.04	0.19

* = Ratio variation attributed to significant weathering of the specimen

C_{27} Dia / (Dia + Reg) steranes = (C_{27} βα 20*S* + 20*R*) / [(C_{27} βα 20*S* + 20*R*) + (C_{27} ααα 20*S* + 20*R*)]

C_{35} homohopane index = [C_{35} 17α(H),21β(H)-homohopanes (22*S* + 22*R*) / ∑ $C_{31\text{-}35}$ 17α(H),21β(H)-homohopanes (22*S* + 22*R*)] x 10

The lithofacies of the asphaltite's source rock has previously been interpreted as a shale containing little to no carbonate, based on their C_{29}/C_{30} αβ hopane ratio being < 1 (Fig. 4, Table 1), their high relative abundance of diasteranes and the complete absence of 2α-methylhopanes (Edwards et al., 1998). Abundant 2α-methylhopanes are observed in oils derived from carbonate source rocks (Summons et al., 1999), while lower abundances are reported in deeper water facies, a trend attributed to the distribution of their precursor cyanobacteria which predominantly reside in shallow-water ecosystems (Eigenbrode et al., 2008). The unusual absence of 2α-methylhopanes in the asphaltites could therefore support the interpretation that the source rock was deposited in a deepwater setting, consistent with their complete lack of molecular markers indicating terrestrial or freshwater organic matter inputs.

Unlike the asphaltites, the asphaltic tars contain 2α-methylhopanes in low abundance. However, the significance of their presence is uncertain, as 2α-methylhopanes appear to require cracking from kerogen and are hence strongly affected by burial temperature (Peters et al. 2005). Additionally, the 17α-22,29,30-trisnorhopane (Tm) occurs in much higher abundance relative to the 18α-22,29,30-trisnorneohopane (Ts). These compounds are usually compared in the Ts/(Ts+Tm) ratio, which is commonly employed as a thermal maturity parameter (Seifert and Moldowan, 1978). However, the low values of this ratio obtained from the asphaltic tars (0.19–0.27) are inconsistent with other thermal maturity parameters which indicate that these samples originated from the late oil window (discussed in Section 3.3). In addition to thermal maturity, the relative influence of lithology and redox conditions of the source rock on the Ts/(Ts+Tm) ratio is not fully understood, with several studies reporting systematically lower values in oils derived from carbonate source rocks deposited under anoxic conditions (McKirdy et al., 1983, 1984; Rullkötter et al., 1985; Price et al., 1987). Aside from this anomalous parameter, the composition of the asphaltic tars appears consistent with their derivation from an anoxic shale. To explain their abnormal Ts/(Ts+Tm) values, we tentatively propose that the source rock composition has a relatively high carbonate content, lying between the endmembers of shale and carbonate (i.e. a calcareous shale). In an anoxic setting, this may have been sufficient to account for their unusually low Ts/(Ts+Tm) values, despite the high thermal maturity of the parent oil.

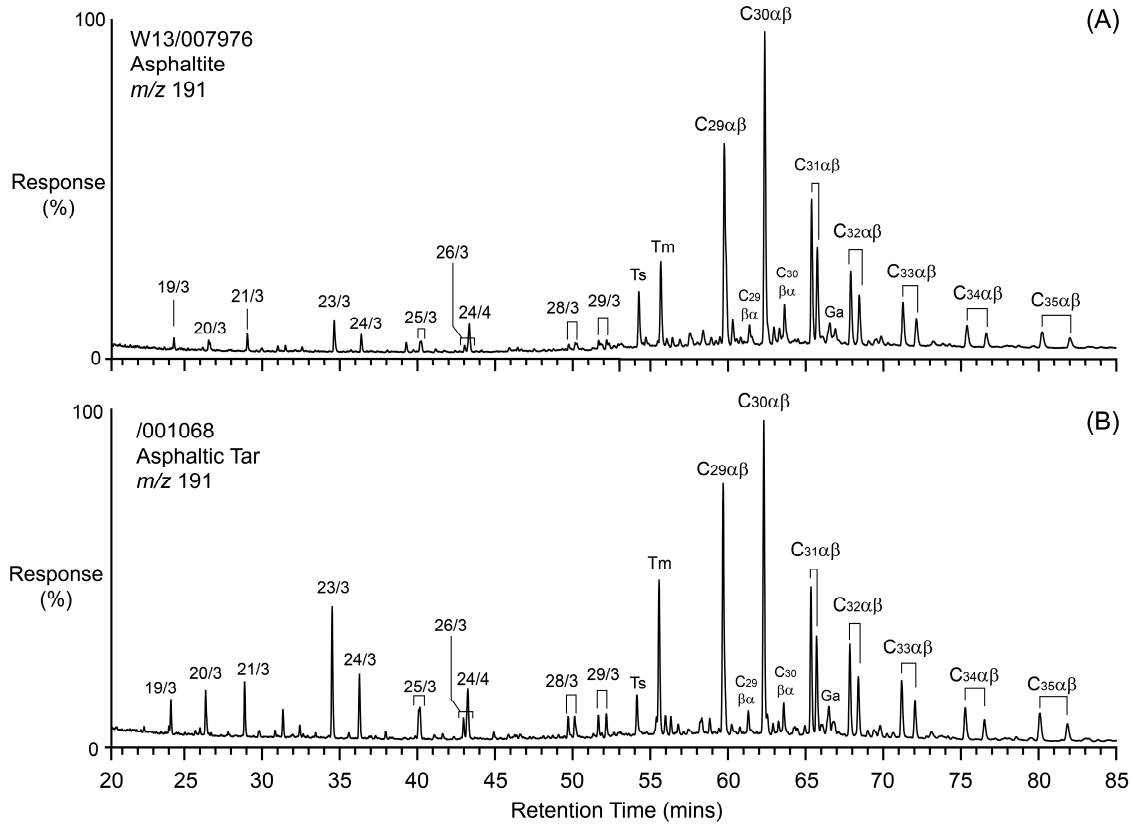


Figure 4: Partial *m/z* 191 chromatograms of (A) asphaltite sample W13/007976; and (B) asphaltic tar sample /001068. See Supplementary Information for full list of compound abbreviations.

3.2. Comparison of stable isotopic composition

The overall similarity of the asphaltic tars and asphaltites indicated by their near-identical source-specific sterane compositions is further reinforced by their internally consistent *n*-alkane $\delta^{13}C$ profiles, a valuable tool in the geochemical correlation of crude oils (e.g. Murray et al., 1994; Dowling et al., 1995; Blevin et al., 1998). The carbon isotopic composition of individual hydrocarbons in a crude oil is controlled principally by the primary organic matter inputs to its source rock. Hence oils derived from similar sources share comparable compound-specific $\delta^{13}C$ values (Hayes et al., 1990; Murray et al., 1994). The *n*-alkane $\delta^{13}C$ profiles of representative asphaltites and asphaltic tars, and of selected examples of Indonesian-derived waxy bitumens which also strand on the South Australian coastline (Ross et al., 2017) are shown in Figure 5. The isotopic values for each individual *n*-alkane in these specimens are listed in Table S2. The waxy bitumens, products of distal petroleum systems with source characteristics notably different to those of the asphaltites (cf. Edwards et al., 2018), contain C_{15+} *n*-alkanes with $\delta^{13}C$ values ranging between approximately –25.5 and –32‰. These results align with those of a previous assessment of the waxy bitumens' *n*-alkane isotopic composition, which demonstrated

their similarity to the Minas and Duri oils from the Central Sumatra Basin (Dowling et al., 1995). In contrast, the *n*-alkane $\delta^{13}C$ values of the asphaltites and asphaltic tars are more uniform, with values between –30 and –34‰. Similarly, flat *n*-alkane $\delta^{13}C$ profiles are observed in other oils derived from marine source rocks (Murray et al., 1994).

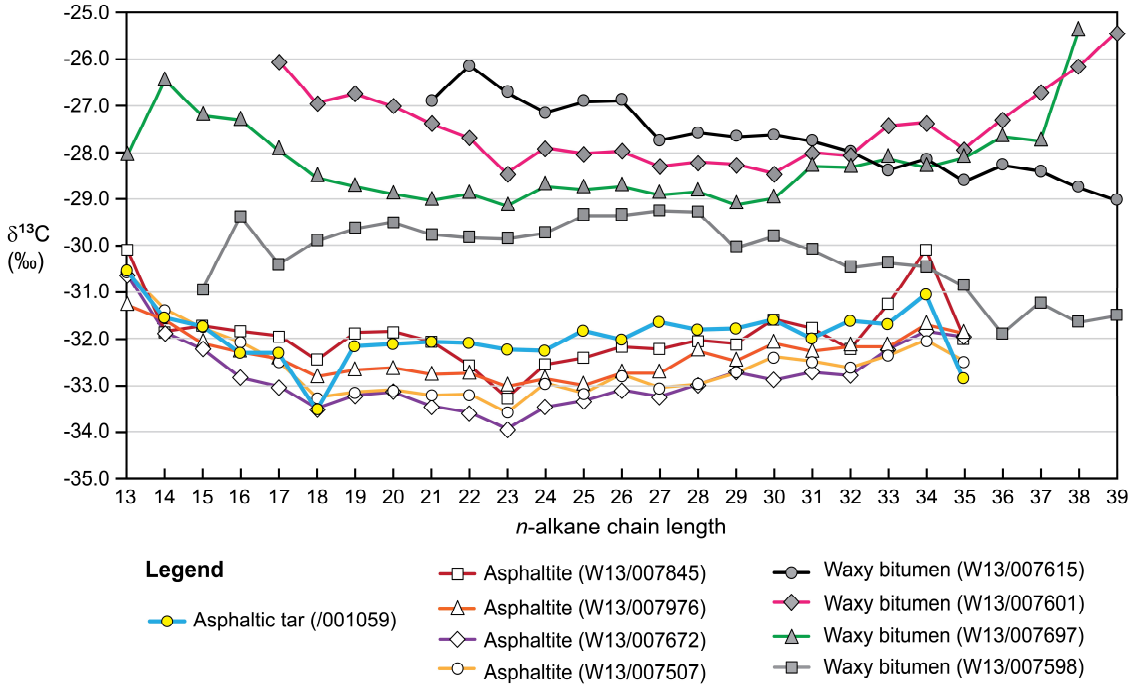


Figure 5: CSIA data on *n*-alkanes from interior subsamples of different coastal bitumen oil families collected from the South Australian coastline. The carbon isotopic profile of the asphaltic tar specimen plots in the same region as those of numerous asphaltites but differs markedly from those of waxy coastal bitumens derived from petroleum systems in Southeast Asia. Each of the waxy bitumen varieties shown are derived from different oil families identified using the presence/absence and abundance of key biomarker alkanes identifiable using whole-oil GC-MS (Corrick et al., 2016; Ross et al., 2017).

Although the carbon isotopic values of the two oil families are highly consistent, their bulk sulphur isotopic compositions ($\delta^{34}S$) differ considerably. The $\delta^{34}S$ signature of an oil may be used to aid oil-oil and oil-source correlations, as the unaltered value typically reflects that of the source kerogen (Thode et al., 1961; Thode and Monster, 1970; Orr, 1986). Although the primary source of the sulphur in marine organic matter is seawater sulphate, the process of bacterial sulphate reduction in the sediment prior to deeper burial results in organically-bound sulphur becoming depleted in ^{34}S (Jones and Starkey, 1957; Harrison and Thode, 1958; Thode et al., 1960). Hence, the $\delta^{34}S$ values of petroleum generated from this organic matter are typically ca. 15‰ lighter than contemporaneous inorganically precipitated sulphur minerals such as gypsum, which may either accurately preserve the composition of seawater or be

enriched in ^{34}S (Thode and Monster, 1965). In asphaltites, bulk $\delta^{34}S$ values range between -3.6 and -4.6‰, while the values for the asphaltic tars are between +2.61 and +4.85‰, reflecting a much greater enrichment in the heavier isotope (Table 1). Given the variability in the $\delta^{34}S$ composition of seawater sulphate during the Cretaceous, these heavier values remain geologically reasonable (cf. Paytan et al., 2004). However, the sulphur isotopic composition of crude oil may also be altered to heavier values under certain conditions (discussed in Section 4.2).

3.3. Comparison of thermal maturity parameters

The maturity parameters of the asphaltite and asphaltic tar samples are summarised in Table 2. As discussed previously, although the Ts/(Ts+Tm) ratio may often constrain thermal maturity, it is unreliable in this case due to likely source interference. The methylphenanthrene index (MPI-1), arguably the most robust molecular measure of thermal maturity (Radke, 1987), varies between 0.49 and 0.62 across the asphaltite samples. Using the relationship between MPI-1 and vitrinite reflectance defined by Radke and Welte (1983), the calculated vitrinite reflectance (R_c) of the asphaltites' source rock falls between 0.7 and 0.8%, indicating a thermal maturity in the early/main oil window, consistent with previous studies (Volkman et al., 1992; Edwards et al., 1998; Hall et al., 2014; Scarlett et al., 2019). Other aromatic maturity indices, namely the methylnaphthalene ratio (MNR) and dimethylnaphthalene ratio (DNR-1), yield slightly higher maturities in the range 0.9–1.0% R_c. This may be the result of mixing with a more mature oil charge, which will influence the methylnaphthalenes of the oil more than the higher-molecular-weight methylphenanthrenes.

The asphaltites used for comparison in this study were collected from widely separated stranding locations along the coastline (Fig. 1A) and, with few exceptions, preserve phenanthrene, comparable to those in previous studies (cf. Volkman et al., 1992; Edwards et al., 1998; Hall et al., 2014). Therefore, most asphaltites within the sample suite have undergone minimal alteration due to water-washing, supporting the interpretation that they are the product of a local seafloor seep (Hall et al., 2014). However, degraded asphaltites do occur (e.g. samples W13/007493 and W13/007668). Such mild to moderately degraded examples exhibit significant alteration to the methyl- and dimethylnaphthalenes, while the MPI-1 ratio appears relatively unaffected (Corrick et al., 2019).

Table 2: Thermal maturity parameters and calculated vitrinite reflectance (R_c) values of asphaltites and asphaltic tars. MPI-1 ratio after Cassani et al. (1988). Relationship between MPI-1 and R_c after Radke and Welte (1983). MNR, DNR-1 ratios and their respective relationships to R_c after Radke et al. (1984). See Supplementary Information for all compound abbreviations.

Sample	Tricyclics / 17α-hopanes	MPI-1	R_c (%) from MPI-1	MNR	R_c (%) from MNR	DNR-1	R_c (%) from DNR-1
Asphaltites							
W13/007472	0.08	0.49	0.7	0.63	0.9	2.57	1.0
W13/007475	0.10	0.62	0.8	0.75	0.9	2.20	1.0
W13/007476	0.09	0.51	0.7	0.81	1.0	2.39	1.0
W13/007488	0.09	0.49	0.7	0.81	1.0	2.20	1.0
W13/007493	0.07	0.60	0.8	*	*	*	*
W13/007507	0.12	0.49	0.7	0.98	1.0	2.43	1.0
W13/007516	0.10	0.53	0.7	0.72	0.9	2.46	1.0
W13/007668	0.11	0.61	0.8	*	*	*	*
W13/007671	0.10	0.55	0.7	0.72	0.9	2.31	1.0
W13/007672	0.10	0.53	0.7	0.77	1.0	2.31	1.0
W13/007845	0.15	0.51	0.7	0.83	1.0	2.58	1.0
W13/007976	0.11	0.54	0.7	0.93	1.0	2.98	1.0
Asphaltic Tars							
/001056	0.31	1.28	1.2	1.76	1.1	6.82	1.2
/001063	0.33	1.26	1.2	1.73	1.1	7.22	1.2
/001067	0.31	1.23	1.1	1.66	1.1	7.10	1.2
/001068	0.34	1.25	1.1	1.59	1.1	6.24	1.2
/001076	0.24	1.33	1.2	1.62	1.1	6.07	1.2
/001079	0.26	1.34	1.2	1.71	1.1	7.29	1.2
/001081	0.27	1.31	1.2	1.55	1.1	6.42	1.2

* Ratio altered due to significant water washing and removal of key aromatic compounds.
Tricyclics/17α-hopanes = $\sum C_{19\text{-}30}$ tricyclic terpanes / $\sum C_{29\text{-}35}$ αβ hopanes
MPI-1 = [1.89 x (2-MP + 3-MP)] / [P + 1.26 (1-MP + 9-MP)]
R_c (%) from MPI-1 = 0.60 x MPI-1 + 0.40
MNR = 2-MN / 1-MN
R_c (%) from MNR = 0.17 x MNR + 0.82
DNR-1 = (2,6-DMN + 2,7-DMN) / 1,5-DMN
R_c (%) from DNR = 0.046 x DNR-1 + 0.89

The aromatic hydrocarbon fraction of the asphaltic tars differs notably from that of the asphaltites (Fig. S2, Table 2). Their MPI-1 values of 1.23–1.34 are equivalent to R_c values of 1.1–1.2%, indicating a thermal maturity within the late oil window. MNR and DNR-1 likewise yield R_c values of 1.1 and 1.2% respectively. This consistency between aromatic maturity indicators suggests the asphaltic tars are unlikely to represent a mix of earlier and later expulsion products (cf. the higher R_c values from MNR and DNR-1 vs. MPI-1 in the asphaltites). Like the asphaltites, the preservation of somewhat water-soluble naphthalenes, despite exposure to the marine environment, supports the interpretation that the asphaltic tars also originated from a nearby petroleum system.

The abundance of tricyclic terpanes relative to 17α-hopanes has been shown to increase at higher thermal maturities due to the preferential release of tricyclic terpanes from kerogen (Aquino Neto et al., 1983; van Graas, 1990; Farrimond et al., 1999). The tricyclic terpanes/17α-hopanes ratios of the asphaltites are low (0.07–0.15), consistent with their other maturity parameters which suggest generation and expulsion from a source rock in the early oil window. The markedly higher thermal maturity of the asphaltic tars indicated by their aromatic maturity parameters is further supported by their higher tricyclic terpanes/17α-hopanes ratio of 0.24–0.34 (Table 2). However, the abundance and composition of tricyclic and tetracyclic terpanes can also reflect source input (Peters et al., 2005). This makes distinguishing the influence of source and thermal maturity difficult when comparing two oils of markedly different maturities.

3.4. Comparison of Re-Os systematics

The Re-Os geochronology of crude oils has been demonstrated to constrain the timing of oil generation and expulsion from the source rock (Selby et al., 2005; Selby and Creaser, 2005; Finlay et al., 2011; Lillis and Selby, 2013; Liu et al., 2018). Application of the Re-Os geochronometer to asphaltites recently collected from the South Australian coastline provided a generation age of 74 ± 26 Ma (n =16; Corrick et al., 2019), while analysis of a smaller suite of archival specimens collected in the 1990's yielded a set of data points with lower analytical uncertainty which define an age of 103 ± 22 Ma (n = 5; Scarlett et al., 2019). These generation ages show 19 Myr of potential overlap when considering their respective uncertainties. However, the remaining variation between these two determined ages is unlikely to be soley attributable to the differences in analytical uncertainty between these two studies, as the results obtained from numerous asphaltites analysed by Corrick et al. (2019), despite their higher analytical uncertaintly, do not overlap with, or plot along the isochron defined by Scarlett et al. (2019). This suggests that a geologic component to the variation is also likely. The overall high uncertainty present in both of the determined ages may be associated with the mixing of increasingly mature oil, given the variation observed between the aromatic maturity parameters used herein (Table 2).

The asphaltic tars contain 30.1–31.4 parts per billion (ppb) Re and 599.9–627.6 parts per trillion (ppt) Os, concentrations significantly greater than in the asphaltites, which contain between 2.6-4.2 ppb Re and 24.6-45.0 ppt Os (Corrick et al., 2019; Scarlett et al., 2019). Such high abundances of Re and Os are unusual, particularly as these elements predominantly reside within the asphaltene fraction of crude oil (Selby et al., 2007; Georgiev et al., 2016; Liu and

Selby, 2018; Liu et al., 2019) and the asphaltic tars contain less asphaltenes (22–35% versus 51–59% in the asphaltites; Table 1). The $^{187}Re/^{188}Os$ and $^{187}Os/^{188}Os$ ratios of the analysed asphaltic tars are highly uniform at 332.2–333.9 and 3.057–3.063, respectively (Table S3). These values overlap when considering the range of analytical uncertainty. Thus, insufficient variation exists to apply a linear regression to these data points to determine a meaningful generation age for the asphaltic tars. Their homogenous Re and Os composition is likely due to both the small number of samples analysed (n = 3), and the high probability that the specimens analysed represent individual fragments of a single larger piece of tar, as discussed previously. Whilst internally consistent, these values differ from those obtained from the asphaltites (Fig. 6), which yield $^{187}Re/^{188}Os$ values between 400.5–547.8 and $^{187}Os/^{188}Os$ values of 1.122–1.334 (Corrick et al., 2019; Scarlett et al., 2019).

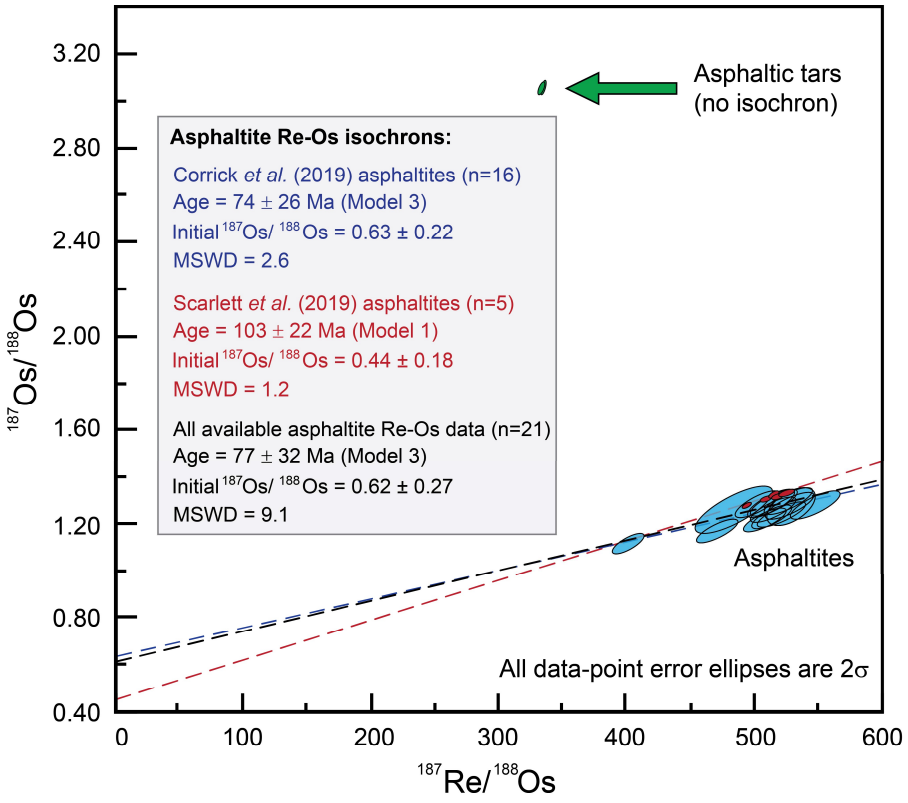


Figure 6: Comparison of Re-Os ratios of asphaltic tars with those of asphaltites analysed by Corrick et al. (2019) and Scarlett et al. (2019). Results for individual samples are listed in Table S3. MSWD = mean square of weighted deviates.

4. DO BOTH OILS ORIGINATE FROM THE SAME SOURCE ROCK?

The geochemistries of these two varieties of asphaltic crude oil exhibit several source-related similarities, such as their highly comparable sterane distributions and *n*-alkane $\delta^{13}C$ values. However, clear and systematic differences are also evident between these two oil types, most notably in their respective Ts/(Ts+Tm) ratios, bulk $\delta^{34}S$ values and Re-Os systematics. Oil-oil and oil-source correlations can become particularly complex when taking into account possible lateral variations in both the organic facies and thermal maturity of the source rock. Therefore, the relationship between these two oil types must be considered in terms of two competing interpretations: (1) The asphaltic tars and asphaltites were derived from separate source rocks which contained similar organic facies; or (2) both oil types originated from lateral equivalents of the same source rock unit. In the latter interpretation, the observed geochemical variations reflect minor lateral variability in the source rock composition, combined with increased thermal maturity and possible alteration by thermochemical sulphate reduction (TSR; discussed below).

In both scenarios, correlation of the two oil types based on multiple source-specific parameters supports their derivation from organic-rich rocks which contained highly comparable organic matter inputs. Thus, these two asphaltic oils are likely to have originated from within the same basin, presently considered to be the offshore Bight Basin. However, the implications of the two potential interpretations for the quality and location of the petroleum system of the asphaltic tars may differ considerably.

4.1. The case for two separate source rocks

Multiple marine intervals with high source potential are proposed to occur throughout the Blue Whale, White Pointer, Tiger and Hammerhead supersequences of the Bight Basin (Blevin et al., 2000; Totterdell et al., 2000; Struckmeyer et al., 2001; Totterdell et al., 2008); and many of these now lie within different stages of the hydrocarbon generation window, depending on their location. For example, in the depocentre of the Ceduna Sub-basin, the proposed source rocks in the Blue Whale and White Pointer supersequences reside in the gas window or overmature zones, while laterally these intervals pass through both the main and late oil window in both the marginal and basinward areas (Fig. 7). It is reasonable to consider that organic matter inputs to a marine sedimentary basin would be similar, though not necessarily identical through time. An interpretation of two discrete marine source rock intervals with similar organic matter inputs

would permit the near-identical compound-specific $\delta^{13}C$ values and sterane distributions of the asphaltites and asphaltic tars. However, the observed differences in $\delta^{34}S$ values and Re-Os systematics may be attributed to variations of seawater chemistry through time (e.g. Paytan et al., 2004; Du Vivier et al., 2014). Although this may account for different $^{187}Re/^{188}Os$ and $^{187}Os/^{188}Os$ values between the two oils, it does not explain the unusually high abundance of Re and Os present in the asphaltic tars. Whilst the possibility of two separate sources cannot be discounted, this interpretation relies predominantly on attributing all observed variations between these two asphaltic oil strandings to differences in source rock composition, with little to no acknowledgement of the role that lateral facies variation and differing thermal maturity may also have had on the composition of the oil generated throughout the basin.

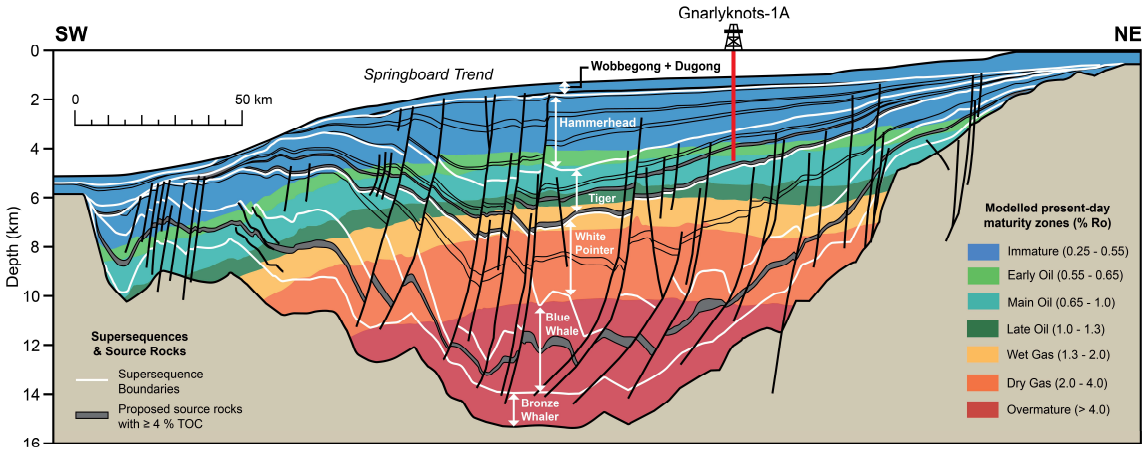


Figure 7: Cross-section of the Ceduna Sub-basin of the Bight Basin with supersequence boundaries, proposed source intervals (> 4% TOC) and modelled present-day maturity (% R_o) zones. Figure modified after Totterdell et al. (2008).

4.2. The case for a single source rock

The geochemical differences between the asphaltic tars and asphaltites may also be attributed to a combination of minor lateral variation in source rock facies, differences in thermal maturity and alteration of the asphaltic tars by TSR. This latter process occurs when oil comes into contact with a source of dissolved sulphate at temperatures at or above 100–140°C (Goldhaber and Orr, 1995; Machel, 2001). Potential sources of dissolved sulphate include buried seawater, basin brines (groundwater) or dissolved evaporite deposits of gypsum or anhydrite (Machel, 2001). During TSR, low-molecular-weight hydrocarbons are oxidised in order to reduce the dissolved sulphate. Branched and *n*-alkanes are the most reactive, followed by cyclic and monoaromatic compounds (Krouse et al., 1988; Manzano et al., 1997; Machel, 2001). Products of this reaction include hydrogen sulphide (H_2S), carbonate, metal sulphides and pyrobitumen

(Machel, 2001). The release of H_2S in particular can also have important technical implications for oil production, as the oxidation reduces the overall hydrocarbon potential and production costs are increased due to the toxicity of H_2S and its associated corrosion of drilling equipment.

Both the sulphur isotopic composition and Re-Os systematics of a crude oil, two parameters typically inherited from seawater at the time of source rock deposition, are severely altered during TSR. Alteration of primary $\delta^{34}S$ values occurs due to the back reaction of the resulting H_2S with the oil. This incorporates sulphur derived from the dissolved sulphate, driving the $\delta^{34}S$ composition towards heavier values (e.g. Orr, 1974; Lillis and Selby, 2013). This is consistent with the observed difference in $\delta^{34}S$ composition between the asphaltic tars and asphaltites (Table 1). TSR has also been observed to reset the Re-Os systematics of crude oils, with the resulting age representing the cessation of this alteration process (Lillis and Selby, 2013). Oils affected by TSR are enriched in both Re and Os relative to the parent oil and possess different $^{187}Re/^{188}Os$ and $^{187}Os/^{188}Os$ ratios (Lillis and Selby, 2013). This suggests that during TSR both Re and Os are also transferred from the dissolved sulphate phase to the oil, though the exact nature of this process remains unclear. The resulting $^{187}Re/^{188}Os$ and $^{187}Os/^{188}Os$ values of the oil will therefore represent mixed signatures of the original oil and the dissolved sulphate. The nature of this alteration is unlikely to be systematic in all cases (i.e. $^{187}Os/^{188}Os$ will not always increase), as the composition of the dissolved sulphate will vary in different settings according to the sources of Re and Os (e.g. balance of Re and Os derived from mantle inputs vs. continental weathering). Disruption of the Re-Os systematics due to TSR is consistent with the differences observed between the asphaltites and asphaltic tars. In particular, the significant enrichment of both Re and Os in the latter, despite their lower asphaltene content. Although the asphaltic tars lacked the necessary variation to produce a meaningful isochron, it is likely that their Re-Os systematics actually constrain the cessation of TSR. Hence, their marked departure from those of the asphaltites, which are considered to record a generation age (Corrick et al., 2019; Scarlett et al., 2019).

A second potential explanation for resetting Re-Os systematics is oil-water interaction without TSR. Laboratory experiments have also shown Re and Os may be rapidly transferred to liquid oil when in contact with a solution enriched in Re and Os (Mahdaoui et al., 2015; Hurtig et al., 2019). Though these studies cannot fully mimic natural oil-water interactions in a geologic setting, their results suggest that interaction of oil with formation waters, which contain much lower abundances of Re and Os, may be capable of altering and resetting the Re-Os composition

of an oil, given sufficiently high water/oil ratios (ca. 250). In this case, such formation waters would require highly radiogenic Os in order to alter the $^{187}Os/^{188}Os$ ratios of the asphaltic tars to their observed values (3.057–3.063), which are much higher than those reported for the asphaltites (1.122–1.334: Corrick et al., 2019; Scarlett et al., 2019). However, the influence of basinal water on the Re-Os systematics of crude oils and their application to constraining the timing of generation has been demonstrated to be limited or negligible in the Duvernay petroleum system of the West Canada Sedimentary Basin (Liu et al., 2018) wherein certain oils contain very low concentrations of both Re (0.04–3.78 ppb) and Os (0.6–41.2 ppt). Such examples should be extremely sensitive to any Re-Os contamination, but such alteration is not observed. Therefore, overprinting from typical interaction with formation waters is unlikely, given the evidence supportive of their alteration by TSR.

Definitive identification that a crude oil has been altered by TSR typically requires identification of thiaadamantanes (Wei et al., 2012), or a combination of evidence from obtained from complementary analyses, notably assessment of the resulting gases (H_2S and CO_2), low-molecular-weight hydrocarbons and precipitated phases including carbonates, pyrobitumens and metal sulphides (e.g. Machel et al., 1995; Machel, 2001; Li et al., 2005; Hao et al., 2008; Liu et al., 2016). Unfortunately, the asphaltic tars do not appear to contain any compounds with mass spectra consistent with thiaadamantane or its various methylated homologues. However, if thiaadamantanes were originally present, they would likely have been lost along with the other low-molecular-weight hydrocarbons due to weathering in the marine environment. Therefore, without fresh examples for comparison, the absence of thiaadamantanes does not definitively preclude TSR in this case. Furthermore, as these oils were collected from the coastline, complementary analyses of the other products of TSR discussed above are not available for comparison as the location of the reservoir is not known. Given this ambiguity, we cannot conclusively determine that TSR has altered the asphaltic tars, although we note it would be consistent with their bulk $\delta^{34}S$ values and Re-Os systematics. Analysis of these oils in a more concentrated form using GC-MS-MS targeting the 2-thiaadamantane and the methlated thiaadamantanes may be able to assess this interpretation further. Alternatively, comparison of the compoud-specific sulphur isotopic composition of the benzothiophenes and dibenzothiophenes may also be diagnostic (Amrani et al., 2012).

The other noted differences between the asphaltites and asphaltic tars are consistent with minor lateral variation in organic facies and the expulsion of the latter from the source rock later in

the oil generation window. The carbonate content and redox conditions of a source rock formation may vary laterally across a basin due to its proximity to shallow water carbonate systems and variations in seafloor topography beneath a stratified water column, respectively. Such variability would be consistent with the minor variations in redox parameters (e.g. Pr/Ph, C_{35} homohopane index) between the two oil types and a calcareous shale source for the asphaltic tars, as indicated by their unusually low Ts/(Ts+Tm) values for an oil generated in the late oil window. The higher thermal maturity of the asphaltic tars is also consistent with their greater abundance of tricyclic terpanes relative to hopanes when compared to the asphaltites. Finally, both increasing thermal maturity and TSR are known to affect the $\delta^{13}C$ composition of the oil. Mature oils contain individual low-molecular-weight hydrocarbons which are 1–3‰ more enriched in ^{13}C relative to their less mature equivalents, while alteration by TSR results in even greater enrichment (> +15‰: Rooney, 1995). The light hydrocarbons affected by these processes are not preserved in the asphaltic tars, and therefore neither of these diagnostic changes can be assessed based on the isotopic composition of their C_{13}–C_{35} *n*-alkanes (Fig. 5).

In summary, whilst the differences between the asphaltites and asphaltic tars could be attributted to their derivation from separate source rocks, the specific points of variation are also consistent with the latter's higher thermal maturity, alteration by TSR and minor lateral variation in source facies (Table 3).

4.3. Potential mechanisms of heavy petroleum formation

Naturally occurring viscous tars/bitumen may form in response to a variety of different processes. These include: (1) extensive biodegradation of crude oil in a shallow subsurface reservoir; (2) weathering and amalgamation of a sea-surface oil slick, leaving a viscous residue which may be subsequently separated by wave action (Logan et al., 2010; Warnock et al., 2015); (3) *in situ* thermal maturation of a crude oil resulting in the formation of pyrobitumen (Machel, 2001); (4) separation of heavy petroleum to form subsurface tar mats, which may occur in several different ways (Dahl and Speers, 1986; Wilhelms and Larter, 1994a, 1994b); and (5) direct seepage of heavy petroleum onto the seafloor (e.g. Brüning et al., 2010), where it then becomes immobile.

Table 3: Summary of processes capable of creating the observed geochemical differences between the asphaltic tars and asphaltites under the single source rock interpretation.

Deviation from asphaltite geochemistry	Potential mechanisms
(1) Higher abundance of tricyclic terpanes relative to hopanes	• Preferential expulsion of terpanes from kerogen at higher thermal maturities (Aquino Neto et al., 1983; van Graas, 1990; Farrimond et al., 1999)
(2) Lower sulphur content	• Lateral variability in euxinic conditions across basin • Thermal decomposition of organosulphur compounds in oil to gases (Orr, 1974; Tissot and Welte, 1984)
(3) Heavier $\delta^{34}S$ values	• Uptake of sulphur from dissolved sulphates and/or back reaction of H_2S during TSR (Orr, 1974; Lillis and Selby, 2013)
(4) Enriched Re and Os abundance and highly different Re-Os ratios	• Alteration due to TSR (Lillis and Selby, 2013)
(5) Pr/Ph < 1	• Lateral variability of source rock redox conditions
(6) Minor variation in C_{29}/C_{30} αβ hopane ratio	• Minor lateral variability in source rock carbonate content • Preferential thermal degradation of C_{30} αβ hopane (Peters et al., 2005)
(7) Presence of 2α-methylhopanes	• Minor increase in carbonate content • Increased thermal maturity
(8) Lower Ts / (Ts+Tm)	• Greater relative abundance of Tm attributed to higher carbonate content and anoxic conditions rather than thermal maturity (e.g. McKirdy et al., 1983, 1984; Rullkötter et al., 1985; Price et al., 1987)

Many of these potential mechanisms are inconsistent with the composition of the asphaltic tars and may therefore be discounted. Firstly, although they have a slightly lower *n*-alkane content than the freshest examples of asphaltite, the asphaltic tars do not appear to be heavily biodegraded, as they still contain C_{10+} *n*-alkanes. The preservation of the somewhat water-soluble naphthalenes in the least altered asphaltites and the entire suite of asphaltic tars also suggests that, despite their interaction with seawater, water washing has not been extensive. This likely precludes their formation from the weathering and amalgamation of an oil slick, whether from a spilled oil or natural seepage. Liquid oil in seawater will disperse into a thin surface slick with an extremely high surface area to volume ratio, making the oil extremely vulnerable to water washing, oxidation and microbial action. Generally, such oil in the marine environment will lose the majority of its low-molecular-weight components in a matter of hours (Head et al., 2006). Additionally, other known examples of marine tars amalgamating from sea surface oil slicks notably required calm oceanic conditions to form (e.g. Lorenson et al., 2009). The high energy environment of the Great Australian Bight, including the intense storm which occurred prior to the collection of the asphaltic tars, is unlikely to be supportive of this process.

In-situ thermal maturation of reservoired crude oil or alteration by TSR are known to form pyrobitumen. These solid residues are only weakly soluble in organic solvents (Wilhelms and Larter, 1994b) and are unlikely to seep. Previous assessment of their origin by Hall et al. (2014) demonstrated that the asphaltites are not pyrobitumen as they readily dissolve in dichloromethane. Although the asphaltic tars were generated and expelled during the late oil window, they are similarly soluble in dichloromethane and therefore they, too, cannot be considered residues of thermal maturation.

Hall et al. (2014) proposed that the asphaltites are transported remnants of subsurface tar mats, also known as viscous oil zones, polar-enriched zones (Larter et al., 1990) or heavy oil tar zones (Haldorsen et al., 1985). These deposits of heavy petroleum are reported in both clastic and carbonate settings and may range in thickness from <1 m to as much as 6 m (Larter et al., 1990; Wilhelms and Larter, 1994a, 1994b). Well characterised examples demonstrate these emplacements of heavy petroleum share comparable biomarker geochemistry with their parent oils but are more enriched in asphaltenes (20–60 wt %; cf. 1–5 wt % in the oil leg: Wilhelms and Larter, 1994a, 1994b). Tar mats are readily soluble in organic solvents, clearly distinguishing them from weakly soluble pyrobitumen formed during reservoir maturation (Milner et al., 1977; Wilhelms and Larter, 1994a). These deposits may separate from the main oil charge in response to several different processes, including gravity segregation, introduction of gas to the reservoir and decreasing reservoir pressures, or are due to permeability barriers (Milner et al., 1977; Dahl and Speers, 1986; Wilhelms and Larter, 1994a, 1994b). In particular, deasphalting of the oil in response to gas generation from a maturing reservoired oil could account for the formation of the asphaltic tars, given that their thermal maturity (R_c = 1.1–1.2%) lies at the boundary of the wet gas window (R_c = 1.3%). Migration of gas into the reservoir is also possible, given the faulting which may connect to regions of the basin in the gas window (Fig. 7). However, ultimately none of the processes listed above can be discounted, as the resulting heavy petroleum in each case displays no diagnostic changes to its geochemistry. A more detailed knowledge of the geologic context of their parent petroleum system is therefore required to assess these mechanisms further.

Considering the asphaltic tars and asphaltite strandings as pieces of previously emplaced tar mats is also problematic, as it also requires facilitating their migration to the seafloor, despite their tendency to remain in place in the subsurface. Hall et al. (2014) suggested that following their formation as tar mats, the asphaltites escaped the subsurface by way of submarine canyon

incision. However, it is more likely that seepage of both the asphaltites and the asphaltic tars is analogous to the asphalt flows observed on the seafloor in the Gulf of Mexico (Brüning et al., 2010). In this case, heavy petroleum that has not yet become immobile reaches the seafloor in a viscous state and flows away from the seepage site. The loss of volatile components, oxidation and other processes progressively increases the viscosity of the oil to the point where it becomes immobile and ultimately solidifies. The deposit forms deep fissures and cracks due to the loss of its low-molecular-weight hydrocarbons. The bitumen eventually fragments, releasing material into the overlying water column where it can become entrained in ocean currents. This process is certainly consistent with the shrinkage cracks seen in the larger asphaltites (Fig. 1B). The asphaltic tars, which have not solidified, may be more analogous to the seafloor tar mounds/whips observed off the southern coast of Santa Barbara (Lorenson et al., 2009). In this case, however, the oil has not been extensively biodegraded like that encountered in the Santa Barbara seeps.

4.4. Constraining the location of the asphaltic tar petroleum system

The prior coastal surveys conducted in November 2014 and September 2015 found no examples of this new variety of asphaltic crude oil across the 30 systematically surveyed beaches (Ross et al., 2017). There are similarly no reports of any oil matching their geochemical signature in previous studies of Australian coastal bitumen (McKirdy, 1984a, 1984b; Currie et al., 1992; Volkman et al., 1992; Summons et al., 1993; Alexander et al., 1994; Padley, 1995; Edwards et al., 1998, Hall et al., 2014; Edwards 2016, 2018). The beach where the asphaltic tars were found, Number 1 and 2 Rocks, is also the most prominent collection point for coastal bitumen identified on the South Australian coastline (Padley, 1995; Edwards et al., 2016; Ross et al., 2017). Despite the abundance of coastal bitumen recovered from this site, no asphaltites were found there during the three annual surveys conducted in 2014–2016 (Ross et al., 2017), nor during the systematic bi-monthly surveys conducted in 1990 and 1991 (Padley, 1995; Edwards et al., 2016). However, it is important to acknowledge that the asphaltic tar strandings were collected just 24 days after a one-in-fifty-year storm event which affected much of the South Australian coastline (Bureau of Meteorology, 2016; Burns et al., 2017). The resulting abnormal wind and wave behaviour likely caused a significant departure from their traditional oceanic transport pathway and ultimate stranding location. Therefore, the single stranding location of the asphaltic tars presently provides little constraint on their point of origin.

If the asphaltic tars were derived from an oil affected by TSR then the parent oil must reside within a region of the subsurface which meets the required minimum onset temperature of 100–140° (Goldhaber and Orr, 1995; Machel, 2001). This may permit assessment of potential reservoirs based on the general increase in temperature with depth (e.g. Fig. 7). However, locally increased temperatures will also occur in proximity to volcanism and circulating hydrothermal fluids. The Bight Basin hosts an approximately 50,000 km^2 complex of volcanic intrusions in the Ceduna Sub-basin and the overlying Eucla Basin, with isolated igneous bodies also reported in the adjacent Duntroon Sub-basin (Schofield and Totterdell, 2008). Thus, circulating hydrothermal fluids could also provide the necessary temperatures and dissolved sulphate for TSR to occur within shallower regions of the basin. This is further supported by the recent identification of hydrocarbon-containing fluid inclusion assemblages in the Duntroon Sub-basin which appear to have been altered by hydrothermal fluids (Bourdet et al., 2020). However, no hydrocarbons extracted from fluid inclusions in the Bight Basin have a composition consistent with the asphaltites or asphaltic tars (Kempton et al., 2020; Gong et al., *submitted*).

Oils altered by TSR are primarily encountered in reservoirs with limited clay content such as clean sandstones or carbonates, as the presence of iron within clay minerals will react with available H_2S to form pyrite, rather than permitting it to accumulate to high concentrations (Worden and Smalley, 2011; Machel, 2001). In order for TSR to occur in clastic sediments containing clays, a larger source of dissolved sulphate is required (e.g. dissolved evaporite deposits) to exhaust all of the available iron before H_2S can accumulate. Presently there are no proposed carbonate reservoirs or evaporite deposits within the Bight Basin. Therefore, if the asphaltic tars have been altered by TSR, the reservoir would likely reside within clean sandstones deposited as part of the Ceduna delta, using sulphate sourced from groundwaters or circulating hydrothermal fluids. However, as the evidence for alteration by TSR is not conclusive, proposing an exact location for the parent petroleum system within this frontier basin remains speculative.

5. CONCLUSIONS

A new type of stranded crude oil termed ‘asphaltic tar’ was encountered during coastal surveys of South Australia in October 2016. These strandings share source-specific features with the well-studied asphaltites, also found on the South Australian coastline. Thermal maturity

parameters constrain the asphaltic tar to the late oil window, unlike the asphaltites which were generated within the early oil window. The contrasting thermal maturity of the two oil types renders their correlation uncertain. Despite their source-specific similarities, differences in several geochemical parameters of the two oil types suggest that each may have originated from separate source rocks with comparable marine organic matter inputs. However, the most prominent differences accord with the higher thermal maturity of the asphaltic tar and its alteration by thermochemical sulphate reduction. Both interpretations are consistent with these two oil types originating from within the same basin. As the asphaltites are presently attributed to an undiscovered petroleum system in the nearby Bight Basin, we consider these newly discovered asphaltic tars to have a similar origin.

ACKNOWLEDGEMENTS

CSIA data were collected by the Davis Isotope Laboratory, University of California. Re-Os data were collected at the Laboratory for Source Rock Geochronology and Geochemistry and Arthur Holmes Laboratory at Durham University (UK). A.J.C. acknowledges the financial support of the Bernold M. “Bruno” Hanson Memorial Environmental Grant from the AAPG Foundation's Grants-In-Aid Program, The D R Stranks Travelling Fellowship, a University of Adelaide postgraduate scholarship and additional funding from the Great Australian Bight Research Program. D.S. acknowledges the Total Endowment Fund and the CUG Wuhan Dida Scholarship. We thank Zachary Angelini, Chris Dyt, Richard Kempton, Cameron White, April Pickard, Stacey Maslin, Stephane Armand, Les Tucker and Su Margot for their assistance in completing the 2014–2016 beach surveys. We also thank Mark Rollog and Robyn Williamson for conducting the EA-IRMS analyses; Antonia Hofmann and Geoff Nowell for assistance with the Re-Os determinations; and Stuart Valladares for the donation of asphaltites from his personal collection for this research. Finally, we thank Charlotte Stalvies, Chris Boreham, Herbert Volk and Jennifer Totterdell for their constructive feedback on our manuscript.

The Great Australian Bight Research Program is a collaboration between BP, CSIRO, the South Australian Research and Development Institute (SARDI), the University of Adelaide, and Flinders University. The program aims to provide a whole-of-system understanding of the environmental and social values of the region; providing an information source for all to use.

SUPPLEMENTARY INFORMATION AND PUBLISHED MANUSCRIPT

The supplementary information for this chapter may be found in pages 231–237.

The published version of this chapter may be found in pages 319–333.

REFERENCES

Alexander, R., Currie, T.J., Kagi, R.I., 1994. The origins of coastal bitumens from Western Australia. Aust. Pet. Expor. Assoc. J. 34 (1), 787–798.

Amrani, A., Deev, A., Sessions, A.L., Tang, Y., Adkins, J.F., Hill, R.J., Moldowan, J.M., Wei, Z., 2012. The sulfur-isotopic compositions of benzothiophenes and dibenzothiophenes as a proxy for thermochemical sulfate reduction. Geochim. Cosmochim. Acta 84, 152–164. doi:10.1016/J.GCA.2012.01.023

Aquino Neto, F.R., Trendel, J.M., Restle, A., Connan, J., Albrecht, P.A., 1983. Occurrence and formation of tricyclic and tetracyclic terpanes in sediments and petroleum. In: Bjoröy, M., Albrecht, P., Cornford, C., de Groot, K., Eglinton, G., Galimov, E., Leythaeuser, D., Pelet, R., Speers, G. (Eds.), Advances in Organic Geochemistry 1981. John Wiley & Sons Limited, Chichester, pp. 659–676.

Bastow, T.P., van Aarssen, B.G.K., Lang, D., 2007. Rapid small-scale separation of saturate, aromatic and polar components in petroleum. Org. Geochem. 38, 1235–1250. doi:10.1016/j.orggeochem.2007.03.004

Blevin, J.E., Boreham, C.J., Summons, R.E., Struckmeyer, H.I.M., Loutit, T.S., 1998. An effective Lower Cretaceous petroleum system on the North West Shelf: Evidence from the Browse Basin. In: Purcell, P.G., Purcell, R.R. (Eds.), The Sedimentary Basins of Western Australia II. Petroleum Exploration Society of Australia, pp. 397–420.

Blevin, J.E., Boreham, C.J., Summons, R.E., Struckmeyer, H.I.M., Loutit, T.S., 2000. Hydrocarbon prospectivity of the Bight Basin - petroleum systems analysis in a frontier basin. In: Wood, G.R. (compiler), 2nd Sprigg Symposium - Frontier Basins, Frontier Ideas. Geological Society of Australia Abstracts 60, pp. 24–26.

Boreham, C., 2009. Organic geochemistry – source rock characterisation. In: Totterdell, J., Mitchell, C. (Eds.), Bight Basin geological sampling and seepage survey: RV Southern Surveyor SS01/2007. Geoscience Australia Record 2009/24, pp. 36-60. http://pid.geoscience.gov.au/dataset/ga/68689

Boreham, C.J., Krassay, A.A., Totterdell, J.M., 2001. Geochemical comparisons between asphaltites on the southern Australian margin and Cretaceous source rock analogues. In: Hill, K.C., Bernecker, T. (Eds.), Eastern Australasian Basins Symposium, A Refocused Energy Perspective for the Future. Petroleum Exploration Society of Australia Special Publication, pp. 531–541

Boult, P.J., McKirdy, D., Blevin, J., Heggeland, R., Lang, S., Vinall, D., 2005. The oil-prone Morum Sub-basin petroleum system, Otway Basin, South Australia. MESA J. 38, 28–33.

Bourdet, J., Kempton, R.H., Dvia, V., Pironon, J., Gong, S., Ross, A.S., (2020). Constraining the timing and evolution of hydrocarbon migration in the Bight Basin. Mar. Pet. Geol. 114, 104193. doi: 10.1016/j.marpetgeo.2019.104193

Brüning, M., Sahling, H., MacDonald, I.R., Ding, F., Bohrmann, G., 2010. Origin, distribution, and alteration of asphalts at Chapopote Knoll, Southern Gulf of Mexico. Mar. Pet. Geol. 27, 1093–1106. doi:10.1016/j.marpetgeo.2009.09.005

Bureau of Meteorology, 2016. Severe thunderstorm and tornado outbreak South Australia, 28 September 2016.

Burns, G., Adams, L., Buckley, G., 2017. Independent review of the extreme weather event South Australia 28 September – 5 October 2016. Report presented to the Premier of South Australia.

Cassani, F., Gallango, O., Talukdar, S., Vallejos, C., Ehrmann, U., 1988. Methylphenanthrene maturity index of marine source rock extracts and crude oils from the Maracaibo Basin. Org. Geochem. 13, 73–80. doi:10.1016/0146-6380(88)90027-7

Corrick, A.J., Hall, P.A., McKirdy, D.M., Gong, S., Trefry, C., Dyt, C., Angelini, Z., Ross, A.S., Kempton, R., Armand, S., White, C., 2016. A revised oil family classification scheme and geochemical weathering proxies for South Australian coastal bitumen strandings. In: 19th Australian Organic Geochemistry Conference, Program and Abstracts. Fremantle, pp. 30–31.

Corrick, A.J., Selby, D., McKirdy, D.M., Hall, P.A., Gong, S., Trefry, C., Ross, A.S., 2019. Remotely constraining the temporal evolution of offshore oil systems. Sci. Rep. 9, 1327. doi:10.1038/s41598-018-37884-x

Currie, T.J., Alexander, R., Kagi, R.I., 1992. Coastal bitumens from Western Australia - long distance transport by ocean currents. Org. Geochem. 18, 595–601.

Dahl, B., Speers, G.C., 1986. Geochemical characterization of a tar mat in the Oseberg field Norwegian sector, North Sea. Org. Geochem. 10, 547–558. doi:10.1016/0146-6380(86)90053-7

Dowling, L.M., Boreham, C.J., Hope, J.M., Murray, A.P., Summons, R.E., 1995. Carbon isotopic composition of hydrocarbons in ocean-transported bitumens from the coastline of Australia. Org. Geochem. 23, 729–737. doi:10.1016/0146-6380(95)00061-I

Du Vivier, A.D.C., Selby, D., Sageman, B.B., Jarvis, I., Gröcke, D.R., Voigt, S., 2014. Marine 187Os/188Os isotope stratigraphy reveals the interaction of volcanism and ocean circulation during Oceanic Anoxic Event 2. Earth Planet. Sci. Lett. 389, 23–33. doi:10.1016/j.epsl.2013.12.024

Edwards, D., McKirdy, D.M., Summons, R.E., 1998. Enigmatic asphaltites from the southern Australian margin: molecular and carbon isotopic composition. PESA J. 26, 397–420.

Edwards, D.S., Vinall, D.R., Corrick, A.J., McKirdy, D.M., 2016. Natural bitumen stranding on the ocean beaches of Southern Australia: a historical and geospatial review. Trans. R. Soc. South Aust. 140, 152–185. doi:10.1080/03721426.2016.1203532

Edwards, D.S., McKirdy, D.M., Rowland, S.J., Heath, D.J., Gray, P.S., 2018. Waxy bitumen stranding in southern Australia: A geochemical study of multiple oil families and their likely origins. Org. Geochem. 118, 132–151. doi:10.1016/j.orggeochem.2017.12.010

Eigenbrode, J.L., Freeman, K.H., Summons, R.E., 2008. Methylhopane biomarker hydrocarbons in Hamersley Province sediments provide evidence for Neoarchean aerobiosis. Earth Planet. Sci. Lett. 273, 323–331. doi:10.1016/J.EPSL.2008.06.037

Farrimond, P., Bevan, J.C., Bishop, A.N., 1999. Tricyclic terpane maturity parameters: response to heating by an igneous intrusion. Org. Geochem. 30, 1011–1019. doi:10.1016/S0146-6380(99)00091-1

Finlay, A.J., Selby, D., Osborne, M.J., 2011. Re-Os geochronology and fingerprinting of United Kingdom Atlantic margin oil: Temporal implications for regional petroleum systems. Geology 39, 475–478. doi:10.1130/G31781.1

Fraser, A.R., Tilbury, L.A., 1979. Structure and stratigraphy of the Ceduna Terrace region, Great Australian Bight Basin. Aust. Pet. Explor. Assoc. J. 19(1), 53–65. doi:10.1071/AJ78007

Georgiev, S. V., Stein, H.J., Hannah, J.L., Galimberti, R., Nali, M., Yang, G., Zimmerman, A., 2016. Re-Os dating of maltenes and asphaltenes within single samples of crude oil. Geochim. Cosmochim. Acta. doi:10.1016/j.gca.2016.01.016

Goldhaber, M.B., Orr, W.L., 1995. Kinetic controls on thermochemical sulfate reduction as a source of sedimentary H2S. In: Vairavamurthy, M.A., Schoonen, M.A.A., Eglinton, T.I., Luther, G.W., Manowitz, B. (Eds.), Geochemical Transformations of Sedimentary Sulfur. American Chemical Society, pp. 412–425. doi:10.1021/bk-1995-0612.ch023

Gong, S., Kempton, R.H., Ross, A.S., Bourdet, J., (in review). Characterisation of migrated hydrocarbons reveal insights into the source rocks of the Bight Basin. Mar. Pet. Geol.

Haldorsen, H.H., Mayson, H.J., Howarth, S.M., 1985. The heavy oil/tar mat in the Prudhoe Bay Field, Alaska - characterization and impacts on reservoir performance. In: 3rd International UNITAR/UNDP Heavy Crude and Tar Sands Conference, Preprints, Vol. 2. Information Centre New York, pp. 481–503.

Hall, P.A., McKirdy, D.M., Grice, K., Edwards, D.S., 2014. Australasian asphaltite strandings: Their origin reviewed in light of the effects of weathering and biodegradation on their biomarker and isotopic profiles. Mar. Pet. Geol. 57, 572–593. doi:10.1016/j.marpetgeo.2014.06.013

Hao, F., Guo, T., Zhu, Y., Cai, X., Zou, H., Li, P., 2008. Evidence for multiple stages of oil cracking and thermochemical sulfate reduction in the Puguang gas field, Sichuan Basin, China. Am. Assoc. Pet. Geol. Bull. 92, 611–637. doi:10.1306/01210807090

Harrison, A.G., Thode, H.G., 1958. Mechanism of the bacterial reduction of sulphate from isotope fractionation studies. Trans. Faraday Soc. 54, 84–92.

Hayes, J.M., Freeman, K.H., Popp, B.N., Hoham, C.H., 1990. Compound-specific isotopic analyses: A novel tool for reconstruction of ancient biogeochemical processes. Org. Geochem. 16, 1115–1128. doi:10.1016/0146-6380(90)90147-R

Head, I.M., Jones, D.M., Röling, W.F.M., 2006. Marine microorganisms make a meal of oil. Nat. Rev. Microbiol. 4, 173–182. doi:10.1038/nrmicro1348

Holba, A.G., Tegelaar, E., Ellis, L., Singletary, M.S., Albrecht, P., 2000. Tetracyclic polyprenoids: Indicators of freshwater (lacustrine) algal input. Geology 28, 251–254. doi:10.1130/0091-7613(2000)28<251:TPIOFL>2.0.CO;2

Hurtig, N.C., Georgiev, S.V., Stein, H.J., Hannah, J.L., 2019. Re-Os systematics in petroleum during water-oil interaction: The effects of oil chemistry. Geochim. Cosmochim. Acta 247, 142–161. doi:10.1016/J.GCA.2018.12.021

Jones, G.E., Starkey, R.L., 1957. Fractionation of stable isotopes of sulfur by microorganisms and their role in deposition of native sulfur. Appl. Microbiol. 5, 111–118.

Kempton, R.H., Bourdet, J., Gong, S., Ross A.S., 2020. Revealing hidden oil migration in the frontier Bight Basin, Australia. Mar. Pet. Geol. 113, 104124. doi:10.1016/j.marpetgeo.2019.104124

Krouse, H.R., Viau, C.A., Eliuk, L.S., Ueda, A., Halas, S., 1988. Chemical and isotopic evidence of thermochemical sulphate reduction by light hydrocarbon gases in deep carbonate reservoirs. Nature 333, 415–419. doi:10.1038/333415a0

Larter, S.R., Bjørlykke, K.O., Karlsen, D.A., Nedkvitne, T., Eglinton, T., Johansen, P.E., Leythaeuser, D., Mason, P.C., Mitchell, A.W., Newcombe, G.A., 1990. Determination of petroleum accumulation histories: Examples from the Ula Field, Central Graben, Norwegian North Sea. In: Buller, A.T., Berg, E., Hjelmeland, O., Kleppe, J., Torsæter, O., Aasen, J.O. (Eds.), North Sea Oil and Gas Reservoirs—II. Graham and Trotman, London, Dordrecht, pp. 319–330. doi:10.1007/978-94-009-0791-1_27

Li, J., Xie, Z., Dai, J., Zhang, S., Zhu, G., Liu, Z., 2005. Geochemistry and origin of sour gas accumulations in the northeastern Sichuan Basin, SW China. Org. Geochem. 36, 1703–1716. doi:10.1016/J.ORGGEOCHEM.2005.08.006

Lillis, P.G., Selby, D., 2013. Evaluation of the rhenium–osmium geochronometer in the Phosphoria petroleum system, Bighorn Basin of Wyoming and Montana, USA. Geochim. Cosmochim. Acta 118, 312–330. doi:10.1016/j.gca.2013.04.021

Liu, J., Selby, D., 2018. A matrix-matched reference material for validating petroleum Re-Os measurements. Geostand. Geoanalytical Res. 42, 97–113. doi:10.1111/ggr.12193

Liu, Q., Zhu, D., Jin, Z., Liu, C., Zhang, D., He, Z., 2016. Coupled alteration of hydrothermal fluids and thermal sulfate reduction (TSR) in ancient dolomite reservoirs – An example from Sinian Dengying Formation in Sichuan Basin, southern China. Precamb. Res. 285, 39–57. doi:10.1016/J.PRECAMRES.2016.09.006

Liu, J., Selby, D., Obermajer, M., Mort, A., 2018. Re-Os geochronology and oil-source correlation of Duvernay Petroleum System, Western Canada Sedimentary Basin: Implications for the application of the Re-Os geochronometer to petroleum systems. Am. Assoc. Pet. Geol. Bull. 102, 1627–1656. doi:10.1306/12081717105

Liu, J., Selby, D., Zhou, H., Pujol, M., 2019. Further evaluation of the Re-Os systematics of crude oil: Implications for Re-Os geochronology of petroleum systems. Chem. Geol. 513, 1–22. doi:10.1016/J.CHEMGEO.2019.03.004

Logan, G.A., Jones, A.T., Kennard, J.M., Ryan, G.J., Rollet, N., 2010. Australian offshore natural hydrocarbon seepage studies, a review and re-evaluation. Mar. Pet. Geol. 27, 26–45. doi:10.1016/j.marpetgeo.2009.07.002

Lorenson, T.D., Hostettler, F.D., Rosenbauer, R.J., Peters, K.E., Dougherty, J.A., Kvenvolden, K.A., Gutmacher, C.E., Wong, F.L., Normark, W.R., 2009. Natural Offshore Oil Seepage and Related Tarball Accumulation on the California Coastline; Santa Barbara Channel and the Southern Santa Maria Basin; source identification and inventory. U.S. Geological Survey Open-File Report 2009-1225 and MMS report 2009-030.

Machel, H.G., 2001. Bacterial and thermochemical sulfate reduction in diagenetic settings — old and new insights. Sediment. Geol. 140, 143–175. doi:10.1016/S0037-0738(00)00176-7

Machel, H.G., Krouse, H.R., Sassen, R., 1995. Products and distinguishing criteria of bacterial and thermochemical sulfate reduction. Appl. Geochemistry 10, 373–389. doi:10.1016/0883-2927(95)00008-8

Mahdaoui, F., Michels, R., Reisberg, L., Pujol, M., Poirier, Y., 2015. Behavior of Re and Os during contact between an aqueous solution and oil: Consequences for the application of the Re–Os geochronometer to petroleum. Geochim. Cosmochim. Acta 158, 1–21. doi:10.1016/j.gca.2015.02.009

Manzano, B.K., Fowler, M.G., Machel, H.G., 1997. The influence of thermochemical sulphate reduction on hydrocarbon composition in Nisku reservoirs, Brazeau river area, Alberta, Canada. Org. Geochem. 27, 507–521. doi:10.1016/S0146-6380(97)00070-3

McKirdy, D.M., 1984a. Coastal bitumens and potential source rocks, Duntroon Basin, South Australia (AMDEL Report F 5769/84 for Getty Oil Development Company Ltd., South Australian Department of Mines and Energy Open File Envelope No. 5876).

McKirdy, D.M., 1984b. Coastal bitumens and potential source rocks in the western Otway Basin, South Australia and Victoria (AMDEL Report F 5840/84 for Australian Aquitaine Petroleum Pty Ltd. and Ultramar Australia Inc., South Australian Department of Mines and Energy Open File.

McKirdy, D.M., Aldridge, A.K., Ypma, P.J.M., 1983. A geochemical comparison of some crude oils from pre-Ordovician carbonate rocks. In: Bjoröy, M., Albrecht, P., Cornford, C., de Groot, K., Eglinton, G., Galimov, E., Leythaeuser, D., Pelet, R., Speers, G. (Eds.), Advances in Organic Geochemistry 1981. John Wiley & Sons Limited, Chichester, pp. 99–107.

McKirdy, D.M., Cox, R.E., Volkman, J.K., Howell, V.J., 1986. Botryococcane in a new class of Australian non-marine crude oils. Nature 320, 57–59. doi:10.1038/320057a0

McKirdy, D.M., Kantsler, A.J., Emmett, J.K., Aldridge, A.K., 1984. Hydrocarbon genesis and organic facies in Cambrian carbonates of the Eastern Officer Basin, South Australia. In: Palacas, J.G. (Ed.), Petroleum Geochemistry and Source Rock Potential of Carbonate Rocks. AAPG Studies in Geology 18, pp. 13–31. doi:https://doi.org/10.1306/St18443C2

McKirdy, D., Summons, R., Padley, D., Serafini, K., Boreham, C., Struckmeyer, H., 1994. Molecular fossils in coastal bitumens from southern Australia: signatures of precursor biota and source rock environments. Org. Geochem. 21, 265–286.

Milner, C.W.D., Rogers, M.A., Evans, C.R., 1977. Petroleum transformations in reservoirs. J. Geochem. Explor. 7, 101–153. doi:10.1016/0375-6742(77)90079-6

Moldowan, J.M., Seifert, W.K., 1980. First discovery of botryococcane in petroleum. J. Chem. Soc. Chem. Commun. 19, 912–914.

Moldowan, J.M., Fago, F.J., Lee, C.Y., Jacobson, S.R., Watt, D.S., Slougui, N.-E., Jeganathan, A., Young, D.C., 1990. Sedimentary 24-n-propylcholestanes, molecular fossils diagnostic of marine algae. Science 247, 309–312. doi:10.2307/2873627

Murray, A.P., Summons, R.E., Boreham, C.J., Dowling, L.M., 1994. Biomarker and *n*-alkane isotope profiles for Tertiary oils: relationship to source rock depositional setting. Org. Geochem. 22, 521–542. doi:10.1016/0146-6380(94)90124-4

Orr, W.L., 1974. Changes in sulfur content and isotopic ratios of sulfur during petroleum maturation - study of Big Horn Basin Paleozoic oils. Am. Assoc. Pet. Geol. Bull. 58, 2295–2318.

Orr, W.L., 1986. Kerogen/asphaltene/sulfur relationships in sulfur-rich Monterey oils. Org. Geochem. 10, 499–516. doi:10.1016/0146-6380(86)90049-5

Padley, D., 1995. Petroleum geochemistry of the Otway Basin and the significance of coastal bitumen strandings on adjacent southern Australian beaches (PhD thesis). University of Adelaide.

Paytan, A., Kastner, M., Campbell, D., Thiemens, M.H., 2004. Seawater sulfur isotope fluctuations in the Cretaceous. Science 304, 1663–1665. doi:10.1126/science.1095258

Peters, K.E., Walters, C.C., Moldowan, J.M., 2005. The Biomarker Guide, Vol. 2: Biomarkers and Isotopes in Petroleum Exploration and Earth History, 2nd edition. Cambridge University Press.

Powell, T.G., McKirdy, D.M., 1973. Relationship between ratio of pristane to phytane, crude oil composition and geological environment in Australia. Nat. Phys. Sci. 243, 37–39.

Price, P.L., O'Sullivan, T., Alexander, R., 1987. The nature and occurrence of oil in Seram, Indonesia. in: Proceedings of the Indonesian Petroleum Association, 16th Annual Convention. Indonesian Petroleum Association, Jakarta, Indonesia, pp. 141–173.

Radke, M., 1987. Organic geochemistry of aromatic hydrocarbons. In: Brooks, J., Welte, D.H. (Eds.), Advances in Petroleum Geochemistry, Vol. 2. Academic Press, London, pp. 141–207.

Radke, M., Welte, D.H., 1983. The methylphenanthrene index (MPI). A maturity parameter based on aromatic hydrocarbons. In: Bjoröy, M., Albrecht, P., Cornford, C., de Groot, K., Eglinton, G., Galimov, E., Leythaeuser, D., Pelet, R., Speers, G. (Eds.), Advances in Organic Geochemistry 1981. John Wiley & Sons Limited, Chichester, pp. 504–512.

Radke, M., Leythaeuser, D., Teichmüller, M., 1984. Relationship between rank and composition of aromatic hydrocarbons for coals of different origins. Org. Geochem. 6, 423–430. doi:10.1016/0146-6380(84)90065-2

Rooney, M.A., 1995. Carbon isotopic data of light hydrocarbons as indicators of thermochemical sulfate reduction. In: Grimalt, J.O., Dorronsoro, C. (Eds.), Organic Geochemistry: Development and Applications to Energy, Climate, Environment and Human History 1995. A.I.G.O.A. Donostia-San Sebastian, pp. 523-525

Ross, A., Corrick, A., Trefry, C., Gong, S., McKirdy, D., Hall, T., Dyt, C., Angelini, Z., Kempton, R., Pickard, A., White, C., Maslin, S., Griffin, D., Middleton, J., Luick, J., Armand, S., Vergara, T., Schinteie, R., 2017. Asphaltite and tarball surveys. Final Report GABRP Project 5.2. Research Report Series Number 25a.

Rullkötter, J., Spiro, B., Nissenbaum, A., 1985. Biological marker characteristics of oils and asphalts from carbonate source rocks in a rapidly subsiding graben, Dead Sea, Israel. Geochim. Cosmochim. Acta 49, 1357–1370. doi:10.1016/0016-7037(85)90286-8

Scarlett, A.G., Holman, A.I., Georgiev, S. V., Stein, H.J., Summons, R.E., Grice, K., 2019. Multi-spectroscopic and elemental characterization of southern Australian asphaltites. Org. Geochem. doi:10.1016/J.ORGGEOCHEM.2019.04.006

Schofield, A., Totterdell, J.M., 2008. Distribution, Timing and Origin of Magmatism in the Bight and Eucla Basins. Geoscience Australia Record 2008/24.

Seifert, W.K., Moldowan, J.M., 1978. Applications of steranes, terpanes and monoaromatics to the maturation, migration and source of crude oils. Geochim. Cosmochim. Acta 42, 77–95. doi:10.1016/0016-7037(78)90219-3

Selby, D., Creaser, R.A., 2005. Direct radiometric dating of hydrocarbon deposits using rhenium-osmium isotopes. Science 308, 1293–1295. doi:10.1126/science.1111081

Selby, D., Creaser, R., Dewing, K., Fowler, M., 2005. Evaluation of bitumen as a Re–Os geochronometer for hydrocarbon maturation and migration: A test case from the Polaris MVT deposit, Canada. Earth Planet. Sci. Lett. 235, 1–15. doi:10.1016/j.epsl.2005.02.018

Selby, D., Creaser, R.A., Fowler, M.G., 2007. Re–Os elemental and isotopic systematics in crude oils. Geochim. Cosmochim. Acta 71, 378–386. doi:10.1016/j.gca.2006.09.005

Sprigg, R.C., Woolley, J.B., 1963. Coastal bitumen in southern Australia with special reference to observations at Geltwood Beach, south-east South Australia. Trans. R. Soc. South Aust. 86, 67–103.

Struckmeyer, H.I.M., Totterdell, J.M., Blevin, J.E., Logan, G.A., Boreham, C.J., Deighton, I., Krassay, A.A., Bradshaw, M.T., 2001. Character, maturity and distribution of potential Cretaceous oil source rocks in the Ceduna Sub-Basin, Bight Basin, Great Australian Bight. In: Hill, K.C., Bernecker, T. (Eds.), Eastern Australian Basins Symposium: a refocused energy perspective for the future. Petroleum Exploration Society of Australia, Special Publication, pp. 543–552.

Summons, R.E., Volkman, J.K., Boreham, C.J., 1987. Dinosterane and other steroidal hydrocarbons of dinoflagellate origin in sediments and petroleum. Geochim. Cosmochim. Acta 51, 3075–3082. doi:10.1016/0016-7037(87)90381-4

Summons, R.E., Bradshaw, J., Brooks, D.M., Goody, A.K., Murray, A.P., Foster, C.B., 1993. Hydrocarbon composition and origins of coastal bitumens from the Northern Territory, Australia. PESA J. 21, 31–42.

Summons, R.E., Jahnke, L.L., Hope, J.M., Logan, G.A., 1999. 2-Methylhopanoids as biomarkers for cyanobacterial oxygenic photosynthesis. Nature 400, 554–557. doi:10.1038/23005

Summons, R.E., Logan, G.A., Edwards, D.S., Boreham, C.J., Bradshaw, M.T., Blevin, J.E., Totterdell, J.M., Zumberge, J.E., 2001. Geochemical analogs for Australian coastal asphaltites - search for the source rock. In: Abstracts, AAPG Annual Convention, Denver, Colorado. Am. Assoc. Pet. Geol. Bull. 85 (Suppl.).

Thode, H.G., Harrison, A.G., Monster, J., 1960. Sulphur isotope fractionation in early diagenesis of Recent sediments of Northeast Venezuela. Am. Assoc. Pet. Geol. Bull. 44, 1809–1817.

Thode, H.., Monster, J., Dunford, H., 1961. Sulphur isotope geochemistry. Geochim. Cosmochim. Acta 25, 159–174. doi:10.1016/0016-7037(61)90074-6

Thode, H.G., Monster, J., 1965. Sulfur-isotope geochemistry of petroleum, evaporites, and ancient seas. In: Young, A., Galley, J.E. (Eds.), Fluids in Subsurface Environments. Am. Assoc. Pet. Geol. Mem. 4, pp. 367–3677. doi:https://doi.org/10.1306/M4360

Thode, H.G., Monster, J., 1970. Sulfur isotope abundances and genetic relations of oil accumulations in Middle East Basin. Am. Assoc. Pet. Geol. Bull. 54, 627–637.

Tissot, B.P., Welte, D.H., 1984. Petroleum Formation and Occurrence, 2nd ed., Springer-Verlag, Berlin.

Tolmer, A., 1882. Reminiscences of an Adventurous and Chequered Career at Home and in the Antipodes. Sampson Low, Marston, Searle & Rivington, London.

Totterdell, J.M., Blevin, J.E., Struckmeyer, H.I.M., Bradshaw, B.E., Colwell, J.B., Kennard, J.M., 2000. A new sequence framework for the Great Australian Bight: Starting with a clean slate. Aust. Pet. Prod. Explor. J. 40, 95–118. doi:10.1071/AJ99007

Totterdell, J.M., Bradshaw, B.E., 2004. The structural framework and tectonic evolution of the Bight Basin. In: Boult, P.J., Johns, D.R., Lang, S.C. (Eds.), Eastern Australasian Basins Symposium II. Petroleum Exploration Society of Australia Special Publication, pp. 41–61.

Totterdell, J.M., Struckmeyer, H.I.M., Boreham, C.J., Mitchell, C.H., Monteil, E., Bradshaw, B.E., 2008. Mid-Late Cretaceous organic-rich rocks from the eastern Bight Basin : implications for prospectivity. In: Blevin, J.E., Bradshaw, B.E., Uruski, E. (Eds.), Eastern Australasian Basins Symposium III. Petroleum Exploration Society of Australia Special Publication. pp. 137–158.

Trewartha, J., 1850. South Australian Government Gazette, 25 April 282.

van Graas, G.W., 1990. Biomarker maturity parameters for high maturities: Calibration of the working range up to the oil/condensate threshold. Org. Geochem. 16, 1025–1032. doi:10.1016/0146-6380(90)90139-Q

Volkman, J.K., O'Leary, T., Summons, R.E., Bendall, M.R., 1992. Biomarker composition of some asphaltic coastal bitumens from Tasmania, Australia. Org. Geochem. 18, 669–682. doi:10.1016/0146-6380(92)90092-C

Warnock, A.M., Hagen, S.C., Passeri, D.L., 2015. Marine Tar Residues: a Review. Water, Air, Soil Pollut. 226, 24. doi:10.1007/s11270-015-2298-5

Edwards, D.S., McKirdy, D.M., Rowland, S.J., Heath, D.J., Gray, P.S., 2018. Waxy bitumen stranding in southern Australia: A geochemical study of multiple oil families and their likely origins. Org. Geochem. 118, 132–151. doi:10.1016/j.orggeochem.2017.12.010

Edwards, D.S., Vinall, D.R., Corrick, A.J., McKirdy, D.M., 2016. Natural bitumen stranding on the ocean beaches of Southern Australia: a historical and geospatial review. Trans. R. Soc. South Aust. 140, 152–185. doi:10.1080/03721426.2016.1203532

Padley, D., 1995. Petroleum geochemistry of the Otway Basin and the significance of coastal bitumen strandings on adjacent southern Australian beaches (PhD thesis). University of Adelaide.

Wilhelms, A., Larter, S.R., 1994a. Origin of tar mats in petroleum reservoirs. Part I: introduction and case studies. Mar. Pet. Geol. 11, 418–441. doi:10.1016/0264-8172(94)90077-9

Wilhelms, A., Larter, S.R., 1994b. Origin of tar mats in petroleum reservoirs. Part II: Formation mechanisms for tar mats. Mar. Pet. Geol. 11, 442–456. doi:10.1016/0264-8172(94)90078-7

Worden, R.H., Smalley, P.C., 2001. H2S in North Sea oil fields: importance of thermochemical sulphate reduction in clastic reservoirs. In: Cidu, R. (Ed.), Water-Rock Interaction: Proceedings of the tenth international symposium on water-rock interaction, WRI-10, Villasimius, Italy, 10-15 July 2001. Swets & Zeitlinger, Lisse. pp. 659–662.

CHAPTER 4

The identification and provenance of crude oils stranded on the South Australian coastline

Statement of Authorship

Title of Paper	The identification and provenance of crude oils stranded on the South Australian coastline	
Publication Status	☐ Published ☐ Accepted for Publication	☐ Submitted for Publication ☑ Unpublished and Unsubmitted w ork w ritten in manuscript style
Publication Details	Written in the appropriate style for publication in *Marine Pollution Bulletin*.	

Principal Author

Name of Principal Author (Candidate)	Alexander J. Corrick		
Contribution to the Paper	Fieldwork, sample preparation, geochemical analysis, data processing and interpretation. Wrote the manuscript and drafted all figures.		
Overall percentage (%)	80		
Certification:	This paper reports on original research I conducted during the period of my Higher Degree by Research candidature and is not subject to any obligations or contractual agreements with a third party that would constrain its inclusion in this thesis. I am the primary author of this paper.		
Signature		Date	4/1/2019

Co-Author Contributions

By signing the Statement of Authorship, each author certifies that:

i. the candidate's stated contribution to the publication is accurate (as detailed above);
ii. permission is granted for the candidate in include the publication in the thesis; and
iii. the sum of all co-author contributions is equal to 100% less the candidate's stated contribution.

Name of Co-Author	Philip A. Hall		
Contribution to the Paper	Assistance with geochemical analysis, data processing and interpretations. Provided input to the final manuscript.		
Signature		Date	4/1/2019

Name of Co-Author	Se Gong		
Contribution to the Paper	Fieldwork, assistance with sample preparation, geochemical data collection and interpretation. Provided input to the final manuscript.		
Signature		Date	23/1/2019

Name of Co-Author	David M. McKirdy		
Contribution to the Paper	Project design, fieldwork and assistance with data interpretation. Provided input to the final manuscript.		
Signature		Date	4/1/2019

Name of Co-Author	Christine Trefry		
Contribution to the Paper	Fieldwork, database management. Provided input to the final manuscript.		
Signature		Date	4/1/2019

Name of Co-Author	Andrew S. Ross		
Contribution to the Paper	Project design, fieldwork, assistance with data interpretation. Provided input to the final manuscript.		
Signature		Date	31/1/2019

Journal format: ***Marine Pollution Bulletin***
Status: Unpublished work written in manuscript-style

The identification and provenance of crude oils stranded on the South Australian coastline

Alexander J. Corrick[1*], Philip A. Hall[1], Se Gong[2], David M. McKirdy[1], Christine Trefry[3] and Andrew S. Ross[3]

[1] Department of Earth Sciences, School of Physical Sciences, University of Adelaide, SA 5005, Australia

[2] Energy, CSIRO, North Ryde, NSW 2113, Australia

[3] Energy, CSIRO, Kensington, WA 6151, Australia

*** Corresponding author**

HIGHLIGHTS

1) Presents a summary of data on 633 coastal oil strandings
2) Whole-oil GC-MS can separate these oils into eight general types
3) Source-specific biomarkers distinguish at least 16 unique oils
4) Asphaltic oils are presently thought to originate from the nearby Bight Basin
5) Waxy oils are consistent with multiple petroleum systems across SE Asia

KEYWORDS

Coastal bitumen; asphaltite; waxy bitumen; tarballs; hydrocarbon seepage; South Australia

ABSTRACT

Semi-solid crude oil has been known to wash ashore along the South Australian coastline for over 120 years, with different oils attributed to various basins in Southeast Asia and potentially a local undiscovered oil system in the nearby Bight Basin. The early reports pre-date offshore petroleum exploration and tanker shipping activities in Australian waters, suggesting that the stranded oils originate from natural seepage. In order to distinguish this natural "background" contamination of the coastline from any potential anthropogenic sources of oil, such as oil spills, we summarise the key visual and geochemical attributes which may be used to identify at least 16 different oils collected from the coastline between 2014 and 2016. Two of these oils are presently thought to originate from the nearby Bight Basin, while the remaining 14 show geochemical similarities to petroleum systems across Southeast Asia. These latter oils are transported to the Australian coastline through a combination of regional ocean currents, most notably the North Pacific thermocline and Leeuwin Current.

1. INTRODUCTION

Natural seepage of crude oil from offshore petroleum systems currently represents the single largest input of oil into the global ocean, estimated at over 45% of the total annual input (NAS, 2003). It is therefore unsurprising that oil released from natural seeps may eventually strand along adjacent or more distant coastlines as either liquid oil, semi-solid tar or bitumen (e.g. Henry et al., 1993; Lorenson et al., 2009; Edwards et al., 2016). While some of the largest natural seeps, such as those located within the Gulf of Mexico (e.g. Brüning et al., 2010) and off the coastline of southern California (e.g. Lorenson et al., 2009), have been extensively documented, many remain unidentified. When such oil is encountered in a coastal environment it can understandably lead to questioning whether or not it is the result of a spill from human-induced activities, particularly if the oil strands in high abundance. Therefore, it is important to document which areas of a given coastline are known to collect crude oil emitted through natural seepage, and how those oils may be recognised, so that they may be distinguished from anthropogenic spillage.

In Australian waters, the overall frequency of oil spills has declined in response to stringent environmental and maritime laws (Hook et al., 2016). However, increasing oil and gas exploration and shipping activities in the region does raise the likelihood of future oil spills

(Hook et al., 2016). When assessing the impact of an oil spill in an area also affected by natural seepage, it can be difficult to separate the two oils if no pre-existing baseline data are available. For example, following the Mega Borg oil spill in the Gulf of Mexico in June 1990, the prior accumulation of tar balls and oil patties on the Louisiana coastline caused considerable confusion for both the response and damage assessment activities when attempting to distinguish the spilled oil from background inputs (Henry et al., 1993). Furthermore, an established baseline for the natural occurrence of oils in a particular region also allows for a more robust assessment of oil spill remediation, enabling clean-up activities to demonstrate when the concentration of oil in a given area has returned to well-documented, pre-spill conditions.

Reports of semi-solid crude oil, also known locally as 'coastal bitumen' stranding on the coastline of South Australia date back to the mid-late 1800s (Trewartha, 1850; Tolmer, 1882; Howchin, 1903, 1919; Ward, 1913, 1944; Sprigg and Woolley, 1963). These early reports pre-date petroleum shipping by tanker in South Australian waters, thus suggesting that these oils result from natural seepage from offshore petroleum systems, rather than anthropogenic oil spillage (Edwards et al., 1998, 2016, 2018). Geochemical assessment of these coastal bitumens began in earnest in the 1970s (McKirdy and Horvath, 1976), with subsequent studies reporting coastal bitumens of identical or similar compositions along the coastlines of the Northern Territory (Summons et al., 1993), Western Australia (Alexander et al., 1994), South Australia and Victoria (McKirdy et al., 1986, 1994; Padley, 1995; Edwards et al., 2016, 2018) and Tasmania (Volkman et al., 1992). Using various combinations of source-specific biomarker assemblages, elemental data (e.g. sulphur content) and stable isotopic assessments, the number of geochemically distinct oils identified from the Australian coastline has increased over time more specimens were analysed (Table 1).

South Australia has previously been considered to collect two main varieties of coastal bitumen: asphaltite, formerly known as 'asphaltum' (Edwards et al., 1998) and waxy bitumen, also referred to as tar balls (Edwards et al., 2018). A number of oil slicks have also been reported previously, although unlike the various coastal bitumens, these were attributed to anthropogenic sources and their occurrence on the coastline was relatively short-lived (Edwards et al., 2016). Asphaltites collected pre-1900 through to the present day have a highly reproducible geochemistry and thus represent a single oil family (Volkman et al., 1992; Edwards et al., 1998; Hall et al., 2014; Scarlett et al., 2019; Corrick et al., 2020a). These bitumens are thought to

originate from an undiscovered offshore petroleum system on Australia's southern margin, most likely the Bight Basin (Boreham et al., 2001; Totterdell et al., 2008; Corrick et al., 2020a). Unlike the asphaltites, the waxy bitumens comprise a wide variety of different oil families (Edwards et al., 2018). However, their content of specific biomarkers characteristic of Cenozoic lacustrine green algae and terrestrial angiosperms, compounds which are not commonly associated with Australian oils, suggests that they originate from petroleum systems in Southeast Asia and are then transported to the Australian coastline by regional ocean currents (Padley, 1995; Edwards et al., 2016, 2018).

Table 1: Summary of previous oil family classifications of Australian coastal bitumens.

Sample locations	Time of Collection	No. of samples analysed	No. of oil families	References
South Australia, western Victoria, Northern Territory	1961–1972	11	2 waxy oil families*	McKirdy and Horvath (1976)
South Australia	1983	27	3 waxy oil families + asphaltite	McKirdy (1984a, 1984b)
Tasmania	1880–1915	10	Asphaltite	Volkman et al. (1992)
Northern Territory	≤1993‡	22	2 waxy oil families*	Summons et al. (1993)
Western Australia	≤1994‡	83	8 waxy oil families	Alexander et al. (1994)
South Australia, Victoria	1990–1991†	126	5 waxy oil families + asphaltite	Edwards et al. (1998, 2018)

* = Sample suite also included a weathered crude oil which was considered anthropogenic in origin.
† = Also included donated specimens collected previously over a wider time period.
‡= Actual time of sample collection not provided in associated reference; date of publication is used.

This is the first of two research articles intended to establish an environmental baseline for the natural occurrence of a variety of different crude oils which strand on the South Australian coastline due to natural offshore seepage. Here we document the different types of oil encountered on the coastline based on a suite of 633 oil strandings collected between 2014 and 2016. We outline the visual, physical and geochemical parameters which may be used to distinguish these different oils, how these features may be altered by progressive weathering in the marine environment and discuss their potential points of origin. The second article then uses the oil classifications defined herein to determine the spatial distribution and abundance of these oils across the coastline and thereby establish a hydrocarbon loading baseline (Corrick et al., 2020b).

2. MATERIALS AND METHODS

2.1. Sample suite

A total of 508 semi-solid to solid oil strandings were collected during three annual surveys of 30 ocean beaches on Australia's southern margin as part of the Great Australian Bight Research Program (Baghurst et al., 2017; Ross et al., 2017; Corrick et al., 2020b). Of these survey sites, 29 are located along the coastline of South Australia and one is in Western Australia near the state border, although no samples were found at the latter (Fig. 1). The details and oil classifications for all collected specimens from the 2014, 2015 and 2016 surveys are provided in Tables S2. The spatial distribution and relative abundances of the oils collected during these surveys are discussed in detail in the accompanying study (Corrick et al., 2020b). The sample suite was supplemented with a further 125 bitumen specimens donated from private collections accrued during the study period or encountered outside the zones systematically surveyed in 2014–2016 (Table S3).

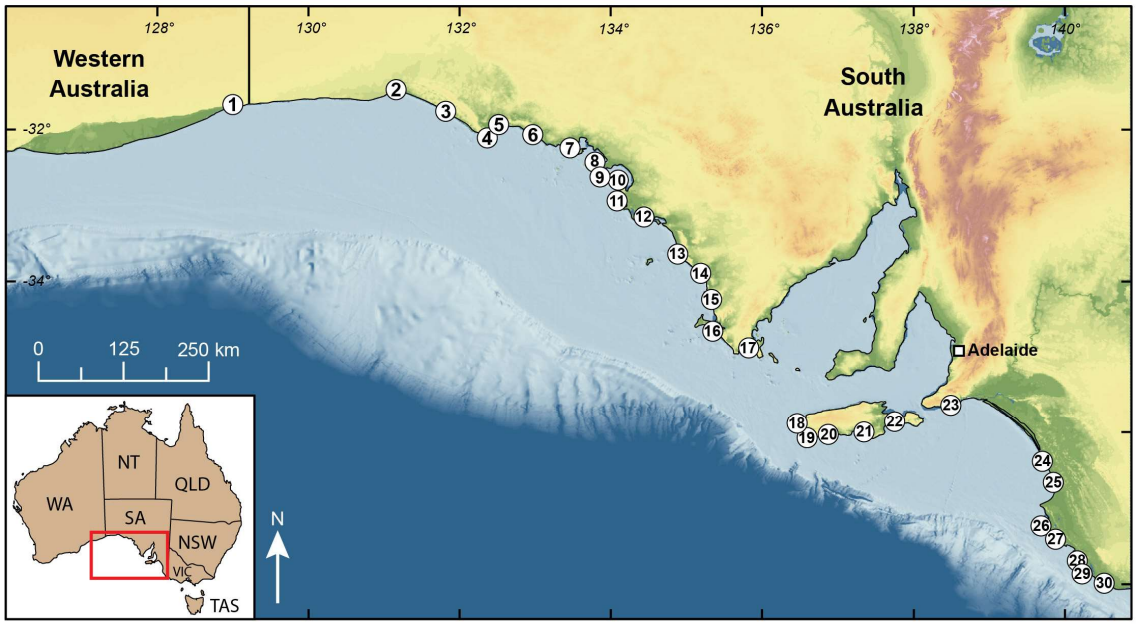


Figure 1: Survey sites visited in 2014, 2015 and 2016. The names and access point co-ordinates for each site are provided in Table S1.

2.2. Oil classification rationale

Oil classification was conducted in three stages of increasing analytical complexity: (1) inspection of visual/physical attributes; (2) bulk geochemical analysis using whole-oil gas chromatography-mass spectrometry (GC-MS); and (3) source-specific biomarker analysis

using selected ion monitoring gas chromatography-mass spectrometry (SIM GC-MS). Each subsequent assessment required a greater investment in sample preparation, data processing and interpretation, but resolved a greater number of unique oils. The entire suite of 633 oils was assessed visually upon collection and analysed by whole-oil GC-MS. A representative subset of samples from each whole-oil classification was then analysed by SIM GC-MS to identify their source-specific biomarker assemblages.

2.3. Whole-oil gas chromatography-mass spectrometry

All the sample preparation and analyses were conducted in the Biogeochemistry Laboratory at the University of Adelaide. A sub-sample (≤200 mg) was removed from each bitumen specimen and dissolved in 10 mL of dichloromethane/methanol (93:7, v:v). An aliquot of this solution was used for whole-oil GC-MS. Note that any specimen which was not soluble in dichloromethane/methanol was categorised as an inorganic/false sample and not analysed further. Analyses of bitumen samples collected in 2014 and 2015 were performed on an Agilent 6890 gas chromatograph interfaced with a 5973N MSD (electron energy 70 eV) and tuned using automatic setup parameters for each sequence. Chromatography was carried out on an Agilent HP-5MS fused silica column (30 m x 0.25 mm i.d. x 0.25 µm film thickness), using either a split (50 mL/min) or splitless injection mode, the latter employed if split injection data showed low responses. The oven was held at an initial temperature of 50°C for 1 min, followed by heating at 8°C/min to 300°C. The carrier gas was helium at a flow rate of 1 mL/min. GC-MS analyses of the samples collected in 2016 were performed on an Agilent 7890B gas chromatograph interfaced with a 5977B MSD (electron energy 70 eV) and tuned using automatic setup parameters for each sequence. Chromatography was undertaken on a J&W DB-5MS fused silica column (30 m x 0.25 mm i.d. x 0.25 µm film thickness), using the same operating conditions as employed for the 2014 and 2015 samples. In both cases, whole-oil GC-MS was conducted in the scan mode (scan interval 45-500 AMU at approx. 3 scans/sec). All data were processed using MSD ChemStation (Agilent Technologies, Inc.).

2.4. Isolation of saturated hydrocarbon fractions

The saturated hydrocarbons were separated from 20 mg aliquots of whole bitumen using the silica gel liquid chromatography procedure of Bastow et al. (2007). The recovered saturated hydrocarbons were stored in 2 mL chromatography vials prior to analysis.

2.5. Separation of branched/cyclic saturated hydrocarbons by molecular sieve

The high *n*-alkane content in many of the collected oils resulted in a suppression of the specified target ions entering the source chamber during SIM GC-MS analysis, resulting in significant drops in the baseline response in the resulting chromatograms. Additionally, condensation of the high wax components onto the stationary phase of the GC column resulted in the gradual phase change which affected the separation efficiency of the capillary after repeated analyses. This necessitated the separation of the branched/cyclic saturated fraction from the *n*-alkanes for reliable results. The saturates fractions were dissolved in cyclohexane and transferred on to 5Å molecular sieve (pre-baked at 350°C) before heating at 80°C in an oven for approximately 16 hours to ensure complete *n*-alkane absorption. The resulting branched/cyclic alkane fraction was then used for biomarker analyses.

2.6. Selected ion monitoring gas chromatography-mass spectrometry (SIM GC-MS)

GC-MS analysis of the branched/cyclic alkane fractions was performed on an Agilent 7890A gas chromatograph interfaced with a 5975C MSD (electron energy 70 eV) tuned using automatic setup parameters on the day of the analysis. Chromatography was carried out on a J&W DB-5MS fused silica column (60 m x 0.25 mm i.d. x 0.25 µm film thickness). A 1µL aliquot of branched/cyclic in *n*-pentane was injected into the split/splitless injector at 300°C operating in splitless mode. After being held at an initial temperature of 40°C for 2 min., the oven was heated at 20°C/min to 200°C and then ramped to 310°C at 2°C/min. The carrier gas was helium at a flow rate of 1.5 mL/min.

3. CLASSIFICATION FROM VISUAL ASSESSMENT

Crude oils found on the South Australian coastline were initially classified as asphaltite, waxy bitumen or tar based on the key features described below. In instances where a specimen could not be readily assigned to one of these categories, it was classified as ‘unknown/other’ pending geochemical assessment.

3.1. Asphaltites

Asphaltites are the most visually distinctive type of crude oil recognised on the South Australian coastline. These large bitumens (up to 7 kg : Edwards et al., 1998) are jet black in colour, have a strong petroliferous odour and commonly display deep shrinkage cracks across their outer surface. These cracks preferentially accumulate sand relative to the outer surface, which at least at the time of collection, is not sufficiently sticky to retain a uniform coating (Fig. 2A). Asphaltite interiors do not contain visible amounts of sand; and while a previous study documented a rare example of asphaltite which exhibited an internal fabric (Hall et al., 2014 : their figure 2D), no examples of similar textures were observed in the 37 asphaltites analysed during this study.

The least weathered asphaltites are predominantly solid but have a mildly pliable interior. Examples of fresh, soft asphaltites were rare, with only three collected in total between 2014 and 2016, all of which solidified during storage over several weeks/months. All but these freshest asphaltites are brittle and will break apart with a characteristic conchoidal fracture (Fig. 2B). Aside from notably soft examples, indicating that they are relatively fresh, the extent an asphaltite may be weathered is not immediately obvious from a visual standpoint and requires geochemical assessment. Of the different varieties of bitumen described herein, conchoidal fracturing is unique to the asphaltites, permitting their identification even in weathered examples which contain highly altered biomarker assemblages. The tendency of the asphaltites to break with a conchoidal fracture when other bitumens do not results from their exceptionally high asphaltene content (>50 %: Hall et al., 2014; Corrick et al., 2020a), as after the separated asphaltene fractions were dried, they were observed to fracture in the same manner. Their brittle nature of the asphaltites and their deep shrinkage cracks ultimately lead to fragmentation. Hence, weathered asphaltites usually occur as much smaller pieces (ca. 1–9 cm in diameter) than fresh specimens, although exceptions do occur.

3.2. Waxy bitumens

Waxy bitumens are semi-rounded to rounded tarballs with a mild petroliferous odour (Figs. 2C, D). The majority of strandings are dull black in colour, but fresh examples may retain a slight greasy lustre. Typical examples are 1–5 cm in diameter, although larger examples can occur. The different types of waxy bitumen are not distinguishable on the basis of their visual characteristics and their physical response to weathering differs markedly from that of the

asphaltites. Waxy bitumens do not become entirely brittle, although they commonly develop a brown and brittle outer surface (Fig. 2E–F), which can cover the entire bitumen in highly degraded crude oil. This is presumably attributable to photo-oxidation because, notwithstanding their hardened surface, such examples retain a pliable interior. As oxidation is only one of several possible weathering processes, the extent of surficial browning is an inconsistent indicator that without geochemical assessment regularly fails to distinguish highly degraded specimens.

3.3. Tars

Tar strandings (Fig. 2G) are sticky, viscous oils with a strong petroliferous odour and a sheen comparable to liquid oil (cf. the dull black colour of the asphaltites and waxy bitumens) that leaves a greasy mark on contact. These oils differ from asphaltite and waxy bitumen in that they are sufficiently soft to readily deform even under mild pressure, such as during handling upon their collection from the beach. Additionally, since their collection these oils have not solidified during storage in the same manner as observed for fresh asphaltites. Two varieties of tar were found on two separate beaches during the final survey in 2016, where at each location they accumulated in high abundance (Corrick et al., 2020a, 2020b). Assessment of their geochemistry was necessary to confirm that they belong to two separate oil families; they cannot be distinguished on the basis of their visual appearance alone.

4. CLASSIFICATION USING BULK GEOCHEMISTRY

Whole-oil GC-MS of the aforementioned 633 individual oil strandings collected from the South Australian coastline has allowed their subdivision into several ‘types’ on the basis of shared characteristics in their respective total ion chromatograms (TICs). The whole-oil classification scheme outlined below is intended to provide rapid discrimination of the different inputs to the natural hydrocarbon loading of its ocean beaches. As conducting detailed analyses across the entire suite was not practical, this provides a reasonable approach to identifying representative specimens for further molecular and isotopic analyses. While some oils (e.g. asphaltite) may be readily identified from their whole-oil TICs and subsequently confirmed to represent a single oil family on the basis of selected source-specific biomarkers (e.g. normal and acyclic isoprenoid alkanes), other types distinguished by this approach do not necessarily indicate a genetic grouping. Such relationships can only be established using more comprehensive

assessments based such as assessment of source-specific biomarkers using SIM GC-MS (discussed in Section 6).

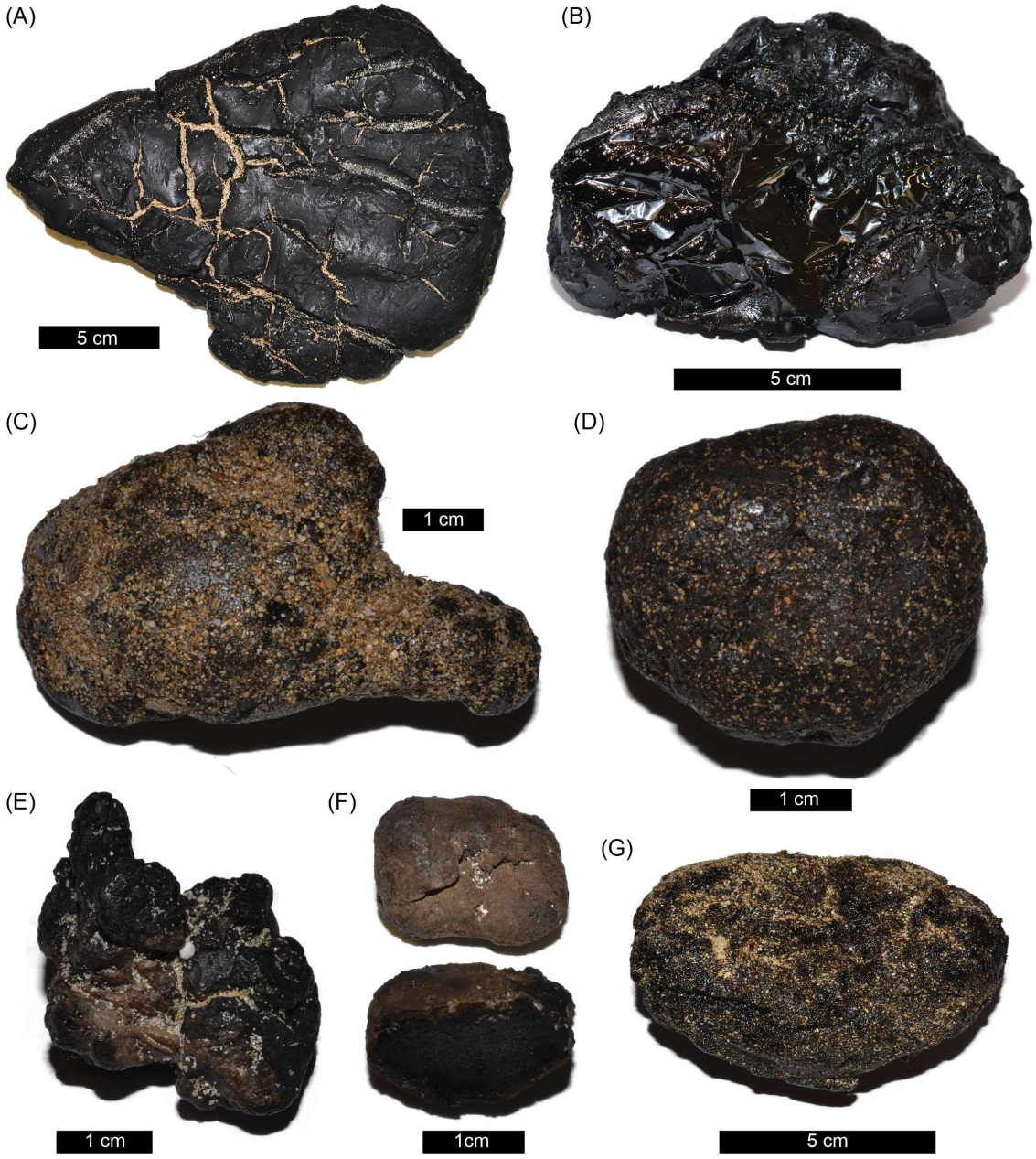


Figure 2: Representative photographs of various types of oil strandings recognised on the South Australian coastline. (A) Asphaltite with abundant devolatilisation cracks (sample W13/007507). (B) Broken asphaltite demonstrating diagnostic conchoidal fracture pattern (sample W13/007742). (C) Semi-rounded waxy bitumen (sample W13/007697). (D) Rounded waxy bitumen (sample W13/007680). (E) Moderately weathered waxy bitumen exhibiting partial surficial browning and loss of sand coating (sample W13/007625). (F) Highly weathered waxy bitumen with a completely hardened and oxidised outer surface resulting in the near total loss of surficial sand (sample W13/007521). Bisecting this waxy bitumen reveals that despite its solid brown exterior, the bitumen retains a semi-solid black interior. (G) Asphaltic tar with sticky, black lustre comparable to liquid oil (sample /001059).

On the basis of their bulk geochemistry, seven general types of oil may be distinguished: asphaltite, asphaltic tar, waxy bitumen types I-IV and Sandy River tar. A further two types: degraded high wax bitumen and unknown/other were also used in instances where classification was uncertain due to weathering. The proportion that each of these categories represents in terms of the total sample suite is shown in Figure 3. Despite the relatively large number of different oils, the geochemical classifications of these oil strandings may be broadly divided into two distinct groups: asphaltic oils and waxy oils. Asphaltic oils, which contain abundant an asphaltene fraction, include the asphaltites and asphaltic tars. Waxy oils, defined by their abundant *n*-alkane content, include waxy bitumen types I-IV and the Sandy River tars, in addition to the degraded high wax bitumen for which the exact classification is uncertain.

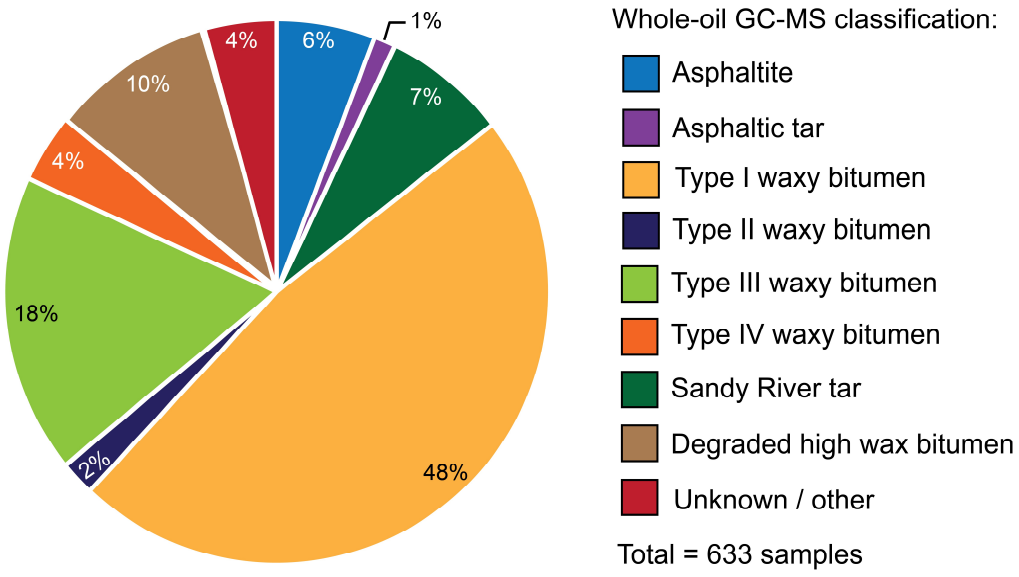


Figure 3: Relative contribution of each oil type based on classification by whole-oil GC-MS for the entire sample suite collected from 2014–2016 including specimens donated from private collections.

4.1. Asphaltic oils

The asphaltites and asphaltic tars are distinguished from the numerous waxy oil types by their abundance of branched/cyclic alkanes relative to n-alkanes and their low/trace abundances of C_{33+} *n*-alkanes (Fig. 4). The similarities and differences between these two oil types, in terms of bulk geochemistry, source-specific biomarkers and isotopic composition (carbon, sulphur, Re-Os), is discussed in greater detail in a separate investigation utilising the samples from the present study (Corrick et al., 2020a). These two oils differ in their relative abundances of pristane (Pr) and phytane (Ph). Asphaltites contain Pr/Ph ratios of 1.1–1.4, while the asphaltic tars have systematically lower values of 0.7–0.8 (Corrick et al., 2020a). Other bulk geochemical parameters which may distinguish these two oils from one another include their asphaltene content (51–59% in the asphaltites compared with 22–35% in the asphaltic tars) and their sulphur isotopic composition ($\delta^{34}S$). The asphaltic tars are enriched in the heavier isotope, with $\delta^{34}S$ values in the range +2.61 to +4.84 ‰, whereas the asphaltites are enriched in the lighter isotope, with $\delta^{34}S$ values between -8.82 and -5.30 ‰ (Corrick et al., 2020a).

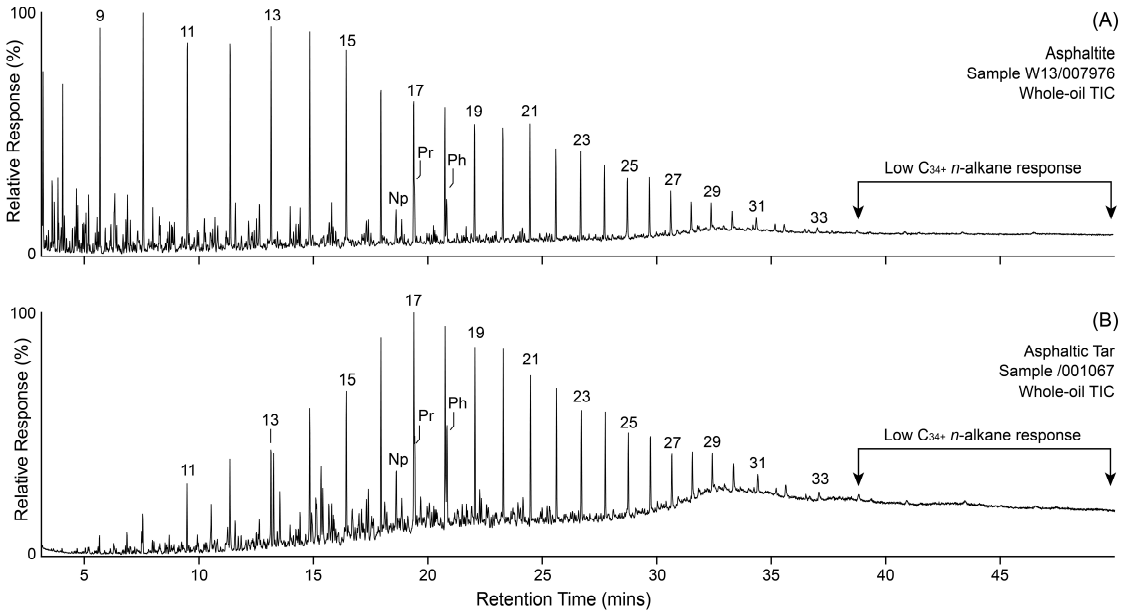


Figure 4: Whole-oil total ion chromatograms for asphaltic oils collected from the South Australian coastline. (A) Fresh asphaltite. (B) Asphaltic tar. Peak numbers correspond to *n*-alkane chain length, Np = norpristane, Pr = pristane, Ph = phytane.

4.2. Waxy oils

The waxy bitumens may be divided into four types on the basis of the presence/absence and relative abundance of the rare biomarker botryococcane, and the high or low abundance of high-molecular-weight *n*-alkanes in the $C_{35–39}$ range. Representative whole-oil total ion chromatograms for each type of waxy oil is shown in Figure 5. The type I and II waxy bitumens are defined by the presence of the rare biomarker botryococcane, which elutes between the C_{28} and C_{29} *n*-alkanes. These two oils may be distinguished by comparing their abundance of botryococcane relative to the $C_{35–39}$ *n*-alkanes. The type I waxy bitumens contain abundant botryococcane and display low individual responses for the $C_{35–39}$ *n*-alkanes (Fig. 5A), while the type II waxy bitumens contain little botryococcane, but abundant C_{35+} *n*-alkanes (Fig. 5B). The type III and IV waxy bitumens do not contain botryococcane and are distinguished by their low and high abundances of $C_{35–39}$ *n*-alkanes, respectively (Fig. 5C, D). Notably, these latter two types of waxy bitumen actually represent multiple oils as revealed by differences in their source-specific biomarker signatures (discussed in Section 6). This is unsurprising given that their key classification features rely on the absence of an extremely rare biomarker (botryococcane) and the abundance of high-molecular-weight *n*-alkanes, which is not highly source-specific. Finally, the Sandy River tars are recognisable in whole-oil GC-MS by their pristane or phytane maxima, bimodal unresolved complex mixture (UCM) and low/trace C_{33+} *n*-alkanes (Fig. 5E). The rapid removal of front-end *n*-alkanes resulting in a pristane or phytane maxima is not observed in the variously degraded waxy bitumens, although it is a common feature of biodegraded liquid oils. This may indicate that the Sandy River tars represent the weathered residue of a biodegraded liquid oil. Although their present *n*-alkane content is low due to biodegradation, the Sandy River tars are considered waxy oils on the basis of their source-specific biomarkers, which show prominent similarities to several other types of waxy bitumen (discussed in Section 6).

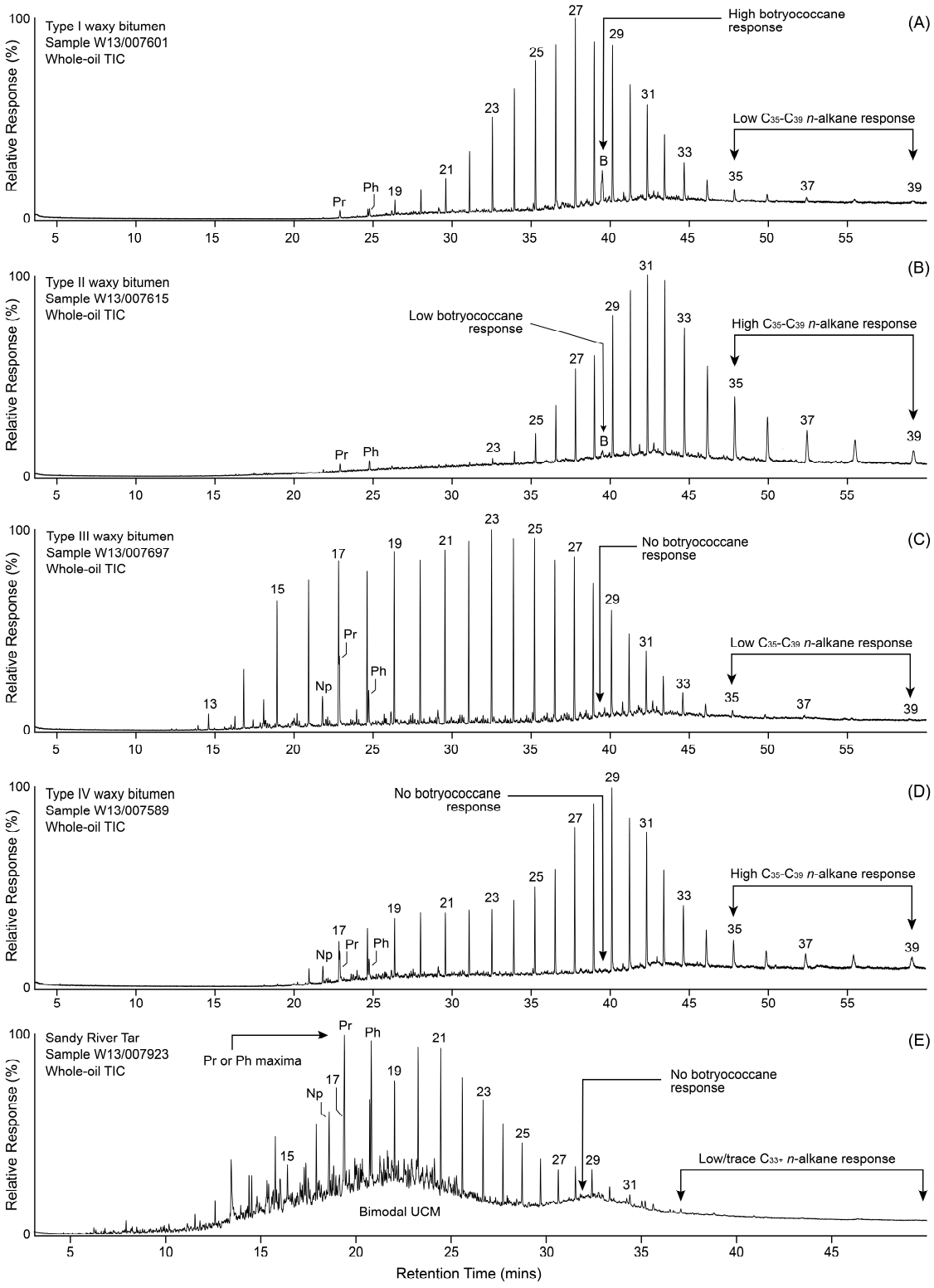


Figure 5: Whole-oil total ion chromatograms of various waxy oils collected from the South Australian coastline. (A) Type I waxy bitumen. (B) Type II waxy bitumen. (C) Type III waxy bitumen. (D) Type IV waxy bitumen. (E) Sandy River tar. Peak numbers correspond to *n*-alkane chain length, Np = pristane, Pr = pristane, Ph = phytane, B = botryococcane.

5. GEOCHEMICAL ALTERATION DUE TO WEATHERING

The duration of a semi-solid oil's exposure to the open marine and coastal environments may be highly variable. In particular, oils which originated from seeps associated with petroleum systems proximal to the coastline may spend significantly less time in the ocean than those transported by long-distance ocean currents. The complex combination of geochemical alteration due to photo-oxidation, biodegradation, water-washing and evaporation, which are referred to collectively as weathering, results in the progressive degradation and removal of different compounds from the oil (e.g. Palmer, 1993; Fingas, 1997; Garrett et al., 1998; Peters et al., 2005; Head et al., 2006). Eventually the key geochemical markers used to characterise these oils are also affected, complicating their identification.

Studies of liquid oils exposed to the marine environment demonstrate rapid degradation occurs within hours to days (Head et al., 2006). However, bitumens are more resistant to such degradation, and are reported to survive in the marine environment for over a year (Blumer et al., 1973; Butler et al., 1976; Lee, 1980; Warnock et al., 2015). This recalcitrance to various weathering processes is presumably related to both their semi-solid to solid nature and their resulting lower surface area, in contrast to liquid oil which disperses into a thin film on the sea surface and is highly reactive. The level of degradation across the suite of oils collected in this study varies significantly. However, two of the oil types collected in this study may still be identified even when extensively weathered. Asphaltites may be reliably identified visually on the basis of their diagnostic conchoidal fracture. Additionally, type I waxy bitumens remain identifiable due to the unusual recalcitrance of botryococcane to weathering. By comparing increasingly degraded examples of both these oils, a series of reproducible alteration trends may be observed.

5.1. Assessing weathering in whole-oil GC-MS

Representative whole-oil TICs of several types of highly degraded coastal bitumen are provided in Figure 6. All but the most weathered strandings will preserve *n*-alkanes in the $<C_{39}$ range, permitting a straightforward assessment based on their extent of preservation. Branched alkanes such as norpristane, pristane and phytane may be slightly more resistant than the $<C_{19}$ *n*-alkanes (Fig. 6A), but in many instances these compounds are also lost along with the adjacent *n*-alkanes. The aforementioned recalcitrance of botryococcane permits the identification of type I waxy bitumens after the complete removal of $<C_{37}$ *n*-alkanes (Fig. 6B). This may be similarly

reflected in the type II waxy bitumens, although there are only 13 specimens of this oil within the sample suite, and only a few highly weathered examples in comparison to the type I oils. Coastal bitumens which preserved only high-molecular-weight *n*-alkanes were classified as 'degraded high wax bitumen' (Fig. 6C). These likely represent heavily weathered type II or IV waxy bitumens, as evidenced by their abundant C_{35+} *n*-alkanes. Analysis of source-specific biomarkers may permit re-classification of these samples. However, alteration of their source-specific biomarkers may also have occurred at this level of weathering (discussed in Section 5.2).

In some instances, oil strandings may simply be too weathered to classify on the basis of their whole-oil TIC, due to the near- or complete removal of *n*-alkanes and other compounds. The TICs of such oils typically feature a large unresolved complex mixture (UCM), with peaks corresponding to biomarkers such as hopanes due to the complete removal of the *n*-alkane fraction. (Fig. 6D). Such oils lacking diagnostic features or exhibiting near-zero responses in whole-oil GC-MS were classified as 'unknown/other'. The biomarker assemblages of these samples can be assessed on a case-by-case basis to determine if they resemble those of any of the presently identified families. However, in most instances these compounds have also undergone some level of alteration.

5.2. Assessing weathering of source-specific biomarkers in SIM GC-MS

Failure to recognise the compositional changes which result from weathering may subsequently lead to the misinterpretation of the nature of the parent petroleum system, thereby potentially defining weathered oils as "new" oil families. The most prominent alteration of source-specific biomarkers observed between fresh and weathered coastal bitumens is the preferential loss of lighter compounds. For example, comparison of the freshest asphaltite specimen with a highly weathered example demonstrates the trend of reduced responses or total removal of compounds of lower mass/retention time (Fig. 7). This same trend is also observed when comparing fresh and highly weathered type I waxy bitumens (Fig. S1). However, the magnitude of alteration to the biomarkers is not always highly consistent with the extent of n-alkane removal observed in whole-oil GC-MS, with some examples entirely lacking in $<C_{37}$ *n*-alkanes preserving less altered sterane distributions than samples which still contain a significant *n*-alkane fraction. Therefore, identification of weathered equivalents of different oils is often best achieved by using their *m/z* 191 chromatograms, which appear less susceptible to alteration. Comparison of

the sterane and diasterane distributions to those in the least weathered example of a given oil type may be used to determine, on a case-by-case basis, the differences that may reasonably be attributed to weathering, as opposed to primary compositional variation.

Alteration of the steranes and diasteranes is particularly evident in highly weathered specimens, where those eluting prior to the C_{29} steranes in the *m/z* 217 (or 218 and 259) chromatograms are heavily attenuated (Fig. 7A–B). In most instances, this alteration is observed prior to visible changes in the distribution of terpanes and hopanes in the *m/z* 191 chromatogram. This may in part be due to the low primary abundance of steranes in the majority of oils identified here. However, it could also be the result of preferential consumption by the local microbial populations. Where alteration due to weathering is observed in the *m/z* 191 chromatogram, it typically involves a decrease in the response of the tricyclic and tetracyclic terpanes relative to hopanes, and preferential loss of the C_{30} αβ hopane relative to the C_{29} αβ hopane and $C_{31–35}$ homohopanes (Fig. 7C–D).

These alteration trends differ from many examples of traditional petroleum biodegradation. In particular, the tricyclic terpanes are commonly considered highly resistant to biodegradation and will persist following biodegradation of the hopanes (e.g. Reed, 1977; Seifert and Moldowan, 1979). Yet, the opposite is observed in the oils collected in this study. Similarly, steranes are generally considered to be more susceptible to biodegradation than diasteranes (Seifert and Moldowan, 1979; Peters et al., 2005), yet the C_{27} βα diasteranes (peaks a and b in Fig. 7A–B) are among the first biomarkers within the *m/z* 217 chromatogram to be altered in weathered coastal bitumens. While such compositional changes would traditionally be attributed to primary variation in source rock composition, in this case they co-occur exclusively with increased weathering. Furthermore, these same alteration patterns may be observed by comparing the interior and highly weathered exterior of the same sample, although the extent of variation within a single sample is subtle compared to the total range of weathering states summarised in Figure 7. Therefore, care should be taken to avoid interpreting these changes as primary variation within the source rock, when they are instead an atypical weathering style at odds with the existing literature on petroleum biodegradation. The difference is presumably due to the differing balance of biodegradation, water washing, photo-oxidation and evaporation for semi-solid bitumens in the marine environment, as compared to liquid oil degraded within the reservoir or during an oil spill.

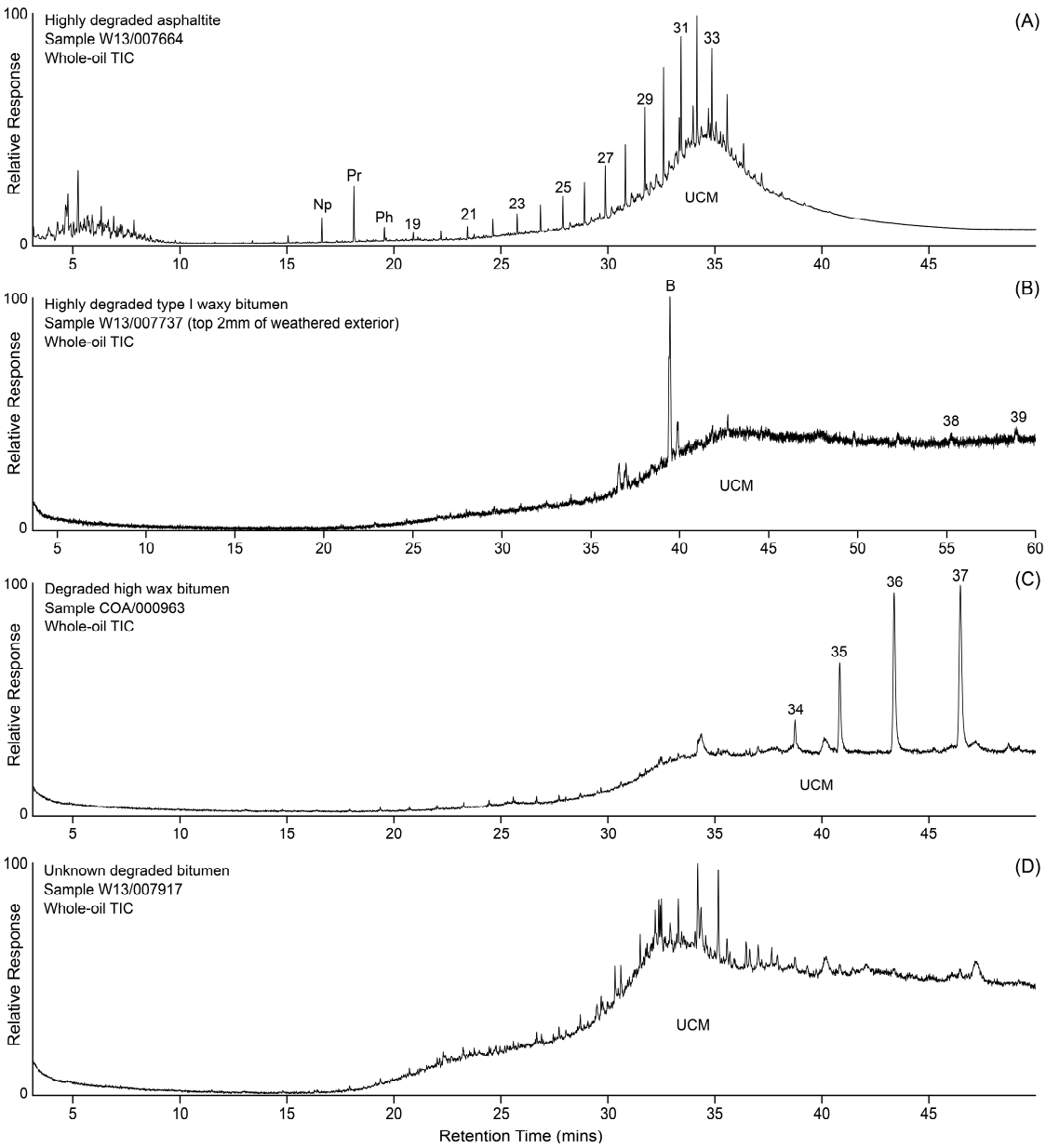


Figure 6: Examples of highly weathered coastal bitumen assessed using whole-oil GC-MS. (A) Highly degraded asphaltite, identified as asphaltite only due to its high asphaltene content and diagnostic conchoidal fracture; (B) Type I waxy bitumen which remains identifiable due to the extremely recalcitrant nature of botryococcane; (C) A highly degraded bitumen which now preserves only C_{34+} *n*-alkanes. This specimen may represent a weathered type II or IV waxy bitumen; (D) Bitumen sample too heavily degraded to reliably classify. Numbered peaks correspond to *n*-alkane chain length, Np = norpristane, Pr = pristane, Ph = phytane, UCM = unresolved complex mixture, B = botryococcane.

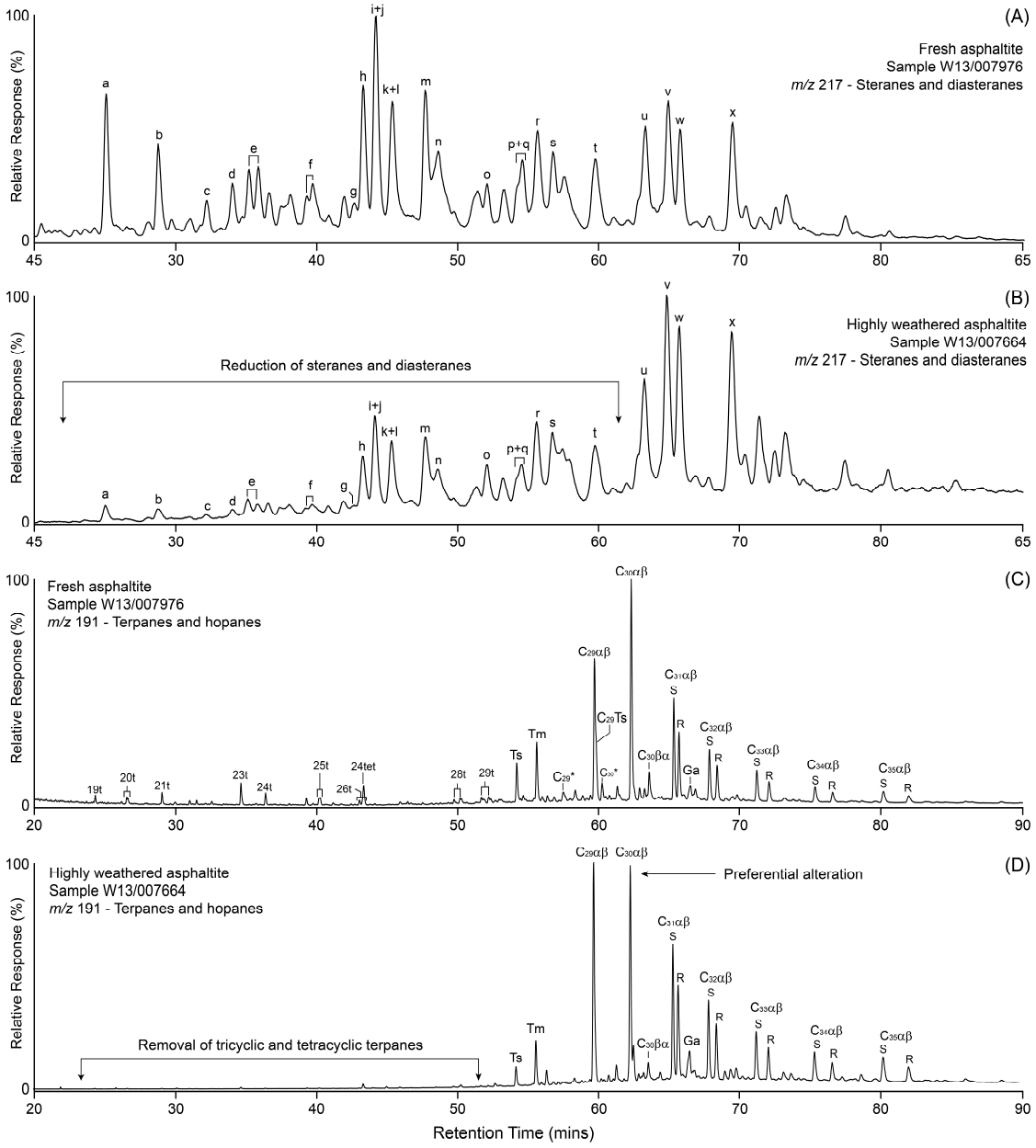


Figure 7: Comparison of source-specific biomarker distributions between fresh and highly weathered asphaltite specimens (W13/007976 vs. W13/007664). (A) Unaltered sterane and diasterane distribution in a fresh asphaltite. (B) Altered sterane and diasterane distribution in a highly weathered asphaltite. (C) Unaltered terpane and hopane distribution in a fresh asphaltite. (D) Altered terpane and hopane distribution in a highly weathered asphaltite.

6. CLASSIFICATION USING SOURCE-SPECIFIC GEOCHEMISTRY AND ASSESSING POTENTIAL PARENT PETROLEUM SYSTEMS

Representative whole-oil TIC and saturated fraction SIM GC-MS chromatograms (*m/z* 191, 217, 218, 259) for each of the oil families identified in this study are provided in the supplementary information (Figs. S2-S18). It was generally observed that the distribution of

terpanes and hopanes in the *m/z* 191 chromatograms for each family were the most useful in distinguishing the different oil families. Although the steranes and diasteranes are also informative and may aid in the assessment, alteration associated with weathering requires comparison with the least weathered example on a case-by-case basis. Furthermore, as biomarker assemblages were assessed primarily by SIM GC-MS, steranes were more vulnerable to variation introduced by co-eluting compounds, particularly the bicadinanes in certain waxy oils. Issues with co-eluting compounds may be resolved in future assessments by utilising multiple reaction monitoring (MRM) or gas chromatography-tandem mass spectrometry (GC-MS-MS) to separate the various co-eluting steranes and the bicadinanes for more reliable integration.

Due to the large size of the sample suite, assessment of the source-specific biomarker assemblages of all collected oil strandings was not practical. It is therefore important to consider that the oils documented here may not encompass all of the different oils which may strand on the South Australian coastline. Analysis of the saturated hydrocarbon fraction of 127 individual specimens was conducted. Of these, oils classified as asphaltite, asphaltic tar, type I and II waxy bitumen and Sandy River tar contained reproducible biomarker assemblages, indicating that these oils each class represent a single genetic family. However, the type III and IV waxy bitumens exhibited a wide range of different combinations of source-specific biomarkers, indicating that their prior whole-oil classifications encompass multiple oil families. These are referred to as types IIIA–F and IVA–F. Identification of multiple oils within the type III and IV whole-oil classifications is not entirely unexpected, as the key characteristics used to distinguish them (viz. lack of the rare biomarker botryococcane and high vs. low wax content) are not highly source-specific.

A summary of selected biomarker ratios from the least altered example of each identified oil type is provided in Table 2. Data from all analysed samples, including interior/exterior comparisons and examples significantly altered by weathering, are included in the supplementary information for reference. Many of the oils identified in this study have not previously been reported on the South Australian coastline. Where geochemical data from prior studies of other types of stranded bitumen are available, they are also briefly discussed here. The key source-specific biomarkers and thermal maturity/hydrocarbon generation parameters discussed below are summarised in Tables 3 and 4, respectively.

Table 2: Selected source-specific biomarker parameters from the least altered sample of each identified oil type. See supplementary information for data from all samples. Note that two examples of the type IVA waxy bitumen are provided as the least weathered example (W13/007589) exhibited low biomarker responses atypical of the other oils which fall under this classification.

Oil classification	Pr/Ph	C19t/ C23t	C22t/ C21t	C22t/ C24t	C24t/ C23t	C26t/ C25t	C24Tet/ C23t	C23t/ C30 αβ	C24Tet/ C30αβ	C28BNH/ C30 αβ	Ts/ (Ts+Tm)	C29 αβ/ C30 αβ	C30*/ C30 αβ	Ole/ C30 αβ	C30Ts/ C30 αβ	Gam/ C30 αβ	Gam/ C31 αβ (R)	C35 αβ/ C34 αβ	C35 Homohopane Index	C29Ts/ (C29Ts+ C29 αβ)
Asphaltic oils																				
Asphaltite (W13/007976)	1.2	0.25	0.39	0.30	0.53	0.76	0.91	0.08	0.07	0.06	0.41	0.62	0.09	n.d.	0.01	0.08	0.26	0.82	8	0.22
Asphaltic Tar (/001067)	0.7	0.16	0.11	0.09	0.51	0.77	0.36	0.30	0.11	0.00	0.22	0.78	0.04	n.d.	0.06	0.12	0.36	1.03	11	0.09
Waxy oils																				
Lacustrine/brackish shale																				
Type I (W13/007601)	w	0.37	0.38	0.32	0.85	1.82	0.38	0.08	0.03	0.03	0.71	0.60	0.18	0.11	0.01	0.04	0.25	0.44	4	0.31
Type IIIA (W13/007877)	1.5	0.17	0.17	0.14	0.87	1.99	0.32	0.07	0.02	0.03	0.65	0.75	0.07	0.07	0.00	0.07	0.40	0.45	4	0.20
Type IIIB (W13/007895)	1.5	0.70	0.20	0.26	0.72	1.69	0.65	0.11	0.07	0.06	0.64	0.53	0.32	0.22	0.00	0.12	0.74	0.46	4	0.35
Type IIIC (W13/007697)	1.7	0.04	0.06	0.04	0.88	1.81	0.09	0.26	0.02	0.09	0.60	0.67	0.09	0.06	0.00	0.06	0.45	0.38	5	0.21
Type IIIF (W13/007867)	w	0.09	0.04	0.03	0.89	0.92	0.05	0.76	0.04	0.12	0.64	0.74	0.16	0.11	0.00	0.07	0.48	0.34	4	0.21
Type IVC (W13/007857A)	w	0.23	0.06	0.07	0.77	1.96	0.30	0.16	0.05	0.07	0.67	0.50	0.20	0.29	0.00	0.08	0.46	0.47	5	0.34
Fluvio-deltaic shale (terrestrial/marine)																				
Type IIID (W13/007499)	w	1.20	0.90	0.64	0.88	0.96	3.14	0.02	0.06	0.06	0.41	0.50	0.07	0.75	0.00	0.06	0.19	0.45	3	0.12
Type IVB (W13/007909)	w	0.12	0.48	0.32	0.55	0.79	0.83	0.18	0.15	0.07	0.50	0.73	0.05	0.82	0.05	0.06	0.24	0.84	6	0.17
Sandy River tar (W13/007923)	1.2†	0.23	0.01	0.01	0.53	0.97	0.46	0.23	0.11	0.10	0.49	0.61	0.02	0.79	0.07	0.06	0.29	0.80	6	0.19
Marine shale																				
Type IIIE (W13/007503)	w	0.17	0.21	0.18	0.61	1.51	0.21	0.35	0.07	0.06	0.58	0.64	0.16	0.19	0.00	0.01	0.05	0.78	7	0.20
Type IVA (W13/007506)	w	0.14	0.30	0.20	0.56	1.05	0.55	0.17	0.09	0.00	0.53	0.63	0.09	0.01	0.01	0.05	0.16	0.83	8	0.21
Type IVA (W13/007589)	1.2†	0.23	0.14	0.08	0.60	1.25	0.12	0.61	0.07	0.00	0.56	0.65	0.25	0.04	0.03	0.08	0.29	0.63	9	0.25
Marine carbonate																				
Type IVD (W13/007564A)	w	0.10	0.64	0.34	0.36	0.82	1.01	0.18	0.18	0.00	0.24	1.26	0.01	0.04	0.18	0.11	0.31	0.97	9	0.07
Type IVE (W13/007712)	w	0.11	0.47	0.25	0.52	0.69	0.98	0.50	0.49	0.06	0.43	1.10	0.04	0.18	0.11	0.10	0.29	1.07	10	0.15
Mixed marine/lacustrine carbonate																				
Type II (W13/007615)	w	0.13	0.64	0.39	0.48	1.01	0.75	0.20	0.15	0.00	0.46	1.05	0.06	0.04	0.12	0.06	0.20	0.91	8	0.15

w = Compounds significantly altered or absent due to weathering.

† = Ratio potentially altered by weathering.

n.d. = Required compound not detected.

Table 2 (cont.): Selected source-specific biomarker parameters from the least altered sample of each identified oil type. See supplementary information for data from all samples. Note that two examples of the type IVA waxy bitumen are provided as the least weathered example (W13/007589) exhibited low biomarker responses atypical of the other oils which fall under this classification.

Oil classification	% C27 ααα 20R	% C28 ααα 20R	% C29 ααα 20R	C27 Dia/ (Dia+Reg) Steranes	(C21+C22)/ (C27+C28+C29) Steranes	C27 Dia/Reg Steranes	% C27 αββ 20(R+S)	% C28 αββ 20(R+S)	% C29 αββ 20 (R+S)	C29/C27 αββ Steranes	Tricyclic terpanes/ hopanes	Steranes/ Tricyclic terpanes	Steranes/ Hopanes
Asphaltic oils													
Asphaltite (W13/007976)	38	26	36	0.45	0.15	0.47	38	25	37	0.98	0.10	0.29	0.32
Asphaltic Tar (/001067)	34	29	37	0.43	0.23	0.40	35	25	40	1.14	0.27	0.24	0.31
Waxy oils													
Lacustrine/brackish shale													
Type I (W13/007601)	49	15	37	0.72	0.08	1.36	50	19	31	0.62	0.15	0.06	0.07
Type IIIA (W13/007877)	43	14	43	0.53	0.08	0.61	38	17	45	1.20	0.14	0.04	0.04
Type IIIB (W13/007895)	31	16	53	0.59	0.13	0.76	34	25	40	1.18	0.20	0.04	0.05
Type IIIC (W13/007697)	39	21	40	0.47	0.09	0.50	42	22	37	0.87	0.47	0.03	0.05
Type IIIF (W13/007867)	25	22	53	0.59	0.28	0.62	25	28	47	1.84	0.92	0.03	0.06
Type IVC (W13/007857A)	25	23	52	0.64	0.14	0.85	35	20	44	1.25	0.25	0.07	0.08
Fluvio-deltaic shale (terrestrial/marine)													
Type IIID (W13/007499)	26	16	58	0.30	0.04	0.30	25	19	56	2.25	0.07	0.09	0.10
Type IVB (W13/007909)	38	18	44	0.40	0.15	0.37	31	28	41	1.29	0.19	0.22	0.26
Sandy River tar (W13/007923)	38	27	35	0.34	0.15	0.30	37	27	37	1.01	0.31	0.18	0.23
Marine shale													
Type IIIE (W13/007503)	35	32	33	0.69	0.39	0.90	35	33	32	0.92	0.39	0.90	1.25
Type IVA (W13/007506)	35	31	34	0.58	0.28	0.66	37	29	34	0.91	0.19	0.63	0.75
Type IVA (W13/007589)	33	37	30	0.72	0.62	0.91	38	31	31	0.83	0.52	1.48	2.26
Marine carbonate													
Type IVD (W13/007564A)	42	24	34	0.24	0.20	0.18	33	25	42	1.28	0.13	0.21	0.24
Type IVE (W13/007712)	43	26	31	0.39	0.21	0.38	35	30	35	1.02	0.43	0.52	0.74
Mixed marine/lacustrine carbonate													
Type II (W13/007615)	40	24	36	0.38	0.13	0.33	35	25	39	1.13	0.18	0.20	0.23

= Compounds significantly altered or absent due to weathering.

† = Ratio potentially altered by weathering.

n.d. = Required compound not detected.

Table 3: Summary of discussed biomarker parameters.

Characterisation	Parameter	Significance
Organic matter inputs to source rock (terrestrial, freshwater / brackish, marine)	% Regular steranes (C_{27}, C_{28}, C_{29})	Low specificity for marine vs. terrestrial inputs. A high relative abundance of C_{29} steranes is associated with terrestrial organic matter, while a dominance of C_{27} steranes indicates marine organic matter (Huang and Meinschein, 1979; Czochanska et al., 1987).
	Oleanane	Indicative of angiosperm organic matter input (flowering higher plants); oleanane/C_{30} hopane >0.2 indicative of Late Cretaceous or younger (Ekweozor and Telnaes, 1990; Moldowan et al., 1994). Its abundance may be enhanced by interaction with seawater during early diagenesis (Murray et al., 1997).
	Bicadinanes	Indicative of organic matter input from tropical angiosperms of the family *Dipterocarpacae* (van Aarssen et al., 1990). May be present in low abundance in Mesozoic oils. Occur in high abundance in Oligocene and younger sediments and oils from SE Asia (Dutta et al., 2011).
	Taraxastane	Derived from diagenetic rearrangement of higher plant inputs (Perkins et al., 1995).
	Botryococcane	Derived from the freshwater/brackish green algae Botryococcus braunii (Moldowan and Seifert, 1980; McKirdy et al., 1986). Jurassic or younger (Peters et al., 2005).
	Tetracyclic polyprenoids	Occur in high abundance in oils derived from source rocks deposited in fresh to brackish environments (Holba et al., 2000, 2003).
	24-*n*-propylcholestanes	Specific for marine chrysophyte algae (Moldowan et al., 1990).
	Dinosterane	Derived from marine dinoflagellates (Summons et al., 1987). Abundant in Triassic or younger source rocks, though older examples occur (Peters et al., 2005).
	C_{26} / C_{25} tricyclic terpanes	Values >1 are typically observed in oils derived from lacustrine source rocks, although exceptions do occur (Zumberge, 1987).
	C_{24} tetracyclic / C_{23} tricyclic terpane	High C_{24} tetracyclic terpane abundance attributed to terrestrial organic matter input (Philp and Gilbert, 1986). Also observed in source rocks deposited in evaporitic/carbonate environments (Connan et al., 1986).
	Steranes/hopanes	Values ≥1 indicate significant marine planktonic or benthic algae inputs; low values suggest terrigenous or lacustrine organic matter (Tissot and Welte, 1984; Moldowan et al., 1985; Peters et al., 2005).
Source lithofacies (carbonate / evaporite vs. shale)	C_{29} / C_{30} αβ hopane ≥ 1	Values ≥1 indicative of carbonate/evaporative source rock (Peters et al., 2005).
	C_{24} tetracyclic terpane	As described above.
	2α-methylhopanes	Abundant in carbonate source rocks; some interference due to high thermal maturity (Summons et al., 1999; Peters et al., 2005).
	17α-diahopane (C_{30}*)	Abundant in sub-oxic to oxic, clay-rich source rocks with terrestrial organic matter input (Peters et al., 2005).
	Diasteranes/steranes	High ratios typical of clay-rich source rocks (e.g. shales); low ratios typical of carbonate source rocks. Some interference by pH, Eh and thermal maturation (Peters et al., 2005).
Source redox conditions (anoxic, sub-oxic, oxic)	Pristane / phytane	Low specificity for depositional redox conditions of source rock. High values (>3.0) indicate oxic conditions; low values (<0.8) suggest anoxia. Some interference due to thermal maturity and source input/environment (Peters et al., 2005).
	17α-diahopane (C_{30}*)	As described above.
	C_{35}/(∑$C_{31–35}$) homohopanes × 100	Also known as the C_{35} homohopane index. High values (>10) are associated with organic matter deposited under anoxic conditions (Peters et al., 2005).

Table 4: Summary of discussed maturity and hydrocarbon generation parameters.

Characterisation	Parameter	Significance
Thermal Maturity	Methylphenanthrene Index (MPI-1)	MPI-1 = 1.89(2-MP + 3-MP) / P + 1.26(1-MP + 9-MP) after Cassani et al. (1988). May be converted to a calculated vitrinite reflectance (R_c) using relationship defined by Radke and Welte (1983).
	Methylnaphthalene Index (MNR)	MNR = 2-MN/1-MN. May be converted to Rc using relationship defined by Radke et al. (1984).
	Dimethylnaphthalene Index (DNR-1)	DNR-1 = (2,6-DMN + 2,7-DMN)/1,5-DMN. May be converted to Rc using relationship defined by Radke et al. (1984).
	Tricyclic terpanes / 17α-hopanes	Tricyclic terpane abundance increases relative to hopanes with advancing thermal maturity (Farrimond et al., 1999). Potential interference due to migration, as tricyclics migrate faster than hopanes (Seifert and Moldowan, 1986) and source rock composition (Peters et al., 2005).
	Ts/(Ts+Tm)	Tm is less stable than Ts at high thermal maturities (Peters et al., 2005). However, interference associated with high carbonate content and anoxic conditions may occur (e.g. McKirdy et al., 1983).
Timing of petroleum generation	Re-Os geochronology	Decay of ^{187}Re to ^{187}Os may be used to determine the timing of hydrocarbon generation when applied to crude oil (Selby and Creaser, 2005).

6.1. Asphaltic oils

6.1.1. Asphaltite

Representative chromatograms from the least weathered asphaltite specimen collected in this study are provided in Figure S2. All associated biomarker data are provided in Table S4. As a large body of literature already exists for the asphaltites, the following discussion is effectively a brief review. For a comprehensive discussion of the geochemistry of the asphaltites, the reader is referred to Volkman et al. (1992); McKirdy et al. (1994); Edwards et al. (1998); Boreham et al. (2001); Hall et al. (2014); Corrick et al. (2019, 2020a) and Scarlett et al. (2019).

The asphaltites are considered to originate from a source rock containing exclusively marine organic matter. This interpretation is based on their C_{26}/C_{25} tricyclic terpane values <1; a lack of lacustrine or terrestrial biomarkers; a greater proportion of regular C_{27} ααα steranes (relative to the C_{28} and C_{29} homologues); and the presence of diagnostic marine markers 24-*n*-propylcholestane and dinosterane, as confirmed by MRM or GC-MS-MS analysis (see Edwards et al., 1998 for representative MRM data). The presence of dinosterane also constrains the age of the asphaltite's source to the Mesozoic (Triassic or younger). Their C_{29}/C_{30} αβ hopane values are <1, a feature consistent with their unusual lack of methylhopanes and their derivation from a shale lithofacies (Volkman et al., 1992; Edwards et al., 1998; Corrick et al., 2020a). Their

Pr/Ph ratios of 1.1–1.4, suggest that their source rock was deposited under sub-oxic conditions, consistent with C_{35} homohopane index values <10. However, their high sulphur content (ca. 4%) suggests euxinic conditions (Hall et al., 2014; Corrick et al., 2020a). The identification of isorenieratane and chlorobactane, molecular markers of the green sulphur bacteria and photic zone euxinia (Summons and Powell, 1987; Grice et al., 1996), along with elevated concentrations of redox-sensitive trace metals such as selenium and vanadium in a recently reanalysed archival suite of asphaltites (Scarlett et al., 2019), suggests that their source rock was deposited under conditions expected of an ocean anoxic event (OAE). Presently, interpretations of the source rock age range from the Cenomanian-Turonian OAE2 (Totterdell et al., 2008; Hall et al., 2014; Corrick et al., 2019), through the Albian OAE1d (Boult et al., 2005; Hall et al., 2014), to the Aptian OAE1a/Albian OAE1b (Scarlett et al., 2019).

Comparison of the asphaltite's geochemistry to that of approximately 4000 produced oils using the GeoMark^{TM} global petroleum database revealed no direct analogues, suggesting that their parent petroleum system has not yet been identified (Summons et al., 2001). Presently, these asphaltic oils are proposed to originate from the nearby Bight Basin (Boreham et al., 2001; Totterdell et al., 2008; Hall et al., 2014; Corrick et al., 2019). This interpretation is supported by the occurrence of extremely fresh strandings on the South Australian coastline, indicating a short exposure to the marine environment. Furthermore, the distribution of regular steranes resembles that in immature, organic-rich rocks dredged from incised canyons within the Bight Basin, notwithstanding other minor differences in geochemistry which have been attributed to natural variation within the same depositional system (Totterdell et al., 2008).

Assessment of both the methylphenanthrene index and compound-specific hydrogen isotopic composition (δ^2H) of *n*-alkanes and isoprenoids suggests that the asphaltites are products of the early oil window (Edwards et al., 1998; Hall et al., 2014; Scarlett et al., 2019; Corrick et al., 2020a). However, the methylnaphthalene (MNR) and dimethylnaphthalene (DNR-1) ratios differ slightly, yielding calculated vitrinite reflectance (R_c) values of 1.0% compared to 0.7–0.8% from MPI-1. This disparity between the aromatic maturity parameters may indicate that the asphaltites actually represent an oil from the early oil window which mixed with a more mature charge. However, more work is required to further assess this possibility (Corrick et al., 2020a).

Recent application of the Re-Os geochronometer to the asphaltites has also provided constraints on the timing of hydrocarbon generation in this undiscovered petroleum system. Using samples from the same suite of asphaltites analysed herein, Corrick et al. (2019) constrained the timing of oil generation for the asphaltites to 74 ± 26 Ma (with a subset of the data favouring an age of 68 ± 15 Ma), concluding that the asphaltites most likely originate from an OAE2 source rock in the Bight Basin. It is significant that petroleum systems modelling of a potential OAE2 source rock in the Ceduna sub-basin of the Bight Basin is consistent with petroleum generation from 74 Ma to the present (Totterdell et al., 2008). A subsequent study using archival asphaltite specimens collected in the early 1990s by Scarlett et al. (2019) yielded a significantly older generation age of 103 ± 22 Ma, introducing a new interpretation that the asphaltites may be associated with one of the earlier anoxic events, namely OAE1a (~125 Ma) or OAE1b (~112 Ma). Although these two studies offer differing conclusions regarding the age of the asphaltite's source rock, it is also important to acknowledge that the large uncertainties associated with the ages from each respective study share 19 Myr of potential overlap. Additionally, further investigation of the aforementioned possibility that the asphaltites may represent a mixture of two oil charges is required, as any mixing would undoubtably affect the resulting generation age obtained by Re-Os radiometric dating.

6.1.2. Asphaltic Tar

The geochemistry of the asphaltic tar strandings collected as part of this study are documented in detail by Corrick et al. (2020a). These strandings were only found at a single stranding location, Number 1 and 2 Rocks (site 29 in Fig. 1) during the 2016 survey, which was conducted immediately following a severe storm event that significantly altered the traditional distributions and abundance of crude oil strandings across the coastline (Corrick et al., 2020b). All collected examples of the asphaltic tars are similarly weathered and therefore there is no preferred sample for comparison. Representative chromatograms of this oil are provided in Figure S3 and the associated biomarker data for all analysed specimens are summarised in Table S5.

The asphaltic tars show numerous source-specific similarities to the asphaltites. The C_{29}/C_{30} αβ hopane ratios of the asphaltic tars are <1, consistent with an argillaceous source lithofacies (although see the discussion below regarding potential evidence for the source being a calcareous shale). Like the asphaltites, these oils lack diagnostic terrestrial or lacustrine markers but do contain 24-*n*-propylcholestane, confirming their marine source affinity (Corrick et al.,

2020a). Their Pr/Ph values of 0.7–0.8 and C_{35} homohopane index values of 10–12 are also consistent with anoxic conditions. Significantly, the two oil types have comparable *n*-alkane carbon isotopic profiles (Fig. 8) and similar sterane distributions, although the asphaltic tars do contain slightly lower abundances of C_{27} regular steranes.

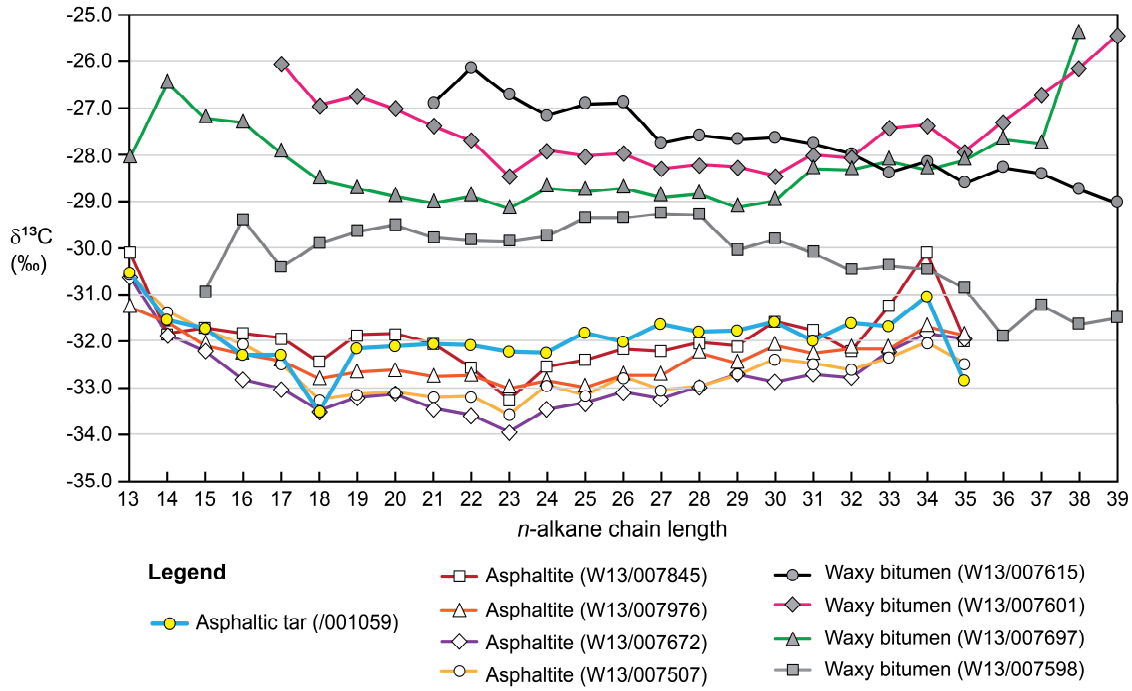


Figure 8: Comparison of *n*-alkane $\delta^{13}C$ profiles of various South Australian coastal bitumen specimens after Corrick et al. (2020a).

Whilst similar in certain aspects, reliable correlation of the asphaltites and asphaltic tars is complicated by their different thermal maturities and significant differences in their respective bulk sulphur isotopic compositions and Re-Os systematics. The MNR, DNR-1 and MPI-1 aromatic maturity parameters constrain the asphaltic tars to the late oil/early gas window, with a highly reproducible calculated vitrinite reflectance of 1.2%. As many source-specific parameters are also sensitive to thermal maturity, this complicates the assessment of what are otherwise source-related molecular signatures. For example, an elevated thermal maturity in the asphaltic tars is consistent with their higher abundance of tricyclic terpanes relative to hopanes. However, this could also represent a difference in the original source rock composition. One unusual feature of the asphaltic tars is that Tm>>Ts, despite the fact that Tm is less stable at high thermal maturities. This led to the tentative conclusion that their source rock may be slightly calcareous, containing sufficient carbonate to affect the Ts/(Ts+Tm) ratio

in the same manner as evident in other oils derived from anoxic carbonates (e.g. McKirdy et al., 1983), while still retaining a C_{29}/C_{30} αβ hopane ratio of <1.

The asphaltic tars are noticeably enriched in ^{34}S, with $\delta^{34}S$ values of up to +4.84 ‰, significantly exceeding the heaviest value obtained from the asphaltites (-5.79 ‰: see Corrick et al., 2020a for the values of all samples). As the sulphur isotopic composition of an oil usually approximates that of its source rock, this large variation between these two asphaltic oils casts doubt on their correlation. Furthermore, the asphaltic tars are highly enriched in both Re and Os, with $^{187}Re/^{188}Os$ and $^{187}Os/^{188}Os$ values which differ significantly from those of the asphaltites. However, the shift of $\delta^{34}S$ towards heavier values, and enrichment of Re and Os resulting in reset Re-Os systematics, are both observed characteristics of crude oils altered by thermochemical sulphate reduction (Lillis and Selby, 2013). Therefore, whilst these prominent deviations in geochemistry could indicate that these oils originate from separate source rocks, it is also possible they represent diagenetic alteration. Further research into these two conflicting interpretations, preferably aided by a more detailed geologic context for the petroleum systems of the Bight Basin, is required before their relationship to one another may be confidently determined.

Despite the aforementioned variations between the asphaltites and asphaltic tars, the strong similarities in many of their source-specific parameters do suggest that these oils either originate from lateral equivalents of the same source rock, or from two separate source rocks with highly comparable organic matter inputs. Therefore, the asphaltic tars are similarly proposed to originate from the nearby Bight Basin.

6.2. Waxy oils

The waxy oils display the largest compositional variability due to the numerous different oils which fall within the type III and IV whole-oil classifications. These oils originate from parent petroleum systems of lacustrine, deltaic and marine source affinity and are broadly consistent with what is known of the petroleum systems in SE Asia. However, whilst hundreds of exploration and production wells have been drilled across the Indonesian Archipelago, information regarding the composition of the produced oils is not always released with the level of detail required for robust basin-scale oil-oil or oil-source correlation. The relevant literature on Indonesian petroleum systems broadly summarises their key geological features, in some

instances including statistical treatment of large geochemical datasets, but the exact locations of specific oils may be de-identified for commercial reasons, or associated biomarker data not provided. Therefore, in assessing the origins of the various waxy oils collected from the South Australian coastline, we demonstrate that their geochemistry is consistent with the general character of the various petroleum systems in the Indonesian Archipelago. However, definitive geochemical correlations at a basin-specific scale are not possible due to both the high degree of geochemical similarity in produced oils from different basins across the region; and the further limitation of comparing our data solely to published geochemical datasets, which represent only a fraction of the total amount of proprietary geochemical information from producing wells in the region.

6.2.1. Waxy oils of lacustrine/brackish shale source affinity (types I, IIIA-C, IIIF, IVC)

Representative chromatograms of waxy bitumen types I, IIIA–C, IIIF and IVC are shown in Figures S4–S9. Biomarker data from all the analysed samples are collated in Table S6. Each of these oil types are considered to originate from a Cenozoic lacustrine or brackish shale. Evidence of its freshwater/brackish depositional environment is provided by the high relative abundance in these oils of C_{30} tetracyclic polyprenoids (labelled TPP in *m/z* 259 chromatograms in the supplementary information). However, we note that a robust assessment of these compounds requires assessing their abundance relative to the 27-norcholestanes, the reliable identification of which would require GC-MS-MS analysis to reliably identify due to their low generally low abundance (Holba et al., 2003). A freshwater/brackish depositional environment is further supported by C_{26}/C_{25} tricyclic terpane ratios generally >1 and the lowest sterane/hopane ratios of all the oils collected, with values <0.1 in all but the most altered specimens. A shale source lithofacies is indicated by their C_{29}/C_{30} αβ hopane ratios <1 and the presence of diahopanes (e.g. C_{30}*) in varying abundance, which also suggests that their source rocks were deposited under sub-oxic conditions. Aside from the type IIIC waxy bitumens, which have Pr/Ph ratios of 1.7–1.9, consistent with sub-oxic conditions, the other waxy oils of lacustrine affinity identified herein no longer preserve their original pristane and phytane signatures because of weathering. Fresh examples of the type I waxy bitumens collected in the 1990s have highly variable Pr/Ph ratios, with values of 0.2–2.6 indicating some instances of anoxia, but a predominance of sub-oxic conditions (Edwards et al., 2018: their families 1 and 2, discussed below). Each of the respective types of waxy bitumen also exhibit low oleanane/C_{30} αβ ratios, with values slightly >0.2 occurring only in the IIIB and IVC examples. All of them

contain bicadinanes in varying abundance, indicative of dipterocarp higher plant input to the lacustrine settings of their source rocks and constraining their age to the Cenozoic.

Although each of these oils have a lacustrine shale source affinity, each may be distinguished on the basis of several key features of their biomarker assemblages. The type I waxy bitumens are readily identified by the presence of abundant botryococcane, which is absent from the other lacustrine waxy oils. The type IIIA waxy bitumens contain notably low abundances of tricyclic terpanes (tricyclic terpanes/hopanes = 0.19–0.23: Table 2). The type IIIB oils likewise have low tricyclic/hopane values of 0.20–0.27, but also contain taraxastane and exhibit prominent responses for the C_{29} and C_{30} diahopanes and the T1 bicadinane in their *m/z* 191 chromatograms. The relative concentration of tricyclic terpanes is higher in the type IIIC and IIIF waxy bitumens (tricyclic terpanes/hopanes = 0.47–0.76 and 0.92, respectively) than in the other lacustrine oils. Additionally, the tricyclic homologues in these two oil types extend out to C_{33}, which is not observed in the other lacustrine oils. The single example of a type IIIF waxy bitumen also exhibits a predominance of C_{29} αββ steranes. However, given its extent of degradation, this may also be the result of weathering. Finally, the one sample classified as a type IVC waxy bitumen contained taraxastane, a slightly higher oleanane/C_{30} αβ hopane ratio of 0.29 and abundant bicadinanes.

The type I waxy bitumens are the most common type of crude oil found along the South Australian coastline (Corrick et al., 2020b). Highly recognisable due to their abundant botryococcane, these oils have been previously recovered from multiple locations along the Australian coastline. In a suite of specimens collected from ocean beaches in South Australia and western Victoria during the early 1990s, Edwards et al. (2018) classified oils of this type as their Family 1 and 2 bitumens, distinguished by the presence or absence of trace abundances of 24-*n*-propylcholestane and dinosterane. The presence of these marine algal markers may indicate lateral variation in the source rock lithofacies resulting from a marine incursion into the lacustrine environment, and/or post-depositional mixing during migration to or within the reservoir. Similar bitumens have also been reported on the coastlines of Western Australia (Alexander et al., 1994: their Group 1 oils) and the Northern Territory (McKirdy and Horvath, 1976: their Type 1; Summons et al., 1993: their Family 2). However, despite their consistent occurrence and high overall abundance, all specimens of the type I waxy bitumens analysed in this study are significantly more degraded than those collected in the 1960s and 1990s (Fig. 9). The lack of any well-preserved examples across our entire sample suite (a total of 301 type I

waxy bitumens), suggests that fresh oil is no longer being released from the parent petroleum system into the marine environment. This is also consistent with the fact that the overall abundance of waxy crude oil accumulating on the coastline of South Australia has decreased dramatically since the early 1990s, when fresh strandings still occurred (Corrick et al., 2020b). The other oils of lacustrine source affinity identified in this study have not been previously reported during any of the prior geochemical investigations of coastal bitumen strandings on the Australian coastline.

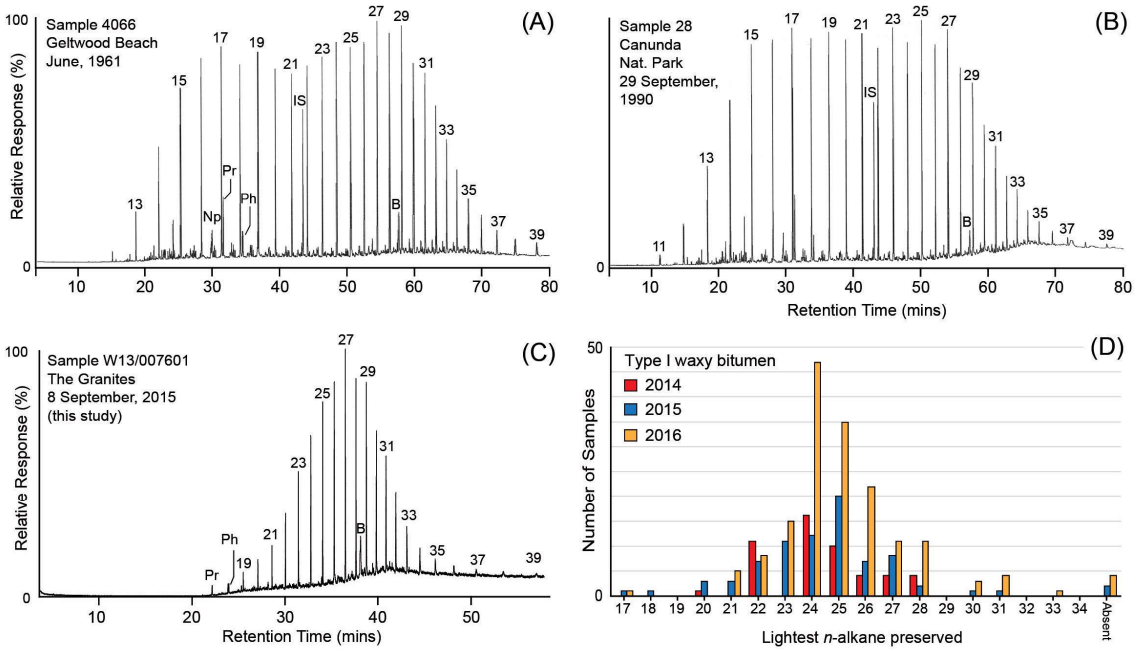


Figure 9: Comparison of historical and modern type I waxy bitumens. (A) Saturated hydrocarbon fraction TIC of waxy bitumen sample 4066 collected in 1961. (B) Saturated hydrocarbon fraction TIC of waxy bitumen sample 28 collected in 1990. (C) Whole-oil TIC of the freshest type I waxy bitumen, sample W13/007601, collected in 2015. (D) Range of weathering extent for all type I waxy bitumens collected between 2014 and 2016 (including samples donated from private collections). Chromatograms of archival samples in parts A and B modified from Padley (1995). Numbered peak responses correspond to *n*-alkane chain length, Np = norpristane, Pr = pristane, Ph = phytane, B = botryococcane, IS = 3-methylhenicosane internal standard (AC 22; 10µg ml^{-1}). The minor variation in relative elution position of botryococcane between archival specimens and those collected in 2015 is the result of differences in chromatography, not sample composition.

Lacustrine oils containing the biomarkers botryococcane, oleanane and bicadinanes are not typically associated with offshore Australian petroleum systems. However, such oils are recognised in the western half of the Indonesian Archipelago, with examples reported from the North Sumatra, Central Sumatra, South Sumatra, Sunda, NW Java, East Java and West Natuna basins (Robinson, 1987; Matchette-Downes et al., 1994; ten Haven and Schiefelbein, 1995;

Napitupulu et al., 1997; Schiefelbein and Cameron, 1997; Hwang et al., 2002). Of these, botryococcane is only reported in the Central Sumatra, South Sumatra, Sunda and NW Java basins (Moldowan and Seifert, 1980; ten Haven and Schiefelbein, 1995; Hwang et al., 2002). Currently, no exact correlations have been established between the type I waxy bitumens and any produced Indonesian oils containing botryococcane, as there are significant differences in their respective geochemistries (Edwards et al., 2018). This likely reflects the lack of uniformity in the lacustrine organic facies of the region, where lateral variations in source rock geochemistry are thought to result from subtle differences in lake chemistry (e.g. Hwang et al., 2002).

The *m/z* 191 chromatograms of a type IIIA waxy bitumen and a representative lacustrine oil from SE Asia do show strong similarities (Fig. 10). However, we do not anticipate any of the oils documented herein will perfectly correlate with the published geochemistry of produced oils obtained predominantly from onshore drilling activities. Rather, reliable correlations will most likely require comparison to seafloor seeps, because of the aforementioned lateral variability frequently observed in SE Asian lacustrine source rocks.

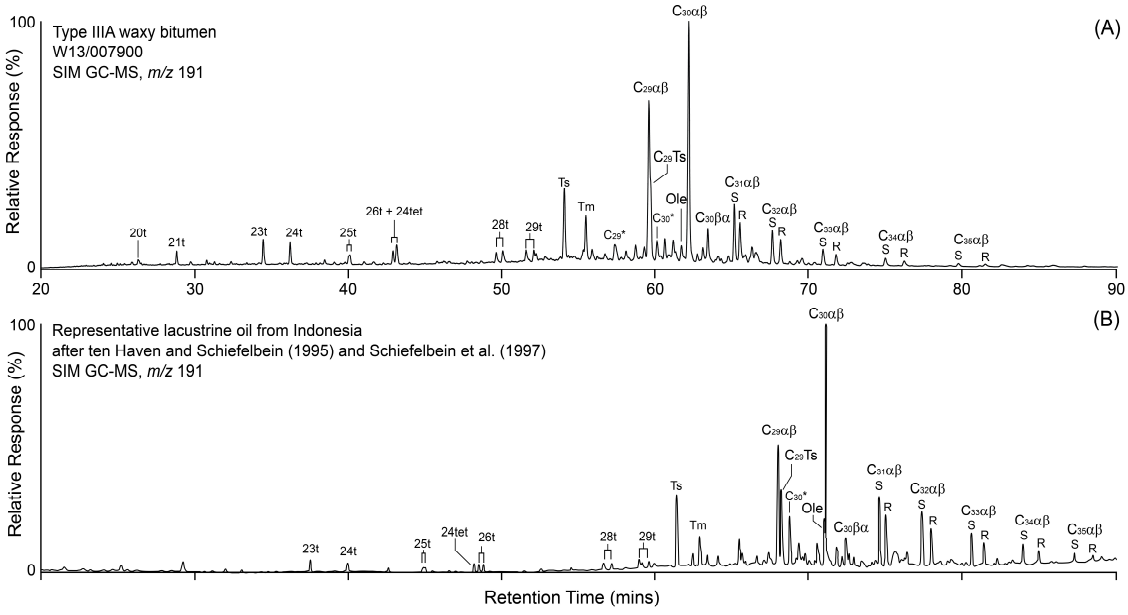


Figure 10: Comparison of *m/z* 191 chromatograms from a waxy bitumen and an Indonesian oil of lacustrine shale source affinity. (A) Waxy bitumen type IIIA sample W13/007900. (B) Representative Indonesian lacustrine oil (exact location not specified) modified after ten Haven and Schiefelbein (1995) and Schiefelbein et al. (1997). Note: differences in compound retention times between studies are the result of differing chromatography.

6.2.2. Waxy oils of fluvio-deltaic source affinity (types IIID, IVB, Sandy River tars)

Representative chromatograms of the least weathered type IIID and IVB waxy bitumens are shown in Figures S10 and S11, respectively. All documented examples of the Sandy River tar are similarly weathered and therefore no one example is preferable; a representative example is shown in Figure S12. Associated biomarker parameters from all analysed samples of these oil types are provided in Table S7.

Waxy oils of fluvio-deltaic source affinity are readily recognised by their high abundance of terrestrial markers, including oleanane/C_{30} αβ hopane ratios >0.7, taraxastane and abundant bicadinanes. The high abundances of oleanane in these oils suggests the original plant matter interacted with seawater during early diagenesis, supporting a marine origin for these oils (Murray et al., 1997). Additionally, each of these oils contain a series of unidentified compounds eluting between Tm and the C_{29} αβ hopane. These may correspond to a combination of bisnorlupanes, bisnoroleanane and bisnorhopane. However, given the close elution of these compounds (see Nytoft et al., 2002: their figure 4), comparison to an authentic analytical standard or oil known to contain these compounds is recommended for confident identification. Both the type IIID and IVB waxy bitumens exhibit C_{29}>C_{27}>C_{28} steranes, consistent with a high terrestrial organic matter input to their source rocks. However, given that even the least weathered examples of these oils are moderately degraded, alteration of the sterane distributions due to weathering may also be possible. The Sandy River tars show approximately equal C_{27} and C_{29} sterane abundances in many examples, but this parameter can be somewhat variable. Both pristane and phytane are either significantly depleted or removed entirely in the type IIID and IVB waxy bitumens. Both compounds are present in the Sandy River tars, where they represent the largest peaks in the whole-oil TIC and return Pr/Ph ratio values of 1.2, consistent with sub-oxic conditions. However, given the extent of degradation in these oils, their Pr/Ph ratios may be altered. Therefore, the most reliable indicator of source redox conditions in these oils is the C_{35} homohopane index, the values of which were uniformly low (3–6), indicating that their source rocks were likely deposited under sub-oxic to oxic conditions. Finally, all three oils have C_{29}/C_{30} αβ hopane ratios <1, consistent with a shale source lithofacies.

As each these oils have been assigned to different whole-oil classifications, they may be distinguished using the following features: low vs. high abundance of n-alkanes >C_{35} and the bimodal UCM of the Sandy River tars. Alternatively, if assessed solely on their biomarker assemblages, they may be readily distinguished by their abundance of tricyclic terpanes, with

tricyclic/hopane ratios ≤0 .1 for the type IIIB oils, 0.22 for the single example of type IVB waxy bitumen and 0.32–0.44 for the Sandy River tars.

Oils containing such high oleanane/C_{30} αβ hopane ratios have not previously been reported on the South Australian coastline. They may correspond to the Family 5 bitumens defined by Edwards et al. (2018), which were attributed to a coal-rich fluvial to deltaic source rock. Unfortunately, minimal GC-MS data are available for these particular bitumens and therefore an informed comparison is not currently possible. However, bitumens of similar character have previously been reported on the coastline of Western Australia by Alexander et al. (1994). Classified as their Group 2 (Deltaic A) bitumens, these oils were attributed to petroleum systems in SE Asia.

In Figure 11 the *m/z* 191 chromatograms of type IIID and IVB waxy bitumens are compared with representative fluvio-deltaic oils from SE Asia. The oils in question exhibit particular similarity with respect to their abundant terrestrial markers (e.g. oleanane, taraxastane) but differences become apparent when comparing their tricyclic terpane distributions. As was the case for the waxy oils of lacustrine source affinity, the presence of abundant Cenozoic terrestrial markers such as oleanane and bicadinanes strongly supports their linkage to SE Asia. Oils with a deltaic source affinity were considered by ten Haven and Schiefelbein (1995) to be restricted to western Indonesia, but still have the largest geographical extent of oils in the region. However, more recent studies have demonstrated that comparable oils are also found in basins further to the east, where predominantly Mesozoic basins also contain Cenozoic source rocks. For example, the Salawati, Seram and Tomori basins also host oils of similar composition (Peters et al., 1999: their Group 3 oils). Moreover, coring of the seafloor above the Salawati Basin demonstrates that seepage of this deltaic oil does occur (Misool seep, Fig. 11E; Noble et al., 2009). Hence, the distribution of deltaic oils throughout SE Asia is now known to be far greater than originally envisaged. Given the strong similarities of these stranded waxy oils to those of fluvio-deltaic source affinity in the Indonesian Archipelago, we consider them to share the same provenance. However, given the large number of basins hosting such oils, we do not propose any basin- or seep-specific correlations at this time.

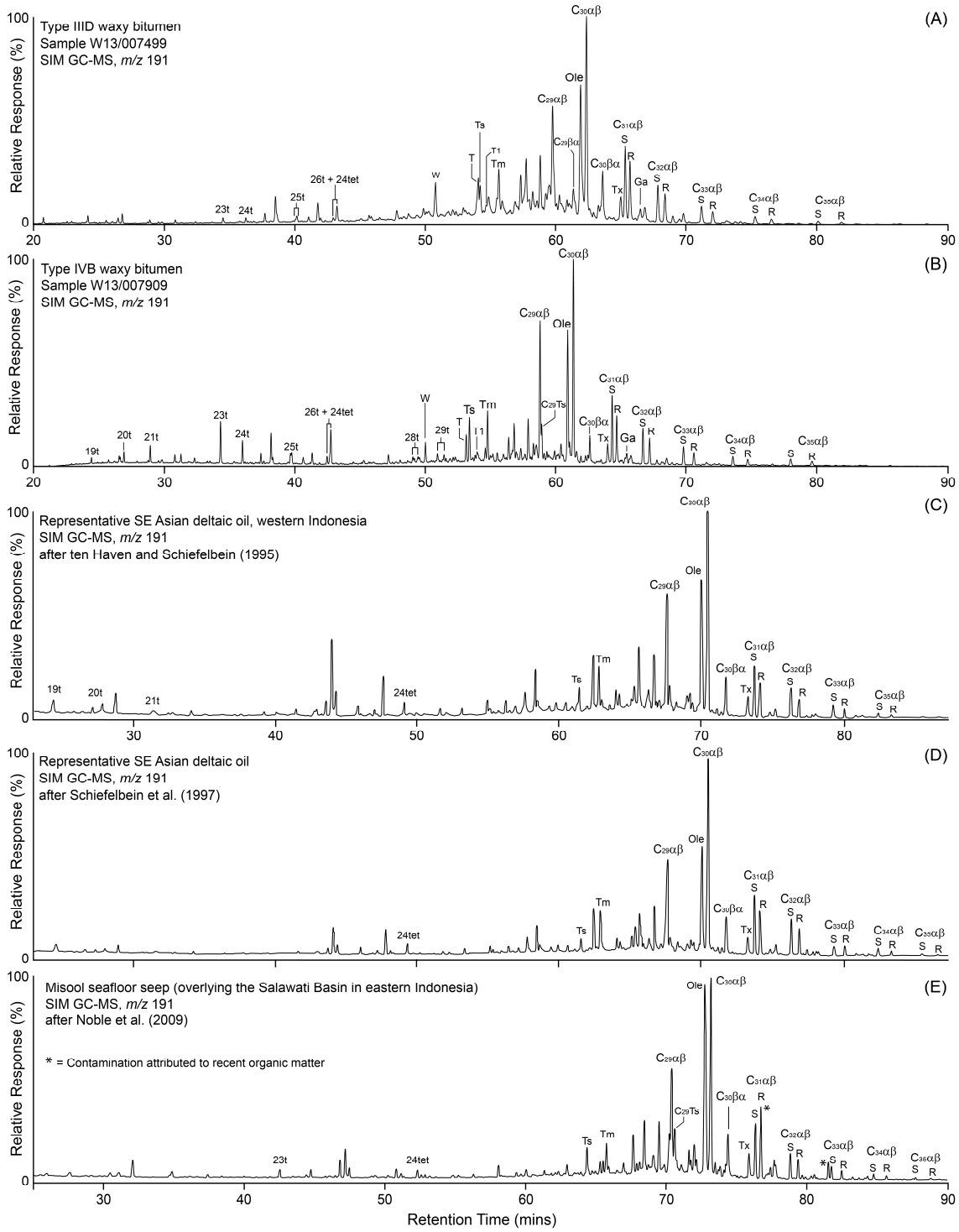


Figure 11: Comparison of *m/z* 191 chromatograms of waxy bitumen types IIID, IVE and Sandy River tars to those of deltaic- and marine/terrigenous-sourced oils from the Indonesian archipelago. (A) Type IIID waxy bitumen sample W13/007499. (B) Type IVB waxy bitumen sample W13/007909. (C) Representative Indonesian deltaic oil (basin not specified) after ten Haven and Schiefelbein (1995). (D) Representative Indonesian deltaic oil (basin not specified) after Schiefelbein et al. (1997). (E) Piston core extract from the Misool seafloor seep overlying the Salawati Basin in the eastern Indonesian Archipelago, modified after Noble et al. (2009). Note: differences in compound retention times between samples is the result of differing chromatography.

6.2.3. Waxy oils of marine shale source affinity (types IIIE and IVA)

Representative chromatograms of type IIIE and IVA waxy bitumens are provided in Figures S13–S15. Biomarker data on all the analysed examples are collated in Table S8. Note that two different samples are selected as examples of type IVA. The least weathered example returned low biomarker responses, which particularly affected its *m/z* 191 chromatogram. Hence, the biomarker ratios from the samples in question (W13/007589 and W13/007506) are included in both Table 2 and the chromatograms from both examples are provided in the supplementary information. These waxy bitumens are considered to originate from a shale lithofacies based on their C_{29}/C_{30} αβ hopane values <1, abundant diasteranes and the presence of rearranged hopanes (C_{30}*), which also suggest its deposition under sub-oxic redox conditions. Aside from the least weathered type IVA waxy bitumen (W13/007589), which preserves a Pr/Ph value of 1.2, consistent with the aforementioned redox conditions, all other examples of these oils lacked both pristane and phytane due to significant weathering. Although these oils generally contain C_{26}/C_{25} tricyclic terpane values ≥1, which could be interpreted as indicative of a lacustrine depositional environment, in this case the elevated values are due to co-elution of the C_{26} tricyclic and C_{24} tetracyclic terpanes and is therefore not appropriate for interpretation. Given that these oils lack freshwater markers (e.g. abundant tetracyclic polyprenoids), contain a predominance of C_{27} steranes, and with few exceptions have sterane/hopane values >1, they are considered marine in origin.

The single identified type IIIE waxy bitumen (W13/007503) may be distinguished from the type IVA waxy bitumens by its lower abundance of high-molecular-weight *n*-alkanes >C_{37} and a higher oleanane/C_{30} αβ hopane ratio of 0.19 (cf. ≤0.03 in type IVA). Otherwise, the type IIIE and IVA waxy bitumens contain near-identical biomarker distributions, suggesting that they are likely to be genetically related.

Aside from the asphaltites, previous studies of South Australian coastal bitumens have not reported any oils with a marine shale source. However, the type IVA waxy bitumen, which contains only trace amounts of oleanane may be equivalent to the Group 8 (marine clastic) bitumens from the coastline of Western Australia analysed by Alexander et al. (1994).

Marine petroleum systems in SE Asia are mostly restricted to depocentres in the eastern half of the Indonesian Archipelago, such as the Bintuni, Seram, Timor and Banggai basins, which contain both marine shale and carbonate source rocks (Robinson, 1987; ten Haven and

Schiefelbein, 1995; Schiefelbein et al., 1997). Exceptions are the East Natuna and North Sumatra basins located in the western part of Indonesia, which also host marine oils (ten Haven and Schiefelbein, 1995). Marine oils with oleanane/C_{30} αβ hopane ratios ≥0.25, indicating their derivation from Cenozoic source rocks, are reported from the North Sumatra, Banggai and Bintuni basins (ten Haven and Schiefelbein, 1995). As the type IIIE and IVA waxy bitumens do not contain comparably abundant oleanane, with the highest oleanane/C_{30} αβ hopane value being 0.19 in the single type IIIE specimen, these oils are unlikely to have originated from these basins. However, the Bintuni Basin is also noted to contain oils derived from both Mesozoic and Cenozoic source rocks and therefore should not be discounted entirely (ten Haven and Schiefelbein, 1995). The *m/z* 191 chromatograms of a type IVA waxy bitumen and an oil derived from marine shale in the eastern half of the Indonesian Archipelago (location/basin not specified) are compared in Figure 12A–B. These oils appear similar, although minor differences include elevated responses for the 17α-diahopane (C_{30}*) and tricyclic terpanes in the produced oil. Despite its poor-quality, the *m/z* 191 chromatogram of the type IIIE waxy bitumen reveals an oleanane abundance and distribution of hopanes and tricyclic terpanes that are similar to those of a marine oil recovered from the Kumuwa Seep overlying the Aru Trough (Fig. 12C–D). However, unlike the seep oil, Ts ≈ Tm and the bicadinane T is identifiable in the *m/z* 191 chromatogram of the type IIIE waxy bitumen.

The presence of low amounts of oleanane and potential bicadinanes in the type IIIE waxy bitumen, and its overall similarity to the IVA waxy bitumens, suggests that both of these oils are likely to share a common origin somewhere in the eastern half of the Indonesian Archipelago. However, further research is required to characterise these oils in greater detail and better constrain their most likely basin(s) of origin.

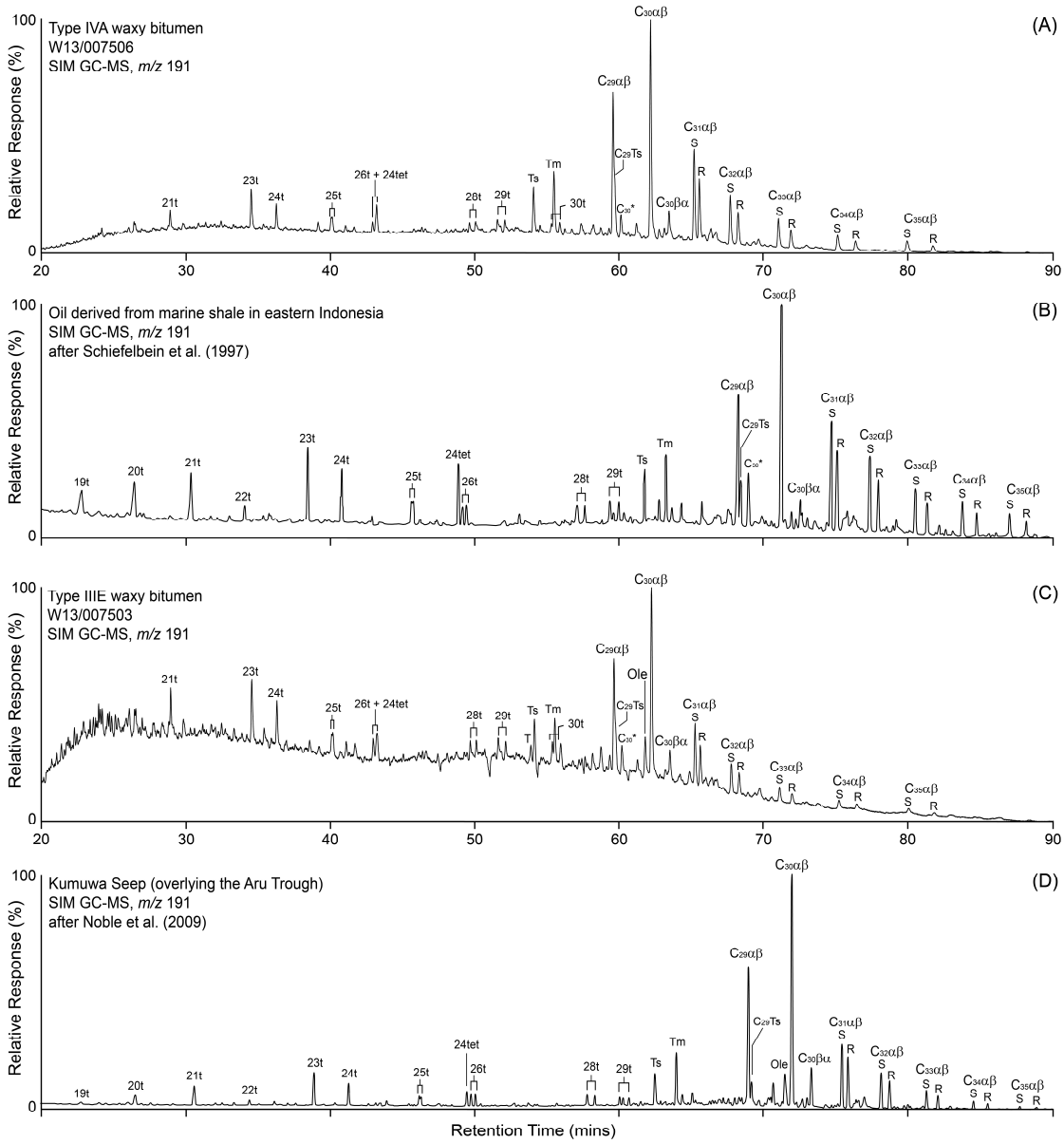


Figure 12: Comparison of the *m/z* 191 chromatograms of waxy bitumens of marine shale affinity and two marine oils from eastern Indonesia. (A) Type IVA waxy bitumen sample W13/007506. (B) Representative example of an eastern Indonesian oil derived from a marine shale, modified after Schiefelbein et al. (1997). (C) Type IIIE waxy bitumen sample W13/007503, which contains minor oleanane. (D) Example of oil emitted from the Kumuwa Seep consistent a marine shale source which also contains minor oleanane, modified after Noble et al. (2009). Note: differences in compound retention times between studies are the result of differing chromatography.

6.2.4. Waxy oils of marine carbonate source affinity (types IVD, IVE)

Representative chromatograms of waxy bitumen types IVD and IVE are shown in Figures S16–S17. Biomarker data on all the analysed examples are collated in Table S9. These oils are considered to originate from a carbonate source lithofacies on the basis of their C_{29}/C_{30} αβ hopane ratio values of <1. A marine origin is inferred from their C_{26}/C_{25} tricyclic terpane values of <1 and low abundance of tetracyclic polyprenoids.

These two oil types may be distinguished from one another on the basis of their oleanane contents. The type IVD waxy bitumens contain little or no oleanane, with oleanane/C30 αβ hopane ratios of 0.00–0.08. By comparison, the type IVE waxy bitumens contain slightly greater abundances, with oleanane/C_{30} αβ hopane ratios of 0.18. No identified examples of these oils preserved pristane or phytane. C_{35} homohopane index values of 7–9 in type IVD, and a value of 10 in type IVE, are consistent with sub-oxic conditions approaching anoxia.

The type IVD waxy bitumens likely correspond to the Family 4 bitumens defined by Edwards et al. (2018), which were highly variable in composition and thought to comprise multiple oils originating from several different source rocks of varying marine lithofacies. A waxy bitumen of similar composition has also been reported from the coastline of Western Australia (Alexander et al., 1994 : their Group 4). The type IVE waxy bitumens do not appear to have been previously reported on the South Australian coastline, although they may be comparable to the Group 7 waxy bitumens from Western Australia identified by Alexander et al. (1994). Shared biomarker characteristics of the type IVE and Group 7 waxy bitumens include comparable oleanane/C_{30} αβ hopane and C_{23} tricyclic/C_{24} tetracyclic terpane values. However, most examples of their Group 7 waxy bitumens have C_{29}-dominant sterane distributions and generally lower abundances of the C_{28} sterane, neither feature being consistent with the sterane signatures of the type IVE waxy bitumens.

The type IVD waxy bitumens display strong source-dependent similarities with Mesozoic produced and seep oils from the Seram Basin (Fig. 13A–C), including abundant 29,30-norhopanes, a general lack of oleanane and $C_{29}>C_{27}>C_{28}$ steranes (cf. ten Haven and Schiefelbein, 1995; Peters et al., 1999). The type IVD waxy bitumens do have higher tricyclic terpane/hopane and Ts/Tm ratios than the produced oil shown in Figure 13B. However, as both of these parameters are affected by thermal maturity, and it is likely that the type IVD waxy

bitumens represent a slightly more mature equivalent of the example from the Seram Basin. Oils from the Timor, East Natuna and Banggai basins have similar biomarker assemblages (ten Haven and Schiefelbein, 1995; Peters et al., 1999) and therefore these depocentres also represent potential regions for correlation. The presence of trace oleanane within certain examples of the type IVD waxy bitumen may be attributed to minor migration-contamination, The *m/z* 191 chromatogram of oil from the seafloor seep in the Seram Basin (Fig. 13C) contains a low response peak at the approximate elution position of oleanane, although it was not identified as such by Noble et al. (2009) in their original study.

The type IVE waxy bitumens, which also contain low amounts of oleanane, have similar hopane distributions to that of a representative example of oil derived from a carbonate source rock in the Indonesian Archipelago (Fig. 13D–E). Unfortunately, the exact location of this particular oil was not specified. Like the type IVD comparison above, the type IVE waxy bitumen also demonstrates higher abundances of terpanes relative to hopanes and lower Tm responses consistent with differences in thermal maturity.

Given the overall similarities between the type IVD waxy bitumens and the two oils from the Seram Basin, we suggest that they are related. That said, oils of comparable biomarker geochemistry are known elsewhere in the region and therefore their correlation remains uncertain. The presence of broadly similar oils derived from a carbonate source and likewise containing a low abundance of oleanane supports the notion that the type IVE and type IVD waxy bitumens also originate from the eastern Indonesian Archipelago, although their exact points of origin are less clear.

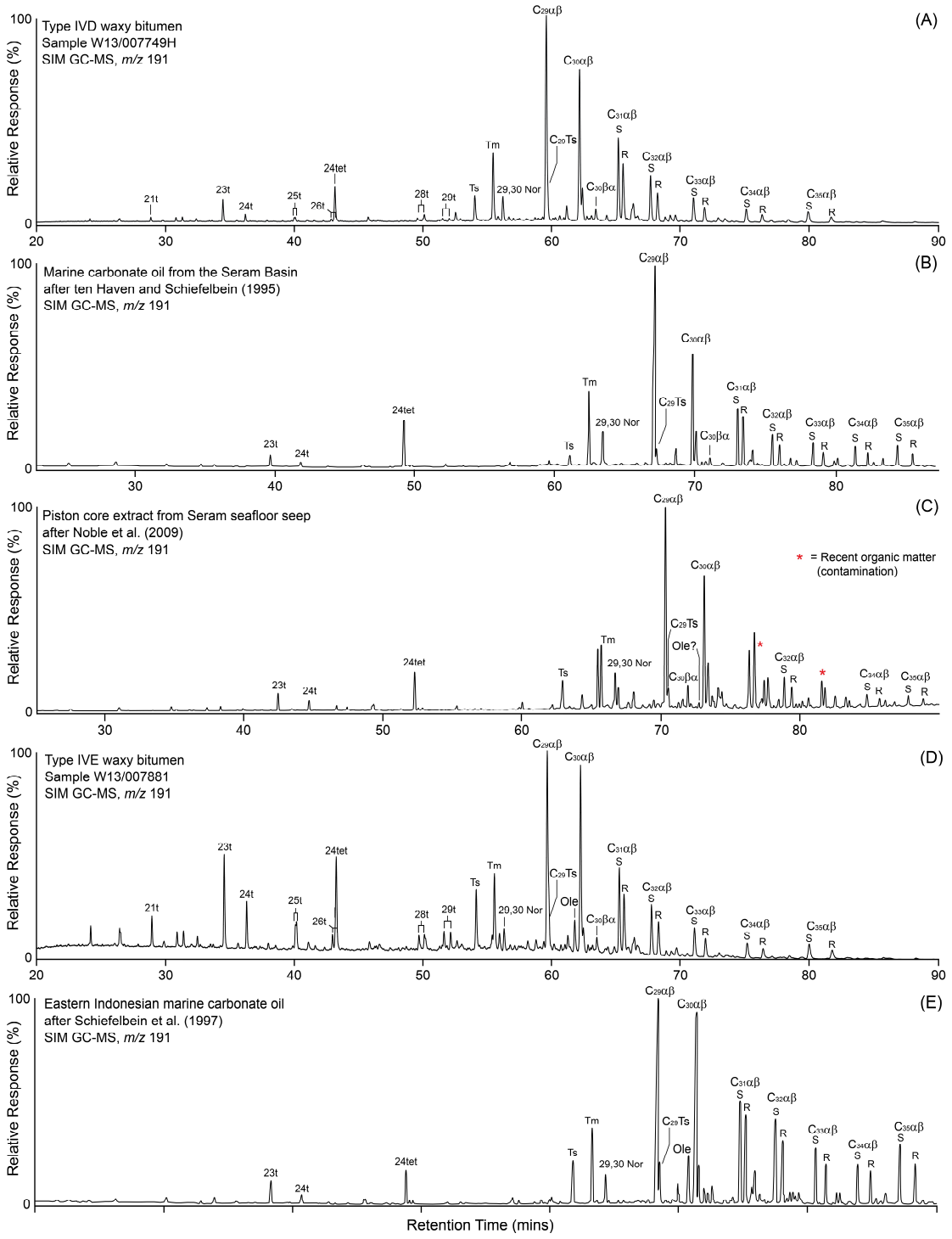


Figure 13: Comparison of the hopane and terpane distributions (*m/z* 191) of type IVD and IVE waxy bitumens with those of two eastern Indonesian marine carbonate oils. (A) Type IVD waxy bitumen sample W13/007749H. (B) Representative marine carbonate oil collected from the Seram Basin, modified after ten Haven and Schiefelbein (1995). (C) Petroleum collected from a piston core extract from the Seram seafloor seep, modified after Noble et al. (2009). (D) Type IVE waxy bitumen sample W13/007881. (E) Eastern Indonesian marine carbonate oil (basin/location not specified) with minor oleanane similar to the type IVE waxy bitumen; modified after Schiefelbein et al. (1997). Note: variations in compound retention times in each chromatogram are due to differences in chromatography between each of the studies.

6.2.5. Waxy oil of mixed lacustrine/marine carbonate source affinity (type II)

Representative chromatograms from the least weathered type II waxy bitumen are provided in Fig. S18 and all the associated biomarker data are included in Table S10. These bitumens are readily identifiable on the basis of the low abundance of botryococcane in their whole-oil TIC chromatograms and their C_{29}/C_{30} αβ hopane values >1, the latter consistent with a carbonate source. However, unlike the previously discussed oils with carbonate sources, the type II waxy bitumens appear to be of a mixed lacustrine/marine origin.

The presence of botryococcane, albeit in low abundance, indicates the source rock of the type II waxy bitumens contained lacustrine organic matter. The presence of this rare marker also makes these bitumens recognisable in previous studies. Specifically, the type II waxy bitumens correspond to the Family 3 bitumens defined by Edwards et al. (2018). Their comparison to these equivalent bitumens collected from the South Australian and Victorian coastlines during the early 1990s demonstrates that, like the type I waxy bitumens, modern type II waxy bitumen strandings are significantly weathered (Fig. 14). This lack of fresh strandings, in addition to the overall low abundance of these oils, comprising only 13 specimens across the entire sample suite, suggests that the seep responsible for these particular oils may no longer be active. MRM GC-MS analysis by Edwards et al. (2018) confirmed that these waxy bitumens contain the marine biomarkers 24-*n*-propylcholestane and dinosterane, in addition to trace bicadinanes. As the type II waxy bitumens contain both lacustrine and marine biomarkers, they either originated from a source rock deposited in a Cenozoic lacustrine environment which was subject to marine incursion, or they represent a mixture of oils derived from both lacustrine and marine carbonate sources. Previous assessment by Edwards et al. (2018) favoured the mixed oil interpretation on the basis of a naphthene 'hump' in their saturated hydrocarbon chromatograms, a feature which they attributed to mixing with a biodegraded oil.

Oils containing a low abundance of botryococcane are reported in the Central Sumatra Basin (Hwang et al., 2002, their Group 3 oils). These oils have botryococcane/*n*-C_{29} values of 0.05–0.09, comparable to the values obtained by Edwards et al. (2018) from fresh samples of their Family 3 bitumens (0.04–0.14). Additionally, both the Group 3 oils ands and the waxy bitumens contain C_{27}>C_{29}>C_{28} sterane signatures. However, despite these similarities, other source-specific parameters do not support their correlation. No oils containing botryococcane in the Central Sumatra Basin have been linked to a carbonate source. Furthermore, the Pr/Ph ratios of the Group III oils analysed by Hwang et al. (2002) are in the range 2.6–2.9, values significantly

higher than those obtained from fresh type II waxy bitumens (viz. 0.5–1.1: Edwards et al., 2018).

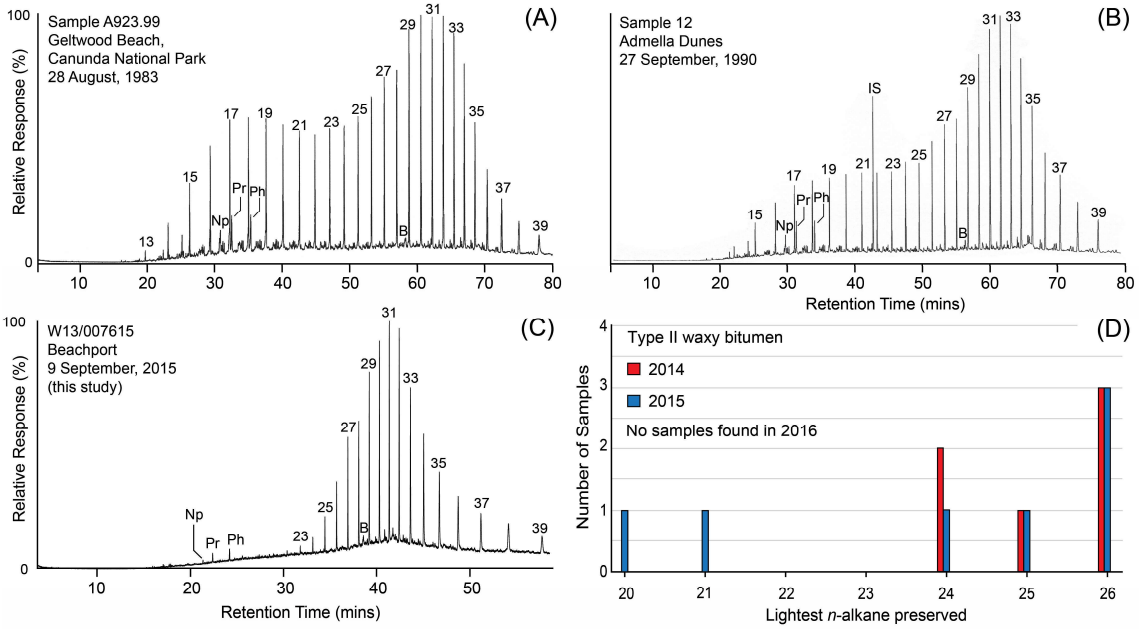


Figure 14: Comparison of historical and modern type II waxy bitumens. (A) Saturates TIC chromatogram of waxy bitumen sample A923.99 collected in 1983. (B) Saturates TIC chromatogram of waxy bitumen sample 12 collected in 1990. (C) Whole-oil TIC of the freshest type II waxy bitumen, sample W13/007615, collected in 2015. (D) Range of weathering extent for the type II waxy bitumens collected in 2014–2016. Chromatograms of archival samples in parts A and B, modified after Padley (1995). Numbered peak responses correspond to n-alkane chain length, Np = norpristane, Pr = pristane, Ph = phytane, B = botryococcane, IS = 3-methylhenicosane internal standard (AC 22; 10µg ml^{-1}). Note: minor variation in the relative elution position of botryococcane between the archival specimens and those collected in 2015 is the result of differences in chromatography, not sample composition.

To the best of our knowledge, there no reports of produced oils or seeps in SE Asia consistent with the source affinity of the type II waxy bitumen. Given that oils derived from lacustrine source rocks in this region are geographically restricted to the basins in the western half of the Indonesian Archipelago (Robinson, 1987; ten Haven and Schiefelbein, 1995), the parent petroleum system likely resides in this area. Of these basins, only the NW Java Basin hosts both oil containing botryococcane and oil derived from a marine carbonate source rock, the latter of which may already be of mixed composition in the reported examples (Napitupulu et al., 1997). Although ten Haven and Schiefelbein (1995) also noted that a carbonate source rock had been proposed in the Central Sumatra Basin based on the geochemical results provided by Kjellgren and Sugiharto (1989) from the Tonjol-1 well, this well actually resides within the North Sumatra Basin. Furthermore, whilst oil attributed to a lacustrine source environment subject to marine incursion has been interpreted for the North Sumatra Basin (Matchette-Downes et al.,

1994), no oils containing botryococcane are have been recognised within the basin. Therefore, based on the limited supporting evidence available, we propose two potential interpretations regarding the origin of the type II waxy bitumens: 1) they originate from a mixture of oils derived from both marine carbonate and lacustrine source rock within the NW Java Basin; or 2) their parent petroleum system has yet to be reported/discovered.

6.3. Classification and provenance summary

The potential classifications from each assessment stage (visual, whole-oil, biomarkers) and the interpretation of source affinity for each identified oil are summarised in Figure 15. Presently the asphaltic oils are attributed to an undiscovered petroleum system(s) in the Bight Basin, while the waxy oils are proposed to originate from a wide variety of potential petroleum systems across the Indonesian Archipelago. The basins in SE Asia reported to host oils similar to the various waxy oils collected from the South Australian coastline are summarised in Table 5. In general, oils of lacustrine source affinity are geographically restricted to Cenozoic basins in the western half of the archipelago, while marine oils attributed to clastic and carbonate source rocks primarily originate from Mesozoic and Cenozoic source rocks within sedimentary basins in the east, with the notable exceptions of the North Sumatra and East Natuna basins, which reside in the western half of the archipelago. Finally, oils associated with fluvio-deltaic coals/shales are the most geographically widespread type of oil observed in SE Asia and hence are the most difficult to correlate at basin-scale.

The comparisons provided herein of various stranded waxy bitumens with produced or seep oils from SE Asia are intended to demonstrate their broad correlation to the region, thereby establishing the distant provenance of the natural petroleum contamination of the South Australian coastline. However, the geochemical similarities are not sufficient in most cases to link them to specific Indonesian oil fields, particularly given the comparable geochemistry of oils in different basins across the archipelago. Thus, to obtain more precise correlations, direct comparison of these waxy oils to a greater number of seafloor seeps will likely be required.

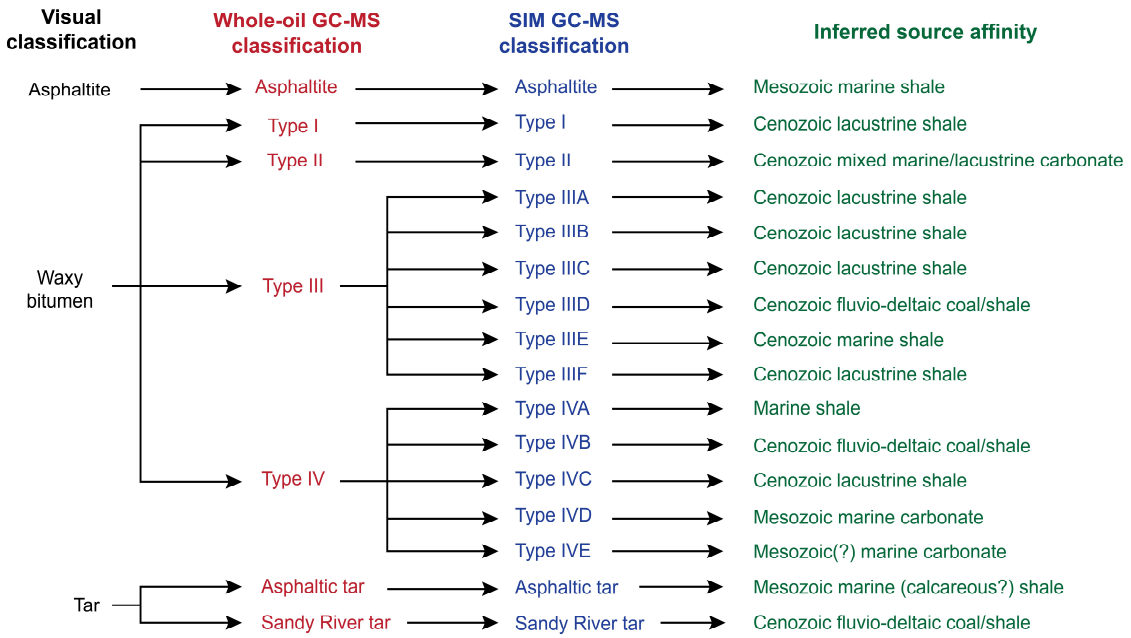


Figure 15: Summary of classifications and inferred source affinity for all stranded oil types, excluding those reserved for degraded samples of uncertain origin. Note that most oils considered marine in origin presently lack reliable age constraints and require further assessment by MRM GC-MS.

6.4. Oceanic transportation of SE Asian crude oils to the Australian coastline

Following their release into the marine environment the waxy oils are entrained in a complex series of regional ocean currents, most notably the North Pacific thermocline and the Leeuwin Current, which deliver them to numerous sites along the Australian coastline, extending from the Northern Territory to Victoria (Fig. 16). This oceanic transportation pathway has previously been invoked to explain the occurrence of oils consistent with an Indonesian origin arriving on the coastlines of Western Australia, South Australia and Victoria (Currie et al., 1992; McKirdy et al., 1994; Padley, 1995; Edwards et al., 2016). Further evidence that these currents transport flotsam from SE Asia may also be found in the occurrence of fossilised tree resins (resinites) which originate from Southeast Asian tropical angiosperms of the family Dipterocarpaceae which similarly strand along the South Australian coastline (Murray et al., 1994). After arriving in the Great Australian Bight the oils are carried by local ocean currents, in particular the Coastal Current (Fig.16) , which flows east during winter and west during summer, consistent with the observed lower abundance of coastal bitumen strandings in the summer months (Edwards et al., 2016).

Table 5: Summary of biomarker characteristics of Indonesian oils which share features in common with waxy oils recovered from the South Australian coastline.

Waxy oil strandings	Source affinity	Possible basins of origin	Characteristics of reported oils	References
Type I Type IIIA Type IIIB Type IIIC Type IIIF Type IVC	Lacustrine/ brackish shale	North Sumatra Central Sumatra South Sumatra Sunda NW Java East Java West Natuna	High botryococcane (type I only) Abundant C_{30} tetracyclic polyprenoids* C_{30} 4-methylsteranes¶ C_{26}/C_{25} tricyclic terpanes >>1 Ts > Tm Oleanane (higher in brackish) Bicadinanes (higher in brackish) Steranes / hopanes <1 Pristane/phytane = 1.5–3 24-*n*-propylcholestane absent¶	Robinson, 1987; Matchette-Downes et al., 1994; ten Haven and Schiefelbein, 1995; Schiefelbein and Cameron, 1997; Napitupulu et al., 1997; Hwang et al., 2002
Type IIID Type IVB Sandy River tars	Fluvio-deltaic shale	North Sumatra Central Sumatra South Sumatra Sunda NW Java East Java Kutei Tarakan Salawati/Misool Seep Seram Tomori	C_{29} steranes dominant Abundant bicadinanes Abundant oleanane Bisnorlupanes Taraxastane† C_{26}/C_{25} tricyclic terpanes < 1 Low C_{30} tetracyclic polyprenoids* Pristane/phytane > 3	Robinson, 1987; Napitupulu et al., 1997; Schiefelbein et al., 1997; Peters et al., 1999; Satyana and Purwaningsih, 2003; Curiale et al., 2005; Noble et al., 2009
Type IIIE Type IVA	Marine shale	Salawati North Sumatra‡ Banggai-Sula§ Bintuni§ Timor	24-*n*-propylcholestane present Steranes/hopanes generally >1 Abundant C_{27} steranes C_{29}/C_{30} αβ hopane <1 Oleanane abundant (Cenozoic) Oleanane absent (Mesozoic)	Robinson, 1987; ten Haven and Schiefelbein, 1995; Schiefelbein et al., 1997
Type IVD Type IVE	Marine carbonate	North Sumatra‡ East Natuna Banggai-Sula§ Salawati Bintuni§ Seram Timor NW Java	C_{29}/C_{30} αβ hopane > 1 C_{27} steranes dominant 24-*n*-propylcholestane present Pristane/phytane = 1–2.5 Abundant 29,30-Norhopane Oleanane abundant (Cenozoic) Oleanane absent (Mesozoic)	Robinson, 1987; Price et al., 1987; Kjellgren and Sugiharto, 1989; ten Haven and Schiefelbein, 1995; Napitupulu et al., 1997; Schiefelbein et al., 1997; Peters et al., 1999; Satyana and Zaitun, 2016
Type II	Mixed lacustrine/ marine carbonate	Mixture of individually reported oils derived from marine carbonate and lacustrine source rocks in NW Java Basin (?)	C_{29}/C_{30} αβ hopane >1 Trace oleanane and bicadinanes Low botryococcane 24-*n*-propylcholestane¶ Dinosterane¶	Napitupulu et al., 1997

* Tetracyclic polyprenoids were originally reported as an unknown 'lacustrine classifier' by ten Haven and Schiefelbein (1995); later identified by Holba et al. (2000).
¶ Based on previous analysis of equivalent samples collected in the early 1990's and analysed using MRM by Edwards et al. (2018).
† Taraxastane appears in reported chromatograms, although is not always explicitly identified.
‡ Reported oils contained high oleanane content and are thus less likely to account for the waxy bitumens.
§ Basin contains both Mesozoic and Cenozoic marine source rocks.

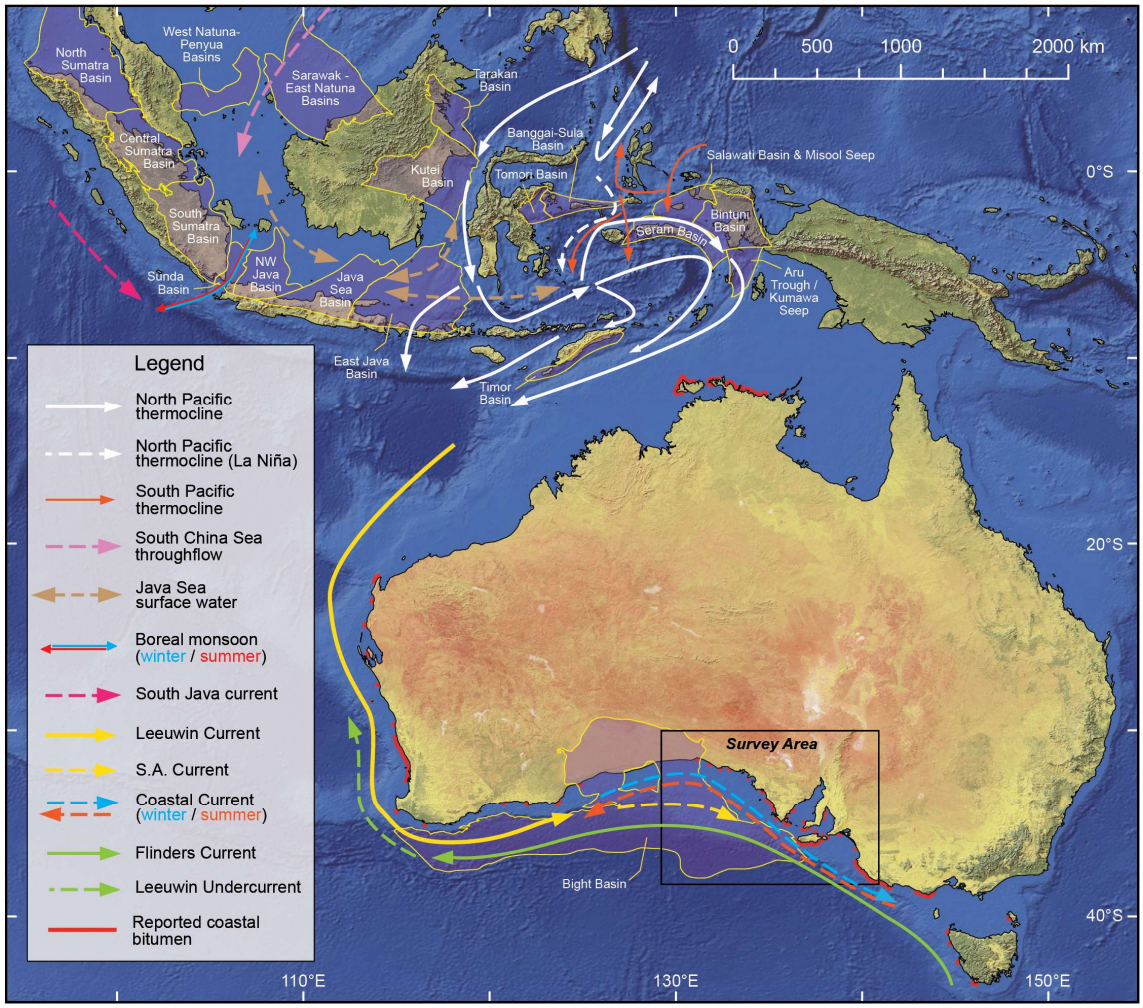


Figure 16: Selected sedimentary basins and simplified regional ocean currents attributed to the transportation of crude oils to the South Australian coastline. Distribution of reported coastal bitumens modified after Edwards et al. (2016) to include those collected in this study. Simplified ocean currents after Lukas et al., (1996); Cirano and Middleton, (2004); Gordon, (2005); Middleton and Bye, (2007); Gordon et al., (2012) and Susanto et al., (2016). For a more complex representation of the various inputs feeding into the Leeuwin Current, including the Eastern Gyral and Subtropical Indian currents not shown here, see Domingues et al. (2007).

6.5. Could any of these oils represent anthropogenic discharges or spills?

Anthropogenic oil spills which reach the coastline typically result in a high abundance of liquid oil in the form of liquid droplets or a thin film of oil coating the stranding site. Although several oil slicks were encountered on the South Australian coastline during the 1990–1991 surveys (Padley, 1995; Edwards et al., 2016 and references therein), no similar occurrences were encountered during this study. The most abundant oils on the coastline, both in terms of total weight recovered, and by number of individual strandings, have a consistent historical record of stranding and thus can be reliably considered products of natural seepage. Asphaltites, which have been stranding on the coastline since at least the late 1800s (Volkman et al., 1992; Edwards

et al., 1998), contribute the most crude oil to the coastline by weight due to their large size; whereas the type I waxy bitumens, recognised from at least the 1960s (e.g. Fig. 9A), are the most commonly occurring variety of coastal bitumen, comprising approximately half of all specimens collected during the 2014–2016 surveys (Corrick et al., 2020b). Furthermore, although numerous small shipping incidents were reported, no large oil discharges or spills occurred in proximity to the path of the Leeuwin Current along the Western Australian or South Australian coastline during the study period which might otherwise account for the oils described herein (Australian Maritime Safety Authority, 2014, 2015, 2016, 2019). Given the lack of significant anthropogenic sources of oil, and the fact that the majority of the stranded oils have geochemistries consistent with petroleum systems in SE Asia, a region where numerous seafloor seeps are recognised and well-documented ocean currents are known to transport material, we presently consider all of the oils documented herein to originate from natural seepage.

7. CONCLUSIONS

Geochemical analysis of 633 pieces of semi-solid crude oil collected from South Australian beaches between 2014 and 2016 demonstrate that the coastline accumulates bitumen and tar strandings from a far wider variety of petroleum systems than previously reported. These oils are considered the result of natural offshore seepage. Thus, by outlining their defining characteristics herein, we show that these oils represent natural “background” contamination that can be readily distinguished from other potential anthropogenic sources of hydrocarbons which may impact the coastline in the future, such as oil spills.

The various oils may be classified with increasing detail using a combination of visual features, whole-oil GC-MS and source-specific biomarker assemblages. The latter are capable of distinguishing at least 16 unique oils. Two of these, referred to as asphaltite and asphaltic tar, are presently thought to originate from the nearby Bight Basin. However, a greater understanding of the petroleum systems in this frontier basin is required before this interpretation can be verified. The remaining oils have source-specific biomarker characteristics similar to those found in lacustrine, fluvio-deltaic and marine petroleum systems located across SE Asia. While the occurrence of oil seepage from SE Asia arriving on the South Australian coastline due to a combination of regional ocean currents has been well established in previous studies, our results demonstrate that the number of different petroleum systems contributing to

this process is far greater than previously recognised. Of these waxy oils, those of lacustrine source affinity are likely products of Cenozoic basins in the western half of the Indonesian Archipelago, while those derived from marine carbonates and shales most likely come from sedimentary basins further east. By far the most problematic oils to link to a parent petroleum system are those derived from predominantly terrigenous organic matter deposited in fluvio-deltaic settings, as reports of petroleum of this composition are particularly widespread across the archipelago. Unfortunately, the majority of proposed correlations for these far-travelled SE Asian oils are provisional, due to the limited available geochemical datasets and the occurrence of oils of similar source affinity across multiple basins in the region.

Comparison of the oils found on the coastline today with those analysed in the previous study, conducted in the early-mid 1990s, demonstrates that some of the same oils continue to strand along South Australian beaches after approximately 25 years. The asphaltites appear unchanged, with the freshest example recovered to date analysed herein, demonstrating that their parent seep remains active today. However, all modern examples of the waxy bitumen families defined by their content of the rare biomarker botryococcane are significantly more weathered compared to their historical counterparts. This suggests that their parent seeps may no longer be active. Finally, in order to establish a robust historical continuity for the new waxy oil families which have been identified during this study, further comprehensive analysis of archival suites of South Australian coastal bitumen will be required.

ACKNOWLEDGEMENTS

We thank Chris Dyt, Zachary Angelini, Richard Kempton, Cameron White, April Pickard, Stacey Maslin, Stephane Armand, Les Tucker and Su Margot for their assistance in completing the 2014–2016 beach surveys. We also thank Stuart Valladares for the donation of asphaltite and waxy bitumen specimens from his personal collection for this research and Robyn Williamson for assistance in the preparation of chromatography columns for oil fractionations.

The Great Australian Bight Research Program is a collaboration between BP, CSIRO, the South Australian Research and Development Institute (SARDI), the University of Adelaide, and Flinders University. The program aims to provide a whole-of-system understanding of the environmental and social values of the region; providing an information source for all to use.

SUPPLEMENTARY INFORMATION

The supplementary information for this chapter may be found in pages 238–289.

REFERENCES

Alexander, R., Currie, T.J., Kagi, R.I., 1994. The origins of coastal bitumens from Western Australia. Aust. Pet. Explor. Assoc. J. 34, 787–798.

Australian Maritime Safety Authority, 2014. National plan for maritime environmental emergencies: Year in review 2013-14.

Australian Maritime Safety Authority, 2015. National plan for maritime environmental emergencies: Year in review 2014-2015.

Australian Maritime Safety Authority, 2016. National plan for maritime environmental emergencies: Year in review 2015-2016.

Australian Maritime Safety Authority, 2019. Major historical incidents. URL https://www.amsa.gov.au/marine-environment/incidents-and-exercises/major-historical-incidents

Baghurst, B., Lukatelich, R., Smith, D., Begg, G., Lewis, R., Smith, R., 2017. Findings from the Great Australian Bight Research Program – an integrated study of environmental, economic and social values. APPEA J. 57, 388–392. doi:10.1071/AJ16144

Bastow, T.P., van Aarssen, B.G.K., Lang, D., 2007. Rapid small-scale separation of saturate, aromatic and polar components in petroleum. Org. Geochem. 38, 1235–1250. doi:10.1016/j.orggeochem.2007.03.004

Blumer, M., Ehrhardt, M., Jones, J.H., 1973. The environmental fate of stranded crude oil. Deep Sea Res. 20, 239–259. doi:10.1016/0011-7471(73)90014-4

Boreham, C.J., Krassay, A.A., Totterdell, J.M., 2001. Geochemical comparisons between asphaltites on the southern Australian margin and Cretaceous source rock analogues, in: Hill, K.C., Bernecker, T. (Eds.), Eastern Australasian Basins Symposium, A Refocused Energy Perspective for the Future. Petroleum Exploration Society of Australia Special Publication. pp. 531–541.

Boult, P.J., McKirdy, D., Blevin, J., Heggeland, R., Lang, S., Vinall, D., 2005. The oil-prone Morum Sub-basin petroleum system, Otway Basin, South Australia. MESA J. 38, 28–33.

Brüning, M., Sahling, H., MacDonald, I.R., Ding, F., Bohrmann, G., 2010. Origin, distribution, and alteration of asphalts at Chapopote Knoll, Southern Gulf of Mexico. Mar. Pet. Geol. 27, 1093–1106. doi:10.1016/j.marpetgeo.2009.09.005

Butler, J.N., Morris, B.F., Sleeter, T.D., 1976. The fate of petroleum in the open ocean, in: Sources, Effects and Sinks of Hydrocarbons in the Aquatic Environment: Proceedings of the Symposium, American University, Washington DC, 9-11. American Institute of Biological Sciences, Washington, D.C., pp. 287–297.

Cassani, F., Gallango, O., Talukdar, S., Vallejos, C., Ehrmann, U., 1988. Methylphenanthrene maturity index of marine source rock extracts and crude oils from the Maracaibo Basin. Org. Geochem. 13, 73–80. doi:10.1016/0146-6380(88)90027-7

Cirano, M., Middleton, J.F., 2004. Aspects of the Mean Wintertime Circulation along Australia's Southern Shelves: Numerical Studies. J. Phys. Oceanogr. 34, 668–684. doi:10.1175/2509.1

Connan, J., Bouroullec, J., Dessort, D., Albrecht, P., 1986. The microbial input in carbonate-anhydrite facies of a sabkha palaeoenvironment from Guatemala: A molecular approach. Org. Geochem. 10, 29–50. doi:10.1016/0146-6380(86)90007-0

Corrick, A.J., Hall, P.A., Gong, S., McKirdy, D.M., Selby, D., Trefry, C., Ross, A.S., 2020a. A second type of highly asphaltic crude oil seepage stranded on the South Australian coastline. Mar. Pet. Geol. 112, 104062. doi:10.1016/J.MARPETGEO.2019.104062

Corrick, A.J., Hall, P.A., Trefry, C., Gong, S., McKirdy, D.M., Ross, A.S., 2020b. The hydrocarbon loading of the South Australian coastline, in: Studies on the nature of crude oil strandings collected from the South Australian coastline. PhD Thesis, unpublished. University of Adelaide.

Corrick, A.J., Selby, D., McKirdy, D.M., Hall, P.A., Gong, S., Trefry, C., Ross, A.S., 2019. Remotely constraining the temporal evolution of offshore oil systems. Sci. Rep. 9, 1327. doi:10.1038/s41598-018-37884-x

Curiale, J., Lin, R., Decker, J., 2005. Isotopic and molecular characteristics of Miocene-reservoired oils of the Kutei Basin, Indonesia. Org. Geochem. 36, 405–424. doi:10.1016/j.orggeochem.2004.09.007

Currie, T.J., Alexander, R., Kagi, R.I., 1992. Coastal bitumens from Western Australia - long distance transport by ocean currents. Org. Geochem. 18, 595–601.

Czochanska, Z., Sheppard, C.M., Weston, R.J., Woolhouse, A.D., 1987. A biological marker study of oils and sediments from the West Coast, South Island, New Zealand. New Zeal. J. Geol. Geophys. 30, 1–17.

Domingues, C.M., Maltrud, M.E., Wijffels, S.E., Church, J.A., Tomczak, M., 2007. Simulated Lagrangian pathways between the Leeuwin Current System and the upper-ocean circulation of the southeast Indian Ocean. Deep Sea Res. Part II Top. Stud. Oceanogr. 54, 797–817. doi:10.1016/J.DSR2.2006.10.003

Dutta, S., Tripathi, S.M., Mallick, M., Mathews, R.P., Greenwood, P.F., Rao, M.R., Summons, R.E., 2011. Eocene out-of-India dispersal of Asian dipterocarps. Rev. Palaeobot. Palynol. 166, 63–68. doi:10.1016/J.REVPALBO.2011.05.002

Edwards, D., McKirdy, D.M., Summons, R.E., 1998. Enigmatic asphaltites from the southern Australian margin: molecular and carbon isotopic composition. Pet. Explor. Soc. Aust. J. 26, 397–420.

Edwards, D.S., McKirdy, D.M., Rowland, S.J., Heath, D.J., Gray, P.S., 2018. Waxy bitumen stranding in southern Australia: A geochemical study of multiple oil families and their likely origins. Org. Geochem. 118, 132–151. doi:10.1016/j.orggeochem.2017.12.010

Edwards, D.S., Vinall, D.R., Corrick, A.J., McKirdy, D.M., 2016. Natural bitumen stranding on the ocean beaches of Southern Australia: a historical and geospatial review. Trans. R. Soc. South Aust. 140, 152–185. doi:10.1080/03721426.2016.1203532

Ekweozor, C.M., Telnaes, N., 1990. Oleanane parameter: Verification by quantitative study of the biomarker occurrence in sediments of the Niger delta. Org. Geochem. 16, 401–413. doi:10.1016/0146-6380(90)90057-7

Farrimond, P., Bevan, J.C., Bishop, A.N., 1999. Tricyclic terpane maturity parameters: response to heating by an igneous intrusion. Org. Geochem. 30, 1011–1019. doi:10.1016/S0146-6380(99)00091-1

Fingas, M.F., 1997. Studies on the evaporation of crude oil and petroleum products: I. the relationship between evaporation rate and time. J. Hazard. Mater. 56, 227–236. doi:10.1016/S0304-3894(97)00050-2

Garrett, R.M., Pickering, I.J., Haith, C.E., Prince, R.C., 1998. Photooxidation of Crude Oils. Environ. Sci. Technol. 32, 3719–3723. doi:10.1021/ES980201R

Gordon, A.L., 2005. Oceanography of the Indonesian Seas and their throughflow. Oceanography 18, 14–27.

Gordon, A.L., Huber, B.A., Metzger, E.J., Susanto, R.D., Hurlburt, H.E., Adi, T.R., 2012. South China Sea throughflow impact on the Indonesian throughflow. Geophys. Res. Lett. 39. doi:10.1029/2012GL052021

Grice, K., Cao, C., Love, G.D., Böttcher, M.E., Twitchett, R.J., Grosjean, E., Summons, R.E., Turgeon, S.C., Dunning, W., Jin, Y., 2005. Photic zone euxinia during the Permian-Triassic superanoxic event. Science. 307, 706–709. doi:10.1126/science.1104323

Hall, P.A., McKirdy, D.M., Grice, K., Edwards, D.S., 2014. Australasian asphaltite strandings: Their origin reviewed in light of the effects of weathering and biodegradation on their biomarker and isotopic profiles. Mar. Pet. Geol. 57, 572–593. doi:10.1016/j.marpetgeo.2014.06.013

Head, I.M., Jones, D.M., Röling, W.F.M., 2006. Marine microorganisms make a meal of oil. Nat. Rev. Microbiol. 4, 173–182. doi:10.1038/nrmicro1348

Henry, C.B., Roberts, P.O., Overton, E.B., 1993. Characterization of chronic sources and impacts of tar along the Louisiana Coast.

Holba, A.., Dzou, L.., Wood, G.., Ellis, L., Adam, P., Schaeffer, P., Albrecht, P., Greene, T., Hughes, W., 2003. Application of tetracyclic polyprenoids as indicators of input from fresh-brackish water environments. Org. Geochem. 34, 441–469. doi:10.1016/S0146-6380(02)00193-6

Holba, A.G., Tegelaar, E., Ellis, L., Singletary, M.S., Albrecht, P., 2000. Tetracyclic polyprenoids: Indicators of freshwater (lacustrine) algal input. Geology 28, 251–254. doi:10.1130/0091-7613(2000)28<251:TPIOFL>2.0.CO;2

Hook, S., Batley, G., Holloway, M., Irving, P., Ross, A. (Eds.), 2016. Oil spill monitoring handbook. CSIRO Publishing.

Howchin, W., 1919. Geological memoranda (first contributions). Trans. R. Soc. South Aust. 43, 45–48.

Howchin, W., 1903. Further notes on the geology of Kangaroo Island. Trans. R. Soc. South Aust. 27, 75–90.

Huang, W.-Y., Meinschein, W.G., 1979. Sterols as ecological indicators. Geochim. Cosmochim. Acta 43, 739–745. doi:10.1016/0016-7037(79)90257-6

Hwang, R.J., Heidrick, T., Mertani, B., Qivayanti, Li, M., 2002. Correlation and migration studies of North Central Sumatra oils. Org. Geochem. 33, 1361–1379. doi:10.1016/S0146-6380(02)00104-3

Kjellgren, G.M., Sugiharto, H., 1989. Oil Geochemistry: A Clue to the Hydrocarbon History and Prospectivity of the Southeastern North Sumatra Basin, Indonesia, in: Indonesian Petroleum Association 18th Annual Convention Proceeding. Indonesian Petroleum Association, pp. 363–384.

Lee, R.F., 1980. Processes Affecting the Fate of Oil in the Sea. Elsevier Oceanogr. Ser. doi:10.1016/S0422-9894(08)71389-8

Lillis, P.G., Selby, D., 2013. Evaluation of the rhenium–osmium geochronometer in the Phosphoria petroleum system, Bighorn Basin of Wyoming and Montana, USA. Geochim. Cosmochim. Acta 118, 312–330. doi:10.1016/j.gca.2013.04.021

Lorenson, T.D., Hostettler, F.D., Rosenbauer, R.J., Peters, K.E., Dougherty, J.A., Kvenvolden, K.A., Gutmacher, C.E., Wong, F.L., Normark, W.R., 2009. Natural Offshore Oil Seepage and Related Tarball Accumulation on the California Coastline; Santa Barbara Channel and the Southern Santa Maria Basin; source identification and inventory, U.S. Geological Survey Open-File Report 2009-1225 and MMS report 2009-030.

Lukas, R., Yamagata, T., McCreary, J.P., 1996. Pacific low-latitude western boundary currents and the Indonesian throughflow. J. Geophys. Res. 101, 12209–12216. doi:10.1029/96JC01204

Matchette-Downes, C.J., Fallick, A.E., Rowland, S., 1994. A maturity and palaeoenvironmental assessment of condensates and oils from the North Sumatra Basin, Indonesia. Geol. Soc. London, Spec. Publ. 77, 139–148. doi:10.1144/GSL.SP.1994.077.01.08

McKirdy, D.M., 1984a. Coastal bitumens and potential source rocks in the western Otway Basin, South Australia and Victoria. AMDEL Report F 5840/84 for Australian Aquitaine Petroleum Pty Ltd. and Ultramar Australia Inc., South Australian Department of Mines and Energy Open File Envelope No. 5876.

McKirdy, D.M., 1984b. Coastal bitumens and potential source rocks, Duntroon Basin, South Australia. AMDEL Report F 5769/84 for Getty Oil Development Company Ltd., South Australian Department of Mines and Energy Open File Envelope No. 5876.

McKirdy, D.M., Aldridge, A.K., Ypma, P.J.M., 1983. A geochemical comparison of some crude oils from pre-Ordovician carbonate rocks, in: Bjoröy, M., Albrecht, P., Cornford, C., de Groot, K., Eglinton, G., Galimov, E., Leythaeuser, D., Pelet, R., Speers, G. (Eds.), Advances in Organic Geochemistry 1981. John Wiley & Sons Limited, Chichester, Chichester, pp. 99–107.

McKirdy, D.M., Cox, R.E., Volkman, J.K., Howell, V.J., 1986. Botryococcane in a new class of Australian non-marine crude oils. Nature 320, 57–59. doi:10.1038/320057a0

McKirdy, D.M., Horvath, Z., 1976. Geochemistry and significance of coastal bitumen from Southern and Northern Australia. APPEA J. 123–135.

Middleton, J.F., Bye, J.A.T., 2007. A review of the shelf-slope circulation along Australia's southern shelves: Cape Leeuwin to Portland. Prog. Oceanogr. 75, 1–41. doi:10.1016/j.pocean.2007.07.001

Moldowan, J.M., Dahl, J., Huizinga, B.J., Fago, F.J., Hickey, L.J., Peakman, T.M., Taylor, D.W., 1994. The molecular fossil record of oleanane and its relation to angiosperms. Science (80-.). 265, 768–771. doi:10.1126/science.265.5173.768

Moldowan, J.M., Fago, F.J., Lee, C.Y., Jacobson, S.R., Watt, D.S., Slougui, N.-E., Jeganathan, A., Young, D.C., 1990. Sedimentary 24-n-propylcholestanes, molecular fossils diagnostic of marine algae. Science (80-.). 247, 309–312. doi:10.2307/2873627

Moldowan, J.M., Seifert, W.K., 1980. First discovery of Botryococcane in petroleum. J. Chem. Soc. Chem. Commun. 19, 912–914.

Moldowan, J.M., Seifert, W.K., Gallegos, E.J., 1985. Relationship Between Petroleum Composition and Depositional Environment of Petroleum Source Rocks. Am. Assoc. Pet. Geol. Bull. 69, 1255–1268.

Murray, A.P., Padley, D., McKirdy, D.M., Booth, W.E., Summons, R.E., 1994. Oceanic transport of fossil dammar resin: The chemistry of coastal resinites from South Australia. Geochim. Cosmochim. Acta 58, 3049–3059. doi:10.1016/0016-7037(94)90178-3

Murray, A.P., Sosrowidjojo, I.B., Alexander, R., Kagi, R.I., Norgate, C.M., Summons, R.E., 1997. Oleananes in oils and sediments: Evidence of marine influence during early diagenesis? Geochim. Cosmochim. Acta 61, 1261–1276. doi:10.1016/S0016-7037(96)00408-5

Napitupulu, H., Mitterer, R.M., Morelos-Garcia, J.A., 1997. Differentiation of Oils from the NW Java Basin into Three Oil Types Based on Biomarker Composition, in: Proceedings of an International Conference on Petroleum Systems of SE Asia and Australasia. Indonesian Petroleum Association, pp. 667–679.

NAS, 2003. Oil in the Sea III: Inputs, Fates and Effects. The National Academies Press, Washington DC. doi:10.17226/10388

Noble, R., Orange, D., Decker, J., Teas, P., Baillie, P., 2009. Oil and Gas Seeps in Deep Marine Sea Floor Cores as Indicators of Active Petroleum Systems in Indonesia, in: Indonesian Petroleum Association Thirty-Third Annual Convention & Exhibition. Indonesian Petroleum Association, p. 10.

Nytoft, H.P., Bojesen-Koefoed, J.A., Christiansen, F.G., Fowler, M.G., 2002. Oleanane or lupane? Reappraisal of the presence of oleanane in Cretaceous–Tertiary oils and sediments. Org. Geochem. 33, 1225–1240. doi:10.1016/S0146-6380(02)00138-9

Padley, D., 1995. Petroleum geochemistry of the Otway Basin and the significance of coastal bitumen strandings on adjacent southern Australian beaches (PhD thesis). University of Adelaide.

Palmer, S.E., 1993. Effect of biodegradation and water washing on crude oil composition, in: Engel, M.H., Macko, S.A. (Eds.), Organic Geochemistry. Plenum Press, New York, pp. 511–533. doi:10.1007/978-1-4615-2890-6_23

Perkins, G.M., Bull, I.D., Ten Haven, H.L., Rullötter, J., Smith, Z.E.F., Peakman, T.M., 1995. First positive identification of triterpenes of the Taraxastane Family in petroleums and oil shales: 19α(H)-Taraxastane and 24-nor-19α(H)-Taraxastane. Evidence for a previously unrecognised diagenetic alteration pathway of Lup-20(29)-ene derivatives, in: Grimalt, J.O., Dorronsoro, C. (Eds.), Organic Geochemistry: Developments and Applications to Energy, Climate, Environment and Human History. pp. 247–249.

Peters, K.E., Fraser, T.H., Amris, W., Rustanto, B., Hermanto, E., 1999. Geochemistry of Crude Oils from Eastern Indonesia. Am. Assoc. Pet. Geol. Bull. 83, 1927–1942.

Peters, K.E., Walters, C.C., Moldowan, J.M., 2005. The Biomarker Guide Volume 2: Biomarkers and Isotopes in Petroleum Exploration and Earth History, 2nd editio. ed. Cambridge University Press.

Philp, R.P., Gilbert, T.D., 1986. Biomarker distributions in Australian oils predominantly derived from terrigenous source material. Org. Geochem. 10, 73–84. doi:10.1016/0146-6380(86)90010-0

Price, P.L., O'Sullivan, T., Alexander, R., 1987. The nature and occurrence of oil in Seram, Indonesia, in: Indonesian Petroleum Associated 16th Annual Convention Proceedings (Volume 1). Indonesian Petroleum Association, pp. 141–173.

Radke, M., Leythaeuser, D., Teichmüller, M., 1984. Relationship between rank and composition of aromatic hydrocarbons for coals of different origins. Org. Geochem. 6, 423–430. doi:10.1016/0146-6380(84)90065-2

Radke, M., Welte, D.H., 1983. The methylphenanthrene index (MPI). A maturity parameter based on aromatic hydrocarbons, in: Bjoröy, M., Albrecht, P., Cornford, C., de Groot, K., Eglinton, G., Galimov, E., Leythaeuser, D., Pelet, R., Speers, G. (Eds.), Advances in Organic Geochemistry 1981. John Wiley & Sons Limited, Chichester, pp. 504–512.

Reed, W.E., 1977. Molecular compositions of weathered petroleum and comparison with its possible source. Geochim. Cosmochim. Acta 41, 237–247. doi:10.1016/0016-7037(77)90231-9

Robinson, K.M., 1987. An Overview of Source Rocks and Oils in Indonesia, in: Indonesian Petroleum Association Sixteenth Annual Convention. Indonesian Petroleum Association, pp. 97–122.

Ross, A., Corrick, A., Trefry, C., Gong, S., McKirdy, D., Hall, T., Dyt, C., Angelini, Z., Kempton, R., Pickard, A., White, C., Maslin, S., Griffin, D., Middleton, J., Luick, J., Armand, S., Vergara, T., Schinteie, R., 2017. Asphaltite and tarball surveys. Final Report GABRP Project 5.2. Research Report Series Number 25a.

Satyana, A.H., Purwaningsih, M.E.M., 2003. Geochemistry of the East Java Basin: new observations on oil grouping, genetic gas types and trends of hydrocarbon habitats, in: Indonesian Petroleum Association 29th Annual Convention & Exhibition. Indonesian Petroleum Association.

Satyana, A.H., Zaitun, S., 2016. Origins of oils and gases at Banggai-Sula microcontinent, Eastern Sulawesi - North Moluccas: Constraints from biomarkers and isotope geochemistry - implications for further exploration of Cenozoic and Pre-Cenozoic objectives, in: Indonesian Petroleum Association 40th Annual Convention & Exhibition. Indonesian Petroleum Association.

Scarlett, A.G., Holman, A.I., Georgiev, S. V., Stein, H.J., Summons, R.E., Grice, K., 2019. Multi-spectroscopic and elemental characterization of southern Australian asphaltites. Org. Geochem. 133, 77–91. doi:10.1016/J.ORGGEOCHEM.2019.04.006

Schiefelbein, C., Cameron, N., 1997. Sumatra/Java oil families. Geol. Soc. London, Spec. Publ. 126, 143–146. doi:10.1144/GSL.SP.1997.126.01.11

Schiefelbein, C.F., Zumberge, J.E., Brown, S.W., 1997. Petroleum Systems in the Far East, in: Proceedings of an International Conference on Petroleum Systems of SE Asia and Australiasia Conference, May 1997. Indonesian Petroleum Association, pp. 101–113.

Seifert, W.K., Michael Moldowan, J., 1979. The effect of biodegradation on steranes and terpanes in crude oils. Geochim. Cosmochim. Acta 43, 111–126. doi:10.1016/0016-7037(79)90051-6

Seifert, W.K., Moldowan, J.M., 1986. Use of biological markers in petroleum exploration, in: Johns, R.B. (Ed.), Methods in Geochemistry and Geophysics Vol. 24. Elsevier, Amsterdam, pp. 261–290.

Selby, D., Creaser, R.A., 2005. Direct radiometric dating of hydrocarbon deposits using rhenium-osmium isotopes. Science (80-.). 308, 1293–1295. doi:10.1126/science.1111081

Sprigg, R.C., Woolley, J.B., 1963. Coastal bitumen in southern Australia with special reference to observations at Geltwood Beach, south-east South Australia. Trans. R. Soc. South Aust. 86, 67–103.

Summons, R.E., Bradshaw, J., Brooks, D.M., Goody, A.K., Murray, A.P., Foster, C.B., 1993. Hydrocarbon composition and origins of coastal bitumens from the Northern Territory, Australia. PESA J. 21, 31–42.

Summons, R.E., Jahnke, L.L., Hope, J.M., Logan, G.A., 1999. 2-Methylhopanoids as biomarkers for cyanobacterial oxygenic photosynthesis. Nature 400, 554–557. doi:10.1038/23005

Summons, R.E., Logan, G.A., Edwards, D.S., Boreham, C.J., Bradshaw, M.T., Blevin, J.E., Totterdell, J.M., Zumberge, J.E., 2001. Geochemical analogs for australian coastal asphaltites - search for the source rock, in: Abstracts, AAPG Annual Convention, Denver, Colorado. American Association of Petroleum Geologists.

Summons, R.E., Powell, T.G., 1987. Identification of aryl isoprenoids in source rocks and crude oils: Biological markers for the green sulphur bacteria. Geochim. Cosmochim. Acta 51, 557–566. doi:10.1016/0016-7037(87)90069-X

Summons, R.E., Volkman, J.K., Boreham, C.J., 1987. Dinosterane and other steroidal hydrocarbons of dinoflagellate origin in sediments and petroleum. Geochim. Cosmochim. Acta 51, 3075–3082. doi:10.1016/0016-7037(87)90381-4

Susanto, R.D., Wei, Z., Adi, T.R., Zheng, Q., Fang, G., Fan, B., Supangat, A., Agustiadi, T., Li, S., Trenggono, M., Setiawan, A., 2016. Oceanography Surrounding Krakatau Volcano in the Sunda Strait, Indonesia. Oceanography 29, 264–272. doi:10.2307/24862689

ten Haven, H.L., Schiefelbein, C., 1995. The Petroleum Systems of Indonesia, in: Proceedings Indonesian Petroleum Association: Twenty Fourth Annual Convention Proceedings. pp. 443–459.

Tissot, B.P., Welte, D.H., 1984. Petroleum formation and occurrence, 2nd ed. ed. Springer-Verlag, Berlin.

Tolmer, A., 1882. Reminiscences of an adventurous and chequered career at home and at the antipodes. Sampson Low, Marston, Searle & Rivington, London.

Totterdell, J.M., Struckmeyer, H.I.M., Boreham, C.J., Mitchell, C.H., Monteil, E., Bradshaw, B.E., 2008. Mid-Late Cretaceous organic-rich rocks from the eastern Bight Basin : implications for prospectivity, in: Blevin, J.E., Bradshaw, B.E., Uruski, E. (Eds.), PESA Eastern Australasian Basins Symposium III Special Publication. pp. 137–158.

Trewartha, J., 1850. South Australian Government Gazette, 25 April 282.

van Aarssen, B.G.K., Cox, H.C., Hoogendoorn, P., De Leeuw, J.W., 1990. A cadinene biopolymer in fossil and extant dammar resins as a source for cadinanes and bicadinanes in crude oils from South East Asia. Geochim. Cosmochim. Acta 54, 3021–3031. doi:10.1016/0016-7037(90)90119-6

Volkman, J.K., O'Leary, T., Summons, R.E., Bendall, M.R., 1992. Biomarker composition of some asphaltic coastal bitumens from Tasmania, Australia. Org. Geochem. 18, 669–682. doi:10.1016/0146-6380(92)90092-C

Ward, L.K., 1944. The Search For Oil In South Australia, Geological Survey of South Australia Bulletin. Adelaide.

Ward, L.K., 1913. The Possibilities of the Discovery of Petroleum on Kangaroo Island and the Western Coast of Eyre's Peninsula, Geological Survey Bulletin. Adelaide.

Zumberge, J.E., 1987. Prediction of source rock characteristics based on terpane biomarkers in crude oils: A multivariate statistical approach. Geochim. Cosmochim. Acta 51, 1625–1637. doi:10.1016/0016-7037(87)90343-7

CHAPTER 5

The hydrocarbon loading of the South Australian coastline

Statement of Authorship

Title of Paper	The hydrocarbon loading of the South Australian coastline	
Publication Status	☐ Published ☐ Accepted for Publication	☐ Submitted for Publication ☑ Unpublished and Unsubmitted w ork w ritten in manuscript style
Publication Details	Written in the appropriate style for publication in *Marine Pollution Bulletin.*	

Principal Author

Name of Principal Author (Candidate)	Alexander J. Corrick		
Contribution to the Paper	Fieldwork, sample preparation, geochemical analysis, data interpretation, wrote the manuscript and drafted all figures.		
Overall percentage (%)	75		
Certification:	This paper reports on original research I conducted during the period of my Higher Degree by Research candidature and is not subject to any obligations or contractual agreements with a third party that would constrain its inclusion in this thesis. I am the primary author of this paper.		
Signature		Date	23/1/2019

Co-Author Contributions

By signing the Statement of Authorship, each author certifies that:

i. the candidate's stated contribution to the publication is accurate (as detailed above);
ii. permission is granted for the candidate in include the publication in the thesis; and
iii. the sum of all co-author contributions is equal to 100% less the candidate's stated contribution.

Name of Co-Author	Philip A. Hall		
Contribution to the Paper	Assistance with geochemical data collection and interpretation. Provided input to the final manuscript.		
Signature		Date	23/1/2019

Name of Co-Author	Se Gong		
Contribution to the Paper	Fieldwork, assistance with geochemical data interpretation. Provided input to the final manuscript.		
Signature		Date	23/1/2019

Name of Co-Author	David M. McKirdy		
Contribution to the Paper	Project design, fieldwork and assistance with data interpretation. Provided input to the final manuscript.		
Signature		Date	23/1/2019

Name of Co-Author	Christine Trefry		
Contribution to the Paper	Fieldwork, database management. Provided input to the final manuscript.		
Signature		Date	23/1/2019

Name of Co-Author	Andrew S. Ross		
Contribution to the Paper	Project design, fieldwork and assistance with data interpretation. Provided input to the final manuscript.		
Signature		Date	31/1/2019

Journal Format: ***Marine Pollution Bulletin***
Status: Unpublished work written in manuscript-style

The hydrocarbon loading of the South Australian coastline

Alexander J. Corrick[1*], Philip A. Hall[1], Christine Trefry[2], Se Gong[3], David M. McKirdy[1], and Andrew S. Ross[2]

[1] Department of Earth Sciences, School of Physical Sciences, University of Adelaide, SA 5005, Australia

[2] Energy, CSIRO, Kensington, WA 6151, Australia

[3] Energy, CSIRO, North Ryde, NSW 2113, Australia

*** Corresponding author**

HIGHLIGHTS

1) Annual surveys of 30 beaches in 2014 to 2016 collected 508 pieces of stranded oil
2) Asphaltites contributed the most oil to the coastline in terms of weight
3) Waxy bitumen with abundant botryococcane represents half of all the strandings
4) The hydrocarbon loading of the coastline has declined significantly since 1990/1991
5) This decline in seep activity is likely due to prolonged oil production in SE Asia

KEYWORDS

Coastal bitumen; asphaltite; waxy bitumen; tarball; oil seepage; hydrocarbon loading; South Australia; environmental baseline

ABSTRACT

Crude oil released from natural offshore seeps may strand in coastal environments. Understanding the different types of oil which accumulate on a given coastline, in addition to their spatial distribution and abundance, may be used to establish an environmental baseline for the natural "background" petroleum contamination. Here we summarise the hydrocarbon loading of thirty beaches on Australia's southern margin based on three annual surveys in 2014–2016. Comparison to the results of surveys conducted between 1990–1991 demonstrates a marked reduction in hydrocarbon loading has occurred. Furthermore, modern samples of the most commonly encountered oil, presently attributed to a lacustrine petroleum system in the Indonesian Archipelago, are significantly more degraded than those of prior studies. We attribute this reduction in hydrocarbon loading to prolonged oil production in Southeast Asia, with reduced reservoir pressures resulting causing a cessation of formerly active offshore seepage.

1. INTRODUCTION

Crude oil can be released into the marine environment through accidental spillage during petroleum extraction, transportation and consumption or from natural seepage. Present estimates of the annual worldwide input of petroleum to the ocean exceed 1,300,000 metric tonnes, with >45% attributed to natural seepage (NAS, 2003). As a result, natural seeps are currently considered to the largest single source of oil input introduced to the global ocean (Kvenvolden and Cooper, 2003). Petroleum released into the marine environment, whether by natural or anthropogenic means, may become entrained in local or regional ocean currents, resulting in the accumulation of oil along different coastlines (e.g. Lorenson et al., 2009; Warnock et al., 2015; Edwards et al., 2016; Shirneshan et al., 2016; Suneel et al., 2016). Such oils may strand as liquid sheets or droplets (e.g. Edwards et al., 2016), a viscous tar residue resulting from the weathering of liquid oil (Warnock et al., 2015), or oil released into the ocean in an already viscous state such as tar or asphalt (Lorenson et al., 2009; Brüning et al., 2010).

Previous studies have reported tar in the waters and on nearby beaches across various coastlines worldwide (e.g. Morris and Butler, 1973; Ohya et al., 1973; Curtis and Saner, 1974; Dwivedi and Parulekar, 1974; Burns et al., 1982; Golik, 1982; Georges and Oostdam, 1983; Corbin et al., 1993; Henry et al., 1993; Lorenson et al., 2009; Edwards et al., 2016; Shirneshan et al., 2016; Suneel et al., 2016). In many of these studies, particularly those conducted between the

1970s and 1990s, the majority of oil strandings were linked to anthropogenic sources, such as the flushing of oil shipping tankers with seawater during cleaning, or oil spills. Assessment of the inputs of oil into the global ocean from 1975 to 2002 suggests that the relative proportion of oil contributed to the ocean by human activity has declined (NAS, 2003), either due to improvements in environmental constraints or unrecognised errors in the previous assessments of global oil seepage (Kvenvolden and Cooper, 2003). While large oil slicks in the ocean may be identified and potentially quantified using remote sensing tools (e.g. MacDonald et al., 1993, 1996; Brekke and Solberg, 2005; Fingas and Brown, 2014), assessment of the environmental impact of oil on the coastal environment typically requires surveying to assess the abundance of oil at each location. In the event of an oil spill, a lack of characterisation of the "background" oil inputs to a given coastline from natural seeps can cause confusion and significant difficulty when assessing the environmental impact of the spill itself and managing the clean-up activities (Henry et al., 1993). Identifying the different types of oil released from offshore seepage which accumulate along a given coastline, in addition to their spatial distribution and abundance may be used to define the natural baseline conditions or "background" petroleum contamination levels in the region, which may act as a metric for comparison against pollution from other anthropogenic sources of oil such as spills (Kvenvolden and Cooper, 2003). Such baselines may also be used to assess the effectiveness of environmental remediation following an oil spill by ensuring the concentration of hydrocarbons in the affected area has returned to pre-incident levels (Hook et al., 2016).

This is the second of two research articles intended to summarise the present understanding of the occurrence of crude oil strandings along the South Australian coastline. The first article outlined the visual/physical and geochemical parameters which may be used to identify the different types of oils collected from the coastline (Corrick et al., 2020a). Here we document the spatial distribution and abundance of these different oils and use this information to construct a hydrocarbon loading baseline for the region.

1.1. The occurrence of crude oil on the South Australian coastline

Historical reports of semi-solid crude oils stranding on the coastline of South Australia date back to the mid-late 1800's (Trewartha, 1850; Tolmer, 1882; Howchin, 1903; Ward 1913; Howchin 1919; Ward, 1944; Sprigg and Woolley, 1963). Commonly referred to as 'coastal bitumens', many of these strandings pre-date offshore oil exploration and/or the shipping of petroleum by tanker in South Australian waters, supporting the interpretation that these

particular oils originated from natural seepage, rather than anthropogenic sources (Edwards et al., 2016).

The majority of research associated with Australian coastal bitumens has sought to use their geochemistry to characterise and locate their parent petroleum systems. The most recent classification scheme for South Australian oil strandings is based on the same suite of samples collected in this study, in addition to specimens donated from private collections (Corrick et al., 2020a). This scheme divides identification into three stages of increasing detail and analytical complexity. An initial assessment can be completed upon collection of the oil from the coastline. Based on their visual characteristics the stranded oils may be separated into three general varieties: asphaltites, waxy bitumens and soft tars (Fig. 1). Bulk geochemical screening using whole-oil gas chromatography mass-spectrometry (GC-MS) may further separate these into nine different types (two of which correspond to highly degraded variants which cannot be reliably classified), while detailed geochemical assessment using source-specific biomarkers has presently identified at least 16 unique oils (Corrick et al., 2020a).

Asphaltites are the most visually distinctive variety of coastal bitumen observed on the coastline (Fig. 1A). Defined by their jet-black colour, petroliferous odour and devolatilization cracks, these large bitumens can reach up to 7 kg in weight (Edwards et al., 1998). They may be slightly soft and pliable when fresh, but upon mild weathering or devolatilization during storage they quickly become brittle and will break with a diagnostic conchoidal fracture not observed in any of the other types of oil encountered on the South Australian coastline. Geochemical assessment of all the asphaltites collected from pre-1900 to the present day demonstrate their highly uniform composition and occurrence on the coastline prior to offshore oil exploration or tanker shipping in the region (Padley, 1995; Volkman et al., 1992; Edwards et al., 1998; Boreham et al., 2001; Hall et al., 2014; Scarlett et al., 2019; Corrick et al., 2020a, 2020b). Source- and maturity-specific parameters indicate that the asphaltites originated from a Mesozoic marine shale deposited under anoxic conditions, most likely an ocean anoxic event (OAE), which expelled hydrocarbons during the early oil window (Edwards et al., 1998; Boreham et al., 2001; Hall et al., 2014; Scarlett et al., 2019; Corrick et al., 2020b). Inspection of approximately 4000 oils using the GeoMark^{TM} global petroleum database revealed that the composition of the asphaltites is not consistent with any known petroleum system (Summons et al., 2001). However, they are presently thought to originate from the nearby Bight Basin (Boreham et al., 2001; Totterdell et al., 2008; Hall et al., 2014; Corrick et al., 2020b).

Waxy bitumens, also commonly referred to as tar balls, have been reported on the South Australian coastline for over a century (Edwards et al., 2018; Sprigg and Woolley, 1963). These rounded bitumens are semi-solid to solid and typically 1–5cm in diameter, although larger examples can occur. These strandings are coated with a surficial layer of sand, which is commonly shed in highly weathered examples as the exterior solidifies (e.g. Figs. 1B, 1C). The number of oil families identified from waxy bitumens recovered from Australia's southern margin has progressively increased through time as a greater number of samples could be collected and analysed (McKirdy and Horvath, 1976; McKirdy, 1984a, 1984b; Padley, 1995; Edwards et al., 2016, 2018; Corrick et al., 2020a).

The most recent geochemical assessment of South Australian waxy bitumens defines four types (I–IV) on the basis of key features recognisable in a total ion chromatogram of the whole-oil (summarised in section 2.2). Further assessment on the basis of source-specific biomarker assemblages revealed and a total of fourteen distinct oils derived from source rocks deposited in a range of different depositional environments (Corrick et al., 2020a). The majority of these different waxy oils are thought to originate from petroleum systems in Southeast Asia (Edwards et al., 2016, 2018; Corrick et al., 2020a). In particular, the most abundant type of waxy bitumen (type I), defined by its high abundance of the freshwater algal biomarker botryococcane, is correlated to the region on the basis that this rare molecular fossil, derived from race B of the freshwater green alga Botryococcus braunii, has only been reported in Cenozoic lacustrine oils from Central Sumatra, South Sumatra, Sunda and NW Java basins in the Indonesian Archipelago (Moldowan and Seifert, 1980; Seifert and Moldowan, 1981; ten Haven and Schiefelbein, 1995; Hwang et al., 2002) and the Eocene Maoming oil shale in the Maonan Basin, China (Brassell et al., 1986). Many of the other waxy bitumen oil families also contain terrestrial molecular markers such as oleanane, bicadinanes and taraxastane. These markers are not typically associated with oils recognised from Australian sedimentary basins but are common in oils produced in SE Asia (ten Haven and Schiefelbein, 1995; Edwards et al., 2018). However, whilst the majority of the different waxy bitumen oil families contain markers characteristic of sedimentary basins in SE Asia, there are several marine oil families which lack these compounds and therefore could potentially be originate from an Australian basin, however further study is required to assess this in greater detail (Corrick et al., 2020a; Edwards et al., 2018).

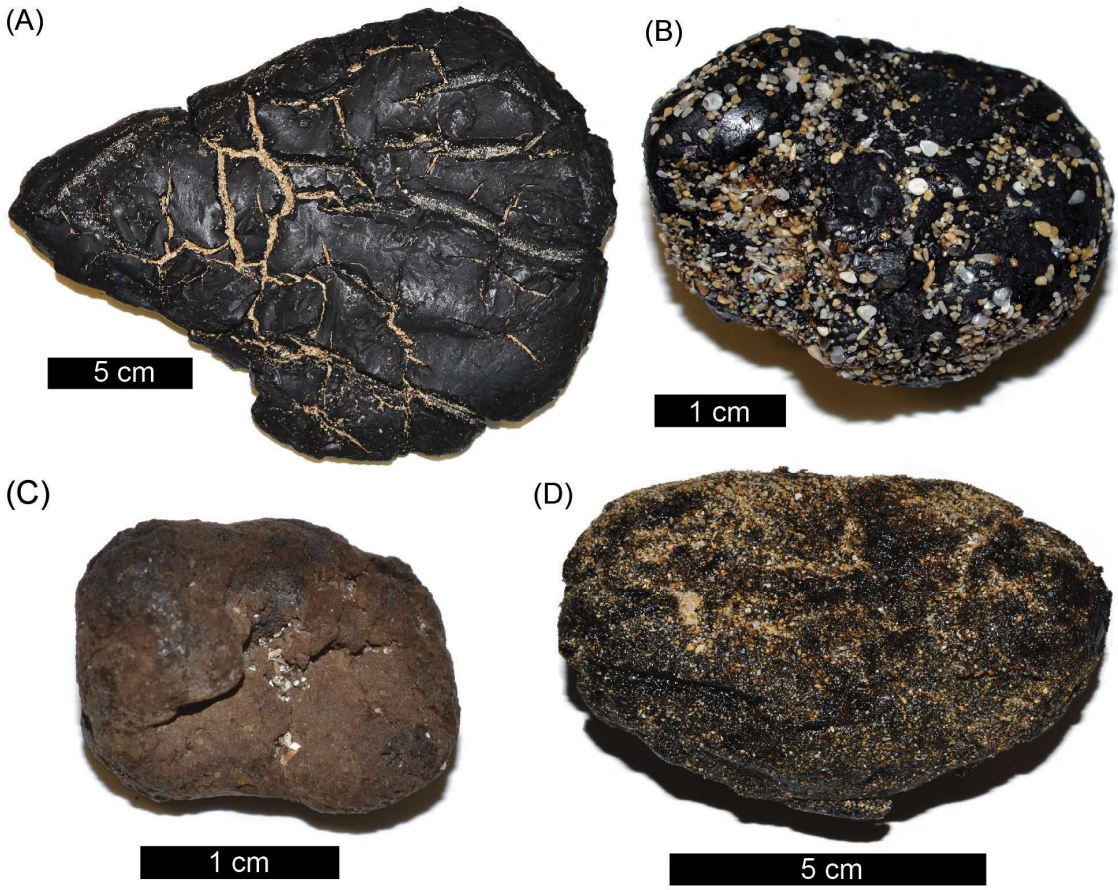


Figure 1: Examples of crude oils found on the South Australian coastline. (A) Asphaltite sample W13/007507. (B) Asphaltic tar sample /001059. (C) Waxy bitumen sample W13/007499. (D) Highly weathered waxy bitumen sample W13/007521, which has oxidised and formed a solid brown exterior.

Although the numerous different waxy bitumens are geochemically consistent with the general geochemical characteristics of petroleum systems across the Indonesian Archipelago, there are few direct correlations linking these strandings from the Australian coastline to a specific produced oil in the region (Edwards et al., 2018; Corrick et al., 2020a). This may be attributed to the fact that many oils across the region demonstrate broadly comparable geochemistry and thus isolating a specific basin for an oil is not always straightforward (Corrick et al., 2020a). Furthermore, detailed assessments against the available geochemical datasets from produced oils will often demonstrate that despite a high degree of similarity, sufficient variations exist between the coastal strandings and produced oils to question the validity of the correlation (e.g. Edwards et al., 2018). This is not entirely unexpected, as lateral variations in the source-specific biomarker ratios from oils obtained across basins in this region can be substantial (e.g. Hwang et al., 2002; Curiale et al., 2005). Therefore, definitive correlations in most cases will likely require identification of the parent seafloor seep and a direct comparison of its emitted oil to

examples recovered from the Australian coastline, rather than comparison of coastal oil strandings to those obtained predominantly from onshore oil production.

In addition to the asphaltites and waxy bitumens, a third variety of stranded oil recently identified by Corrick et al. (2020a, 2020b) is referred to as tars (Fig. 1D). These strandings are soft and viscous, unlike the predominantly semi-solid to solid waxy bitumens or asphaltites. Only two types of tar were identified, each recovered from a single respective stranding site in 2016 following severe storm activity. The first type, referred to as Sandy River tars, after their stranding site on Kangaroo Island, show strong geochemical similarities to other oils attributed to SE Asia. Unlike the relatively solid waxy bitumens attributed to the region, the Sandy River tars also show degradation characteristics indicating they likely formed via biodegradation and emulsification of a liquid oil due to weathering in the marine environment (Corrick et al., 2020a). The second type, referred to as asphaltic tars, show a strong degree of geochemical similarity to the asphaltites and hence are likewise thought to originate from the Bight Basin (Corrick et al., 2020b).

The oils attributed to seepage from petroleum systems in SE Asia are delivered to the Australian coastline by regional ocean currents, most notably the North Pacific thermocline, which feeds into the headwaters of the Leeuwin Current, transporting the oils to the Great Australian Bight (Fig. 2). This is supported by the occurrence of waxy bitumens along the coastlines of the Northern Territory (McKirdy and Horvath, 1976; Summons et al., 1993) and Western Australia (Currie et al., 1992; Alexander et al., 1994) adjacent to the pathway of the Leeuwin Current before it reaches the Great Australian Bight. After arriving in the Great Australian Bight, the coastal current then carries the bitumens on to the waters of South Australia and western Victoria (Edwards et al., 2016). Further evidence of this oceanic transportation pathway is also provided by strandings of fossilised tree resins (resinites) along the South Australian coastline which originate from resinous hardwoods not found in Australia, but are common in SE Asia (Murray et al., 1994).

Finally, previous coastal surveys of South Australia and Victoria undertaken in the 1990's identified oil slicks which were attributed to local spillage and maritime traffic (Padley et al., 1993; Padley, 1995; Edwards et al., 2016). These oils occurred as thin sheets up to 5 mm thick or liquid globules approximately 10–20 mm in diameter. They resulted from discrete spill events with little temporal continuity. When revisited two to four months following the initial

stranding, little evidence of the oil remained aside from solidified oil spots on rocks and hard discs of oil-cemented sand (Edwards et al., 2016). Although several oil slicks occurred during the course of the previous coastal surveys, no significant oil spills were reported between 2014–2016 in Australian waters (Australian Maritime Safety Authority, 2014, 2015, 2016, 2019) and therefore no examples of such liquid oils are included within the current classification schemes (Corrick et al., 2020a). The two tar varieties could potentially be considered oil slicks based on the definition by Edwards et al., (2016) which included the occurrence of sticky tars, although neither of the two varieties identified between 2014–2016 have been demonstrated as anthropogenic in origin (Corrick et al., 2020a, 2020b).

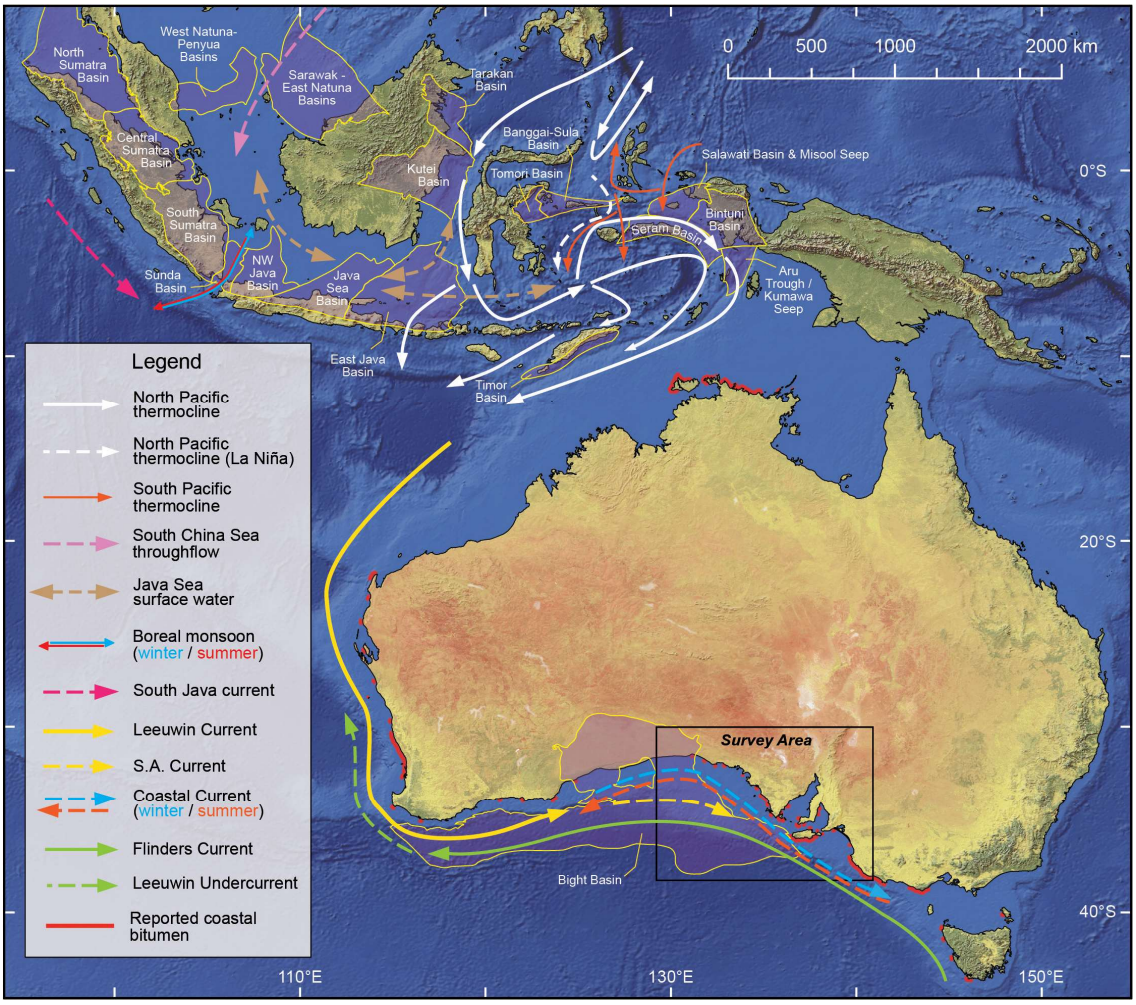


Figure 2: Sites of bitumen stranding on the Australian coastline, selected sedimentary basins and simplified relevant ocean currents after Corrick et al., (2020b).

1.2. The 1990–1991 hydrocarbon loading baseline

All previous geospatial surveys of South Australian coastal bitumen are of limited extent and reproducibility, particularly given the lack of handheld global positioning systems (GPS) to assist with surveying at the time. The first such studies were undertaken by the South Australian Department of Mines and Energy (SADME) in 1983 (McKirdy, 1984a, 1984b). However, they did not record the distance surveyed at each site and therefore their findings could not be used to determine an environmental baseline. A series of follow-up surveys conducted in 1990–1991 compiled an extensive suite of samples from the South Australian and western Victorian coastlines in addition to historical examples donated from private collections (Padley, 1995; Padley et al., 1993). Although samples were collected from a wide geographic area, systematic surveying was limited to six ocean beaches where lengths of 200–300 m of coastline were revisited every 2–4 months. The highly variable abundances of bitumen collected during these surveys demonstrated that the amount of oil stranding on the coastline is seasonally controlled, with the highest number of pieces recovered in September/October (Padley, 1995; Edwards et al., 2016). As the first surveys to document the distance logged at each location, and the total number of samples and weight of oil collected, the results from these surveys were recently used to retroactively establish the historical environmental baseline for the occurrence of waxy bitumens along the south-eastern portion of the South Australian coastline (Edwards et al., 2016). The hydrocarbon loading from these six beaches is summarised in Figure 3 and associated data listed in Table S1.

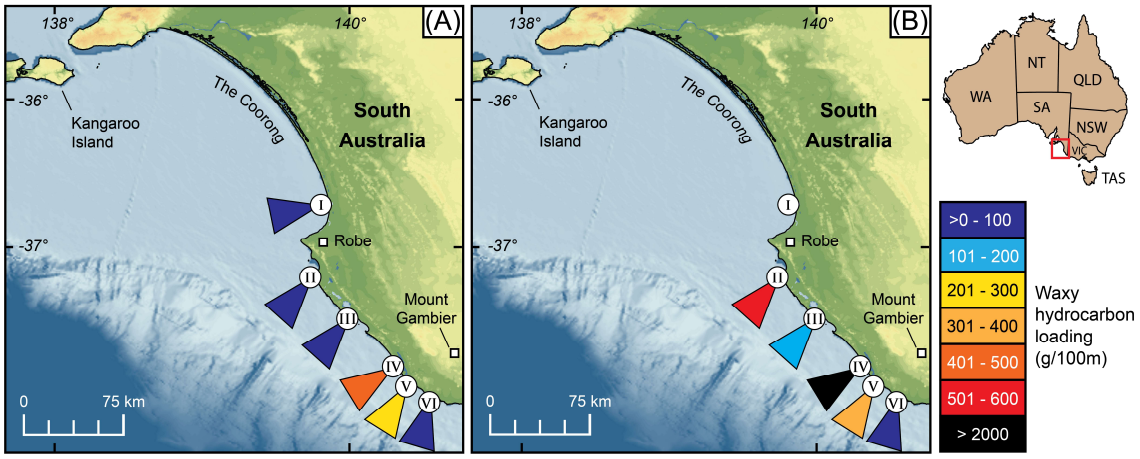


Figure 3: The hydrocarbon loading, expressed as the average weight of oil in grams per 100m of coastline for six beaches (I-VI) on the southeast of the South Australian coastline based on the results of Edwards et al. (2016). (A) Waxy hydrocarbon loading from September 1990. (B) Waxy hydrocarbon loading from September 1991. The results of these surveys are summarised for reference in Table S1.

1.3. Present investigation

To establish a modern hydrocarbon loading baseline across the South Australian coastline, three annual surveys were conducted between 2014–2016 as part of the Great Australian Bight Research Program (Baghurst et al., 2017; Ross et al., 2017). This provides the first quantitative assessment of hydrocarbon loading for Kangaroo Island and the coastline west of the Eyre Peninsula. It also significantly revises the existing baseline for the south-eastern coastline defined by the results of the aforementioned surveys conducted in 1990 and 1991 (Edwards et al., 2016).

2. MATERIALS AND METHODS

2.1. Coastal surveying

Coastal surveys were conducted in November 2014, September 2015 and October 2016. Their timing was influenced by the observation that the abundance of bitumen strandings is greatest in September/October, based on surveys conducted at 2–4 month intervals throughout 1990 and 1991 (Padley, 1995; Edwards et al., 2016). However, these prior surveys were restricted to south-eastern South Australia and hence there was no existing systematic survey data for the occurrence of crude oil strandings west of the southern tip of Eyre Peninsula. A total of 30 beaches were selected for systematic surveying on the basis of accessibility, distance from the previous/subsequent sites and beach aspect. The location of each survey site is shown in Figure 4, while the co-ordinates for beach access points and the distance surveyed each year are provided in Table S2. The survey area provides wide coverage of the state's coastline, with the exception of Spencer’s Gulf and the Gulf of St. Vincent. These areas were excluded because of their assumed greater potential for anthropogenic influence on the survey results arising from local maritime traffic and large numbers of beachgoers (discussed further in Section 4.3.3.). At each location a team of surveyors used an ‘Emu Parade’ approach, walking along the beach between the shoreline and the backshore to obtain the highest possible visual coverage. For each location the co-ordinates of the survey start and end points were logged using a GPS. The stranding co-ordinates of each individual bitumen specimen were recorded before the sample was retrieved while wearing nitrile gloves and placed in aluminium foil to prevent potential contamination. Other metadata collected for each survey site included wind direction; beach shape, aspect and slope; backshore type; dominant substrate; intertidal zone lengths; wave height; weather status; and the abundance of marine debris. These metadata are compiled in the supplementary data files of Ross et al., (2017) but are not discussed in further detail here.

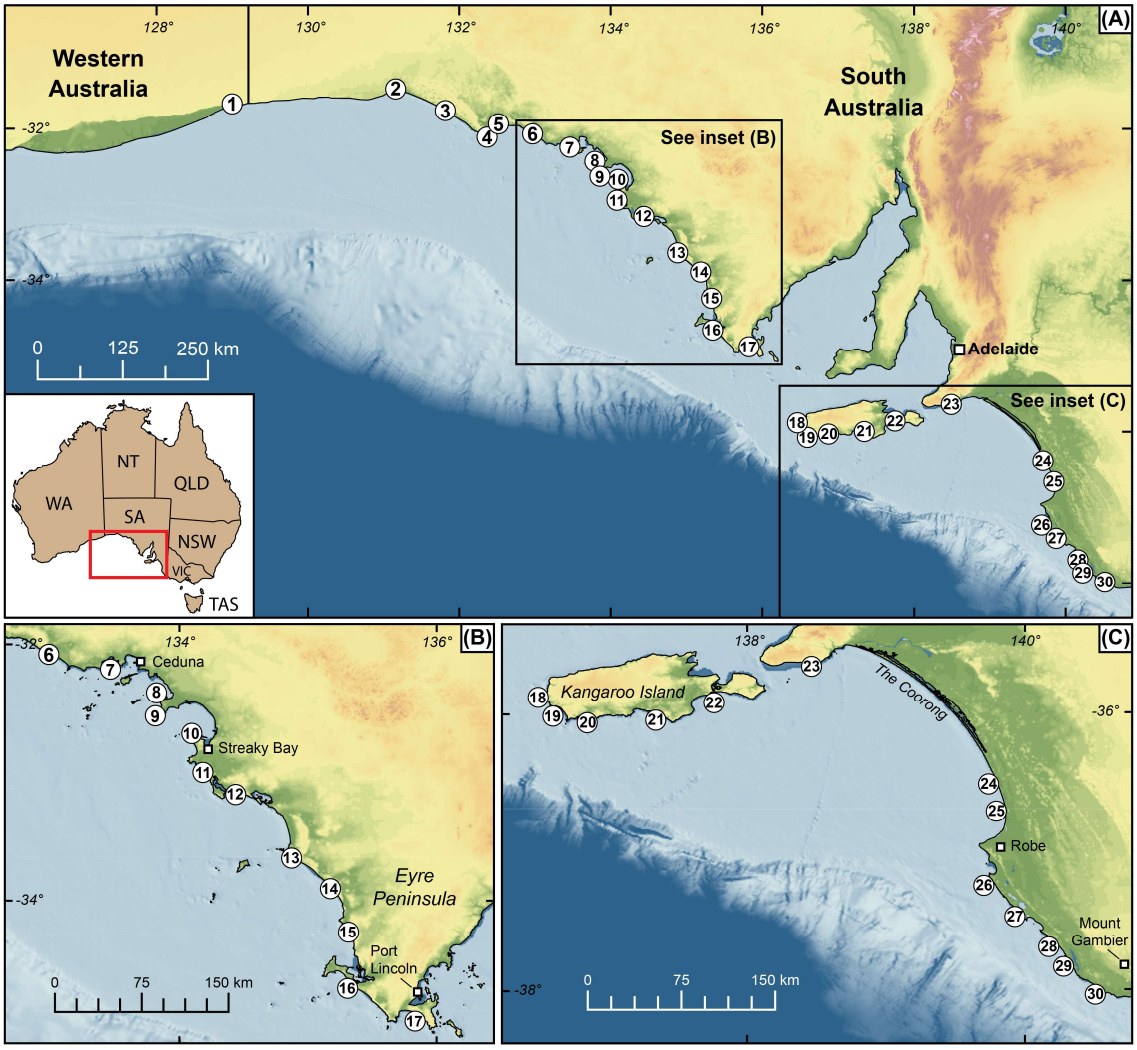


Figure 4: Survey sites visited annually in 2014–2016. Beach names, co-ordinates and survey lengths are listed in Table S2.

2.2. Sample classification by whole-oil GC-MS

All collected bitumens were classified using a whole-oil GC-MS screening approach defined by Corrick et al. (2020a), which is summarised below. For the purposes of establishing an environmental baseline, the whole-oil classification scheme is a practical compromise between visual assessment of oil strandings and detailed geochemical assessments utilising analysis of source-specific biomarker assemblages. The latter approach requires a greater investment in sample preparation, analysis and data processing for each individual sample that is impractical when assessing a large sample suite, such as that in the present study. Although it cannot distinguish all seventeen of the oil types which may be identified by assessing source-specific biomarker assemblages, assessment via whole-oil GC-MS is rapid, requiring minimal sample preparation and data processing. The resulting classification relies on the recognition of

reproducible features unique to each category and is sufficient to separate the oils into several types: asphaltites, asphaltic tars, waxy bitumen types I–IV and Sandy River tars. A further two classifications, known as degraded high-wax bitumen and unknown/other were also reserved for highly weathered strandings for which classification was uncertain.

Asphaltites and asphaltic tars may be distinguished from the waxy oils recovered from the South Australian coastline on the basis of their abundant branched/cyclic fraction relative to *n*-alkanes and their consistently low abundance of C_{33+} *n*-alkanes (Fig. 5). Additionally, both asphaltic oil types typically preserve *n*-alkanes in the range $<C_{13}$, the few exceptions being extensively weathered specimens. Preservation of such low-molecular-weight *n*-alkanes was not observed in the various waxy oil families. Notwithstanding their similar unimodal *n*-alkane profiles, which may vary due to weathering, these two asphaltic oils may be differentiated by their respective pristane/phytane ratios. Asphaltites systematically contain more pristane than phytane, while the opposite is true for the asphaltic tars.

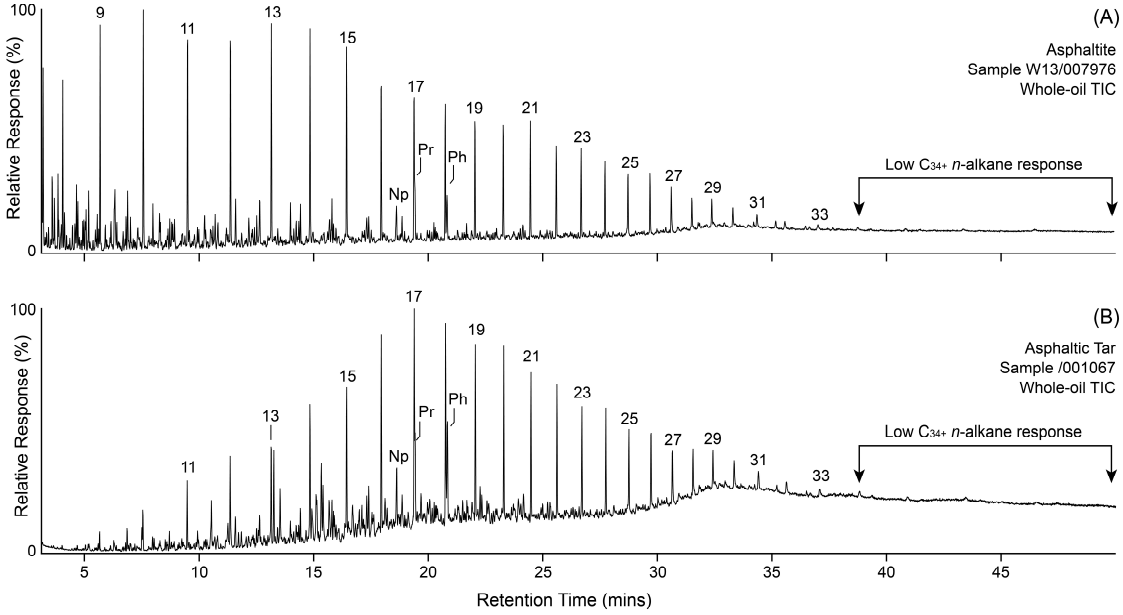


Figure 5: Whole-oil total ion chromatograms for asphaltic oils collected from the South Australian coastline after Corrick et al. (2020a). (A) Fresh asphaltite. (B) Asphaltic tar. Peak numbers correspond to *n*-alkane chain length, Np = norpristane, Pr = pristane, Ph = phytane.

The waxy oil strandings may be classified into several different types on the basis of reproducible features in their whole-oil total ion chromatograms (Fig. 6). Type I and II waxy bitumens are readily identifiable by the presence of botryococcane. In type I waxy bitumens,

the abundance of botryococcane exceeds that of the high-molecular-weight *n*-alkanes in the $C_{35–39}$ range. The type II waxy bitumens contain a higher abundance of these high-molecular-weight *n*-alkanes relative to botryococcane, which exhibits a lower response. The type III and IV waxy bitumens are defined by their lack of botryococcane and distinguished from one another by their relative abundances of $C_{35–39}$ *n*-alkanes. These two varieties of waxy oil require further assessment, as both appear to comprise multiple oil families when examined in greater detail using source-specific molecular markers.

The Sandy River tar strandings are also considered to be waxy oils, despite their extensive degradation which has resulted in a low abundance of *n*-alkanes in all recovered specimens. The whole-oil chromatograms of these tars exhibit a bimodal unresolved complex mixture (UCM) and a pristane or phytane maximum, a feature rarely observed in weathered coastal bitumens where these two acyclic isoprenoids are usually lost shortly after the adjacent *n*-alkanes (Corrick et al., 2020a). Additionally, these tars lack *n*-alkanes $>C_{33}$, distinguishing them from waxy bitumen types II and IV. Although their extensively degraded nature has removed the majority of their *n*-alkane fraction, these tar strandings are considered waxy oils on the basis of the similarity of their source-specific biomarker composition to that of several other types of waxy bitumen (Corrick et al., 2020a).

Finally, highly weathered bitumens lacking *n*-alkanes $<C_{29}$ were typically classified as degraded high-wax bitumens. These likely represent weathered examples of type II or IV waxy bitumens which could not be distinguished without further analysis. Other stranded crude oils which could not be classified into one of the above types were categorised as unknown/other. Oils assigned to this latter category were typically too weathered to reliably identify. For further discussion of alteration associated with weathering see Corrick et al. (2020a).

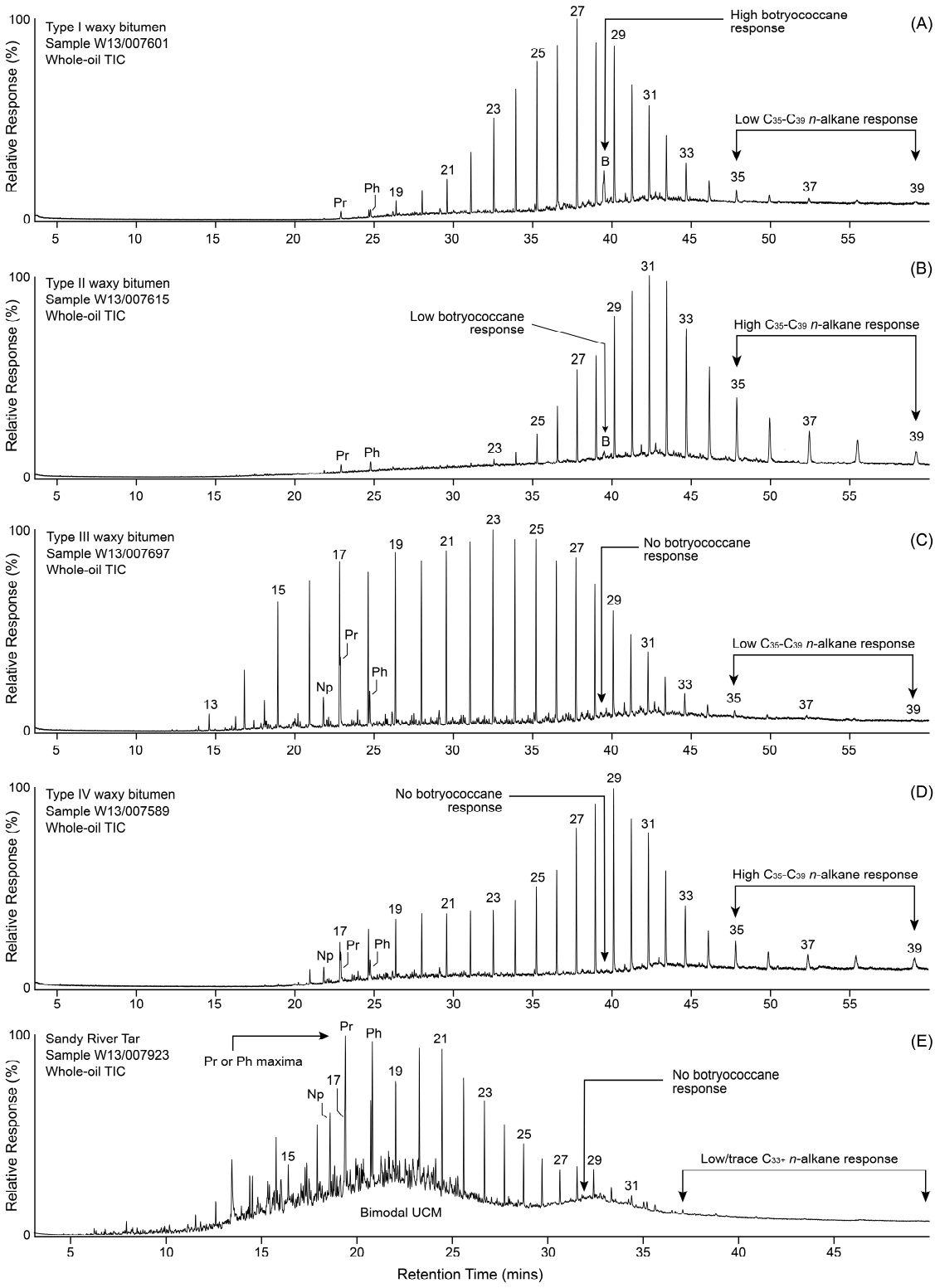


Figure 6: Representative whole-oil total ion chromatograms of various waxy oils collected from the South Australian coastline after Corrick et al., (2020a). (A) Type I waxy bitumen. (B) Type II waxy bitumen. (C) Type III waxy bitumen. (D) Type IV waxy bitumen. (E) Sandy River tar. Peak numbers correspond to *n*-alkane chain length, Np = pristane, Pr = pristane, Ph = phytane, B = botryococcane.

2.3. Quantification of hydrocarbon loading

The abundance of crude oil found at each survey site can be expressed in several ways. Because all of the oil found on the South Australian coastline between 2014 and 2016 was semi-solid or solid and hence could be easily removed from the beach (unlike liquid oil), its hydrocarbon loading may be expressed using three metrics: (1) the number of pieces of oil recovered; (2) the total weight of oil collected at each site; or (3) the average weight of oil collected per 100m. As these oil strandings vary significantly in size, from <1 g up to several kilograms, use of only one of the above parameters can easily misrepresent the true nature of the loading of a particular portion of the coastline. For example, if a single large asphaltite is collected during a survey, the hydrocarbon loading of that site may seem low if expressed in terms of the number of samples but high in terms of total weight of oil, while the average weight of oil per 100 m would vary considerably depending the survey length. Therefore, in order to accurately describe each site, all three metrics are provided for each site in the supplementary information.

Hydrocarbon loading is separated into two categories: asphaltic and waxy, given the former tend to strand as larger pieces than the latter. The asphaltic oil classification encompasses both the asphaltites and the recently discovered asphaltic tars, while the waxy oil classification encompasses the waxy bitumen types I–IV, degraded high wax bitumens and the Sandy River tar strandings. As both varieties of asphaltic oil are presently considered to originate from the nearby Bight Basin (Corrick et al., 2020b), while the waxy oils are attributed petroleum systems in SE Asia (Edwards et al., 2018; Corrick et al., 2020a), this approach also distinguishes the impact of seepage from local versus distant petroleum systems on the coastline. Furthermore, the separation of the asphaltic and waxy oils allows the results to be directly comparable to the 1990/1991 surveys, which did not encounter any asphaltic oils at their six systematic surveyed beaches (Edwards et al., 2016). The few specimens classified as unknown/other were excluded from the asphaltic and waxy loading estimates as they could not be reliably assigned to either category. However, their details are included within the supplementary information for reference.

3. RESULTS

Summaries of the total number of samples and total weight of oil collected in each whole-oil classification during the 2014–2016 surveys are listed in Tables S3 and S4, respectively. The waxy and asphaltic and hydrocarbon loading values for each survey site are provided in Tables

S5 and S6. The hydrocarbon loading from the few oils classified as unknown/other is provided in Table S7 for reference but is not discussed further. Finally, the details of each individual oil specimen collected during each of the surveys are included in Tables S8–S10.

3.1. November 2014 hydrocarbon loading

The November 2014 hydrocarbon loading distribution across the survey area is shown in Figure 7. It comprises 94 bitumen specimens weighing a combined total of 2727 g. The co-ordinates, weight and classification of each individual sample may be found in Table S8. The distribution of oil recovered from the coastline during this survey is more limited than that observed during the subsequent surveys conducted in September 2015 and October 2016, with 15 of the 30 survey sites containing no asphaltites or waxy oils. This is attributed to seasonal variability, as historically less coastal bitumens have been reported on the southeastern beaches during November compared to September/October (Padley, 1995; Edwards et al., 2016). With the notable exception of Waitpinga Beach (site 23), asphaltites were predominantly found on beaches along the west coast of Eyre Peninsula. Waxy bitumens were primarily observed along the southeastern coast, with the most prominent collection point being Number 1 and 2 rocks (site 29).

Figure 8 summarises the relative proportion of each bitumen type, based on the whole-oil GC-MS classification scheme, in terms of number of samples collected and contribution to the total weight of oil recovered. A total of 51 type I waxy bitumens were collected, accounting for 54% of the 2014 sample suite. However, these abundant waxy bitumens contributed only 187 g or 7 wt % of the total oil collected during the 2014 survey. By comparison, the eight asphaltites recovered during this survey weighed 2302 g, or 84 wt % of the crude oil collected during this survey, due to their larger size in comparison to other bitumen types. Other waxy bitumen varieties (types II, III, IV and degraded high wax) represented the remaining 35% of collected specimens, but comprised <7 wt % of the oil collected during this survey. Only two samples weighing a combined total of 63 g were classified as unknown/other and excluded from the asphaltic and waxy hydrocarbon loading calculations. These samples were collected from Bales Beach (site 21) and Eve's Cove (site 26).

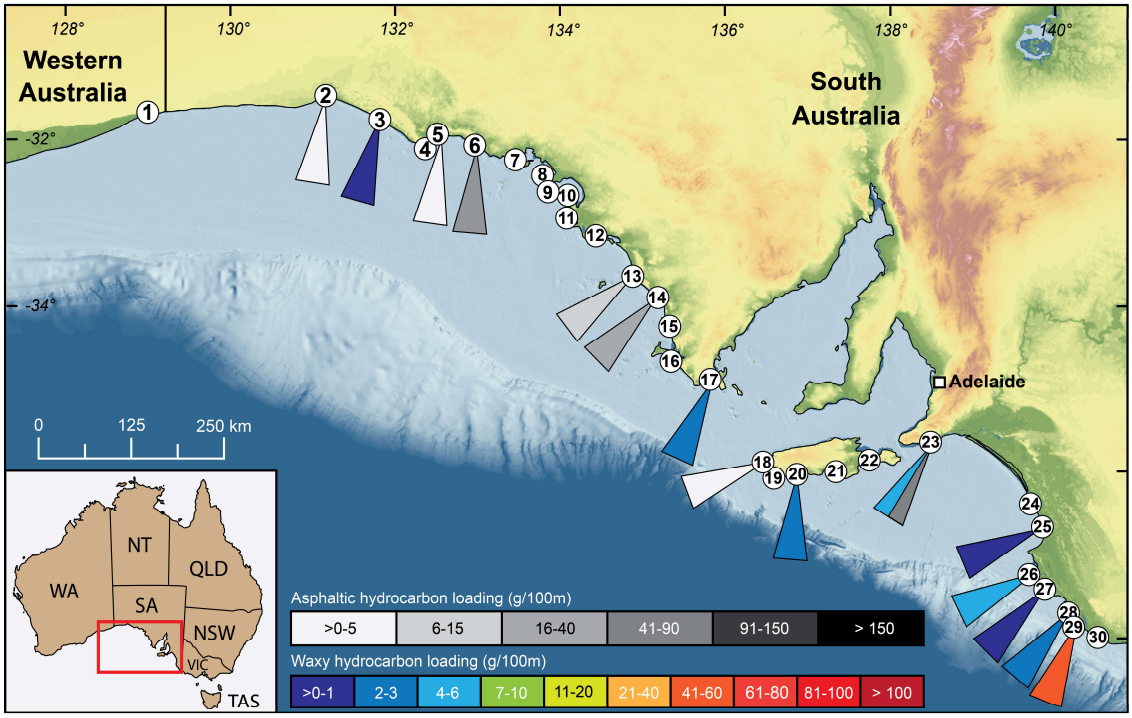


Figure 7: Summary of the hydrocarbon loading (in g/100 m) of the South Australian coastline based on the November 2014 survey.

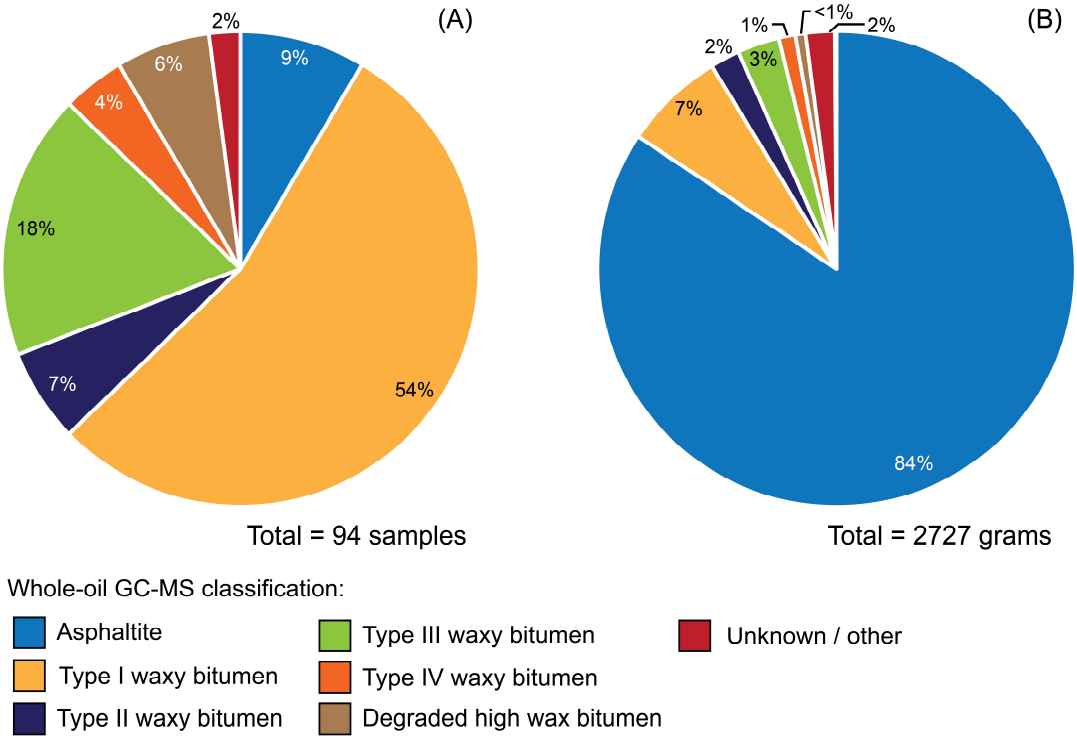


Figure 8: (A) Relative proportion of each whole-oil type collected during the 2014 survey based on number of pieces found. (B) Relative proportion of each whole-oil type collected during the 2014 survey by total weight.

3.2. September 2015 hydrocarbon loading

The September 2015 hydrocarbon loading distribution across the survey area is shown in Figure 9. This second survey recovered 97 bitumen specimens weighing a combined total of 2054 g. The co-ordinates, weight and classification of each individual sample are listed in Table S9. As in the 2014 survey, asphaltites were only found at survey sites on the western side of Eyre Peninsula. Waxy bitumen was collected from a larger number of western beaches, particularly Dogfence Beach (site 3), although strandings also remained concentrated along the southeastern coastline where the highest number of samples was again collected from Number 1 and 2 Rocks (site 29). The waxy hydrocarbon loading at this location doubled that observed in 2014 (109 g/100 m versus 53 g/100 m); and most other beaches along the southeastern coastline also exhibited elevated waxy hydrocarbon loadings relative to the previous survey.

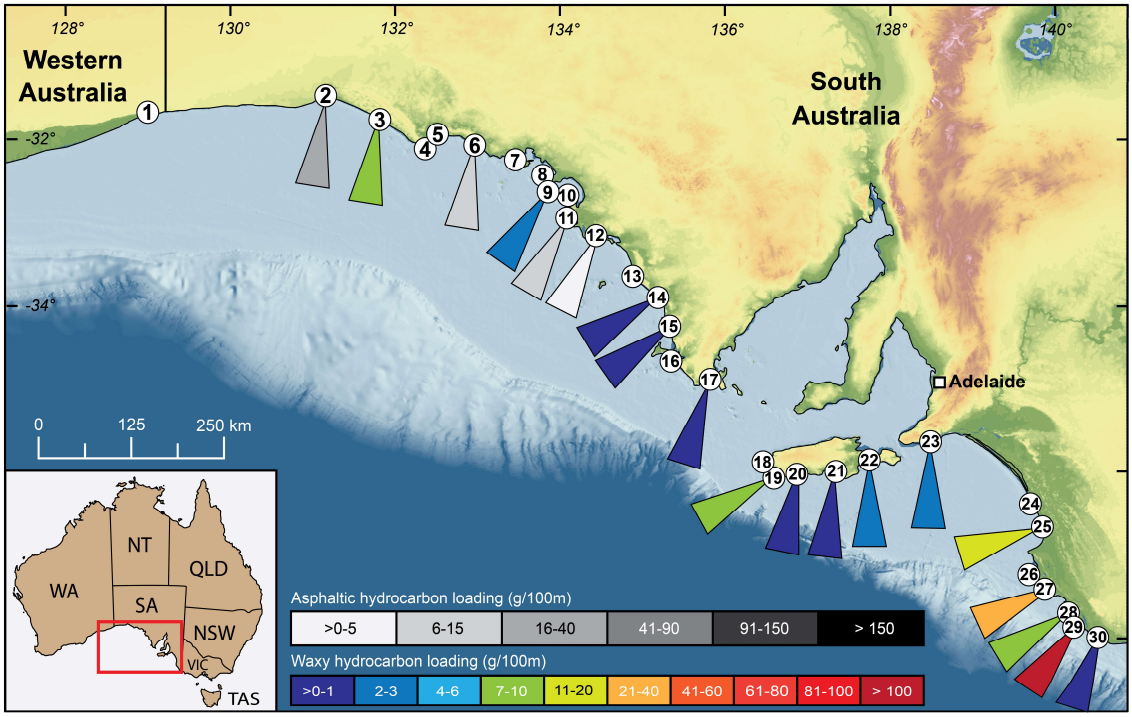


Figure 9: Summary of the hydrocarbon loading (in g/100 m) of the South Australian coastline based on the September 2015 survey.

The proportions of different bitumen varieties, in terms of the number of specimens and their contribution to the total weight of oil recovered in September 2015, are shown in Figure 10. Type I waxy bitumen remained the most commonly encountered type of crude oil, with 52 samples found, representing 54% of the total collection for that year. Although the number of type I waxy bitumens collected was comparable to the 2014 survey, the individual specimens

were larger, together weighing 607 g or 30 wt % of the total oil recovered for the 2015 survey. Thirteen asphaltites were collected, five more than in the previous survey but weighing only 830 g, compared to the previous survey's 2302 g. This difference is due to the fact that ten small pieces of asphaltite were recovered from Tractor Beach (site 11) which likely represent fragments of a larger original asphaltite. These fragments weighed between 1 and 31.5 g, and were heavily degraded in comparison to typical asphaltites. Most were not readily recognisable based on their whole-oil TIC chromatogram, due to the significant removal of selected compounds (see Corrick et al. 2020b: their Figure 6A). However, these samples remained identifiable as asphaltite due to their characteristic conchoidal fracture. Most of the total weight of asphaltite collected during 2015 is attributed to two individual specimens collected from Eyre Well (site 2) and Cactus Beach (site 6) weighing 276 and 429 g, respectively. The combined weight of asphaltites collected in 2015 represented 40% of the total oil by weight found during that survey, the smallest annual contribution of asphaltites to the coastline during the three surveys. As in the 2014 survey, only two of the collected bitumen specimens were classified as unknown/other (2% of the sample suite, <1% by weight) and they are excluded from the asphaltic and waxy hydrocarbon loading calculations. The two samples in question weighed a total of 17 g and were collected from Dogfence Beach (site 3) and Geltwood Beach (site 28) respectively.

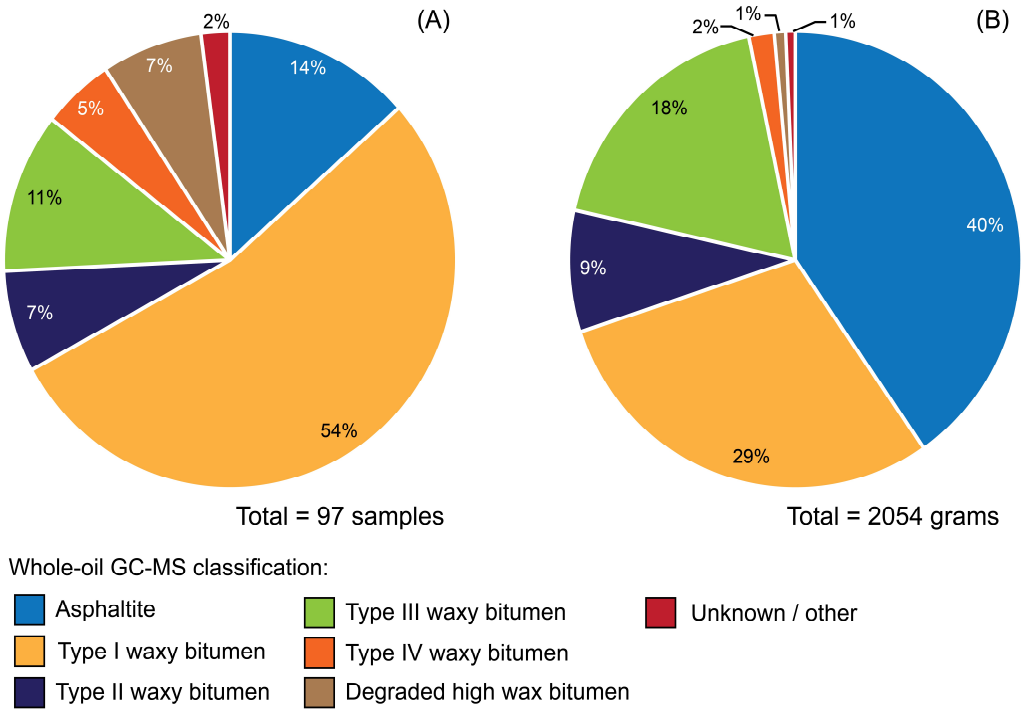


Figure 10: (A) Relative proportion of each whole-oil type collected during the 2015 survey based on number of pieces found. (B) Relative proportion of each whole-oil type collected during the 2015 survey by total weight.

3.3. October 2016 hydrocarbon loading

During the afternoon and evening of the 28th of September 2016, the Great Australian Bight and the entire South Australian coastline were affected by a severe storm event (Bureau of Meteorology, 2016; Burns et al., 2017). This storm gave rise to reports of hailstones up to 5 cm in diameter, localised intense rainfall and flooding, at least seven tornados and destructive winds which unearthed electrical transmission towers, resulting in widespread blackouts across the state (Bureau of Meteorology, 2016). These highly abnormal conditions clearly affected the results of the 2016 survey, which began eight days later on October 4th. Numerous beaches across the survey area were impacted, particularly those along west coast of Eyre Peninsula. Some beaches were stripped of sand, exposing underlying beachrock or bedrock and preventing safe access at points used in the prior two surveys (Fig. 11A). At many of the survey locations highly vegetated dune systems had undergone metre-scale erosion and received an abnormal amount of flotsam in the form of both oil strandings and/or marine debris (Fig. 11B). In certain locations the storm activity was also sufficient to cause significant damage to local coastal infrastructure (Fig. 11C). These abnormal conditions immediately prior to the 2016 survey undoubtedly altered the distribution and abundance of oil strandings along the South Australian coastline from that produced by the normal metocean regime. Therefore, the results of the 2016 survey should be considered atypical.

The October 2016 hydrocarbon loading distribution across the survey area is shown in Figure 12. The survey collected 317 pieces of crude oil with a combined weight of 5936 g. These values exceed the total number of strandings and weight of oil recovered during the 2014 and 2015 surveys. Notably, over half of the total weight of oil collected during the 2016 survey was contributed by a single asphaltite specimen (W13/007976) recovered from Waitpinga Beach (site 23), which weighed 3188 g. Whilst smaller than the largest reported asphaltite (viz. 7 kg: Edwards et al., 1998), this specimen from Waitpinga Beach was the largest individual oil stranding recovered during the 2014–2016 survey period and represents the least weathered asphaltite analysed to date.

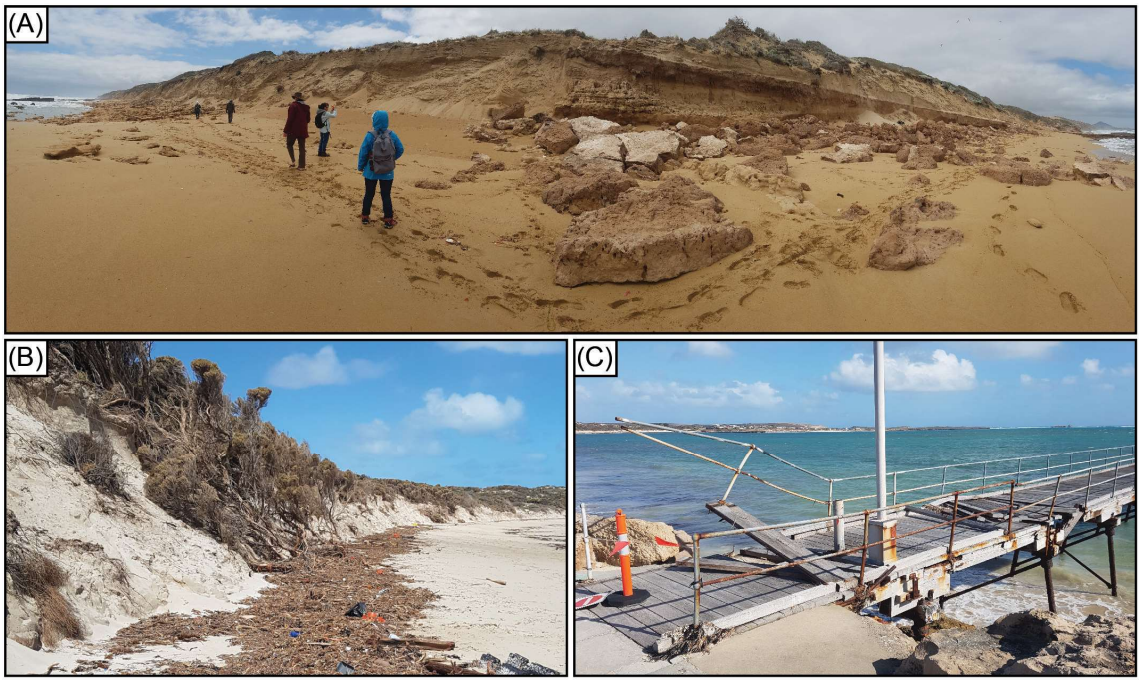


Figure 11: Photographs illustrating the impact of storm damage to coastal areas along the western Eyre Peninsula following the severe storm activity on 28 September 2016. (A) Prominent erosion of vegetated dune system and exposure of underlying beachrock at Mount Drummond (site 15). Previously these dunes continued to the beach at a low angle with no exposure of the underlying beachrock, but now the dunes end in unstable, metre-scale vertical sand faces. (B) Erosion and collapse of a heavily vegetated dune system at Elliston Beach (site 13) in addition to a large increase ocean-derived floatsam delivered to the backshore. (C) Significant structural damage to the jetty at Elliston following the storm event.

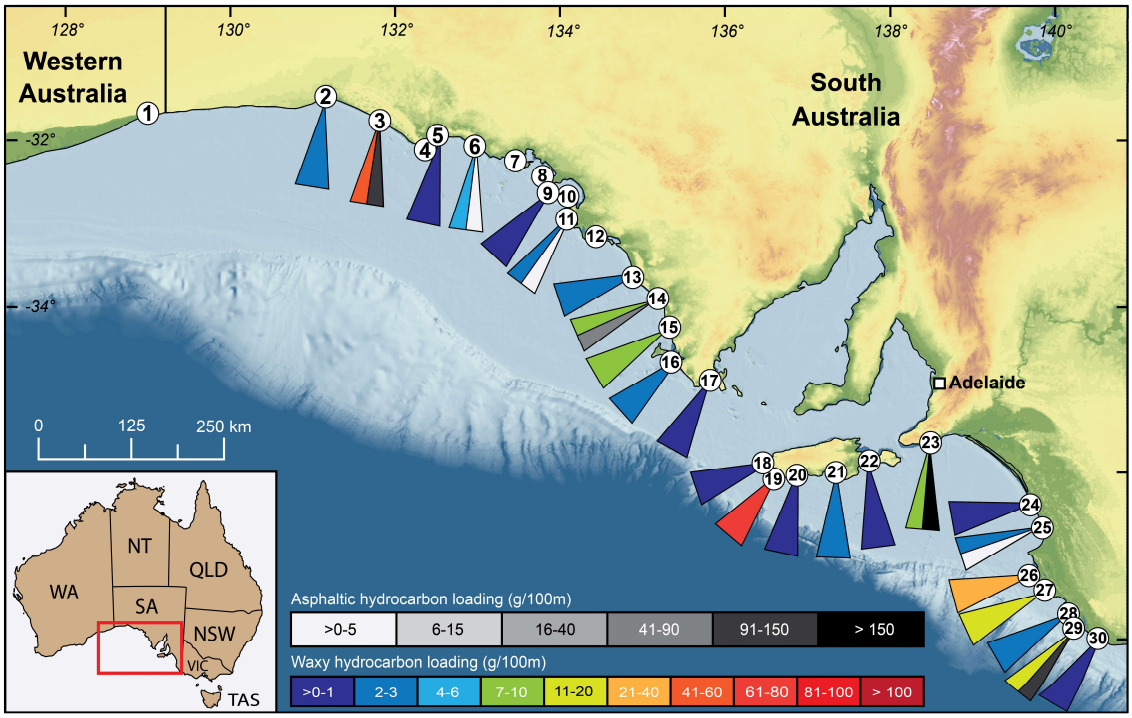


Figure 12: Summary of the average hydrocarbon loading (in g/100 m) for each survey site following the October 2016 survey.

Oil strandings were encountered at 25 of the 30 beaches visited. As in the 2015 survey, waxy bitumens were found in low abundance at sites along the western coastline of Eyre Peninsula, with the notable exception of a large number of strandings again accumulating at Dogfence Beach (site 3). Whilst such strandings were again common on the southeastern beaches, the most prominent collection point was Eve's Cove (site 26) rather than Number 1 and 2 Rocks (site 29). This was likely the result of the recent storm activity since the latter beach had undergone significant erosion and was stripped clean, as evidenced by the absence of other marine debris which typically occurs in extremely high abundance. The scoured beach contained less waxy bitumen strandings than either of the previous surveys. Unlike the surveys conducted during 2014 and 2016, no type II waxy bitumens were collected. However, two varieties of tar not found during the previous surveys (asphaltic tar and Sandy River tar) did occur in high abundance at Number 1 and 2 Rocks (site 29) and Sandy River (site 19), respectively.

The relative proportions of each oil type recovered in October 2016, expressed as the number of samples and their contribution to the total weight of stranded bitumen, are summarised in Figure 13. Despite the abnormal conditions and significantly reduced overall abundance of waxy bitumen at Number 1 and 2 Rocks (site 29), the type I waxy bitumens remained the most commonly encountered variety of crude oil, comprising 160 samples with a total weight of 720 g and representing 12% of all the specimens collected and 14% of the total oil by weight. Twelve asphaltites were collected weighing a total of 4220 g or 71% of the total weight of oil recovered during the survey, with the majority contributed by the aforementioned single specimen (3188 g) found on Waitpinga Beach (site 23). The larger population of oil strandings in 2016 also included a number of highly weathered samples classified as either degraded high wax bitumen or unknown/other. This is presumably due to storm activity bringing ashore specimens which had resided in the marine environment for a greater period of time and/or the unearthing of long-buried bitumens due to the severe erosion of shorelines and dune systems. A total of ten samples weighing a combined total of 45 g (3% of the 2016 sample suite, <1% by weight) were classified as unknown/other and excluded from the determined hydrocarbon loading values. These strandings were recovered from Dogfence Beach (site 3), Cactus Beach (site 6), Tractor Beach (site 11), Mount Drummond (site 15), Avoid Bay (site 16), Bales Beach (site 21), Eve's Cove (site 26) and Number 1 and 2 Rocks (site 29).

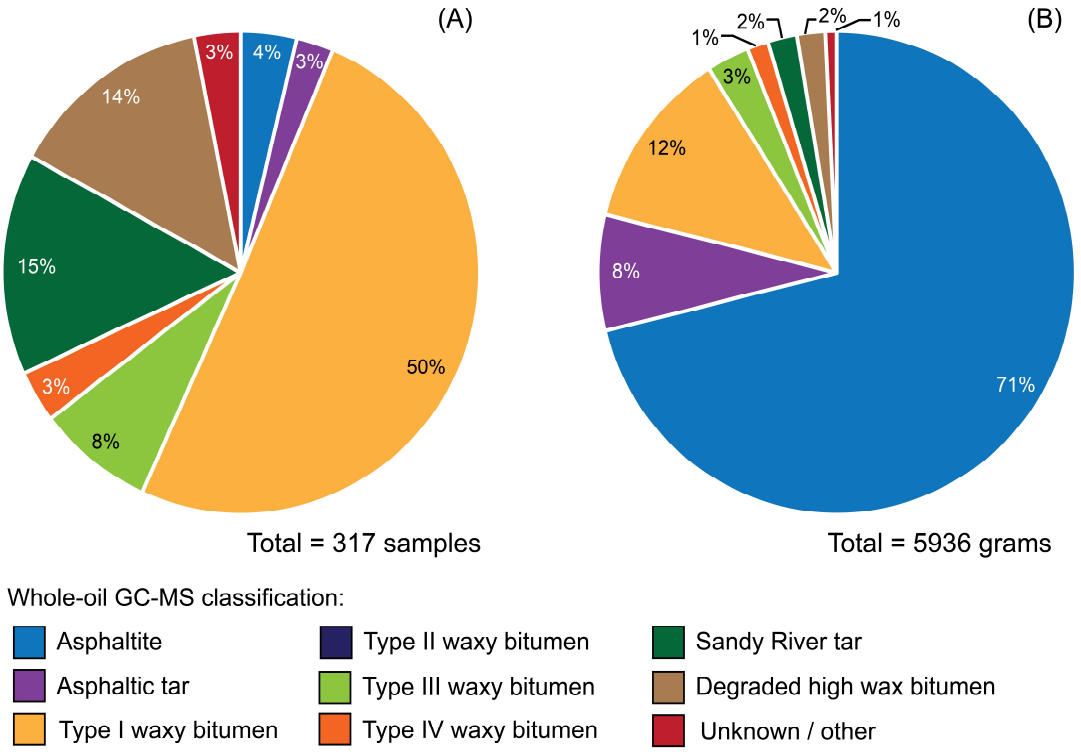


Figure 13: (A) Relative proportion of each whole-oil type collected during the 2016 survey based on number of pieces found. (B) Relative proportion of each whole-oil type collected during the 2016 survey by total weight.

3.4. 2014–2016 total summary

Across the three annual surveys a total of 508 pieces of crude oil were collected. The populations of different oil types in terms of number of pieces found and total weight collected for the entire sample suite from all three surveys is summarised in Figure 14. Consistently across all three surveys, the waxy bitumen containing abundant botryococcane (type I) was the most commonly encountered type of oil on the South Australian coastline, accounting for 52% of all stranded specimens. Asphaltites, whilst only representing 6% of the total sample suite, contributed 69% of the total weight of oil recovered from the coastline due to the generally larger size of individual specimens. The other oil types provided smaller contributions both in terms of the number of pieces collected and total weight of oil recovered. The remaining waxy bitumen varieties (types II-IV) combined represented 17% of the sample suite and 10% by weight. Degraded high wax bitumen was the second most abundant type of oil, representing 11% of all samples collected. However, oils in this category only account for 1% of the oil recovered in terms of weight. This is consistent with the fact that highly degraded pieces of oil are typically smaller than fresh examples. Similarly, the Sandy River tar strandings, found only during 2016, accounted for 9% of all collected oils due to their extremely high abundance at

their single stranding location. However, the small size of these tars resulted in their low total contribution by weight, accounting for only 1%. The asphaltic tars, which were larger than the tars found at Sandy River, contributed 4% of the total oil by weight and 2% in terms of number of pieces collected. This may be partly attributed to the short length of surveyed coastline at Number 1 and 2 Rocks (site 29), the only location where these oils were found. A longer survey would have undoubtably raised the relative contribution of this oil type based on the high frequency and moderate size of samples recovered within the short distance surveyed. Finally, oils classified as unknown/other represented only 3% of all oils collected, and 1% in terms of weight.

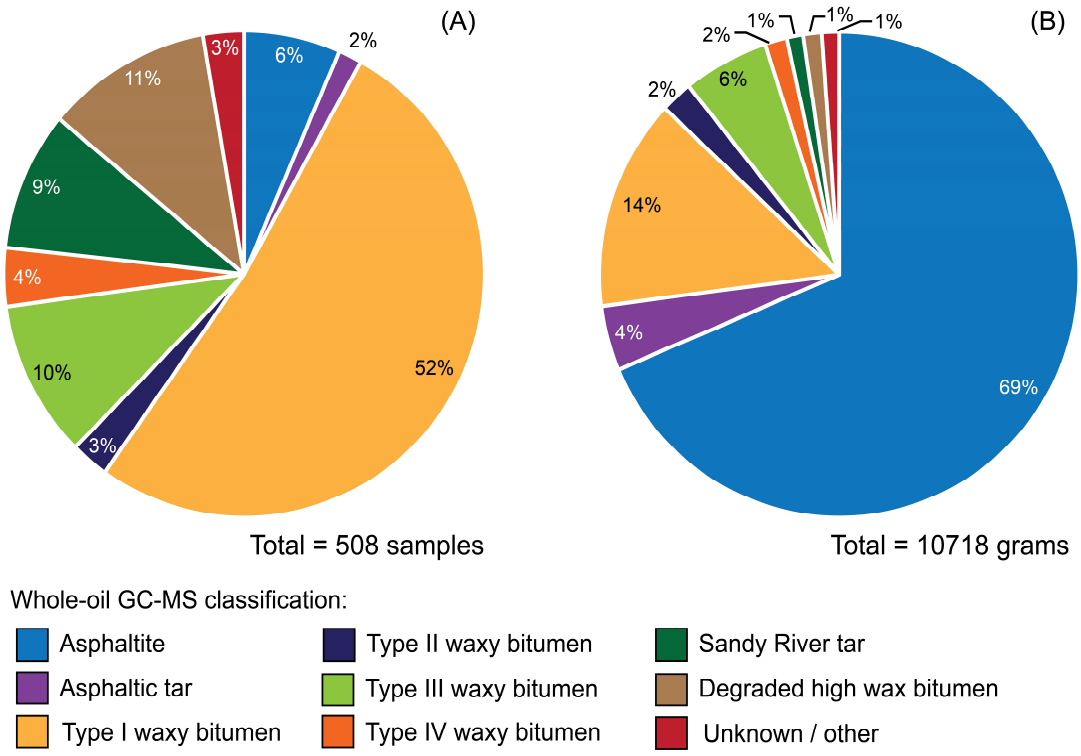


Figure 14: Comparison of the relative proportion of each whole-oil type by number of pieces collected and total weight contribution across the entire 2014–2016 sample suite. (A) Proportions of the number of samples. (B) Proportions of overall weight of material collected.

4. DISCUSSION

4.1. Comparison to the 1990–1991 hydrocarbon loading baseline

Four of the six beaches surveyed in September of 1990 and 1991 were also visited during this study: The Granites (site 25), Beachport Conservation Park (site 27), Number 1 and 2 Rocks (site 29) and Nene Valley (site 30). These correspond to sites labelled I, III, IV and VI in Figure 3. Due to the previously established seasonal variability in terms of the abundance of oil strandings on the coastline (Edwards et al., 2016), the most suitable comparison to these prior surveys are the results from September 2015, as this survey is both seasonally appropriate for comparison and was not affected by abnormal weather conditions like the 2016 results. These prior surveys did not find examples of asphaltic crude oil (solid asphaltite or soft tar) at any of the specified sites. Therefore, only the waxy hydrocarbon loading values may be compared.

In both the 1990/1991 and 2015 surveys, the Number 1 and 2 Rocks beach in the Canunda National Park was the most prominent collection point for waxy crude oil strandings (Figs. 3 and 9). However, the magnitude of hydrocarbon loading differs significantly between the past and present results. The waxy hydrocarbon loading of this site was 496 g/100 m in 1990 and 2046 g/100 m in 1991 (Fig. 3; Table S1). Notwithstanding the difference in these two values, it is significant that they originate from the same location at the same time of year and greatly exceed those obtained during the 2015 survey, which returned an average waxy hydrocarbon loading of 109 g/100 m (Fig. 9, Table S5). Although a significant reduction compared to the previous surveys, this represents the single highest waxy hydrocarbon loading value (in g/100 m) for any surveyed site during the present study. This demonstrates a remarkable reduction in the overall abundance of waxy oils currently accumulating on the South Australian coastline compared to the early 1990's. The reduction in waxy hydrocarbon loading may be further exemplified by comparing the sample suites amassed during both studies. The two surveys of six beaches in 1990 and 1991 collected a total of 871 waxy bitumens weighing a total of 10988 g. By comparison, the three surveys of thirty beaches between 2014–2016, which included four of those previously visited in 1990/1991, collected only 453 pieces of waxy oil, weighing a combined total of 2779 g.

Finally, the lack of oils stranding as sheets of oil or liquid globules, like several examples identified in the early 1990s (Padley, 1995; Edwards et al., 2016), is consistent with global trends suggesting that modern maritime practices have improved and hence reduced the amount of anthropogenically-derived oil contaminating the coastline.

4.2. Linking changes in geochemistry with hydrocarbon loading

In addition to the overall reduction in waxy bitumen abundance on the South Australian coastline, those specimens containing botryococcane (types I and II) collected between 2014 and 2016 are significantly more degraded than their historical counterparts from previous surveys (Fig. 15). Although the type II waxy bitumens are much less abundant than the type I examples, they are similarly thought to originate from SE Asia and further demonstrate the decline in preservation of specific waxy oils since the early 1990's. The lack of well-preserved type I and II waxy bitumens suggests that their respective petroleum systems are no longer seeping fresh oil into the marine environment.

This lack of fresh oil seepage is likely due to the decades of oil production in SE Asia, where the type I and II waxy bitumens are considered to originate (Edwards et al., 2018; Corrick et al., 2020a). Comparison of oil seepage from Coal Oil Point in the Santa Barbara Channel in 1973, 1995 and 1996 revealed a >50% decline in the extent of seepage across the area and an overall reduction in emission volumes above the producing reservoir due to declining reservoir pressures (Quigley et al., 1999). Given that oil production in SE Asia has been active since the 1940s, with the first oils containing abundant botryococcane reported in 1980 (Moldowan and Seifert, 1980), the ongoing extraction of petroleum across the region has most likely caused sufficient decreases in reservoir pressures to cause a cessation of natural seeps associated with both the type I and II waxy bitumens.

Alternatively, some oil seeps are demonstrably episodic (e.g. MacDonald et al., 2000). Thus, the present lack of fresh seep emissions could also be attributed to a temporary period of inactivity. However, the lack of any fresh oil emissions collected across the entire three-year survey period makes this option unlikely. Further assessment regarding seep emission periodicity would require a greater understanding of the mechanics of the seeps themselves, which have not yet been identified. Therefore, future coastal surveys will likely be required to demonstrate a continued lack of fresh type I and II waxy bitumens stranding on the South Australian coastline before this explanation can be ruled out.

Although secular variation in the abundance of asphaltic oil accumulating on the coastline cannot be assessed due to a lack of previous asphaltic hydrocarbon loading assessments, continuity may still be assessed in terms of their geochemistry. The oldest asphaltites

geochemically analysed were collected in the late 1800s and although weathered, their biomarker and isotopic geochemistry remained comparable to those of asphaltites collected in the 1990s (Volkman et al., 1992; Edwards et al., 1998). The exceptional preservation of gasoline-range *n*-alkanes in the freshest asphaltites collected as part of this study (e.g. W13/007976; Fig. 5A) represent the least weathered asphaltites to be geochemically analysed to date. Thus, while asphaltites strand on the South Australian coastline in systematically lower numbers than the various types of waxy oils, the seep responsible for these large bitumen specimens must still be active. Notwithstanding their generally low abundance, the large size of these strandings (up to 7 kg; Edwards et al., 1998) and their retention of volatile components continues to support their origin from a nearby seep on Australia's southern margin which either releases petroleum episodically or at an extremely low rate.

Many of the remaining types of oil now known to strand on the South Australian coastline (viz. those within the type III and IV classifications, the Sandy River tars and the asphaltic tars) have only been recently identified (Corrick et al., 2020a). Identification of many these oils requires examination of their biomarker assemblages, a procedure that could not feasibly be applied to all the specimens collected in the 2014–2016 surveys, and therefore the least degraded examples may not yet be recognised. Previously identified waxy bitumens lacking botryococcane were considered to be derived from a variety of marine source rocks but were classified together (Family 4; Edwards et al., 2018). Therefore, detailed assessment of the as-yet unanalysed waxy bitumen specimens collected during both the 1990–1991 and 2014–2016 surveys will be required to confidently establish a record of historical continuity for these newly discovered oils.

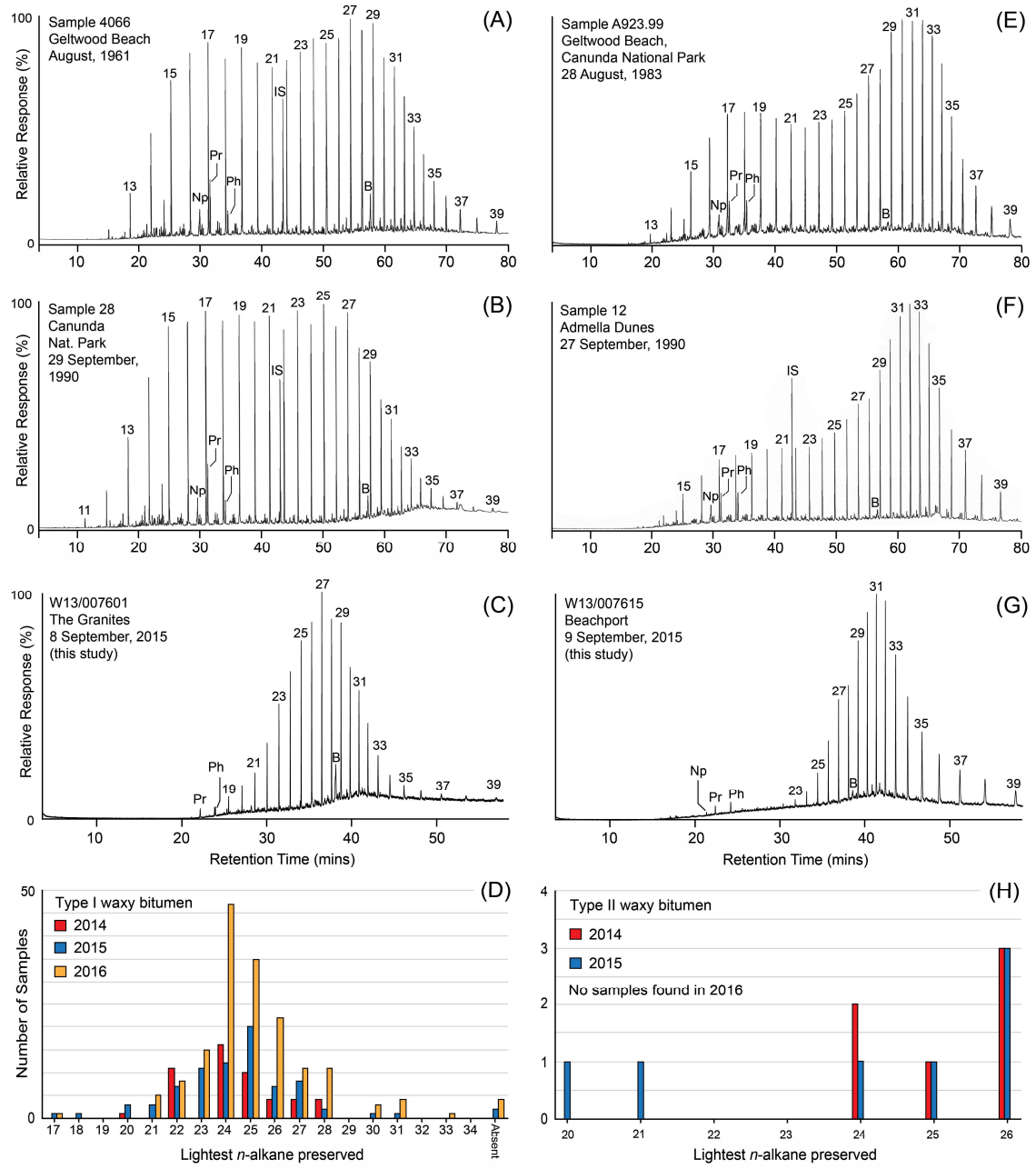


Figure 15: Comparison of GC-MS results from historical vs. modern type I and II waxy bitumens adapted from Corrick et al., (2020a). (A) Saturated hydrocarbon fraction TIC of waxy bitumen sample 4066 (type I equivalent) collected in 1961. (B) Saturated hydrocarbon fraction TIC of waxy bitumen sample 28 (type I equivalent) collected in 1990. (C) Whole-oil TIC of the freshest type I waxy bitumen in the present study, sample W13/007601, collected in 2015. (D) Range of weathering extent for all type I waxy bitumens collected between 2014-2016 (including samples donated from private collections). (E) Saturated hydrocarbons fraction TIC of waxy bitumen sample A923.99 (type II equivalent) collected in 1983. (F) Saturated hydrocarbons fraction TIC of waxy bitumen sample 12 (type II equivalent) collected in 1990. (G) Whole-oil TIC of the least weathered type II waxy bitumen from the present study, sample W13/007615, collected in 2015. (H) Range of weathering extent for all type II waxy bitumens collected between 2014-206 (including samples donated from private collections). Chromatograms of archival samples in parts A, B, E and F after Padley (1995). Numbered peak responses correspond to *n*-alkane chain length, Np = norpristane, Pr = pristane, Ph = phytane, B = botryococcane, IS = 3-methylhenicosane internal standard (AC 22; 10µg ml^{-1}). Note the minor variation in relative elution position of botryococcane between archival specimens and those collected in 2015 is the result of differences in chromatography, not sample composition.

4.3. Considerations regarding the hydrocarbon loading baseline

The hydrocarbon loading baseline established herein may be of use for future monitoring of both anthropogenic pollution and the impact of natural oil seepage on the South Australian coastline. However, when using this dataset as baseline for comparison, a number of potentially limiting factors must also be considered.

4.3.1. Seasonal variability

The annual surveys conducted as part of this study were restricted to between September and November of each year, with the intention of maximising the number of samples collected. Therefore, using the results of this study as a baseline for a particular location during a different time of the year is unlikely to be meaningful (cf. the seasonal surveys by Edwards et al., 2016). Larger-scale surveying throughout the year could assist in addressing this issue, although systematic surveying of the South Australian coastline in all seasons is impractical, particularly in remote areas during summer where temperatures frequently exceed 40 °C. Furthermore, given the previous evidence that the most bitumen collects on the coastline during September/October, surveying outside of this period is unlikely to be considered given the economic costs associated with such surveys. Hence, comparisons to this baseline should be as seasonally appropriate as possible.

4.3.2. Abnormal weather conditions

A representative environmental baseline cannot account for abnormal conditions such as the severe storm which affected the results of the 2016 survey. Although surveys immediately following extreme weather events are not representative of typical conditions, the results may still be useful for other purposes. For example, the high number of oils collected during the 2016 survey aided in the identification of several new types of oil not previously recognised on the coastline (Corrick et al., 2020a). However, the spatial distribution and abundance of stranded oil resulting from such events are not directly comparable to those eventuating under normal conditions.

4.3.3. Alteration by local beach activities

The hydrocarbon loading value of a particular stretch of coastline is also highly susceptible to alteration by local beachgoers. Beaches in close proximity to populated areas are less likely to

accurately represent natural conditions due to activities such as beach cleaning, the turnover of sand by motorised vehicles, and the dumping of sand on popular beaches in order to compensate for its removal by longshore drift. The majority of beaches selected for this study were sufficiently remote to minimise the influence of human activity. However, even in remote areas evidence of human activity can still be evident (e.g. car tracks from beach driving). There is no straightforward approach to mitigating this potential source of random error within the survey results. Thus, the potential impact of human activity should be assessed on a case-by-case basis at each site.

4.3.4. Potential for extrapolation between survey areas

Although the surveyed sites were intended to create an accurate representation of the occurrence of stranded oil across the South Australian coastline, extrapolation of hydrocarbon loading results to areas between survey sites is unlikely to be accurate. Variations in the surface ocean currents and wind direction can drive significant variability even on relatively small scales. For example, both Geltwood Beach (site 28) and Nene Valley (site 30) typically returned low hydrocarbon loading values, despite their close proximity to the most prominent waxy oil collection point, Number 1 and 2 Rocks (site 29). Therefore, future studies intending to compare the abundance of crude oil accumulation on the coastline are recommended to visit the same survey sites at the same time of year in order to make reliable comparisons.

4.1.1. A hydrocarbon loading baseline is not comparable to oil spill forecasting

The distribution of naturally seeped petroleum accumulating on the coastline should also not be considered as a tool to predict regions likely to be affected in the event of an offshore oil spill. Although this study documents the occurrence of oil stranding along the South Australian coastline, it does not identify which areas may potentially be impacted by an oil spill within the Great Australian Bight or elsewhere in the region. Prediction of the oceanographic transport of spilled liquid hydrocarbons from offshore oil exploration, production or shipping requires a combination of stochastic and deterministic modelling, usually conducted as part of an environmental impact assessment (e.g. Equinor, 2019). Forecasting which areas may potentially be affected by an oil spill requires an understanding of the physical properties of the hydrocarbons released (approximated in frontier basins with no produced oils for reference), the point and time of release, spill size and duration, wind velocity, waves, currents, water

temperature and many other variables to construct an accurate representation of the full complexity inherent to the natural environment.

Liquid oils in the marine environment may strand as a slick, or weather to form a viscous, emulsified tar residue (Warnock et al., 2015). This does not mean that the oil strandings discussed herein represent a valid approximation for spilled hydrocarbons. Liquid hydrocarbons are typically less dense than seawater, forming a slick on the sea surface which cannot be expected to migrate in a perfectly analogous manner to individual pieces of bitumen or amalgamated tar. Semi-solid to solid bitumens, viscous tars and liquid oils will differ in size, density and viscosity, all of which will ultimately affect how they traverse the marine environment prior to stranding on the coastline. For example, the asphaltites are likely analogous to the asphalt seeps observed on the seafloor in the Gulf of Mexico, where heavy petroleum flows onto the seafloor, solidifies and fragments (Brüning et al., 2010). The waxy bitumens could also result from the weathering of liquid oil. However, given the historical record of coastal bitumens which are well preserved, with very little biodegradation (Fig. 15) despite their long travel distance from SE Asia. It is therefore more likely that these oils were already semi-solid upon their release into the marine environment. The exception to this is the Sandy River tar strandings, which demonstrate a bimodal UCM characteristic of a liquid crude oil weathered in the marine environment, however without an understanding of their point of release from the subsurface and the rate at which the oils transitioned from liquid to semi-solid, any consideration of their migration is highly speculative..

In the event of an oil spill proximal to the South Australian coastline, locations documented herein with consistently high hydrocarbon loading values, such as Dogfence Beach or Number 1 and 2 Rocks, may be worthy of particular investigation for the purposes of comparison. However, their environmental baseline should be used only as a measure of natural conditions (e.g. what types of oil have been found pre-spill on the coastline and in what abundance) and not as a predictive tool.

5. CONCLUSIONS

Australia's southern margin is known to collect oil strandings attributed to natural offshore seepage from petroleum systems in both Australia and the Indonesian Archipelago. Over the course of three annual surveys of 30 ocean beaches conducted from 2014–2016, a total of 508 individual pieces of semi-solid to solid oil were recovered and used to construct a modern hydrocarbon loading baseline for the South Australian coastline. This baseline may be considered in terms of asphaltic oils, attributed to seepage from the nearby Bight Basin and waxy oils, which originate from a variety of different petroleum systems across SE Asia and are delivered to the Australian coastline by the Leeuwin Current.

Asphaltites contribute the most oil to the coastline by total weight due to their large size, despite their relative scarcity in comparison to other identified oil varieties. The exceptional preservation of low-molecular-weight compounds in recently collected asphaltites suggests that, notwithstanding their rare occurrence on the coastline, seepage from their parent petroleum system remains active.

Waxy bitumens containing a high abundance of the rare biomarker botryococcane are by far the most commonly encountered type of oil on the coastline, comprising approximately half of all collected specimens. However, these strandings are significantly weathered in comparison to their historical counterparts from prior surveys. This suggests a lack of fresh oil seepage from their parent petroleum system thought to reside in Western Indonesia. This is further reinforced by the observation that the overall waxy hydrocarbon loading of the South Australian coastline has markedly declined since 1990–1991. We attribute both the lack of fresh waxy oil strandings containing abundant botryococcane and the overall reduction in waxy hydrocarbon loading to reduced reservoir pressures, presumably associated with the long history of oil production in SE Asia, causing a cessation of formerly active offshore seepage. We therefore anticipate that the waxy hydrocarbon loading of the South Australian coastline will continue to decline as the remaining oil from this particular system continues to break down in the marine environment.

ACKNOWLEDGEMENTS

We thank Chris Dyt, Zachary Angelini, Richard Kempton, Cameron White, April Pickard, Stacey Maslin, Stephane Armand, Les Tucker and Su Margot for their assistance in completing the 2014–2016 beach surveys. We also thank Stuart Valladares for the donation of asphaltite and waxy bitumen specimens from his personal collection for this research.

The Great Australian Bight Research Program is a collaboration between BP, CSIRO, the South Australian Research and Development Institute (SARDI), the University of Adelaide, and Flinders University. The program aims to provide a whole-of-system understanding of the environmental and social values of the region; providing an information source for all to use.

SUPPLEMENTARY INFORMATION

The supplementary information for this chapter may be found in pages 290–305.

REFERENCES

Alexander, R., Currie, T.J., Kagi, R.I., 1994. The origins of coastal bitumens from Western Australia. Aust. Pet. Explor. Assoc. J. 34, 787–798.

Australian Maritime Safety Authority, 2014. National plan for maritime environmental emergencies: Year in review 2013-14.

Australian Maritime Safety Authority, 2015. National plan for maritime environmental emergencies: Year in review 2014-2015.

Australian Maritime Safety Authority, 2016. National plan for maritime environmental emergencies: Year in review 2015-2016.

Australian Maritime Safety Authority, 2019. Major historical incidents. URL https://www.amsa.gov.au/marine-environment/incidents-and-exercises/major-historical-incidents

Baghurst, B., Lukatelich, R., Smith, D., Begg, G., Lewis, R., Smith, R., 2017. Findings from the Great Australian Bight Research Program – an integrated study of environmental, economic and social values. APPEA J. 57, 388–392. doi:10.1071/AJ16144

Boreham, C.J., Krassay, A.A., Totterdell, J.M., 2001. Geochemical comparisons between asphaltites on the southern Australian margin and Cretaceous source rock analogues, in: Hill, K.C., Bernecker, T. (Eds.), Eastern Australasian Basins Symposium, A Refocused Energy

Perspective for the Future. Petroleum Exploration Society of Australia Special Publication. pp. 531–541.

Brassell, S.C., Eglinton, G., Mo, F.J., 1986. Biological marker compounds as indicators of the depositional history of the Maoming oil shale. Org. Geochem. 10, 927–941. doi:10.1016/S0146-6380(86)80030-4

Brekke, C., Solberg, A.H.S., 2005. Oil spill detection by satellite remote sensing. Remote Sens. Environ. 95, 1–13. doi:10.1016/J.RSE.2004.11.015

Brüning, M., Sahling, H., MacDonald, I.R., Ding, F., Bohrmann, G., 2010. Origin, distribution, and alteration of asphalts at Chapopote Knoll, Southern Gulf of Mexico. Mar. Pet. Geol. 27, 1093–1106. doi:10.1016/j.marpetgeo.2009.09.005

Burns, G., Adams, L., Buckley, G., 2017. Independent review of the extreme weather event South Australia 28 September - 5 October 2016. Report presented to the Premier of South Australia.

Burns, K.A., Villeneuve, J.P., Anderlin, V.C., Fowler, S.W., 1982. Survey of tar, hydrocarbon and metal pollution in the coastal waters of Oman. Mar. Pollut. Bull. 13, 240–247. doi:10.1016/0025-326X(82)90347-2

Corbin, C.J., Singh, J.G., Ibiebele, D.D., 1993. Tar ball survey of six Eastern Caribbean countries. Mar. Pollut. Bull. 26, 482–486. doi:10.1016/0025-326X(93)90464-U

Corrick, A.J., Hall, P.A., Gong, S., McKirdy, D.M., Trefry, C., Ross, A.S., 2020a. The identification and provenance of crude oils stranded on the South Australian coastline, in: Studies on the nature of crude oil strandings collected from the South Australian coastline. PhD Thesis, Unpublished. University of Adelaide.

Corrick, A.J., Hall, P.A., Gong, S., McKirdy, D.M., Selby, D., Trefry, C., Ross, A.S., 2020b. A second type of highly asphaltic crude oil seepage stranded on the South Australian coastline. Mar. Pet. Geol. 112, 104062. doi:10.1016/J.MARPETGEO.2019.104062

Curiale, J., Lin, R., Decker, J., 2005. Isotopic and molecular characteristics of Miocene-reservoired oils of the Kutei Basin, Indonesia. Org. Geochem. 36, 405–424. doi:10.1016/j.orggeochem.2004.09.007

Currie, T.J., Alexander, R., Kagi, R.I., 1992. Coastal bitumens from Western Australia - long distance transport by ocean currents. Org. Geochem. 18, 595–601.

Curtis, M., Saner, A., 1974. Tar ball loadings on Golden Beach, Florida. US Dep. Commer. Washington, DC (National Bur. Stand. Spec. Publ. 79–81.

Dwivedi, S.N., Parulekar, A.H., 1974. Oil pollution along the Indian coastline, in: Marine Pollution Monitoring (Petroleum) Symposium and Workshop, National Bureau of Standards, Maryland. pp. 101–105.

Edwards, D., McKirdy, D.M., Summons, R.E., 1998. Enigmatic asphaltites from the southern Australian margin: molecular and carbon isotopic composition. Pet. Explor. Soc. Aust. J. 26, 397–420.

Edwards, D.S., McKirdy, D.M., Rowland, S.J., Heath, D.J., Gray, P.S., 2018. Waxy bitumen stranding in southern Australia: A geochemical study of multiple oil families and their likely origins. Org. Geochem. 118, 132–151. doi:10.1016/j.orggeochem.2017.12.010

Edwards, D.S., Vinall, D.R., Corrick, A.J., McKirdy, D.M., 2016. Natural bitumen stranding on the ocean beaches of Southern Australia: a historical and geospatial review. Trans. R. Soc. South Aust. 140, 152–185. doi:10.1080/03721426.2016.1203532

Equinor, 2019. Environment Plan for the Stromlo-1 Exploration Drilling Program (Revision 1).

Fingas, M., Brown, C., 2014. Review of oil spill remote sensing. Mar. Pollut. Bull. 83, 9–23. doi:10.1016/J.MARPOLBUL.2014.03.059

Georges, C., Oostdam, B.L., 1983. The characteristics and dynamics of tar pollution on the beaches of Trinidad and Tobago. Mar. Pollut. Bull. 14, 170–178. doi:10.1016/0025-326X(83)90228-X

Golik, A., 1982. The distribution and behaviour of tar balls along the Israeli coast. Estuar. Coast. Shelf Sci. 15, 267–276. doi:10.1016/0272-7714(82)90063-4

Hall, P.A., McKirdy, D.M., Grice, K., Edwards, D.S., 2014. Australasian asphaltite strandings: Their origin reviewed in light of the effects of weathering and biodegradation on their biomarker and isotopic profiles. Mar. Pet. Geol. 57, 572–593. doi:10.1016/j.marpetgeo.2014.06.013

Henry, C.B., Roberts, P.O., Overton, E.B., 1993. Characterization of chronic sources and impacts of tar along the Louisiana Coast.

Hook, S., Batley, G., Holloway, M., Irving, P., Ross, A. (Eds.), 2016. Oil spill monitoring handbook. CSIRO Publishing.

Howchin, W., 1919. Geological memoranda (first contributions). Trans. R. Soc. South Aust. 43, 45–48.

Howchin, W., 1903. Further notes on the geology of Kangaroo Island. Trans. R. Soc. South Aust. 27, 75–90.

Hwang, R.J., Heidrick, T., Mertani, B., Qivayanti, Li, M., 2002. Correlation and migration studies of North Central Sumatra oils. Org. Geochem. 33, 1361–1379. doi:10.1016/S0146-6380(02)00104-3

Kvenvolden, K.A., Cooper, C.K., 2003. Natural seepage of crude oil into the marine environment. Geo-Marine Lett. 23, 140–146. doi:10.1007/s00367-003-0135-0

Lorenson, T.D., Hostettler, F.D., Rosenbauer, R.J., Peters, K.E., Dougherty, J.A., Kvenvolden, K.A., Gutmacher, C.E., Wong, F.L., Normark, W.R., 2009. Natural Offshore Oil Seepage and Related Tarball Accumulation on the California Coastline; Santa Barbara Channel and the Southern Santa Maria Basin; source identification and inventory, U.S. Geological Survey Open-File Report 2009-1225 and MMS report 2009-030.

MacDonald, I.R., Buthman, D.B., Sager, W.W., Peccini, M.B., Guinasso, N.L., 2000. Pulsed oil discharge from a mud volcano. Geology 28, 907. doi:10.1130/0091-7613(2000)28<907:PODFAM>2.0.CO;2

MacDonald, I.R., Guinasso, N.L., Ackleson, S.G., Amos, J.F., Duckworth, R., Sassen, R., Brooks, J.M., 1993. Natural oil slicks in the Gulf of Mexico visible from space. J. Geophys. Res. 98, 16351–16364. doi:10.1029/93JC01289

MacDonald, I.R., Reilly, Jr., J.F., Best, S.E., Venkataramaiah, R., Sassen, R., Guinasso, Jr., N.L., Amos, J., 1996. Remote Sensing Inventory of Active Oil Seeps and Chemosynthetic Communities in the Northern Gulf of Mexico, in: D. Schumacher, M.A. Abrams (Eds.), Hydrocarbon Migration and Its Near-Surface Expression: AAPG Memoir 66. AAPG Special Volumes, pp. 27–37.

McKirdy, D.M., 1984a. Coastal bitumens and potential source rocks in the western Otway Basin, South Australia and Victoria. AMDEL Report F 5840/84 for Australian Aquitaine Petroleum Pty Ltd. and Ultramar Australia Inc., South Australian Department of Mines and Energy Open File Envelope No. 5876.

McKirdy, D.M., 1984b. Coastal bitumens and potential source rocks, Duntroon Basin, South Australia. AMDEL Report F 5769/84 for Getty Oil Development Company Ltd., South Australian Department of Mines and Energy Open File Envelope No. 5876.

McKirdy, D.M., Horvath, Z., 1976. Geochemistry and significance of coastal bitumen from Southern and Northern Australia. APPEA J. 123–135.

Meteorology, B. of, 2016. Severe thunderstorm and tornado outbreak South Australia 28 September 2016.

Moldowan, J.M., Seifert, W.K., 1980. First discovery of Botryococcane in petroleum. J. Chem. Soc. Chem. Commun. 19, 912–914.

Morris, B.F., Butler, J.N., 1973. Petroleum Residues in the Sargasso Sea and on Bermuda Beaches, in: International Oil Spill Conference Proceedings: March 1973. American Petroleum Institute, pp. 521–529. doi:10.7901/2169-3358-1973-1-521

Murray, A.P., Padley, D., McKirdy, D.M., Booth, W.E., Summons, R.E., 1994. Oceanic transport of fossil dammar resin: The chemistry of coastal resinites from South Australia. Geochim. Cosmochim. Acta 58, 3049–3059. doi:10.1016/0016-7037(94)90178-3

NAS, 2003. Oil in the Sea III: Inputs, Fates and Effects. The National Academies Press, Washington DC. doi:10.17226/10388

Ohya, M., Otsuki, T., Saito, M., 1973. Oil pollution in the Izu Islands waters. J. Oceanogr. 29, 121–129. doi:10.1007/BF02109154

Padley, D., 1995. Petroleum geochemistry of the Otway Basin and the significance of coastal bitumen strandings on adjacent southern Australian beaches (PhD thesis). University of Adelaide.

Padley, D., McKirdy, D.M., Murray, A., Summons, R.E., 1993. Oil strandings on the beaches of Southern Australia: Origins from natural seepage and shipping, in: Øygard, K. (Ed.), Poster Sessions from the 16th International Meeting On Organic Geochemistry, Stavanger 1993. Falch Hurtigtrykk, pp. 660–663.

Quigley, D.C., Scott Hornafius, J., Luyendyk, B.P., Francis, R.D., Clark, J., Washburn, L., 1999. Decrease in natural marine hydrocarbon seepage near Coal Oil Point, California, associated with offshore oil production. Geology 27, 1047. doi:10.1130/0091-7613(1999)027<1047:DINMHS>2.3.CO;2

Ross, A., Corrick, A., Trefry, C., Gong, S., McKirdy, D., Hall, T., Dyt, C., Angelini, Z., Kempton, R., Pickard, A., White, C., Maslin, S., Griffin, D., Middleton, J., Luick, J., Armand, S., Vergara, T., Schinteie, R., 2017. Asphaltite and tarball surveys. Final Report GABRP Project 5.2. Research Report Series Number 25a.

Scarlett, A.G., Holman, A.I., Georgiev, S. V., Stein, H.J., Summons, R.E., Grice, K., 2019. Multi-spectroscopic and elemental characterization of southern Australian asphaltites. Org. Geochem. 133, 77–91. doi:10.1016/J.ORGGEOCHEM.2019.04.006

Seifert, W.K., Moldowan, J.M., 1981. Paleoreconstruction by biological markers. Geochim. Cosmochim. Acta 45, 783–794. doi:10.1016/0016-7037(81)90108-3

Shirneshan, G., Bakhtiari, A.R., Memariani, M., 2016. Identification of sources of tar balls deposited along the Southwest Caspian Coast, Iran using fingerprinting techniques. Sci. Total Environ. 568, 979–989. doi:10.1016/j.scitotenv.2016.04.203

Sprigg, R.C., Woolley, J.B., 1963. Coastal bitumen in southern Australia with special reference to observations at Geltwood Beach, south-east South Australia. Trans. R. Soc. South Aust. 86, 67–103.

Summons, R.E., Bradshaw, J., Brooks, D.M., Goody, A.K., Murray, A.P., Foster, C.B., 1993. Hydrocarbon composition and origins of coastal bitumens from the Northern Territory, Australia. PESA J. 21, 31–42.

Summons, R.E., Logan, G.A., Edwards, D.S., Boreham, C.J., Bradshaw, M.T., Blevin, J.E., Totterdell, J.M., Zumberge, J.E., 2001. Geochemical analogs for australian coastal asphaltites - search for the source rock, in: Abstracts, AAPG Annual Convention, Denver, Colorado. American Association of Petroleum Geologists.

Suneel, V., Ciappa, A., Vethamony, P., 2016. Backtrack modeling to locate the origin of tar balls depositing along the west coast of India. Sci. Total Environ. 569–570, 31–39. doi:10.1016/j.scitotenv.2016.06.101

ten Haven, H.L., Schiefelbein, C., 1995. The Petroleum Systems of Indonesia, in: Proceedings Indonesian Petroleum Association: Twenty Fourth Annual Convention Proceedings. pp. 443–459.

Tolmer, A., 1882. Reminiscences of an adventurous and chequered career at home and at the antipodes. Sampson Low, Marston, Searle & Rivington, London.

Totterdell, J.M., Struckmeyer, H.I.M., Boreham, C.J., Mitchell, C.H., Monteil, E., Bradshaw, B.E., 2008. Mid-Late Cretaceous organic-rich rocks from the eastern Bight Basin : implications for prospectivity, in: Blevin, J.E., Bradshaw, B.E., Uruski, E. (Eds.), PESA Eastern Australasian Basins Symposium III Special Publication. pp. 137–158.

Trewartha, J., 1850. South Australian Government Gazette, 25 April 282.

Volkman, J.K., O'Leary, T., Summons, R.E., Bendall, M.R., 1992. Biomarker composition of some asphaltic coastal bitumens from Tasmania, Australia. Org. Geochem. 18, 669–682. doi:10.1016/0146-6380(92)90092-C

Ward, L.K., 1944. The Search For Oil In South Australia, Geological Survey of South Australia Bulletin. Adelaide.

Ward, L.K., 1913. The Possibilities of the Discovery of Petroleum on Kangaroo Island and the Western Coast of Eyre's Peninsula, Geological Survey Bulletin. Adelaide.

Warnock, A.M., Hagen, S.C., Passeri, D.L., 2015. Marine Tar Residues: a Review. Water, Air, Soil Pollut. 226, 24. doi:10.1007/s11270-015-2298-5

CHAPTER 6

Conclusions and future research directions

1. CONCLUSIONS

The key objectives of this study were to further our understanding of potential petroleum systems in the frontier Bight Basin and establish an updated environmental baseline for the occurrence of crude oil on the South Australian coastline. This thesis provides several significant advances in addressing these aims. As each of the chapters comprising this thesis contain their own respective conclusions, this section will be comparatively brief.

Chapter 2 demonstrates the first successful application of Re-Os radiometric dating to natural oil seepage, demonstrating that the technique has the potential to be utilised as an exploration tool to aid in the characterisation of offshore petroleum systems. Analysis of a suite of asphaltites (n = 16) was able to constrain the age of their generation to 74 ± 26 Ma, with a preferred trend within the dataset yielding an age of 68 ± 15 Ma (n = 9). These results support the hypothesis that the asphaltites originate from the Bight Basin, in which modelling of the Ceduna Sub-basin suggests it generated oil from ~74 Ma to the present (Totterdell et al., 2008).

Chapter 3 documents a new variety of highly asphaltic oil referred to as asphaltic tar, which arrived on the coastline in 2016. These oils exhibit several source-specific similarities to the asphaltites, suggesting that they may also originate from the Bight Basin. However, the possibility that this new oil may have been altered by thermochemical sulphate reduction requires further assessment, given the implications this process can have for oil exploration and production.

Chapter 4 outlines several procedures to identify the different types of crude oil encountered on the South Australian coastline and assesses their likely provenance. Source-specific biomarker assemblages of the various waxy oils collected demonstrated that the number of different oils delivered to the South Australian coastline from petroleum systems across Southeast Asia is far greater than previously recognised in the early-mid 1990's (Edwards et al., 2018). Furthermore, comparison of the type I and II waxy bitumens with those collected in prior studies demonstrates that the modern examples are significantly more weathered, suggesting a lack of fresh seepage from these particular petroleum systems.

Finally, Chapter 5 provided a quantified assessment of the occurrence of crude oil accumulating along the South Australian coastline, due to both local (asphaltic) and distant (waxy) petroleum

systems. The asphaltites, attributed to the Bight Basin, account for the majority by weight of crude oil recovered from the coastline due to their large size. However, the various waxy oils represent the vast majority of individual strandings recovered from the survey area. Furthermore, despite the larger number of different waxy oils identified in this study, their overall contribution to the hydrocarbon loading of the coastline has declined significantly compared to the historical baseline established using the 1990–1991 survey results (Edwards et al., 2016). This is likely due to a lack of fresh seepage from the petroleum systems associated with the type I and II waxy bitumens in the Indonesian Archipelago, as all of the modern samples collected were significantly weathered compared to examples analysed in prior studies.

2. FUTURE RESEARCH DIRECTIONS

2.1. The application of Re-Os geochronology to crude oil seepage

Given that the majority of Re and Os in crude oil resides within its asphaltene fraction (Selby et al., 2007), the asphaltites, and to a lesser extent the asphaltic tars, were the most appropriate oils in the sample suite to test if Re-Os radiometric dating could be successfully applied to oil seepage. However, given that the parent petroleum systems of these oils have not yet been located, the interpretations of their Re-Os systematics could not be independently verified. This has subsequently led to differing interpretations regarding the source rock responsible for the asphaltites (discussed below). Therefore, whilst the results of Chapter 2 demonstrate a proof-of-concept regarding the application of Re-Os radiometric dating to hydrocarbon seepage, further case studies will be required. Ideally, such studies will utilise seepage emitted from a well-studied petroleum system, one where the timing of oil generation is independently constrained and, if possible, samples of the source rock available to compare $^{187}Os/^{188}Os$ values at the time of generation.

2.2. The Re-Os generation age of the asphaltites

With a specific focus on the Re-Os systematics of the asphaltites, two potential research directions are recommended. Firstly, the possibility that the asphaltites may represent a mixture of two oil charges of differing maturities should be investigated. This possibility is indicated by their conflicting aromatic thermal maturity indices (methylnaphthalene and dimethylnaphthalene ratios versus methylphenanthrene index) based on analysis of the freshest collected asphaltites analysed in Chapter 3. If the asphaltites do indeed represent a mixed oil,

their resulting Re-Os systematics will undoubtedly no longer accurately represent either of the two original oils. Unravelling such mixing to assess viable generation ages for each individual charge would require far greater knowledge of the petroleum system(s) within the Bight Basin than is presently available.

Secondly, should the Re-Os systematics of the asphaltites be considered unaffected by the aforementioned potential subsurface mixing, the variation in Re-Os generation ages obtained between different studies should be assessed. The results of Chapter 2 differ from those of a subsequent study which obtained a significantly older mean generation age of 103 ± 22 Ma (Scarlett et al., 2019). Given its difference from the mean age reported in Chapter 2 (74 ± 26 Ma, with a subset of data points defining an isochron of 68 ± 15 Ma), it is unsurprising that these two studies propose different source rocks to account for the asphaltites (OAE2 and OAE1a/b, respectively). Scarlett and co-workers obtained significantly lower analytical uncertainties for each individual asphaltite, but a lack of significant variation in $^{187}Re/^{188}Os$ and $^{187}Os/^{188}Os$ values, due to the small number of samples they analysed (n = 5), resulted in a high uncertainty in their final generation age. However, consideration of the full range of uncertainty in the generation age obtained in Chapter 2 from all the available data points (74 ± 26 Ma) does show 19 Myr of potential overlap with this new result. Given that the asphaltites analysed in Chapter 2 demonstrate a greater range in $^{187}Re/^{188}Os$ and $^{187}Os/^{188}Os$ values than those analysed by Scarlett et al. (2019), future studies are recommended to re-analyse samples from both studies to obtain results with reduced analytical uncertainties and independently reassess the validity of the competing interpretations proposed by both studies.

2.3. Linking the asphaltic oils to the Bight Basin

The correlation of the asphaltites to the Bight Basin currently relies on their observed spatial distribution along the South Australian coastline, exceptional preservation suggesting minimal oceanic transport and geochemical constraints suggesting a source rock depositional environment consistent with our present understanding of the basin. However, to date, no viable petroleum systems have yet been identified in the Bight Basin. Therefore, assigning the origin of the asphaltites, and by extension the asphaltic tars, to the Bight Basin should continue to be treated as an interpretation rather than a direct correlation, until an oil of comparable composition is recovered from the basin.

2.4. Assessing if thermochemical sulphate reduction occurred in the Bight Basin

The most significant difficulty regarding the potential correlation of the asphaltites to the newly discovered asphaltic tar strandings in Chapter 3 is the fact that significant points of geochemical variation could be interpreted to represent either primary differences in source rock composition or secondary diagenetic alteration of the parent oil by thermochemical sulphate reduction. As discussed within the main text of Chapter 3, the future research most likely to resolve this outstanding issue would be to utilise compound-specific sulphur isotope analysis, comparing the $\delta^{34}S$ values of benzothiophenes and dibenzothiophenes in these samples (e.g. Amrani et al., 2012). Given the costly complications associated with extraction of hydrocarbons from sour reservoirs, resolving these conflicting interpretations may have important ramifications for the exploration prospects of the Bight Basin.

2.5. Assessment of unanalysed coastal bitumens

Although this study is based on the largest suite of analysed oil strandings collected from the Australian coastline to date, the majority of collected bitumens were not analysed beyond whole-oil GC-MS screening. While certain oils such as the asphaltites demonstrated highly reproducible biomarker assemblages indicative of a single oil family, the wide variety of different oils identified within the type III and IV waxy bitumen classifications raises the possibility that further undocumented oil families exist within the present sample suite that have yet to be identified. As the newly identified oils remain consistent with the reported types of petroleum recognised in Southeast Asia, it is highly likely that other commonly occurring oils associated with Indonesian sedimentary basins also arrive on the South Australian coastline. These include the terrestrial oil sub-families referred to as “Resinitic” and “Oleanane” oils, respectively (Fig. 1). Resinitic oils are reported primarily from the South Sumatra, Central Sumatra, Sarawak, West Natuna and NW Java basins, while the oleanane-rich oils are recognised in the South Makassar, East Java and North Sumatra basins where they are thought to represent highly biodegraded equivalents of the fluvio-deltaic oils in the region (ten Haven and Schiefelbein, 1995; Schiefelbein et al., 1997).

Similarly, the prior study based on surveys conducted in 1990–1991 assembled a suite bitumens so large that it was impractical to analyse every sample (cf. the hundreds of waxy bitumens reported by Padley (1995) and Edwards et al. (2016) versus the representative 96 waxy bitumens and 30 asphaltites analysed in detail by Edwards et al. (2018) and Edwards et al.

(1998), respectively). Given the large number of oils identified in the present study that have not previously been reported on the South Australian coastline, geochemical assessment of unanalysed archival specimens could assist in establishing a historical continuity for these new oils. A composite record of these strandings from the early 1990s would further support the interpretation that all these stranded oils originate from natural seepage, as opposed to anthropogenic spills, justifying their inclusion in an environmental baseline.

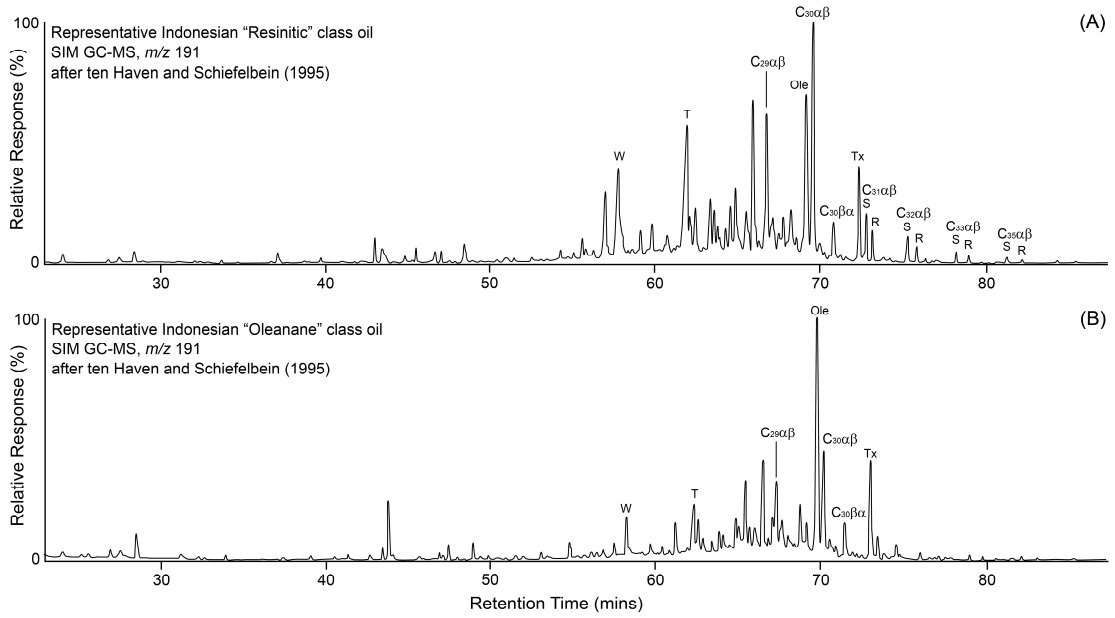


Figure 1: Representative *m/z* 191 chromatograms of common terrestrial sub-classes of Indonesian oils (after ten Haven and Schiefelbein, 1995) which have not yet been reported on the South Australian coastline. (A) "Resinitic" oil. (B) "Oleanane" oil, proposed to represent a heavily biodegraded equivalent to the typical fluvio-deltaic oils from the region. The chromatograms are modified with additional peak identifications. Ole = oleanane; W and T = bicadinanes; Tx = taraxastane.

The oils analysed in this study would also greatly benefit from further geochemical characterisation. Ideally each oil family could also be analysed using MRM or GC-MS-MS to target biomarkers which occur in low abundances or are known to co-elute with other compounds when analysed using SIM GC-MS. As interference by co-eluting compounds affected the assessment of other source-specific compounds, for example bicadinanes and steranes. This approach would also have the added benefit of assessing the presence or absence of diagnostic marine biomarkers such as 24-*n*-propylcholestane and dinosteranes in all the identified oil families. The waxy oils would also benefit from further detailed assessment utilising high temperature GC-MS, which would permit an assessment of the high molecular weight compounds which occur in these oils that are notably resistant to biodegradation.

2.6. Further comparisons to produced oils and seafloor seeps in Southeast Asia

In order to determine the origin of specific oils with a higher degree of certainty than the interpretations provided in Chapter 4, a greater understanding of the geochemistry of oils across the Indonesian Archipelago will be required. Given the large amount of proprietary geochemical data from across the region that has not been publicly released, collaboration with oil producers in the region will likely be required to obtain more robust correlations for many of the waxy oils found on the South Australian coastline. Such comparisons should include assessment of both offshore oil reservoirs and known seafloor seeps where possible, ideally utilising oil samples analysed with the same analytical instruments under the same operating conditions to facilitate clearer correlations.

2.7. Maintaining and expanding the hydrocarbon loading baseline

The results of the 2014–2016 coastal surveys summarised in Chapter 5 show a significant reduction in waxy hydrocarbon loading compared to that found by the previous systematic surveys conducted during the early 1990s (Edwards et al., 2016). This result was not anticipated at the outset of the present study and demonstrates the need to maintain an up-to-date environmental baseline in order for it to remain representative and therefore of use in the event of an oil spill. As discussed in Chapter 5, the waxy hydrocarbon loading across the South Australian coastline is expected to continue declining as the abundant type I waxy bitumen now in the marine environment continues to break down with no fresh seepage to replace it. However, the possibility remains that the observed decline may also be associated with temporary seep inactivity, as oil seeps are often episodic and ephemeral (Kvenvolden and Cooper, 2003). Therefore, the established environmental baseline, specifically in terms of the abundance of waxy oil strandings, is likely to continue changing through time and future surveying will be required to assess this. Such surveys would be well advised to continue assessing both the abundance of the various waxy oils on the coastline and their extent of weathering, compared to the results in Chapters 4 and 5 of this study, to ascertain if the oils are associated with fresh seepage.

Finally, it would also be beneficial for future studies to expand the geographic extent of the survey area to assess the hydrocarbon loading of other areas of the Australian coastline, particularly along the pathway of the Leeuwin Current. Embayed beaches subject to high energy wave action along the Naturaliste coastline in Western Australia are most likely to collect waxy

bitumen strandings, as would islands along the coastline such as Rottnest Island, which are directly exposed to the Leeuwin Current compared to other areas of the coastline which are protected by offshore reefs.

REFERENCES

Amrani, A., Deev, A., Sessions, A.L., Tang, Y., Adkins, J.F., Hill, R.J., Moldowan, J.M., Wei, Z., 2012. The sulfur-isotopic compositions of benzothiophenes and dibenzothiophenes as a proxy for thermochemical sulfate reduction. Geochim. Cosmochim. Acta 84, 152–164. doi:10.1016/J.GCA.2012.01.023

Edwards, D., McKirdy, D.M., Summons, R.E., 1998. Enigmatic asphaltites from the southern Australian margin: molecular and carbon isotopic composition. Pet. Explor. Soc. Aust. J. 26, 397–420.

Edwards, D.S., McKirdy, D.M., Rowland, S.J., Heath, D.J., Gray, P.S., 2018. Waxy bitumen stranding in southern Australia: A geochemical study of multiple oil families and their likely origins. Org. Geochem. 118, 132–151. doi:10.1016/j.orggeochem.2017.12.010

Edwards, D.S., Vinall, D.R., Corrick, A.J., McKirdy, D.M., 2016. Natural bitumen stranding on the ocean beaches of Southern Australia: a historical and geospatial review. Trans. R. Soc. South Aust. 140, 152–185. doi:10.1080/03721426.2016.1203532

Kempton, R., Bourdet, J., Gong, S., 2017. Petroleum migration in the Bight Basin: a fluid inclusion approach to constraining source, composition and timing. Final Report GABRP Project 5.3. GABRP Research Report Series Number 14.

Kempton, R.H., Bourdet, J., Gong, S., Ross, A.S., 2020. Revealing oil migration in the frontier Bight Basin, Australia. Mar. Pet. Geol. 113. doi:10.1016/J.MARPETGEO.2019.104124

Kvenvolden, K.A., Cooper, C.K., 2003. Natural seepage of crude oil into the marine environment. Geo-Marine Lett. 23, 140–146. doi:10.1007/s00367-003-0135-0

Padley, D., 1995. Petroleum geochemistry of the Otway Basin and the significance of coastal bitumen strandings on adjacent southern Australian beaches. PhD thesis, University of Adelaide.

Scarlett, A.G., Holman, A.I., Georgiev, S. V., Stein, H.J., Summons, R.E., Grice, K., 2019. Multi-spectroscopic and elemental characterization of southern Australian asphaltites. Org. Geochem. 133, 77–91. doi:10.1016/J.ORGGEOCHEM.2019.04.006

Schiefelbein, C.F., Zumberge, J.E., Brown, S.W., 1997. Petroleum Systems in the Far East, in: Proceedings of an International Conference on Petroleum Systems of SE Asia and Australiasia Conference, May 1997. Indonesian Petroleum Association, pp. 101–113.

Selby, D., Creaser, R.A., Fowler, M.G., 2007. Re–Os elemental and isotopic systematics in crude oils. Geochim. Cosmochim. Acta 71, 378–386. doi:10.1016/j.gca.2006.09.005

ten Haven, H.L., Schiefelbein, C., 1995. The Petroleum Systems of Indonesia, in: Proceedings Indonesian Petroleum Association: Twenty Fourth Annual Convention Proceedings. pp. 443–459.

Totterdell, J.M., Struckmeyer, H.I.M., Boreham, C.J., Mitchell, C.H., Monteil, E., Bradshaw, B.E., 2008. Mid-Late Cretaceous organic-rich rocks from the eastern Bight Basin : implications for prospectivity, in: Blevin, J.E., Bradshaw, B.E., Uruski, E. (Eds.), PESA Eastern Australasian Basins Symposium III Special Publication. pp. 137–158.

SUPPLEMENTARY INFORMATION

Chapter 2: Remotely constraining the temporal evolution of offshore oil systems

SUPPLEMENTARY INFORMATION

1. Supplementary data tables

Table S1: Sample collection details. Co-ordinates use WGS84 datum and unless otherwise stated have a maximum error of ± 5m.

Sample	Stranding Location	Latitude	Longitude	Date Collected	Weight (g)
Asphaltites					
W13/007476	Cactus Beach	-32.0739	132.9761	10-Nov-14	813
W13/007477	Cactus Beach	-32.0689	132.9706	10-Nov-14	219
W13/007507	Waitpinga Beach	-35.6362	138.5061	22-Nov-14	601
W13/007516	The Granites	-36.6517	139.8520	23-Nov-14	170
W13/007668	Tractor Beach	-32.8675	134.1178	21-Sep-15	25
W13/007671	Cactus Beach	-32.5328	133.8636	23-Sep-15	276
W13/007672	Avoid Bay*	-34.66	135.49	31-May-15	1357
W13/007742	Greenly Beach*	-34.46	135.36	22-Aug-15	392
W13/007764	Eyre Well	-31.4651	131.1338	26-Sep-15	429
W13/007845	Sheringa Beach	-33.8744	135.1781	11-Oct-16	500
W13/007976	Waitpinga Beach	-35.6374	138.5103	19-Oct-16	3188
Waxy bitumen (for comparison)					
W13/007697	Avoid Bay*	-34.64	135.35	13-Jul-15	35

* = Sample donated from private collection. Location co-ordinates are approximate.

Table S2: Re-Os data.

Sample	Re (ppb)	±	Os (ppt)	±	^{192}Os (ppt)	±	^{187}Re / ^{188}Os	±	^{187}Os / ^{188}Os	±	Rho	% Re Blank	% ^{187}Os Blank	% ^{188}Os Blank	Osi (@ 74 Ma)	Osi (@ 53 Ma)	Osi (@ 68 Ma)	Osi (@ 83 Ma)	±
Asphaltites																			
W13/007476 (exterior)	3.11	0.01	33.5	0.5	12.1	0.3	514.1	14.7	1.263	0.046	0.776	1.2	1.7	8.7	0.63	0.81	0.68	0.55	0.07
W13/007477 (exterior)	3.09	0.01	32.5	0.5	11.7	0.3	527.7	15.2	1.280	0.047	0.776	1.2	1.7	8.8	0.63	0.81	0.68	0.55	0.07
W13/007477 (interior)	2.95	0.01	32.6	0.5	11.7	0.3	502.5	14.2	1.288	0.046	0.773	1.2	1.6	8.4	0.67	0.84	0.72	0.59	0.07
W13/007507 (interior)	2.65	0.01	28.0	0.4	10.1	0.3	521.4	15.4	1.244	0.045	0.798	0.5	0.8	4.0	0.60	0.78	0.65	0.52	0.07
W13/007507 (interior replicate)	2.15	0.01	24.6	0.6	8.8	0.5	483.7	24.8	1.265	0.083	0.771	0.7	0.4	2.1	0.67	0.84	0.72	0.60	0.09
W13/007516 (exterior)	3.01	0.01	31.7	0.5	11.4	0.3	526.3	15.3	1.303	0.047	0.781	1.2	1.7	8.9	0.65	0.84	0.71	0.58	0.07
W13/007516 (interior)	3.00	0.01	30.3	0.5	10.9	0.3	547.8	16.0	1.285	0.047	0.776	1.1	1.7	8.9	0.61	0.80	0.66	0.53	0.07
W13/007668 (interior)	3.08	0.01	32.3	0.6	11.6	0.3	528.6	15.5	1.278	0.068	0.539	1.2	1.8	9.2	0.63	0.81	0.68	0.55	0.09
W13/007671 (exterior)	2.99	0.01	32.4	0.5	11.6	0.3	512.6	15.1	1.291	0.048	0.776	1.2	1.8	9.1	0.66	0.84	0.71	0.58	0.07
W13/007671 (interior)	4.02	0.01	43.1	0.6	15.6	0.4	513.6	12.9	1.233	0.040	0.756	0.3	0.5	2.7	0.60	0.78	0.65	0.52	0.06
W13/007672 (interior)	2.68	0.01	36.4	0.5	13.3	0.3	400.5	10.3	1.122	0.037	0.758	0.4	0.6	2.8	0.63	0.77	0.67	0.57	0.05
W13/007742 (interior)	2.85	0.01	30.3	0.5	10.9	0.3	521.5	16.2	1.299	0.050	0.794	1.4	2.0	10.4	0.66	0.84	0.71	0.58	0.08
W13/007764 (exterior)	3.07	0.02	32.2	0.5	11.5	0.3	529.6	15.3	1.294	0.047	0.772	1.1	1.7	8.7	0.64	0.83	0.69	0.56	0.07
W13/007764 (interior)	3.04	0.01	33.0	0.5	11.9	0.3	508.0	13.8	1.219	0.042	0.775	0.4	0.7	3.3	0.59	0.77	0.64	0.52	0.06
W13/007845 (interior)	2.89	0.01	31.2	0.5	11.2	0.3	515.5	15.1	1.296	0.048	0.783	1.2	1.8	9.2	0.66	0.84	0.71	0.58	0.07
W13/007976 (interior)	2.59	0.01	30.1	0.4	10.9	0.3	470.7	13.0	1.176	0.041	0.780	0.4	0.7	3.5	0.60	0.76	0.64	0.52	0.06
Waxy Bitumen (for comparison)																			
W13/007697 (interior)	0.02	0.01	1.34	0.3	0.5	0.3	84.4	60.8	0.486	0.279	0.544	65.0	16.5	32.3	N/A	N/A	N/A	N/A	N/A

Individual ratio uncertainties are given at the 2σ level.

Rho = error correlation value between ^{187}Re/^{188}Os and ^{187}Os/^{188}Os

Os_i uncertainties are determined through full propagation of uncertainties in Re and Os mass spectrometry, spike, blanks and std Rd and Os isotopic values.

Table S3: Asphaltite Re-Os deviation assessment.

Sample	^{187}Re / ^{188}Os	±	^{187}Os / ^{188}Os	±	^{187}Os / ^{188}Os calculated from data best-fit initial	Difference	% deviation from regression #1	Comments
W13/007476 (exterior)	514.1	14.7	1.263	0.046	1.247	0.017	1.3	
W13/007477 (exterior)	527.7	15.2	1.280	0.047	1.263	0.017	1.3	
W13/007477 (interior)	502.5	14.2	1.288	0.046	1.233	0.055	4.4	>2% deviation. Excluded from regression #2
W13/007507 (interior)	521.4	15.4	1.244	0.045	1.256	-0.012	-0.9	
W13/007507 (interior replicate)	483.7	24.8	1.265	0.083	1.210	0.054	4.5	>2% deviation. Excluded from regression #2
W13/007516 (exterior)	526.3	15.3	1.303	0.047	1.262	0.042	3.3	>2% deviation. Excluded from regression #2
W13/007516 (interior)	547.8	16.0	1.285	0.047	1.287	-0.003	-0.2	
W13/007668 (interior)	528.6	15.5	1.278	0.068	1.264	0.013	1.0	
W13/007671 (exterior)	512.6	15.1	1.291	0.048	1.245	0.046	3.7	>2% deviation. Excluded from regression #2
W13/007671 (interior)	513.6	12.9	1.233	0.040	1.246	-0.013	-1.1	
W13/007672 (interior)	400.5	10.3	1.122	0.037	1.111	0.011	1.0	
W13/007742 (interior)	521.5	16.2	1.299	0.050	1.256	0.043	3.4	>2% deviation. Excluded from regression #2
W13/007764 (exterior)	529.6	15.3	1.294	0.047	1.266	0.028	2.3	>2% deviation. Excluded from regression #2
W13/007764 (interior)	508.0	13.8	1.219	0.042	1.240	-0.020	-1.6	
W13/007845 (interior)	515.5	15.1	1.296	0.048	1.249	0.047	3.8	>2% deviation. Excluded from regression #2
W13/007976 (interior)	470.7	13.0	1.176	0.041	1.195	-0.019	-1.6	

Isochron equation for regression #1 (all data): $^{187}Os/^{188}Os_{\text{calculated from data best-fit initial}} = 0.63 + 0.0012 \times {}^{187}Re/^{188}Os$
Samples which deviated >2% from regression #1 were excluded from regression #2.

Table S4: Selected geochemical parameters and assigned degradation levels for analysed samples.

Sample	Asphaltene content (%)	Relative degradation level	Soft vs. Brittle*	Lightest *n*-alkane preserved	Pr/ Ph	MNR (*m/z* 142)	DNR-1 (*m/z* 156)	Ts/ (Ts+Tm)	C_{29} / C_{30} αβ hopane	27 : 28 : 29 ααα 20*R* steranes (*m/z* 217)	27: 28 : 29 αββ (20*R*+*S*) steranes (*m/z* 218)	C_{27} Dia / (Dia + Regular)	C_{35} homohopane index (%)
Asphaltites													
W13/007476	53	Moderate	Brittle	10	1.3	0.81	2.39	0.41	0.60	43 : 20 : 38	38 : 25 : 37	0.42	7.6
W13/007477	56	Moderate	Brittle	10	1.1	0.72	2.03	0.40	0.59	47 : 18 : 36	38 : 24 : 37	0.44	7.4
W13/007507	54	Moderate	Brittle	10	1.2	0.98	2.43	0.40	0.65	40 : 27 : 33	39 : 25 : 36	0.43	7.4
W13/007516	55	Moderate	Brittle	10	1.3	0.72	2.46	0.38	0.66	44 : 19 : 37	38 : 25 : 37	0.42	8.0
W13/007668	59	High	Brittle	14	1.1	0.30	1.20	0.38	0.67	37 : 27 : 36	37: 26 : 37	0.45	7.7
W13/007671	54	Moderate	Brittle	9	1.1	0.72	2.31	0.41	0.65	37 : 23 : 39	37 : 25 : 38	0.42	7.9
W13/007672	54	Moderate	Brittle	9	1.2	0.77	2.31	0.38	0.65	43 : 20 : 37	39 : 25 : 36	0.43	8.4
W13/007742	54	Moderate	Brittle	10	1.0	0.78	1.56	0.39	0.64	39 : 23 : 38	39 : 23 : 38	0.45	8.3
W13/007764	56	Moderate	Brittle	9	1.2	0.69	2.41	0.35	0.61	38 : 25 : 37	36 : 24 : 40	0.42	10.9
W13/007845	51	Low	Soft	< 8‡	1.2	0.83	2.58	0.37	0.64	39 : 27 : 34	39 : 26 : 35	0.46	7.2
W13/007976	51	Low	Soft	< 8‡	1.2	0.93	2.98	0.41	0.62	39 : 26 : 36	38 : 25 : 37	0.45	7.6
Waxy bitumen													
W13/007697	32	Moderate / High	Soft†	12	1.8	0.84§	5.84§	0.60	0.67	39 : 21 : 40	42 : 22 : 37	0.47	4.7

* At the time of initial sub-sampling. Asphaltites devolatilise their low-molecular-weight hydrocarbons during storage and will eventually become brittle like their weathered counterparts.

† Waxy bitumen remain semi-solid and will only develop a brittle exterior if extremely degraded.

‡ *n*-alkanes lighter than C_8 (octane) were outside the detection limit of the whole-oil GC-MS analysis.

§ Compounds present in low abundance.

MN = Methylnaphthalene ratio = 2-MN / 1-MN

DNR = Dimethylnaphthalene ratio = (2,6-DMN + 2,7-DMN) / 1,5-DMN

C_{27} Dia / Dia + Regular = C_{27} βα (20S+R) diacholestanes / (C_{27} βα (20S+R) diacholestanes + C_{27} ααα (20S+R) cholestanes

C_{35} homohopane index (%) = (C_{35} αβ (S+R) homohopanes / $C_{31\text{-}35}$ αβ (S+R) homohopanes) x 100

Table S5: Degradation level classification criteria. Classification for each sample is based on the characteristics of the interior sub-sample.

Degradation Level	Physical characteristics (soft / brittle)*	*n*-alkanes <C_{10}	*n-alkanes* <C_{14}	Water-soluble compounds (e.g. alkylnaphthalenes)	Steranes and hopanes
Low	Soft	Preserved/Altered	Preserved	Preserved	Preserved
Moderate	Brittle	Altered/Lost	Preserved/Altered	Preserved / Mild Alteration	Preserved
High	Brittle	Lost	Lost	Significant alteration	Potential minor alteration to the C_{30} αβ hopane and C_{27} steranes

* Only asphaltites become brittle due to weathering. The waxy bitumen used for comparison remains semi-solid despite moderate degradation.

Table S6: Compiled Re-Os data for OAE2 sections and calculated Os_g values for asphaltite generation window (68 ± 15 Ma).

Sample ID	Reference	Depth (m)	Re (ppb)	±	Os (ppt)	±	^{187}Re / ^{188}Os	±	^{187}Os / ^{188}Os	±	^{192}Os (ppt)	Os_g (@ 53 Ma)	Os_g (@ 68 Ma)	Os_g (@83 Ma)	±
Portland #1 Core, Colorado, USA (Fig. 6A)															
AD117-09	(27)	9.30	47.5	0.15	298.4	1.19	983.5	4.2	2.295	0.008	96.0	1.427	1.181	0.935	0.004
AD115-09	(27)	8.71	49.4	0.16	290.3	1.17	1071.7	4.7	2.472	0.008	91.8	1.525	1.257	0.989	0.004
AD114-09	(27)	8.46	75.2	0.24	303.3	1.32	1714.1	7.5	3.453	0.011	87.3	1.939	1.510	1.081	0.004
AD112-09	(27)	8.25	55.9	0.18	277.8	1.19	1306.5	5.9	2.794	0.010	85.1	1.640	1.313	0.986	0.004
AD111-09	(27)	7.92	69.5	0.22	399.2	1.46	1093.0	4.3	2.442	0.007	126.6	1.477	1.203	0.930	0.004
AD110-09	(27)	7.65	1.3	0.01	14.6	0.35	500.4	26.2	1.494	0.084	5.1	1.052	0.927	0.801	0.055
AD109-09	(27)	7.49	52.5	0.17	296.8	1.28	1111.8	5.0	2.466	0.009	93.9	1.484	1.206	0.928	0.004
AD108-09	(27)	7.25	66.3	0.21	366.2	1.42	1146.5	4.7	2.540	0.008	115.0	1.527	1.241	0.954	0.004
AD107-09	(27)	6.98	50.9	0.16	323.7	1.25	964.7	4.1	2.229	0.007	104.9	1.376	1.135	0.894	0.004
AD106-09	(27)	6.69	8.3	0.03	90.9	0.65	516.6	5.3	1.504	0.017	31.8	1.048	0.919	0.789	0.011
AD105-09	(27)	6.37	12.6	0.04	129.2	0.77	558.6	4.3	1.583	0.013	44.8	1.090	0.950	0.810	0.008
AD104-09	(27)	6.07	2.0	0.01	27.4	0.45	414.2	13.5	1.317	0.050	9.8	0.951	0.848	0.744	0.034
AD103-09	(27)	5.47	5.3	0.02	88.5	0.77	327.4	4.5	1.143	0.020	32.2	0.854	0.772	0.690	0.014
AD102-09	(27)	5.11	17.7	0.06	189.0	0.91	521.2	3.1	1.325	0.009	67.5	0.865	0.734	0.604	0.005
AD101-09	(27)	4.80	7.2	0.03	98.0	0.74	407.4	4.6	1.282	0.017	35.2	0.923	0.821	0.719	0.011
AD99-09	(27)	4.17	35.0	0.11	319.0	1.08	627.9	2.6	1.572	0.005	110.8	1.018	0.861	0.704	0.003
AD98-09	(27)	3.85	4.8	0.02	111.6	0.75	229.3	2.5	0.955	0.012	41.6	0.752	0.695	0.637	0.010
AD96-09	(27)	3.52	3.9	0.02	77.5	0.63	267.7	3.7	0.948	0.016	28.9	0.712	0.645	0.578	0.012
AD95-09	(27)	3.10	4.6	0.02	134.2	0.92	175.9	2.1	0.697	0.011	51.6	0.542	0.498	0.454	0.008
AD93-09	(27)	2.40	5.4	0.02	100.9	0.67	278.8	3.1	0.792	0.011	38.3	0.546	0.476	0.406	0.006
AD90-09	(27)	1.90	17.0	0.06	532.6	1.41	160.2	0.7	0.468	0.002	210.5	0.327	0.286	0.246	0.001
AD88-09	(27)	1.67	16.9	0.06	570.4	1.47	148.6	0.7	0.438	0.002	226.3	0.307	0.270	0.232	0.001
AD87-09	(27)	1.50	4.7	0.02	670.3	3.46	34.1	0.4	0.210	0.003	273.7	0.180	0.171	0.162	0.003
AD84-09	(27)	1.25	4.1	0.02	621.4	4.12	32.0	0.5	0.210	0.004	253.8	0.181	0.173	0.165	0.004
AD83-09	(27)	1.10	3.7	0.02	213.8	1.52	86.5	1.2	0.344	0.007	85.8	0.268	0.246	0.224	0.005
AD68-09	(27)	0.30	1.9	0.01	592.8	5.62	15.3	0.3	0.216	0.006	241.9	0.202	0.199	0.195	0.007
AD69-09	(27)	0.20	18.6	0.06	1116.0	2.51	81.9	0.4	0.296	0.001	450.8	0.224	0.203	0.183	0.001

Sample ID	Reference	Depth (m)	Re (ppb)	±	Os (ppt)	±	^{187}Re / ^{188}Os	±	^{187}Os / ^{188}Os	±	^{192}Os (ppt)	Os_g (@ 53 Ma)	Os_g (@ 68 Ma)	Os_g (@83 Ma)	±
AD70-09	(27)	0.10	35.4	0.12	1716.0	2.90	102.1	0.4	0.328	0.001	690.3	0.238	0.213	0.187	0.001
AD71-09	(27)	0.00	111.9	0.55	554.6	1.68	1280.3	6.6	2.558	0.005	173.9	1.427	1.106	0.786	0.003
AD72-09	(27)	-0.10	58.3	0.19	324.1	1.38	1146.2	5.0	2.591	0.009	101.3	1.578	1.292	1.005	0.005
AD73-09	(27)	-0.20	66.7	0.22	262.4	1.26	1788.0	8.5	3.646	0.013	74.3	2.067	1.619	1.172	0.005
AD74-09	(27)	-0.30	51.8	0.17	320.5	1.25	1009.9	4.3	2.397	0.008	102.1	1.505	1.253	1.000	0.004
AD75-09	(27)	-0.30	71.8	0.24	301.0	1.35	1646.9	7.4	3.447	0.011	86.7	1.992	1.581	1.168	0.005
AD76-09	(27)	-0.50	59.0	0.19	290.0	1.27	1350.9	6.0	3.034	0.010	86.8	1.840	1.502	1.164	0.005
AD77-09	(27)	-0.60	72.7	0.23	371.9	1.48	1288.4	5.2	2.951	0.008	112.2	1.813	1.491	1.169	0.005
AD78-09	(27)	-0.70	70.7	0.23	323.0	1.42	1481.7	6.4	3.232	0.011	94.9	1.923	1.552	1.182	0.005
AD118-09	(27)	-1.10	87.3	0.28	346.6	1.49	1776.5	7.5	3.678	0.011	97.8	2.109	1.664	1.220	0.002
AD119-09	(27)	-1.25	84.3	0.27	332.2	1.47	1792.6	7.7	3.702	0.011	93.6	2.118	1.670	1.221	0.002
AD79-09	(27)	-1.84	82.4	0.27	326.5	1.43	1775.8	7.6	3.660	0.011	92.3	2.092	1.647	1.203	0.005
AD120-09	(27)	-1.98	67.7	0.22	269.4	1.27	1766.0	8.1	3.644	0.013	76.3	2.084	1.642	1.200	0.003
AD121-09	(27)	-2.26	58.2	0.19	251.0	1.23	1597.1	7.7	3.423	0.013	72.5	2.012	1.613	1.213	0.003
AD80-09	(27)	-2.81	83.5	0.27	328.7	1.71	1796.2	8.3	3.711	0.016	95.7	2.124	1.675	1.226	0.006
AD122-09	(27)	-2.87	70.0	0.23	295.3	1.36	1642.9	7.4	3.492	0.012	84.7	2.041	1.630	1.219	0.003
AD123-09	(27)	-2.95	67.2	0.22	256.8	1.32	1866.9	9.2	3.817	0.015	71.6	2.168	1.701	1.233	0.003
AD124-09	(27)	-3.18	76.3	0.25	276.7	1.80	1999.3	13.0	3.993	0.025	75.9	2.227	1.727	1.227	0.004
AD81-09	(27)	-3.79	91.0	0.29	391.3	1.58	1576.1	6.3	3.246	0.009	114.8	1.854	1.460	1.065	0.004
AD126-09	(27)	-3.82	125.7	0.41	497.0	2.25	1770.4	7.8	3.598	0.012	141.2	2.034	1.591	1.148	0.002
AD128-09	(27)	-4.25	84.4	0.27	333.4	1.87	1768.1	9.9	3.576	0.018	94.9	2.014	1.571	1.129	0.003
AD82-09	(27)	-4.80	69.7	0.22	365.6	1.51	1226.8	5.1	2.692	0.009	113.1	1.608	1.301	0.994	0.004
AD130-09	(27)	-5.16	85.1	0.27	400.9	2.28	1389.3	7.6	2.878	0.016	121.8	1.651	1.303	0.956	0.003
AD132-09	(27)	-5.36	68.1	0.22	305.4	2.52	1529.8	12.3	3.375	0.034	88.6	2.024	1.641	1.258	0.006
AD133-09	(27)	-5.59	73.5	0.24	299.3	1.91	1715.9	10.7	3.582	0.022	85.2	2.067	1.637	1.208	0.004
501.61	(27)	-7.09	90.0	0.29	366.6	2.40	1724.6	11.8	3.638	0.024	103.8	2.114	1.683	1.251	0.004
AD134-09	(27)	-7.26	82.7	0.27	319.1	1.90	1850.8	10.8	3.821	0.020	88.9	2.186	1.723	1.260	0.004
505.9	(27)	-8.53	64.6	0.21	328.2	2.15	1301.8	9.5	2.986	0.021	98.7	1.836	1.510	1.185	0.005

Sample ID	Reference	Depth (m)	Re (ppb)	±	Os (ppt)	±	^{187}Re / ^{188}Os	±	^{187}Os / ^{188}Os	±	^{192}Os (ppt)	Os_g (@ 53 Ma)	Os_g (@ 68 Ma)	Os_g (@83 Ma)	±
509.5	(27)	-9.65	45.0	0.15	278.4	1.94	1029.1	8.6	2.597	0.022	87.0	1.688	1.431	1.173	0.006
512	(27)	-10.43	56.8	0.19	271.3	2.04	1415.7	12.4	3.215	0.029	79.9	1.964	1.610	1.256	0.006
516	(27)	-11.65	52.2	0.17	227.6	1.85	1583.0	15.9	3.453	0.034	65.6	2.055	1.659	1.263	0.007
DSDP Site 530, Hole 530A, South Atlantic (Fig. 6B)															
AD80-10	(27)	1017.18	0.2	0.01	14.3	0.38	70.3	6.00	0.530	0.041	5.6	0.468	0.450	0.433	0.024
AD86-10	(27)	1021.88	11.6	0.04	682.2	3.05	87.5	0.62	0.665	0.006	263.2	0.588	0.566	0.544	0.003
AD88-10	(27)	1023.53	10.7	0.04	331.6	1.79	169.9	1.41	0.808	0.008	125.7	0.658	0.616	0.573	0.004
AD90-10	(27)	1024.58	2.8	0.01	215.5	1.72	66.0	0.97	0.671	0.013	83.1	0.613	0.597	0.580	0.007
AD92-10	(27)	1027.29	35.4	0.13	1025.7	5.04	181.0	1.34	0.816	0.007	388.5	0.656	0.611	0.566	0.003
AD94-10	(27)	1028.16	156.2	0.51	2385.9	6.56	355.6	1.38	1.100	0.003	874.1	0.786	0.697	0.608	0.001
AD95-10	(27)	1028.78	183.4	0.60	1663.0	5.29	627.4	2.54	1.514	0.004	581.4	0.959	0.802	0.646	0.001
AD97-10	(27)	1029.65	198.2	0.65	1817.4	5.89	627.5	2.50	1.616	0.005	628.3	1.062	0.905	0.748	0.002
AD99-10	(27)	1031.35	18.8	0.07	455.1	2.32	217.5	1.69	0.821	0.008	172.3	0.629	0.575	0.520	0.003
AD100-10	(27)	1031.56	34.2	0.13	642.2	4.03	283.1	2.72	0.926	0.011	240.1	0.676	0.605	0.534	0.004
AD101-10	(27)	1031.87	79.1	0.26	1599.1	6.46	265.5	1.37	1.004	0.006	592.4	0.769	0.703	0.637	0.002
AD102-10	(27)	1035.28	0.3	0.01	39.8	1.44	39.6	3.59	0.282	0.033	16.1	0.247	0.238	0.228	0.016
AD103-10	(27)	1035.50	1.7	0.01	200.8	1.97	42.9	0.93	0.301	0.009	81.0	0.263	0.252	0.241	0.004
AD104-10	(27)	1035.69	1.8	0.02	348.9	4.40	25.5	0.74	0.292	0.011	141.0	0.269	0.263	0.256	0.006
AD105-10	(27)	1035.89	2.5	0.01	354.7	3.42	34.1	0.72	0.260	0.007	143.9	0.230	0.221	0.212	0.004
AD106-10	(27)	1036.10	12.4	0.05	1042.3	5.34	58.5	0.59	0.282	0.004	421.8	0.230	0.216	0.201	0.002
AD108-10	(27)	1036.51	11.4	0.05	1868.2	8.10	29.8	0.27	0.226	0.003	761.5	0.200	0.192	0.185	0.001
AD109-10	(27)	1036.72	48.1	0.16	6144.1	12.50	38.2	0.17	0.216	0.001	2507.5	0.182	0.173	0.163	0.000
AD110-10	(27)	1036.97	6.6	0.04	2465.9	16.09	13.0	0.19	0.177	0.003	1011.5	0.166	0.162	0.159	0.002
AD111-10	(27)	1037.21	13.7	0.05	2195.9	11.35	30.3	0.33	0.216	0.003	896.2	0.190	0.182	0.174	0.002
AD112-10	(27)	1037.41	51.4	0.17	5239.7	12.02	48.1	0.22	0.272	0.001	2123.1	0.230	0.218	0.206	0.001
AD113-10	(27)	1037.54	104.6	0.35	4429.2	10.05	117.3	0.51	0.357	0.001	1775.3	0.254	0.225	0.195	0.001
AD114-10	(27)	1037.69	122.5	0.40	8478.9	17.56	71.2	0.30	0.305	0.001	3420.9	0.243	0.225	0.207	0.001

Sample ID	Reference	Depth (m)	Re (ppb)	±	Os (ppt)	±	^{187}Re / ^{188}Os	±	^{187}Os / ^{188}Os	±	^{192}Os (ppt)	Os_g (@ 53 Ma)	Os_g (@ 68 Ma)	Os_g (@83 Ma)	±
AD115-10	(27)	1037.89	122.9	0.40	9101.5	18.69	65.9	0.28	0.223	0.001	3711.4	0.164	0.148	0.131	0.000
AD116-10	(27)	1038.12	0.5	0.01	571.5	10.23	4.6	0.21	0.171	0.010	234.6	0.167	0.166	0.165	0.006
AD117-10	(27)	1038.35	177.5	0.58	9451.3	14.93	92.6	0.34	0.304	0.001	3814.2	0.222	0.199	0.176	0.000
AD118-10	(27)	1038.50	280.3	0.95	14395.4	24.15	96.5	0.36	0.346	0.001	5778.3	0.261	0.236	0.212	0.000
AD119-10	(27)	1038.87	356.4	1.16	12387.3	16.94	142.6	0.49	0.348	0.001	4970.8	0.222	0.187	0.151	0.000
AD120-10	(27)	1039.26	77.4	0.26	1713.0	5.29	236.1	1.08	0.772	0.003	652.3	0.564	0.505	0.445	0.001
AD121-10	(27)	1039.62	0.4	0.01	45.8	0.87	46.8	2.03	0.548	0.031	17.9	0.507	0.495	0.484	0.017
AD122-10	(27)	1039.78	13.9	0.05	394.9	2.22	185.3	1.62	0.864	0.009	148.7	0.700	0.653	0.607	0.004
AD123-10	(27)	1044.20	1.0	0.01	105.7	2.07	51.1	2.17	0.773	0.044	40.2	0.728	0.715	0.703	0.025
AD124-10	(27)	1044.43	0.9	0.01	36.6	0.58	122.2	4.31	0.774	0.033	13.9	0.666	0.636	0.605	0.016
AD125-10	(27)	1044.86	0.4	0.01	38.2	0.79	60.1	3.10	0.720	0.043	14.7	0.667	0.652	0.636	0.025
AD126-10	(27)	1045.44	0.8	0.01	88.4	1.71	46.4	2.03	0.670	0.038	34.1	0.629	0.618	0.606	0.022
AD127-10	(27)	1045.51	1.1	0.01	125.9	2.42	45.2	1.90	0.656	0.037	48.6	0.616	0.605	0.593	0.021
AD129-10	(27)	1045.83	2.3	0.01	112.3	0.96	107.1	1.69	0.781	0.016	42.7	0.686	0.659	0.633	0.008
AD131-10	(27)	1046.52	0.3	0.01	56.3	0.80	23.2	1.28	0.551	0.022	22.0	0.531	0.525	0.519	0.018
AD137-10	(27)	1048.51	2.4	0.01	111.0	0.97	112.9	1.78	0.851	0.017	41.9	0.751	0.723	0.695	0.009
AD139-10	(27)	1048.97	1.4	0.02	73.9	1.51	99.5	4.51	0.804	0.047	28.0	0.716	0.691	0.666	0.024
AD141-10	(27)	1050.59	13.2	0.05	456.3	2.16	154.5	1.02	0.973	0.007	169.7	0.837	0.798	0.759	0.004
AD143-10	(27)	1051.23	18.4	0.07	576.1	2.97	171.0	1.26	0.972	0.008	214.3	0.821	0.778	0.735	0.004
Vocontian Basin (Pont d'Issole (Adx-10 and ISLx) and Vergons (VGN) sections), SE France (Fig. 6C)															
AD41-10	(27)	17.22	0.2	0.02	306.2	1.59	3.8	0.3	1.128	0.009	111.8	1.124	1.123	1.122	0.050
AD43-10	(27)	15.55	0.1	0.02	228.8	1.47	3.1	0.4	0.937	0.012	85.4	0.934	0.934	0.933	0.066
AD45-10	(27)	15.26	13.2	0.05	324.4	1.72	217.8	1.7	0.994	0.009	120.3	0.802	0.747	0.693	0.004
AD47-10	(27)	14.86	0.1	0.02	284.4	1.93	2.1	0.4	0.943	0.013	106.1	0.941	0.940	0.940	0.080
AD49-10	(27)	14.46	0.3	0.02	6.5	0.45	227.7	41.1	0.963	0.168	2.4	0.762	0.705	0.648	0.076
AD51-10	(27)	14.06	1.2	0.02	83.8	1.62	69.0	3.1	0.427	0.025	33.3	0.366	0.349	0.331	0.012
AD55-10	(27)	13.26	0.8	0.02	109.3	3.89	37.0	3.1	0.524	0.060	42.9	0.491	0.482	0.472	0.033

Sample ID	Reference	Depth (m)	Re (ppb)	±	Os (ppt)	±	^{187}Re / ^{188}Os	±	^{187}Os / ^{188}Os	±	^{192}Os (ppt)	Os_g (@ 53 Ma)	Os_g (@ 68 Ma)	Os_g (@83 Ma)	±
AD59-10	(27)	12.46	12.5	0.05	340.7	1.71	188.4	1.6	0.629	0.006	132.0	0.463	0.415	0.368	0.002
AD61-10	(27)	12.06	1.4	0.03	149.1	5.27	47.5	3.9	0.405	0.046	59.4	0.363	0.351	0.339	0.023
AD63-10	(27)	11.66	12.8	0.05	600.9	2.56	108.5	0.8	0.558	0.005	234.9	0.463	0.436	0.408	0.002
AD64-10	(27)	11.46	14.0	0.05	461.8	2.04	154.9	1.1	0.574	0.005	180.1	0.437	0.398	0.359	0.002
AD65-10	(27)	11.26	7.5	0.03	293.4	1.85	129.8	1.5	0.520	0.008	115.2	0.406	0.373	0.341	0.003
AD67-10	(27)	10.86	10.3	0.04	366.1	2.00	143.9	1.3	0.582	0.007	142.7	0.455	0.419	0.383	0.003
AD69-10	(27)	10.46	1.5	0.01	671.1	12.09	11.1	0.5	0.220	0.012	273.8	0.210	0.207	0.205	0.007
AD71-10	(27)	10.06	2.3	0.02	733.7	13.23	15.2	0.6	0.218	0.012	299.4	0.204	0.201	0.197	0.007
AD73-10	(27)	9.66	2.4	0.01	697.4	12.52	16.8	0.7	0.189	0.011	285.6	0.174	0.170	0.166	0.006
AD75-10	(27)	9.45	0.4	0.01	1642.1	57.51	1.1	0.1	0.162	0.018	674.9	0.161	0.161	0.161	0.011
VGN 437	(27)	8.00	7.6	0.03	362.9	6.83	106.5	4.3	0.537	0.030	142.2	0.443	0.416	0.390	0.013
AD02-10	(27)	7.75	0.4	0.01	461.2	8.27	4.7	0.2	0.189	0.011	188.9	0.185	0.184	0.183	0.007
AD05-10	(27)	7.15	0.2	0.00	269.8	9.46	3.2	0.3	0.210	0.024	110.2	0.207	0.206	0.205	0.014
AD07-10	(27)	6.75	14.4	0.05	1294.0	4.82	55.3	0.4	0.361	0.003	518.4	0.312	0.298	0.284	0.001
AD09-10	(27)	6.35	4.4	0.03	670.8	6.37	31.8	0.7	0.223	0.006	273.5	0.195	0.187	0.179	0.003
AD11-10	(27)	5.95	5.9	0.02	748.4	3.22	38.2	0.3	0.215	0.002	305.5	0.181	0.171	0.162	0.001
AD13-10	(27)	5.55	4.0	0.04	651.2	2.75	29.7	0.4	0.184	0.002	266.9	0.158	0.150	0.143	0.001
AD15-10	(27)	5.15	463.9	1.50	37827.0	42.56	60.3	0.2	0.287	0.000	15297.3	0.234	0.219	0.204	0.000
AD17-10	(27)	4.75	5.1	0.02	790.9	7.30	31.2	0.6	0.175	0.005	324.5	0.147	0.139	0.132	0.002
AD19-10	(27)	4.35	11.5	0.04	2853.1	8.39	19.6	0.1	0.223	0.002	1163.4	0.206	0.201	0.196	0.001
AD21-10	(27)	3.95	5.4	0.02	1675.3	7.06	15.7	0.1	0.178	0.002	687.1	0.164	0.160	0.156	0.001
AD22-10	(27)	3.75	2.0	0.01	602.4	5.73	16.0	0.3	0.206	0.006	246.2	0.191	0.187	0.183	0.003
AD23-10	(27)	3.55	1.3	0.01	623.4	11.20	10.3	0.4	0.201	0.011	254.9	0.192	0.189	0.187	0.006
AD24-10	(27)	3.35	4.4	0.02	275.3	2.90	80.2	1.7	0.430	0.013	109.3	0.359	0.339	0.319	0.006
ISL8	(27)	2.80	18.5	0.06	4084.2	10.75	22.1	0.1	0.250	0.001	1659.5	0.231	0.225	0.220	0.001
ISL7	(27)	2.30	0.4	0.01	179.6	3.37	11.7	0.6	0.510	0.029	70.6	0.500	0.497	0.494	0.019
VGN 436.5	(27)	1.50	0.9	0.03	167.2	0.85	25.9	0.9	0.257	0.004	67.9	0.234	0.228	0.221	0.004
VGN 436	(27)	1.00	0.3	0.01	31.2	0.63	52.2	2.4	0.896	0.052	11.7	0.850	0.837	0.823	0.030

Sample ID	Reference	Depth (m)	Re (ppb)	±	Os (ppt)	±	^{187}Re / ^{188}Os	±	^{187}Os / ^{188}Os	±	^{192}Os (ppt)	Os_g (@ 53 Ma)	Os_g (@ 68 Ma)	Os_g (@83 Ma)	±
VGN 435	(27)	0.00	0.2	0.01	30.2	0.61	36.4	1.8	0.825	0.048	11.4	0.793	0.784	0.775	0.030
AD27-10	(27)	-0.78	0.4	0.01	31.1	1.12	66.0	5.5	0.896	0.102	11.7	0.838	0.821	0.805	0.056
AD29-10	(27)	-1.07	0.3	0.00	35.7	1.29	40.2	3.3	0.902	0.102	13.4	0.866	0.856	0.846	0.059
AD33-10	(27)	-1.84	0.3	0.00	57.0	1.53	28.1	1.6	0.975	0.079	21.2	0.950	0.943	0.936	0.046
VGN 431	(27)	-4.00	0.5	0.01	33.8	0.72	74.4	3.8	0.892	0.054	12.7	0.826	0.808	0.789	0.031
Wunstorf, NW Germany (Fig. 6D)															
AD44-09	(27)	-27.17	2.6	0.01	70.7	0.46	194.9	2.0	0.919	0.012	26.5	0.747	0.698	0.649	0.010
AD42-09	(27)	-28.76	1.0	0.01	53.6	0.36	95.6	1.2	0.818	0.011	20.3	0.734	0.710	0.686	0.012
AD41-09	(27)	-29.4	1.6	0.01	44.2	0.32	191.9	2.3	0.949	0.013	16.5	0.779	0.731	0.683	0.012
AD40-09	(27)	-30.06	14.9	0.05	505.8	1.43	156.3	0.6	0.907	0.003	189.5	0.769	0.730	0.691	0.003
AD38-09	(27)	-32.72	1.1	0.01	118.7	0.68	48.1	0.5	0.688	0.008	45.7	0.646	0.634	0.622	0.010
AD30-09	(27)	-36.53	38.8	0.13	398.1	0.97	551.6	1.9	1.456	0.003	140.1	0.969	0.831	0.693	0.002
AD28-09	(27)	-37.63	0.5	0.01	88.2	0.34	30.4	0.4	0.608	0.004	34.3	0.582	0.574	0.566	0.008
AD27-09	(27)	-38.34	1.7	0.01	253.9	0.81	34.4	0.2	0.596	0.003	98.8	0.566	0.557	0.549	0.004
AD26-09	(27)	-39.84	5.2	0.02	288.0	0.78	93.2	0.4	0.631	0.002	111.6	0.548	0.525	0.502	0.003
AD25-09	(27)	-40.47	9.9	0.03	270.7	0.64	192.4	0.7	0.812	0.002	102.6	0.642	0.594	0.546	0.002
AD24-09	(27)	-41.1	12.4	0.04	296.7	0.65	220.6	0.8	0.837	0.002	112.1	0.642	0.587	0.532	0.002
AD23-09	(27)	-42.05	1.2	0.01	133.1	0.69	46.1	0.5	0.490	0.006	52.5	0.449	0.438	0.426	0.007
AD21-09	(27)	-43.15	6.9	0.02	737.4	2.20	47.2	0.2	0.465	0.002	291.6	0.423	0.412	0.400	0.003
AD19-09	(27)	-43.78	16.8	0.05	485.0	1.00	177.1	0.7	0.617	0.001	188.2	0.460	0.416	0.372	0.002
AD17-09	(27)	-44.33	5.0	0.02	2247.3	4.86	10.8	0.1	0.199	0.001	919.2	0.189	0.186	0.184	0.001
AD12-09	(27)	-47.7	3.4	0.01	1375.3	5.03	12.1	0.1	0.198	0.002	562.6	0.187	0.184	0.181	0.002
AD11-09	(27)	-47.97	0.7	0.01	223.7	2.13	14.5	0.3	0.232	0.007	91.1	0.220	0.216	0.212	0.008
AD10-09	(27)	-48.1	8.5	0.03	801.8	1.58	52.1	0.2	0.267	0.001	325.1	0.221	0.208	0.195	0.001
AD9-09	(27)	-48.32	3.7	0.01	551.0	1.69	32.9	0.2	0.246	0.002	224.0	0.217	0.209	0.201	0.002

Sample ID	Reference	Depth (m)	Re (ppb)	±	Os (ppt)	±	^{187}Re / ^{188}Os	±	^{187}Os / ^{188}Os	±	^{192}Os (ppt)	Os_g (@ 53 Ma)	Os_g (@ 68 Ma)	Os_g (@83 Ma)	±
ODP207, Site 1260 (Hole 1260B), Demerara Rise (Fig. 6E)															
04W/57-58.5	(26)	-424.89	NS	NS	802.6	NS	564.59	3.72	1.4695	0.0132	NS	0.971	0.83	0.688	NS
04W/67-68.5	(26)	-424.99	NS	NS	517.8	NS	512.02	2.30	1.3816	0.0045	NS	0.929	0.80	0.673	NS
04W/73-74.5R	(26)	-425.05	NS	NS	752.0	NS	1231.05	6.34	2.54	0.0103	NS	1.453	1.14	0.837	NS
04W/81-83	(26)	-425.13	NS	NS	774.9	NS	1434.53	6.14	2.7445	0.0091	NS	1.477	1.12	0.759	NS
04W/96.5-98	(26)	-425.28	NS	NS	1073.8	NS	207.27	1.14	0.6308	0.0041	NS	0.448	0.40	0.344	NS
04W/102-103.5	(26)	-425.34	NS	NS	1145.7	NS	200.49	0.78	0.6187	0.0013	NS	0.442	0.39	0.341	NS
04W/108.5-110	(26)	-425.40	NS	NS	1792.3	NS	367.38	1.59	0.8694	0.0034	NS	0.545	0.45	0.361	NS
04W/112-114R	(26)	-425.44	NS	NS	1481.5	NS	161.1	0.68	0.5106	0.0018	NS	0.368	0.33	0.288	NS
04W/122-124	(26)	-425.54	NS	NS	1314.3	NS	169.08	0.73	0.5444	0.0018	NS	0.395	0.35	0.310	NS
05W/11-13.5	(26)	-425.93	NS	NS	2115.3	NS	208.88	0.88	0.5089	0.0020	NS	0.324	0.27	0.220	NS
05W/22-24R	(26)	-426.04	NS	NS	11696.4	NS	86.75	0.33	0.2672	0.0006	NS	0.191	0.17	0.147	NS
05W/31-34R	(26)	-426.14	NS	NS	4198.6	NS	269.62	1.06	0.5813	0.0014	NS	0.343	0.28	0.208	NS
05A/43-45	(26)	-426.25	NS	NS	3531.9	NS	113.33	0.43	0.345	0.0006	NS	0.245	0.22	0.188	NS
05A/55-57	(26)	-426.37	NS	NS	8989.6	NS	163.02	0.76	0.4331	0.0022	NS	0.289	0.25	0.208	NS
05A/59-61	(26)	-426.41	NS	NS	14122.1	NS	53.26	0.22	0.2464	0.0007	NS	0.199	0.19	0.173	NS
05A/61-63	(26)	-426.43	NS	NS	5219.1	NS	94.38	0.36	0.3272	0.0007	NS	0.244	0.22	0.197	NS
05A/64-66	(26)	-426.46	NS	NS	1230.8	NS	474.33	2.02	1.1303	0.0033	NS	0.711	0.59	0.474	NS
05A/70-72	(26)	-426.52	NS	NS	649.9	NS	855.77	4.33	1.8756	0.0097	NS	1.120	0.91	0.691	NS
05A/95-97	(26)	-426.77	NS	NS	550.4	NS	1172.7	6.24	2.4651	0.0140	NS	1.429	1.14	0.842	NS
05A/110-112	(26)	-426.92	NS	NS	468.4	NS	617.98	3.35	1.6099	0.0094	NS	1.064	0.91	0.755	NS
05A/125-127	(26)	-427.07	NS	NS	460.3	NS	643.26	3.62	1.7312	0.0111	NS	1.163	1.00	0.841	NS
05A/142-144	(26)	-427.24	NS	NS	594.8	NS	2029.38	10.29	4.1732	0.0203	NS	2.381	1.87	1.365	NS
06A/10-12	(26)	-427.42	NS	NS	481.9	NS	975.96	5.07	2.2706	0.0108	NS	1.408	1.16	0.920	NS
06A/25-27	(26)	-427.57	NS	NS	334.2	NS	670.49	5.11	1.7364	0.0187	NS	1.144	0.98	0.809	NS
06A/37-38.5	(26)	-427.69	NS	NS	107.5	NS	2023.11	29.97	4.0005	0.0615	NS	2.213	1.71	1.201	NS
35/05W/125-127	(27)	-427.07	62.9	0.20	571.5	2.16	642.3	2.8	1.744	0.006	194.9	1.176	1.02	0.855	0.002
35/05W/144-147	(27)	-427.26	146.7	0.47	473.0	2.46	2316.7	11.1	4.348	0.017	125.9	2.374	1.80	1.233	0.003

Sample ID	Reference	Depth (m)	Re (ppb)	±	Os (ppt)	±	^{187}Re / ^{188}Os	±	^{187}Os / ^{188}Os	±	^{192}Os (ppt)	Os_g (@ 53 Ma)	Os_g (@ 68 Ma)	Os_g (@83 Ma)	±
35/06W/01-03	(27)	-427.32	125.2	0.40	411.4	2.21	2281.4	11.4	4.390	0.018	109.2	2.374	1.80	1.233	0.003
35/06W/55-57	(27)	-427.87	35.5	0.12	246.2	1.49	874.2	6.3	2.104	0.016	80.8	1.331	1.11	0.894	0.004
36/01W/14-17	(27)	-428.24	33.7	0.11	112.2	1.25	2214.0	32.8	4.197	0.067	30.3	2.241	1.69	1.133	0.008
36/01W/54-56	(27)	-428.64	186.6	0.60	699.2	3.00	1925.4	7.8	3.938	0.011	192.8	2.238	1.76	1.274	0.002
36/01W/135-138	(27)	-429.45	68.6	0.22	565.3	2.50	717.6	3.4	1.873	0.009	190.1	1.239	1.06	0.880	0.002
36/02W/23-25	(27)	-429.83	111.4	0.36	538.3	2.49	1360.9	6.1	2.925	0.011	162.8	1.723	1.38	1.042	0.002
36/02W/83-85	(27)	-430.43	62.1	0.20	513.7	2.07	712.1	3.2	1.829	0.007	173.5	1.200	1.02	0.844	0.002
36/02W/105-108	(27)	-430.65	629.9	2.03	5126.8	29.87	717.9	4.3	1.757	0.014	1745.5	1.123	0.94	0.764	0.003
36/03W/10-12	(27)	-431.20	65.3	0.21	585.3	2.38	646.5	3.0	1.684	0.007	200.9	1.113	0.95	0.789	0.002
36/03W/51-53	(27)	-431.61	184.8	0.60	759.6	2.86	1635.5	6.3	3.157	0.008	224.8	1.713	1.30	0.894	0.001
Furlo, Italy (Fig. 6F)															
BON-16	(26)	-3.05	NS	NS	1451	NS	302.62	1.22	0.9341	0.0020	NS	0.515	0.591	0.667	NS
BON-14	(26)	-3.14	NS	NS	1654	NS	454.07	1.85	1.1783	0.0030	NS	0.550	0.664	0.777	NS
BON-12	(26)	-3.20	NS	NS	2344	NS	412.42	1.85	1.0822	0.0048	NS	0.512	0.615	0.718	NS
BON-10	(26)	-3.29	NS	NS	854	NS	152.21	0.73	0.6415	0.0027	NS	0.431	0.469	0.507	NS
BON-9	(26)	-3.40	NS	NS	2764	NS	169.87	0.64	0.5821	0.0010	NS	0.347	0.390	0.432	NS
BON-8	(26)	-3.48	NS	NS	2492	NS	201.51	0.80	0.603	0.0015	NS	0.324	0.375	0.425	NS
BON-6	(26)	-3.56	NS	NS	1471	NS	234.36	0.97	0.643	0.0018	NS	0.319	0.377	0.436	NS
BON-5	(26)	-3.75	NS	NS	5060	NS	156.38	0.60	0.424	0.0009	NS	0.208	0.247	0.286	NS
BON-4	(26)	-3.85	NS	NS	15002	NS	86.68	0.32	0.2922	0.0004	NS	0.172	0.194	0.216	NS
BON-3	(26)	-3.94	NS	NS	6893	NS	45.3	0.17	0.2347	0.0004	NS	0.172	0.183	0.195	NS
BON-2	(26)	-3.98	NS	NS	10691	NS	59.12	0.22	0.2452	0.0004	NS	0.163	0.178	0.193	NS
BON-1	(26)	-4.03	NS	NS	10385	NS	77.59	0.32	0.2716	0.0008	NS	See Furlo 3.6	See Furlo 3.6	See Furlo 3.6	NS
BON-A1	(26)	-4.45	NS	NS	114	NS	64.6	0.67	0.7567	0.0079	NS	0.667	0.683	0.700	NS
BON-B1	(26)	-9.17	NS	NS	117	NS	116.33	2.21	0.8864	0.0214	NS	0.725	0.755	0.784	NS
BON-C1	(26)	-13.15	NS	NS	126	NS	85.72	0.84	0.9824	0.0097	NS	0.864	0.885	0.907	NS
BON-D1	(26)	-16.06	NS	NS	141	NS	185.61	2.80	1.2059	0.0183	NS	0.949	0.996	1.042	NS

Sample ID	Reference	Depth (m)	Re (ppb)	±	Os (ppt)	±	^{187}Re / ^{188}Os	±	^{187}Os / ^{188}Os	±	^{192}Os (ppt)	Os_g (@ 53 Ma)	Os_g (@ 68 Ma)	Os_g (@83 Ma)	±
BON-E1	(26)	-20.54	NS	NS	138	NS	131.03	1.16	1.0436	0.0093	NS	0.862	0.895	0.928	NS
Furlo 8.1	(27)	-3.99	81.1	0.27	10316.0	17.40	38.4	0.2	0.235	0.001	0.4	0.182	0.192	0.201	0.000
Furlo 3.6	(27)	-4.03	130.4	0.43	11355.4	16.46	56.4	0.2	0.272	0.001	0.3	0.194	0.208	0.222	0.000
Furlo 0	(27)	-4.07	0.3	0.01	163.8	2.06	8.1	0.3	0.291	0.011	0.5	0.279	0.281	0.283	0.007
Furlo -42	(27)	-4.49	3.4	0.02	55.3	0.51	330.0	5.4	1.059	0.020	0.8	0.603	0.685	0.768	0.007
Furlo -70	(27)	-4.77	1.0	0.01	42.1	0.64	126.9	4.2	0.743	0.031	0.7	0.568	0.600	0.631	0.014
Furlo -90	(27)	-4.97	1.5	0.01	57.2	0.69	134.7	3.3	0.754	0.023	0.7	0.568	0.602	0.635	0.011
Yezo Group, Japan (Fig. 6G)															
T740A	(28)	138.10	0.30	0.01	39.27	0.55	39.6	1.4	0.669	0.026	15.14	0.63	0.62	0.61	0.02
T738A	(28)	136.53	0.34	0.01	45.96	0.51	38.2	1.1	0.669	0.020	17.72	0.63	0.63	0.62	0.01
T736A	(28)	133.96	0.34	0.01	48.05	0.66	36.0	1.2	0.654	0.025	18.56	0.62	0.61	0.60	0.02
T733A	(28)	130.55	0.33	0.01	51.12	0.70	33.4	1.1	0.653	0.025	19.75	0.62	0.62	0.61	0.02
T730A	(28)	127.25	0.42	0.01	41.83	0.47	52.0	1.3	0.671	0.020	16.13	0.63	0.61	0.60	0.01
T728A	(28)	125.40	0.35	0.01	52.53	0.73	34.4	1.1	0.683	0.026	20.22	0.65	0.64	0.64	0.02
T726A	(28)	123.60	0.32	0.01	46.17	0.64	36.1	1.2	0.656	0.025	17.83	0.62	0.62	0.61	0.02
T724A	(28)	121.20	0.43	0.01	41.02	0.46	54.3	1.4	0.684	0.020	15.79	0.64	0.62	0.61	0.01
T719A	(28)	116.00	0.40	0.01	47.67	0.66	42.9	1.4	0.686	0.026	18.34	0.65	0.64	0.63	0.02
T717A	(28)	113.96	0.25	0.01	37.26	0.73	35.0	1.7	0.658	0.038	14.39	0.63	0.62	0.61	0.02
T715A	(28)	111.75	0.29	0.01	38.82	0.55	38.2	1.3	0.673	0.026	14.96	0.64	0.63	0.62	0.02
T713A	(28)	110.00	0.32	0.01	41.11	0.57	40.4	1.4	0.655	0.026	15.88	0.62	0.61	0.60	0.02
T710A	(28)	104.36	0.30	0.01	35.53	0.50	43.5	1.5	0.679	0.027	13.68	0.64	0.63	0.62	0.02
AD90-11	(28)	98.75	0.23	0.01	27.86	0.55	42.0	2.1	0.695	0.040	10.71	0.66	0.65	0.64	0.02
AD92-11	(28)	92.50	0.32	0.01	47.22	0.92	34.7	1.6	0.684	0.039	18.17	0.65	0.64	0.64	0.02
AD94-11	(28)	84.10	0.28	0.01	41.37	0.81	35.2	1.6	0.690	0.040	15.91	0.66	0.65	0.64	0.02
AD96-11	(28)	77.10	0.45	0.01	42.20	0.82	54.8	2.4	0.629	0.036	16.35	0.58	0.57	0.55	0.02
AD98-11	(28)	71.85	0.23	0.01	33.33	0.65	35.4	1.7	0.662	0.038	12.86	0.63	0.62	0.61	0.02
AD100-11	(28)	64.85	0.25	0.01	42.66	0.83	30.2	1.4	0.678	0.039	16.43	0.65	0.64	0.64	0.02

Sample ID	Reference	Depth (m)	Re (ppb)	±	Os (ppt)	±	^{187}Re / ^{188}Os	±	^{187}Os / ^{188}Os	±	^{192}Os (ppt)	Os_g (@ 53 Ma)	Os_g (@ 68 Ma)	Os_g (@83 Ma)	±
AD102-11	(28)	59.25	0.29	0.01	40.54	0.79	37.5	1.7	0.663	0.038	15.64	0.63	0.62	0.61	0.02
AD104-11	(28)	50.75	0.28	0.01	40.28	0.78	35.1	1.6	0.600	0.035	15.67	0.57	0.56	0.55	0.02
AD106-11	(28)	44.00	0.16	0.01	29.15	0.58	27.4	1.6	0.640	0.038	11.28	0.62	0.61	0.60	0.02
AD108-11	(28)	36.90	0.17	0.01	34.34	0.67	25.2	1.4	0.646	0.037	13.28	0.62	0.62	0.61	0.02
AD110-11	(28)	29.50	0.32	0.01	40.30	0.78	40.4	1.8	0.645	0.037	15.58	0.61	0.60	0.59	0.02
AD112-11	(28)	22.75	0.20	0.01	28.27	0.56	36.2	1.9	0.629	0.037	10.95	0.60	0.59	0.58	0.02
AD114-11	(28)	15.80	0.16	0.01	30.29	0.59	27.7	1.5	0.605	0.035	11.77	0.58	0.57	0.57	0.02
AD116-11	(28)	7.90	0.26	0.01	32.99	0.64	39.6	1.9	0.563	0.033	12.89	0.53	0.52	0.51	0.02
AD118-11	(28)	0.25	0.32	0.01	35.19	0.68	46.4	2.1	0.614	0.035	13.66	0.57	0.56	0.55	0.02
AD120-11	(28)	-7.15	1.10	0.01	307.60	5.54	17.4	0.7	0.205	0.012	125.71	0.19	0.19	0.18	0.01
AD121-11	(28)	-11.25	1.17	0.01	580.82	10.41	9.8	0.4	0.179	0.010	238.18	0.17	0.17	0.17	0.01
AD122-11	(28)	-15.20	1.40	0.01	738.64	13.25	9.2	0.4	0.187	0.011	302.60	0.18	0.18	0.17	0.01
CT056	(28)	-16.15	1.43	0.01	236.71	2.24	29.3	0.6	0.195	0.006	96.87	0.17	0.16	0.15	0.00
CT055	(28)	-17.40	0.73	0.01	11.45	0.35	331.1	23.5	0.708	0.059	4.39	0.42	0.33	0.25	0.01
CT053	(28)	-18.60	0.55	0.01	8.98	0.32	322.5	27.4	0.787	0.076	3.41	0.50	0.42	0.34	0.02
AD123-11	(28)	-19.35	1.24	0.01	61.92	1.25	105.8	4.5	0.860	0.050	23.33	0.77	0.74	0.71	0.03
AD124-11	(28)	-21.00	1.19	0.01	57.71	1.17	109.0	4.7	0.875	0.051	21.71	0.78	0.75	0.72	0.03
AD125-11	(28)	-23.25	1.01	0.01	39.24	0.83	136.3	6.2	0.914	0.055	14.69	0.79	0.76	0.73	0.03
AD126-11	(28)	-24.95	1.04	0.01	60.22	1.19	90.9	3.8	0.838	0.048	22.75	0.76	0.73	0.71	0.02
AD128-11	(28)	-28.55	1.50	0.01	63.65	1.29	125.5	5.3	0.920	0.053	23.82	0.81	0.78	0.75	0.03
AD130-11	(28)	-33.70	1.04	0.01	58.92	1.18	93.1	4.0	0.819	0.048	22.31	0.74	0.71	0.69	0.02
AD132-11	(28)	-37.10	0.92	0.01	58.15	1.15	83.2	3.5	0.840	0.048	21.96	0.77	0.75	0.72	0.03
AD134-11	(28)	-40.65	1.10	0.01	64.79	1.30	89.2	3.8	0.845	0.049	24.46	0.77	0.74	0.72	0.03
AD136-11	(28)	-44.60	1.21	0.01	49.14	1.01	130.1	5.7	0.876	0.051	18.48	0.76	0.73	0.70	0.02
AD138-11	(28)	-47.95	0.90	0.01	56.73	1.13	82.9	3.6	0.816	0.047	21.49	0.74	0.72	0.70	0.02
AD140-11	(28)	-51.25	1.63	0.02	70.38	1.42	122.4	5.3	0.850	0.049	26.55	0.74	0.71	0.68	0.02
AD142-11	(28)	-56.10	0.83	0.01	65.26	1.29	65.8	2.9	0.737	0.043	24.96	0.68	0.66	0.65	0.02
AD144-11	(28)	-59.85	1.10	0.01	87.96	1.23	64.8	1.9	0.686	0.027	33.85	0.63	0.61	0.60	0.01

Sample ID	Reference	Depth (m)	Re (ppb)	±	Os (ppt)	±	^{187}Re / ^{188}Os	±	^{187}Os / ^{188}Os	±	^{192}Os (ppt)	Os_g (@ 53 Ma)	Os_g (@ 68 Ma)	Os_g (@83 Ma)	±
AD146-11	(28)	-63.80	1.08	0.01	101.45	1.39	54.6	1.6	0.603	0.023	39.44	0.56	0.54	0.53	0.01
AD148-11	(28)	-67.00	0.72	0.01	50.78	1.03	74.5	3.4	0.835	0.049	19.19	0.77	0.75	0.73	0.03
AD150-11	(28)	-71.25	0.80	0.01	50.47	1.03	83.6	3.8	0.868	0.051	19.00	0.79	0.77	0.75	0.03
AD152-11	(28)	-75.00	0.89	0.01	64.57	0.60	72.1	1.6	0.787	0.017	24.55	0.72	0.71	0.69	0.01
AD154-11	(28)	-79.75	0.55	0.01	40.34	0.84	71.6	3.5	0.834	0.050	15.25	0.77	0.75	0.73	0.03
AD156-11	(28)	-83.45	1.15	0.01	64.68	0.96	94.5	2.9	0.891	0.035	24.28	0.81	0.78	0.76	0.02
AD158-11	(28)	-88.00	0.82	0.01	45.48	0.93	94.3	4.3	0.828	0.049	17.20	0.74	0.72	0.70	0.03
AD160-11	(28)	-91.20	0.58	0.01	47.51	0.97	64.3	3.1	0.832	0.049	17.96	0.78	0.76	0.74	0.03
AD162-11	(28)	-94.40	0.59	0.01	44.56	0.92	70.8	3.4	0.913	0.054	16.68	0.85	0.83	0.82	0.03
AD164-11	(28)	-97.70	0.93	0.01	47.92	0.98	101.7	4.5	0.814	0.048	18.16	0.72	0.70	0.67	0.02
AD166-11	(28)	-101.60	0.72	0.01	46.59	0.96	81.8	3.8	0.845	0.050	17.59	0.77	0.75	0.73	0.03
AD168-11	(28)	-105.10	0.67	0.01	42.54	0.88	83.3	3.9	0.823	0.049	16.10	0.75	0.73	0.71	0.03
AD170-11	(28)	-109.60	0.75	0.01	46.35	0.94	85.1	3.9	0.796	0.047	17.60	0.72	0.70	0.68	0.02
AD172-11	(28)	-112.70	0.83	0.01	57.31	1.16	76.4	3.4	0.864	0.050	21.58	0.80	0.78	0.76	0.03
AD174-11	(28)	-116.10	0.67	0.01	40.82	0.85	85.6	4.0	0.810	0.048	15.48	0.73	0.71	0.69	0.03
AD176-11	(28)	-120.30	0.76	0.01	44.90	0.92	89.7	4.1	0.840	0.050	16.96	0.76	0.74	0.72	0.03
AD178-11	(28)	-124.30	0.76	0.01	54.98	1.12	72.6	3.3	0.837	0.049	20.77	0.77	0.75	0.74	0.03
AD180-11	(28)	-131.70	0.33	0.01	30.16	1.13	57.7	5.3	0.801	0.094	11.45	0.75	0.74	0.72	0.05
Great Valley Sequence, California, USA (Fig. 6H)															
US 908	(28)	312.50	1.03	0.01	85.03	1.68	63.5	2.7	0.818	0.047	32.20	0.76	0.75	0.73	0.03
US 903	(28)	296.00	0.76	0.01	65.38	1.30	61.0	2.7	0.765	0.044	24.92	0.71	0.70	0.68	0.02
US 089	(28)	279.50	0.87	0.01	74.35	1.47	60.9	2.6	0.765	0.046	28.34	0.71	0.70	0.68	0.02
US 613	(28)	261.00	0.32	0.01	24.10	0.38	71.9	2.6	1.008	0.041	8.92	0.94	0.93	0.91	0.02
US 621	(28)	244.50	0.48	0.01	53.99	0.75	45.9	1.4	0.681	0.026	20.79	0.64	0.63	0.62	0.01
US 626	(28)	227.50	0.38	0.01	40.95	0.81	48.7	2.1	0.764	0.044	15.61	0.72	0.71	0.70	0.02
US 632	(28)	212.80	0.45	0.01	49.77	0.70	46.6	1.4	0.746	0.029	19.01	0.71	0.69	0.68	0.02
US 637	(28)	195.50	0.61	0.01	56.59	1.13	56.4	2.6	0.730	0.043	21.66	0.68	0.67	0.65	0.02

Sample ID	Reference	Depth (m)	Re (ppb)	±	Os (ppt)	±	^{187}Re / ^{188}Os	±	^{187}Os / ^{188}Os	±	^{192}Os (ppt)	Os_g (@ 53 Ma)	Os_g (@ 68 Ma)	Os_g (@83 Ma)	±
US 648	(28)	175.20	0.29	0.01	54.13	1.03	27.7	1.3	0.588	0.034	21.08	0.56	0.56	0.55	0.02
US 653	(28)	159.50	1.05	0.01	82.73	1.60	65.2	2.8	0.606	0.035	32.15	0.55	0.53	0.52	0.02
US 084	(28)	142.00	0.89	0.01	140.46	2.65	32.0	1.4	0.462	0.027	55.56	0.43	0.43	0.42	0.01
US 662	(28)	124.50	0.48	0.01	156.16	1.98	15.1	0.4	0.333	0.013	62.78	0.32	0.32	0.31	0.01
US 666	(28)	106.20	0.62	0.01	179.10	3.26	16.9	0.8	0.262	0.015	72.66	0.25	0.24	0.24	0.01
US 674	(28)	88.50	1.05	0.01	154.02	2.85	34.0	1.4	0.388	0.022	61.50	0.36	0.35	0.34	0.01
US 675	(28)	84.10	0.86	0.01	223.71	4.09	18.9	0.8	0.298	0.017	90.35	0.28	0.28	0.27	0.01
US 061	(28)	82.00	0.92	0.01	176.47	3.25	25.9	1.1	0.346	0.020	70.84	0.32	0.32	0.31	0.01
US 676	(28)	78.90	0.80	0.01	32.30	0.65	122.7	5.8	0.309	0.020	13.03	0.20	0.17	0.14	0.00
US 677	(28)	75.60	0.81	0.01	30.52	0.62	130.2	6.2	0.311	0.020	12.30	0.20	0.16	0.13	0.00
US 062	(28)	72.30	1.28	0.01	424.53	5.26	14.7	0.4	0.239	0.009	172.75	0.23	0.22	0.22	0.01
US 678	(28)	68.50	1.58	0.01	108.22	1.08	71.7	1.6	0.259	0.008	43.92	0.20	0.18	0.16	0.00
US 679	(28)	65.00	0.59	0.01	67.24	1.25	43.1	2.0	0.218	0.013	27.43	0.18	0.17	0.16	0.01
US 680	(28)	60.70	1.34	0.01	88.28	0.91	75.0	1.7	0.305	0.009	35.62	0.24	0.22	0.20	0.00
US 681	(28)	60.40	0.92	0.01	39.94	0.78	113.3	5.1	0.317	0.019	16.09	0.22	0.19	0.16	0.01
US 682	(28)	59.90	1.94	0.01	36.54	0.48	270.3	7.4	0.558	0.019	14.28	0.32	0.25	0.18	0.00
US 684	(28)	58.90	1.31	0.01	121.25	1.37	56.7	1.3	0.790	0.023	46.07	0.74	0.73	0.71	0.01
US 063	(28)	58.00	1.49	0.01	28.23	0.42	274.9	8.7	0.752	0.028	10.78	0.51	0.44	0.37	0.01
US 687	(28)	57.00	1.24	0.01	20.34	0.37	322.1	12.6	0.889	0.039	7.64	0.60	0.52	0.44	0.01
US 688	(28)	55.71	1.30	0.01	28.38	0.42	237.8	7.5	0.726	0.027	10.87	0.52	0.46	0.40	0.01
US 064	(28)	55.60	1.07	0.01	14.23	0.39	396.3	24.7	0.840	0.063	5.38	0.49	0.39	0.29	0.01
US 065	(28)	55.30	2.34	0.01	30.70	0.40	397.1	10.7	0.761	0.024	11.71	0.41	0.31	0.21	0.00
US 066	(28)	54.20	0.98	0.01	40.23	0.43	126.4	3.1	0.686	0.018	15.48	0.57	0.54	0.51	0.01
US 690	(28)	52.70	0.56	0.01	12.30	0.36	240.6	16.8	0.827	0.066	4.65	0.61	0.55	0.49	0.02
US 067	(28)	52.30	0.97	0.01	9.93	0.32	534.7	39.4	1.134	0.090	3.62	0.66	0.53	0.39	0.02
US 691	(28)	51.60	0.75	0.01	17.71	0.44	218.9	12.4	0.680	0.048	6.82	0.49	0.43	0.38	0.02
US 692	(28)	50.40	0.99	0.01	92.01	1.31	56.4	1.7	0.810	0.031	34.88	0.76	0.75	0.73	0.02
US 068	(28)	50.20	0.67	0.01	17.58	0.44	199.5	11.5	0.752	0.052	6.71	0.58	0.53	0.48	0.02

Sample ID	Reference	Depth (m)	Re (ppb)	±	Os (ppt)	±	^{187}Re / ^{188}Os	±	^{187}Os / ^{188}Os	±	^{192}Os (ppt)	Os_g (@ 53 Ma)	Os_g (@ 68 Ma)	Os_g (@83 Ma)	±
US 069	(28)	49.50	1.17	0.01	13.93	0.34	443.1	24.2	0.827	0.052	5.27	0.44	0.32	0.21	0.01
US 694	(28)	48.10	1.10	0.01	12.77	0.33	457.2	26.9	0.875	0.058	4.80	0.47	0.36	0.24	0.01
US 070	(28)	47.70	1.22	0.01	21.53	0.40	290.3	12.0	0.640	0.032	8.33	0.38	0.31	0.24	0.01
US 071	(28)	45.20	0.57	0.01	17.82	0.43	160.8	9.3	0.530	0.037	6.99	0.39	0.35	0.31	0.01
US 072	(28)	44.50	3.74	0.02	61.54	0.62	322.0	5.7	0.898	0.022	23.08	0.61	0.53	0.45	0.01
US 698	(28)	43.90	2.21	0.01	36.81	0.42	316.1	7.2	0.827	0.022	13.93	0.55	0.47	0.39	0.01
US 1002	(28)	43.20	0.69	0.01	15.18	0.40	235.8	14.5	0.744	0.055	5.80	0.54	0.48	0.42	0.02
US 1005	(28)	40.40	1.45	0.01	31.97	0.45	236.6	7.0	0.751	0.027	12.21	0.54	0.48	0.42	0.01
US 1007	(28)	34.50	0.63	0.01	32.40	0.72	106.6	5.3	1.119	0.068	11.85	1.03	1.00	0.97	0.04
US 1009	(28)	27.00	1.57	0.01	22.33	0.39	377.4	13.8	0.988	0.042	8.29	0.65	0.56	0.47	0.01
US 075	(28)	25.50	1.12	0.01	36.12	0.61	170.1	5.9	1.188	0.051	13.10	1.04	1.00	0.95	0.03
US 1011	(28)	22.10	1.11	0.01	14.97	0.35	396.4	20.8	0.936	0.056	5.59	0.59	0.49	0.39	0.01
US 1012	(28)	19.40	1.35	0.01	72.41	1.46	99.6	4.2	0.949	0.055	27.00	0.86	0.84	0.81	0.03
US 076	(28)	11.00	0.82	0.01	20.56	0.40	208.7	9.2	0.794	0.040	7.81	0.61	0.56	0.51	0.02
US 077	(28)	0.00	2.74	0.01	78.35	0.61	192.2	2.5	1.212	0.018	28.34	1.04	0.99	0.95	0.01

NS = Data not specified in associated reference.

Chapter 3: A second type of highly asphaltic crude oil seepage stranded on the South Australian coastline

SUPPLEMENTARY INFORMATION

1. Supplementary figures

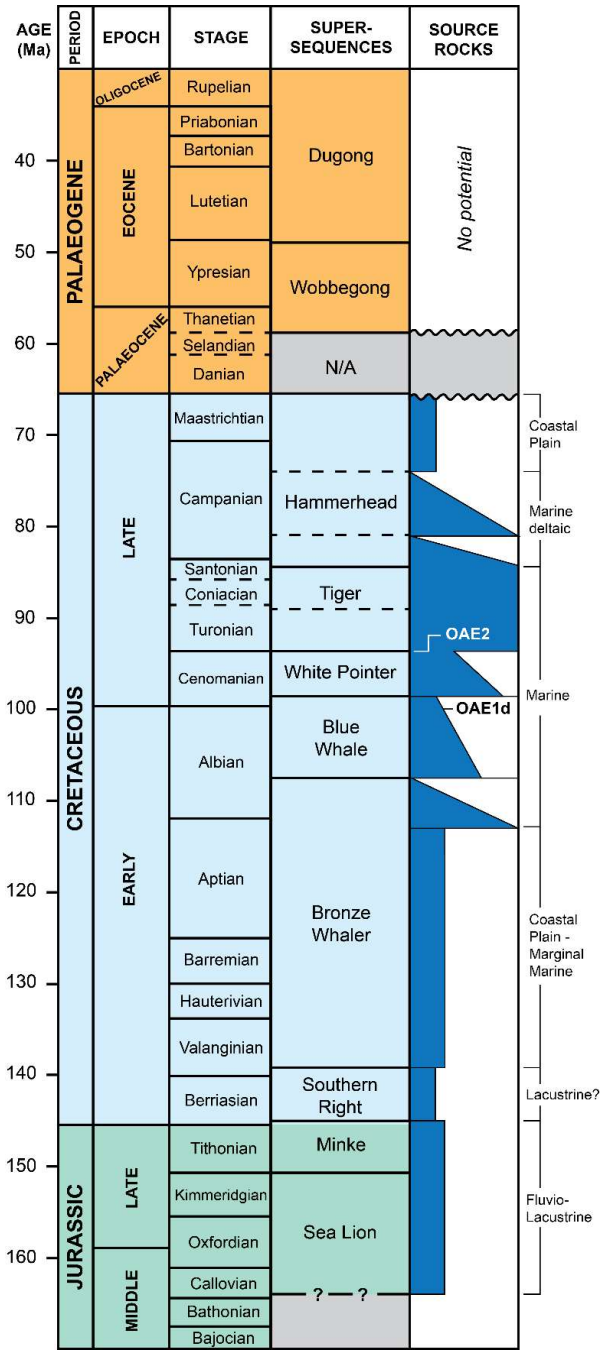


Figure S1: Summary of the stratigraphy of the Jurassic-Cretaceous Bight Basin and overlying Eucla Basin showing potential source rocks and their depositional environments. Figure modified after Totterdell et al. (2008).

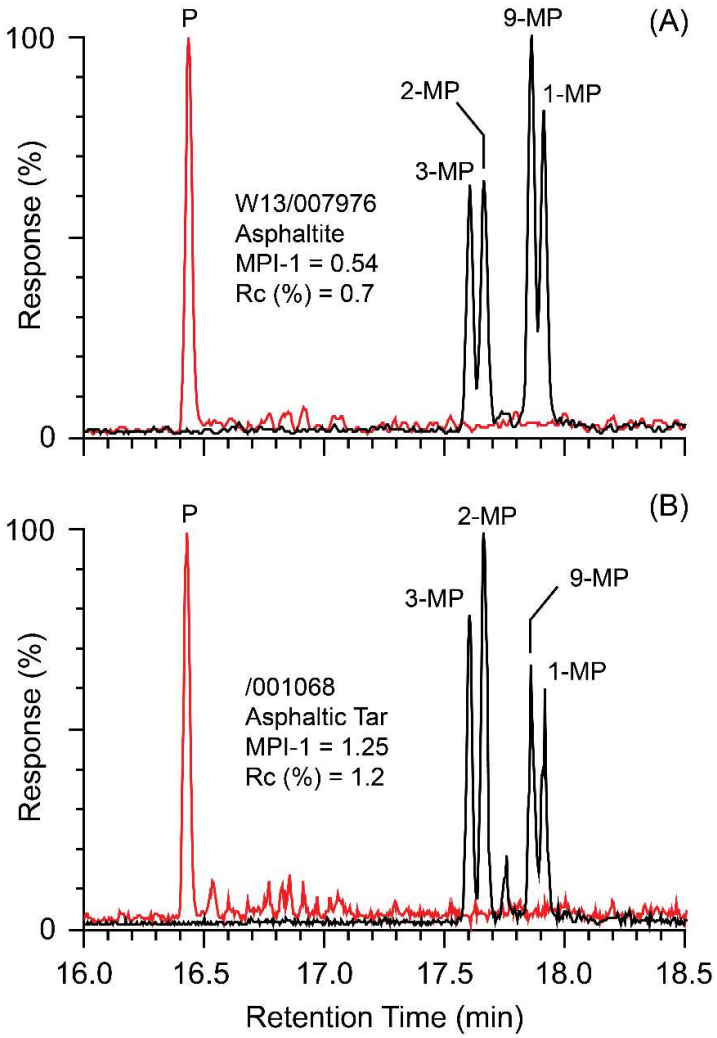


Figure S2: Comparison of phenanthrene (*m/z* 178 - red) and methylphenanthrene (*m/z* 192 - black) abundances in (A) asphaltite sample W13/007976; and (B) asphaltic tar sample /001068. See Supplementary Information for all peak abbreviations.

2. Compound identification lists

Sterane and diasteranes peak identification for Figure 3:

Peak label	Peak assignment	Common Abbreviation
1	13β(H),17α(H)-diacholestane (20*S*)	C_{27} βα 20*S* diasterane
2	13β(H),17α(H)-diacholestane (20*R*)	C_{27} βα 20*R* diasterane
3	13α(H),17β(H)-diacholestane (20*S*)	C_{27} αβ 20*S* diasterane
4	13α(H),17β(H)-diacholestane (20*R*)	C_{27} αβ 20*R* diasterane
5	24-methyl-13β(H),17α(H)-diacholestane (20*S*)*	C_{28} βα 20*S* diasterane
6	24-methyl-13β(H),17α(H)-diacholestane (20*R*)*	C_{28} βα 20*R* diasterane
7	24-methyl-13α(H),17β(H)-diacholestane (20*S*)	C_{28} αβ 20*S* diasterane
8	5α(H),14α(H),17α(H)-cholestane (20*S*)	C_{27} ααα 20*S* sterane
9	5α(H),14β(H),17β(H)-cholestane (20*R*)	C_{27} αββ 20*R* sterane
10	24-ethyl-13β(H),17α(H)-diacholestane (20*S*)	C_{29} βα 20*S* diasterane
11	5α(H),14β(H),17β(H)-cholestane (20*S*)	C_{27} αββ 20*S* sterane
12	24-methyl-13α(H),17β(H)-diacholestane (20*R*)*	C_{28} αβ 20*R* diasterane
13	5α(H),14α(H),17α(H)-cholestane (20*R*)	C_{27} ααα 20*R* sterane
14	24-ethyl-13β(H),17α(H)-diacholestane (20*R*)	C_{29} βα 20*R* diasterane
15	24-ethyl-13α(H),17β(H)-diacholestane (20*S*)	C_{29} αβ 20*S* diasterane
16	24-methyl-5α(H),14α(H),17α(H)-cholestane (20*S*)*	C_{28} ααα 20*S* sterane
17	24-ethyl-13α(H),17β(H)-diacholestane (20*R*)	C_{29} αβ 20*R* diasterane
18	24-methyl-5α(H),14β(H),17β(H)-cholestane (20*R*)	C_{28} αββ 20*R* sterane
19	24-methyl-5α(H),14β(H),17β(H)-cholestane (20*S*)	C_{28} αββ 20*S* sterane
20	24-methyl-5α(H),14α(H),17α(H)-cholestane (20*R*)	C_{28} ααα 20*R* sterane
21	24-ethyl-5α(H),14α(H),17α(H)-cholestane (20*S*)	C_{29} ααα 20*S* sterane
22	24-ethyl-5α(H),14β(H),17β(H)-cholestane (20*R*)	C_{29} αββ 20*R* sterane
23	24-ethyl-5α(H),14β(H),17β(H)-cholestane (20*S*)	C_{29} αββ 20*S* sterane
24	24-ethyl-5α(H),14α(H),17α(H)-cholestane (20*R*)	C_{29} ααα 20*R* sterane
25	24-*n*-propyl-5α(H),14α(H),17α(H)-cholestane (20*S*)	C_{30} ααα 20*S* sterane
26	24-*n*-propyl-5α(H),14β(H),17β(H)-cholestane (20*R*)	C_{30} αββ 20*R* sterane
27	24-*n*-propyl-5α(H),14β(H),17β(H)-cholestane (20*S*)	C_{30} αββ 20*S* sterane
28	24-*n*-propyl-5α(H),14α(H),17α(H)-cholestane (20*R*)	C_{30} ααα 20*R* sterane

***** isomeric peaks (24*S* and 24*R*)

Terpane and hopane peak identification for Figure 4:

Peak label	Peak Assignment
19/3	C_{19} tricyclic diterpane
20/3	C_{20} tricyclic diterpane
21/3	C_{21} tricyclic diterpane
23/3	C_{23} tricyclic terpane
24/3	C_{24} tricyclic terpane
25/3	C_{25} tricyclic terpane
26/3	C_{26} tricyclic terpane
24/4	C_{24} tetracyclic terpane
25/3	C_{25} tricyclic terpane
26/3	C_{26} tricyclic terpane
28/3	C_{28} tricyclic terpane
29/3	C_{29} tricyclic terpane
Ts	C_{27} 18α(H),22,29,30-trisnorneohopane
Tm	C_{27} 17α(H),22,29,30-trisnorhopane
C_{29}αβ	17α(H),21β(H)-30-norhopane
C_{29}βα	17β(H),21α(H)-30-norhopane
C_{30}αβ	17α(H),21β(H)-hopane
C_{30}βα	17β(H),21α(H)-hopane
C_{31}αβ	17α(H),21β(H)-homohopane (22*S* and 22*R*)
Ga	Gammacerane
C_{32}αβ	17α(H),21β(H)-bishomohopane (22*S* and 22*R*)
C_{33}αβ	17α(H),21β(H)-trishomohopane (22*S* and 22*R*)
C_{34}αβ	17α(H),21β(H)-tetrakishomohopane (22*S* and 22*R*)
C_{35}αβ	17α(H),21β(H)-pentakishomohopane (22*S* and 22*R*)

Aromatic compound identification for Figure S2:

Peak	Peak Assignment	*m/z*
P	Phenanthrene	178
3-MP	3-methylphenanthrene	192
2-MP	2-methylphenanthrene	192
9-MP	9-methylphenanthrene	192
1-MP	1-methylphenanthrene	192
2-MN	2-methylnaphthalene	142
1-MN	1-methylnaphthalene	142
2,6-DMN	2,6-dimethylnaphthalene	156
2,7-DMN	2,7-dimethylnaphthalene	156
1,5-DMN	1,5-dimethylnaphthalene	156

3. Supplementary data tables

Table S1: Details of analysed asphaltic bitumen samples. All co-ordinates correspond to the WGS84 datum.

Sample	Location	Year	Latitude	Longitude	Weight (g)
Asphaltites					
W13/007472	Eyre Well	2014	-31.4639	131.1422	18
W13/007475	Fowlers Bay (west)	2014	-31.9928	132.4375	60
W13/007476	Cactus Beach	2014	-32.0739	132.9761	813
W13/007488	Elliston	2014	-33.6350	134.8753	78
W13/007493	West Bay	2014	-35.8858	136.5512	18
W13/007507	Waitpinga Beach	2014	-35.6362	138.5061	601
W13/007516	The Granites	2014	-36.6517	139.8520	170
W13/007668	Tractor Beach	2015	-32.8675	134.1178	25
W13/007671	Cactus Beach	2015	-32.0774	132.9791	276
W13/007672*	Avoid Bay	2015	-34.66	135.49	1357
W13/007845	Sheringa Beach	2016	-33.8744	135.1781	500
W13/007976	Waitpinga Beach	2016	-35.6374	138.5103	3188
Asphaltic Tars					
/001056	Number 1 and 2 Rocks	2016	-37.7955	140.3205	9
/001063	Number 1 and 2 Rocks	2016	-37.7977	140.3228	52
/001067	Number 1 and 2 Rocks	2016	-37.7979	140.3231	27
/001068	Number 1 and 2 Rocks	2016	-37.7980	140.3231	27
/001076	Number 1 and 2 Rocks	2016	-37.7982	140.3232	3
/001079	Number 1 and 2 Rocks	2016	-37.7985	140.3235	196
/001081	Number 1 and 2 Rocks	2016	-37.7986	140.3236	17

* = Sample donated from private collection (GPS co-ordinates are approximated)

Table S2: Carbon isotopic composition ($\delta^{13}C$) of individual *n*-alkanes for representative asphaltite, asphaltic tar and waxy bitumen specimens. Waxy bitumen sub-classifications after Corrick et al. (2016) and Ross et al. (2017).

***n*-Alkane carbon chain length**	**Asphaltites**				**Asphaltic Tar**	**Waxy Bitumen***			
	W13/007517	W13/007672	W13/007976	W13/007845	/001063	W13/007601 (Type I)	W13/007615 (Type II)	W13/007697 (Type III)	W13/007589 (Type IV)
13	-30.6	-30.6	-31.3	-30.1	-30.5	†	†	-28.1	†
14	-31.9	-31.4	-31.6	-31.9	-31.6	†	†	-26.4	†
15	-32.2	-31.8	-32.1	-31.7	-31.7	†	-28. 8	-27.2	-30.9
16	-32.8	-32.1	-32.3	-31.8	-32.3	†	-31.5	-27.3	-29.4
17	-33.0	-32.5	-32.4	-31.9	-32.3	†	-26.6	-28.0	-30.4
18	-33.5	-33.3	-32.8	-32.4	-33.5	-26.9	-28.1	-28.5	-29.9
19	-33.2	-33.1	-32.7	-31.9	-32.2	-26.7	-26.2	-28.7	-29.6
20	-33.1	-33.1	-32.6	-31.9	-32.1	-27.0	-25.9	-28.9	-29.5
21	-33.4	-33.2	-32.8	-32.1	-32.1	-27.4	-26.9	-29.0	-29.8
22	-33.6	-33.2	-32.8	-32. 6	-32.1	-27.7	-26.1	-28.9	-29.8
23	-34.0	-33.6	-33.0	-33.3	-32.2	-28. 5	-26.7	-29.1	-29.8
24	-33.5	-33.0	-32.9	-32.5	-32.2	-27.9	-27.1	-28.7	-29.7
25	-33.3	-33.2	-33.0	-32.4	-31.8	-28.0	-26.9	-28.8	-29.3
26	-33.1	-32.8	-32.7	-32.2	-32.0	-28.0	-26.9	-28.7	-29.3
27	-33.2	-33.1	-32.7	-32.2	-31.6	-28.3	-27.7	-28.9	-29.2
28	-33.0	-33.0	-32.3	-32.0	-31.8	-28.2	-27.6	-28.8	-29.3
29	-32.7	-32.7	-32.5	-32.1	-31.8	-28.3	-27.6	-29.1	-30.0
30	-32.9	-32.4	-32.1	-31.6	-31.6	-28.5	-27.6	-29.0	-29.8
31	-32.7	-32.5	-32.3	-31.8	-32.0	-28.0	-27.7	-28.3	-30.1
32	-32.8	-32.6	-32.2	-32.2	-31.6	-28.1	-28.0	-28.3	-30.5
33	-32.2	-32.4	-32.2	-31.3	-31.7	-27.4	-28.4	-28.1	-30.4

* Least altered examples of each waxy bitumen family defined by whole-oil GC-MS.
† *n*-Alkane not present in specimen due to weathering.

Table S3: Re-Os data from asphaltites after Corrick et al. (2019) and asphaltic tars (this study). Int = interior sub-sample, ext = exterior subsample. Rho = error correlation value between $^{187}Re/^{188}Os$ and $^{187}Os/^{188}Os$. Individual ratio uncertainties are given at the 2σ level.

Sample	Re (ppb)	±	Os (ppt)	±	^{192}Os (ppt)	±	$^{187}Re/^{188}Os$	±	$^{187}Os/^{188}Os$	±	rho	% Re Blank	% ^{187}Os Blank	% ^{188}Os Blank
Asphaltites														
W13/007507 (int replicate)	2.15	0.01	24.6	0.6	8.8	0.5	483.7	24.8	1.265	0.083	0.771	0.7	0.4	2.1
W13/007976 (int)	2.59	0.01	30.1	0.4	10.9	0.3	470.7	13.0	1.176	0.041	0.780	0.4	0.7	3.5
W13/007764 (int)	3.04	0.01	33.0	0.5	11.9	0.3	508.0	13.8	1.219	0.042	0.775	0.4	0.7	3.3
W13/007671 (int)	4.02	0.01	43.1	0.6	15.6	0.4	513.6	12.9	1.233	0.040	0.756	0.3	0.5	2.7
W13/007507 (int)	2.65	0.01	28.0	0.4	10.1	0.3	521.4	15.4	1.244	0.045	0.798	0.5	0.8	4.0
W13/007672 (int)	2.68	0.01	36.4	0.5	13.3	0.3	400.5	10.3	1.122	0.037	0.758	0.4	0.6	2.8
W13/007476 (ext)	3.11	0.01	33.5	0.5	12.1	0.3	514.1	14.7	1.263	0.046	0.776	1.2	1.7	8.7
W13/007668 (int)	3.08	0.01	32.3	0.6	11.6	0.3	528.6	15.5	1.278	0.068	0.539	1.2	1.8	9.2
W13/007671 (ext)	2.99	0.01	32.4	0.5	11.6	0.3	512.6	15.1	1.291	0.048	0.776	1.2	1.8	9.1
W13/007742 (int)	2.85	0.01	30.3	0.5	10.9	0.3	521.5	16.2	1.299	0.050	0.794	1.4	2.0	10.4
W13/007764 (ext)	3.07	0.02	32.2	0.5	11.5	0.3	529.6	15.3	1.294	0.047	0.772	1.1	1.7	8.7
W13/007845 (int)	2.89	0.01	31.2	0.5	11.2	0.3	515.5	15.1	1.296	0.048	0.783	1.2	1.8	9.2
W13/007477 (int)	2.95	0.01	32.6	0.5	11.7	0.3	502.5	14.2	1.288	0.046	0.773	1.2	1.6	8.4
W13/007477 (ext)	3.09	0.01	32.5	0.5	11.7	0.3	527.7	15.2	1.280	0.047	0.776	1.2	1.7	8.8
W13/007516 (int)	3.00	0.01	30.3	0.5	10.9	0.3	547.8	16.0	1.285	0.047	0.776	1.1	1.7	8.9
W13/007516 (ext)	3.01	0.01	31.7	0.5	11.4	0.3	526.3	15.3	1.303	0.047	0.781	1.2	1.7	8.9
Asphaltic Tars														
/001059 (int)	30.1	0.1	599.9	4.1	179.2	1.0	333.9	2.0	3.057	0.023	0.648	0.1	0.01	0.1
/001068 (int)	31.4	0.1	627.6	4.2	187.4	1.0	333.7	2.0	3.063	0.023	0.648	0.1	0.01	0.1
/001079 (int)	31.2	0.1	626.2	4.2	187.0	1.0	332.2	2.0	3.059	0.023	0.650	0.1	0.01	0.1

Chapter 4: The identification and provenance of crude oils stranded on the South Australian coastline

SUPPLEMENTARY INFORMATION

1. Survey details

Table S1: Survey locations visited annually from 2014-2016. All co-ordinates correspond to the WGS84 datum. Site numbers correspond to Figure 1 in the main text. For further details and discussion of the survey results see Corrick et al. (2020b).

Survey site	Beach access point	
	Latitude	Longitude
(1) Delisser Sandhills	-31.6916	128.9772
(2) Eyre Well	-31.4636	131.1444
(3) Dogfence Beach	-31.7715	131.8424
(4) Scott Bay	-32.0039	132.3891
(5) Fowlers Bay West	-32.0051	132.4405
(6) Cactus Beach	-32.0545	132.9467
(7) Point Peter	-32.1772	133.4399
(8) St. Mary Bay	-32.5319	133.8589
(9) St. Mary Bay (South)	-32.536	133.857
(10) Cape Bauer	-32.7141	134.0935
(11) Tractor Beach	-32.8561	134.132
(12) Tyringa Beach	-33.147	134.4176
(13) Elliston	-33.6465	134.888
(14) Sheringa Beach	-33.8962	135.1924
(15) Mount Drummond	-34.2404	135.3341
(16) Avoid Bay	-34.6587	135.3503
(17) Sleaford Bay	-34.882	135.8464
(18) West Bay	-35.8877	136.5527
(19) Sandy River	-35.9509	136.6343
(20) Hanson Bay	-36.0167	136.853
(21) Bales Beach	-35.9939	137.3491
(22) Pennington Bay	-35.8525	137.7442
(23) Waitpinga Beach	-35.6346	138.4989
(24) 28 Mile Crossing	-36.2	139.6414
(25) The Granites	-36.6575	139.854
(26) Eve's Cove	-37.1821	139.7443
(27) Beachport Conservation Park	-37.4481	139.9636
(28) Geltwood Beach	-37.6587	140.2228
(29) Number 1 & 2 Rocks	-37.7965	140.3213
(30) Nene Valley	-37.9862	140.5144

2. Chromatogram peak assignments

2.1. Whole-oil GC-MS total ion chromatograms

Peak label/ abbreviation	Peak assignment
8–39	*n*-alkanes, number corresponds to carbon chain length
Np	Norpristane
Pr	Pristane
Ph	Phytane
B	Botryococcane
UCM	Unresolved complex mixture

2.2. Saturated fraction SIM GC-MS *m/z* 191 (terpanes and hopanes)

Peak label/ abbreviation	Peak assignment
19t	C_{19} tricyclic diterpane
20t	C_{20} tricyclic diterpane
21t	C_{21} tricyclic diterpane
23t	C_{23} tricyclic terpane
24t	C_{24} tricyclic terpane
25t	C_{25} tricyclic terpane
26t	C_{26} tricyclic terpane
24tet	C_{24} tetracyclic terpane
25t	C_{25} tricyclic terpane
26t	C_{26} tricyclic terpane
28t	C_{28} tricyclic terpane
29t	C_{29} tricyclic terpane
30t	C_{30} tricyclic terpane
31t	C_{31} tricyclic terpane
32t	C_{32} tricyclic terpane
33t	C_{33} tricyclic terpane
34t	C_{34} tricyclic terpane
35t	C_{35} tricyclic terpane
36t	C_{36} tricyclic terpane
Ts	C_{27} 18α(H),22,29,30-trisnorneohopane
Tm	C_{27} 17α(H),22,29,30-trisnorhopane
29,30-Nor	C_{28} 29,30-bisnorhopane
25-Nor	C_{29} 25-nor-17α(H)-hopane
C_{29}αβ	17α(H),21β (H)-30-norhopane
C_{29}βα	17β(H),21α (H)-30-norhopane
Ole	Oleanane
C_{30}αβ	17α(H),21β (H)-hopane
C_{30}βα	17β(H),21α (H)-hopane
C_{30}*	17α-diahopane
C_{29}Ts	18α-30-norneohopane
C_{31}αβ	17α (H),21β (H)-homohopane*
Ga	Gammacerane
Tx	19α(H)-taraxastane
C_{32}αβ	17α (H),21β (H)-bishomohopane*
C_{33}αβ	17α (H),21β (H)-trishomohopane*
C_{34}αβ	17α (H),21β (H)-tetrakishomohopane*
C_{35}αβ	17α (H),21β (H)-pentakishomohopane*

* isomeric peaks (22*S* and 22*R*)

2.3. Saturated fraction SIM GC-MS *m/z* 217, 218 and 258 (steranes and diasteranes)

Peak label	Peak assignment	Common Abbreviation
a	13β(H),17α(H)-diacholestane (20*S*)	C_{27} βα 20*S* diasterane
b	13β(H),17α(H)-diacholestane (20*R*)	C_{27} βα 20*R* diasterane
c	13α(H),17β(H)-diacholestane (20*S*)	C_{27} αβ 20*S* diasterane
d	13α(H),17β(H)-diacholestane (20*R*)	C_{27} αβ 20*R* diasterane
e	24-methyl-13β(H),17α(H)-diacholestane (20*S*)*	C_{28} βα 20*S* diasterane
f	24-methyl-13β(H),17α (H)-diacholestane (20*R*)*	C_{28} βα 20*R* diasterane
g	24-methyl-13α(H),17β (H)-diacholestane (20*S*)	C_{28} αβ 20*S* diasterane
h	5α(H),14α(H),17α(H)-cholestane (20*S*)	C_{27} ααα 20*S* sterane
i	5α(H),14β(H), 17β(H)-cholestane (20*R*)	C_{27} αββ 20*R* sterane
j	24-ethyl-13β(H),17α(H)-diacholestane (20*S*)	C_{29} βα 20*S* diasterane
k	5α(H),14β(H), 17β(H)-cholestane (20*S*)	C_{27} αββ 20*S* sterane
l	24-methyl-13α(H),17β(H)-diacholestane (20*R*)*	C_{28} αβ 20*R* diasterane
m	5α(H),14α(H), 17α(H)-cholestane (20*R*)	C_{27} ααα 20*R* sterane
n	24-ethyl-13β(H),17α(H)-diacholestane (20*R*)	C_{29} βα 20*R* diasterane
o	24-ethyl-13α(H),17β(H)-diacholestane (20*S*)	C_{29} αβ 20*S* diasterane
p	24-methyl-5α(H),14α(H), 17α(H)-cholestane (20*S*)*	C_{28} ααα 20*S* sterane
q	24-ethyl-13α(H),17β(H)-diacholestane (20*R*)	C_{29} αβ 20*R* diasterane
r	24-methyl-5α(H),14β(H), 17β(H)-cholestane (20*R*)	C_{28} αββ 20*R* sterane
s	24-methyl-5α(H),14β(H), 17β(H)-cholestane (20*S*)	C_{28} αββ 20*S* sterane
t	24-methyl-5α(H),14α(H), 17α(H)-cholestane (20*R*)	C_{28} ααα 20*R* sterane
u	24-ethyl-5α(H),14α(H), 17α(H)-cholestane (20*S*)	C_{29} ααα 20*S* sterane
v	24-ethyl-5α(H),14β(H), 17β(H)-cholestane (20*R*)	C_{29} αββ 20*R* sterane
w	24-ethyl-5α(H),14β(H), 17β(H)-cholestane (20*S*)	C_{29} αββ 20*S* sterane
x	24-ethyl-5α (H),14α(H), 17α(H)-cholestane (20*R*)	C_{29} ααα 20*R* sterane

* isomeric peaks (24*S* and 24*R*)

2.4. Bicadinanes (minor fragment ions in saturated fraction SIM GC-MS *m/z* 191, 217, 218 and 259)

Peak label/ abbreviation	Peak assignment
W	*Cis-cis-trans* bicadinane
T, T1	*Trans-trans-trans* bicadinanes

3. Sample collection and classification details

Table S2: Details of all crude oil samples collected during the 2014–2016 coastal surveys.

Sample ID	Survey Site	Collection Date	Weight (g)	Latitude	Longitude	Whole-oil classification	Biomarker Classification
2014 survey samples							
W13/007472	Eyre Well	8/11/2014	17.6	-31.4639	131.1422	Asphaltite	Asphaltite
W13/007473	Dogfence Beach	8/11/2014	19.3	-31.7708	131.8417	Type I waxy bitumen	Type I waxy bitumen
W13/007475	Fowlers Bay West	10/11/2014	60.2	-31.9928	132.4375	Asphaltite	Asphaltite
W13/007476	Cactus Beach	10/11/2014	813	-32.0739	132.9761	Asphaltite	Asphaltite
W13/007477	Cactus Beach	10/11/2014	219	-32.0689	132.9706	Asphaltite	Asphaltite
W13/007488	Elliston	13/11/2014	78.0	-33.6350	134.8753	Asphaltite	Asphaltite
W13/007490	Sheringa Beach	13/11/2014	495	-33.8736	135.1758	Asphaltite	n.d.
W13/007491	Sleaford Bay	15/11/2014	16.9	-34.8858	135.8506	Type IV waxy bitumen	Type IVA waxy bitumen
W13/007493	West Bay	19/11/2014	18.3	-35.8858	136.5512	Asphaltite	Asphaltite
W13/007495	Hanson Bay	20/11/2014	2.8	-36.0172	136.8576	Type I waxy bitumen	n.d.
W13/007497	Hanson Bay	20/11/2014	4.3	-36.0174	136.8608	Type I waxy bitumen	n.d.
W13/007498A	Hanson Bay	20/11/2014	0.4	-36.0174	136.8608	Type III waxy bitumen	n.d.
W13/007498B	Hanson Bay	20/11/2014	0.2	-36.0174	136.8608	Type III waxy bitumen	n.d.
W13/007499	Hanson Bay	20/11/2014	8.8	-36.0178	136.8620	Type III waxy bitumen	Type IIID
W13/007500	Bales Beach	21/11/2014	10.2	-35.9937	137.3521	Unknown/other	n.d.
W13/007502	Waitpinga Beach	22/11/2014	4.2	-35.6353	138.5028	Type III waxy bitumen	n.d.
W13/007503	Waitpinga Beach	22/11/2014	6.7	-35.6354	138.5034	Type III waxy bitumen	Type IIIE
W13/007504A	Waitpinga Beach	22/11/2014	10.7	-35.6357	138.5048	Type IV waxy bitumen	n.d.
W13/007504B	Waitpinga Beach	22/11/2014	1.6	-35.6357	138.5048	Type I waxy bitumen	n.d.
W13/007505	Waitpinga Beach	22/11/2014	5.6	-35.6359	138.5053	Type IV waxy bitumen	n.d.
W13/007506	Waitpinga Beach	22/11/2014	1.6	-35.6360	138.5055	Type IV waxy bitumen	Type IVA waxy bitumen
W13/007507	Waitpinga Beach	22/11/2014	601	-35.6362	138.5061	Asphaltite	Asphaltite
W13/007508	Waitpinga Beach	22/11/2014	4.6	-35.6363	138.5068	Type III waxy bitumen	n.d.
W13/007509	Waitpinga Beach	22/11/2014	6.5	-35.6368	138.5084	Type III waxy bitumen	n.d.
W13/007510	Waitpinga Beach	22/11/2014	1.7	-35.6369	138.5089	Type III waxy bitumen	n.d.
W13/007511	Waitpinga Beach	22/11/2014	10.5	-35.6375	138.5106	Type I waxy bitumen	Type I waxy bitumen
W13/007512	Waitpinga Beach	22/11/2014	2.7	-35.6375	138.5106	Type III waxy bitumen	n.d.
W13/007513	Waitpinga Beach	22/11/2014	10.7	-35.6380	138.5115	Type III waxy bitumen	n.d.
W13/007514	The Granites	23/11/2014	15.6	-36.6573	139.8536	Type II waxy bitumen	Type II waxy bitumen
W13/007515	The Granites	23/11/2014	1.5	-36.6561	139.8533	Degraded high wax bitumen	n.d.
W13/007517	Eve's Cove	24/11/2014	3.4	-37.1826	139.7443	Type I waxy bitumen	Type I waxy bitumen
W13/007518	Eve's Cove	24/11/2014	53.0	-37.1838	139.7461	Unknown/other (Sooty bitumen?)	n.d.
W13/007519	Eve's Cove	24/11/2014	16.6	-37.1839	139.7462	Type I waxy bitumen	n.d.
W13/007520	Eve's Cove	24/11/2014	4.0	-37.1843	139.7465	Type I waxy bitumen	n.d.
W13/007521	Beachport Conservation Park	24/11/2014	6.0	-37.4499	139.9659	Type I waxy bitumen	Type I waxy bitumen
W13/007522	Beachport Conservation Park	24/11/2014	1.5	-37.4441	139.9615	Type I waxy bitumen	n.d.
W13/007523	Beachport Conservation Park	24/11/2014	3.6	-37.4446	139.9618	Type I waxy bitumen	n.d.
W13/007524	Geltwood Beach	25/11/2014	0.6	-37.6586	140.2216	Type I waxy bitumen	n.d.
W13/007525	Geltwood Beach	25/11/2014	4.2	-37.6595	140.2227	Type III waxy bitumen	n.d.
W13/007526	Geltwood Beach	25/11/2014	9.6	-37.6595	140.2227	Type II waxy bitumen	Type II waxy bitumen
W13/007527	Geltwood Beach	25/11/2014	5.4	-37.6601	140.2235	Type I waxy bitumen	n.d.
W13/007528	Geltwood Beach	25/11/2014	6.0	-37.6638	140.2273	Type I waxy bitumen	Type I waxy bitumen
W13/007529	Number 1 & 2 Rocks	25/11/2014	3.5	-37.7954	140.3204	Type I waxy bitumen	n.d.
W13/007530	Number 1 & 2 Rocks	25/11/2014	4.2	-37.7955	140.3205	Type I waxy bitumen	Type I waxy bitumen
W13/007531A	Number 1 & 2 Rocks	25/11/2014	1.8	-37.7955	140.3205	Type I waxy bitumen	n.d.
W13/007531B	Number 1 & 2 Rocks	25/11/2014	1.0	-37.7955	140.3205	Type I waxy bitumen	n.d.
W13/007531C	Number 1 & 2 Rocks	25/11/2014	0.6	-37.7955	140.3205	Type I waxy bitumen	n.d.

Sample ID	Survey Site	Collection Date	Weight (g)	Latitude	Longitude	Whole-oil classification	Biomarker Classification
W13/007531D	Number 1 & 2 Rocks	25/11/2014	0.4	-37.7955	140.3205	Type I waxy bitumen	n.d.
W13/007532A	Number 1 & 2 Rocks	25/11/2014	2.4	-37.7956	140.3205	Type I waxy bitumen	n.d.
W13/007532B	Number 1 & 2 Rocks	25/11/2014	1.3	-37.7956	140.3205	Type I waxy bitumen	n.d.
W13/007533	Number 1 & 2 Rocks	25/11/2014	1.9	-37.7956	140.3205	Type I waxy bitumen	n.d.
W13/007534	Number 1 & 2 Rocks	25/11/2014	5.6	-37.7956	140.3206	Type I waxy bitumen	n.d.
W13/007535	Number 1 & 2 Rocks	25/11/2014	17.6	-37.7957	140.3206	Type III waxy bitumen	n.d.
W13/007536	Number 1 & 2 Rocks	25/11/2014	3.9	-37.7957	140.3205	Type I waxy bitumen	n.d.
W13/007537	Number 1 & 2 Rocks	25/11/2014	10.3	-37.7957	140.3207	Type I waxy bitumen	n.d.
W13/007538A	Number 1 & 2 Rocks	25/11/2014	7.9	-37.7959	140.3208	Type II waxy bitumen	Type II waxy bitumen
W13/007538B	Number 1 & 2 Rocks	25/11/2014	0.9	-37.7959	140.3208	Type I waxy bitumen	n.d.
W13/007539A	Number 1 & 2 Rocks	25/11/2014	2.7	-37.7959	140.3209	Type III waxy bitumen	n.d.
W13/007539B	Number 1 & 2 Rocks	25/11/2014	0.6	-37.7959	140.3209	Type III waxy bitumen	n.d.
W13/007540	Number 1 & 2 Rocks	25/11/2014	7.5	-37.7961	140.3210	Type I waxy bitumen	n.d.
W13/007541	Number 1 & 2 Rocks	25/11/2014	4.6	-37.7962	140.3211	Type III waxy bitumen	Type IIIA waxy bitumen
W13/007542	Number 1 & 2 Rocks	25/11/2014	7.9	-37.7962	140.3212	Type II waxy bitumen	Type II waxy bitumen
W13/007543	Number 1 & 2 Rocks	25/11/2014	1.2	-37.7963	140.3212	Type I waxy bitumen	n.d.
W13/007544	Number 1 & 2 Rocks	25/11/2014	3.8	-37.7963	140.3211	Type I waxy bitumen	n.d.
W13/007545	Number 1 & 2 Rocks	25/11/2014	10.5	-37.7963	140.3214	Type II waxy bitumen	Type II waxy bitumen
W13/007546	Number 1 & 2 Rocks	25/11/2014	0.7	-37.7964	140.3214	Type I waxy bitumen	n.d.
W13/007547	Number 1 & 2 Rocks	25/11/2014	0.5	-37.7965	140.3215	Type I waxy bitumen	n.d.
W13/007548	Number 1 & 2 Rocks	25/11/2014	5.7	-37.7968	140.3218	Type I waxy bitumen	n.d.
W13/007549	Number 1 & 2 Rocks	25/11/2014	0.6	-37.7968	140.3218	Type I waxy bitumen	n.d.
W13/007550	Number 1 & 2 Rocks	25/11/2014	2.6	-37.7969	140.3219	Type I waxy bitumen	n.d.
W13/007551	Number 1 & 2 Rocks	25/11/2014	5.0	-37.7970	140.3219	Type I waxy bitumen	n.d.
W13/007552A	Number 1 & 2 Rocks	25/11/2014	3.1	-37.7970	140.3220	Type I waxy bitumen	n.d.
W13/007552B	Number 1 & 2 Rocks	25/11/2014	0.5	-37.7970	140.3220	Type I waxy bitumen	n.d.
W13/007553	Number 1 & 2 Rocks	25/11/2014	1.5	-37.7970	140.3221	Type I waxy bitumen	Type I waxy bitumen
W13/007554	Number 1 & 2 Rocks	25/11/2014	3.1	-37.7971	140.3222	Type II waxy bitumen	n.d.
W13/007556	Number 1 & 2 Rocks	25/11/2014	0.9	-37.7973	140.3224	Type I waxy bitumen	n.d.
W13/007557A	Number 1 & 2 Rocks	25/11/2014	2.3	-37.7974	140.3225	Type I waxy bitumen	n.d.
W13/007557B	Number 1 & 2 Rocks	25/11/2014	0.5	-37.7974	140.3225	Type I waxy bitumen	n.d.
W13/007557C	Number 1 & 2 Rocks	25/11/2014	0.5	-37.7974	140.3225	Type III waxy bitumen	n.d.
W13/007558	Number 1 & 2 Rocks	25/11/2014	4.3	-37.7975	140.3226	Type I waxy bitumen	n.d.
W13/007559	Number 1 & 2 Rocks	25/11/2014	7.7	-37.7975	140.3226	Type I waxy bitumen	n.d.
W13/007560A	Number 1 & 2 Rocks	25/11/2014	0.5	-37.7977	140.3227	Type I waxy bitumen	n.d.
W13/007560B	Number 1 & 2 Rocks	25/11/2014	0.3	-37.7977	140.3227	Degraded high wax bitumen	n.d.
W13/007561	Number 1 & 2 Rocks	25/11/2014	3.6	-37.7977	140.3227	Type I waxy bitumen	n.d.
W13/007562	Number 1 & 2 Rocks	25/11/2014	1.0	-37.7977	140.3228	Degraded high wax bitumen	n.d.
W13/007563A	Number 1 & 2 Rocks	25/11/2014	2.6	-37.7978	140.3229	Type I waxy bitumen	n.d.
W13/007563B	Number 1 & 2 Rocks	25/11/2014	1.0	-37.7978	140.3229	Type I waxy bitumen	n.d.
W13/007564A	Number 1 & 2 Rocks	25/11/2014	4.0	-37.7978	140.3229	Degraded high wax bitumen	Type IVD waxy bitumen
W13/007564B	Number 1 & 2 Rocks	25/11/2014	0.9	-37.7978	140.3229	Type III waxy bitumen	n.d.
W13/007564C	Number 1 & 2 Rocks	25/11/2014	1.4	-37.7978	140.3229	Degraded high wax bitumen	n.d.

Sample ID	Survey Site	Collection Date	Weight (g)	Latitude	Longitude	Whole-oil classification	Biomarker Classification
W13/007564D	Number 1 & 2 Rocks	25/11/2014	0.5	-37.7978	140.3229	Type I waxy bitumen	n.d.
W13/007564E	Number 1 & 2 Rocks	25/11/2014	0.2	-37.7978	140.3229	Degraded high wax bitumen	n.d.
W13/007564F	Number 1 & 2 Rocks	25/11/2014	0.2	-37.7978	140.3229	Type I waxy bitumen	n.d.
W13/007565	Number 1 & 2 Rocks	25/11/2014	6.5	-37.7979	140.3229	Type I waxy bitumen	n.d.
2015 survey samples							
W13/007573	Sandy River	5/09/2015	20.4	-35.9559	136.6292	Type III waxy bitumen	n.d.
W13/007578	Sandy River	5/09/2015	3.7	-35.9551	136.6276	Type III waxy bitumen	n.d.
W13/007579	Sandy River	5/09/2015	9.0	-35.9542	136.6261	Type III waxy bitumen	n.d.
W13/007581	Hanson Bay	5/09/2015	8.2	-36.0172	136.8594	Type III waxy bitumen	n.d.
W13/007584	Bales Beach	6/09/2015	0.5	-35.9936	137.3485	Type I waxy bitumen	n.d.
W13/007587	Pennington Bay	6/09/2015	7.9	-35.8532	137.7407	Type I waxy bitumen	n.d.
W13/007588	Waitpinga Beach	7/09/2015	2.0	-35.6354	138.5035	Type IV waxy bitumen	n.d.
W13/007589	Waitpinga Beach	7/09/2015	32.1	-35.6354	138.5035	Type IV waxy bitumen	Type IVA waxy bitumen
W13/007590	Waitpinga Beach	7/09/2015	1.1	-35.6362	138.5067	Type IV waxy bitumen	Type IVA waxy bitumen
W13/007593	Waitpinga Beach	7/09/2015	3.2	-35.6359	138.5058	Type IV waxy bitumen	Type IVA waxy bitumen
W13/007594	The Granites	8/09/2015	24.5	-36.6625	139.8551	Type I waxy bitumen	n.d.
W13/007595	The Granites	8/09/2015	14.8	-36.6597	139.8543	Type I waxy bitumen	n.d.
W13/007596	The Granites	8/09/2015	1.2	-36.6594	139.8542	Type I waxy bitumen	n.d.
W13/007597	The Granites	8/09/2015	5.0	-36.6563	139.8533	Type I waxy bitumen	n.d.
W13/007598	The Granites	8/09/2015	3.3	-36.6561	139.8533	Type I waxy bitumen	n.d.
W13/007600	The Granites	8/09/2015	3.8	-36.6560	139.8533	Type I waxy bitumen	n.d.
W13/007601	The Granites	8/09/2015	25.0	-36.6552	139.8530	Type I waxy bitumen	Type I waxy bitumen
W13/007602	The Granites	8/09/2015	3.8	-36.6552	139.8530	Type I waxy bitumen	n.d.
W13/007603	The Granites	8/09/2015	1.8	-36.6543	139.8528	Type I waxy bitumen	n.d.
W13/007604	The Granites	8/09/2015	2.2	-36.6543	139.8528	Type I waxy bitumen	n.d.
W13/007605	The Granites	8/09/2015	91	-36.6535	139.8526	Type III waxy bitumen	Type IIIB waxy bitumen
W13/007606	The Granites	8/09/2015	2.9	-36.6525	139.8523	Type I waxy bitumen	n.d.
W13/007607	The Granites	8/09/2015	3.8	-36.6524	139.8523	Type I waxy bitumen	n.d.
W13/007608	The Granites	8/09/2015	5.6	-36.6519	139.8522	Type I waxy bitumen	n.d.
W13/007609	Beachport	9/09/2015	2.9	-37.4443	139.9616	Type I waxy bitumen	n.d.
W13/007610	Beachport	9/09/2015	1.0	-37.4443	139.9616	Type I waxy bitumen	n.d.
W13/007611	Beachport	9/09/2015	3.0	-37.4444	139.9616	Type I waxy bitumen	n.d.
W13/007612	Beachport	9/09/2015	0.4	-37.4445	139.9617	Type I waxy bitumen	n.d.
W13/007613	Beachport	9/09/2015	7.0	-37.4445	139.9618	Type I waxy bitumen	n.d.
W13/007614	Beachport	9/09/2015	13.0	-37.4446	139.9618	Type I waxy bitumen	n.d.
W13/007615	Beachport	9/09/2015	154.3	-37.4450	139.9621	Type II waxy bitumen	Type II waxy bitumen
W13/007616	Geltwood Beach	10/09/2015	71.4	-37.6592	140.2222	Type I waxy bitumen	n.d.
W13/007617	Geltwood Beach	10/09/2015	4.6	-37.6606	140.2238	Type I waxy bitumen	n.d.
W13/007618	Geltwood Beach	10/09/2015	14.8	-37.6603	140.2235	Unknown/other (Sooty bitumen?)	n.d.
W13/007619	Geltwood Beach	10/09/2015	1.2	-37.6601	140.2234	Type II waxy bitumen	Type II waxy bitumen
W13/007620	Number 1 and 2 Rocks	10/09/2015	72.8	-37.7952	140.3202	Type I waxy bitumen	n.d.
W13/007621	Number 1 and 2 Rocks	10/09/2015	3.3	-37.7952	140.3202	Type III waxy bitumen	n.d.
W13/007622	Number 1 and 2 Rocks	10/09/2015	5.4	-37.7953	140.3202	Type I waxy bitumen	n.d.
W13/007623	Number 1 and 2 Rocks	10/09/2015	5.4	-37.7954	140.3204	Type I waxy bitumen	n.d.
W13/007624	Number 1 and 2 Rocks	10/09/2015	18.9	-37.7954	140.3203	Type I waxy bitumen	n.d.
W13/007625	Number 1 and 2 Rocks	10/09/2015	5.7	-37.7954	140.3203	Type I waxy bitumen	Type I waxy bitumen
W13/007626	Number 1 and 2 Rocks	10/09/2015	4.4	-37.7954	140.3204	Type I waxy bitumen	n.d.
W13/007627	Number 1 and 2 Rocks	10/09/2015	208.3	-37.7955	140.3205	Type III waxy bitumen	n.d.
W13/007628	Number 1 and 2 Rocks	10/09/2015	14.6	-37.7955	140.3205	Type I waxy bitumen	n.d.
W13/007629	Number 1 and 2 Rocks	10/09/2015	2.5	-37.7956	140.3204	Type I waxy bitumen	n.d.
W13/007630	Number 1 and 2 Rocks	10/09/2015	1.9	-37.7958	140.3205	Type II waxy bitumen	n.d.

Sample ID	Survey Site	Collection Date	Weight (g)	Latitude	Longitude	Whole-oil classification	Biomarker Classification
W13/007631	Number 1 and 2 Rocks	10/09/2015	7.5	-37.7959	140.3208	Type I waxy bitumen	n.d.
W13/007632	Number 1 and 2 Rocks	10/09/2015	10.3	-37.7960	140.3209	Type I waxy bitumen	n.d.
W13/007633	Number 1 and 2 Rocks	10/09/2015	4.0	-37.7961	140.3210	Type II waxy bitumen	n.d.
W13/007634	Number 1 and 2 Rocks	10/09/2015	57.4	-37.7961	140.3211	Type I waxy bitumen	n.d.
W13/007635	Number 1 and 2 Rocks	10/09/2015	9.4	-37.7964	140.3215	Type I waxy bitumen	n.d.
W13/007637	Number 1 and 2 Rocks	10/09/2015	10.6	-37.7966	140.3218	Type II waxy bitumen	n.d.
W13/007638	Number 1 and 2 Rocks	10/09/2015	1.6	-37.7969	140.3219	Type I waxy bitumen	n.d.
W13/007639	Number 1 and 2 Rocks	10/09/2015	2.7	-37.7971	140.3221	Type II waxy bitumen	n.d.
W13/007641	Number 1 and 2 Rocks	10/09/2015	2.1	-37.7976	140.3225	Type II waxy bitumen	n.d.
W13/007642	Number 1 and 2 Rocks	10/09/2015	8.1	-37.7976	140.3227	Type I waxy bitumen	n.d.
W13/007643	Nene Valley	11/09/2015	0.5	-37.9832	140.5085	Type I waxy bitumen	n.d.
W13/007646	Sleaford Bay	18/09/2015	5.8	-34.8837	135.8497	Type III waxy bitumen	n.d.
W13/007649	Mount Drummond	19/09/2015	3.3	-34.2571	135.3420	Type III waxy bitumen	n.d.
W13/007651	Sheringa Beach	20/09/2015	0.8	-33.8735	135.1760	Type I waxy bitumen	n.d.
W13/007655	Sheringa Beach	20/09/2015	21.6	-33.8768	135.1817	Type I waxy bitumen	n.d.
W13/007658	Tyringa Beach	21/09/2015	1.0	-33.1488	134.4157	Degraded asphaltite	n.d.
W13/007659	Tractor Beach	21/09/2015	8.5	-32.8699	134.1112	Degraded asphaltite	Asphaltite
W13/007660	Tractor Beach	21/09/2015	3.8	-32.8697	134.1120	Degraded asphaltite	Asphaltite
W13/007661	Tractor Beach	21/09/2015	19.9	-32.8697	134.1123	Asphaltite	Asphaltite
W13/007662	Tractor Beach	21/09/2015	0.9	-32.8697	134.1124	Degraded asphaltite	Asphaltite
W13/007663	Tractor Beach	21/09/2015	1.0	-32.8696	134.1125	Degraded asphaltite	Asphaltite
W13/007664	Tractor Beach	21/09/2015	31.5	-32.8693	134.1134	Degraded asphaltite	Asphaltite
W13/007665	Tractor Beach	21/09/2015	16.8	-32.8687	134.1154	Degraded asphaltite	Asphaltite
W13/007666	Tractor Beach	21/09/2015	12.6	-32.8685	134.1159	Degraded asphaltite	Asphaltite
W13/007667	Tractor Beach	21/09/2015	4.4	-32.8683	134.1166	Degraded asphaltite	Asphaltite
W13/007668	Tractor Beach	21/09/2015	24.5	-32.8675	134.1178	Asphaltite	Asphaltite
W13/007669	St Mary Bay (South)	22/09/2015	24.0	-32.5328	133.8636	Type I waxy bitumen	n.d.
W13/007671	Cactus Beach	23/09/2015	275.7	-32.0774	132.9791	Asphaltite	Asphaltite
W13/007746	Dogfence Beach	25/09/2015	20.9	-31.7718	131.8421	Type I waxy bitumen	n.d.
W13/007747	Dogfence Beach	25/09/2015	1.9	-31.7718	131.8422	Degraded high wax bitumen	n.d.
W13/007749A	Dogfence Beach	25/09/2015	2.4	-31.7718	131.8421	Type I waxy bitumen	n.d.
W13/007749B	Dogfence Beach	25/09/2015	1.9	-31.7718	131.8421	Unknown/other	n.d.
W13/007749C	Dogfence Beach	25/09/2015	1.8	-31.7718	131.8421	Type I waxy bitumen	n.d.
W13/007749D	Dogfence Beach	25/09/2015	3.9	-31.7718	131.8421	Degraded high wax bitumen	n.d.
W13/007749E	Dogfence Beach	25/09/2015	2.3	-31.7718	131.8421	Type I waxy bitumen	n.d.
W13/007749F	Dogfence Beach	25/09/2015	1.4	-31.7718	131.8421	Type III waxy bitumen	n.d.
W13/007749H	Dogfence Beach	25/09/2015	0.8	-31.7718	131.8421	Type IV waxy bitumen	Type IVD waxy bitumen
W13/007749K	Dogfence Beach	25/09/2015	0.4	-31.7718	131.8421	Degraded high wax bitumen	n.d.
W13/007749M	Dogfence Beach	25/09/2015	0.2	-31.7718	131.8421	Degraded high wax bitumen	n.d.
W13/007749N	Dogfence Beach	25/09/2015	0.3	-31.7718	131.8421	Type I waxy bitumen	n.d.
W13/007751	Dogfence Beach	25/09/2015	19.3	-31.7717	131.8421	Type III waxy bitumen	n.d.
W13/007752	Dogfence Beach	25/09/2015	1.0	-31.7716	131.8422	Degraded high wax bitumen	n.d.
W13/007753	Dogfence Beach	25/09/2015	1.3	-31.7716	131.8422	Degraded high wax bitumen	n.d.
W13/007754	Dogfence Beach	25/09/2015	3.1	-31.7717	131.8422	Degraded high wax bitumen	n.d.
W13/007755	Dogfence Beach	25/09/2015	3.0	-31.7716	131.8421	Type I waxy bitumen	n.d.
W13/007756	Dogfence Beach	25/09/2015	40.4	-31.7716	131.8422	Type I waxy bitumen	n.d.
W13/007757	Dogfence Beach	25/09/2015	14.1	-31.7714	131.8421	Type I waxy bitumen	n.d.
W13/007758	Dogfence Beach	25/09/2015	1.7	-31.7688	131.8394	Type I waxy bitumen	n.d.
W13/007759	Dogfence Beach	25/09/2015	27.8	-31.7653	131.8346	Type I waxy bitumen	n.d.
W13/007760	Dogfence Beach	25/09/2015	11.5	-31.7628	131.8311	Type I waxy bitumen	n.d.
W13/007764	Eyre Well	26/09/2015	429	-31.4651	131.1338	Asphaltite	n.d.

Sample ID	Survey Site	Collection Date	Weight (g)	Latitude	Longitude	Whole-oil classification	Biomarker Classification
2016 survey samples							
W13/007769	Eyre Well	06-Oct-16	41.8	-31.4652	131.1361	Type I waxy bitumen	n.d.
W13/007770	Eyre Well	06-Oct-16	1.2	-31.4647	131.1319	Type I waxy bitumen	n.d.
W13/007772	Dogfence Beach	06-Oct-16	2.0	-31.7717	131.8422	Type I waxy bitumen	n.d.
W13/007774	Dogfence Beach	06-Oct-16	1.5	N.R.	N.R.	Type I waxy bitumen	n.d.
W13/007775	Dogfence Beach	06-Oct-16	2.1	-31.7716	131.8422	Degraded high wax bitumen	n.d.
W13/007776	Dogfence Beach	06-Oct-16	2.5	-31.7716	131.8422	Unknown	n.d.
W13/007778	Dogfence Beach	06-Oct-16	24.6	-31.7716	131.8421	Type III waxy bitumen	Type IIIA waxy bitumen
W13/007779	Dogfence Beach	06-Oct-16	34.3	-31.7715	131.8421	Asphaltite	n.d.
W13/007780	Dogfence Beach	06-Oct-16	2.9	-31.7715	131.8422	Type III waxy bitumen	n.d.
W13/007781	Dogfence Beach	06-Oct-16	5.7	-31.7715	131.8421	Type I waxy bitumen	n.d.
W13/007782	Dogfence Beach	06-Oct-16	8.6	-31.7714	131.8421	Type III waxy bitumen	n.d.
W13/007783	Dogfence Beach	06-Oct-16	4.9	-31.7714	131.8421	Degraded high wax bitumen	n.d.
W13/007784	Dogfence Beach	06-Oct-16	11.9	-31.7713	131.8421	Degraded high wax bitumen	n.d.
W13/007785	Dogfence Beach	06-Oct-16	13.6	-31.7713	131.8421	Type I waxy bitumen	n.d.
W13/007786	Dogfence Beach	06-Oct-16	2.6	-31.7713	131.8420	Type I waxy bitumen	n.d.
W13/007788	Dogfence Beach	06-Oct-16	0.9	-31.7713	131.8420	Type I waxy bitumen	n.d.
W13/007789	Dogfence Beach	06-Oct-16	5.0	-31.7713	131.8420	Type I waxy bitumen	n.d.
W13/007790	Dogfence Beach	06-Oct-16	3.1	-31.7712	131.8420	Type I waxy bitumen	n.d.
W13/007792	Dogfence Beach	06-Oct-16	2.3	-31.7712	131.8420	Unknown	n.d.
W13/007794A	Dogfence Beach	06-Oct-16	4.2	-31.7712	131.8419	Type I waxy bitumen	n.d.
W13/007794B	Dogfence Beach	06-Oct-16	1.7	-31.7712	131.8419	Type I waxy bitumen	n.d.
W13/007794C	Dogfence Beach	06-Oct-16	1.1	-31.7712	131.8419	Type I waxy bitumen	n.d.
W13/007796	Dogfence Beach	06-Oct-16	2.1	-31.7709	131.8417	Degraded high wax bitumen	n.d.
W13/007797	Dogfence Beach	06-Oct-16	14.0	-31.7708	131.8416	Degraded high wax bitumen	n.d.
W13/007798	Dogfence Beach	06-Oct-16	1.0	-31.7708	131.8416	Type I waxy bitumen	n.d.
W13/007801	Dogfence Beach	06-Oct-16	140.4	-31.7707	131.8415	Asphaltite	n.d.
W13/007802	Dogfence Beach	06-Oct-16	21.2	-31.7707	131.8415	Asphaltite	n.d.
W13/007804	Dogfence Beach	06-Oct-16	3.3	-31.7706	131.8415	Type I waxy bitumen	n.d.
W13/007806	Dogfence Beach	06-Oct-16	2.6	-31.7706	131.8414	Type I waxy bitumen	n.d.
W13/007807	Dogfence Beach	06-Oct-16	38.9	-31.7706	131.8414	Asphaltite	n.d.
W13/007808	Dogfence Beach	06-Oct-16	1.3	-31.7705	131.8414	Type I waxy bitumen	n.d.
W13/007809	Dogfence Beach	06-Oct-16	7.9	-31.7706	131.8414	Type I waxy bitumen	n.d.
W13/007811	Dogfence Beach	06-Oct-16	1.9	-31.7701	131.8410	Degraded high wax bitumen	Type IVE waxy bitumen
W13/007812	Dogfence Beach	06-Oct-16	3.9	-31.7700	131.8408	Degraded high wax bitumen	n.d.
W13/007813A	Dogfence Beach	06-Oct-16	5.7	-31.7700	131.8408	Type III waxy bitumen	n.d.
W13/007813B	Dogfence Beach	06-Oct-16	2.0	-31.7700	131.8408	Type I waxy bitumen	n.d.
W13/007813C	Dogfence Beach	06-Oct-16	2.6	-31.7700	131.8408	Type I waxy bitumen	n.d.
W13/007813D	Dogfence Beach	06-Oct-16	0.9	-31.7700	131.8408	Type I waxy bitumen	n.d.
W13/007813E	Dogfence Beach	06-Oct-16	1.5	-31.7700	131.8408	Type I waxy bitumen	n.d.
W13/007813F	Dogfence Beach	06-Oct-16	1.0	-31.7700	131.8408	Type I waxy bitumen	n.d.
W13/007815	Scott Bay	07-Oct-16	9.6	N.R.	N.R.	Type I waxy bitumen	n.d.
W13/007817A	Cactus Beach	08-Oct-16	0.9	-32.0795	132.9800	Type I waxy bitumen	n.d.
W13/007817B	Cactus Beach	08-Oct-16	0.7	-32.0795	132.9800	Degraded high wax bitumen	n.d.
W13/007817C	Cactus Beach	08-Oct-16	1.1	-32.0795	132.9800	Degraded high wax bitumen	n.d.
W13/007817D	Cactus Beach	08-Oct-16	0.4	-32.0795	132.9800	Degraded high wax bitumen	n.d.
W13/007818A	Cactus Beach	08-Oct-16	4.4	-32.0777	132.9797	Type III waxy bitumen	n.d.
W13/007818B	Cactus Beach	08-Oct-16	1.4	-32.0777	132.9797	Degraded high wax bitumen	Type IVD waxy bitumen
W13/007819	Cactus Beach	08-Oct-16	14.0	-32.0729	132.9755	Type I waxy bitumen	Type I waxy bitumen
W13/007820	Cactus Beach	08-Oct-16	4.9	-32.0712	132.9734	Asphaltite	Asphaltite
W13/007821	Cactus Beach	08-Oct-16	11.6	-32.0706	132.9730	Type III waxy bitumen	n.d.
W13/007822	Cactus Beach	08-Oct-16	7.6	-32.0704	132.9727	Type I waxy bitumen	n.d.
W13/007824	Cactus Beach	08-Oct-16	15.3	-32.0674	132.9686	Type I waxy bitumen	n.d.
W13/007825	Cactus Beach	08-Oct-16	21.2	-32.0673	132.9685	Unknown	n.d.
W13/007826	Cactus Beach	08-Oct-16	27.9	-32.0671	132.9681	Type I waxy bitumen	n.d.
W13/007827	Cactus Beach	08-Oct-16	7.4	-32.0714	132.9734	Asphaltite	Asphaltite

Sample ID	Survey Site	Collection Date	Weight (g)	Latitude	Longitude	Whole-oil classification	Biomarker Classification
W13/007829	St Mary Bay Sth	09-Oct-16	3.2	-32.5337	133.8559	Type I waxy bitumen	n.d.
W13/007830	Tractor Beach	09-Oct-16	19.4	-32.8698	134.1118	Asphaltite	Asphaltite
W13/007831	Tractor Beach	09-Oct-16	5.3	-32.8698	134.1119	Unknown	n.d.
W13/007832	Tractor Beach	09-Oct-16	16.9	-32.8697	134.1121	Asphaltite	Asphaltite
W13/007833	Tractor Beach	09-Oct-16	20.5	-32.8696	134.1126	Degraded high wax bitumen	n.d.
W13/007835	Elliston	10-Oct-16	1.2	-33.6369	134.8803	Degraded high wax bitumen	n.d.
W13/007836	Elliston	10-Oct-16	7.2	-33.6353	134.8772	Type I waxy bitumen	n.d.
W13/007837	Elliston	10-Oct-16	4.6	-33.6425	134.8863	Type IV waxy bitumen	Type IVD waxy bitumen
W13/007838	Elliston	10-Oct-16	10.2	-33.6395	134.8848	Type I waxy bitumen	n.d.
W13/007839	Elliston	10-Oct-16	7.3	-33.6385	134.8833	Type I waxy bitumen	n.d.
W13/007841	Sheringa Beach	11-Oct-16	2.7	-33.8735	135.1762	Type III waxy bitumen	n.d.
W13/007842	Sheringa Beach	11-Oct-16	0.4	-33.8734	135.1763	Type I waxy bitumen	n.d.
W13/007845	Sheringa Beach	11-Oct-16	500	-33.8744	135.1781	Asphaltite	Asphaltite
W13/007846	Sheringa Beach	11-Oct-16	242	-33.8746	135.1782	Asphaltite	n.d.
W13/007847	Sheringa Beach	11-Oct-16	10.9	-33.8758	135.1805	Type III waxy bitumen	Type IIIA waxy bitumen
W13/007848	Sheringa Beach	11-Oct-16	15.3	-33.8763	135.1807	Type III waxy bitumen	Type IIIA waxy bitumen
W13/007849	Sheringa Beach	11-Oct-16	3.7	-33.8765	135.1811	Type I waxy bitumen	n.d.
W13/007850	Sheringa Beach	11-Oct-16	114.7	-33.8781	135.1826	Type I waxy bitumen	n.d.
W13/007851A	Sheringa Beach	11-Oct-16	2.0	-33.8791	135.1832	Degraded high wax bitumen	n.d.
W13/007852A	Mount Drummond Beach	11-Oct-16	4.4	-34.2568	135.3419	Type III waxy bitumen	n.d.
W13/007852B	Mount Drummond Beach	11-Oct-16	0.6	-34.2568	135.3419	Type III waxy bitumen	n.d.
W13/007853A	Mount Drummond Beach	11-Oct-16	2.7	-34.2568	135.3420	Type I waxy bitumen	n.d.
W13/007853B	Mount Drummond Beach	11-Oct-16	3.0	-34.2568	135.3420	Type I waxy bitumen	n.d.
W13/007855	Mount Drummond Beach	11-Oct-16	9.4	-34.2575	135.3424	Unknown	n.d.
W13/007856	Mount Drummond Beach	11-Oct-16	5.5	-34.2576	135.3425	Type I waxy bitumen	n.d.
W13/007857A	Mount Drummond Beach	11-Oct-16	7.9	-34.2576	135.3425	Type IV waxy bitumen	Type IVC waxy bitumen
W13/007858	Mount Drummond Beach	11-Oct-16	2.6	-34.2576	135.3425	Type I waxy bitumen	n.d.
W13/007859	Mount Drummond Beach	11-Oct-16	4.5	-34.2582	135.3427	Type III waxy bitumen	n.d.
W13/007860	Mount Drummond Beach	11-Oct-16	2.3	-34.2589	135.3430	Type I waxy bitumen	n.d.
W13/007861	Avoid Bay	12-Oct-16	0.3	-34.6685	135.3455	Type I waxy bitumen	n.d.
W13/007862	Avoid Bay	12-Oct-16	1.4	-34.6684	135.3456	Unknown	n.d.
W13/007863	Avoid Bay	12-Oct-16	4.0	-34.6681	135.3460	Type I waxy bitumen	Type I waxy bitumen
W13/007864	Avoid Bay	12-Oct-16	11.0	-34.6670	135.3469	Type III waxy bitumen	n.d.
W13/007865	Avoid Bay	12-Oct-16	0.9	-34.6669	135.3470	Type I waxy bitumen	n.d.
W13/007866	Avoid Bay	12-Oct-16	0.6	-34.6667	135.3470	Unknown	n.d.
W13/007867	Avoid Bay	12-Oct-16	0.7	-34.6663	135.3472	Type III waxy bitumen	Type IIIF waxy bitumen
W13/007868	Sleaford Bay	12-Oct-16	1.1	-34.8845	135.8502	Type I waxy bitumen	Type I waxy bitumen
W13/007869	Sleaford Bay	12-Oct-16	1.0	-34.8838	135.8498	Type III waxy bitumen	Type IIID waxy bitumen
W13/007872	Sleaford Bay	12-Oct-16	1.1	-34.8800	135.8459	Degraded high wax bitumen	n.d.
W13/007874	Sleaford Bay	12-Oct-16	0.3	-34.8799	135.8455	Degraded high wax bitumen	n.d.
W13/007922	West Bay	16-Oct-16	2.6	-35.8873	136.5534	Type I waxy bitumen	Type I waxy bitumen
W13/007923	Sandy River	17-Oct-16	11.8	-35.9560	136.6294	Sandy River Tar	Sandy River Tar
W13/007924	Sandy River	17-Oct-16	1.3	-35.9559	136.6292	Sandy River Tar	n.d.
W13/007925	Sandy River	17-Oct-16	1.7	-35.9558	136.6293	Sandy River Tar	n.d.
W13/007926	Sandy River	17-Oct-16	0.3	-35.9557	136.6292	Degraded high wax bitumen	n.d.

Sample ID	Survey Site	Collection Date	Weight (g)	Latitude	Longitude	Whole-oil classification	Biomarker Classification
W13/007927	Sandy River	17-Oct-16	1.9	-35.9557	136.6292	Sandy River Tar	n.d.
W13/007928	Sandy River	17-Oct-16	1.0	-35.9557	136.6292	Sandy River Tar	Sandy River Tar
W13/007929	Sandy River	17-Oct-16	2.0	-35.9556	136.6291	Sandy River Tar	Sandy River Tar
W13/007930	Sandy River	17-Oct-16	0.5	-35.9556	136.6291	Sandy River Tar	n.d.
W13/007931	Sandy River	17-Oct-16	10.6	-35.9556	136.6291	Sandy River Tar	n.d.
W13/007932	Sandy River	17-Oct-16	26.0	-35.9555	136.6291	Sandy River Tar	Sandy River Tar
W13/007933	Sandy River	17-Oct-16	1.3	-35.9555	136.6291	Sandy River Tar	n.d.
W13/007934	Sandy River	17-Oct-16	1.1	-35.9555	136.6291	Sandy River Tar	n.d.
W13/007935	Sandy River	17-Oct-16	0.3	-35.9555	136.6291	Sandy River Tar	n.d.
W13/007936A	Sandy River	17-Oct-16	0.5	-35.9555	136.6290	Sandy River Tar	n.d.
W13/007936B	Sandy River	17-Oct-16	0.2	-35.9555	136.6290	Sandy River Tar	n.d.
W13/007936C	Sandy River	17-Oct-16	0.2	-35.9555	136.6290	Sandy River Tar	n.d.
W13/007937A	Sandy River	17-Oct-16	4.8	-35.9555	136.6290	Sandy River Tar	Sandy River Tar
W13/007937B	Sandy River	17-Oct-16	0.2	-35.9555	136.6290	Sandy River Tar	Sandy River Tar
W13/007938	Sandy River	17-Oct-16	32.7	-35.9554	136.6291	Type III waxy bitumen	Type IIIB waxy bitumen
W13/007939	Sandy River	17-Oct-16	0.8	-35.9552	136.6292	Type I waxy bitumen	n.d.
W13/007940	Sandy River	17-Oct-16	1.2	-35.9554	136.6290	Type III waxy bitumen	n.d.
W13/007941	Sandy River	17-Oct-16	0.7	-35.9554	136.6289	Sandy River Tar	n.d.
W13/007942	Sandy River	17-Oct-16	0.3	-35.9555	136.6290	Sandy River Tar	n.d.
W13/007943	Sandy River	17-Oct-16	17.6	-35.9554	136.6289	Sandy River Tar	n.d.
W13/007944	Sandy River	17-Oct-16	0.5	-35.9555	136.6289	Sandy River Tar	Sandy River Tar
W13/007945A	Sandy River	17-Oct-16	0.3	-35.9554	136.6289	Sandy River Tar	n.d.
W13/007945B	Sandy River	17-Oct-16	0.2	-35.9554	136.6289	Sandy River Tar	n.d.
W13/007946A	Sandy River	17-Oct-16	1.1	-35.9554	136.6289	Sandy River Tar	n.d.
W13/007946B	Sandy River	17-Oct-16	1.2	-35.9554	136.6289	Sandy River Tar	n.d.
W13/007946C	Sandy River	17-Oct-16	0.5	-35.9554	136.6289	Sandy River Tar	n.d.
W13/007947	Sandy River	17-Oct-16	0.6	-35.9554	136.6288	Sandy River Tar	n.d.
W13/007948	Sandy River	17-Oct-16	1.1	-35.9554	136.6288	Sandy River Tar	n.d.
W13/007949	Sandy River	17-Oct-16	7.2	-35.9554	136.6288	Sandy River Tar	n.d.
W13/007950A	Sandy River	17-Oct-16	0.8	-35.9554	136.6288	Sandy River Tar	n.d.
W13/007950B	Sandy River	17-Oct-16	0.3	-35.9554	136.6288	Sandy River Tar	n.d.
W13/007950C	Sandy River	17-Oct-16	0.2	-35.9554	136.6288	Sandy River Tar	n.d.
W13/007950D	Sandy River	17-Oct-16	0.2	-35.9554	136.6288	Sandy River Tar	n.d.
W13/007951	Sandy River	17-Oct-16	0.3	-35.9554	136.6288	Sandy River Tar	n.d.
W13/007952A	Sandy River	17-Oct-16	1.5	-35.9554	136.6287	Sandy River Tar	n.d.
W13/007952B	Sandy River	17-Oct-16	0.8	-35.9554	136.6287	Sandy River Tar	n.d.
W13/007952C	Sandy River	17-Oct-16	0.8	-35.9554	136.6287	Sandy River Tar	n.d.
W13/007952D	Sandy River	17-Oct-16	0.4	-35.9554	136.6287	Sandy River Tar	n.d.
W13/007953	Sandy River	17-Oct-16	12.7	-35.9554	136.6287	Sandy River Tar	Sandy River Tar
W13/007954A	Sandy River	17-Oct-16	0.5	-35.9554	136.6286	Sandy River Tar	n.d.
W13/007954B	Sandy River	17-Oct-16	0.3	-35.9554	136.6286	Sandy River Tar	n.d.
W13/007954C	Sandy River	17-Oct-16	0.1	-35.9554	136.6286	Sandy River Tar	n.d.
W13/007955	Sandy River	17-Oct-16	0.3	-35.9553	136.6286	Sandy River Tar	n.d.
W13/007956A	Sandy River	17-Oct-16	1.2	-35.9553	136.6285	Sandy River Tar	n.d.
W13/007956B	Sandy River	17-Oct-16	0.2	-35.9553	136.6285	Sandy River Tar	n.d.
W13/007957	Sandy River	17-Oct-16	0.3	-35.9553	136.6283	Sandy River Tar	n.d.
W13/007958	Sandy River	17-Oct-16	0.1	-35.9552	136.6283	Sandy River Tar	n.d.
W13/007960	Hanson Bay	17-Oct-16	1.1	-36.0172	136.8576	Degraded high wax bitumen	n.d.
W13/007961	Bales Beach	18-Oct-16	0.5	-35.9950	137.3562	Unknown	n.d.
W13/007962	Bales Beach	18-Oct-16	7.1	-35.9952	137.3567	Type I waxy bitumen	Type I waxy bitumen
W13/007963	Bales Beach	18-Oct-16	16.6	-35.9952	137.3584	Type I waxy bitumen	n.d.
W13/007964	Bales Beach	18-Oct-16	4.2	-35.9951	137.3584	Type I waxy bitumen	n.d.
W13/007965	Bales Beach	18-Oct-16	0.3	-35.9967	137.3607	Type I waxy bitumen	Type I waxy bitumen
W13/007966	Bales Beach	18-Oct-16	1.6	-35.9967	137.3607	Type I waxy bitumen	n.d.
W13/007967	Pennington Bay	18-Oct-16	3.8	-35.8523	137.7445	Type I waxy bitumen	Type I waxy bitumen
W13/007968	Pennington Bay	18-Oct-16	0.6	-35.8525	137.7436	Degraded high wax bitumen	n.d.
W13/007969	Waitpinga Beach	19-Oct-16	21.0	-35.6346	138.5001	Type IV waxy bitumen	Type IVA waxy bitumen
W13/007971	Waitpinga Beach	19-Oct-16	1.8	-35.6359	138.5055	Type I waxy bitumen	n.d.
W13/007972	Waitpinga Beach	19-Oct-16	5.8	-35.6359	138.5056	Degraded high wax bitumen	n.d.

Sample ID	Survey Site	Collection Date	Weight (g)	Latitude	Longitude	Whole-oil classification	Biomarker Classification
W13/007973	Waitpinga Beach	19-Oct-16	5.6	-35.6362	138.5068	Type IV waxy bitumen	Type IVA waxy bitumen
W13/007974	Waitpinga Beach	19-Oct-16	0.9	-35.6373	138.5101	Type IV waxy bitumen	Type IVA waxy bitumen
W13/007975	Waitpinga Beach	19-Oct-16	12.1	-35.6374	138.5103	Type IV waxy bitumen	Type IVA waxy bitumen
W13/007976	Waitpinga Beach	19-Oct-16	3188	-35.6374	138.5103	Asphaltite	Asphaltite
W13/007977	Waitpinga Beach	19-Oct-16	3.0	-35.6376	138.5108	Type I waxy bitumen	n.d.
W13/007978	Waitpinga Beach	19-Oct-16	0.6	-35.6376	138.5108	Type IV waxy bitumen	n.d.
W13/007979	Waitpinga Beach	19-Oct-16	3.9	-35.6376	138.5109	Type IV waxy bitumen	n.d.
W13/007980	Waitpinga Beach	19-Oct-16	0.3	-35.6376	138.5108	Degraded high wax bitumen	n.d.
W13/007981	Waitpinga Beach	19-Oct-16	0.6	-35.6376	138.5109	Type I waxy bitumen	n.d.
W13/007982	Waitpinga Beach	19-Oct-16	0.4	-35.6378	138.5111	Degraded high wax bitumen	n.d.
W13/007984	Waitpinga Beach	19-Oct-16	16.8	-35.6380	138.5115	Type IV waxy bitumen	Type IVA waxy bitumen
W13/007985	Waitpinga Beach	19-Oct-16	9.2	-35.6368	138.5088	Type IV waxy bitumen	Type IVA waxy bitumen
W13/007986	28 Mile Crossing	20-Oct-16	0.9	-36.4370	139.7724	Type I waxy bitumen	n.d.
W13/007987	28 Mile Crossing	20-Oct-16	1.5	-36.4375	139.7726	Type I waxy bitumen	n.d.
W13/007988	28 Mile Crossing	20-Oct-16	0.5	-36.4362	139.7728	Type I waxy bitumen	n.d.
W13/007989	The Granites	20-Oct-16	2.6	-36.6581	139.8537	Type I waxy bitumen	n.d.
W13/007990	The Granites	20-Oct-16	0.7	-36.6577	139.8537	Type I waxy bitumen	n.d.
W13/007991	The Granites	20-Oct-16	5.0	-36.6575	139.8536	Type I waxy bitumen	n.d.
W13/007992	The Granites	20-Oct-16	0.4	-36.6573	139.8535	Type I waxy bitumen	n.d.
W13/007993	The Granites	20-Oct-16	2.5	-36.6571	139.8535	Type I waxy bitumen	n.d.
W13/007994	The Granites	20-Oct-16	0.5	-36.6570	139.8534	Type I waxy bitumen	n.d.
W13/007995	The Granites	20-Oct-16	4.4	-36.6562	139.8532	Type I waxy bitumen	Type I waxy bitumen
W13/007996	The Granites	20-Oct-16	10.3	-36.6546	139.8528	Type I waxy bitumen	n.d.
W13/007997	The Granites	20-Oct-16	1.9	-36.6529	139.8524	Type I waxy bitumen	Type I waxy bitumen
W13/007998	The Granites	20-Oct-16	1.2	-36.6529	139.8524	Type I waxy bitumen	n.d.
W13/007999	The Granites	20-Oct-16	0.7	-36.6509	139.8519	Type I waxy bitumen	Type I waxy bitumen
COA/000956	The Granites	20-Oct-16	6.4	-36.6521	139.8521	Asphaltite	Asphaltite
COA/000957	Eves Cove	21-Oct-16	6.1	-37.1818	139.7430	Type I waxy bitumen	n.d.
COA/000958	Eves Cove	21-Oct-16	0.7	-37.1819	139.7430	Degraded high wax bitumen	n.d.
COA/000959	Eves Cove	21-Oct-16	1.0	-37.1825	139.7442	Degraded high wax bitumen	n.d.
COA/000960	Eves Cove	21-Oct-16	0.7	-37.1830	139.7447	Degraded high wax bitumen	n.d.
COA/000961	Eves Cove	21-Oct-16	3.3	-37.1833	139.7452	Type I waxy bitumen	n.d.
COA/000962	Eves Cove	21-Oct-16	0.8	-37.1834	139.7453	Degraded high wax bitumen	n.d.
COA/000963	Eves Cove	21-Oct-16	1.2	-37.1838	139.7460	Degraded high wax bitumen	n.d.
COA/000964	Eves Cove	21-Oct-16	1.9	-37.1838	139.7460	Type I waxy bitumen	n.d.
COA/000965	Eves Cove	21-Oct-16	1.0	-37.1838	139.7460	Degraded high wax bitumen	n.d.
COA/000966	Eves Cove	21-Oct-16	2.0	-37.1839	139.7460	Type I waxy bitumen	n.d.
COA/000967	Eves Cove	21-Oct-16	2.1	-37.1839	139.7460	Type I waxy bitumen	n.d.
COA/000968	Eves Cove	21-Oct-16	1.0	-37.1838	139.7461	Degraded high wax bitumen	n.d.
COA/000969	Eves Cove	21-Oct-16	1.8	-37.1838	139.7461	Type I waxy bitumen	n.d.
COA/000970	Eves Cove	21-Oct-16	2.3	-37.1839	139.7461	Degraded high wax bitumen	n.d.
COA/000971	Eves Cove	21-Oct-16	2.1	-37.1839	139.7461	Type I waxy bitumen	n.d.
COA/000972	Eves Cove	21-Oct-16	2.5	-37.1839	139.7462	Type III waxy bitumen	n.d.
COA/000973	Eves Cove	21-Oct-16	0.5	-37.1840	139.7462	Type I waxy bitumen	n.d.
COA/000974	Eves Cove	21-Oct-16	1.0	-37.1840	139.7462	Degraded high wax bitumen	n.d.
COA/000975	Eves Cove	21-Oct-16	1.3	-37.1841	139.7462	Degraded high wax bitumen	n.d.
COA/000976	Eves Cove	21-Oct-16	8.4	-37.1841	139.7462	Type I waxy bitumen	Type I waxy bitumen
COA/000977	Eves Cove	21-Oct-16	0.8	-37.1840	139.7463	Degraded high wax bitumen	n.d.
COA/000978	Eves Cove	21-Oct-16	0.6	-37.1840	139.7463	Type I waxy bitumen	n.d.
COA/000979	Eves Cove	21-Oct-16	0.8	-37.1841	139.7463	Type I waxy bitumen	n.d.
COA/000980	Eves Cove	21-Oct-16	1.1	-37.1841	139.7464	Type III waxy bitumen	n.d.
COA/000981	Eves Cove	21-Oct-16	3.7	-37.1841	139.7463	Type I waxy bitumen	n.d.
COA/000982	Eves Cove	21-Oct-16	2.6	-37.1841	139.7464	Type I waxy bitumen	n.d.
COA/000983	Eves Cove	21-Oct-16	1.4	-37.1842	139.7464	Type I waxy bitumen	n.d.

Sample ID	Survey Site	Collection Date	Weight (g)	Latitude	Longitude	Whole-oil classification	Biomarker Classification
COA/000984	Eves Cove	21-Oct-16	12.7	-37.1842	139.7465	Type I waxy bitumen	n.d.
COA/000985	Eves Cove	21-Oct-16	0.7	-37.1844	139.7467	Unknown	n.d.
COA/000986	Eves Cove	21-Oct-16	1.7	-37.1844	139.7467	Type I waxy bitumen	n.d.
COA/000987	Eves Cove	21-Oct-16	2.2	-37.1845	139.7468	Degraded high wax bitumen	n.d.
COA/000988A	Eves Cove	21-Oct-16	2.5	-37.1845	139.7468	Degraded high wax bitumen	n.d.
COA/000988B	Eves Cove	21-Oct-16	0.3	-37.1845	139.7468	Degraded high wax bitumen	n.d.
COA/000989	Eves Cove	21-Oct-16	1.6	-37.1845	139.7468	Type I waxy bitumen	n.d.
COA/000990	Eves Cove	21-Oct-16	3.1	-37.1846	139.7470	Degraded high wax bitumen	n.d.
COA/000991	Eves Cove	21-Oct-16	4.4	-37.1860	139.7484	Type I waxy bitumen	n.d.
COA/000992	Eves Cove	21-Oct-16	6.0	-37.1860	139.7484	Degraded high wax bitumen	n.d.
COA/000993	Eves Cove	21-Oct-16	0.7	-37.1860	139.7484	Degraded high wax bitumen	n.d.
COA/000994	Eves Cove	21-Oct-16	2.6	-37.1861	139.7484	Type I waxy bitumen	n.d.
COA/000995	Eves Cove	21-Oct-16	4.9	-37.1861	139.7485	Type I waxy bitumen	n.d.
COA/000996	Eves Cove	21-Oct-16	4.1	-37.1865	139.7489	Degraded high wax bitumen	n.d.
COA/000997	Eves Cove	21-Oct-16	1.6	-37.1865	139.7489	Type I waxy bitumen	n.d.
COA/000998	Eves Cove	21-Oct-16	1.7	-37.1866	139.7490	Type I waxy bitumen	n.d.
COA/000999	Eves Cove	21-Oct-16	6.1	-37.1867	139.7490	Type I waxy bitumen	n.d.
COA/001000	Eves Cove	21-Oct-16	4.2	-37.1867	139.7490	Type I waxy bitumen	n.d.
/001001	Eves Cove	21-Oct-16	4.2	-37.1867	139.7491	Type I waxy bitumen	n.d.
/001002	Eves Cove	21-Oct-16	10.4	-37.1867	139.7491	Type I waxy bitumen	n.d.
/001003	Eves Cove	21-Oct-16	4.3	-37.1867	139.7491	Type I waxy bitumen	n.d.
/001004	Eves Cove	21-Oct-16	2.3	-37.1867	139.7491	Type I waxy bitumen	n.d.
/001005	Eves Cove	21-Oct-16	0.6	-37.1868	139.7493	Type III waxy bitumen	n.d.
/001006	Eves Cove	21-Oct-16	8.4	-37.1868	139.7492	Type I waxy bitumen	n.d.
/001007	Eves Cove	21-Oct-16	2.2	-37.1868	139.7492	Type I waxy bitumen	n.d.
/001008	Eves Cove	21-Oct-16	7.0	-37.1868	139.7491	Type I waxy bitumen	n.d.
/001009	Eves Cove	21-Oct-16	3.1	-37.1869	139.7491	Type I waxy bitumen	n.d.
/001010	Eves Cove	21-Oct-16	2.6	-37.1869	139.7491	Type I waxy bitumen	n.d.
/001011	Eves Cove	21-Oct-16	11.8	-37.1869	139.7492	Type I waxy bitumen	n.d.
/001012	Beachport Conservation Park	21-Oct-16	1.6	-37.4412	139.9554	Type I waxy bitumen	n.d.
/001013	Beachport Conservation Park	21-Oct-16	1.6	-37.4412	139.9555	Type I waxy bitumen	n.d.
/001014	Beachport Conservation Park	21-Oct-16	2.3	-37.4411	139.9555	Type I waxy bitumen	n.d.
/001015	Beachport Conservation Park	21-Oct-16	2.7	-37.4412	139.9556	Type I waxy bitumen	n.d.
/001016	Beachport Conservation Park	21-Oct-16	1.2	-37.4417	139.9575	Type I waxy bitumen	n.d.
/001017	Beachport Conservation Park	21-Oct-16	1.9	-37.4417	139.9581	Type I waxy bitumen	n.d.
/001019	Beachport Conservation Park	21-Oct-16	5.7	-37.4418	139.9583	Type I waxy bitumen	n.d.
/001020	Beachport Conservation Park	21-Oct-16	1.2	-37.4418	139.9584	Type I waxy bitumen	n.d.
/001021	Beachport Conservation Park	21-Oct-16	7.3	-37.4419	139.9584	Type I waxy bitumen	Type I waxy bitumen
/001022	Beachport Conservation Park	21-Oct-16	16.1	-37.4419	139.9584	Type I waxy bitumen	n.d.
/001024	Beachport Conservation Park	21-Oct-16	1.2	-37.4424	139.9594	Type I waxy bitumen	n.d.
/001025A	Beachport Conservation Park	21-Oct-16	4.1	-37.4432	139.9604	Type I waxy bitumen	n.d.
/001025B	Beachport Conservation Park	21-Oct-16	2.5	-37.4432	139.9604	Type IV waxy bitumen	n.d.

Sample ID	Survey Site	Collection Date	Weight (g)	Latitude	Longitude	Whole-oil classification	Biomarker Classification
/001026	Beachport Conservation Park	21-Oct-16	1.5	-37.4434	139.9607	Degraded high wax bitumen	n.d.
/001027	Beachport Conservation Park	21-Oct-16	1.5	-37.4436	139.9610	Type I waxy bitumen	n.d.
/001028	Beachport Conservation Park	21-Oct-16	2.8	-37.4437	139.9611	Type I waxy bitumen	n.d.
/001029	Beachport Conservation Park	21-Oct-16	1.8	-37.4437	139.9612	Type I waxy bitumen	n.d.
/001030	Beachport Conservation Park	21-Oct-16	0.8	-37.4438	139.9612	Degraded high wax bitumen	n.d.
/001031	Beachport Conservation Park	21-Oct-16	1.5	-37.4445	139.9617	Type I waxy bitumen	n.d.
/001032	Beachport Conservation Park	21-Oct-16	2.1	-37.4448	139.9620	Type III waxy bitumen	Type IIIB waxy bitumen
/001033	Beachport Conservation Park	21-Oct-16	6.4	-37.4449	139.9621	Type I waxy bitumen	n.d.
/001034	Beachport Conservation Park	21-Oct-16	1.0	-37.4450	139.9621	Type I waxy bitumen	n.d.
/001035	Beachport Conservation Park	21-Oct-16	2.8	-37.4450	139.9621	Type I waxy bitumen	n.d.
/001036	Beachport Conservation Park	21-Oct-16	2.6	-37.4451	139.9622	Type I waxy bitumen	n.d.
/001037	Beachport Conservation Park	21-Oct-16	3.6	-37.4452	139.9622	Type I waxy bitumen	n.d.
/001038	Beachport Conservation Park	21-Oct-16	1.3	-37.4452	139.9622	Type I waxy bitumen	n.d.
/001039A	Beachport Conservation Park	21-Oct-16	1.0	-37.4452	139.9622	Type I waxy bitumen	n.d.
/001039B	Beachport Conservation Park	21-Oct-16	0.5	-37.4452	139.9622	Type I waxy bitumen	Type I waxy bitumen
/001040A	Beachport Conservation Park	21-Oct-16	1.1	-37.4453	139.9622	Type I waxy bitumen	n.d.
/001040B	Beachport Conservation Park	21-Oct-16	0.6	-37.4453	139.9622	Type I waxy bitumen	n.d.
/001041	Beachport Conservation Park	21-Oct-16	0.7	-37.4453	139.9623	Type I waxy bitumen	n.d.
/001042	Beachport Conservation Park	21-Oct-16	0.3	-37.4453	139.9623	Type I waxy bitumen	n.d.
/001043	Beachport Conservation Park	21-Oct-16	0.8	-37.4453	139.9623	Type I waxy bitumen	Type I waxy bitumen
/001044A	Beachport Conservation Park	21-Oct-16	0.3	-37.4454	139.9623	Type I waxy bitumen	n.d.
/001044B	Beachport Conservation Park	21-Oct-16	0.2	-37.4454	139.9623	Type III waxy bitumen	Type IIIB waxy bitumen
/001045	Beachport Conservation Park	21-Oct-16	0.6	-37.4455	139.9624	Type I waxy bitumen	n.d.
/001046	Beachport Conservation Park	21-Oct-16	2.9	-37.4455	139.9624	Type I waxy bitumen	n.d.
/001047	Beachport Conservation Park	21-Oct-16	2.3	-37.4459	139.9627	Type I waxy bitumen	n.d.
/001048	Beachport Conservation Park	21-Oct-16	1.1	-37.4459	139.9628	Type I waxy bitumen	n.d.
/001049	Beachport Conservation Park	21-Oct-16	1.3	-37.4460	139.9628	Degraded high wax bitumen	n.d.
/001050	Beachport Conservation Park	21-Oct-16	1.1	-37.4461	139.9629	Type I waxy bitumen	n.d.

Sample ID	Survey Site	Collection Date	Weight (g)	Latitude	Longitude	Whole-oil classification	Biomarker Classification
/001051	Beachport Conservation Park	21-Oct-16	0.8	-37.4463	139.9630	Type I waxy bitumen	n.d.
/001052	Geltwood Beach	22-Oct-16	14.7	-37.6586	140.2215	Type I waxy bitumen	n.d.
/001053	Geltwood Beach	22-Oct-16	3.8	-37.6603	140.2234	Type I waxy bitumen	n.d.
/001054	Geltwood Beach	22-Oct-16	0.7	-37.6603	140.2235	Type I waxy bitumen	n.d.
/001055	Number 1 and 2 Rocks	22-Oct-16	0.5	-37.7954	140.3204	Type III waxy bitumen	Type IIIA waxy bitumen
/001056	Number 1 and 2 Rocks	22-Oct-16	8.8	-37.7956	140.3205	Asphaltic Tar	Asphaltic Tar
/001057	Number 1 and 2 Rocks	22-Oct-16	1.3	-37.7956	140.3206	Type I waxy bitumen	n.d.
/001058	Number 1 and 2 Rocks	22-Oct-16	0.4	-37.7958	140.3206	Type III waxy bitumen	n.d.
/001059	Number 1 and 2 Rocks	22-Oct-16	132	-37.7959	140.3209	Asphaltic Tar	n.d.
/001060	Number 1 and 2 Rocks	22-Oct-16	0.6	-37.7959	140.3209	Type I waxy bitumen	n.d.
/001061	Number 1 and 2 Rocks	22-Oct-16	0.1	-37.7965	140.3217	Type I waxy bitumen	n.d.
/001062	Number 1 and 2 Rocks	22-Oct-16	1.7	-37.7976	140.3226	Degraded high wax bitumen	n.d.
/001063	Number 1 and 2 Rocks	22-Oct-16	52	-37.7977	140.3228	Asphaltic Tar	Asphaltic Tar
/001064A	Number 1 and 2 Rocks	22-Oct-16	1.1	-37.7980	140.3230	Unknown	n.d.
/001064B	Number 1 and 2 Rocks	22-Oct-16	0.5	-37.7980	140.3230	Type I waxy bitumen	n.d.
/001065	Number 1 and 2 Rocks	22-Oct-16	0.3	-37.7979	140.3230	Type I waxy bitumen	n.d.
/001067	Number 1 and 2 Rocks	22-Oct-16	26.6	-37.7980	140.3231	Asphaltic Tar	Asphaltic Tar
/001068	Number 1 and 2 Rocks	22-Oct-16	27.0	-37.7980	140.3231	Asphaltic Tar	Asphaltic Tar
/001069	Number 1 and 2 Rocks	22-Oct-16	1.5	-37.7980	140.3231	Type I waxy bitumen	n.d.
/001070	Number 1 and 2 Rocks	22-Oct-16	8.7	-37.7981	140.3231	Type I waxy bitumen	n.d.
/001071	Number 1 and 2 Rocks	22-Oct-16	2.8	-37.7981	140.3232	Type I waxy bitumen	n.d.
/001072A	Number 1 and 2 Rocks	22-Oct-16	1.0	-37.7981	140.3232	Type I waxy bitumen	n.d.
/001073	Number 1 and 2 Rocks	22-Oct-16	10.3	-37.7982	140.3232	Type I waxy bitumen	n.d.
/001074	Number 1 and 2 Rocks	22-Oct-16	0.6	-37.7983	140.3232	Type I waxy bitumen	n.d.
/001075	Number 1 and 2 Rocks	22-Oct-16	4.3	-37.7982	140.3233	Type I waxy bitumen	n.d.
/001076	Number 1 and 2 Rocks	22-Oct-16	2.9	-37.7982	140.3233	Asphaltic Tar	Asphaltic Tar
/001077	Number 1 and 2 Rocks	22-Oct-16	0.4	-37.7982	140.3233	Type I waxy bitumen	n.d.
/001079	Number 1 and 2 Rocks	22-Oct-16	196	-37.7985	140.3235	Asphaltic Tar	Asphaltic Tar
/001080	Number 1 and 2 Rocks	22-Oct-16	1.0	-37.7986	140.3236	Type I waxy bitumen	n.d.
/001081	Number 1 and 2 Rocks	22-Oct-16	16.9	-37.7986	140.3236	Asphaltic Tar	Asphaltic Tar
/001082	Number 1 and 2 Rocks	22-Oct-16	21.5	-37.7962	140.3217	Type III waxy bitumen	n.d.
/001083	Number 1 and 2 Rocks	22-Oct-16	10.0	-37.7962	140.3217	Type I waxy bitumen	n.d.
/001084	Number 1 and 2 Rocks	22-Oct-16	1.3	-37.7962	140.3217	Type I waxy bitumen	n.d.
/001085	Nene Valley	22-Oct-16	6.7	-37.9860	140.5118	Type I waxy bitumen	n.d.

n.d. = Not determined.
N.R. = GPS co-ordinates were not recorded.

Table S3: Details of all crude oil samples donated from private collections. All samples were collected between 2014–2016.

Sample ID	Survey Site	Collection Date	Sample weight (g)	Latitude	Longitude	Whole-oil classification	Biomarker Classification
W13/007516	The Granites	23-Nov-14	169.6639	N.R.	N.R.	Asphaltite	Asphaltite
W13/007566	Unnamed Beach on Kangaroo Island	Easter 2015	180	-36.0179	137.1024	Asphaltite	Asphaltite
W13/007657	Elliston	20-Sep-15	11.2	-34.6439	134.88651	Type I waxy bitumen	n.d.
W13/007672	Avoid Bay	31-May-15	1357.1	-34.66	135.49	Asphaltite	Asphaltite
W13/007673	Avoid Bay	13-Jul-14	8.3	-34.644	135.348	Type III waxy bitumen	n.d.
W13/007674	Avoid Bay	13-Jul-14	10.2	-34.644	135.348	Type III waxy bitumen	n.d.
W13/007675	Avoid Bay	13-Jul-14	9.5	-34.644	135.348	Type I waxy bitumen	n.d.
W13/007676	Avoid Bay	13-Jul-14	34.2	-34.644	135.348	Type I waxy bitumen	n.d.
W13/007677	Avoid Bay	13-Jul-14	26	-34.644	135.348	Type III waxy bitumen	n.d.
W13/007678	Avoid Bay	13-Jul-14	12	-34.644	135.348	Type III waxy bitumen	n.d.
W13/007679	Avoid Bay	13-Jul-14	24.2	-34.644	135.348	Type III waxy bitumen	n.d.
W13/007680	Avoid Bay	13-Jul-14	17	-34.644	135.348	Type III waxy bitumen	n.d.
W13/007681	Avoid Bay	13-Jul-14	9.2	-34.644	135.348	Type I waxy bitumen	n.d.
W13/007682	Avoid Bay	13-Jul-14	11.9	-34.644	135.348	Type III waxy bitumen	n.d.
W13/007683	Avoid Bay	13-Jul-14	9.7	-34.644	135.348	Type III waxy bitumen	Type IIIA waxy bitumen
W13/007684	Avoid Bay	13-Jul-14	4.7	-34.644	135.348	Type III waxy bitumen	Type IIIA waxy bitumen
W13/007685	Avoid Bay	13-Jul-14	4.1	-34.644	135.348	Type III waxy bitumen	n.d.
W13/007686	Avoid Bay	13-Jul-14	6.7	-34.644	135.348	Type I waxy bitumen	n.d.
W13/007687	Avoid Bay	13-Jul-14	4.8	-34.644	135.348	Type III waxy bitumen	n.d.
W13/007688	Avoid Bay	13-Jul-14	3.9	-34.644	135.348	Type I waxy bitumen	n.d.
W13/007689	Avoid Bay	13-Jul-14	3.6	-34.644	135.348	Type III waxy bitumen	n.d.
W13/007690	Avoid Bay	13-Jul-14	5.8	-34.644	135.348	Type III waxy bitumen	n.d.
W13/007691	Avoid Bay	13-Jul-14	5	-34.644	135.348	Type III waxy bitumen	n.d.
W13/007692	Avoid Bay	13-Jul-14	6.1	-34.644	135.348	Type III waxy bitumen	Type IIIA waxy bitumen
W13/007693	Avoid Bay	13-Jul-14	4.8	-34.644	135.348	Type III waxy bitumen	n.d.
W13/007694	Avoid Bay	13-Jul-14	8	-34.644	135.348	Type III waxy bitumen	n.d.
W13/007695	Avoid Bay	13-Jul-14	4	-34.644	135.348	Type III waxy bitumen	Type IIIC waxy bitumen
W13/007696	Avoid Bay	13-Jul-14	3.6	-34.644	135.348	Type III waxy bitumen	n.d.
W13/007697	Avoid Bay	13-Jul-14	34.6	-34.644	135.348	Type III waxy bitumen	Type IIIC waxy bitumen
W13/007698	Avoid Bay	13-Jul-14	6.7	-34.644	135.348	Type III waxy bitumen	Type IIIA waxy bitumen
W13/007699	Avoid Bay	13-Jul-14	9	-34.644	135.348	Type I waxy bitumen	Type I waxy bitumen
W13/007700	Avoid Bay	13-Jul-14	5.4	-34.644	135.348	Type III waxy bitumen	Type IIIC waxy bitumen
W13/007701	Avoid Bay	13-Jul-14	3.8	-34.644	135.348	Type III waxy bitumen	n.d.
W13/007702	Avoid Bay	13-Jul-14	4	-34.644	135.348	Type I waxy bitumen	n.d.
W13/007703	Avoid Bay	13-Jul-14	3.6	-34.644	135.348	Type III waxy bitumen	n.d.
W13/007704	Avoid Bay	13-Jul-14	4.9	-34.644	135.348	Type I waxy bitumen	n.d.
W13/007705	Avoid Bay	13-Jul-14	4.8	-34.644	135.348	Type I waxy bitumen	n.d.
W13/007706	Avoid Bay	13-Jul-14	3	-34.644	135.348	Type I waxy bitumen	n.d.
W13/007707	Avoid Bay	13-Jul-14	3.1	-34.644	135.348	Type III waxy bitumen	n.d.
W13/007708	Avoid Bay	13-Jul-14	3.2	-34.644	135.348	Type I waxy bitumen	n.d.
W13/007709	Avoid Bay	13-Jul-14	1.8	-34.644	135.348	Type I waxy bitumen	n.d.

Sample ID	Survey Site	Collection Date	Sample weight (g)	Latitude	Longitude	Whole-oil classification	Biomarker Classification
W13/007710	Avoid Bay	13-Jul-14	3.2	-34.644	135.348	Unknown/other	n.d.
W13/007711	Avoid Bay	13-Jul-14	1.7	-34.644	135.348	Type I waxy bitumen	n.d.
W13/007712	Avoid Bay	13-Jul-14	0.7	-34.644	135.348	Type IV waxy bitumen	Type IVE waxy bitumen
W13/007713	Avoid Bay	13-Jul-14	3	-34.644	135.348	Type III waxy bitumen	n.d.
W13/007714	Avoid Bay	13-Jul-14	1.8	-34.644	135.348	Type III waxy bitumen	n.d.
W13/007715	Avoid Bay	13-Jul-14	1.2	-34.644	135.348	Unknown/other	n.d.
W13/007716	Avoid Bay	13-Jul-14	1	-34.644	135.348	Type I waxy bitumen	n.d.
W13/007717	Avoid Bay	13-Jul-14	1.3	-34.644	135.348	Type I waxy bitumen	n.d.
W13/007718	Avoid Bay	13-Jul-14	2.7	-34.644	135.348	Type III waxy bitumen	n.d.
W13/007719	Avoid Bay	13-Jul-14	1.1	-34.644	135.348	Type III waxy bitumen	n.d.
W13/007720	Avoid Bay	13-Jul-14	1.8	-34.644	135.348	Type III waxy bitumen	n.d.
W13/007721	Avoid Bay	13-Jul-14	0.6	-34.644	135.348	Type I waxy bitumen	Type I waxy bitumen
W13/007722	Avoid Bay	13-Jul-14	0.4	-34.644	135.348	Unknown/other	n.d.
W13/007723	Avoid Bay	13-Jul-14	0.8	-34.644	135.348	Type III waxy bitumen	n.d.
W13/007724	Avoid Bay	13-Jul-14	0.3	-34.644	135.348	Type I waxy bitumen	n.d.
W13/007725	Avoid Bay	13-Jul-14	2.1	-34.644	135.348	Type I waxy bitumen	n.d.
W13/007726	Avoid Bay	13-Jul-14	1.4	-34.644	135.348	Type I waxy bitumen	n.d.
W13/007727	Avoid Bay	13-Jul-14	2	-34.644	135.348	Type I waxy bitumen	n.d.
W13/007728	Avoid Bay	13-Jul-14	1	-34.644	135.348	Degraded high wax bitumen	n.d.
W13/007729	Avoid Bay	13-Jul-14	1.7	-34.644	135.348	Unknown	n.d.
W13/007730	Avoid Bay	13-Jul-14	0.7	-34.644	135.348	Type III waxy bitumen	n.d.
W13/007731	Avoid Bay	13-Jul-14	1	-34.644	135.348	Type I waxy bitumen	n.d.
W13/007732	Avoid Bay	13-Jul-14	0.7	-34.644	135.348	Type I waxy bitumen	n.d.
W13/007733	Avoid Bay	13-Jul-14	1.3	-34.644	135.348	Type I waxy bitumen	n.d.
W13/007734	Avoid Bay	13-Jul-14	0.6	-34.644	135.348	Type III waxy bitumen	n.d.
W13/007735	Avoid Bay	13-Jul-14	1.9	-34.644	135.348	Type III waxy bitumen	n.d.
W13/007736	Avoid Bay	13-Jul-14	2.4	-34.644	135.348	Degraded high wax bitumen	Type IVD waxy bitumen
W13/007737	Avoid Bay	13-Jul-14	2.8	-34.644	135.348	Type I waxy bitumen	Type I waxy bitumen
W13/007738	Avoid Bay	13-Jul-14	0.8	-34.644	135.348	Unknown/other	n.d.
W13/007739	Avoid Bay	13-Jul-14	2	-34.644	135.348	Type I waxy bitumen	n.d.
W13/007740	Avoid Bay	13-Jul-14	2.7	-34.644	135.348	Type III waxy bitumen	n.d.
W13/007741	Avoid Bay	13-Jul-14	0.8	-34.644	135.348	Type III waxy bitumen	n.d.
W13/007742	Greenly Beach	22-Aug-15	392	-34.462	135.358	Asphaltite	Asphaltite
W13/007743	Avoid Bay	22-Aug-15	1.1	-34.384	135.365	Type III waxy bitumen	n.d.
W13/007744	Avoid Bay	22-Aug-15	1.7	-34.384	135.365	Type III waxy bitumen	n.d.
W13/007745	Avoid Bay	22-Aug-15	28	-34.384	135.365	PAH (Unknown)	n.d.
W13/007768A	Avoid Bay	31-May-15	154.4	-34.66	135.49	Type I waxy bitumen	n.d.
W13/007768B	Avoid Bay	31-May-15	83.6	-34.66	135.49	Type IV waxy bitumen	n.d.
W13/007768C	Avoid Bay	31-May-15	31.2	-34.66	135.49	PAH (Unknown)	n.d.
2016 samples:							
W13/007876	Greenly Beach	N.R.	13.6576	N.R.	N.R.	Type III waxy bitumen	n.d.
W13/007877	Greenly Beach	N.R.	23.93225	N.R.	N.R.	Type III waxy bitumen	Type IIIA waxy bitumen
W13/007878	Greenly Beach	N.R.	4.65619	N.R.	N.R.	Type III waxy bitumen	Type IIIA waxy bitumen
W13/007879	Greenly Beach	N.R.	5.71246	N.R.	N.R.	Type III waxy bitumen	n.d.
W13/007880	Greenly Beach	N.R.	1.33622	N.R.	N.R.	Type III waxy bitumen	n.d.

Sample ID	Survey Site	Collection Date	Sample weight (g)	Latitude	Longitude	Whole-oil classification	Biomarker Classification
W13/007881	Greenly Beach	N.R.	4.6015	N.R.	N.R.	Type IV waxy bitumen	Type IVE waxy bitumen
W13/007882	Sleaford Bay	N.R.	96.0363	N.R.	N.R.	Unknown	n.d.
W13/007883	Sleaford Bay	N.R.	14.04316	N.R.	N.R.	Type III waxy bitumen	n.d.
W13/007884	Sleaford Bay	N.R.	22.08063	N.R.	N.R.	Degraded high wax bitumen	n.d.
W13/007885	Sleaford Bay	N.R.	7.63894	N.R.	N.R.	Type I waxy bitumen	n.d.
W13/007886	Sleaford Bay	N.R.	10.31384	N.R.	N.R.	Type III waxy bitumen	n.d.
W13/007887	Sleaford Bay	N.R.	14.52705	N.R.	N.R.	Type I waxy bitumen	Type I waxy bitumen
W13/007888	Sleaford Bay	N.R.	2.98093	N.R.	N.R.	Type I waxy bitumen	n.d.
W13/007889	Sleaford Bay	N.R.	2.10492	N.R.	N.R.	Type I waxy bitumen	n.d.
W13/007890	Sleaford Bay	N.R.	1.29782	N.R.	N.R.	Unknown	n.d.
W13/007891	Sleaford Bay	N.R.	3.65363	N.R.	N.R.	Type IV waxy bitumen	Type IVB waxy bitumen
W13/007892	Sleaford Bay	N.R.	1.32991	N.R.	N.R.	Type I waxy bitumen	n.d.
W13/007893	Sleaford Bay	N.R.	1.33209	N.R.	N.R.	Unknown	n.d.
W13/007894	Avoid Bay	N.R.	100.8504	N.R.	N.R.	PAH	n.d.
W13/007895	Avoid Bay	N.R.	120.2403	N.R.	N.R.	Type III waxy bitumen	Type IIIB waxy bitumen
W13/007896	Avoid Bay	N.R.	19.86261	N.R.	N.R.	Type III waxy bitumen	n.d.
W13/007897	Avoid Bay	N.R.	6.6111	N.R.	N.R.	Type III waxy bitumen	n.d.
W13/007898	Avoid Bay	N.R.	9.12093	N.R.	N.R.	Type I waxy bitumen	n.d.
W13/007899	Avoid Bay	N.R.	5.47266	N.R.	N.R.	Type III waxy bitumen	n.d.
W13/007900	Avoid Bay	N.R.	5.56357	N.R.	N.R.	Type III waxy bitumen	Type IIIA waxy bitumen
W13/007901	Avoid Bay	N.R.	13.31812	N.R.	N.R.	Type III waxy bitumen	n.d.
W13/007902	Avoid Bay	N.R.	9.45986	N.R.	N.R.	Type III waxy bitumen	Type IIIA waxy bitumen
W13/007903	Avoid Bay	N.R.	4.39969	N.R.	N.R.	Type I waxy bitumen	n.d.
W13/007904	Avoid Bay	N.R.	6.37354	N.R.	N.R.	Type III waxy bitumen	n.d.
W13/007905	Avoid Bay	N.R.	2.63177	N.R.	N.R.	Type III waxy bitumen	n.d.
W13/007906	Avoid Bay	N.R.	7.04158	N.R.	N.R.	Type I waxy bitumen	n.d.
W13/007907	Avoid Bay	N.R.	5.30119	N.R.	N.R.	Type I waxy bitumen	n.d.
W13/007908	Avoid Bay	N.R.	3.73999	N.R.	N.R.	Type III waxy bitumen	n.d.
W13/007909	Avoid Bay	N.R.	5.05494	N.R.	N.R.	Type IV waxy bitumen	Type IVB waxy bitumen
W13/007910	Avoid Bay	N.R.	4.64371	N.R.	N.R.	Type III waxy bitumen	Type IIID waxy bitumen
W13/007911	Avoid Bay	N.R.	6.13425	N.R.	N.R.	Type IV waxy bitumen	n.d.
W13/007912	Avoid Bay	N.R.	5.55696	N.R.	N.R.	Type I waxy bitumen	n.d.
W13/007913	Avoid Bay	N.R.	2.58272	N.R.	N.R.	Not bitumen (false sample)	n.d.
W13/007914	Avoid Bay	N.R.	2.40648	N.R.	N.R.	Type III waxy bitumen	n.d.
W13/007915	Avoid Bay	N.R.	3.84604	N.R.	N.R.	Type III waxy bitumen	n.d.
W13/007916	Avoid Bay	N.R.	2.16323	N.R.	N.R.	Type I waxy bitumen	n.d.
W13/007917	Avoid Bay	N.R.	2.22084	N.R.	N.R.	Unknown	n.d.
W13/007918	Avoid Bay	N.R.	1.15803	N.R.	N.R.	Degraded high wax bitumen	n.d.
W13/007919	Avoid Bay	N.R.	1.56032	N.R.	N.R.	Type III waxy bitumen	n.d.
W13/007920	Avoid Bay	N.R.	0.95987	N.R.	N.R.	Type III waxy bitumen	Type IIIC waxy bitumen
W13/007921	West Bay	N.R.	7.16484	N.R.	N.R.	Unknown/other (Sooty bitumen?)	n.d.

n.d. = Not determined
N.R. = Not recorded.

4. Supplementary geochemical data

4.1. Biomarker degradation in type I waxy bitumen

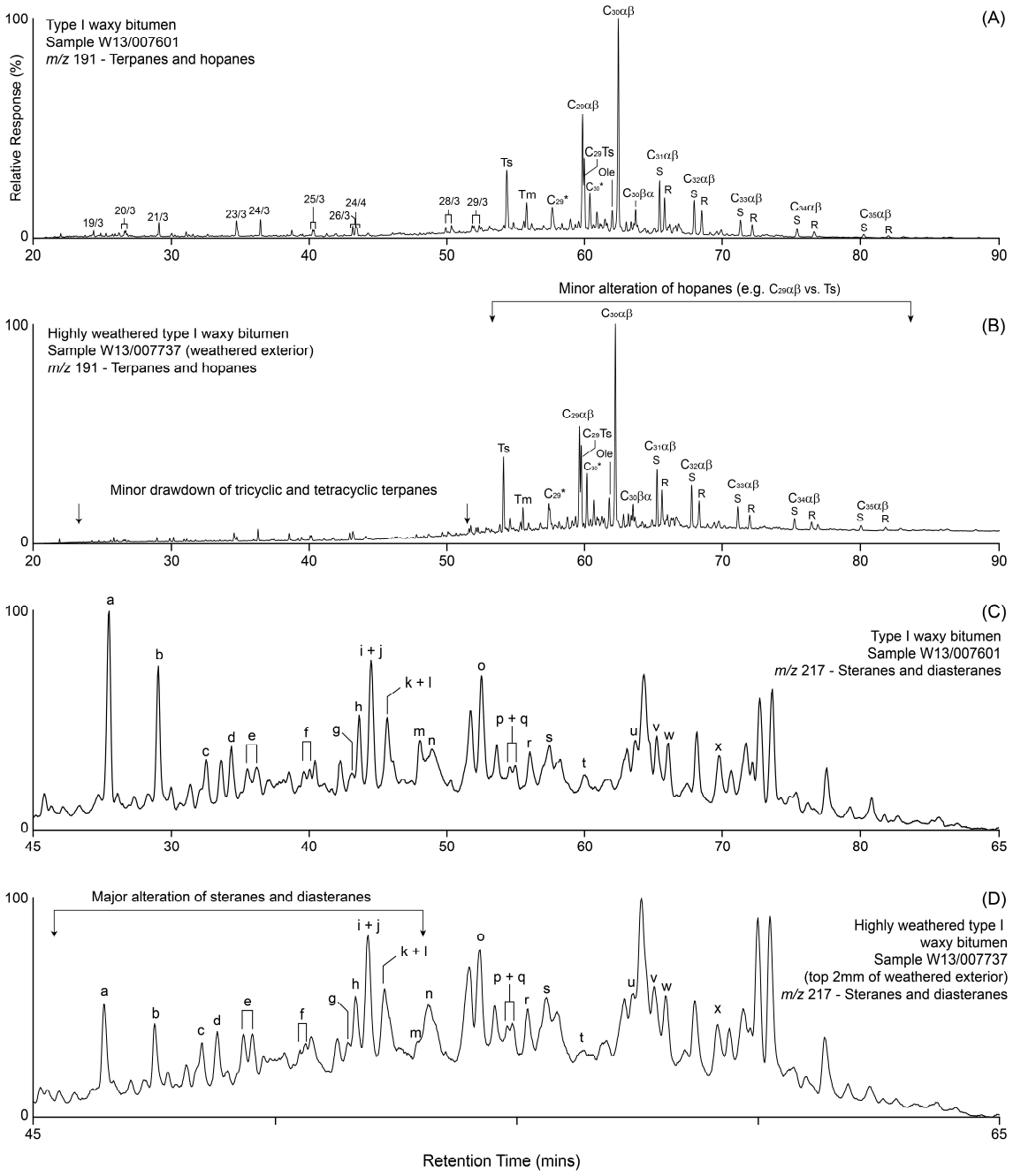


Figure S1: Comparison of fresh and highly weathered type I waxy bitumens. (A) Sterane and diasterane distribution in the least weathered type I waxy bitumen sample W13/007601. (B) Altered distribution of steranes and diasteranes in highly weathered asphaltite sample W13/007737 (weathered sample exterior). (C) Unaltered terpane and hopane distribution in the least weathered type I waxy bitumen sample. (D) Altered terpane and hopane distribution in the highly weathered type I waxy bitumen (weathered sample exterior).

4.2. Asphaltites

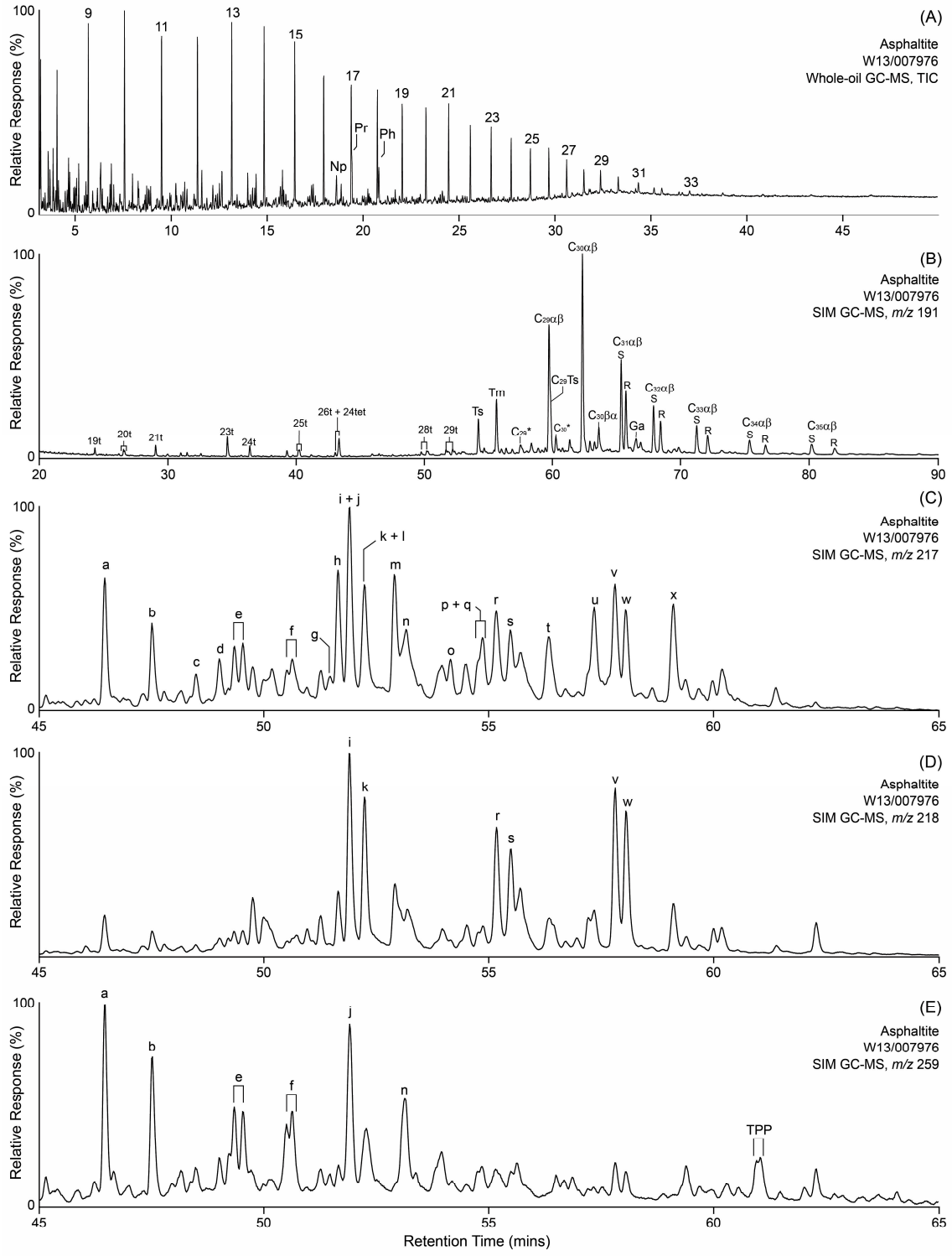


Figure S2: Representative chromatograms from the least weathered collected asphaltite (sample W13/007976). (A) Whole-oil GC-MS total ion chromatogram. (B) Saturated fraction SIM GC-MS *m/z* 191 chromatogram. (C) Saturated fraction SIM GC-MS *m/z* 217 chromatogram. (D) Saturated fraction SIM GC-MS *m/z* 218 chromatogram. (E) Saturated fraction SIM GC-MS *m/z* 259 chromatogram.

Table S4: Selected biomarker parameters from analysed asphaltites, int = sample interior, ext = sample exterior (top 2mm).

Sample ID	C19t/ C23t	C22t/ C21t	C22t/ C24t	C24t/ C23t	C26t/ C25t	C24tet /C23t	C23t/ C30 αβ	C24tet/ C30 αβ	C28BNH /C30 αβ	25-Nor/ C30 αβ	C29 αβ /C30 αβ	C30*/ C30 αβ	Ole/ C30 αβ	C30Ts/ C30 αβ	Gam/ C30 αβ	Gam/ C31 αβ (R)	C35 αβ/ C34 αβ	C35 Homohopane Index	Ts/ (Ts+Tm)	C29Ts/ (C29Ts +C29 αβ)
W13/007472 (ext)	0.24	0.32	0.28	0.56	0.89	0.72	0.08	0.06	0.03	0.02	0.63	0.08	n.d.	0.04	0.07	0.23	0.92	8	0.39	0.20
W13/007472 (int)	0.29	0.37	0.31	0.54	0.95	0.72	0.06	0.04	0.05	0.02	0.64	0.08	n.d.	0.04	0.06	0.17	0.95	9	0.40	0.18
W13/007475 (ext)	0.30	0.35	0.30	0.55	1.19	1.06	0.07	0.07	0.05	0.03	0.65	0.09	n.d.	0.03	0.07	0.20	0.90	8	0.41	0.17
W13/007476 (ext)	0.30	0.36	0.30	0.57	1.06	1.16	0.06	0.07	0.05	0.03	0.62	0.08	n.d.	0.02	0.07	0.22	0.88	8	0.41	0.19
W13/007476 (int)	0.22	0.38	0.29	0.55	0.81	0.95	0.06	0.06	0.04	0.03	0.60	0.09	n.d.	0.04	0.07	0.19	0.90	8	0.41	0.20
W13/007477 (ext)	0.15	0.38	0.27	0.56	1.05	0.95	0.07	0.06	0.04	0.03	0.64	0.09	n.d.	0.04	0.07	0.21	0.86	8	0.40	0.19
W13/007477 (int)	0.18	0.36	0.28	0.54	0.85	0.94	0.06	0.06	0.04	0.03	0.59	0.09	n.d.	0.04	0.05	0.13	0.90	7	0.40	0.20
W13/007488 (ext)	0.29	0.37	0.31	0.56	0.89	0.88	0.07	0.06	0.05	0.03	0.63	0.09	n.d.	0.02	0.06	0.19	0.93	9	0.40	0.20
W13/007488 (int)	0.29	0.33	0.28	0.55	0.79	0.99	0.07	0.07	0.04	0.03	0.64	0.08	n.d.	0.04	0.07	0.20	0.92	9	0.39	0.17
W13/007493 (ext)	0.41	0.30	0.29	0.64	0.79	1.37	0.04	0.06	0.07	0.03	0.68	0.06	n.d.	0.04	0.09	0.28	0.85	8	0.35	0.17
W13/007493 (int)	0.37	0.30	0.28	0.65	0.90	1.26	0.04	0.05	0.08	0.03	0.69	0.06	n.d.	0.03	0.06	0.19	0.91	8	0.35	0.16
W13/007507 (ext)	0.08	0.37	0.28	0.37	1.00	0.40	0.13	0.05	0.05	0.02	0.67	0.07	n.d.	0.01	0.05	0.16	0.84	7	0.43	0.20
W13/007507 (int)	0.29	0.35	0.29	0.55	0.68	0.85	0.08	0.07	0.01	0.03	0.65	0.08	n.d.	0.04	0.07	0.22	0.79	7	0.40	0.18

Sample ID	% C27 ααα 20R	% C28 ααα 20R	% C29 ααα 20R	C27 Dia/ (Dia+Reg)	(C21+C22)/ (C27+C28 +C29)	C27 Dia /Ster	% C27 αββ 20(R+S)	% C28 αββ 20(R+S)	% C29 αββ 20(R+S)	C29/C27 αββ Sterane Ratio	Tricyclic Terpanes/ Hopanes	Steranes/ Terpanes	% Tricyclic Terpanes	% Pentacyclic Terpanes	% Steranes	Steranes/ hopanes
W13/007472 (ext)	42	24	34	0.41	0.09	0.40	36	24	40	1.10	0.13	0.29	9	69	22	0.33
W13/007472 (int)	40	23	36	0.44	0.11	0.43	37	25	37	1.00	0.07	0.25	6	74	20	0.27
W13/007475 (ext)	38	23	39	0.43	0.09	0.42	38	26	37	0.96	0.10	0.25	7	73	20	0.28
W13/007476 (ext)	36	25	39	0.44	0.08	0.43	37	26	37	1.01	0.09	0.25	7	73	20	0.27
W13/007476 (int)	43	20	38	0.42	0.09	0.41	38	25	37	0.99	0.09	0.25	6	74	20	0.27
W13/007477 (ext)	42	20	38	0.42	0.08	0.42	38	25	37	0.97	0.09	0.28	6	71	22	0.31
W13/007477 (int)	47	18	36	0.44	0.10	0.45	38	24	37	0.97	0.08	0.25	6	74	20	0.27
W13/007488 (ext)	37	25	38	0.45	0.10	0.44	38	26	36	0.95	0.10	0.27	7	71	22	0.30
W13/007488 (int)	43	20	37	0.43	0.10	0.43	38	25	37	0.97	0.09	0.28	6	72	22	0.30
W13/007493 (ext)	47	18	35	0.33	0.07	0.35	38	24	38	0.99	0.07	0.27	5	73	21	0.29
W13/007493 (int)	44	19	36	0.34	0.06	0.36	37	25	38	1.01	0.07	0.28	5	73	22	0.30
W13/007507 (ext)	36	28	35	0.46	0.09	0.49	39	24	37	0.95	0.12	0.31	8	68	24	0.34
W13/007507 (int)	40	27	33	0.43	0.14	0.45	39	25	36	0.93	0.11	0.30	8	69	23	0.34

Table S4 (continued).

Sample ID	C19t/ C23t	C22t/ C21t	C22t/ C24t	C24t/ C23t	C26t/ C25t	C24tet /C23t	C23t/ C30 αβ	C24tet/ C30 αβ	C28BNH /C30 αβ	25-Nor/ C30 αβ	C29 αβ /C30 αβ	C30*/ C30 αβ	Ole/ C30 αβ	C30Ts/ C30 αβ	Gam/ C30 αβ	Gam/ C31 αβ (R)	C35 αβ/ C34 αβ	C35 Homohopane Index	Ts/ (Ts+Tm)	C29Ts/ (C29Ts +C29 αβ)
W13/007516 (ext)	0.28	0.36	0.30	0.55	1.01	1.00	0.07	0.07	0.04	0.03	0.67	0.09	n.d.	0.04	0.08	0.23	0.83	8	0.41	0.20
W13/007516 (int)	0.28	0.34	0.28	0.56	0.85	1.10	0.07	0.07	0.04	0.03	0.66	0.08	n.d.	0.04	0.08	0.25	0.91	8	0.38	0.17
W13/007566 (ext)	0.61	0.48	0.31	0.80	0.82	1.44	0.01	0.02	0.04	0.03	0.66	0.08	n.d.	0.04	0.09	0.27	0.84	7	0.40	0.18
W13/007566 (int)	0.33	0.35	0.31	0.55	1.02	0.87	0.07	0.06	0.04	0.03	0.66	0.09	n.d.	0.04	0.09	0.26	0.85	8	0.41	0.18
W13/007659 (ext)	0.16	0.47	0.32	0.38	1.97	1.29	0.02	0.02	0.01	0.01	0.95	0.02	n.d.	0.14	0.08	0.20	0.95	9	0.36	0.10
W13/007659 (int)	0.26	0.43	0.33	0.27	1.37	2.36	0.01	0.02	0.02	0.01	1.03	0.02	n.d.	0.15	0.08	0.20	1.04	10	0.32	0.07
W13/007660 (ext)	0.33	0.43	0.33	0.34	1.37	3.32	0.01	0.02	0.02	0.01	1.04	0.01	n.d.	0.16	0.09	0.21	1.00	9	0.33	0.06
W13/007660 (int)	0.06	0.67	0.38	0.19	1.87	1.58	0.01	0.02	0.02	0.01	1.00	0.02	n.d.	0.13	0.10	0.23	1.00	9	0.32	0.06
W13/007661 (ext)	0.16	0.31	0.23	0.46	0.78	0.76	0.10	0.08	0.05	0.02	0.70	0.06	n.d.	0.01	0.06	0.20	0.83	7	0.37	0.16
W13/007661 (int)	0.19	0.36	0.25	0.53	0.80	0.82	0.08	0.07	0.04	0.02	0.64	0.07	n.d.	0.01	0.05	0.17	0.79	7	0.39	0.14
W13/007662 (ext)	0.30	0.43	0.33	0.42	1.86	2.58	0.01	0.02	0.02	0.01	0.96	0.02	n.d.	0.16	0.09	0.21	1.01	10	0.32	0.05
W13/007662 (int)	0.19	0.40	0.32	0.74	1.43	1.26	0.02	0.02	0.01	0.02	0.92	0.04	n.d.	0.12	0.08	0.22	1.00	10	0.43	0.15
W13/007663 (ext)	0.28	0.44	0.34	0.44	1.48	2.98	0.01	0.02	0.02	0.01	0.95	0.02	n.d.	0.15	0.09	0.19	0.98	9	0.32	0.07

Sample ID	% C27 ααα 20R	% C28 ααα 20R	% C29 ααα 20R	C27 Dia/ (Dia+Reg)	(C21+C22)/ (C27+C28 +C29)	C27 Dia /Ster	% C27 αββ 20(R+S)	% C28 αββ 20(R+S)	% C29 αββ 20(R+S)	C29/C27 αββ Sterane Ratio	Tricyclic Terpanes/ Hopanes	Steranes/ Terpanes	% Tricyclic Terpanes	% Pentacyclic Terpanes	% Steranes	Steranes/ hopanes
W13/007516 (ext)	37	25	38	0.44	0.10	0.43	38	26	36	0.95	0.10	0.26	7	72	21	0.29
W13/007516 (int)	44	19	37	0.42	0.10	0.41	38	25	37	0.96	0.09	0.28	7	72	22	0.30
W13/007566 (ext)	13	25	62	0.30	0.06	0.19	14	31	55	3.95	0.03	0.17	2	83	15	0.18
W13/007566 (int)	38	25	38	0.44	0.11	0.42	38	26	36	0.93	0.10	0.28	7	71	22	0.30
W13/007659 (ext)	30	24	46	0.26	0.03	0.20	23	21	56	2.49	0.02	0.06	2	92	6	0.06
W13/007659 (int)	23	21	56	0.18	0.01	0.13	21	20	59	2.86	0.01	0.06	1	93	5	0.06
W13/007660 (ext)	29	24	47	0.18	0.02	0.13	20	22	57	2.84	0.01	0.06	1	93	5	0.06
W13/007660 (int)	29	22	49	0.17	0.01	0.12	22	16	62	2.81	0.01	0.06	1	93	5	0.06
W13/007661 (ext)	43	26	31	0.45	0.15	0.48	41	23	36	0.88	0.12	0.33	8	67	25	0.36
W13/007661 (int)	45	24	31	0.45	0.14	0.47	41	24	35	0.87	0.11	0.32	7	68	24	0.36
W13/007662 (ext)	31	22	47	0.23	0.02	0.17	23	21	56	2.49	0.02	0.06	1	93	6	0.06
W13/007662 (int)	28	23	49	0.34	0.02	0.28	24	21	54	2.24	0.03	0.06	3	91	6	0.06
W13/007663 (ext)	25	23	51	0.18	0.01	0.12	22	22	56	2.50	0.01	0.06	1	93	6	0.06

Table S4 (continued).

Sample ID	C19t/ C23t	C22t/ C21t	C22t/ C24t	C24t/ C23t	C26t/ C25t	C24tet /C23t	C23t/ C30 αβ	C24tet/ C30 αβ	C28BNH /C30 αβ	25-Nor/ C30 αβ	C29 αβ /C30 αβ	C30*/ C30 αβ	Ole/ C30 αβ	C30Ts/ C30 αβ	Gam/ C30 αβ	Gam/ C31 αβ (R)	C35 αβ/ C34 αβ	C35 Homohopane Index	Ts/ (Ts+Tm)	C29Ts/ (C29Ts +C29 αβ)
W13/007663 (int)	0.24	0.48	0.37	0.28	1.37	2.59	0.01	0.02	0.02	0.01	0.99	0.02	n.d.	0.15	0.10	0.21	1.08	10	0.32	0.08
W13/007664 (ext)	0.29	0.45	0.35	0.40	1.14	3.61	0.00	0.02	0.02	0.01	1.04	0.02	n.d.	0.15	0.12	0.26	1.01	10	0.32	0.06
W13/007664 (int)	0.19	0.45	0.33	0.32	1.27	2.69	0.00	0.01	0.02	0.01	1.01	0.01	n.d.	0.14	0.10	0.23	1.03	10	0.33	0.06
W13/007665 (ext)	0.01	0.47	0.07	0.69	0.83	1.95	0.06	0.12	0.03	0.04	0.88	0.02	n.d.	0.09	0.06	0.17	0.90	8	0.41	0.09
W13/007665 (int)	0.01	0.47	0.08	0.67	1.03	1.56	0.04	0.07	0.03	0.04	0.87	0.03	n.d.	0.09	0.06	0.18	0.93	8	0.45	0.12
W13/007666 (ext)	0.21	0.47	0.24	0.35	1.30	2.40	0.01	0.02	0.02	0.01	1.02	0.02	n.d.	0.15	0.10	0.23	1.01	10	0.33	0.09
W13/007666 (int)	0.20	0.44	0.28	0.34	1.44	2.96	0.01	0.02	0.02	0.01	0.99	0.02	n.d.	0.15	0.10	0.22	1.02	11	0.32	0.08
W13/007667 (ext)	0.04	0.57	0.39	0.19	1.25	1.82	0.01	0.01	0.01	0.01	0.97	0.01	n.d.	0.16	0.11	0.22	1.03	11	0.32	0.08
W13/007667 (int)	0.13	0.48	0.38	0.21	1.05	2.34	0.01	0.02	0.02	0.01	1.00	0.02	n.d.	0.15	0.09	0.22	1.04	10	0.32	0.09
W13/007668 (ext)	0.23	0.35	0.28	0.52	0.76	0.77	0.09	0.07	0.05	0.03	0.69	0.08	n.d.	0.01	0.06	0.17	0.84	8	0.39	0.16
W13/007668 (int)	0.21	0.34	0.29	0.52	0.83	0.86	0.07	0.06	0.04	0.02	0.67	0.06	n.d.	0.02	0.06	0.20	0.90	8	0.38	0.16
W13/007671 (ext)	0.29	0.38	0.31	0.55	1.06	0.90	0.07	0.06	0.04	0.03	0.67	0.09	n.d.	0.04	0.09	0.26	0.86	8	0.40	0.19
W13/007671 (int)	0.26	0.42	0.31	0.59	0.86	0.90	0.06	0.06	0.04	0.03	0.65	0.09	n.d.	0.03	0.07	0.23	0.90	8	0.41	0.19

Sample ID	% C27 ααα 20R	% C28 ααα 20R	% C29 ααα 20R	C27 Dia/ (Dia+Reg)	(C21+C22)/ (C27+C28 +C29)	C27 Dia /Ster	% C27 αββ 20(R+S)	% C28 αββ 20(R+S)	% C29 αββ 20(R+S)	C29/C27 αββ Sterane Ratio	Tricyclic Terpanes/ Hopanes	Steranes/ Terpanes	% Tricyclic Terpanes	% Pentacyclic Terpanes	% Steranes	Steranes/ hopanes
W13/007663 (int)	25	23	52	0.16	0.01	0.11	21	22	57	2.74	0.01	0.06	1	94	5	0.06
W13/007664 (ext)	24	22	53	0.18	0.01	0.12	21	21	58	2.75	0.01	0.05	1	94	5	0.05
W13/007664 (int)	25	21	54	0.17	0.01	0.11	20	21	59	2.97	0.01	0.05	1	94	5	0.05
W13/007665 (ext)	31	28	40	0.42	0.03	0.39	31	30	38	1.22	0.14	0.33	9	66	25	0.38
W13/007665 (int)	34	29	36	0.35	0.02	0.30	31	30	40	1.31	0.11	0.31	7	69	24	0.34
W13/007666 (ext)	28	23	49	0.21	0.02	0.15	22	24	54	2.42	0.02	0.07	2	92	6	0.07
W13/007666 (int)	25	23	52	0.17	0.01	0.12	22	23	55	2.54	0.01	0.07	1	92	6	0.07
W13/007667 (ext)	20	22	57	0.17	0.01	0.12	18	23	60	3.41	0.01	0.06	1	94	5	0.06
W13/007667 (int)	25	22	53	0.16	0.01	0.12	21	23	57	2.72	0.01	0.07	1	93	6	0.07
W13/007668 (ext)	37	27	36	0.46	0.11	0.46	37	26	37	0.99	0.11	0.38	7	65	28	0.43
W13/007668 (int)	37	27	36	0.45	0.10	0.45	37	26	37	1.00	0.10	0.35	7	68	26	0.38
W13/007671 (ext)	38	24	38	0.44	0.10	0.44	38	26	36	0.94	0.10	0.28	7	71	22	0.31
W13/007671 (int)	37	23	39	0.42	0.09	0.42	37	25	38	1.04	0.10	0.29	7	71	22	0.31

Table S4 (continued).

Sample ID	C19t/ C23t	C22t/ C21t	C22t/ C24t	C24t/ C23t	C26t/ C25t	C24tet /C23t	C23t/ C30 αβ	C24tet/ C30 αβ	C28BNH /C30 αβ	25-Nor/ C30 αβ	C29 αβ /C30 αβ	C30*/ C30 αβ	Ole/ C30 αβ	C30Ts/ C30 αβ	Gam/ C30 αβ	Gam/ C31 αβ (R)	C35 αβ/ C34 αβ	C35 Homohopane Index	Ts/ (Ts+Tm)	C29Ts/ (C29Ts +C29 αβ)
W13/007672 (ext)	0.34	0.34	0.30	0.56	0.77	1.07	0.07	0.08	0.04	0.03	0.65	0.08	n.d.	0.05	0.08	0.25	0.94	8	0.38	0.18
W13/007672 (int)	0.30	0.37	0.31	0.55	0.96	1.07	0.07	0.08	0.04	0.03	0.64	0.09	n.d.	0.04	0.09	0.26	0.94	8	0.39	0.18
W13/007820 (ext)	0.32	0.34	0.30	0.54	0.94	1.08	0.07	0.08	0.04	0.03	0.67	0.08	n.d.	0.04	0.08	0.26	0.96	8	0.38	0.17
W13/007820 (int)	0.17	0.37	0.26	0.53	0.79	0.76	0.13	0.10	0.01	0.03	0.65	0.10	n.d.	0.01	0.06	0.21	0.85	7	0.42	0.19
W13/007827 (ext)	0.29	0.38	0.33	0.55	0.89	0.89	0.08	0.07	0.05	0.03	0.67	0.09	n.d.	0.04	0.09	0.26	0.85	7	0.41	0.17
W13/007830 (ext)	0.25	0.35	0.28	0.58	1.04	0.93	0.07	0.06	0.05	0.03	0.70	0.09	n.d.	0.04	0.08	0.24	0.87	8	0.41	0.17
W13/007830 (int)	0.26	0.38	0.29	0.57	0.78	0.90	0.08	0.07	0.05	0.03	0.69	0.09	n.d.	0.04	0.08	0.23	0.89	8	0.41	0.19
W13/007832 (ext)	0.25	0.36	0.30	0.57	0.90	0.90	0.07	0.07	0.05	0.03	0.65	0.09	n.d.	0.04	0.07	0.24	0.84	8	0.41	0.19
W13/007832 (int)	0.27	0.37	0.30	0.59	0.84	0.83	0.08	0.07	0.05	0.03	0.69	0.09	n.d.	0.04	0.08	0.24	0.85	8	0.41	0.17
W13/007845 (ext)	0.26	0.30	0.28	0.58	0.77	0.94	0.07	0.07	0.04	0.02	0.65	0.09	n.d.	0.04	0.06	0.18	0.88	8	0.38	0.18
W13/007845 (int)	0.22	0.35	0.21	0.55	0.86	0.85	0.11	0.09	0.07	0.03	0.64	0.09	n.d.	0.03	0.08	0.26	0.82	7	0.37	0.19
W13/007976 (ext)	0.25	0.32	0.24	0.49	0.63	0.88	0.09	0.08	0.05	0.02	0.68	0.08	n.d.	0.01	0.07	0.23	0.82	7	0.38	0.19
W13/007976 (int)	0.25	0.39	0.30	0.53	0.76	0.91	0.08	0.07	0.06	0.02	0.62	0.09	n.d.	0.01	0.08	0.26	0.82	8	0.41	0.22
COA/000956 (ext)	0.21	0.36	0.30	0.55	0.99	0.75	0.08	0.06	0.05	0.03	0.68	0.08	n.d.	0.05	0.07	0.20	0.85	8	0.38	0.17
COA/000956 (int)	0.25	0.32	0.27	0.57	1.04	0.79	0.08	0.06	0.05	0.03	0.66	0.08	n.d.	0.04	0.07	0.21	0.87	8	0.39	0.16

Sample ID	% C27 ααα 20R	% C28 ααα 20R	% C29 ααα 20R	C27 Dia/ (Dia+Reg)	(C21+C22)/ (C27+C28 +C29)	C27 Dia /Ster	% C27 αββ 20(R+S)	% C28 αββ 20(R+S)	% C29 αββ 20(R+S)	C29/C27 αββ Sterane Ratio	Tricyclic Terpanes/ Hopanes	Steranes/ Terpanes	% Tricyclic Terpanes	% Pentacyclic Terpanes	% Steranes	Steranes/ hopanes
W13/007672 (ext)	43	20	37	0.43	0.10	0.43	39	25	36	0.94	0.10	0.29	7	71	23	0.32
W13/007672 (int)	39	23	38	0.45	0.10	0.44	39	25	36	0.93	0.10	0.29	7	70	22	0.32
W13/007820 (ext)	42	21	38	0.43	0.10	0.43	39	25	36	0.94	0.10	0.29	7	71	22	0.32
W13/007820 (int)	40	27	33	0.47	0.17	0.50	40	26	34	0.85	0.15	0.42	9	61	30	0.49
W13/007827 (ext)	37	25	37	0.44	0.10	0.43	38	27	35	0.92	0.11	0.29	7	70	22	0.32
W13/007830 (ext)	37	27	36	0.46	0.12	0.47	37	28	35	0.96	0.10	0.25	7	73	20	0.28
W13/007830 (int)	37	22	40	0.44	0.06	0.45	38	26	36	0.95	0.10	0.31	7	69	24	0.35
W13/007832 (ext)	38	24	38	0.44	0.10	0.42	37	27	36	0.98	0.11	0.32	7	69	24	0.35
W13/007832 (int)	38	23	38	0.45	0.10	0.45	38	26	36	0.96	0.11	0.32	8	68	24	0.36
W13/007845 (ext)	42	20	39	0.43	0.11	0.42	38	25	37	0.96	0.10	0.31	7	69	24	0.34
W13/007845 (int)	39	27	34	0.46	0.14	0.47	39	26	35	0.90	0.14	0.41	9	63	29	0.46
W13/007976 (ext)	43	23	34	0.44	0.13	0.46	39	25	36	0.94	0.10	0.31	7	69	24	0.34
W13/007976 (int)	38	26	36	0.45	0.15	0.47	38	25	37	0.98	0.10	0.29	7	70	23	0.32
COA/000956 (ext)	40	20	40	0.46	0.11	0.46	38	26	36	0.94	0.11	0.31	7	69	24	0.35
COA/000956 (int)	38	28	34	0.44	0.11	0.44	38	25	36	0.95	0.11	0.32	7	68	24	0.36

* = Most representative examples, i.e. least altered results due to low biomarker responses and/or alteration associated with weathering.

4.3. Asphaltic tars

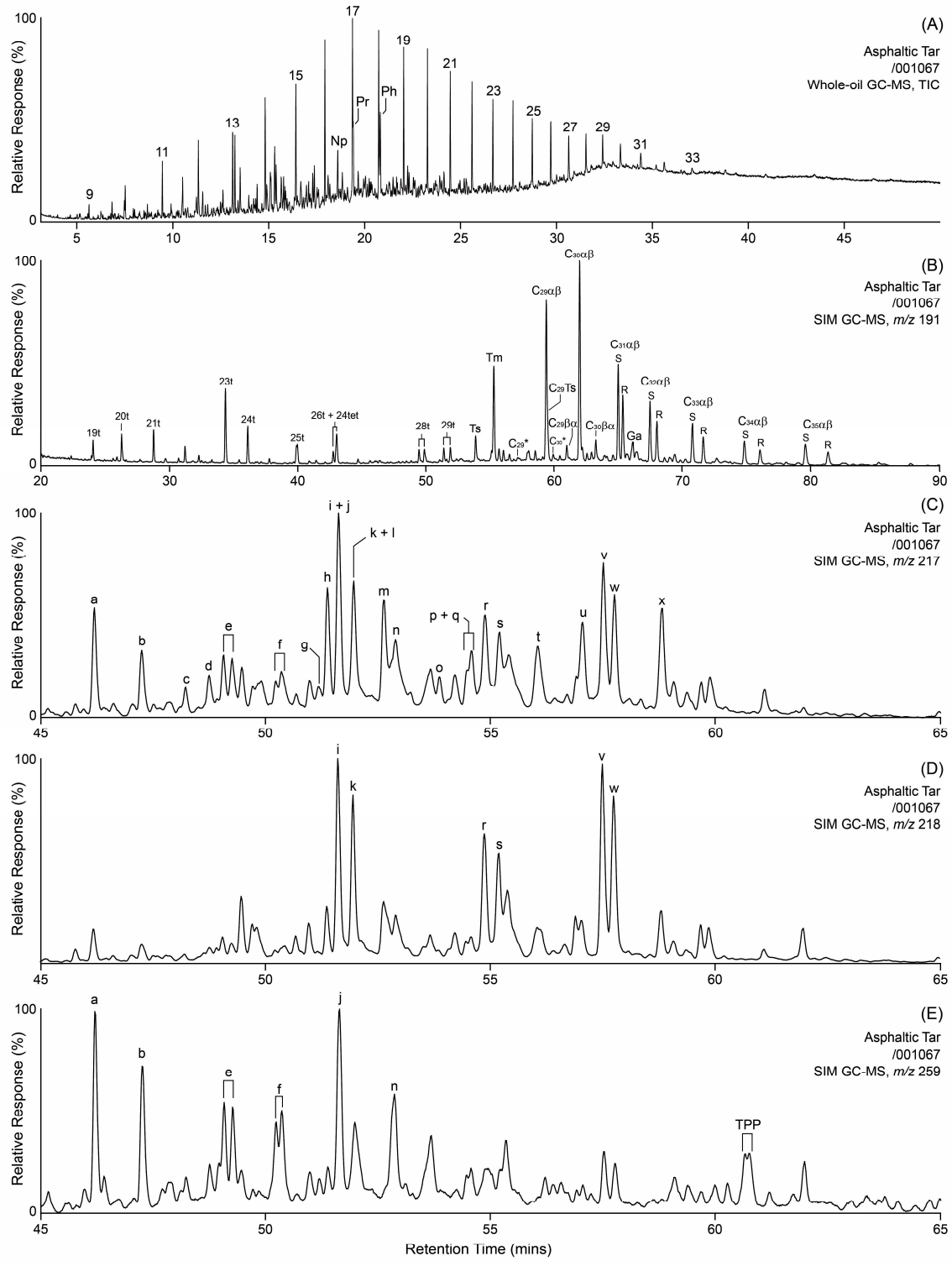


Figure S3: Representative chromatograms from asphaltic tar sample /001067. (A) Whole-oil GC-MS total ion chromatogram. (B) Saturated fraction SIM GC-MS *m/z* 191 chromatogram. (C) Saturated fraction SIM GC-MS *m/z* 217 chromatogram. (D) Saturated fraction SIM GC-MS *m/z* 218 chromatogram. (E) Saturated fraction SIM GC-MS *m/z* 259 chromatogram.

Table S5: Selected biomarker parameters from analysed asphaltic tars, bulk = sample includes interior and exterior.

Sample ID	C19t/ C23t	C22t/ C21t	C22t/ C24t	C24t/ C23t	C26t/ C25t*	C24tet /C23t	C23t/ C30 αβ	C24tet/ C30 αβ	C28BNH /C30 αβ	25-Nor/ C30 αβ	C29 αβ /C30 αβ	C30*/ C30 αβ	Ole/ C30 αβ	C30Ts/ C30 αβ	Gam/ C30 αβ	Gam/ C31 αβ (R)	C35 αβ/ C34 αβ	C35 Homohopane Index	Ts/ (Ts+Tm)	C29Ts/ (C29Ts +C29 αβ)
/001056 (bulk)	0.17	0.13	0.10	0.49	0.57	0.30	0.31	0.09	0.05	0.04	0.82	0.04	n.d.	0.06	0.11	0.34	1.02	0.11	0.22	0.09
/001063 (bulk)	0.18	0.10	0.08	0.47	0.67	0.29	0.31	0.09	0.04	0.04	0.80	0.04	n.d.	0.06	0.12	0.37	1.00	0.10	0.22	0.11
/001067 (bulk)	0.16	0.11	0.09	0.51	0.77	0.36	0.30	0.11	0.00	0.04	0.78	0.04	n.d.	0.06	0.12	0.36	1.03	0.11	0.22	0.09
/001068 (bulk)	0.16	0.01	0.01	0.51	0.66	0.35	0.33	0.12	0.00	0.04	0.75	0.04	n.d.	0.06	0.10	0.33	1.01	0.11	0.22	0.11
/001076 (bulk)	0.13	0.04	0.03	0.52	0.62	0.44	0.26	0.11	0.03	0.06	0.79	0.05	n.d.	0.07	0.10	0.30	1.05	0.11	0.27	0.13
/001079 (bulk)	0.12	0.14	0.09	0.52	0.56	0.40	0.27	0.11	0.03	0.05	0.73	0.04	n.d.	0.07	0.10	0.31	1.02	0.12	0.19	0.08
/001081 (bulk)	0.15	0.12	0.08	0.51	0.62	0.36	0.29	0.10	0.03	0.05	0.76	0.04	n.d.	0.05	0.10	0.31	1.04	0.12	0.19	0.10

Sample ID	% C27 ααα 20R	% C28 ααα 20R	% C29 ααα 20R	C27 Dia/ (Dia+Reg)	(C21+C22)/ (C27+C28 +C29)	C27 Dia /Ster	% C27 αββ 20(R+S)	% C28 αββ 20(R+S)	% C29 αββ 20(R+S)	C29/C27 αββ Sterane Ratio	Tricyclic Terpanes/ Hopanes	Steranes/ Terpanes	% Tricyclic Terpanes	% Pentacyclic Terpanes	% Steranes	Steranes/ hopanes
/001056 (bulk)	35	29	36	0.34	0.20	0.28	36	26	38	1.06	0.27	0.24	17	64	19	0.30
/001063 (bulk)	35	29	36	0.43	0.21	0.41	36	26	38	1.07	0.28	0.25	17	63	20	0.32
/001067 (bulk)	34	29	37	0.43	0.23	0.40	35	25	40	1.14	0.27	0.24	17	64	19	0.31
/001068 (bulk)	35	29	36	0.44	0.25	0.41	36	25	39	1.09	0.29	0.26	18	62	20	0.33
/001076 (bulk)	37	26	37	0.43	0.18	0.39	36	23	42	1.16	0.21	0.22	14	68	18	0.27
/001079 (bulk)	33	29	38	0.43	0.18	0.41	35	25	41	1.17	0.23	0.23	15	66	19	0.28
/001081 (bulk)	32	29	38	0.44	0.20	0.41	35	25	40	1.16	0.23	0.23	15	66	19	0.28

4.4. Waxy oils of lacustrine source affinity (types I, IIIA–C, IIIF and IVC)

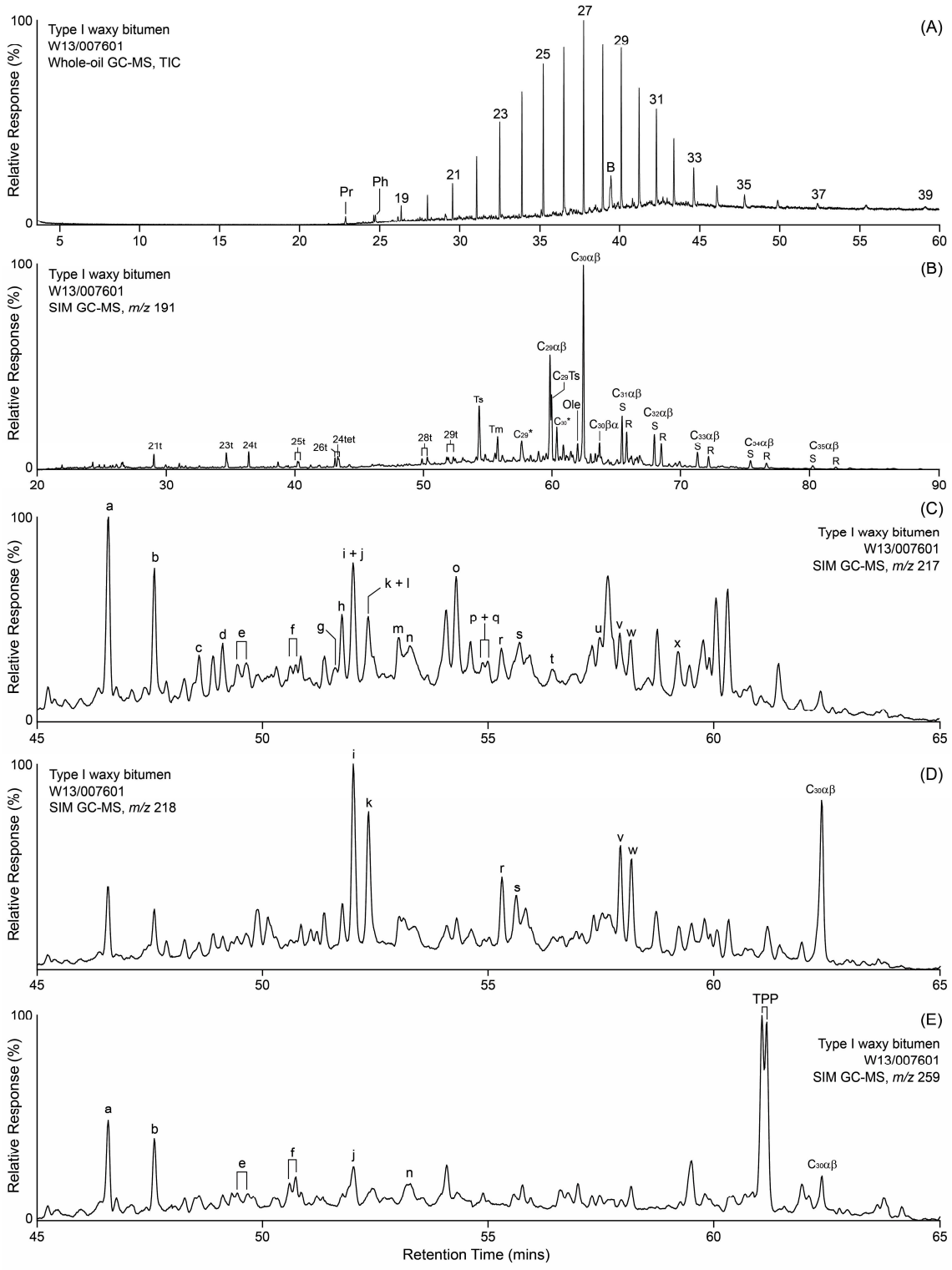


Figure S4: Representative chromatograms from the least weathered type I waxy bitumen (W13/007601). (A) Whole-oil GC-MS total ion chromatogram. (B) Saturated fraction SIM GC-MS *m/z* 191 chromatogram. (C) Saturated fraction SIM GC-MS *m/z* 217 chromatogram. (D) Saturated fraction SIM GC-MS *m/z* 218 chromatogram. (E) Saturated fraction SIM GC-MS *m/z* 259 chromatogram.

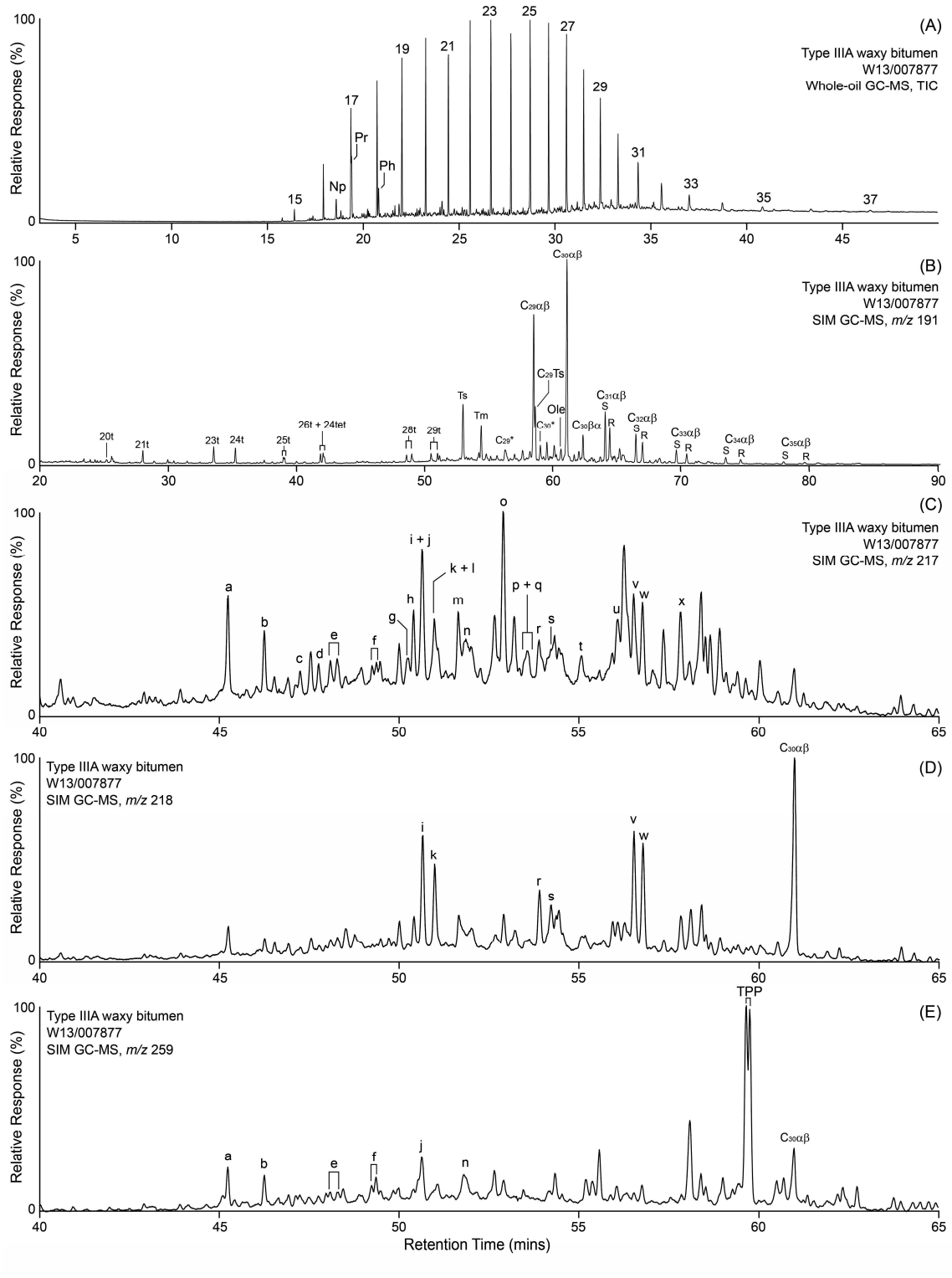


Figure S5: Representative chromatograms from the least weathered type IIIA waxy bitumen (W13/007877). (A) Whole-oil GC-MS total ion chromatogram. (B) Saturated fraction SIM GC-MS *m/z* 191 chromatogram. (C) Saturated fraction SIM GC-MS *m/z* 217 chromatogram. (D) Saturated fraction SIM GC-MS *m/z* 218 chromatogram. (E) Saturated fraction SIM GC-MS *m/z* 259 chromatogram.

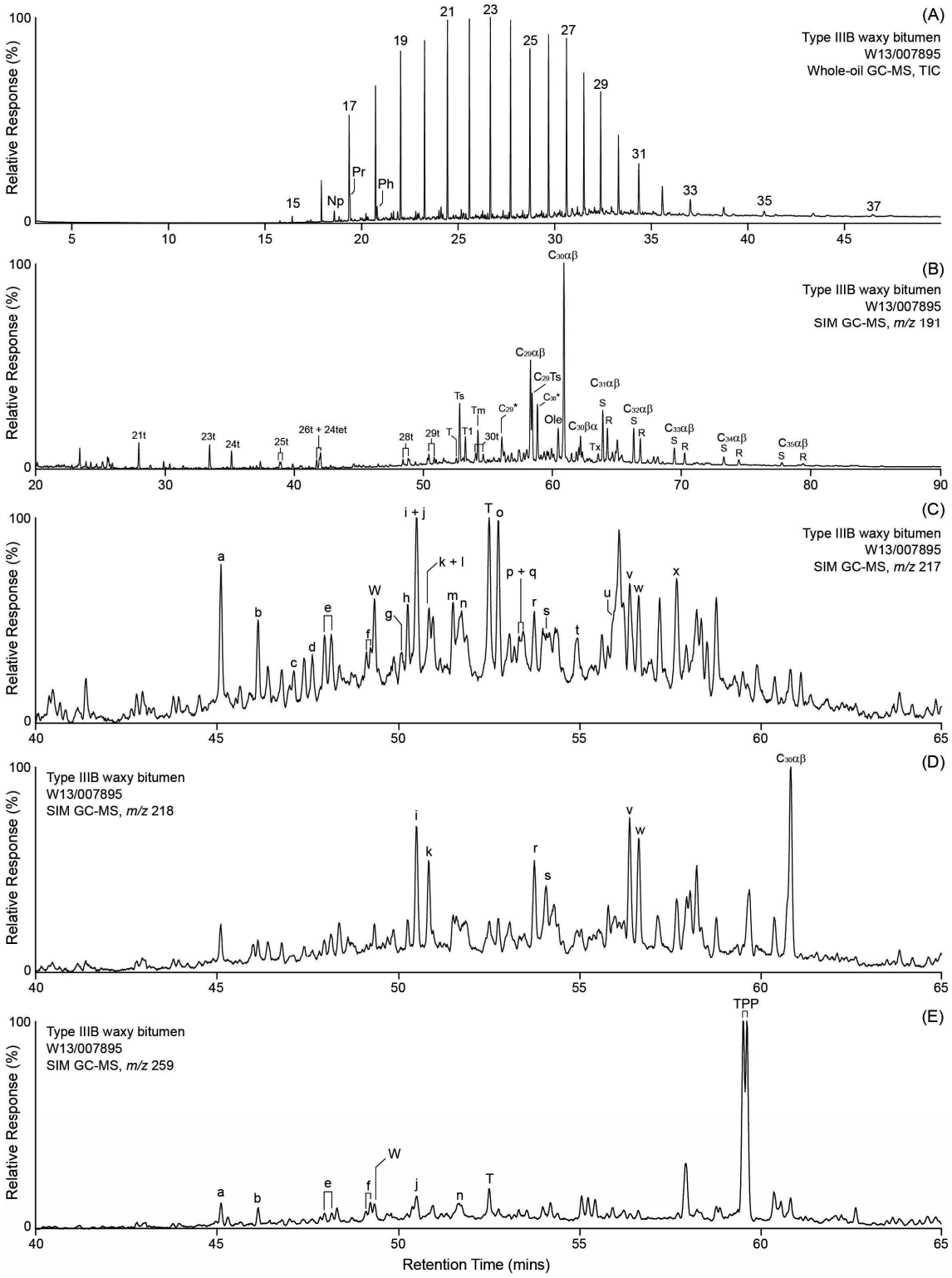


Figure S6: Representative chromatograms from the least weathered type IIIB waxy bitumen (W13/007895). (A) Whole-oil GC-MS total ion chromatogram. (B) Saturated fraction SIM GC-MS *m/z* 191 chromatogram. (C) Saturated fraction SIM GC-MS *m/z* 217 chromatogram. (D) Saturated fraction SIM GC-MS *m/z* 218 chromatogram. (E) Saturated fraction SIM GC-MS *m/z* 259 chromatogram.

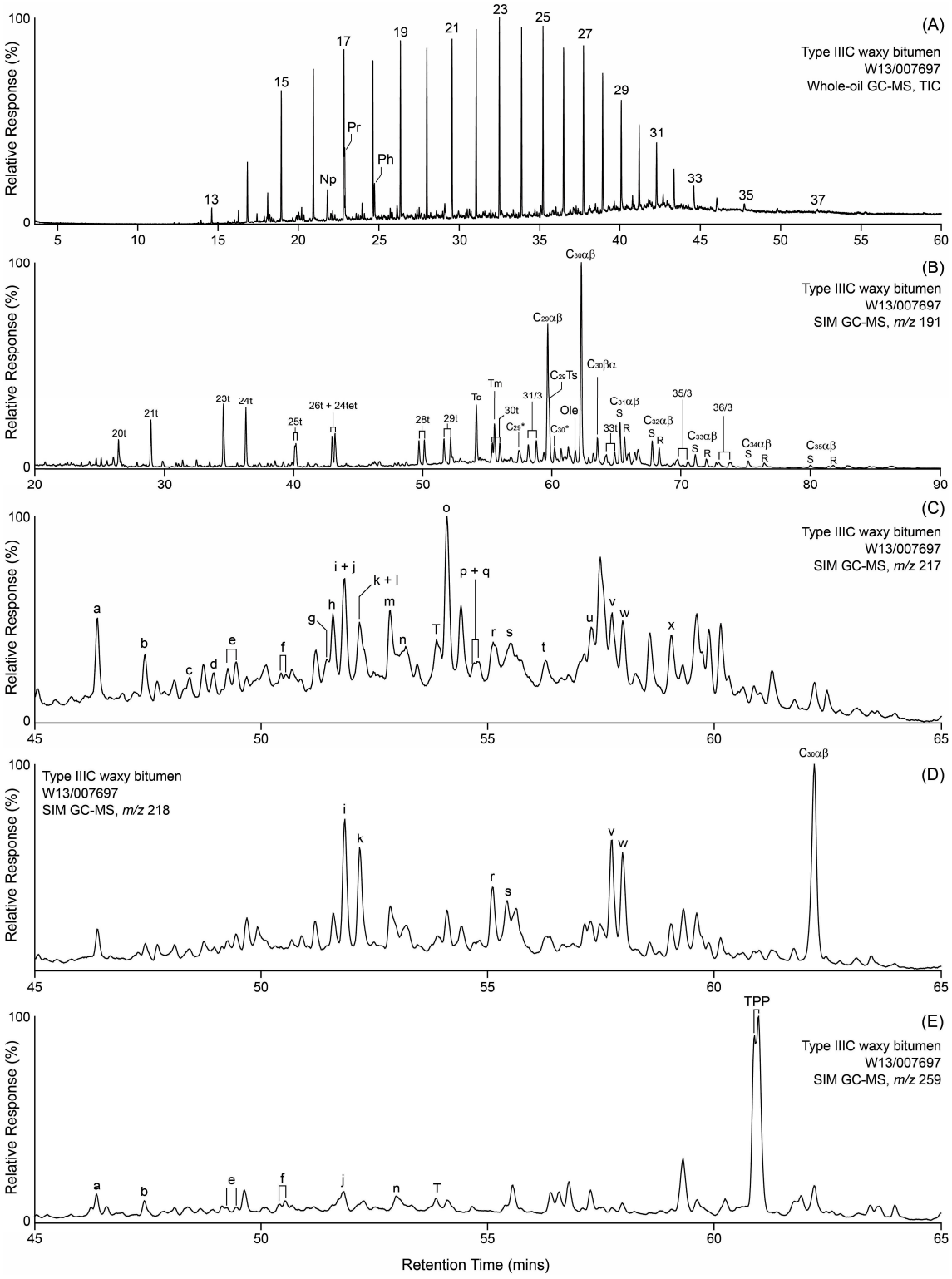


Figure S7: Representative chromatograms from the least weathered type IIIC waxy bitumen (W13/007697). (A) Whole-oil GC-MS total ion chromatogram. (B) Saturated fraction SIM GC-MS *m/z* 191 chromatogram. (C) Saturated fraction SIM GC-MS *m/z* 217 chromatogram. (D) Saturated fraction SIM GC-MS *m/z* 218 chromatogram. (E) Saturated fraction SIM GC-MS *m/z* 259 chromatogram.

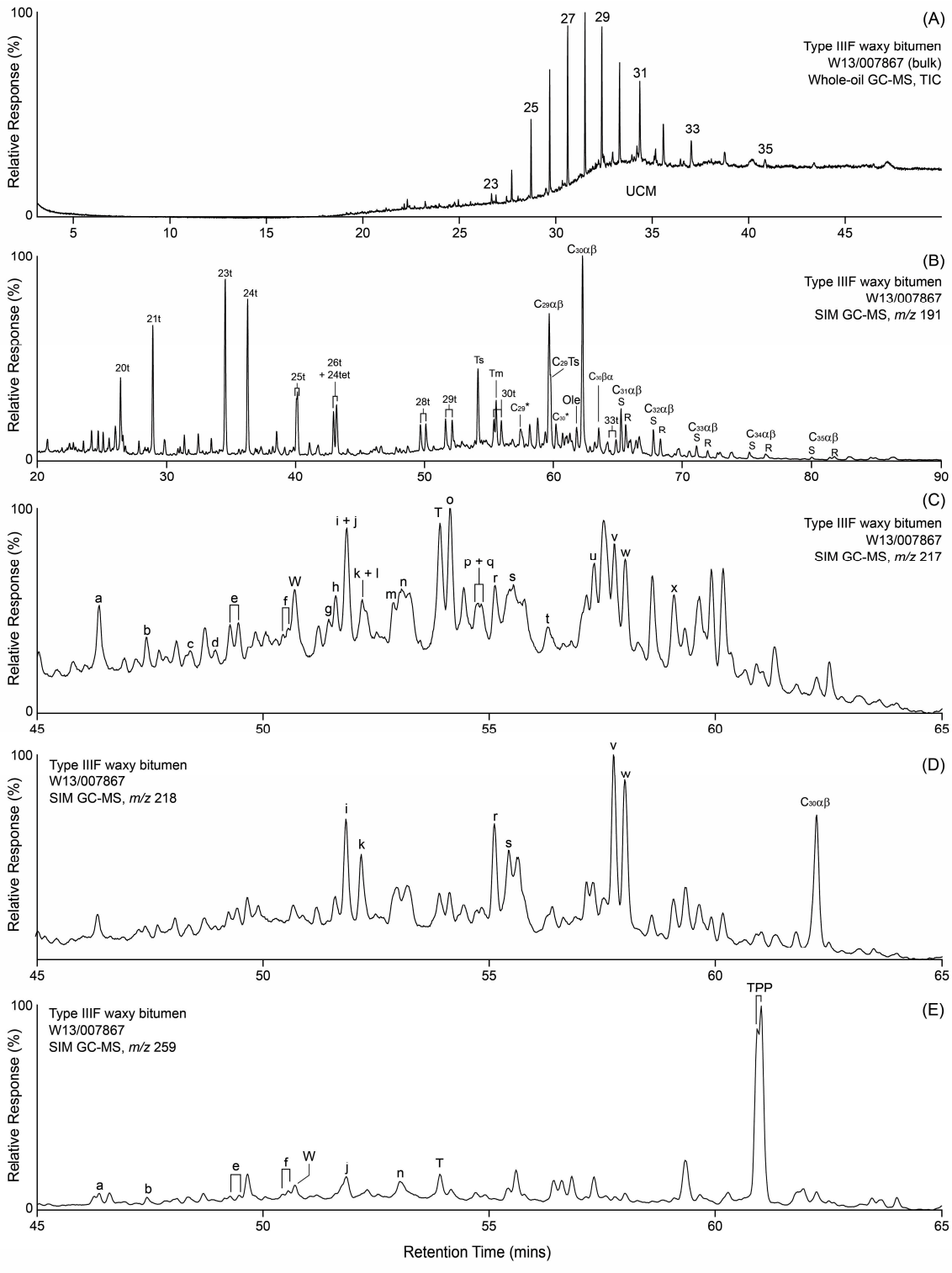


Figure S8: Chromatograms from the only identified type IIIF waxy bitumen (W13/007867). (A) Whole-oil GC-MS total ion chromatogram. (B) Saturated fraction SIM GC-MS *m/z* 191 chromatogram. (C) Saturated fraction SIM GC-MS *m/z* 217 chromatogram. (D) Saturated fraction SIM GC-MS *m/z* 218 chromatogram. (E) Saturated fraction SIM GC-MS *m/z* 259 chromatogram.

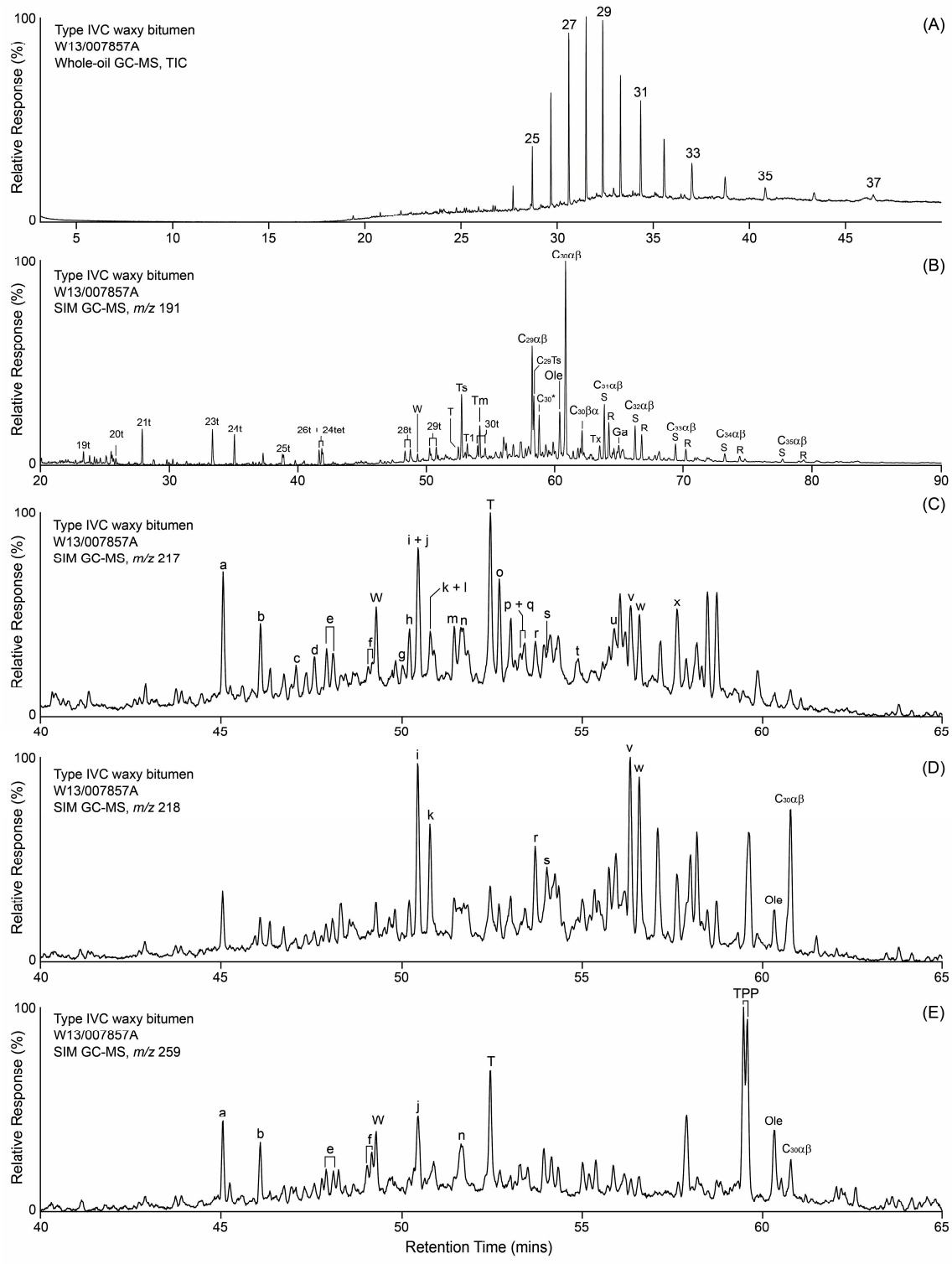


Figure S9: Chromatograms from the only identified type IVC waxy bitumen (W13/007857A). (A) Whole-oil GC-MS total ion chromatogram. (B) Saturated fraction SIM GC-MS *m/z* 191 chromatogram. (C) Saturated fraction SIM GC-MS *m/z* 217 chromatogram. (D) Saturated fraction SIM GC-MS *m/z* 218 chromatogram. (E) Saturated fraction SIM GC-MS *m/z* 259 chromatogram.

Table S6: Selected biomarker parameters from analysed waxy oils of lacustrine shale source affinity (waxy bitumen types I, IIIA–C, IIIF and IVC), int = sample interior, ext = sample exterior (top 2mm), bulk = sample includes interior and exterior.

Sample ID	C19t/ C23t	C22t/ C21t	C22t/ C24t	C24t/ C23t	C26t/ C25t	C24tet /C23t	C23t/ C30 αβ	C24tet/ C30 αβ	C28BNH /C30 αβ	25-Nor/ C30 αβ	C29 αβ /C30 αβ	C30*/ C30 αβ	Ole/ C30 αβ	C30Ts/ C30 αβ	Gam/ C30 αβ	Gam/ C31 αβ (R)	C35 αβ/ C34 αβ	C35 Homohopane Index	Ts/ (Ts+Tm)	C29Ts/ (C29Ts +C29 αβ)
Type I waxy bitumen																				
W13/007473 (int)	0.23	0.34	0.24	0.78	1.88	0.50	0.08	0.04	0.01	0.06	0.52	0.17	0.08	0.00	0.05	0.28	0.47	5	0.72	0.35
W13/007511 (ext)	0.02	0.37	0.20	1.04	2.08	0.46	0.07	0.03	0.03	0.08	0.66	0.17	0.13	0.00	0.04	0.19	0.47	4	0.71	0.31
W13/007511 (int)	0.02	0.41	0.18	0.92	1.71	0.42	0.08	0.03	0.01	0.06	0.58	0.14	0.10	0.00	0.03	0.15	0.47	5	0.69	0.32
W13/007517 (ext)	0.20	0.49	0.31	1.03	1.43	0.70	0.06	0.04	0.02	0.06	0.57	0.22	0.11	0.00	0.04	0.26	0.32	2	0.75	0.37
W13/007521 (ext)	0.42	1.16	0.30	1.33	0.61	0.60	0.03	0.02	0.06	0.13	0.47	0.33	0.38	0.00	0.05	0.27	0.34	2	0.88	0.51
W13/007521 (int)	0.19	0.53	0.19	1.58	1.75	0.56	0.03	0.02	0.03	0.07	0.59	0.26	0.17	0.01	0.04	0.24	0.42	5	0.78	0.42
W13/007528 (ext)	0.36	0.43	0.25	0.92	1.78	0.54	0.03	0.02	0.02	0.04	0.42	0.16	0.10	0.04	0.04	0.21	0.54	4	0.68	0.30
W13/007528 (int)	0.29	0.42	0.30	0.90	1.68	0.54	0.06	0.03	0.03	0.05	0.66	0.19	0.11	0.05	0.05	0.31	0.55	5	0.71	0.27
W13/007530 (ext)	0.25	0.38	0.29	1.03	1.85	0.55	0.06	0.04	0.03	0.07	0.58	0.20	0.11	0.02	0.04	0.25	0.49	4	0.70	0.33
W13/007530 (int)	0.23	0.37	0.31	0.91	1.87	0.51	0.09	0.04	0.04	0.05	0.63	0.21	0.14	0.03	0.04	0.21	0.44	4	0.73	0.35
W13/007553 (ext)	0.35	0.33	0.30	0.94	1.99	0.58	0.07	0.04	0.03	0.07	0.62	0.20	0.12	0.01	0.04	0.21	0.43	4	0.73	0.31
W13/007553 (int)	0.44	0.17	0.16	0.96	1.81	0.58	0.06	0.03	0.03	0.05	0.55	0.20	0.12	0.00	0.04	0.25	0.46	4	0.74	0.32

Sample ID	% C27 ααα 20R	% C28 ααα 20R	% C29 ααα 20R	C27 Dia/ (Dia+Reg)	(C21+C22)/ (C27+C28 +C29)	C27 Dia /Ster	% C27 αββ 20(R+S)	% C28 αββ 20(R+S)	% C29 αββ 20(R+S)	C29/C27 αββ Sterane Ratio	Tricyclic Terpanes/ Hopanes	Steranes/ Terpanes	% Tricyclic Terpanes	% Pentacyclic Terpanes	% Steranes	Steranes/ hopanes
Type I waxy bitumen																
W13/007473 (int)	26.58	11.92	61.50	0.72	0.09	1.04	41.07	23.72	35.21	0.86	0.14	0.06	11.37	83.19	5.44	0.07
W13/007511 (ext)	40.88	17.82	41.31	0.69	0.06	1.07	48.57	19.69	31.74	0.65	0.14	0.06	11.83	82.86	5.30	0.06
W13/007511 (int)	42.75	16.89	40.36	0.68	0.06	0.98	49.53	20.88	29.59	0.60	0.14	0.07	11.38	81.64	6.97	0.09
W13/007517 (ext)	31.87	8.63	59.51	0.70	0.10	0.73	34.72	25.15	40.13	1.16	0.11	0.04	9.68	86.43	3.89	0.04
W13/007521 (ext)	60.28	13.28	26.44	0.26	0.01	0.19	24.17	29.04	46.80	1.94	0.12	0.05	10.15	85.00	4.84	0.06
W13/007521 (int)	27.52	20.74	51.74	0.70	0.04	0.91	31.61	25.88	42.52	1.35	0.09	0.04	7.86	87.87	4.26	0.05
W13/007528 (ext)	18.69	23.94	57.36	0.66	0.04	0.81	29.49	24.32	46.19	1.57	0.08	0.04	7.15	88.69	4.16	0.05
W13/007528 (int)	29.75	11.82	58.44	0.71	0.08	1.19	32.64	22.96	44.40	1.36	0.11	0.05	9.38	86.10	4.53	0.05
W13/007530 (ext)	34.22	16.40	49.38	0.75	0.07	1.33	50.74	19.68	29.58	0.58	0.14	0.05	11.87	82.96	5.17	0.06
W13/007530 (int)	29.22	17.86	52.92	0.78	0.07	1.41	50.70	21.48	27.81	0.55	0.16	0.06	13.13	81.12	5.76	0.07
W13/007553 (ext)	48.68	14.13	37.19	0.71	0.08	1.24	45.82	20.34	33.85	0.74	0.16	0.06	13.14	81.49	5.37	0.07
W13/007553 (int)	43.93	13.54	42.53	0.66	0.05	1.05	46.17	19.89	33.94	0.74	0.14	0.05	11.65	83.34	5.01	0.06

Table S6 (continued).

Sample ID	C19t/ C23t	C22t/ C21t	C22t/ C24t	C24t/ C23t	C26t/ C25t	C24tet /C23t	C23t/ C30 αβ	C24tet/ C30 αβ	C28BNH /C30 αβ	25-Nor/ C30 αβ	C29 αβ /C30 αβ	C30*/ C30 αβ	Ole/ C30 αβ	C30Ts/ C30 αβ	Gam/ C30 αβ	Gam/ C31 αβ (R)	C35 αβ/ C34 αβ	C35 Homohopane Index	Ts/ (Ts+Tm)	C29Ts/ (C29Ts +C29 αβ)
Type I waxy bitumen (cont.)																				
W13/007601 (int)*	0.37	0.38	0.32	0.85	1.82	0.38	0.08	0.03	0.03	0.07	0.60	0.18	0.11	0.01	0.04	0.25	0.44	4	0.71	0.31
W13/007625 (int)	0.21	0.36	0.27	0.94	1.96	0.39	0.08	0.03	0.03	0.06	0.62	0.16	0.11	0.01	0.04	0.27	0.43	4	0.70	0.29
W13/007699 (int)	0.23	0.35	0.24	1.09	2.04	0.38	0.07	0.03	0.03	0.08	0.54	0.20	0.10	0.00	0.03	0.18	0.43	4	0.73	0.39
W13/007721 (bulk)	0.15	0.43	0.26	0.87	1.94	0.29	0.11	0.03	0.04	0.08	0.59	0.18	0.16	0.00	0.03	0.18	0.47	5	0.73	0.42
W13/007737 (ext)	0.26	0.41	0.28	0.98	1.84	0.38	0.10	0.04	0.05	0.12	0.54	0.33	0.20	0.00	0.04	0.23	0.45	5	0.77	0.44
W13/007819 (int)	0.31	0.29	0.28	0.87	1.60	0.32	0.18	0.06	0.04	0.06	0.65	0.17	0.12	0.00	0.06	0.31	0.44	5	0.70	0.31
W13/007838 (int)	0.19	0.45	0.25	0.85	1.94	0.34	0.13	0.04	0.05	0.09	0.60	0.21	0.10	0.00	0.03	0.16	0.42	4	0.71	0.32
W13/007863 (int)	0.27	0.16	0.12	0.89	1.06	0.38	0.13	0.05	0.02	0.05	0.56	0.19	0.08	0.00	0.03	0.16	0.32	2	0.72	0.32
W13/007865 (bulk)	0.67	0.13	0.09	2.59	0.57	1.63	0.03	0.06	0.02	0.04	0.61	0.19	0.09	0.00	0.04	0.23	0.35	2	0.70	0.31
W13/007868 (bulk)	0.00	0.00	0.00	1.10	3.08	0.20	0.05	0.01	0.03	0.05	0.60	0.14	0.09	0.75	0.04	0.29	0.41	4	0.68	0.27
W13/007887 (int)	0.23	0.09	0.07	0.90	1.73	0.19	0.10	0.02	0.04	0.08	0.52	0.15	0.12	0.00	0.04	0.25	0.76	5	0.69	0.33
W13/007898 (int)	0.15	0.46	0.24	0.91	2.54	0.34	0.08	0.03	0.04	0.06	0.58	0.18	0.10	0.00	0.05	0.28	0.44	5	0.72	0.32

Sample ID	% C27 ααα 20R	% C28 ααα 20R	% C29 ααα 20R	C27 Dia/ (Dia+Reg)	(C21+C22)/ (C27+C28 +C29)	C27 Dia /Ster	% C27 αββ 20(R+S)	% C28 αββ 20(R+S)	% C29 αββ 20(R+S)	C29/C27 αββ Sterane Ratio	Tricyclic Terpanes/ Hopanes	Steranes/ Terpanes	% Tricyclic Terpanes	% Pentacyclic Terpanes	% Steranes	Steranes/ hopanes
Type I waxy bitumen (cont.)																
W13/007601 (int)*	48.72	14.73	36.55	0.72	0.08	1.36	50.03	19.08	30.89	0.62	0.15	0.06	12.53	81.72	5.76	0.07
W13/007625 (int)	48.32	12.14	39.54	0.71	0.09	1.20	47.50	18.35	34.15	0.72	0.17	0.06	13.55	80.83	5.63	0.07
W13/007699 (int)	22.37	18.04	59.60	0.72	0.06	1.00	43.06	23.03	33.90	0.79	0.15	0.06	12.58	81.86	5.56	0.07
W13/007721 (bulk)	41.67	15.75	42.57	0.69	0.08	1.03	48.73	21.35	29.92	0.61	0.21	0.08	15.75	76.43	7.82	0.10
W13/007737 (ext)	0.00	17.20	82.80	0.76	0.07	0.82	42.47	23.74	33.79	0.80	0.19	0.06	15.12	78.92	5.96	0.08
W13/007819 (int)	58.44	7.72	33.83	0.69	0.11	1.09	44.66	20.26	35.08	0.79	0.29	0.06	21.29	73.15	5.57	0.08
W13/007838 (int)	47.61	9.09	43.30	0.77	0.06	1.37	53.25	21.09	25.66	0.48	0.23	0.07	17.63	75.76	6.61	0.09
W13/007863 (int)	57.43	13.97	28.60	0.31	0.15	0.28	24.84	30.52	44.63	1.80	0.19	0.04	15.33	80.68	4.00	0.05
W13/007865 (bulk)	30.71	6.85	62.45	0.44	0.10	0.36	16.01	26.57	57.42	3.59	0.12	0.04	10.04	86.40	3.56	0.04
W13/007868 (bulk)	61.34	5.71	32.95	0.68	0.02	1.16	53.14	17.63	29.24	0.55	0.12	0.05	9.94	85.39	4.67	0.05
W13/007887 (int)	31.30	20.54	48.15	0.72	0.10	1.18	47.18	20.39	32.43	0.69	0.19	0.07	14.66	79.01	6.33	0.08
W13/007898 (int)	44.36	15.91	39.73	0.70	0.06	1.05	50.47	20.70	28.83	0.57	0.15	0.07	12.21	81.13	6.66	0.08

* = Most representative examples, i.e. least altered results due to low biomarker responses and/or alteration associated with weathering.

Table S6 (continued).

Sample ID	C19t/ C23t	C22t/ C21t	C22t/ C24t	C24t/ C23t	C26t/ C25t	C24tet /C23t	C23t/ C30 αβ	C24tet/ C30 αβ	C28BNH /C30 αβ	25-Nor/ C30 αβ	C29 αβ /C30 αβ	C30*/ C30 αβ	Ole/ C30 αβ	C30Ts/ C30 αβ	Gam/ C30 αβ	Gam/ C31 αβ (R)	C35 αβ/ C34 αβ	C35 Homohopane Index	Ts/ (Ts+Tm)	C29Ts/ (C29Ts +C29 αβ)
Type I waxy bitumen (cont.)																				
W13/007922 (int)	0.20	0.10	0.07	0.88	1.83	0.31	0.11	0.03	0.04	0.07	0.57	0.19	0.11	0.00	0.05	0.26	0.50	5	0.71	0.34
W13/007962 (int)	0.39	0.61	0.21	1.13	1.55	0.64	0.05	0.03	0.04	0.08	0.54	0.31	0.18	0.00	0.03	0.17	0.49	4	0.75	0.37
W13/007965 (bulk)	0.17	0.47	0.32	0.77	1.70	0.37	0.08	0.03	0.04	0.06	0.49	0.21	0.12	0.00	0.04	0.22	0.44	5	0.70	0.36
W13/007967 (bulk)	0.12	9.06	0.52	0.93	2.35	0.83	0.11	0.09	0.32	0.52	0.56	1.61	0.83	0.08	0.22	1.47	0.56	11	0.74	0.56
W13/007995 (int)	0.22	0.12	0.06	0.79	1.86	0.72	0.08	0.06	0.03	0.05	0.54	0.16	0.09	0.04	0.05	0.25	0.68	6	0.69	0.32
W13/007997 (bulk)	0.12	0.42	0.24	0.87	1.79	0.50	0.08	0.04	0.03	0.07	0.51	0.19	0.12	0.00	0.03	0.19	0.44	4	0.73	0.39
W13/007999 (bulk)	0.03	0.19	0.07	0.78	1.83	0.79	0.08	0.07	0.03	0.06	0.54	0.16	0.10	0.04	0.06	0.29	0.63	7	0.66	0.35
COA/000976 (int)	0.31	0.17	0.11	0.79	1.91	0.58	0.09	0.05	0.03	0.06	0.53	0.20	0.12	0.00	0.04	0.22	0.40	4	0.69	0.32
/001021 (int)	0.32	0.34	0.23	0.94	1.71	0.55	0.10	0.06	0.04	0.07	0.62	0.17	0.10	0.02	0.04	0.20	0.45	4	0.68	0.28
/001039B (bulk)	0.18	0.17	0.10	0.82	1.32	0.60	0.08	0.05	0.01	0.06	0.53	0.22	0.12	0.03	0.05	0.26	0.49	4	0.71	0.36
W13/001043 (bulk)	0.18	0.27	0.10	0.91	1.59	0.05	0.41	0.02	0.04	0.30	0.36	0.76	0.59	0.14	0.15	0.88	0.64	10	0.87	0.75

Sample ID	% C27 ααα 20R	% C28 ααα 20R	% C29 ααα 20R	C27 Dia/ (Dia+Reg)	(C21+C22)/ (C27+C28 +C29)	C27 Dia /Ster	% C27 αββ 20(R+S)	% C28 αββ 20(R+S)	% C29 αββ 20(R+S)	C29/C27 αββ Sterane Ratio	Tricyclic Terpanes/ Hopanes	Steranes/ Terpanes	% Tricyclic Terpanes	% Pentacyclic Terpanes	% Steranes	Steranes/ hopanes
Type I waxy bitumen (cont.)																
W13/007922 (int)	37.77	7.87	54.36	0.69	0.08	1.01	43.77	22.11	34.13	0.78	0.18	0.07	14.08	79.65	6.27	0.08
W13/007962 (int)	63.87	7.17	28.96	0.27	0.07	0.23	19.59	27.34	53.07	2.71	0.10	0.05	8.75	86.61	4.64	0.05
W13/007965 (bulk)	53.12	8.15	38.73	0.89	0.04	3.89	49.07	21.88	29.05	0.59	0.14	0.03	11.66	85.12	3.23	0.04
W13/007967 (bulk)	46.78	9.01	44.21	0.72	0.03	1.00	41.57	23.38	35.05	0.84	0.17	0.14	12.87	74.64	12.49	0.17
W13/007995 (int)	39.49	16.94	43.57	0.67	0.08	1.02	45.75	19.32	34.93	0.76	0.14	0.07	11.20	82.27	6.52	0.08
W13/007997 (bulk)	52.39	8.58	39.02	0.77	0.09	1.50	55.96	18.85	25.19	0.45	0.15	0.05	12.40	82.44	5.16	0.06
W13/007999 (bulk)	36.83	8.85	54.32	0.72	0.08	1.03	45.98	19.45	34.57	0.75	0.13	0.07	10.62	82.76	6.62	0.08
COA/000976 (int)	45.34	6.25	48.40	0.74	0.07	1.18	50.94	22.04	27.01	0.53	0.15	0.06	12.70	81.99	5.30	0.06
/001021 (int)	51.11	13.64	35.25	0.72	0.09	1.10	49.84	19.52	30.64	0.61	0.21	0.06	16.22	77.72	6.06	0.08
/001039B (bulk)	17.19	23.94	58.87	0.70	0.08	0.85	34.50	26.61	38.89	1.13	0.13	0.06	10.55	84.06	5.40	0.06
W13/001043 (bulk)	0.00	17.55	82.45	0.85	0.12	1.21	42.70	24.09	33.22	0.78	0.34	0.14	22.21	65.72	12.07	0.18

Table S6 (continued).

Sample ID	C19t/ C23t	C22t/ C21t	C22t/ C24t	C24t/ C23t	C26t/ C25t	C24tet /C23t	C23t/ C30 αβ	C24tet/ C30 αβ	C28BNH /C30 αβ	25-Nor/ C30 αβ	C29 αβ /C30 αβ	C30*/ C30 αβ	Ole/ C30 αβ	C30Ts/ C30 αβ	Gam/ C30 αβ	Gam/ C31 αβ (R)	C35 αβ/ C34 αβ	C35 Homohopane Index	Ts/ (Ts+Tm)	C29Ts/ (C29Ts +C29 αβ)
Type IIIA waxy bitumen																				
W13/007541 (ext)	0.10	0.31	0.21	0.96	1.72	0.31	0.10	0.03	0.02	0.06	0.90	0.09	0.11	0.03	0.09	0.66	0.40	4	0.65	0.22
W13/007541 (int)	0.12	0.31	0.25	0.90	2.00	0.29	0.08	0.02	0.02	0.05	0.66	0.08	0.06	0.01	0.05	0.42	0.45	4	0.66	0.21
W13/007683 (int)	0.13	0.29	0.21	0.85	1.65	0.34	0.12	0.04	0.04	0.06	0.72	0.09	0.05	0.00	0.06	0.43	0.42	3	0.63	0.23
W13/007684 (int)	0.12	0.29	0.22	0.88	1.88	0.33	0.09	0.03	0.02	0.04	0.77	0.06	0.08	0.02	0.06	0.44	0.45	3	0.65	0.18
W13/007692 (int)	0.05	0.26	0.19	0.85	1.59	0.34	0.12	0.04	0.04	0.06	0.73	0.09	0.06	0.00	0.06	0.42	0.37	3	0.63	0.22
W13/007698 (int)	0.12	0.05	0.05	0.85	1.89	0.22	0.11	0.02	0.03	0.06	0.73	0.09	0.05	0.00	0.06	0.38	0.41	3	0.64	0.20
W13/007698 (int dup)	0.12	0.05	0.04	0.84	1.89	0.25	0.10	0.03	0.03	0.06	0.71	0.09	0.06	0.00	0.06	0.40	0.39	3	0.63	0.16
W13/007778 (int)	0.04	0.21	0.19	0.78	2.19	0.19	0.13	0.02	0.03	0.05	0.82	0.07	0.06	0.00	0.07	0.45	0.46	4	0.63	0.16
W13/007847 (int)	0.11	0.22	0.17	0.76	1.98	0.20	0.08	0.01	0.02	0.03	0.60	0.07	0.05	0.00	0.04	0.21	0.14	3	0.62	0.18
W13/007848 (int)	0.13	0.05	0.04	0.79	1.70	0.30	0.13	0.04	0.04	0.07	0.71	0.08	0.06	0.00	0.07	0.48	0.38	3	0.65	0.18
W13/007877 (int)*	0.17	0.17	0.14	0.87	1.99	0.32	0.07	0.02	0.03	0.03	0.75	0.07	0.07	0.00	0.07	0.40	0.45	4	0.65	0.20
W13/007878 (int)	0.15	0.24	0.19	0.82	2.14	0.19	0.09	0.02	0.04	0.06	0.69	0.09	0.06	0.00	0.08	0.45	0.41	4	0.61	0.19

Sample ID	% C27 ααα 20R	% C28 ααα 20R	% C29 ααα 20R	C27 Dia/ (Dia+Reg)	(C21+C22)/ (C27+C28 +C29)	C27 Dia /Ster	% C27 αββ 20(R+S)	% C28 αββ 20(R+S)	% C29 αββ 20(R+S)	C29/C27 αββ Sterane Ratio	Tricyclic Terpanes/ Hopanes	Steranes/ Terpanes	% Tricyclic Terpanes	% Pentacyclic Terpanes	% Steranes	Steranes/ hopanes
Type IIIA waxy bitumen																
W13/007541 (ext)	31.95	14.47	53.58	0.67	0.09	0.82	35.67	20.70	43.63	1.22	0.20	0.03	16.28	80.51	3.22	0.04
W13/007541 (int)	32.09	17.20	50.71	0.64	0.11	0.74	38.33	22.10	39.56	1.03	0.20	0.04	15.80	80.57	3.63	0.05
W13/007683 (int)	36.23	20.14	43.63	0.59	0.11	0.74	40.69	20.75	38.56	0.95	0.23	0.05	17.95	77.12	4.92	0.06
W13/007684 (int)	35.45	20.23	44.31	0.57	0.13	0.65	40.59	21.95	37.46	0.92	0.19	0.04	15.58	80.41	4.01	0.05
W13/007692 (int)	36.80	19.43	43.76	0.59	0.11	0.75	40.42	20.88	38.70	0.96	0.23	0.05	17.88	77.48	4.65	0.06
W13/007698 (int)	35.33	20.64	44.02	0.60	0.11	0.75	39.44	20.05	40.50	1.03	0.22	0.04	16.99	78.75	4.26	0.05
W13/007698 (int dup)	33.26	20.87	45.87	0.58	0.10	0.68	39.28	21.04	39.68	1.01	0.19	0.05	15.45	79.82	4.72	0.06
W13/007778 (int)	38.31	12.98	48.71	0.60	0.14	0.76	39.98	19.79	40.23	1.01	0.22	0.04	17.38	78.79	3.83	0.05
W13/007847 (int)	27.41	23.30	49.29	0.52	0.06	0.50	34.38	23.48	42.14	1.23	0.13	0.06	10.67	83.68	5.65	0.07
W13/007848 (int)	47.95	12.98	39.07	0.59	0.15	0.80	42.50	19.56	37.94	0.89	0.23	0.04	17.75	78.45	3.81	0.05
W13/007877 (int)*	42.64	13.91	43.45	0.53	0.08	0.61	37.72	16.95	45.33	1.20	0.14	0.04	12.16	84.34	3.50	0.04
W13/007878 (int)	32.28	18.90	48.82	0.61	0.14	0.73	40.50	21.03	38.47	0.95	0.19	0.04	15.28	80.99	3.73	0.05

* = Most representative examples, i.e. least altered results due to low biomarker responses and/or alteration associated with weathering.

Table S6 (continued).

Sample ID	C19t/ C23t	C22t/ C21t	C22t/ C24t	C24t/ C23t	C26t/ C25t	C24tet /C23t	C23t/ C30 αβ	C24tet/ C30 αβ	C28BNH /C30 αβ	25-Nor/ C30 αβ	C29 αβ /C30 αβ	C30*/ C30 αβ	Ole/ C30 αβ	C30Ts/ C30 αβ	Gam/ C30 αβ	Gam/ C31 αβ (R)	C35 αβ/ C34 αβ	C35 Homohopane Index	Ts/ (Ts+Tm)	C29Ts/ (C29Ts +C29 αβ)
Type IIIA waxy bitumen (cont.)																				
W13/007900 (int)	0.06	0.07	0.04	0.84	1.88	0.18	0.09	0.02	0.04	0.06	0.72	0.08	0.05	0.00	0.07	0.43	0.45	4	0.64	0.22
W13/007902 (int)	0.12	0.08	0.05	0.84	2.26	0.36	0.09	0.03	0.04	0.06	0.71	0.09	0.07	0.00	0.08	0.44	0.45	4	0.61	0.19
/001055 (bulk)	0.07	0.09	0.05	0.93	1.77	0.42	0.09	0.04	0.04	0.06	0.71	0.10	0.07	0.00	0.08	0.46	0.42	4	0.66	0.25
Type IIIB waxy bitumen																				
W13/007605 (int)	0.30	0.33	0.35	0.67	1.63	0.55	0.17	0.09	0.04	0.09	0.48	0.34	0.10	0.00	0.10	0.73	0.43	4	0.66	0.39
W13/007895 (int)*	0.36	0.31	0.36	0.58	2.01	0.48	0.16	0.08	0.05	0.10	0.49	0.30	0.29	0.00	0.13	0.86	0.50	5	0.64	0.34
W13/007938 (int)	0.19	0.32	0.31	0.65	1.92	0.53	0.12	0.06	0.06	0.10	0.46	0.32	0.18	0.00	0.13	0.85	0.53	5	0.65	0.39
/001032 (bulk)	0.50	0.27	0.41	0.57	1.62	0.64	0.14	0.09	0.05	0.07	0.49	0.34	0.08	0.00	0.13	0.94	0.49	4	0.68	0.39
/001044B (bulk)	0.78	0.41	0.35	1.70	0.23	0.94	0.03	0.02	0.01	0.06	0.56	0.22	0.14	0.00	0.03	0.20	0.33	1	0.73	0.33

Sample ID	% C27 ααα 20R	% C28 ααα 20R	% C29 ααα 20R	C27 Dia/ (Dia+Reg)	(C21+C22)/ (C27+C28 +C29)	C27 Dia /Ster	% C27 αββ 20(R+S)	% C28 αββ 20(R+S)	% C29 αββ 20(R+S)	C29/C27 αββ Sterane Ratio	Tricyclic Terpanes/ Hopanes	Steranes/ Terpanes	% Tricyclic Terpanes	% Pentacyclic Terpanes	% Steranes	Steranes/ hopanes
Type IIIA waxy bitumen (cont.)																
W13/007900 (int)	34.76	11.97	53.26	0.64	0.08	0.77	40.21	20.75	39.04	0.97	0.18	0.04	14.47	82.09	3.44	0.04
W13/007902 (int)	35.99	17.89	46.12	0.56	0.10	0.63	39.40	22.15	38.45	0.98	0.17	0.04	13.81	82.04	4.14	0.05
/001055 (bulk)	25.88	19.78	54.34	0.63	0.14	0.63	31.66	25.08	43.26	1.37	0.17	0.04	14.16	81.80	4.03	0.05
Type IIIB waxy bitumen																
W13/007605 (int)	28.49	25.17	46.34	0.72	0.21	1.09	36.26	29.26	34.48	0.95	0.27	0.05	20.17	75.16	4.67	0.06
W13/007895 (int)*	32.84	14.58	52.58	0.64	0.18	0.92	39.41	24.48	36.11	0.92	0.24	0.04	18.32	77.83	3.85	0.05
W13/007938 (int)	28.98	21.74	49.27	0.62	0.13	0.83	37.53	24.77	37.70	1.00	0.18	0.04	14.78	81.51	3.71	0.05
/001032 (bulk)	26.82	27.70	45.48	0.69	0.20	0.91	36.03	27.66	36.31	1.01	0.22	0.03	17.82	79.20	2.98	0.04
/001044B (bulk)	37.05	6.24	56.72	0.08	0.11	0.04	15.69	24.12	60.19	3.84	0.10	0.07	8.80	84.79	6.41	0.08

* = Most representative examples, i.e. least altered results due to low biomarker responses and/or alteration associated with weathering.

Table S6 (continued).

Sample ID	C19t/ C23t	C22t/ C21t	C22t/ C24t	C24t/ C23t	C26t/ C25t	C24tet /C23t	C23t/ C30 αβ	C24tet/ C30 αβ	C28BNH /C30 αβ	25-Nor/ C30 αβ	C29 αβ /C30 αβ	C30*/ C30 αβ	Ole/ C30 αβ	C30Ts/ C30 αβ	Gam/ C30 αβ	Gam/ C31 αβ (R)	C35 αβ/ C34 αβ	C35 Homohopane Index	Ts/ (Ts+Tm)	C29Ts/ (C29Ts +C29 αβ)
Type IIIC waxy bitumen																				
W13/007695 (int)	0.09	0.06	0.04	0.85	1.65	0.08	0.48	0.04	0.16	0.20	0.77	0.11	0.12	0.01	0.07	0.48	0.56	7	0.67	0.23
W13/007697 (int)	0.04	0.06	0.04	0.88	1.81	0.09	0.26	0.02	0.09	0.11	0.67	0.09	0.06	0.00	0.06	0.45	0.38	5	0.60	0.21
W13/007700 (int)	0.08	0.05	0.03	0.87	1.70	0.12	0.34	0.04	0.11	0.11	0.71	0.09	0.06	0.00	0.07	0.50	0.36	4	0.59	0.22
W13/007920 (bulk)	0.04	0.15	0.11	0.90	1.56	0.13	0.39	0.05	0.16	0.18	0.76	0.10	0.12	0.00	0.07	0.50	0.46	6	0.62	0.23
Type IIIF waxy bitumen																				
W13/007867 (bulk)	0.09	0.04	0.03	0.89	0.92	0.05	0.76	0.04	0.12	0.17	0.74	0.16	0.11	0.00	0.07	0.48	0.34	4	0.64	0.21
Type IVC waxy bitumen																				
W13/007857A (int)	0.23	0.06	0.07	0.77	1.96	0.30	0.16	0.05	0.07	0.13	0.50	0.20	0.29	0.00	0.08	0.46	0.47	5	0.67	0.34

Sample ID	% C27 ααα 20R	% C28 ααα 20R	% C29 ααα 20R	C27 Dia/ (Dia+Reg)	(C21+C22)/ (C27+C28 +C29)	C27 Dia /Ster	% C27 αββ 20(R+S)	% C28 αββ 20(R+S)	% C29 αββ 20(R+S)	C29/C27 αββ Sterane Ratio	Tricyclic Terpanes/ Hopanes	Steranes/ Terpanes	% Tricyclic Terpanes	% Pentacyclic Terpanes	% Steranes	Steranes/ hopanes
Type IIIC waxy bitumen																
W13/007695 (int)	34.04	25.30	40.66	0.48	0.13	0.46	38.92	24.03	37.05	0.95	0.76	0.04	41.40	54.47	4.13	0.08
W13/007697 (int)*	39.30	21.06	39.63	0.47	0.09	0.50	41.92	21.54	36.54	0.87	0.47	0.03	31.02	65.79	3.19	0.05
W13/007700 (int)*	39.91	21.75	38.34	0.48	0.17	0.48	43.86	21.17	34.98	0.80	0.57	0.04	35.12	61.43	3.45	0.06
W13/007920 (bulk)	43.22	13.15	43.63	0.45	0.11	0.45	39.07	22.60	38.33	0.98	0.69	0.03	39.40	57.45	3.15	0.05
Type IIIF waxy bitumen																
W13/007867 (bulk)*	24.72	22.15	53.13	0.59	0.28	0.62	25.29	28.14	46.57	1.84	0.92	0.03	46.50	50.36	3.15	0.06
Type IVC waxy bitumen																
W13/007857A (int)*	25.05	22.76	52.19	0.64	0.14	0.85	35.48	20.08	44.44	1.25	0.25	0.07	18.97	74.69	6.34	0.08

* = Most representative examples, i.e. least altered results due to low biomarker responses and/or alteration associated with weathering.

4.5. Waxy oils of fluvio-deltaic source affinity (types IIID, IVB and Sandy River tars)

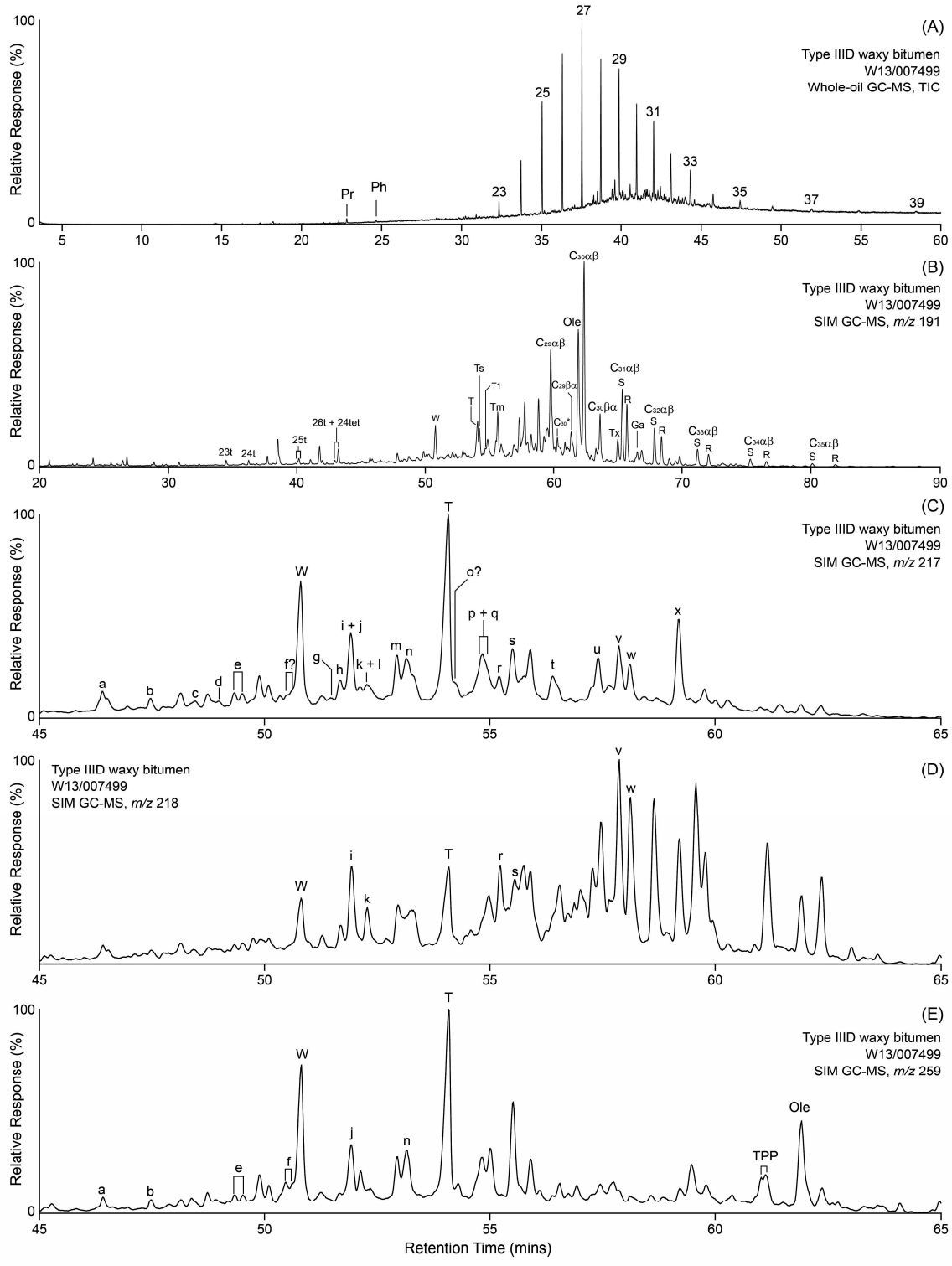


Figure S10: Representative chromatograms of the least weathered type IIID waxy bitumen (W13/007499). (A) Whole-oil GC-MS total ion chromatogram. (B) Saturated fraction SIM GC-MS *m/z* 191 chromatogram. (C) Saturated fraction SIM GC-MS *m/z* 217 chromatogram. (D) Saturated fraction SIM GC-MS *m/z* 218 chromatogram. (E) Saturated fraction SIM GC-MS *m/z* 259 chromatogram.

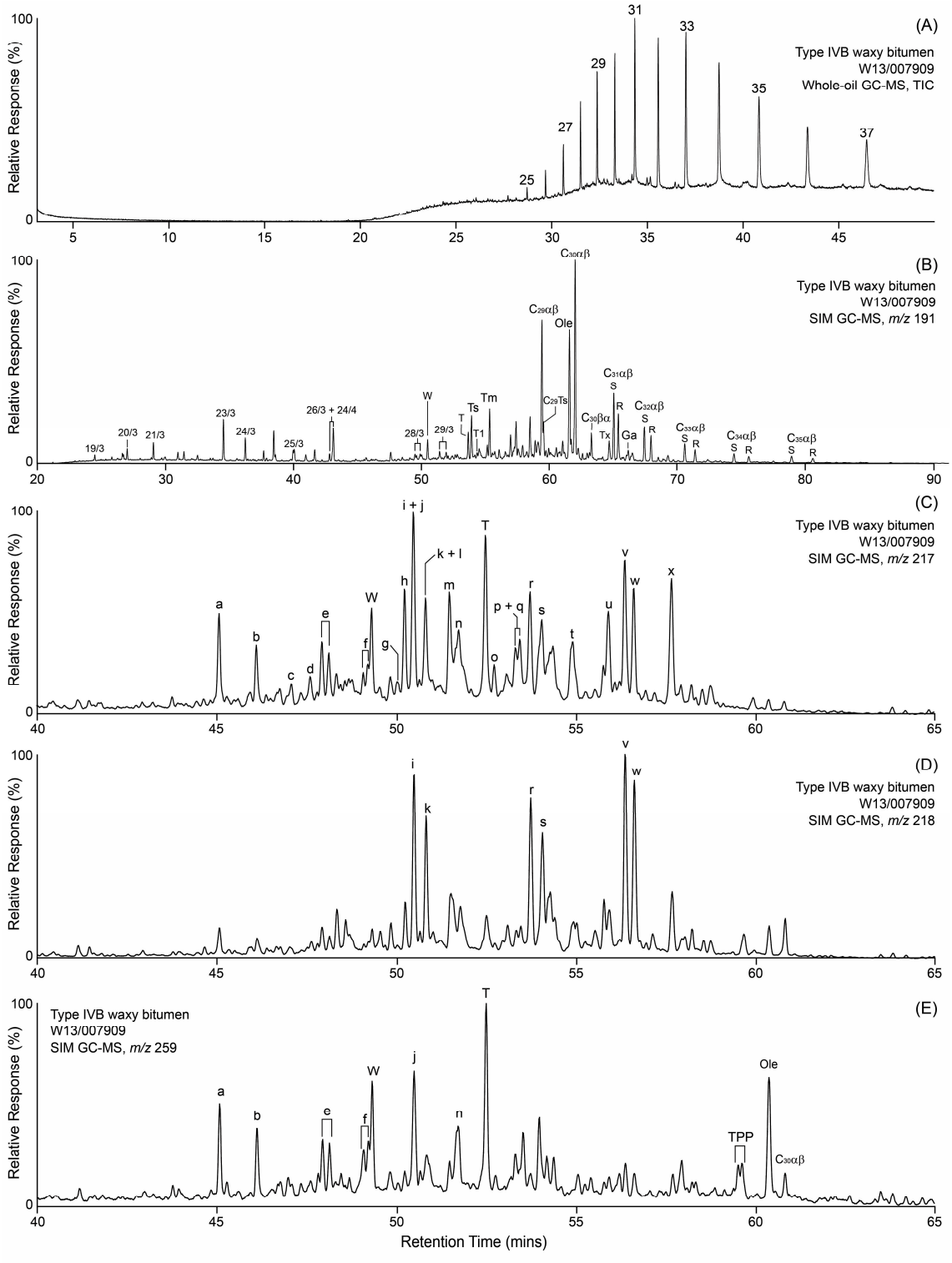


Figure S11: Representative chromatograms of the least weathered type IVB waxy bitumen (W13/007909). (A) Whole-oil GC-MS total ion chromatogram. (B) Saturated fraction SIM GC-MS *m/z* 191 chromatogram. (C) Saturated fraction SIM GC-MS *m/z* 217 chromatogram. (D) Saturated fraction SIM GC-MS *m/z* 218 chromatogram. (E) Saturated fraction SIM GC-MS *m/z* 259 chromatogram.

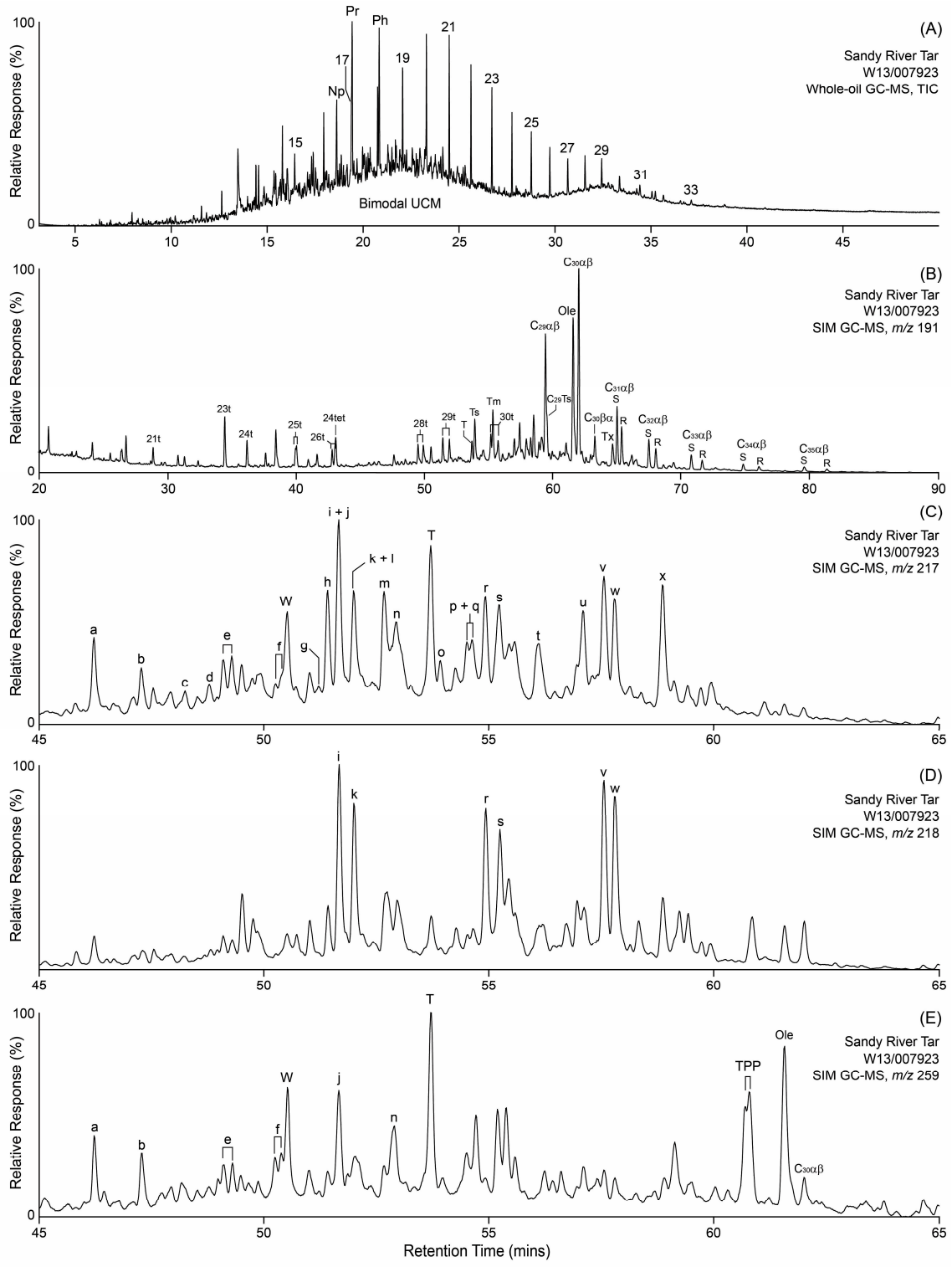


Figure S12: Representative chromatograms from Sandy River tar sample W13/007923. (A) Whole-oil GC-MS total ion chromatogram. (B) Saturated fraction SIM GC-MS *m/z* 191 chromatogram. (C) Saturated fraction SIM GC-MS *m/z* 217 chromatogram. (D) Saturated fraction SIM GC-MS *m/z* 218 chromatogram. (E) Saturated fraction SIM GC-MS *m/z* 259 chromatogram.

Table S7: Selected biomarker parameters from waxy oils of fluvio-deltaic source affinity (waxy bitumen types IIID, IVB and the Sandy River tars), int = sample interior, ext = sample exterior (top 2mm), bulk = sample includes interior and exterior.

Sample ID	C19t/ C23t	C22t/ C21t	C22t/ C24t	C24t/ C23t	C26t/ C25t	C24tet /C23t	C23t/ C30 αβ	C24tet/ C30 αβ	C28BNH /C30 αβ	25-Nor/ C30 αβ	C29 αβ /C30 αβ	C30*/ C30 αβ	Ole/ C30 αβ	C30Ts/ C30 αβ	Gam/ C30 αβ	Gam/ C31 αβ (R)	C35 αβ/ C34 αβ	C35 Homohopane Index	Ts/ (Ts+Tm)	C29Ts/ (C29Ts +C29 αβ)
Type IIID waxy bitumen																				
W13/007499 (ext)	1.13	0.84	0.57	0.89	1.60	2.49	0.01	0.02	0.06	0.19	0.52	0.03	0.76	0.02	0.05	0.21	0.40	2	0.57	0.12
W13/007499 (int)*	1.20	0.90	0.64	0.88	0.96	3.14	0.02	0.06	0.06	0.26	0.50	0.07	0.75	0.00	0.06	0.19	0.45	3	0.41	0.12
W13/007869 (bulk)	1.00	1.07	0.61	0.82	1.22	1.75	0.03	0.06	0.09	0.27	0.60	0.06	0.86	0.03	0.07	0.23	0.43	3	0.31	0.13
W13/007910 (bulk)	1.28	0.08	0.06	0.89	1.21	2.06	0.02	0.04	0.10	0.24	0.50	0.07	0.78	0.05	0.06	0.20	0.43	3	0.23	0.15
Type IVB waxy bitumen																				
W13/007891 (bulk)	1.03	0.19	0.18	0.85	1.11	6.10	0.00	0.01	0.04	0.23	0.44	0.08	0.84	0.00	0.05	0.20	0.61	5	0.40	0.20
W13/007909 (int)*	0.12	0.48	0.32	0.55	0.79	0.83	0.18	0.15	0.07	0.23	0.73	0.05	0.82	0.05	0.06	0.24	0.84	6	0.50	0.17

Sample ID	% C27 ααα 20R	% C28 ααα 20R	% C29 ααα 20R	C27 Dia/ (Dia+Reg)	(C21+C22)/ (C27+C28 +C29)	C27 Dia /Ster	% C27 αββ 20(R+S)	% C28 αββ 20(R+S)	% C29 αββ 20(R+S)	C29/C27 αββ Sterane Ratio	Tricyclic Terpanes/ Hopanes	Steranes/ Terpanes	% Tricyclic Terpanes	% Pentacyclic Terpanes	% Steranes	Steranes/ hopanes
Type IIID waxy bitumen																
W13/007499 (ext)	21	21	58	0.28	0.02	0.26	17	20	63	3.70	0.05	0.07	5	89	7	0.07
W13/007499 (int)*	26	16	58	0.30	0.04	0.30	25	19	56	2.25	0.07	0.09	6	86	9	0.10
W13/007869 (bulk)	31	11	59	0.28	0.05	0.27	22	15	63	2.90	0.10	0.10	8	83	9	0.11
W13/007910 (bulk)	29	11	60	0.34	0.03	0.34	21	16	63	2.95	0.08	0.08	7	85	7	0.09
Type IVB waxy bitumen																
W13/007891 (bulk)	15	26	59	0.23	0.01	0.16	10	21	69	6.90	0.01	0.03	1	96	3	0.03
W13/007909 (int)*	38	18	44	0.40	0.15	0.37	31	28	41	1.29	0.19	0.22	13	69	18	0.26

* = Most representative examples, i.e. least altered results due to low biomarker responses and/or alteration associated with weathering.

Table S7 (continued)

Sample ID	C19t/ C23t	C22t/ C21t	C22t/ C24t	C24t/ C23t	C26t/ C25t	C24tet /C23t	C23t/ C30 αβ	C24tet/ C30 αβ	C28BNH /C30 αβ	25-Nor/ C30 αβ	C29 αβ /C30 αβ	C30*/ C30 αβ	Ole/ C30 αβ	C30Ts/ C30 αβ	Gam/ C30 αβ	Gam/ C31 αβ (R)	C35 αβ/ C34 αβ	C35 Homohopane Index	Ts/ (Ts+Tm)	C29Ts/ (C29Ts +C29 αβ)
Sandy River Tars																				
W13/007923 (bulk)*	0.23	0.01	0.01	0.53	0.97	0.46	0.23	0.11	0.10	0.22	0.61	0.02	0.79	0.07	0.06	0.29	0.80	6	0.49	0.19
W13/007928 (bulk)	0.24	0.66	0.31	0.54	0.95	0.42	0.22	0.09	0.10	0.20	0.62	0.03	0.84	0.06	0.06	0.33	0.79	6	0.49	0.18
W13/007929 (bulk)	0.31	0.47	0.33	0.49	1.17	0.35	0.23	0.08	0.09	0.22	0.60	0.03	0.80	0.06	0.07	0.35	0.77	5	0.48	0.22
W13/007932 (bulk)	0.23	0.63	0.34	0.52	1.07	0.37	0.23	0.09	0.14	0.23	0.62	0.04	0.90	0.06	0.07	0.32	0.73	5	0.47	0.15
W13/007937 (bulk)	0.04	0.53	0.28	0.48	1.01	0.33	0.40	0.13	0.13	0.22	0.59	0.03	0.84	0.04	0.07	0.35	0.70	5	0.47	0.17
W13/007937B (bulk)	0.27	0.62	0.37	0.53	1.14	0.39	0.23	0.09	0.11	0.23	0.63	0.04	0.88	0.06	0.07	0.31	0.73	5	0.46	0.15
W13/007944 (bulk)	0.30	0.66	0.33	0.52	1.22	0.40	0.20	0.08	0.10	0.21	0.62	0.02	0.83	0.07	0.06	0.33	0.70	5	0.46	0.18
W13/007953 (bulk)	0.23	0.76	0.39	0.47	1.11	0.35	0.22	0.08	0.10	0.20	0.57	0.02	0.80	0.06	0.05	0.28	0.76	5	0.46	0.21

Sample ID	% C27 ααα 20R	% C28 ααα 20R	% C29 ααα 20R	C27 Dia/ (Dia+Reg)	(C21+C22)/ (C27+C28 +C29)	C27 Dia /Ster	% C27 αββ 20(R+S)	% C28 αββ 20(R+S)	% C29 αββ 20(R+S)	C29/C27 αββ Sterane Ratio	Tricyclic Terpanes/ Hopanes	Steranes/ Terpanes	% Tricyclic Terpanes	% Pentacyclic Terpanes	% Steranes	Steranes/ hopanes
Sandy River Tars																
W13/007923 (bulk)*	38	27	35	0.34	0.15	0.30	37	27	37	1.01	0.31	0.18	20	65	15	0.23
W13/007928 (bulk)	33	25	41	0.36	0.15	0.33	34	29	37	1.06	0.31	0.18	20	65	15	0.24
W13/007929 (bulk)	35	26	39	0.33	0.15	0.29	36	26	38	1.05	0.31	0.17	20	65	14	0.22
W13/007932 (bulk)	36	26	38	0.36	0.16	0.32	36	26	38	1.04	0.31	0.18	20	65	15	0.23
W13/007937 (bulk)	43	22	34	0.39	0.28	0.38	37	28	35	0.96	0.44	0.19	25	58	16	0.27
W13/007937B (bulk)	38	27	35	0.33	0.16	0.27	36	25	38	1.05	0.31	0.17	20	65	15	0.22
W13/007944 (bulk)	34	24	42	0.35	0.17	0.30	34	27	39	1.13	0.28	0.15	19	68	13	0.19
W13/007953 (bulk)	33	25	42	0.35	0.15	0.32	35	28	37	1.04	0.31	0.18	20	65	15	0.23

* = Most representative examples, i.e. least altered results due to low biomarker responses and/or alteration associated with weathering.

4.6. Waxy oils of marine shale source affinity (types IIIE and IVA)

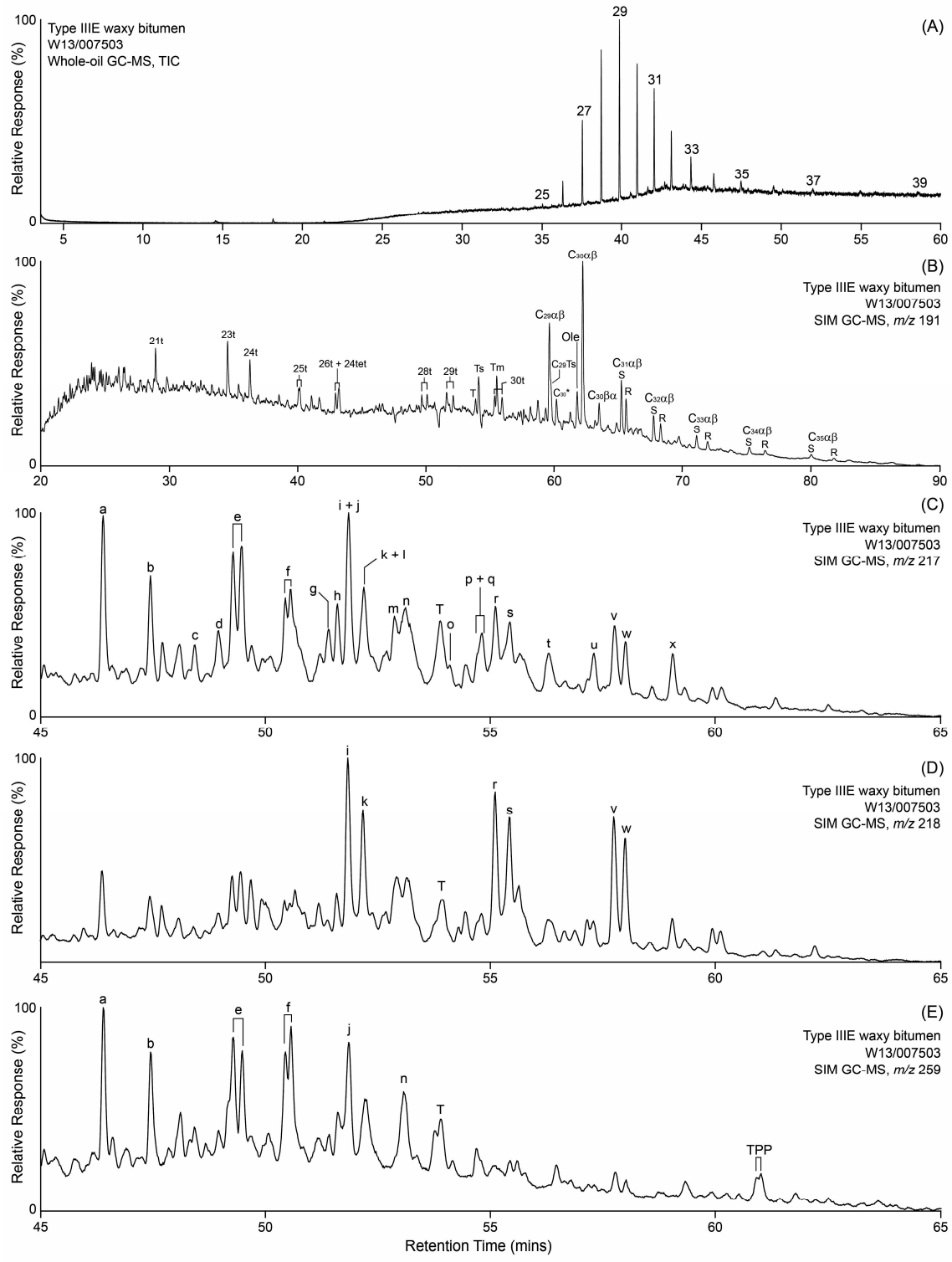


Figure S13: Chromatograms from the only identified type IIIE waxy bitumen (W13/007503). (A) Whole-oil GC-MS total ion chromatogram. (B) Saturated fraction SIM GC-MS *m/z* 191 chromatogram. (C) Saturated fraction SIM GC-MS *m/z* 217 chromatogram. (D) Saturated fraction SIM GC-MS *m/z* 218 chromatogram. (E) Saturated fraction SIM GC-MS *m/z* 259 chromatogram.

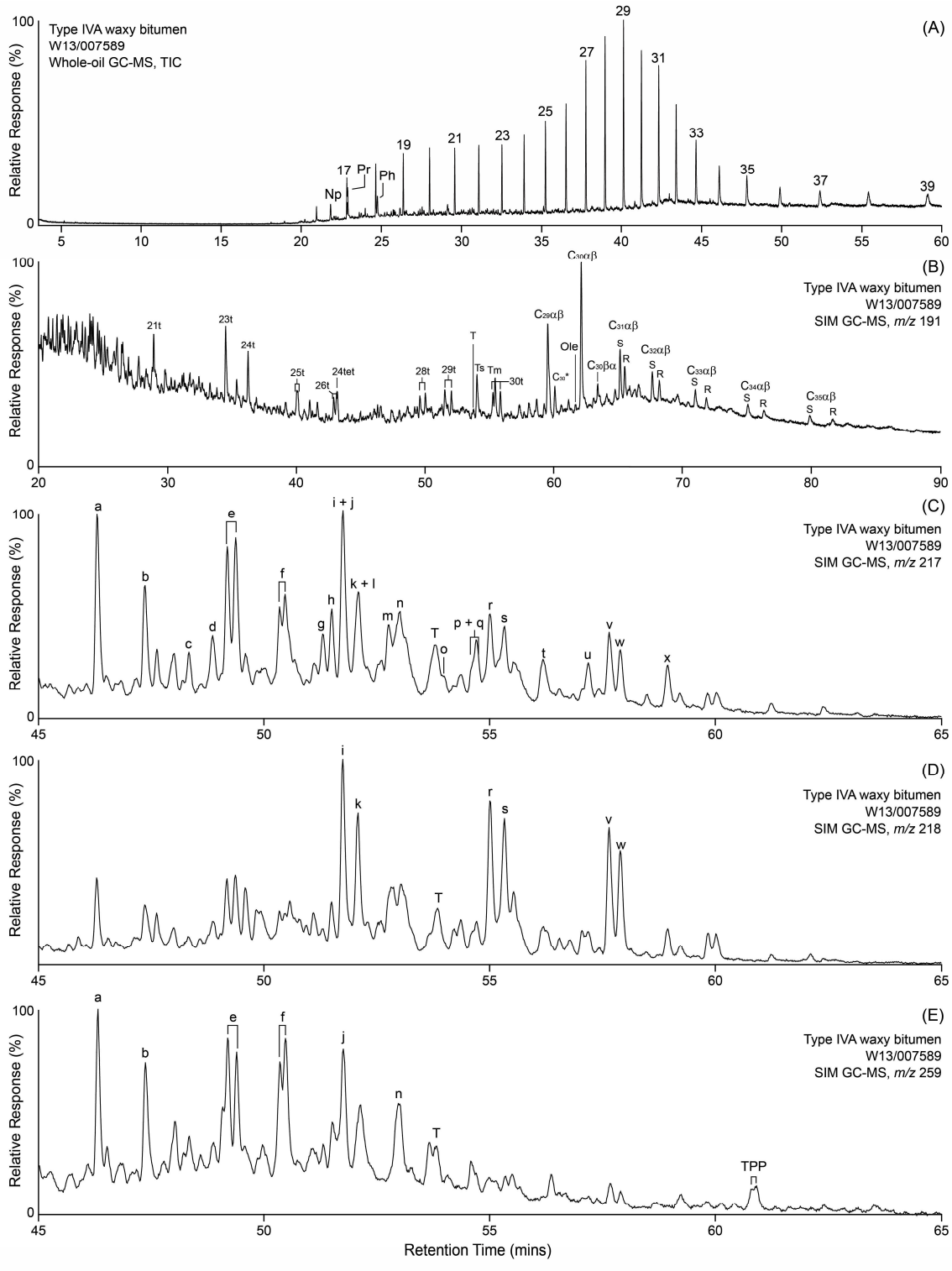


Figure S14: Chromatograms from the least weathered type IVA waxy bitumen (W13/007589). (A) Whole-oil GC-MS total ion chromatogram. (B) Saturated fraction SIM GC-MS *m/z* 191 chromatogram. Note that although this represents the least weathered sample the hopane and terpane responses were low. See Figure S15 for a second example with higher responses. (C) Saturated fraction SIM GC-MS *m/z* 217 chromatogram. (D) Saturated fraction SIM GC-MS *m/z* 218 chromatogram. (E) Saturated fraction SIM GC-MS *m/z* 259 chromatogram.

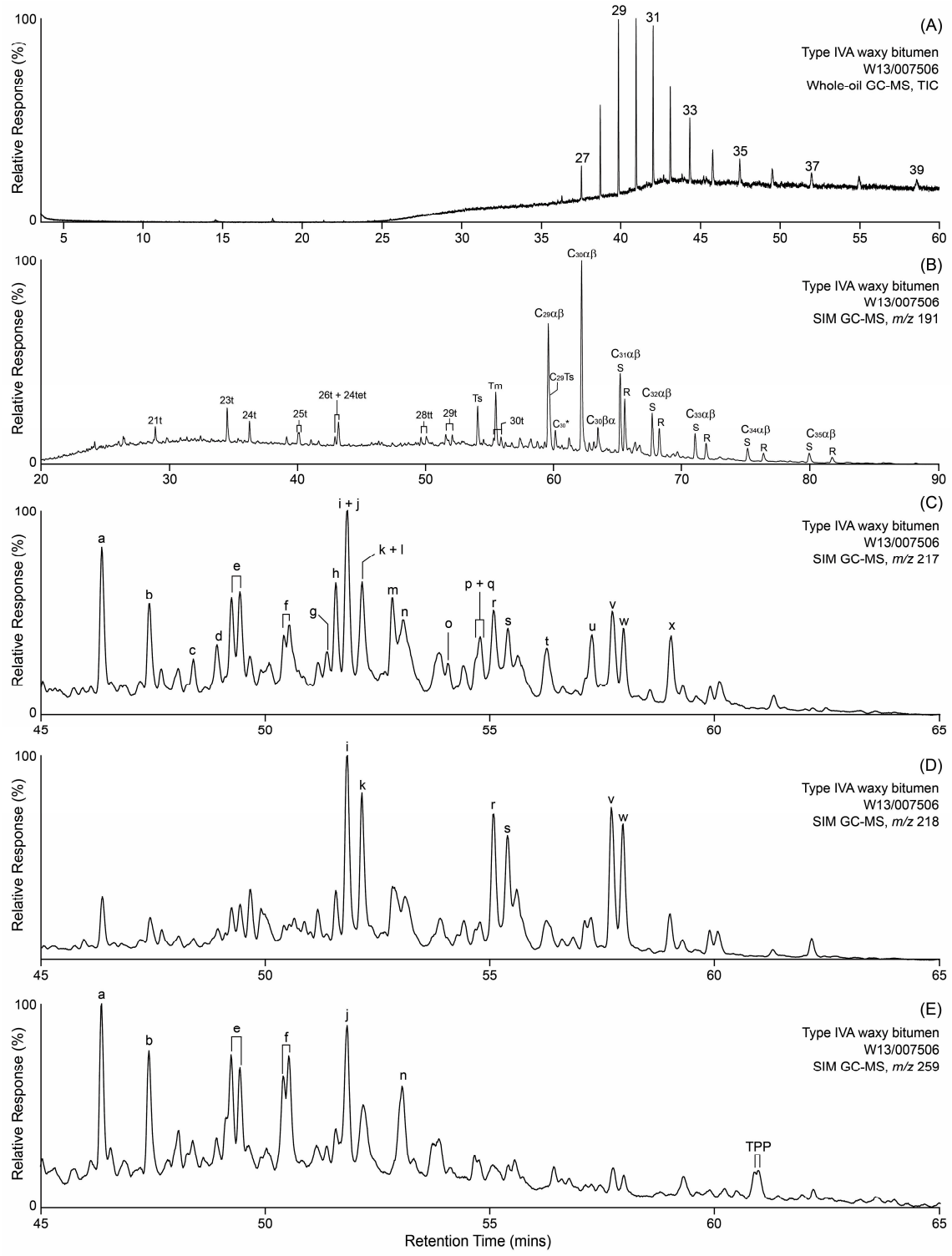


Figure S15: Chromatograms from a type IVA waxy bitumen (W13/007506) which exhibits greater terpane and hopane responses than the least weathered example shown in Figure S14. Note that the majority of type IVA waxy bitumens contained extremely low responses for the terpanes and hopanes. (A) Whole-oil GC-MS total ion chromatogram. (B) Saturated fraction SIM GC-MS *m/z* 191 chromatogram. (C) Saturated fraction SIM GC-MS *m/z* 217 chromatogram. (D) Saturated fraction SIM GC-MS *m/z* 218 chromatogram. (E) Saturated fraction SIM GC-MS *m/z* 259 chromatogram.

Table S8: Selected biomarker parameters from waxy oils of marine shale source affinity (waxy bitumen types IIIE and IVA), int = sample interior, ext = sample exterior (top 2mm).

Sample ID	C19t/ C23t	C22t/ C21t	C22t/ C24t	C24t/ C23t	C26t/ C25t	C24tet /C23t	C23t/ C30 αβ	C24tet/ C30 αβ	C28BNH /C30 αβ	25-Nor/ C30 αβ	C29 αβ /C30 αβ	C30*/ C30 αβ	Ole/ C30 αβ	C30Ts/ C30 αβ	Gam/ C30 αβ	Gam/ C31 αβ (R)	C35 αβ/ C34 αβ	C35 Homohopane Index	Ts/ (Ts+Tm)	C29Ts/ (C29Ts +C29 αβ)
Type IIIE waxy bitumen																				
W13/007503 (ext)	0.29	0.14	0.10	0.63	1.26	0.17	0.37	0.06	0.10	0.10	0.64	0.18	0.05	0.03	0.06	0.26	1.15	20	0.57	0.24
W13/007503 (int)*	0.17	0.21	0.18	0.61	1.51	0.21	0.35	0.07	0.06	0.16	0.64	0.16	0.19	0.00	0.01	0.05	0.78	7	0.58	0.20
Type IVA waxy bitumen																				
W13/007491 (ext)	0.31	0.15	0.13	0.70	0.88	0.87	0.06	0.05	0.00	0.03	0.76	0.02	0.00	0.03	0.05	0.29	0.57	5	0.48	0.16
W13/007491 (int)	0.23	0.30	0.28	0.62	1.25	0.89	0.07	0.06	0.01	0.02	0.67	0.04	0.01	0.00	0.04	0.26	0.53	5	0.43	0.17
W13/007506 (ext)	0.03	0.09	0.05	0.64	1.10	0.24	0.43	0.10	0.13	0.12	0.60	0.21	n.d.	0.08	0.08	0.33	0.77	8	0.50	0.27
W13/007506 (int)*	0.14	0.30	0.20	0.56	1.05	0.55	0.17	0.09	0.00	0.04	0.63	0.09	0.01	0.01	0.05	0.16	0.83	8	0.44	0.21
W13/007589 (int)*	0.23	0.14	0.08	0.60	1.25	0.12	0.61	0.07	0.00	0.13	0.65	0.25	n.d.	0.03	0.08	0.29	0.63	9	0.56	0.25
W13/007590 (ext)	0.09	0.11	0.07	0.61	0.97	0.15	0.69	0.11	0.06	0.15	0.56	0.26	n.d.	0.03	0.02	0.10	0.61	6	0.56	0.23
W13/007590 (int)	0.17	0.07	0.06	0.56	1.09	0.21	0.56	0.12	0.00	0.13	0.54	0.27	n.d.	0.00	0.07	0.36	0.76	9	0.52	0.25
W13/007969 (int)	0.00	N/A	0.00	0.43	2.53	0.14	0.31	0.04	0.06	0.00	0.59	0.21	n.d.	0.01	0.02	0.10	0.75	6	0.40	0.15
W13/007973 (int)	0.00	0.00	0.00	0.79	1.73	0.15	0.36	0.05	0.12	0.08	0.59	0.23	n.d.	0.00	0.03	0.17	0.76	6	0.60	0.19

Sample ID	% C27 ααα 20R	% C28 ααα 20R	% C29 ααα 20R	C27 Dia/ (Dia+Reg)	(C21+C22)/ (C27+C28 +C29)	C27 Dia /Ster	% C27 αββ 20(R+S)	% C28 αββ 20(R+S)	% C29 αββ 20(R+S)	C29/C27 αββ Sterane Ratio	Tricyclic Terpanes/ Hopanes	Steranes/ Terpanes	% Tricyclic Terpanes	% Pentacyclic Terpanes	% Steranes	Steranes/ hopanes
Type IIIE waxy bitumen																
W13/007503 (ext)	37	31	33	0.69	0.46	0.88	35	33	33	0.93	0.35	0.78	15	42	44	1.06
W13/007503 (int)*	35	32	33	0.69	0.39	0.90	35	33	32	0.92	0.39	0.90	15	38	47	1.25
Type IVA waxy bitumen																
W13/007491 (ext)	33	22	45	0.43	0.10	0.37	26	31	44	1.67	0.11	0.22	8	74	18	0.24
W13/007491 (int)	38	26	36	0.49	0.11	0.50	40	25	35	0.87	0.13	0.29	9	68	23	0.33
W13/007506 (ext)	26	41	33	0.73	0.48	0.97	35	34	31	0.90	0.44	1.30	13	30	57	1.87
W13/007506 (int)*	35	31	34	0.58	0.28	0.66	37	29	34	0.91	0.19	0.63	10	52	39	0.75
W13/007589 (int)*	33	37	30	0.72	0.62	0.91	38	31	31	0.83	0.52	1.48	14	26	60	2.26
W13/007590 (ext)	31	41	28	0.74	0.55	1.08	37	34	29	0.79	0.84	1.69	17	20	63	3.10
W13/007590 (int)	28	40	32	0.74	0.43	0.98	36	33	31	0.84	0.62	1.52	15	24	60	2.47
W13/007969 (int)	37	31	32	0.71	0.51	0.96	34	35	30	0.89	0.42	1.65	11	27	62	2.33
W13/007973 (int)	41	29	30	0.72	0.51	0.98	39	33	29	0.74	0.50	1.61	13	25	62	2.43

* = Most representative examples, i.e. least altered results due to low biomarker responses and/or alteration associated with weathering.

Table S8 (continued)

Sample ID	C19t/ C23t	C22t/ C21t	C22t/ C24t	C24t/ C23t	C26t/ C25t	C24tet /C23t	C23t/ C30 αβ	C24tet/ C30 αβ	C28BNH /C30 αβ	25-Nor/ C30 αβ	C29 αβ /C30 αβ	C30*/ C30 αβ	Ole/ C30 αβ	C30Ts/ C30 αβ	Gam/ C30 αβ	Gam/ C31 αβ (R)	C35 αβ/ C34 αβ	C35 Homohopane Index	Ts/ (Ts+Tm)	C29Ts/ (C29Ts +C29 αβ)
Type IVA waxy bitumen (cont.)																				
W13/007974 (bulk)	0.13	0.03	0.02	0.72	0.99	0.16	0.60	0.10	0.13	0.12	0.58	0.28	0.03	0.05	0.03	0.17	0.58	6	0.60	0.22
W13/007975 (int)	0.47	0.19	0.14	0.68	1.26	0.14	0.48	0.07	0.09	0.13	0.59	0.25	n.d.	0.05	0.03	0.15	0.92	8	0.54	0.22
W13/007984 (int)	0.16	0.19	0.19	0.56	1.30	0.18	0.51	0.09	0.08	0.07	0.62	0.22	n.d.	0.00	0.02	0.12	0.58	5	0.59	0.23
W13/007985 (int)	0.13	0.00	0.00	0.61	1.73	0.15	0.46	0.07	0.09	0.10	0.56	0.25	n.d.	0.00	0.02	0.14	0.32	4	0.54	0.24

Sample ID	% C27 ααα 20R	% C28 ααα 20R	% C29 ααα 20R	C27 Dia/ (Dia+Reg)	(C21+C22)/ (C27+C28 +C29)	C27 Dia /Ster	% C27 αββ 20(R+S)	% C28 αββ 20(R+S)	% C29 αββ 20(R+S)	C29/C27 αββ Sterane Ratio	Tricyclic Terpanes/ Hopanes	Steranes/ Terpanes	% Tricyclic Terpanes	% Pentacyclic Terpanes	% Steranes	Steranes/ hopanes
Type IVA waxy bitumen (cont.)																
W13/007974 (bulk)	31	34	35	0.75	0.70	0.82	26	40	34	1.30	0.73	1.47	17	23	60	2.54
W13/007975 (int)	31	39	30	0.72	0.47	0.99	36	36	29	0.80	0.68	1.47	16	24	60	2.47
W13/007984 (int)	30	35	35	0.73	0.63	1.09	33	35	32	0.97	0.64	1.48	16	25	60	2.43
W13/007985 (int)	44	21	35	0.74	0.65	1.07	36	31	33	0.93	0.59	1.49	15	25	60	2.36

4.7. Waxy oils of marine carbonate source affinity (types IVD and IVE)

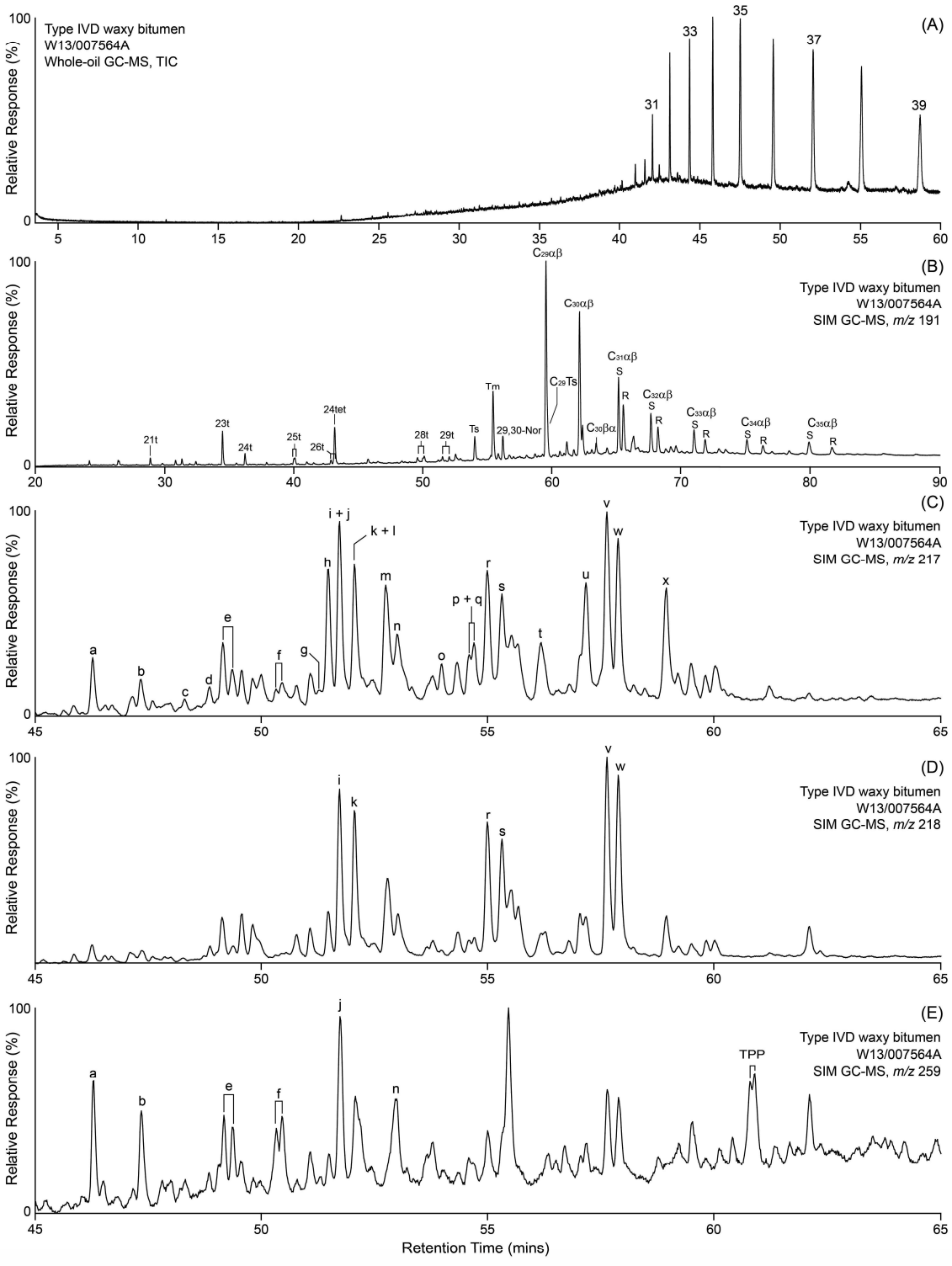


Figure S16: Chromatograms from the most representative type IVD waxy bitumen (W13/007564A). (A) Whole-oil GC-MS total ion chromatogram. (B) Saturated fraction SIM GC-MS *m/z* 191 chromatogram. (C) Saturated fraction SIM GC-MS *m/z* 217 chromatogram. (D) Saturated fraction SIM GC-MS *m/z* 218 chromatogram. (E) Saturated fraction SIM GC-MS *m/z* 259 chromatogram.

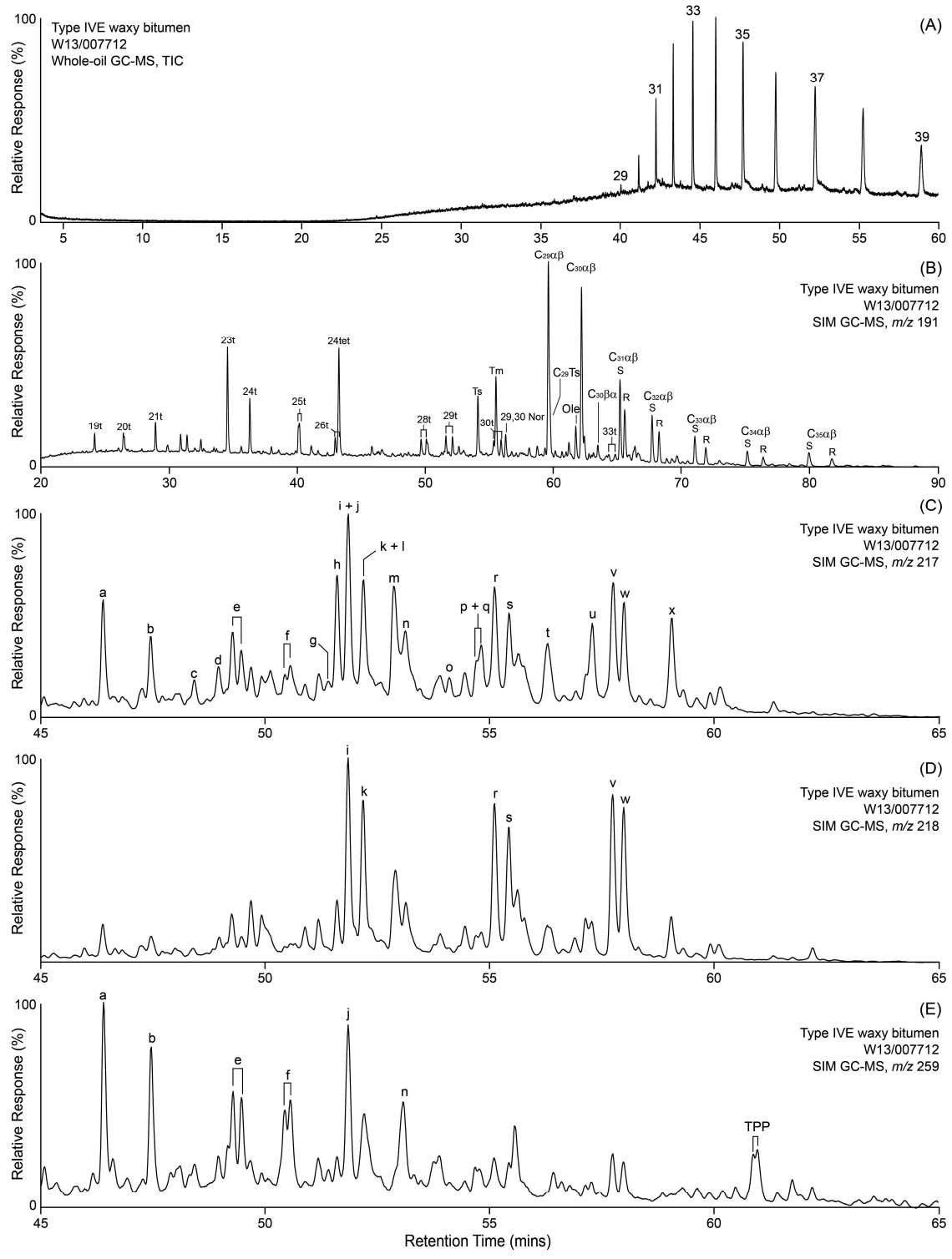


Figure S17: Chromatograms from the least weathered type IVE waxy bitumen (W13/007712). (A) Whole-oil GC-MS total ion chromatogram. (B) Saturated fraction SIM GC-MS *m/z* 191 chromatogram. (C) Saturated fraction SIM GC-MS *m/z* 217 chromatogram. (D) Saturated fraction SIM GC-MS *m/z* 218 chromatogram. (E) Saturated fraction SIM GC-MS *m/z* 259 chromatogram.

Table S9: Selected biomarker parameters from waxy oils of marine carbonate source affinity (waxy bitumen types IVD and IVE), int = sample interior, ext = sample exterior (top 2mm), bulk = sample includes interior and exterior.

Sample ID	C19t/ C23t	C22t/ C21t	C22t/ C24t	C24t/ C23t	C26t/ C25t	C24tet /C23t	C23t/ C30 αβ	C24tet/ C30 αβ	C28BNH /C30 αβ	25-Nor/ C30 αβ	C29 αβ /C30 αβ	C30*/ C30 αβ	Ole/ C30 αβ	C30Ts/ C30 αβ	Gam/ C30 αβ	Gam/ C31 αβ (R)	C35 αβ/ C34 αβ	C35 Homohopane Index	Ts/ (Ts+Tm)	C29Ts/ (C29Ts +C29 αβ)
Type IVD waxy bitumen																				
W13/007564A (int)*	0.10	0.64	0.34	0.36	0.82	1.01	0.18	0.18	0.00	0.02	1.26	0.01	n.d.	0.18	0.11	0.31	0.97	9	0.24	0.07
W13/007736 (int)	0.14	0.42	0.26	0.42	0.57	0.94	0.32	0.30	0.03	0.03	1.43	0.01	n.d.	0.15	0.10	0.31	0.96	9	0.24	0.04
W13/007749H (bulk)	0.09	0.87	0.46	0.34	0.72	1.63	0.12	0.19	0.01	0.02	1.41	0.01	n.d.	0.18	0.12	0.30	0.91	7	0.27	0.05
W13/007818B (bulk)	0.05	1.14	0.38	0.41	0.78	1.12	0.13	0.14	0.01	0.02	1.23	0.03	n.d.	0.18	0.12	0.29	1.00	9	0.38	0.09
W13/007837 (bulk)	0.11	0.79	0.46	0.33	0.88	1.23	0.17	0.21	0.01	0.02	1.47	0.02	n.d.	0.20	0.13	0.29	0.95	7	0.26	0.07
Type IVE waxy bitumen																				
W13/007712 (bulk)	0.11	0.47	0.25	0.52	0.69	0.98	0.50	0.49	0.06	0.06	1.10	0.04	0.18	0.11	0.10	0.29	1.07	10	0.43	0.15
W13/007881 (bulk)*	0.15	0.42	0.26	0.51	0.58	0.99	0.41	0.41	0.06	0.06	1.10	0.03	0.18	0.12	0.10	0.29	1.06	10	0.43	0.12

Sample ID	% C27 ααα 20R	% C28 ααα 20R	% C29 ααα 20R	C27 Dia/ (Dia+Reg)	(C21+C22)/ (C27+C28 +C29)	C27 Dia /Ster	% C27 αββ 20(R+S)	% C28 αββ 20(R+S)	% C29 αββ 20(R+S)	C29/C27 αββ Sterane Ratio	Tricyclic Terpanes/ Hopanes	Steranes/ Terpanes	% Tricyclic Terpanes	% Pentacyclic Terpanes	% Steranes	Steranes/ hopanes
Type IVD waxy bitumen																
W13/007564A (int)*	42.29	23.74	33.97	0.24	0.20	0.18	32.97	24.89	42.14	1.28	0.13	0.21	9.74	72.98	17.29	0.24
W13/007736 (int)	35.40	28.36	36.24	0.20	0.26	0.17	21.46	34.27	44.28	2.06	0.24	0.31	14.92	61.17	23.91	0.39
W13/007749H (bulk)	35.79	19.69	44.52	0.18	0.14	0.13	24.14	24.86	50.99	2.11	0.10	0.16	7.57	79.00	13.42	0.17
W13/007818B (bulk)	21.36	22.99	55.65	0.12	0.03	0.08	7.81	25.95	66.24	8.48	0.10	0.18	7.40	77.61	15.00	0.19
W13/007837 (bulk)	33.49	22.95	43.55	0.18	0.17	0.13	21.88	27.54	50.58	2.31	0.12	0.15	9.14	77.69	13.16	0.17
Type IVE waxy bitumen																
W13/007712 (bulk)	42.63	26.21	31.16	0.39	0.21	0.38	34.77	29.93	35.31	1.02	0.43	0.52	19.76	46.07	34.17	0.74
W13/007881 (bulk)*	40.46	26.06	33.47	0.33	0.22	0.29	32.42	30.54	37.04	1.14	0.37	0.43	18.74	51.00	30.25	0.59

* = Most representative examples, i.e. least altered results due to low biomarker responses and/or alteration associated with weathering.

4.8. Waxy oil of mixed lacustrine/marine carbonate source affinity (type II)

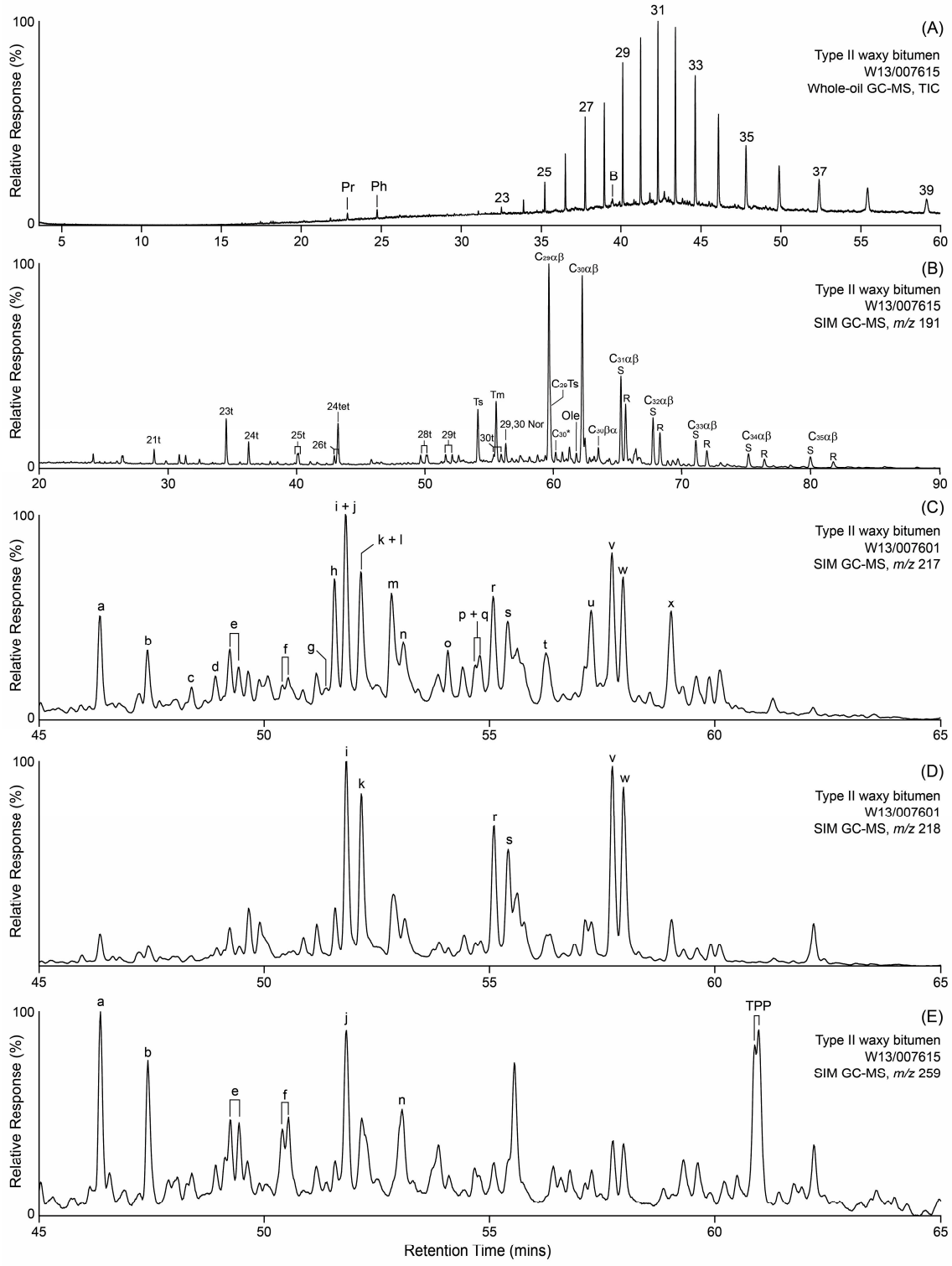


Figure S18: Chromatograms from the least weathered type II waxy bitumen (W13/007615). (A) Whole-oil GC-MS total ion chromatogram. (B) Saturated fraction SIM GC-MS *m/z* 191 chromatogram. (C) Saturated fraction SIM GC-MS *m/z* 217 chromatogram. (D) Saturated fraction SIM GC-MS *m/z* 218 chromatogram. (E) Saturated fraction SIM GC-MS *m/z* 259 chromatogram.

Table S10: Selected biomarker parameters from waxy oil of mixed lacustrine/marine carbonate source affinity (type II waxy bitumen), int = sample interior, ext = sample exterior (top 2mm).

Sample ID	C19t/ C23t	C22t/ C21t	C22t/ C24t	C24t/ C23t	C26t/ C25t	C24tet /C23t	C23t/ C30 αβ	C24tet/ C30 αβ	C28BNH /C30 αβ	25-Nor/ C30 αβ	C29 αβ /C30 αβ	C30*/ C30 αβ	Ole/ C30 αβ	C30Ts/ C30 αβ	Gam/ C30 αβ	Gam/ C31 αβ (R)	C35 αβ/ C34 αβ	C35 Homohopane Index	Ts/ (Ts+Tm)	C29Ts/ (C29Ts +C29 αβ)
W13/007514 (ext)	0.21	0.53	0.41	0.53	1.29	0.99	0.13	0.13	0.02	0.04	1.14	0.06	0.05	0.13	0.08	0.24	0.87	7	0.52	0.12
W13/007514 (int)	0.19	0.54	0.37	0.49	1.27	1.04	0.14	0.15	0.02	0.05	1.14	0.06	0.04	0.10	0.09	0.26	0.92	8	0.52	0.13
W13/007526 (ext)	0.37	0.54	0.41	1.08	0.33	2.86	0.04	0.12	0.00	0.02	1.18	0.07	0.06	0.10	0.12	0.39	0.91	1	0.49	0.14
W13/007526 (int)	0.20	0.53	0.38	0.49	1.17	0.82	0.14	0.11	0.02	0.04	1.11	0.06	0.05	0.14	0.09	0.26	0.98	8	0.49	0.13
W13/007526 (int)	0.23	0.53	0.40	0.52	1.07	1.00	0.13	0.12	0.02	0.04	1.13	0.06	0.05	0.14	0.09	0.26	0.94	8	0.48	0.14
W13/007538A (ext)	0.18	0.54	0.36	0.57	1.07	0.97	0.14	0.14	0.02	0.04	1.13	0.07	0.07	0.14	0.09	0.26	0.91	6	0.51	0.16
W13/007538A (int)*	0.19	0.55	0.43	0.48	1.12	0.89	0.14	0.12	0.02	0.04	1.15	0.05	0.05	0.14	0.09	0.23	0.96	9	0.45	0.14
W13/007542 (ext)	0.21	0.61	0.36	0.54	1.20	1.00	0.11	0.11	0.02	0.04	1.18	0.07	0.07	0.13	0.08	0.25	0.97	7	0.53	0.14
W13/007542 (int)	0.23	0.59	0.30	0.91	0.00	1.38	0.04	0.05	0.00	0.09	0.90	0.05	0.00	0.05	0.00	0.00	1.04	12	0.51	0.16
W13/007545 (ext)	0.11	0.46	0.28	0.92	1.64	1.05	0.05	0.05	0.02	0.06	0.69	0.15	0.09	0.03	0.03	0.14	0.68	6	0.64	0.30
W13/007545 (int)	0.21	0.53	0.42	0.45	1.45	0.79	0.16	0.12	0.02	0.03	1.16	0.05	0.05	0.11	0.09	0.27	0.93	8	0.47	0.11
W13/007615 (int)*	0.13	0.64	0.39	0.48	1.01	0.75	0.20	0.15	0.00	0.04	1.05	0.06	0.04	0.12	0.06	0.20	0.91	8	0.46	0.15
W13/007619 (int)	0.18	0.54	0.40	0.50	1.22	1.01	0.13	0.13	0.02	0.03	1.16	0.05	0.04	0.10	0.08	0.27	0.91	7	0.50	0.10

Sample ID	% C27 ααα 20R	% C28 ααα 20R	% C29 ααα 20R	C27 Dia/ (Dia+Reg)	(C21+C22)/ (C27+C28 +C29)	C27 Dia /Ster	% C27 αββ 20(R+S)	% C28 αββ 20(R+S)	% C29 αββ 20(R+S)	C29/C27 αββ Sterane Ratio	Tricyclic Terpanes/ Hopanes	Steranes/ Terpanes	% Tricyclic Terpanes	% Pentacyclic Terpanes	% Steranes	Steranes/ hopanes
W13/007514 (ext)	28.39	25.38	46.23	0.35	0.15	0.28	23.04	28.93	48.03	2.08	0.15	0.13	11.26	77.04	11.69	0.15
W13/007514 (int)	36.53	25.70	37.76	0.34	0.12	0.28	30.17	26.61	43.21	1.43	0.15	0.15	11.54	75.47	12.99	0.17
W13/007526 (ext)	27.91	17.84	54.25	0.13	0.15	0.07	6.17	39.52	54.30	8.79	0.08	0.18	6.53	78.18	15.29	0.20
W13/007526 (int)	33.67	23.22	43.11	0.35	0.13	0.28	28.17	28.08	43.75	1.55	0.14	0.14	10.88	77.04	12.08	0.16
W13/007526 (int)	38.99	21.38	39.63	0.34	0.14	0.27	28.40	26.41	45.19	1.59	0.13	0.13	10.44	78.11	11.45	0.15
W13/007538A (ext)	26.94	24.44	48.62	0.34	0.15	0.24	18.33	30.69	50.98	2.78	0.14	0.16	10.55	75.93	13.52	0.18
W13/007538A (int)*	44.03	15.67	40.30	0.34	0.13	0.29	31.85	25.01	43.13	1.35	0.13	0.14	9.90	77.64	12.46	0.16
W13/007542 (ext)	32.19	21.86	45.94	0.29	0.11	0.21	13.30	29.91	56.79	4.27	0.11	0.15	8.60	78.02	13.38	0.17
W13/007542 (int)	29.23	14.39	56.38	0.35	0.08	0.26	22.28	26.43	51.29	2.30	0.04	0.07	3.36	89.74	6.90	0.08
W13/007545 (ext)	36.69	11.46	51.85	0.62	0.07	0.81	30.67	25.83	43.50	1.42	0.10	0.07	8.51	85.27	6.21	0.07
W13/007545 (int)	36.62	24.33	39.05	0.35	0.13	0.31	28.42	26.68	44.91	1.58	0.16	0.14	11.86	75.58	12.56	0.17
W13/007615 (int)*	39.72	23.97	36.31	0.38	0.13	0.33	35.07	25.46	39.47	1.13	0.18	0.20	12.77	70.69	16.54	0.23
W13/007619 (int)	29.21	23.90	46.89	0.34	0.14	0.27	19.65	28.78	51.58	2.63	0.13	0.13	10.55	78.17	11.28	0.14

* = Most representative examples, i.e. least altered results due to low biomarker responses and/or alteration associated with weathering.

Chapter 5: The hydrocarbon loading of the South Australian coastline

SUPPLEMENTARY INFORMATION

1. Supplementary data tables

Table S1: Hydrocarbon loading for six South Australian beaches surveyed in 1990-1991 after Edwards et al., 2016. Site labels I-VI correspond to Figure 3 in the main text. Note the locations are referred to as sites 1-6 from west to east in the original reference. They are relabelled I-VI from east to west here to avoid potential confusion with the site numbering for locations surveyed between 2014–2016 as part of this study. No asphaltites were recovered during these surveys (i.e. asphaltic oil loading = 0 g/100m for all six survey sites).

Survey Site	Site number in 2014-2016	Survey Length (m)	Date	No. of waxy oil pieces	Total weight (g)	Waxy oil loading g/100m
(I) The Granites	25	200	01/10/1990	5	56	28
			27/09/1991	0	0	0
(II) Long Gulley, Little Dip Conservation Park	N.S.	200	01/10/1990	7	83	42
			27/09/1991	6	1010	505
(III) Three Mile Rocks, Beachport Cons. Park	27	300	30/09/1990	32	104	35
			26/09/1991	19	527	176
(IV) Number 2 Rocks (aka Number 1 and 2 Rocks)	29	300	28/09/1990	191	1489	496
			25/09/1991	422	6137	2046
(V) Admella Dunes	N.S.	200	27/09/1990	66	580	290
			25/09/1991	103	670	335
(VI) Nene Valley	30	200	27/09/1990	13	136	68
			25/09/1991	7	196	98

N.S. = Not surveyed during 2014-2016.

Table S2: Survey lengths and access points for each visited beach. For satellite imagery and further metadata for each site see Appendix 5 of Ross et al., (2017). GPS use the WGS84 geographic datum.

Survey Site	Beach Access Point		Survey Length			Comments
	Latitude	Longitude	2014	2015	2016	
(1) Delisser Sandhills	-31.6916	128.9772	1.74	1.79	1.83	
(2) Eyre Well	-31.4636	131.1444	2.00	2.49	2.48	2015/2016 surveys included extra ca. 500m west of the access point to include the catchment area.
(3) Dogfence Beach	-31.7715	131.8424	2.03	2.04	0.25	2016 survey was shortened due to the high abundance of material in catchment area and high temperatures.
(4) Scott Bay	-32.0039	132.3891	2.04	2.02	1.95	
(5) Fowlers Bay West	-32.0051	132.4405	1.59	1.68	1.93	
(6) Cactus Beach	-32.0545	132.9467	2.04	1.95	2.02	2016 starting point was 80m before that of 2014/2015 to include remaining beach in eastern catchment.
(7) Point Peter	-32.1772	133.4399	0.83	1.91	1.05	2014 starting point 240 m after 2015/2016 transects. 2016 survey length reduced due to high abundance of vehicles which obscured the beach.
(8) St. Mary Bay	-32.5319	133.8589	0.84	0.87	0.52	2016 starting point is 480m after the start of the 2014/2015 transects.
(9) St. Mary Bay (South)	-32.536	133.857	0.77	0.81	0.77	
(10) Cape Bauer	-32.7141	134.0935	1.33	1.25	0.56	
(11) Tractor Beach	-32.8561	134.1320	0.77	0.82	0.81	
(12) Tyringa Beach	-33.1470	134.4176	0.58	0.58	0.58	
(13) Elliston	-33.6465	134.8880	0.99	1.00	1.00	
(14) Sheringa Beach	-33.8962	135.1924	1.65	1.53	1.47	2014 starting point was 250m before the 2015/2016 transects.
(15) Mount Drummond (aka Convention Beach)	-34.2404	135.3341	1.95	0.99	0.48	2015 survey started 210m after original 2014 transect, total survey length shortened due to lack of daylight. 2016 survey start point 980m after the start of 2014 and shorter than previous surveys due to inaccessibility following heavy beach erosion associated with 2016 storm activity forming steep and unstable sand cliffs.
(16) Avoid Bay	-34.6587	135.3503	1.17	0.89	0.89	
(17) Sleaford Bay	-34.8820	135.8464	0.73	0.93	0.95	2014 starting point is 150m after the start of 2015/2016 transects.
(18) West Bay	-35.8877	136.5527	0.38	0.37	0.36	
(19) Sandy River	-35.9509	136.6343	0.19	0.38	0.20	Longer survey length in 2015 due to low tide permitting further beach access.
(20) Hanson Bay	-36.0167	136.8530	0.94	0.80	0.92	2014 starting point was 85m before the start of the 2015/2016 transects
(21) Bales Beach	-35.9939	137.3491	1.02	0.93	1.52	
(22) Pennington Bay	-35.8525	137.7442	0.59	0.48	0.46	
(23) Waitpinga Beach	-35.6346	138.4989	1.20	1.13	1.20	
(24) 28 Mile Crossing	-36.2000	139.6414	1.02	0.91	1.07	
(25) The Granites*	-36.6575	139.8540	1.52	1.32	1.01	
(26) Eve's Cove (aka Evan's Cove)	-37.1821	139.7443	0.46	0.77	0.76	2014 survey length was shortened by 300m due to deteriorating weather conditions.
(27) Beachport Cons. Park*	-37.4481	139.9636	1.06	0.74	0.88	2014 survey started 450m further along the beach compared with 2015/2016.
(28) Geltwood Beach	-37.6587	140.2228	1.01	0.96	1.08	
(29) Number 1 & 2 Rocks*	-37.7965	140.3213	0.31	0.42	0.49	2014 starting point slightly further south than 2015/2016.
(30) Nene Valley*	-37.9862	140.5144	0.67	0.68	0.69	

Table S3: Number of samples collected from each oil type determined by whole-oil GC-MS. This list does not include samples donated from private collections or those recovered from outside of the surveyed areas.

Whole-oil Classification	No. collected in 2014	% of 2014 samples	No. collected in 2015	% of 2015 samples	No. collected in 2016	% of 2016 samples	Total number collected	% of total number of samples collected
Asphaltite	8	8.5%	13	13.4%	12	3.8%	33	6.5%
Asphaltic Tar	0	0.0%	0	0.0%	8	2.5%	8	1.6%
Type I waxy bitumen	51	54.3%	52	53.6%	160	50.5%	263	51.8%
Type II waxy bitumen	6	6.4%	7	7.2%	0	0.0%	13	2.6%
Type III waxy bitumen	17	18.1%	11	11.3%	25	7.9%	53	10.4%
Type IV waxy bitumen	4	4.3%	5	5.2%	11	3.5%	20	3.9%
Sandy River Tar	0	0.0%	0	0.0%	47	14.8%	47	9.3%
Degraded high wax bitumen	6	6.4%	7	7.2%	44	13.9%	57	11.2%
Unknown/ other	2	2.1%	2	2.1%	10	3.2%	14	2.8%

Table S4: Weight of crude oil collected from each oil type determined by whole-oil GC-MS. This list does not include samples donated from private collections or those recovered from outside of the surveyed areas.

Whole-oil Classification	Weight collected in 2014 (g)	% of 2014 total weight	Weight collected in 2015 (g)	% of 2015 total weight	Weight collected in 2016 (g)	% of 2016 total	Total weight collected (g)	% of total weight collected
Asphaltite	2302	84.4%	830	40.4%	4220	71.1%	7352	68.6%
Asphaltic Tar	0	0.0%	0	0.0%	462	7.8%	462	4.3%
Type I waxy bitumen	187	6.8%	607	29.5%	720	12.1%	1514	14.1%
Type II waxy bitumen	55	2.0%	177	8.6%	0	0.0%	231	2.2%
Type III waxy bitumen	78	2.8%	374	18.2%	172	2.9%	623	5.8%
Type IV waxy bitumen	35	1.3%	39	1.9%	85	1.4%	159	1.5%
Sandy River Tar	0	0.0%	0	0.0%	118	2.0%	118	1.1%
Degraded high wax bitumen	8	0.3%	12	0.6%	114	1.9%	134	1.3%
Unknown/ other	63	2.3%	17	0.8%	45	0.8%	125	1.2%

Table S5: Summary of waxy oil loading for sites surveyed annually from 2014- 2016. See Table S2 for survey length at each site. Note: only locations where waxy oils were recovered are listed (i.e. hydrocarbon loading from waxy oils = 0 for all survey sites not listed)

	2014 Waxy oil loading			2015 Waxy oil loading			2016 Waxy oil loading		
Survey Site	**No. of pieces**	**Total weight (g)**	**g/100m**	**No. of pieces**	**Total weight (g)**	**g/100m**	**No. of pieces**	**Total weight (g)**	**g/100m**
(2) Eyre Well	0	0	0	0	0	0	2	43	2
(3) Dogfence Beach	1	19	1	21	160	8	32	148	59
(4) Scott Bay	0	0	0	0	0	0	1	10	<0.5
(5) Fowlers Bay West	0	0	0	0	0	0	0	0	0
(6) Cactus Beach	0	0	0	0	0	0	11	85	4
(9) St. Mary Bay (South)	0	0	0	1	24	3	1	3	<0.5
(11) Tractor Beach	0	0	0	0	0	0	1	20	3
(13) Elliston	0	0	0	0	0	0	5	30	3
(14) Sheringa Beach	0	0	0	2	22	1	7	150	10
(15) Mount Drummond	0	0	0	1	3	<0.5	9	33	7
(16) Avoid Bay	0	0	0	0	0	0	5	17	2
(17) Sleaford Bay	1	17	2	1	6	1	4	4	<0.5
(18) West Bay	0	0	0	0	0	0	1	3	1
(19) Sandy River	0	0	0	3	33	9	51	153	76
(20) Hanson Bay	5	17	2	1	8	1	1	1	<0.5
(21) Bales Beach	0	0	0	1	1	<0.5	5	30	2
(22) Pennington Bay	0	0	0	1	8	2	2	4	1
(23) Waitpinga Beach	12	67	6	4	38	3	14	82	7
(24) 28 Mile Crossing	0	0	0	0	0	0	3	3	<0.5
(25) The Granites*	2	17	1	14	189	14	11	30	3
(26) Eve's Cove	3	24	5	0	0	0	55	170	22
(27) Beachport Cons. Park*	3	11	1	7	182	25	42	95	11
(28) Geltwood Beach	5	26	3	3	77	8	3	19	2
(29) Number 1 & 2 Rocks*	52	164	53	21	457	109	20	69	14
(30) Nene Valley*	0	0	0	1	1	<0.5	1	7	1

* = Site also surveyed in 1990-1991 (see **Table S1)**.

Table S6*:* Summary of asphaltic oil loading for sites surveyed annually from 2014- 2016. See Table S2 for survey length at each site. Note: only locations where asphaltic oils were recovered are listed (i.e. hydrocarbon loading from asphaltic oils = 0 for all survey sites not listed).

	2014 Asphaltic oil loading			2015 Asphaltic oil loading			2016 Asphaltic oil loading		
Survey Site	**No. of pieces**	**Total weight (g)**	**g/100m**	**No. of pieces**	**Total weight (g)**	**g/100m**	**No. of pieces**	**Total weight (g)**	**g/100m**
(2) Eyre Well	1	18	1	1	429	17	0	0	0
(3) Dogfence Beach	0	0	0	0	0	0	4	235	94
(5) Fowlers Bay West	1	60	4	0	0	0	0	0	0
(6) Cactus Beach	2	1032	51	1	276	14	2	12	1
(11) Tractor Beach	0	0	0	10	124	15	2	36	4
(12) Tyringa Beach	0	0	0	1	1	< 0.5	0	0	0
(13) Elliston	1	78	8	0	0	0	0	0	0
(14) Sheringa Beach	1	495	30	0	0	0	2	742	50
(18) West Bay	1	18	5	0	0	0	0	0	0
(23) Waitpinga Beach	1	601	50	0	0	0	1	3188	266
(25) The Granites*	0	0	0	0	0	0	1	6	1
(29) Number 1 & 2 Rocks*	0	0	0	0	0	0	8	462	94

* = Site also surveyed in 1990-1991, though no asphaltic oils were recovered (i.e. asphaltic loading = 0 g/100m).

Table S7*:* Summary of hydrocarbon loading from oils classified as unknown/other for sites surveyed annually from 2014- 2016. See Table S2 for survey length at each site. Note: only locations where unknown oils were recovered are listed (i.e. hydrocarbon loading from unknown/other oils = 0 for all survey sites not listed).

	2014 unknown/other hydrocarbon loading			2015 unknown/other hydrocarbon loading			2016 unknown/other hydrocarbon loading		
Survey Site	**No. of pieces**	**Total weight (g)**	**g/100m**	**No. of pieces**	**Total weight (g)**	**g/100m**	**No. of pieces**	**Total weight (g)**	**g/100m**
(3) Dogfence Beach	0	0	0	1	2	< 0.5	2	5	2
(6) Cactus Beach	0	0	0	0	0	0	1	21	1
(11) Tractor Beach	0	0	0	0	0	0	1	5	1
(15) Mount Drummond	0	0	0	0	0	0	1	9	2
(16) Avoid Bay	0	0	0	0	0	0	2	2	<0.5
(21) Bales Beach	1	10	1	0	0	0	1	1	<0.5
(26) Eve's Cove	1	53	12	0	0	0	1	1	<0.5
(28) Geltwood Beach	0	0	0	1	15	2	0	0	0
(29) Number 1 & 2 Rocks*	0	0	0	0	0	0	1	1	<0.5

* = Site also surveyed in 1990-1991, (see **Table S1**).

Table S8: Crude oil samples collected during the November 2014 survey. See Corrick et al. 2020b for discussion of biomarker classifications.

Sample ID	Survey Site	Collection Date	Weight (g)	Latitude	Longitude	Whole-oil classification	Biomarker Classification
W13/007472	Eyre Well	8/11/2014	17.6	-31.4639	131.1422	Asphaltite	Asphaltite
W13/007473	Dogfence Beach	8/11/2014	19.3	-31.7708	131.8417	Type I waxy bitumen	Type I waxy bitumen
W13/007475	Fowlers Bay West	10/11/2014	60.2	-31.9928	132.4375	Asphaltite	Asphaltite
W13/007476	Cactus Beach	10/11/2014	813	-32.0739	132.9761	Asphaltite	Asphaltite
W13/007477	Cactus Beach	10/11/2014	219	-32.0689	132.9706	Asphaltite	Asphaltite
W13/007488	Elliston	13/11/2014	78.0	-33.6350	134.8753	Asphaltite	Asphaltite
W13/007490	Sheringa Beach	13/11/2014	495	-33.8736	135.1758	Asphaltite	n.d.
W13/007491	Sleaford Bay	15/11/2014	16.9	-34.8858	135.8506	Type IV waxy bitumen	Type IVA waxy bitumen
W13/007493	West Bay	19/11/2014	18.3	-35.8858	136.5512	Asphaltite	Asphaltite
W13/007495	Hanson Bay	20/11/2014	2.8	-36.0172	136.8576	Type I waxy bitumen	n.d.
W13/007497	Hanson Bay	20/11/2014	4.3	-36.0174	136.8608	Type I waxy bitumen	n.d.
W13/007498A	Hanson Bay	20/11/2014	0.4	-36.0174	136.8608	Type III waxy bitumen	n.d.
W13/007498B	Hanson Bay	20/11/2014	0.2	-36.0174	136.8608	Type III waxy bitumen	n.d.
W13/007499	Hanson Bay	20/11/2014	8.8	-36.0178	136.8620	Type III waxy bitumen	Type IIID
W13/007500	Bales Beach	21/11/2014	10.2	-35.9937	137.3521	Unknown/other	n.d.
W13/007502	Waitpinga Beach	22/11/2014	4.2	-35.6353	138.5028	Type III waxy bitumen	n.d.
W13/007503	Waitpinga Beach	22/11/2014	6.7	-35.6354	138.5034	Type III waxy bitumen	Type IIIE
W13/007504A	Waitpinga Beach	22/11/2014	10.7	-35.6357	138.5048	Type IV waxy bitumen	n.d.
W13/007504B	Waitpinga Beach	22/11/2014	1.6	-35.6357	138.5048	Type I waxy bitumen	n.d.
W13/007505	Waitpinga Beach	22/11/2014	5.6	-35.6359	138.5053	Type IV waxy bitumen	n.d.
W13/007506	Waitpinga Beach	22/11/2014	1.6	-35.6360	138.5055	Type IV waxy bitumen	Type IVA waxy bitumen
W13/007507	Waitpinga Beach	22/11/2014	601	-35.6362	138.5061	Asphaltite	Asphaltite
W13/007508	Waitpinga Beach	22/11/2014	4.6	-35.6363	138.5068	Type III waxy bitumen	n.d.
W13/007509	Waitpinga Beach	22/11/2014	6.5	-35.6368	138.5084	Type III waxy bitumen	n.d.
W13/007510	Waitpinga Beach	22/11/2014	1.7	-35.6369	138.5089	Type III waxy bitumen	n.d.
W13/007511	Waitpinga Beach	22/11/2014	10.5	-35.6375	138.5106	Type I waxy bitumen	Type I waxy bitumen
W13/007512	Waitpinga Beach	22/11/2014	2.7	-35.6375	138.5106	Type III waxy bitumen	n.d.
W13/007513	Waitpinga Beach	22/11/2014	10.7	-35.6380	138.5115	Type III waxy bitumen	n.d.
W13/007514	The Granites	23/11/2014	15.6	-36.6573	139.8536	Type II waxy bitumen	Type II waxy bitumen
W13/007515	The Granites	23/11/2014	1.5	-36.6561	139.8533	Degraded high wax bitumen	n.d.
W13/007517	Eve's Cove	24/11/2014	3.4	-37.1826	139.7443	Type I waxy bitumen	Type I waxy bitumen
W13/007518	Eve's Cove	24/11/2014	53.0	-37.1838	139.7461	Unknown/other (Sooty bitumen?)	n.d.
W13/007519	Eve's Cove	24/11/2014	16.6	-37.1839	139.7462	Type I waxy bitumen	n.d.
W13/007520	Eve's Cove	24/11/2014	4.0	-37.1843	139.7465	Type I waxy bitumen	n.d.
W13/007521	Beachport Conservation Park	24/11/2014	6.0	-37.4499	139.9659	Type I waxy bitumen	Type I waxy bitumen
W13/007522	Beachport Conservation Park	24/11/2014	1.5	-37.4441	139.9615	Type I waxy bitumen	n.d.
W13/007523	Beachport Conservation Park	24/11/2014	3.6	-37.4446	139.9618	Type I waxy bitumen	n.d.
W13/007524	Geltwood Beach	25/11/2014	0.6	-37.6586	140.2216	Type I waxy bitumen	n.d.
W13/007525	Geltwood Beach	25/11/2014	4.2	-37.6595	140.2227	Type III waxy bitumen	n.d.
W13/007526	Geltwood Beach	25/11/2014	9.6	-37.6595	140.2227	Type II waxy bitumen	Type II waxy bitumen
W13/007527	Geltwood Beach	25/11/2014	5.4	-37.6601	140.2235	Type I waxy bitumen	n.d.
W13/007528	Geltwood Beach	25/11/2014	6.0	-37.6638	140.2273	Type I waxy bitumen	Type I waxy bitumen
W13/007529	Number 1 & 2 Rocks	25/11/2014	3.5	-37.7954	140.3204	Type I waxy bitumen	n.d.
W13/007530	Number 1 & 2 Rocks	25/11/2014	4.2	-37.7955	140.3205	Type I waxy bitumen	Type I waxy bitumen
W13/007531A	Number 1 & 2 Rocks	25/11/2014	1.8	-37.7955	140.3205	Type I waxy bitumen	n.d.
W13/007531B	Number 1 & 2 Rocks	25/11/2014	1.0	-37.7955	140.3205	Type I waxy bitumen	n.d.
W13/007531C	Number 1 & 2 Rocks	25/11/2014	0.6	-37.7955	140.3205	Type I waxy bitumen	n.d.
W13/007531D	Number 1 & 2 Rocks	25/11/2014	0.4	-37.7955	140.3205	Type I waxy bitumen	n.d.
W13/007532A	Number 1 & 2 Rocks	25/11/2014	2.4	-37.7956	140.3205	Type I waxy bitumen	n.d.

Sample ID	Survey Site	Collection Date	Weight (g)	Latitude	Longitude	Whole-oil classification	Biomarker Classification
W13/007532B	Number 1 & 2 Rocks	25/11/2014	1.3	-37.7956	140.3205	Type I waxy bitumen	n.d.
W13/007533	Number 1 & 2 Rocks	25/11/2014	1.9	-37.7956	140.3205	Type I waxy bitumen	n.d.
W13/007534	Number 1 & 2 Rocks	25/11/2014	5.6	-37.7956	140.3206	Type I waxy bitumen	n.d.
W13/007535	Number 1 & 2 Rocks	25/11/2014	17.6	-37.7957	140.3206	Type III waxy bitumen	n.d.
W13/007536	Number 1 & 2 Rocks	25/11/2014	3.9	-37.7957	140.3205	Type I waxy bitumen	n.d.
W13/007537	Number 1 & 2 Rocks	25/11/2014	10.3	-37.7957	140.3207	Type I waxy bitumen	n.d.
W13/007538A	Number 1 & 2 Rocks	25/11/2014	7.9	-37.7959	140.3208	Type II waxy bitumen	Type II waxy bitumen
W13/007538B	Number 1 & 2 Rocks	25/11/2014	0.9	-37.7959	140.3208	Type I waxy bitumen	n.d.
W13/007539A	Number 1 & 2 Rocks	25/11/2014	2.7	-37.7959	140.3209	Type III waxy bitumen	n.d.
W13/007539B	Number 1 & 2 Rocks	25/11/2014	0.6	-37.7959	140.3209	Type III waxy bitumen	n.d.
W13/007540	Number 1 & 2 Rocks	25/11/2014	7.5	-37.7961	140.3210	Type I waxy bitumen	n.d.
W13/007541	Number 1 & 2 Rocks	25/11/2014	4.6	-37.7962	140.3211	Type III waxy bitumen	Type IIIA waxy bitumen
W13/007542	Number 1 & 2 Rocks	25/11/2014	7.9	-37.7962	140.3212	Type II waxy bitumen	Type II waxy bitumen
W13/007543	Number 1 & 2 Rocks	25/11/2014	1.2	-37.7963	140.3212	Type I waxy bitumen	n.d.
W13/007544	Number 1 & 2 Rocks	25/11/2014	3.8	-37.7963	140.3211	Type I waxy bitumen	n.d.
W13/007545	Number 1 & 2 Rocks	25/11/2014	10.5	-37.7963	140.3214	Type II waxy bitumen	Type II waxy bitumen
W13/007546	Number 1 & 2 Rocks	25/11/2014	0.7	-37.7964	140.3214	Type I waxy bitumen	n.d.
W13/007547	Number 1 & 2 Rocks	25/11/2014	0.5	-37.7965	140.3215	Type I waxy bitumen	n.d.
W13/007548	Number 1 & 2 Rocks	25/11/2014	5.7	-37.7968	140.3218	Type I waxy bitumen	n.d.
W13/007549	Number 1 & 2 Rocks	25/11/2014	0.6	-37.7968	140.3218	Type I waxy bitumen	n.d.
W13/007550	Number 1 & 2 Rocks	25/11/2014	2.6	-37.7969	140.3219	Type I waxy bitumen	n.d.
W13/007551	Number 1 & 2 Rocks	25/11/2014	5.0	-37.7970	140.3219	Type I waxy bitumen	n.d.
W13/007552A	Number 1 & 2 Rocks	25/11/2014	3.1	-37.7970	140.3220	Type I waxy bitumen	n.d.
W13/007552B	Number 1 & 2 Rocks	25/11/2014	0.5	-37.7970	140.3220	Type I waxy bitumen	n.d.
W13/007553	Number 1 & 2 Rocks	25/11/2014	1.5	-37.7970	140.3221	Type I waxy bitumen	Type I waxy bitumen
W13/007554	Number 1 & 2 Rocks	25/11/2014	3.1	-37.7971	140.3222	Type II waxy bitumen	n.d.
W13/007556	Number 1 & 2 Rocks	25/11/2014	0.9	-37.7973	140.3224	Type I waxy bitumen	n.d.
W13/007557A	Number 1 & 2 Rocks	25/11/2014	2.3	-37.7974	140.3225	Type I waxy bitumen	n.d.
W13/007557B	Number 1 & 2 Rocks	25/11/2014	0.5	-37.7974	140.3225	Type I waxy bitumen	n.d.
W13/007557C	Number 1 & 2 Rocks	25/11/2014	0.5	-37.7974	140.3225	Type III waxy bitumen	n.d.
W13/007558	Number 1 & 2 Rocks	25/11/2014	4.3	-37.7975	140.3226	Type I waxy bitumen	n.d.
W13/007559	Number 1 & 2 Rocks	25/11/2014	7.7	-37.7975	140.3226	Type I waxy bitumen	n.d.
W13/007560A	Number 1 & 2 Rocks	25/11/2014	0.5	-37.7977	140.3227	Type I waxy bitumen	n.d.
W13/007560B	Number 1 & 2 Rocks	25/11/2014	0.3	-37.7977	140.3227	Degraded high wax bitumen	n.d.
W13/007561	Number 1 & 2 Rocks	25/11/2014	3.6	-37.7977	140.3227	Type I waxy bitumen	n.d.
W13/007562	Number 1 & 2 Rocks	25/11/2014	1.0	-37.7977	140.3228	Degraded high wax bitumen	n.d.
W13/007563A	Number 1 & 2 Rocks	25/11/2014	2.6	-37.7978	140.3229	Type I waxy bitumen	n.d.
W13/007563B	Number 1 & 2 Rocks	25/11/2014	1.0	-37.7978	140.3229	Type I waxy bitumen	n.d.
W13/007564A	Number 1 & 2 Rocks	25/11/2014	4.0	-37.7978	140.3229	Degraded high wax bitumen	Type IVD waxy bitumen
W13/007564B	Number 1 & 2 Rocks	25/11/2014	0.9	-37.7978	140.3229	Type III waxy bitumen	n.d.
W13/007564C	Number 1 & 2 Rocks	25/11/2014	1.4	-37.7978	140.3229	Degraded high wax bitumen	n.d.
W13/007564D	Number 1 & 2 Rocks	25/11/2014	0.5	-37.7978	140.3229	Type I waxy bitumen	n.d.
W13/007564E	Number 1 & 2 Rocks	25/11/2014	0.2	-37.7978	140.3229	Degraded high wax bitumen	n.d.

Sample ID	Survey Site	Collection Date	Weight (g)	Latitude	Longitude	Whole-oil classification	Biomarker Classification
W13/007564F	Number 1 & 2 Rocks	25/11/2014	0.2	-37.7978	140.3229	Type I waxy bitumen	n.d.
W13/007565	Number 1 & 2 Rocks	25/11/2014	6.5	-37.7979	140.3229	Type I waxy bitumen	n.d.

n.d. = Not determined.

Table S9: Crude oil samples collected during the September 2015 survey. See Corrick et al. 2020b for discussion of biomarker classifications.

Sample ID	Survey Site	Collection Date	Weight (g)	Latitude	Longitude	Whole-oil classification	Biomarker Classification
W13/007573	Sandy River	5/09/2015	20.4	-35.9559	136.6292	Type III waxy bitumen	n.d.
W13/007578	Sandy River	5/09/2015	3.7	-35.9551	136.6276	Type III waxy bitumen	n.d.
W13/007579	Sandy River	5/09/2015	9.0	-35.9542	136.6261	Type III waxy bitumen	n.d.
W13/007581	Hanson Bay	5/09/2015	8.2	-36.0172	136.8594	Type III waxy bitumen	n.d.
W13/007584	Bales Beach	6/09/2015	0.5	-35.9936	137.3485	Type I waxy bitumen	n.d.
W13/007587	Pennington Bay	6/09/2015	7.9	-35.8532	137.7407	Type I waxy bitumen	n.d.
W13/007588	Waitpinga Beach	7/09/2015	2.0	-35.6354	138.5035	Type IV waxy bitumen	n.d.
W13/007589	Waitpinga Beach	7/09/2015	32.1	-35.6354	138.5035	Type IV waxy bitumen	Type IVA waxy bitumen
W13/007590	Waitpinga Beach	7/09/2015	1.1	-35.6362	138.5067	Type IV waxy bitumen	Type IVA waxy bitumen
W13/007593	Waitpinga Beach	7/09/2015	3.2	-35.6359	138.5058	Type IV waxy bitumen	Type IVA waxy bitumen
W13/007594	The Granites	8/09/2015	24.5	-36.6625	139.8551	Type I waxy bitumen	n.d.
W13/007595	The Granites	8/09/2015	14.8	-36.6597	139.8543	Type I waxy bitumen	n.d.
W13/007596	The Granites	8/09/2015	1.2	-36.6594	139.8542	Type I waxy bitumen	n.d.
W13/007597	The Granites	8/09/2015	5.0	-36.6563	139.8533	Type I waxy bitumen	n.d.
W13/007598	The Granites	8/09/2015	3.3	-36.6561	139.8533	Type I waxy bitumen	n.d.
W13/007600	The Granites	8/09/2015	3.8	-36.6560	139.8533	Type I waxy bitumen	n.d.
W13/007601	The Granites	8/09/2015	25.0	-36.6552	139.8530	Type I waxy bitumen	Type I waxy bitumen
W13/007602	The Granites	8/09/2015	3.8	-36.6552	139.8530	Type I waxy bitumen	n.d.
W13/007603	The Granites	8/09/2015	1.8	-36.6543	139.8528	Type I waxy bitumen	n.d.
W13/007604	The Granites	8/09/2015	2.2	-36.6543	139.8528	Type I waxy bitumen	n.d.
W13/007605	The Granites	8/09/2015	91	-36.6535	139.8526	Type III waxy bitumen	Type IIIB waxy bitumen
W13/007606	The Granites	8/09/2015	2.9	-36.6525	139.8523	Type I waxy bitumen	n.d.
W13/007607	The Granites	8/09/2015	3.8	-36.6524	139.8523	Type I waxy bitumen	n.d.
W13/007608	The Granites	8/09/2015	5.6	-36.6519	139.8522	Type I waxy bitumen	n.d.
W13/007609	Beachport	9/09/2015	2.9	-37.4443	139.9616	Type I waxy bitumen	n.d.
W13/007610	Beachport	9/09/2015	1.0	-37.4443	139.9616	Type I waxy bitumen	n.d.
W13/007611	Beachport	9/09/2015	3.0	-37.4444	139.9616	Type I waxy bitumen	n.d.
W13/007612	Beachport	9/09/2015	0.4	-37.4445	139.9617	Type I waxy bitumen	n.d.
W13/007613	Beachport	9/09/2015	7.0	-37.4445	139.9618	Type I waxy bitumen	n.d.
W13/007614	Beachport	9/09/2015	13.0	-37.4446	139.9618	Type I waxy bitumen	n.d.
W13/007615	Beachport	9/09/2015	154.3	-37.4450	139.9621	Type II waxy bitumen	Type II waxy bitumen
W13/007616	Geltwood Beach	10/09/2015	71.4	-37.6592	140.2222	Type I waxy bitumen	n.d.
W13/007617	Geltwood Beach	10/09/2015	4.6	-37.6606	140.2238	Type I waxy bitumen	n.d.
W13/007618	Geltwood Beach	10/09/2015	14.8	-37.6603	140.2235	Unknown/other (Sooty bitumen?)	n.d.
W13/007619	Geltwood Beach	10/09/2015	1.2	-37.6601	140.2234	Type II waxy bitumen	Type II waxy bitumen
W13/007620	Number 1 and 2 Rocks	10/09/2015	72.8	-37.7952	140.3202	Type I waxy bitumen	n.d.
W13/007621	Number 1 and 2 Rocks	10/09/2015	3.3	-37.7952	140.3202	Type III waxy bitumen	n.d.
W13/007622	Number 1 and 2 Rocks	10/09/2015	5.4	-37.7953	140.3202	Type I waxy bitumen	n.d.
W13/007623	Number 1 and 2 Rocks	10/09/2015	5.4	-37.7954	140.3204	Type I waxy bitumen	n.d.
W13/007624	Number 1 and 2 Rocks	10/09/2015	18.9	-37.7954	140.3203	Type I waxy bitumen	n.d.
W13/007625	Number 1 and 2 Rocks	10/09/2015	5.7	-37.7954	140.3203	Type I waxy bitumen	Type I waxy bitumen
W13/007626	Number 1 and 2 Rocks	10/09/2015	4.4	-37.7954	140.3204	Type I waxy bitumen	n.d.
W13/007627	Number 1 and 2 Rocks	10/09/2015	208.3	-37.7955	140.3205	Type III waxy bitumen	n.d.
W13/007628	Number 1 and 2 Rocks	10/09/2015	14.6	-37.7955	140.3205	Type I waxy bitumen	n.d.

Sample ID	Survey Site	Collection Date	Weight (g)	Latitude	Longitude	Whole-oil classification	Biomarker Classification
W13/007629	Number 1 and 2 Rocks	10/09/2015	2.5	-37.7956	140.3204	Type I waxy bitumen	n.d.
W13/007630	Number 1 and 2 Rocks	10/09/2015	1.9	-37.7958	140.3205	Type II waxy bitumen	n.d.
W13/007631	Number 1 and 2 Rocks	10/09/2015	7.5	-37.7959	140.3208	Type I waxy bitumen	n.d.
W13/007632	Number 1 and 2 Rocks	10/09/2015	10.3	-37.7960	140.3209	Type I waxy bitumen	n.d.
W13/007633	Number 1 and 2 Rocks	10/09/2015	4.0	-37.7961	140.3210	Type II waxy bitumen	n.d.
W13/007634	Number 1 and 2 Rocks	10/09/2015	57.4	-37.7961	140.3211	Type I waxy bitumen	n.d.
W13/007635	Number 1 and 2 Rocks	10/09/2015	9.4	-37.7964	140.3215	Type I waxy bitumen	n.d.
W13/007637	Number 1 and 2 Rocks	10/09/2015	10.6	-37.7966	140.3218	Type II waxy bitumen	n.d.
W13/007638	Number 1 and 2 Rocks	10/09/2015	1.6	-37.7969	140.3219	Type I waxy bitumen	n.d.
W13/007639	Number 1 and 2 Rocks	10/09/2015	2.7	-37.7971	140.3221	Type II waxy bitumen	n.d.
W13/007641	Number 1 and 2 Rocks	10/09/2015	2.1	-37.7976	140.3225	Type II waxy bitumen	n.d.
W13/007642	Number 1 and 2 Rocks	10/09/2015	8.1	-37.7976	140.3227	Type I waxy bitumen	n.d.
W13/007643	Nene Valley	11/09/2015	0.5	-37.9832	140.5085	Type I waxy bitumen	n.d.
W13/007646	Sleaford Bay	18/09/2015	5.8	-34.8837	135.8497	Type III waxy bitumen	n.d.
W13/007649	Mount Drummond	19/09/2015	3.3	-34.2571	135.3420	Type III waxy bitumen	n.d.
W13/007651	Sheringa Beach	20/09/2015	0.8	-33.8735	135.1760	Type I waxy bitumen	n.d.
W13/007655	Sheringa Beach	20/09/2015	21.6	-33.8768	135.1817	Type I waxy bitumen	n.d.
W13/007658	Tyringa Beach	21/09/2015	1.0	-33.1488	134.4157	Degraded asphaltite	n.d.
W13/007659	Tractor Beach	21/09/2015	8.5	-32.8699	134.1112	Degraded asphaltite	Asphaltite
W13/007660	Tractor Beach	21/09/2015	3.8	-32.8697	134.1120	Degraded asphaltite	Asphaltite
W13/007661	Tractor Beach	21/09/2015	19.9	-32.8697	134.1123	Asphaltite	Asphaltite
W13/007662	Tractor Beach	21/09/2015	0.9	-32.8697	134.1124	Degraded asphaltite	Asphaltite
W13/007663	Tractor Beach	21/09/2015	1.0	-32.8696	134.1125	Degraded asphaltite	Asphaltite
W13/007664	Tractor Beach	21/09/2015	31.5	-32.8693	134.1134	Degraded asphaltite	Asphaltite
W13/007665	Tractor Beach	21/09/2015	16.8	-32.8687	134.1154	Degraded asphaltite	Asphaltite
W13/007666	Tractor Beach	21/09/2015	12.6	-32.8685	134.1159	Degraded asphaltite	Asphaltite
W13/007667	Tractor Beach	21/09/2015	4.4	-32.8683	134.1166	Degraded asphaltite	Asphaltite
W13/007668	Tractor Beach	21/09/2015	24.5	-32.8675	134.1178	Asphaltite	Asphaltite
W13/007669	St Mary Bay (South)	22/09/2015	24.0	-32.5328	133.8636	Type I waxy bitumen	n.d.
W13/007671	Cactus Beach	23/09/2015	275.7	-32.0774	132.9791	Asphaltite	Asphaltite
W13/007746	Dogfence Beach	25/09/2015	20.9	-31.7718	131.8421	Type I waxy bitumen	n.d.
W13/007747	Dogfence Beach	25/09/2015	1.9	-31.7718	131.8422	Degraded high wax bitumen	n.d.
W13/007749A	Dogfence Beach	25/09/2015	2.4	-31.7718	131.8421	Type I waxy bitumen	n.d.
W13/007749B	Dogfence Beach	25/09/2015	1.9	-31.7718	131.8421	Unknown/other	n.d.
W13/007749C	Dogfence Beach	25/09/2015	1.8	-31.7718	131.8421	Type I waxy bitumen	n.d.
W13/007749D	Dogfence Beach	25/09/2015	3.9	-31.7718	131.8421	Degraded high wax bitumen	n.d.
W13/007749E	Dogfence Beach	25/09/2015	2.3	-31.7718	131.8421	Type I waxy bitumen	n.d.
W13/007749F	Dogfence Beach	25/09/2015	1.4	-31.7718	131.8421	Type III waxy bitumen	n.d.
W13/007749H	Dogfence Beach	25/09/2015	0.8	-31.7718	131.8421	Type IV waxy bitumen	Type IVD waxy bitumen
W13/007749K	Dogfence Beach	25/09/2015	0.4	-31.7718	131.8421	Degraded high wax bitumen	n.d.
W13/007749M	Dogfence Beach	25/09/2015	0.2	-31.7718	131.8421	Degraded high wax bitumen	n.d.
W13/007749N	Dogfence Beach	25/09/2015	0.3	-31.7718	131.8421	Type I waxy bitumen	n.d.
W13/007751	Dogfence Beach	25/09/2015	19.3	-31.7717	131.8421	Type III waxy bitumen	n.d.
W13/007752	Dogfence Beach	25/09/2015	1.0	-31.7716	131.8422	Degraded high wax bitumen	n.d.
W13/007753	Dogfence Beach	25/09/2015	1.3	-31.7716	131.8422	Degraded high wax bitumen	n.d.
W13/007754	Dogfence Beach	25/09/2015	3.1	-31.7717	131.8422	Degraded high wax bitumen	n.d.
W13/007755	Dogfence Beach	25/09/2015	3.0	-31.7716	131.8421	Type I waxy bitumen	n.d.
W13/007756	Dogfence Beach	25/09/2015	40.4	-31.7716	131.8422	Type I waxy bitumen	n.d.
W13/007757	Dogfence Beach	25/09/2015	14.1	-31.7714	131.8421	Type I waxy bitumen	n.d.
W13/007758	Dogfence Beach	25/09/2015	1.7	-31.7688	131.8394	Type I waxy bitumen	n.d.
W13/007759	Dogfence Beach	25/09/2015	27.8	-31.7653	131.8346	Type I waxy bitumen	n.d.
W13/007760	Dogfence Beach	25/09/2015	11.5	-31.7628	131.8311	Type I waxy bitumen	n.d.

Sample ID	Survey Site	Collection Date	Weight (g)	Latitude	Longitude	Whole-oil classification	Biomarker Classification
W13/007764	Eyre Well	26/09/2015	429	-31.4651	131.1338	Asphaltite	n.d.

n.d. = Not determined.

Table S10: Crude oil samples collected during the October 2016 survey. See Corrick et al. 2020b for discussion of biomarker classifications.

Sample ID	Survey Site	Collection Date	Weight (g)	Latitude	Longitude	Whole-oil classification	Biomarker Classification
W13/007769	Eyre Well	06-Oct-16	41.8	-31.4652	131.1361	Type I waxy bitumen	n.d.
W13/007770	Eyre Well	06-Oct-16	1.2	-31.4647	131.1319	Type I waxy bitumen	n.d.
W13/007772	Dogfence Beach	06-Oct-16	2.0	-31.7717	131.8422	Type I waxy bitumen	n.d.
W13/007774	Dogfence Beach	06-Oct-16	1.5	N.R.	N.R.	Type I waxy bitumen	n.d.
W13/007775	Dogfence Beach	06-Oct-16	2.1	-31.7716	131.8422	Degraded high wax bitumen	n.d.
W13/007776	Dogfence Beach	06-Oct-16	2.5	-31.7716	131.8422	Unknown	n.d.
W13/007778	Dogfence Beach	06-Oct-16	24.6	-31.7716	131.8421	Type III waxy bitumen	Type IIIA waxy bitumen
W13/007779	Dogfence Beach	06-Oct-16	34.3	-31.7715	131.8421	Asphaltite	n.d.
W13/007780	Dogfence Beach	06-Oct-16	2.9	-31.7715	131.8422	Type III waxy bitumen	n.d.
W13/007781	Dogfence Beach	06-Oct-16	5.7	-31.7715	131.8421	Type I waxy bitumen	n.d.
W13/007782	Dogfence Beach	06-Oct-16	8.6	-31.7714	131.8421	Type III waxy bitumen	n.d.
W13/007783	Dogfence Beach	06-Oct-16	4.9	-31.7714	131.8421	Degraded high wax bitumen	n.d.
W13/007784	Dogfence Beach	06-Oct-16	11.9	-31.7713	131.8421	Degraded high wax bitumen	n.d.
W13/007785	Dogfence Beach	06-Oct-16	13.6	-31.7713	131.8421	Type I waxy bitumen	n.d.
W13/007786	Dogfence Beach	06-Oct-16	2.6	-31.7713	131.8420	Type I waxy bitumen	n.d.
W13/007788	Dogfence Beach	06-Oct-16	0.9	-31.7713	131.8420	Type I waxy bitumen	n.d.
W13/007789	Dogfence Beach	06-Oct-16	5.0	-31.7713	131.8420	Type I waxy bitumen	n.d.
W13/007790	Dogfence Beach	06-Oct-16	3.1	-31.7712	131.8420	Type I waxy bitumen	n.d.
W13/007792	Dogfence Beach	06-Oct-16	2.3	-31.7712	131.8420	Unknown	n.d.
W13/007794A	Dogfence Beach	06-Oct-16	4.2	-31.7712	131.8419	Type I waxy bitumen	n.d.
W13/007794B	Dogfence Beach	06-Oct-16	1.7	-31.7712	131.8419	Type I waxy bitumen	n.d.
W13/007794C	Dogfence Beach	06-Oct-16	1.1	-31.7712	131.8419	Type I waxy bitumen	n.d.
W13/007796	Dogfence Beach	06-Oct-16	2.1	-31.7709	131.8417	Degraded high wax bitumen	n.d.
W13/007797	Dogfence Beach	06-Oct-16	14.0	-31.7708	131.8416	Degraded high wax bitumen	n.d.
W13/007798	Dogfence Beach	06-Oct-16	1.0	-31.7708	131.8416	Type I waxy bitumen	n.d.
W13/007801	Dogfence Beach	06-Oct-16	140.4	-31.7707	131.8415	Asphaltite	n.d.
W13/007802	Dogfence Beach	06-Oct-16	21.2	-31.7707	131.8415	Asphaltite	n.d.
W13/007804	Dogfence Beach	06-Oct-16	3.3	-31.7706	131.8415	Type I waxy bitumen	n.d.
W13/007806	Dogfence Beach	06-Oct-16	2.6	-31.7706	131.8414	Type I waxy bitumen	n.d.
W13/007807	Dogfence Beach	06-Oct-16	38.9	-31.7706	131.8414	Asphaltite	n.d.
W13/007808	Dogfence Beach	06-Oct-16	1.3	-31.7705	131.8414	Type I waxy bitumen	n.d.
W13/007809	Dogfence Beach	06-Oct-16	7.9	-31.7706	131.8414	Type I waxy bitumen	n.d.
W13/007811	Dogfence Beach	06-Oct-16	1.9	-31.7701	131.8410	Degraded high wax bitumen	Type IVE waxy bitumen
W13/007812	Dogfence Beach	06-Oct-16	3.9	-31.7700	131.8408	Degraded high wax bitumen	n.d.
W13/007813A	Dogfence Beach	06-Oct-16	5.7	-31.7700	131.8408	Type III waxy bitumen	n.d.
W13/007813B	Dogfence Beach	06-Oct-16	2.0	-31.7700	131.8408	Type I waxy bitumen	n.d.
W13/007813C	Dogfence Beach	06-Oct-16	2.6	-31.7700	131.8408	Type I waxy bitumen	n.d.
W13/007813D	Dogfence Beach	06-Oct-16	0.9	-31.7700	131.8408	Type I waxy bitumen	n.d.
W13/007813E	Dogfence Beach	06-Oct-16	1.5	-31.7700	131.8408	Type I waxy bitumen	n.d.
W13/007813F	Dogfence Beach	06-Oct-16	1.0	-31.7700	131.8408	Type I waxy bitumen	n.d.
W13/007815	Scott Bay	07-Oct-16	9.6	N.R.	N.R.	Type I waxy bitumen	n.d.
W13/007817A	Cactus Beach	08-Oct-16	0.9	-32.0795	132.9800	Type I waxy bitumen	n.d.
W13/007817B	Cactus Beach	08-Oct-16	0.7	-32.0795	132.9800	Degraded high wax bitumen	n.d.
W13/007817C	Cactus Beach	08-Oct-16	1.1	-32.0795	132.9800	Degraded high wax bitumen	n.d.
W13/007817D	Cactus Beach	08-Oct-16	0.4	-32.0795	132.9800	Degraded high wax bitumen	n.d.
W13/007818A	Cactus Beach	08-Oct-16	4.4	-32.0777	132.9797	Type III waxy bitumen	n.d.
W13/007818B	Cactus Beach	08-Oct-16	1.4	-32.0777	132.9797	Degraded high wax bitumen	Type IVD waxy bitumen
W13/007819	Cactus Beach	08-Oct-16	14.0	-32.0729	132.9755	Type I waxy bitumen	Type I waxy bitumen

Sample ID	Survey Site	Collection Date	Weight (g)	Latitude	Longitude	Whole-oil classification	Biomarker Classification
W13/007820	Cactus Beach	08-Oct-16	4.9	-32.0712	132.9734	Asphaltite	Asphaltite
W13/007821	Cactus Beach	08-Oct-16	11.6	-32.0706	132.9730	Type III waxy bitumen	n.d.
W13/007822	Cactus Beach	08-Oct-16	7.6	-32.0704	132.9727	Type I waxy bitumen	n.d.
W13/007824	Cactus Beach	08-Oct-16	15.3	-32.0674	132.9686	Type I waxy bitumen	n.d.
W13/007825	Cactus Beach	08-Oct-16	21.2	-32.0673	132.9685	Unknown	n.d.
W13/007826	Cactus Beach	08-Oct-16	27.9	-32.0671	132.9681	Type I waxy bitumen	n.d.
W13/007827	Cactus Beach	08-Oct-16	7.4	-32.0714	132.9734	Asphaltite	Asphaltite
W13/007829	St Mary Bay Sth	09-Oct-16	3.2	-32.5337	133.8559	Type I waxy bitumen	n.d.
W13/007830	Tractor Beach	09-Oct-16	19.4	-32.8698	134.1118	Asphaltite	Asphaltite
W13/007831	Tractor Beach	09-Oct-16	5.3	-32.8698	134.1119	Unknown	n.d.
W13/007832	Tractor Beach	09-Oct-16	16.9	-32.8697	134.1121	Asphaltite	Asphaltite
W13/007833	Tractor Beach	09-Oct-16	20.5	-32.8696	134.1126	Degraded high wax bitumen	n.d.
W13/007835	Elliston	10-Oct-16	1.2	-33.6369	134.8803	Degraded high wax bitumen	n.d.
W13/007836	Elliston	10-Oct-16	7.2	-33.6353	134.8772	Type I waxy bitumen	n.d.
W13/007837	Elliston	10-Oct-16	4.6	-33.6425	134.8863	Type IV waxy bitumen	Type IVD waxy bitumen
W13/007838	Elliston	10-Oct-16	10.2	-33.6395	134.8848	Type I waxy bitumen	n.d.
W13/007839	Elliston	10-Oct-16	7.3	-33.6385	134.8833	Type I waxy bitumen	n.d.
W13/007841	Sheringa Beach	11-Oct-16	2.7	-33.8735	135.1762	Type III waxy bitumen	n.d.
W13/007842	Sheringa Beach	11-Oct-16	0.4	-33.8734	135.1763	Type I waxy bitumen	n.d.
W13/007845	Sheringa Beach	11-Oct-16	500	-33.8744	135.1781	Asphaltite	Asphaltite
W13/007846	Sheringa Beach	11-Oct-16	242	-33.8746	135.1782	Asphaltite	n.d.
W13/007847	Sheringa Beach	11-Oct-16	10.9	-33.8758	135.1805	Type III waxy bitumen	Type IIIA waxy bitumen
W13/007848	Sheringa Beach	11-Oct-16	15.3	-33.8763	135.1807	Type III waxy bitumen	Type IIIA waxy bitumen
W13/007849	Sheringa Beach	11-Oct-16	3.7	-33.8765	135.1811	Type I waxy bitumen	n.d.
W13/007850	Sheringa Beach	11-Oct-16	114.7	-33.8781	135.1826	Type I waxy bitumen	n.d.
W13/007851A	Sheringa Beach	11-Oct-16	2.0	-33.8791	135.1832	Degraded high wax bitumen	n.d.
W13/007852A	Mount Drummond Beach	11-Oct-16	4.4	-34.2568	135.3419	Type III waxy bitumen	n.d.
W13/007852B	Mount Drummond Beach	11-Oct-16	0.6	-34.2568	135.3419	Type III waxy bitumen	n.d.
W13/007853A	Mount Drummond Beach	11-Oct-16	2.7	-34.2568	135.3420	Type I waxy bitumen	n.d.
W13/007853B	Mount Drummond Beach	11-Oct-16	3.0	-34.2568	135.3420	Type I waxy bitumen	n.d.
W13/007855	Mount Drummond Beach	11-Oct-16	9.4	-34.2575	135.3424	Unknown	n.d.
W13/007856	Mount Drummond Beach	11-Oct-16	5.5	-34.2576	135.3425	Type I waxy bitumen	n.d.
W13/007857A	Mount Drummond Beach	11-Oct-16	7.9	-34.2576	135.3425	Type IV waxy bitumen	Type IVC waxy bitumen
W13/007858	Mount Drummond Beach	11-Oct-16	2.6	-34.2576	135.3425	Type I waxy bitumen	n.d.
W13/007859	Mount Drummond Beach	11-Oct-16	4.5	-34.2582	135.3427	Type III waxy bitumen	n.d.
W13/007860	Mount Drummond Beach	11-Oct-16	2.3	-34.2589	135.3430	Type I waxy bitumen	n.d.
W13/007861	Avoid Bay	12-Oct-16	0.3	-34.6685	135.3455	Type I waxy bitumen	n.d.
W13/007862	Avoid Bay	12-Oct-16	1.4	-34.6684	135.3456	Unknown	n.d.
W13/007863	Avoid Bay	12-Oct-16	4.0	-34.6681	135.3460	Type I waxy bitumen	Type I waxy bitumen
W13/007864	Avoid Bay	12-Oct-16	11.0	-34.6670	135.3469	Type III waxy bitumen	n.d.
W13/007865	Avoid Bay	12-Oct-16	0.9	-34.6669	135.3470	Type I waxy bitumen	n.d.
W13/007866	Avoid Bay	12-Oct-16	0.6	-34.6667	135.3470	Unknown	n.d.
W13/007867	Avoid Bay	12-Oct-16	0.7	-34.6663	135.3472	Type III waxy bitumen	Type IIIF waxy bitumen
W13/007868	Sleaford Bay	12-Oct-16	1.1	-34.8845	135.8502	Type I waxy bitumen	Type I waxy bitumen
W13/007869	Sleaford Bay	12-Oct-16	1.0	-34.8838	135.8498	Type III waxy bitumen	Type IIID waxy bitumen
W13/007872	Sleaford Bay	12-Oct-16	1.1	-34.8800	135.8459	Degraded high wax bitumen	n.d.

Sample ID	Survey Site	Collection Date	Weight (g)	Latitude	Longitude	Whole-oil classification	Biomarker Classification
W13/007874	Sleaford Bay	12-Oct-16	0.3	-34.8799	135.8455	Degraded high wax bitumen	n.d.
W13/007922	West Bay	16-Oct-16	2.6	-35.8873	136.5534	Type I waxy bitumen	Type I waxy bitumen
W13/007923	Sandy River	17-Oct-16	11.8	-35.9560	136.6294	Sandy River Tar	Sandy River Tar
W13/007924	Sandy River	17-Oct-16	1.3	-35.9559	136.6292	Sandy River Tar	n.d.
W13/007925	Sandy River	17-Oct-16	1.7	-35.9558	136.6293	Sandy River Tar	n.d.
W13/007926	Sandy River	17-Oct-16	0.3	-35.9557	136.6292	Degraded high wax bitumen	n.d.
W13/007927	Sandy River	17-Oct-16	1.9	-35.9557	136.6292	Sandy River Tar	n.d.
W13/007928	Sandy River	17-Oct-16	1.0	-35.9557	136.6292	Sandy River Tar	Sandy River Tar
W13/007929	Sandy River	17-Oct-16	2.0	-35.9556	136.6291	Sandy River Tar	Sandy River Tar
W13/007930	Sandy River	17-Oct-16	0.5	-35.9556	136.6291	Sandy River Tar	n.d.
W13/007931	Sandy River	17-Oct-16	10.6	-35.9556	136.6291	Sandy River Tar	n.d.
W13/007932	Sandy River	17-Oct-16	26.0	-35.9555	136.6291	Sandy River Tar	Sandy River Tar
W13/007933	Sandy River	17-Oct-16	1.3	-35.9555	136.6291	Sandy River Tar	n.d.
W13/007934	Sandy River	17-Oct-16	1.1	-35.9555	136.6291	Sandy River Tar	n.d.
W13/007935	Sandy River	17-Oct-16	0.3	-35.9555	136.6291	Sandy River Tar	n.d.
W13/007936A	Sandy River	17-Oct-16	0.5	-35.9555	136.6290	Sandy River Tar	n.d.
W13/007936B	Sandy River	17-Oct-16	0.2	-35.9555	136.6290	Sandy River Tar	n.d.
W13/007936C	Sandy River	17-Oct-16	0.2	-35.9555	136.6290	Sandy River Tar	n.d.
W13/007937A	Sandy River	17-Oct-16	4.8	-35.9555	136.6290	Sandy River Tar	Sandy River Tar
W13/007937B	Sandy River	17-Oct-16	0.2	-35.9555	136.6290	Sandy River Tar	Sandy River Tar
W13/007938	Sandy River	17-Oct-16	32.7	-35.9554	136.6291	Type III waxy bitumen	Type IIIB waxy bitumen
W13/007939	Sandy River	17-Oct-16	0.8	-35.9552	136.6292	Type I waxy bitumen	n.d.
W13/007940	Sandy River	17-Oct-16	1.2	-35.9554	136.6290	Type III waxy bitumen	n.d.
W13/007941	Sandy River	17-Oct-16	0.7	-35.9554	136.6289	Sandy River Tar	n.d.
W13/007942	Sandy River	17-Oct-16	0.3	-35.9555	136.6290	Sandy River Tar	n.d.
W13/007943	Sandy River	17-Oct-16	17.6	-35.9554	136.6289	Sandy River Tar	n.d.
W13/007944	Sandy River	17-Oct-16	0.5	-35.9555	136.6289	Sandy River Tar	Sandy River Tar
W13/007945A	Sandy River	17-Oct-16	0.3	-35.9554	136.6289	Sandy River Tar	n.d.
W13/007945B	Sandy River	17-Oct-16	0.2	-35.9554	136.6289	Sandy River Tar	n.d.
W13/007946A	Sandy River	17-Oct-16	1.1	-35.9554	136.6289	Sandy River Tar	n.d.
W13/007946B	Sandy River	17-Oct-16	1.2	-35.9554	136.6289	Sandy River Tar	n.d.
W13/007946C	Sandy River	17-Oct-16	0.5	-35.9554	136.6289	Sandy River Tar	n.d.
W13/007947	Sandy River	17-Oct-16	0.6	-35.9554	136.6288	Sandy River Tar	n.d.
W13/007948	Sandy River	17-Oct-16	1.1	-35.9554	136.6288	Sandy River Tar	n.d.
W13/007949	Sandy River	17-Oct-16	7.2	-35.9554	136.6288	Sandy River Tar	n.d.
W13/007950A	Sandy River	17-Oct-16	0.8	-35.9554	136.6288	Sandy River Tar	n.d.
W13/007950B	Sandy River	17-Oct-16	0.3	-35.9554	136.6288	Sandy River Tar	n.d.
W13/007950C	Sandy River	17-Oct-16	0.2	-35.9554	136.6288	Sandy River Tar	n.d.
W13/007950D	Sandy River	17-Oct-16	0.2	-35.9554	136.6288	Sandy River Tar	n.d.
W13/007951	Sandy River	17-Oct-16	0.3	-35.9554	136.6288	Sandy River Tar	n.d.
W13/007952A	Sandy River	17-Oct-16	1.5	-35.9554	136.6287	Sandy River Tar	n.d.
W13/007952B	Sandy River	17-Oct-16	0.8	-35.9554	136.6287	Sandy River Tar	n.d.
W13/007952C	Sandy River	17-Oct-16	0.8	-35.9554	136.6287	Sandy River Tar	n.d.
W13/007952D	Sandy River	17-Oct-16	0.4	-35.9554	136.6287	Sandy River Tar	n.d.
W13/007953	Sandy River	17-Oct-16	12.7	-35.9554	136.6287	Sandy River Tar	Sandy River Tar
W13/007954A	Sandy River	17-Oct-16	0.5	-35.9554	136.6286	Sandy River Tar	n.d.
W13/007954B	Sandy River	17-Oct-16	0.3	-35.9554	136.6286	Sandy River Tar	n.d.
W13/007954C	Sandy River	17-Oct-16	0.1	-35.9554	136.6286	Sandy River Tar	n.d.
W13/007955	Sandy River	17-Oct-16	0.3	-35.9553	136.6286	Sandy River Tar	n.d.
W13/007956A	Sandy River	17-Oct-16	1.2	-35.9553	136.6285	Sandy River Tar	n.d.
W13/007956B	Sandy River	17-Oct-16	0.2	-35.9553	136.6285	Sandy River Tar	n.d.
W13/007957	Sandy River	17-Oct-16	0.3	-35.9553	136.6283	Sandy River Tar	n.d.
W13/007958	Sandy River	17-Oct-16	0.1	-35.9552	136.6283	Sandy River Tar	n.d.
W13/007960	Hanson Bay	17-Oct-16	1.1	-36.0172	136.8576	Degraded high wax bitumen	n.d.
W13/007961	Bales Beach	18-Oct-16	0.5	-35.9950	137.3562	Unknown	n.d.
W13/007962	Bales Beach	18-Oct-16	7.1	-35.9952	137.3567	Type I waxy bitumen	Type I waxy bitumen
W13/007963	Bales Beach	18-Oct-16	16.6	-35.9952	137.3584	Type I waxy bitumen	n.d.
W13/007964	Bales Beach	18-Oct-16	4.2	-35.9951	137.3584	Type I waxy bitumen	n.d.
W13/007965	Bales Beach	18-Oct-16	0.3	-35.9967	137.3607	Type I waxy bitumen	Type I waxy bitumen
W13/007966	Bales Beach	18-Oct-16	1.6	-35.9967	137.3607	Type I waxy bitumen	n.d.

Sample ID	Survey Site	Collection Date	Weight (g)	Latitude	Longitude	Whole-oil classification	Biomarker Classification
W13/007967	Pennington Bay	18-Oct-16	3.8	-35.8523	137.7445	Type I waxy bitumen	Type I waxy bitumen
W13/007968	Pennington Bay	18-Oct-16	0.6	-35.8525	137.7436	Degraded high wax bitumen	n.d.
W13/007969	Waitpinga Beach	19-Oct-16	21.0	-35.6346	138.5001	Type IV waxy bitumen	Type IVA waxy bitumen
W13/007971	Waitpinga Beach	19-Oct-16	1.8	-35.6359	138.5055	Type I waxy bitumen	n.d.
W13/007972	Waitpinga Beach	19-Oct-16	5.8	-35.6359	138.5056	Degraded high wax bitumen	n.d.
W13/007973	Waitpinga Beach	19-Oct-16	5.6	-35.6362	138.5068	Type IV waxy bitumen	Type IVA waxy bitumen
W13/007974	Waitpinga Beach	19-Oct-16	0.9	-35.6373	138.5101	Type IV waxy bitumen	Type IVA waxy bitumen
W13/007975	Waitpinga Beach	19-Oct-16	12.1	-35.6374	138.5103	Type IV waxy bitumen	Type IVA waxy bitumen
W13/007976	Waitpinga Beach	19-Oct-16	3188	-35.6374	138.5103	Asphaltite	Asphaltite
W13/007977	Waitpinga Beach	19-Oct-16	3.0	-35.6376	138.5108	Type I waxy bitumen	n.d.
W13/007978	Waitpinga Beach	19-Oct-16	0.6	-35.6376	138.5108	Type IV waxy bitumen	n.d.
W13/007979	Waitpinga Beach	19-Oct-16	3.9	-35.6376	138.5109	Type IV waxy bitumen	n.d.
W13/007980	Waitpinga Beach	19-Oct-16	0.3	-35.6376	138.5108	Degraded high wax bitumen	n.d.
W13/007981	Waitpinga Beach	19-Oct-16	0.6	-35.6376	138.5109	Type I waxy bitumen	n.d.
W13/007982	Waitpinga Beach	19-Oct-16	0.4	-35.6378	138.5111	Degraded high wax bitumen	n.d.
W13/007984	Waitpinga Beach	19-Oct-16	16.8	-35.6380	138.5115	Type IV waxy bitumen	Type IVA waxy bitumen
W13/007985	Waitpinga Beach	19-Oct-16	9.2	-35.6368	138.5088	Type IV waxy bitumen	Type IVA waxy bitumen
W13/007986	28 Mile Crossing	20-Oct-16	0.9	-36.4370	139.7724	Type I waxy bitumen	n.d.
W13/007987	28 Mile Crossing	20-Oct-16	1.5	-36.4375	139.7726	Type I waxy bitumen	n.d.
W13/007988	28 Mile Crossing	20-Oct-16	0.5	-36.4362	139.7728	Type I waxy bitumen	n.d.
W13/007989	The Granites	20-Oct-16	2.6	-36.6581	139.8537	Type I waxy bitumen	n.d.
W13/007990	The Granites	20-Oct-16	0.7	-36.6577	139.8537	Type I waxy bitumen	n.d.
W13/007991	The Granites	20-Oct-16	5.0	-36.6575	139.8536	Type I waxy bitumen	n.d.
W13/007992	The Granites	20-Oct-16	0.4	-36.6573	139.8535	Type I waxy bitumen	n.d.
W13/007993	The Granites	20-Oct-16	2.5	-36.6571	139.8535	Type I waxy bitumen	n.d.
W13/007994	The Granites	20-Oct-16	0.5	-36.6570	139.8534	Type I waxy bitumen	n.d.
W13/007995	The Granites	20-Oct-16	4.4	-36.6562	139.8532	Type I waxy bitumen	Type I waxy bitumen
W13/007996	The Granites	20-Oct-16	10.3	-36.6546	139.8528	Type I waxy bitumen	n.d.
W13/007997	The Granites	20-Oct-16	1.9	-36.6529	139.8524	Type I waxy bitumen	Type I waxy bitumen
W13/007998	The Granites	20-Oct-16	1.2	-36.6529	139.8524	Type I waxy bitumen	n.d.
W13/007999	The Granites	20-Oct-16	0.7	-36.6509	139.8519	Type I waxy bitumen	Type I waxy bitumen
COA/000956	The Granites	20-Oct-16	6.4	-36.6521	139.8521	Asphaltite	Asphaltite
COA/000957	Eves Cove	21-Oct-16	6.1	-37.1818	139.7430	Type I waxy bitumen	n.d.
COA/000958	Eves Cove	21-Oct-16	0.7	-37.1819	139.7430	Degraded high wax bitumen	n.d.
COA/000959	Eves Cove	21-Oct-16	1.0	-37.1825	139.7442	Degraded high wax bitumen	n.d.
COA/000960	Eves Cove	21-Oct-16	0.7	-37.1830	139.7447	Degraded high wax bitumen	n.d.
COA/000961	Eves Cove	21-Oct-16	3.3	-37.1833	139.7452	Type I waxy bitumen	n.d.
COA/000962	Eves Cove	21-Oct-16	0.8	-37.1834	139.7453	Degraded high wax bitumen	n.d.
COA/000963	Eves Cove	21-Oct-16	1.2	-37.1838	139.7460	Degraded high wax bitumen	n.d.
COA/000964	Eves Cove	21-Oct-16	1.9	-37.1838	139.7460	Type I waxy bitumen	n.d.
COA/000965	Eves Cove	21-Oct-16	1.0	-37.1838	139.7460	Degraded high wax bitumen	n.d.
COA/000966	Eves Cove	21-Oct-16	2.0	-37.1839	139.7460	Type I waxy bitumen	n.d.
COA/000967	Eves Cove	21-Oct-16	2.1	-37.1839	139.7460	Type I waxy bitumen	n.d.
COA/000968	Eves Cove	21-Oct-16	1.0	-37.1838	139.7461	Degraded high wax bitumen	n.d.
COA/000969	Eves Cove	21-Oct-16	1.8	-37.1838	139.7461	Type I waxy bitumen	n.d.
COA/000970	Eves Cove	21-Oct-16	2.3	-37.1839	139.7461	Degraded high wax bitumen	n.d.
COA/000971	Eves Cove	21-Oct-16	2.1	-37.1839	139.7461	Type I waxy bitumen	n.d.
COA/000972	Eves Cove	21-Oct-16	2.5	-37.1839	139.7462	Type III waxy bitumen	n.d.
COA/000973	Eves Cove	21-Oct-16	0.5	-37.1840	139.7462	Type I waxy bitumen	n.d.
COA/000974	Eves Cove	21-Oct-16	1.0	-37.1840	139.7462	Degraded high wax bitumen	n.d.
COA/000975	Eves Cove	21-Oct-16	1.3	-37.1841	139.7462	Degraded high wax bitumen	n.d.
COA/000976	Eves Cove	21-Oct-16	8.4	-37.1841	139.7462	Type I waxy bitumen	Type I waxy bitumen
COA/000977	Eves Cove	21-Oct-16	0.8	-37.1840	139.7463	Degraded high wax bitumen	n.d.

Sample ID	Survey Site	Collection Date	Weight (g)	Latitude	Longitude	Whole-oil classification	Biomarker Classification
COA/000978	Eves Cove	21-Oct-16	0.6	-37.1840	139.7463	Type I waxy bitumen	n.d.
COA/000979	Eves Cove	21-Oct-16	0.8	-37.1841	139.7463	Type I waxy bitumen	n.d.
COA/000980	Eves Cove	21-Oct-16	1.1	-37.1841	139.7464	Type III waxy bitumen	n.d.
COA/000981	Eves Cove	21-Oct-16	3.7	-37.1841	139.7463	Type I waxy bitumen	n.d.
COA/000982	Eves Cove	21-Oct-16	2.6	-37.1841	139.7464	Type I waxy bitumen	n.d.
COA/000983	Eves Cove	21-Oct-16	1.4	-37.1842	139.7464	Type I waxy bitumen	n.d.
COA/000984	Eves Cove	21-Oct-16	12.7	-37.1842	139.7465	Type I waxy bitumen	n.d.
COA/000985	Eves Cove	21-Oct-16	0.7	-37.1844	139.7467	Unknown	n.d.
COA/000986	Eves Cove	21-Oct-16	1.7	-37.1844	139.7467	Type I waxy bitumen	n.d.
COA/000987	Eves Cove	21-Oct-16	2.2	-37.1845	139.7468	Degraded high wax bitumen	n.d.
COA/000988A	Eves Cove	21-Oct-16	2.5	-37.1845	139.7468	Degraded high wax bitumen	n.d.
COA/000988B	Eves Cove	21-Oct-16	0.3	-37.1845	139.7468	Degraded high wax bitumen	n.d.
COA/000989	Eves Cove	21-Oct-16	1.6	-37.1845	139.7468	Type I waxy bitumen	n.d.
COA/000990	Eves Cove	21-Oct-16	3.1	-37.1846	139.7470	Degraded high wax bitumen	n.d.
COA/000991	Eves Cove	21-Oct-16	4.4	-37.1860	139.7484	Type I waxy bitumen	n.d.
COA/000992	Eves Cove	21-Oct-16	6.0	-37.1860	139.7484	Degraded high wax bitumen	n.d.
COA/000993	Eves Cove	21-Oct-16	0.7	-37.1860	139.7484	Degraded high wax bitumen	n.d.
COA/000994	Eves Cove	21-Oct-16	2.6	-37.1861	139.7484	Type I waxy bitumen	n.d.
COA/000995	Eves Cove	21-Oct-16	4.9	-37.1861	139.7485	Type I waxy bitumen	n.d.
COA/000996	Eves Cove	21-Oct-16	4.1	-37.1865	139.7489	Degraded high wax bitumen	n.d.
COA/000997	Eves Cove	21-Oct-16	1.6	-37.1865	139.7489	Type I waxy bitumen	n.d.
COA/000998	Eves Cove	21-Oct-16	1.7	-37.1866	139.7490	Type I waxy bitumen	n.d.
COA/000999	Eves Cove	21-Oct-16	6.1	-37.1867	139.7490	Type I waxy bitumen	n.d.
COA/001000	Eves Cove	21-Oct-16	4.2	-37.1867	139.7490	Type I waxy bitumen	n.d.
/001001	Eves Cove	21-Oct-16	4.2	-37.1867	139.7491	Type I waxy bitumen	n.d.
/001002	Eves Cove	21-Oct-16	10.4	-37.1867	139.7491	Type I waxy bitumen	n.d.
/001003	Eves Cove	21-Oct-16	4.3	-37.1867	139.7491	Type I waxy bitumen	n.d.
/001004	Eves Cove	21-Oct-16	2.3	-37.1867	139.7491	Type I waxy bitumen	n.d.
/001005	Eves Cove	21-Oct-16	0.6	-37.1868	139.7493	Type III waxy bitumen	n.d.
/001006	Eves Cove	21-Oct-16	8.4	-37.1868	139.7492	Type I waxy bitumen	n.d.
/001007	Eves Cove	21-Oct-16	2.2	-37.1868	139.7492	Type I waxy bitumen	n.d.
/001008	Eves Cove	21-Oct-16	7.0	-37.1868	139.7491	Type I waxy bitumen	n.d.
/001009	Eves Cove	21-Oct-16	3.1	-37.1869	139.7491	Type I waxy bitumen	n.d.
/001010	Eves Cove	21-Oct-16	2.6	-37.1869	139.7491	Type I waxy bitumen	n.d.
/001011	Eves Cove	21-Oct-16	11.8	-37.1869	139.7492	Type I waxy bitumen	n.d.
/001012	Beachport Conservation Park	21-Oct-16	1.6	-37.4412	139.9554	Type I waxy bitumen	n.d.
/001013	Beachport Conservation Park	21-Oct-16	1.6	-37.4412	139.9555	Type I waxy bitumen	n.d.
/001014	Beachport Conservation Park	21-Oct-16	2.3	-37.4411	139.9555	Type I waxy bitumen	n.d.
/001015	Beachport Conservation Park	21-Oct-16	2.7	-37.4412	139.9556	Type I waxy bitumen	n.d.
/001016	Beachport Conservation Park	21-Oct-16	1.2	-37.4417	139.9575	Type I waxy bitumen	n.d.
/001017	Beachport Conservation Park	21-Oct-16	1.9	-37.4417	139.9581	Type I waxy bitumen	n.d.
/001019	Beachport Conservation Park	21-Oct-16	5.7	-37.4418	139.9583	Type I waxy bitumen	n.d.
/001020	Beachport Conservation Park	21-Oct-16	1.2	-37.4418	139.9584	Type I waxy bitumen	n.d.
/001021	Beachport Conservation Park	21-Oct-16	7.3	-37.4419	139.9584	Type I waxy bitumen	Type I waxy bitumen
/001022	Beachport Conservation Park	21-Oct-16	16.1	-37.4419	139.9584	Type I waxy bitumen	n.d.
/001024	Beachport Conservation Park	21-Oct-16	1.2	-37.4424	139.9594	Type I waxy bitumen	n.d.

Sample ID	Survey Site	Collection Date	Weight (g)	Latitude	Longitude	Whole-oil classification	Biomarker Classification
/001025A	Beachport Conservation Park	21-Oct-16	4.1	-37.4432	139.9604	Type I waxy bitumen	n.d.
/001025B	Beachport Conservation Park	21-Oct-16	2.5	-37.4432	139.9604	Type IV waxy bitumen	n.d.
/001026	Beachport Conservation Park	21-Oct-16	1.5	-37.4434	139.9607	Degraded high wax bitumen	n.d.
/001027	Beachport Conservation Park	21-Oct-16	1.5	-37.4436	139.9610	Type I waxy bitumen	n.d.
/001028	Beachport Conservation Park	21-Oct-16	2.8	-37.4437	139.9611	Type I waxy bitumen	n.d.
/001029	Beachport Conservation Park	21-Oct-16	1.8	-37.4437	139.9612	Type I waxy bitumen	n.d.
/001030	Beachport Conservation Park	21-Oct-16	0.8	-37.4438	139.9612	Degraded high wax bitumen	n.d.
/001031	Beachport Conservation Park	21-Oct-16	1.5	-37.4445	139.9617	Type I waxy bitumen	n.d.
/001032	Beachport Conservation Park	21-Oct-16	2.1	-37.4448	139.9620	Type III waxy bitumen	Type IIIB waxy bitumen
/001033	Beachport Conservation Park	21-Oct-16	6.4	-37.4449	139.9621	Type I waxy bitumen	n.d.
/001034	Beachport Conservation Park	21-Oct-16	1.0	-37.4450	139.9621	Type I waxy bitumen	n.d.
/001035	Beachport Conservation Park	21-Oct-16	2.8	-37.4450	139.9621	Type I waxy bitumen	n.d.
/001036	Beachport Conservation Park	21-Oct-16	2.6	-37.4451	139.9622	Type I waxy bitumen	n.d.
/001037	Beachport Conservation Park	21-Oct-16	3.6	-37.4452	139.9622	Type I waxy bitumen	n.d.
/001038	Beachport Conservation Park	21-Oct-16	1.3	-37.4452	139.9622	Type I waxy bitumen	n.d.
/001039A	Beachport Conservation Park	21-Oct-16	1.0	-37.4452	139.9622	Type I waxy bitumen	n.d.
/001039B	Beachport Conservation Park	21-Oct-16	0.5	-37.4452	139.9622	Type I waxy bitumen	Type I waxy bitumen
/001040A	Beachport Conservation Park	21-Oct-16	1.1	-37.4453	139.9622	Type I waxy bitumen	n.d.
/001040B	Beachport Conservation Park	21-Oct-16	0.6	-37.4453	139.9622	Type I waxy bitumen	n.d.
/001041	Beachport Conservation Park	21-Oct-16	0.7	-37.4453	139.9623	Type I waxy bitumen	n.d.
/001042	Beachport Conservation Park	21-Oct-16	0.3	-37.4453	139.9623	Type I waxy bitumen	n.d.
/001043	Beachport Conservation Park	21-Oct-16	0.8	-37.4453	139.9623	Type I waxy bitumen	Type I waxy bitumen
/001044A	Beachport Conservation Park	21-Oct-16	0.3	-37.4454	139.9623	Type I waxy bitumen	n.d.
/001044B	Beachport Conservation Park	21-Oct-16	0.2	-37.4454	139.9623	Type III waxy bitumen	Type IIIB waxy bitumen
/001045	Beachport Conservation Park	21-Oct-16	0.6	-37.4455	139.9624	Type I waxy bitumen	n.d.
/001046	Beachport Conservation Park	21-Oct-16	2.9	-37.4455	139.9624	Type I waxy bitumen	n.d.
/001047	Beachport Conservation Park	21-Oct-16	2.3	-37.4459	139.9627	Type I waxy bitumen	n.d.
/001048	Beachport Conservation Park	21-Oct-16	1.1	-37.4459	139.9628	Type I waxy bitumen	n.d.
/001049	Beachport Conservation Park	21-Oct-16	1.3	-37.4460	139.9628	Degraded high wax bitumen	n.d.

Sample ID	Survey Site	Collection Date	Weight (g)	Latitude	Longitude	Whole-oil classification	Biomarker Classification
/001050	Beachport Conservation Park	21-Oct-16	1.1	-37.4461	139.9629	Type I waxy bitumen	n.d.
/001051	Beachport Conservation Park	21-Oct-16	0.8	-37.4463	139.9630	Type I waxy bitumen	n.d.
/001052	Geltwood Beach	22-Oct-16	14.7	-37.6586	140.2215	Type I waxy bitumen	n.d.
/001053	Geltwood Beach	22-Oct-16	3.8	-37.6603	140.2234	Type I waxy bitumen	n.d.
/001054	Geltwood Beach	22-Oct-16	0.7	-37.6603	140.2235	Type I waxy bitumen	n.d.
/001055	Number 1 and 2 Rocks	22-Oct-16	0.5	-37.7954	140.3204	Type III waxy bitumen	Type IIIA waxy bitumen
/001056	Number 1 and 2 Rocks	22-Oct-16	8.8	-37.7956	140.3205	Asphaltic Tar	Asphaltic Tar
/001057	Number 1 and 2 Rocks	22-Oct-16	1.3	-37.7956	140.3206	Type I waxy bitumen	n.d.
/001058	Number 1 and 2 Rocks	22-Oct-16	0.4	-37.7958	140.3206	Type III waxy bitumen	n.d.
/001059	Number 1 and 2 Rocks	22-Oct-16	132	-37.7959	140.3209	Asphaltic Tar	n.d.
/001060	Number 1 and 2 Rocks	22-Oct-16	0.6	-37.7959	140.3209	Type I waxy bitumen	n.d.
/001061	Number 1 and 2 Rocks	22-Oct-16	0.1	-37.7965	140.3217	Type I waxy bitumen	n.d.
/001062	Number 1 and 2 Rocks	22-Oct-16	1.7	-37.7976	140.3226	Degraded high wax bitumen	n.d.
/001063	Number 1 and 2 Rocks	22-Oct-16	52	-37.7977	140.3228	Asphaltic Tar	Asphaltic Tar
/001064A	Number 1 and 2 Rocks	22-Oct-16	1.1	-37.7980	140.3230	Unknown	n.d.
/001064B	Number 1 and 2 Rocks	22-Oct-16	0.5	-37.7980	140.3230	Type I waxy bitumen	n.d.
/001065	Number 1 and 2 Rocks	22-Oct-16	0.3	-37.7979	140.3230	Type I waxy bitumen	n.d.
/001067	Number 1 and 2 Rocks	22-Oct-16	26.6	-37.7980	140.3231	Asphaltic Tar	Asphaltic Tar
/001068	Number 1 and 2 Rocks	22-Oct-16	27.0	-37.7980	140.3231	Asphaltic Tar	Asphaltic Tar
/001069	Number 1 and 2 Rocks	22-Oct-16	1.5	-37.7980	140.3231	Type I waxy bitumen	n.d.
/001070	Number 1 and 2 Rocks	22-Oct-16	8.7	-37.7981	140.3231	Type I waxy bitumen	n.d.
/001071	Number 1 and 2 Rocks	22-Oct-16	2.8	-37.7981	140.3232	Type I waxy bitumen	n.d.
/001072A	Number 1 and 2 Rocks	22-Oct-16	1.0	-37.7981	140.3232	Type I waxy bitumen	n.d.
/001073	Number 1 and 2 Rocks	22-Oct-16	10.3	-37.7982	140.3232	Type I waxy bitumen	n.d.
/001074	Number 1 and 2 Rocks	22-Oct-16	0.6	-37.7983	140.3232	Type I waxy bitumen	n.d.
/001075	Number 1 and 2 Rocks	22-Oct-16	4.3	-37.7982	140.3233	Type I waxy bitumen	n.d.
/001076	Number 1 and 2 Rocks	22-Oct-16	2.9	-37.7982	140.3233	Asphaltic Tar	Asphaltic Tar
/001077	Number 1 and 2 Rocks	22-Oct-16	0.4	-37.7982	140.3233	Type I waxy bitumen	n.d.
/001079	Number 1 and 2 Rocks	22-Oct-16	196	-37.7985	140.3235	Asphaltic Tar	Asphaltic Tar
/001080	Number 1 and 2 Rocks	22-Oct-16	1.0	-37.7986	140.3236	Type I waxy bitumen	n.d.
/001081	Number 1 and 2 Rocks	22-Oct-16	16.9	-37.7986	140.3236	Asphaltic Tar	Asphaltic Tar
/001082	Number 1 and 2 Rocks	22-Oct-16	21.5	-37.7962	140.3217	Type III waxy bitumen	n.d.
/001083	Number 1 and 2 Rocks	22-Oct-16	10.0	-37.7962	140.3217	Type I waxy bitumen	n.d.
/001084	Number 1 and 2 Rocks	22-Oct-16	1.3	-37.7962	140.3217	Type I waxy bitumen	n.d.
/001085	Nene Valley	22-Oct-16	6.7	-37.9860	140.5118	Type I waxy bitumen	n.d.

n.d. = Not determined.
N.R. = GPS co-ordinates were not recorded.

PUBLISHED MANUSCRIPTS

www.nature.com/scientificreports

SCIENTIFIC REPORTS

OPEN

Remotely constraining the temporal evolution of offshore oil systems

Alexander J. Corrick[1], David Selby[2,3], David M. McKirdy[1], Philip A. Hall[1], Se Gong[4], Christine Trefry[5] & Andrew S. Ross[5]

Received: 14 August 2018
Accepted: 13 December 2018
Published online: 04 February 2019

An understanding of the temporal evolution of a petroleum system is fundamental to interpreting where hydrocarbons may be trapped in the subsurface. However, traditional exploration methods provide few absolute constraints on the timing of petroleum generation. Here we show that $^{187}Re/^{187}Os$ geochronology may be applied to natural crude oil seepage to determine when petroleum generation occurred in offshore sedimentary basins. Using asphaltites collected from the South Australian coastline, our determined Re-Os age (68 ± 15 million years ago) is consistent with their derivation from a Late Cretaceous source rock in the nearby Bight Basin, an interpretation similarly favoured by source-specific biomarker constraints. Furthermore, the calculated initial $^{187}Os/^{188}Os$ composition of the asphaltites, a value inherited from the source rock at the time of oil generation, suggests that the source rock represents the later stage of Oceanic Anoxic Event 2. Our results demonstrate a new approach to identifying the origin of crude oils encountered in coastal environments by providing direct constraints on the timing of petroleum generation and potential source rock intervals in poorly characterised offshore sedimentary basins prior to exploratory drilling.

Natural seepage is a major contributor of oil to the marine environment, estimated at ~600,000 tonnes per year[1]. When entrained in prevailing ocean currents, this seepage may strand along the coastline as liquid oil, viscous tar or semi-solid bitumen[2–4]. The distance crude oils are transported by ocean currents may be short if the seepage site is near the coastline[5]. However, there is evidence of significantly longer transport, where bitumens are found on distant foreign coastlines[3]. The geochemistry of these crude oils can be used to characterise and identify their respective parent petroleum systems and potentially distinguish them from anthropogenic inputs of oil such as tanker spillage[6].

The traditional approach to geochemically characterising and correlating crude oils utilises carbon isotopes and biomarkers to ascertain the depositional environment and organic facies of their source rocks[7]. Although specific biomarkers may broadly constrain the depositional age of a source rock and provide an estimate of its thermal maturity, none of these analytical tools yields an absolute age. Understanding the timing of oil generation from the source rock is vital to assessing the potential migration pathways and structural traps which form viable hydrocarbon reservoirs. Consequently, petroleum exploration relies heavily on a theoretical timing of hydrocarbon generation determined from basin modelling[8]. These models are generally based on assumptions about the source rocks that may be active in the basin, which in turn introduces a component of uncertainty that may affect exploration prospects.

A major recent advance in petroleum geochemistry has been the ability to directly determine the timing of hydrocarbon generation from the source rock using the decay of ^{187}Re to ^{187}Os within the produced oil[9–14]. Studies using naturally formed oils and those produced via artificial maturation of source rocks in a laboratory setting have also demonstrated that the initial $^{187}Os/^{188}Os$ composition of an oil (Os_i) is inherited directly from the source rock at the time of generation[13–15]. Therefore, comparison of this Os_i value of an oil to the $^{187}Os/^{188}Os$ composition of a proposed source rock at the time of generation (Os_g) may be used to aid oil-to-source correlations, should data on the source rock be available[11,14,16]. However, previous applications of Re-Os dating using oils and bitumens have been restricted to samples collected *in-situ*, rather than examples released from the subsurface into the marine environment through natural seepage. The successful application of Re-Os geochronology to seep emissions will permit the timing of oil generation to be constrained prior to exploratory drilling.

[1]Department of Earth Sciences, School of Physical Sciences, University of Adelaide, Adelaide, SA, 5005, Australia. [2]Department of Earth Sciences, Durham University, Durham, DH1 3LE, UK. [3]State Key Laboratory of Geological Processes and Mineral Resources, School of Earth Resources, China University of Geosciences, Wuhan, 430074, Hubei, China. [4]Energy, CSIRO, North Ryde, NSW, 2113, Australia. [5]Energy, CSIRO, Kensington, WA, 6151, Australia. Correspondence and requests for materials should be addressed to A.J.C. (email: alexander.corrick@adelaide.edu.au)

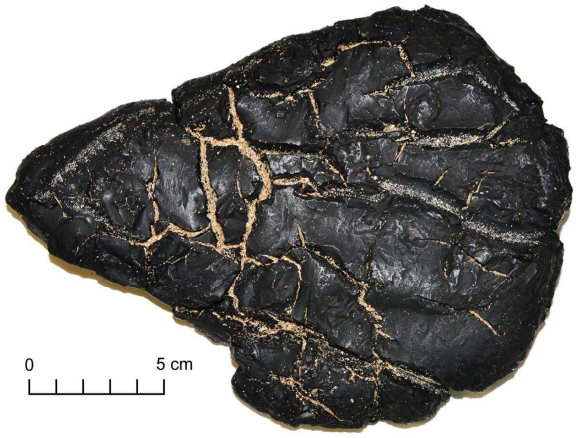


Figure 1. Large asphaltite exhibiting deep shrinkage cracks following devolatilization of low-molecular-weight hydrocarbons. Sample W13/007507, collected from Waitpinga Beach, South Australia in 2014.

Australia's southern margin collects bitumens emitted from a variety of different petroleum systems[2,3,17,18]. One of the rarest, but most distinctive, types encountered is known as asphaltite[2,17]. These bitumens are easily identified by their striking appearance defined by deep shrinkage cracks, conchoidal fracture and jet-black colour (Fig. 1). A combination of highly reproducible source-specific biomarkers and other hydrocarbons constrains the origin of these asphaltites to a single oil family expelled early in the oil generation window from a Mesozoic marine shale deposited under anoxic/sulfidic conditions[2,17]. Their biomarker composition is unique, and yet to be linked to any produced oil worldwide[19]. This suggests that the asphaltites are not the result of anthropogenic spillage, but rather the product of seafloor seepage from an unidentified petroleum system. Despite their prior extended immersion in seawater, recently stranded asphaltite specimens also preserve high abundances of slightly water-soluble aromatic hydrocarbons such as methylnaphthalenes and phenanthrene, indicating that the parent petroleum system is proximal to their region of stranding[2,17]. Presently, the origin of these asphaltite strandings is attributed to a source rock deposited during the Late Cretaceous global oceanic anoxic event (OAE2) at the Cenomanian-Turonian boundary (93.9 Ma) within the nearby Bight Basin[17,20]. This predominantly offshore Jurassic-Cretaceous rift basin formed during the separation of Australia and Antarctica[21,22] and remains relatively unexplored. However, it is proposed to contain marine-derived source rocks deposited during the latest Cenomanian to earliest Turonian[20].

Here we present Re-Os data from asphaltites collected from the South Australian coastline (n = 11; Fig. 2; Table S1) during annual beach surveys in 2014–2016, as part of the Great Australian Bight Research Program[18,23]. We show that the timing of oil generation in an offshore sedimentary basin may be constrained directly using hydrocarbon seepage. This information may then be used to inform, refine or support petroleum systems models for assessing offshore exploration prospects. We then use the calculated asphaltite Os_i value to assess if their origin is consistent with an OAE2 source rock. Our findings demonstrate that the Re-Os isotope systematics of hydrocarbon seepage can provide important information constraining the evolution of offshore oil systems prior to costly exploratory drilling.

Results

Asphaltite Re-Os data. The asphaltites contain between 2.59 and 4.02 parts per billion (ppb) Re and 24.6 to 43.1 parts per trillion (ppt) Os. The $^{187}Re/^{188}Os$ ratios are high (400.5–547.8) and positively correlate with the $^{187}Os/^{188}Os$ ratios (1.122–1.303). Regression of all the asphaltite Re-Os data from sample interiors, exteriors and replicate analyses (n = 16; Table S2) yields a Model 3 age (for which the scatter in the data exceeds that expected from analytical precision)[24] of 74 ± 26 Ma, with an Os_i of 0.63 ± 0.22 and a degree of fit (mean square of weighted deviates; MSWD) value of 2.6 (Fig. 3A). The low precision of this age (35%) can be attributed to specific data points which deviate from the best-fit regression line (i.e. the isochron). A refined Re-Os age may therefore be determined by limiting the regression to the data points with low deviation from the predicted $^{187}Os/^{188}Os$ value determined from the entire dataset[25]. A revised regression restricted to samples with less than 2% deviation from the regression line (n = 9; Table S3) yields a Model 1 age (for which the scatter in data is consistent with the uncertainties attributable to analytical precision)[24] of 68 ± 15 Ma, an Os_i of 0.66 ± 0.12 and a MSWD of 0.95 (Fig. 3B). Of the seven data points excluded, five were replicate analyses of counterparts that deviated <2% from the initial regression and were still included. The remaining two excluded data points were obtained from specimens with no replicate analyses but returned $^{187}Os/^{188}Os$ values comparable to the other excluded data points. Samples with $^{187}Os/^{188}Os$ values that differ from the majority of the dataset could be interpreted as having originated from a

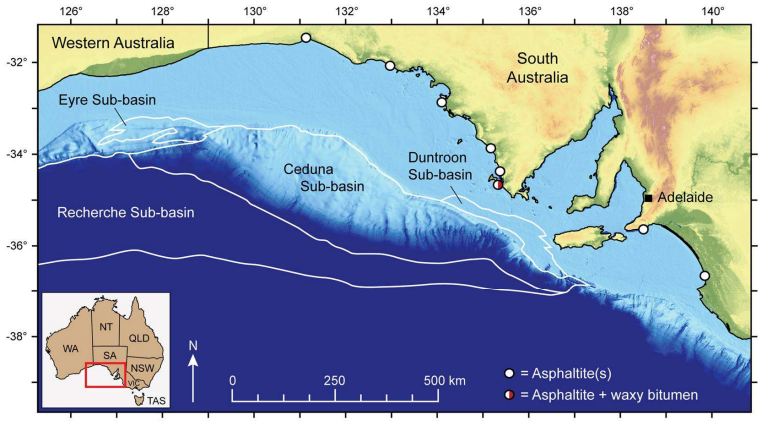


Figure 2. Stranding locations of analysed samples and the offshore Jurassic-Cretaceous sub-basins of the Bight Basin. See Table S1 for further sample collection information.

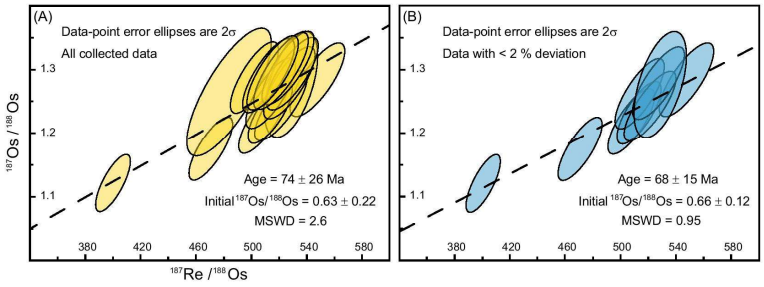


Figure 3. Re-Os isochron diagrams for South Australian asphaltites. (**A**) Regression of all Re-Os data (n = 16) from asphaltite interiors, weathered exteriors and replicate analyses yields an age of 74 ± 26 Ma. (**B**) Regression of asphaltite data with <2% deviation from the regression of all data points (n = 9; Table S3) yields an age of 68 ± 15 Ma.

second source rock. However, this is not the case here because the biomarker geochemistry of all samples analysed is highly consistent (Table S4).

Extent of alteration in the marine environment. The majority of the Re and Os in a crude oil is located in its asphaltene fraction, which is highly resistant to the effects of biodegradation[16]. However, to test if exposure to seawater influenced the Re-Os systematics of the asphaltites, the extent of degradation (Fig. 4) in each specimen was assessed based on the alteration and removal of key compounds by evaporation, water washing and biodegradation (Table S5). This assessment revealed that variation in $^{187}Re/^{188}Os$ and $^{187}Os/^{188}Os$ ratios in the sample suite is not systematic with increasing alteration. Furthermore, comparison of the weathered exteriors (top 2 mm) of four asphaltites with their respective interiors all returned ratios within the range of analytical uncertainty (Table S2). Finally, the Re-Os characteristics of the asphaltites were compared to those of a waxy bitumen specimen (W13/007697) recovered from the same coastline and known to originate from one of several distant Cenozoic lacustrine petroleum systems in the Indonesian archipelago[3]. The waxy bitumen contained very low abundances of Re and Os (0.02 ppb and 1.34 ppt, respectively), with a $^{187}Re/^{188}Os$ ratio of 84.4 and $^{187}Os/^{188}Os$ ratio of 0.486. As only a single waxy bitumen specimen was analysed for comparison, no isochron could be constructed to calculate a generation age for its parent crude oil. Nevertheless, the fact that the asphaltites and waxy bitumen, two distinctly different oil types, have clearly different Re-Os abundances and ratios (Table S2) is significant because it suggests they have retained the signatures of their parent oils, despite their exposure to the same marine environment.

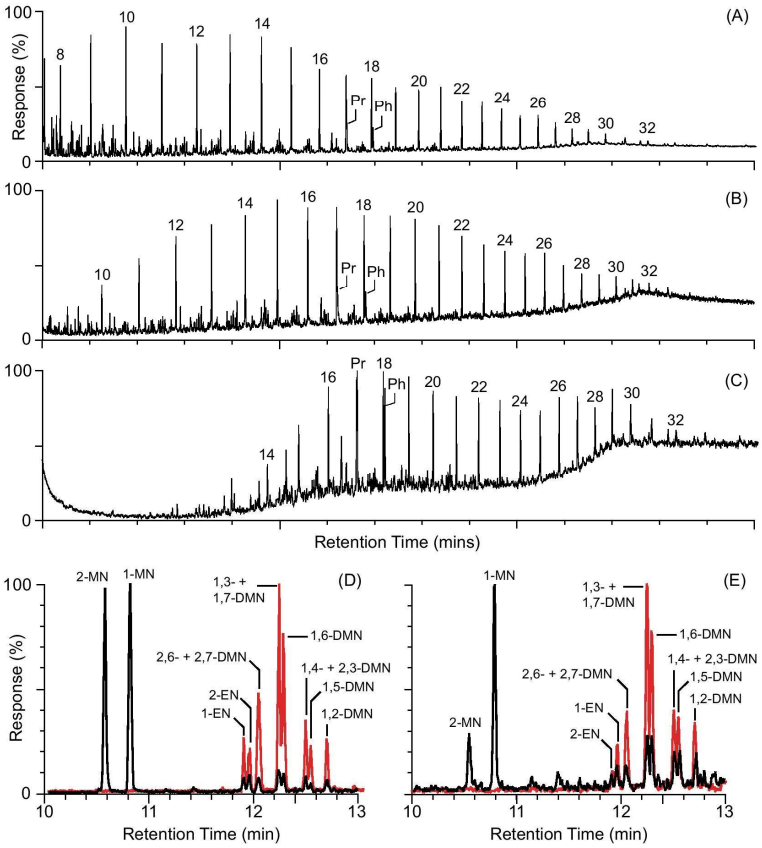


Figure 4. GC-MS chromatograms illustrating the variation in degradation across the suite of analysed asphaltites. (**A**) Whole-oil total ion chromatogram (TIC) of a minimally degraded asphaltite (W13/007976). (**B**) Whole-oil TIC of a moderately degraded asphaltite (W13/007507) showing depletion of low-molecular-weight *n*-alkanes. (**C**) Whole-oil TIC of a highly degraded asphaltite (W13/007668) showing loss of gasoline and kerosene-range alkanes. (**D**) Selected ion monitoring (SIM) chromatograms (black = *m/z* 142, red = *m/z* 156) of the aromatic fraction of a fresh asphaltite (W13/007976), preserving abundant methylnaphthalenes, ethylnaphthalenes and dimethylnaphthalenes. (**E**) SIM chromatograms of the aromatic fraction of a highly degraded asphaltite (W13/007668), displaying prominent loss of 2-MN, 2-EN and 1,5-DMN due to weathering. Key: peak numbers in whole-oil TIC chromatograms correspond to *n*-alkane carbon chain length; Pr = pristane; Ph = phytane; MN = methylnaphthalene; EN = ethylnaphthalene; DMN = dimethylnaphthalene. Geochemical data and assigned level of degradation for each sample is listed in Table S4. The criteria used to define each level of alteration are listed in Table S5.

Comparison with the OAE2 osmium isotope record. Following the generation and expulsion of hydrocarbons, the different abundances of ^{187}Re in the source rock and its expelled oil will cause their ^{187}Os/^{188}Os compositions to gradually diverge as ^{187}Re continues to decay to ^{187}Os. Therefore, in order to use osmium isotopes to assess the correlation of an oil and a potential source rock, the ^{187}Os/^{188}Os values at the time of oil generation must be known (i.e. it is the Os_i and Os_g values that must be compared), as this is the point when the osmium composition of the source rock was imparted directly to the oil. Unfortunately, there is no established osmium isotope record across the Cenomanian-Turonian boundary in the Bight Basin from which to determine an Os_g value for direct correlation. However, OAE2 is associated with an ^{187}Os/^{188}Os anomaly expressed in widely separated palaeogeographic settings[26–28] (Fig. 5). Therefore, to assess if the asphaltite Os_i value (0.66 ± 0.12) is consistent

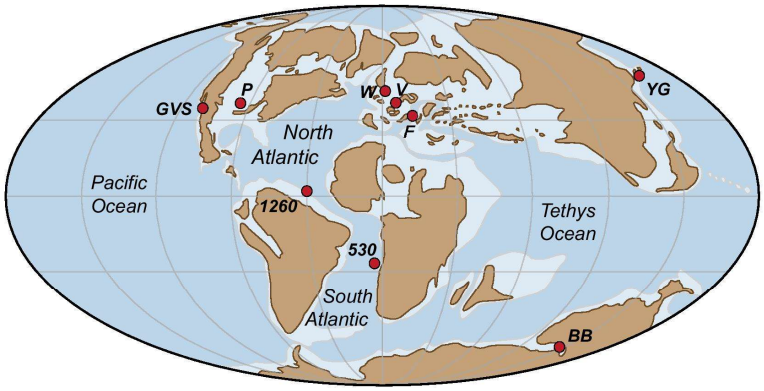


Figure 5. Palaeogeographic map identifying locations of Os isotope records across OAE2 and the location of the Bight Basin. GVS = Great Valley Sequence, P = Portland #1 (GSSP), W = Wunstorf, V = Vocontian Basin, F = Furlo, 1260 = ODP Site 1260, 530 = DSDP Site 530, YG = Yezo Group, BB = Bight Basin. Modified after reference[28].

with that of an OAE2 source rock, we calculated the $^{187}Os/^{188}Os$ composition for each of these published records across the asphaltite generation window of 68 ± 15 Ma (Fig. 6; Table S6). These Os_g profiles preserve an abrupt shift towards non-radiogenic values (~0.2) at the onset of OAE2. The anomalously non-radiogenic conditions are maintained across the A-B stage (94.38–94.23 Ma), prior to a progressive return to radiogenic values within the B-C stage (94.23–93.95 Ma). Despite local variability, the asphaltite Os_i value most commonly intersects these OAE2 records during this B-C stage.

Discussion

To produce a reliable age using Re-Os data three conditions must be met: (1) there must have been no addition or removal of Re or Os, i.e. the samples must remain within a closed system; (2) sufficient variation must exist in the parent/daughter ratios ($^{187}Re/^{188}Os$) to produce an isochron; and (3) the samples analysed must contain the same or near-identical initial $^{187}Os/^{188}Os$ composition[29].

A major concern when assessing material released from hydrocarbon seeps is the continued integrity of its Re-Os system despite exposure to formation waters and the marine environment. Studies of weakly to heavily biodegraded crude oils have repeatedly shown that their Re-Os system is not significantly affected by microbial alteration[10,11,13,14]. However, laboratory experiments have demonstrated rapid transfer of Re and Os to liquid oils from an enriched aqueous solution[30]. The authors of this study note that the concentrations of Re and Os used in their experiments were not intended to accurately mimic the natural environment, and that experiments attempting to do so are unlikely to yield meaningful results due to current technical limitations associated with extremely low Re and Os abundances[31]. However, their results demonstrate that Re and Os from formation waters could potentially be imparted to oil in a natural setting. This presents an alternative mechanism for resetting the Re-Os geochronometer and therefore, what the resulting age constrains. If interaction with formation waters occurred in a geologically short timeframe after generation then Re-Os geochronology may still approximate a generation age, although it would actually represent the timing of formation water interaction. Additionally, if the formation waters comprised contemporaneous seawater from when the source rocks were deposited, the resulting $^{187}Os/^{188}Os$ composition of the oil would still correlate to the average source rock value. However, if interaction with formation waters occurred much later, the resetting of the geochronometer would constrain the timing of this later alteration. Additionally, if the formation waters comprised migrated groundwater containing Os inherited from sources other than seawater from the time of source rock deposition, then oil-source correlation using the oil's Os_i value would be compromised. Understanding the role played by formation waters in the Re-Os systematics of crude oils in a natural setting is clearly a crucial topic which warrants further investigation. However, it is not practical to assess this competing hypothesis here, as the parent petroleum system of the asphaltites remains undiscovered and is thought to reside within a relatively unexplored basin. Therefore, reliably constraining the impact of groundwater-oil interactions in the subsurface for this system is not currently possible.

Similarly, if the asphaltites sequestered Re and Os from seawater during their time exposed to the marine environment, the required closed system may be compromised, progressively altering the $^{187}Os/^{188}Os$ composition of the bitumen towards the present marine value of ~1.06[32]. Such alteration would be expected to increase with continued exposure to seawater. In the case of the asphaltites, their degree of alteration due to both water washing and biodegradation permits an assessment of which specimens have spent the most time in contact with seawater (Fig. 4; Tables S4 and S5). Increasingly degraded asphaltites and interior/exterior comparisons show no systematic trends in their $^{187}Re/^{188}Os$ and $^{187}Os/^{188}Os$ ratios which could reasonably be attributed to weathering.

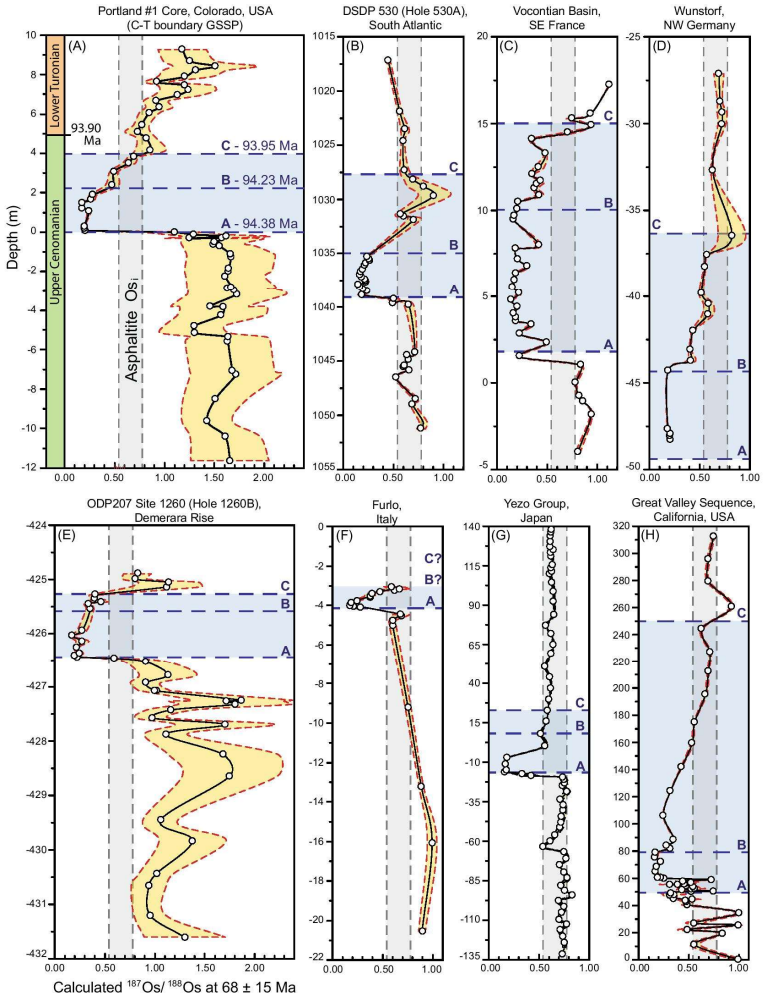


Figure 6. Variation of the calculated $^{187}Os/^{188}Os$ compositions at 68 ± 15 Ma with depth for OAE2 sections during the asphaltite generation window. The asphaltite Os_i value (0.66 ± 0.12) is shown in grey. Data points and black trendline correspond to the calculated Os_g at 68 Ma, while variation in this value due to the uncertainty associated with the generation age is shown in yellow. Areas where asphaltite Os_i value = OAE2 section Os_g value support potential oil-source correlation. Re-Os data from OAE2 sections after references[26–28]. Location of datums A, B and C labelled in blue within each section are defined by references[27,28,37–41]. The ages of these datums in the Portland #1 core were determined by references[27,42] and are supported by comparable ages in the Yezo Group[28]. All compiled Re-Os data from these records is listed in Table S6.

Furthermore, comparison with a second variety of coastal bitumen from a different petroleum system (waxy bitumen sample W13/007697) demonstrates that the oils retain unique values. Therefore, any alteration of the asphaltites due to their contact with seawater, which contains only trace concentrations of Re and Os, does not appear to have caused a quantifiable disruption of their Re-Os system.

Although our asphaltite sample suite displays sufficient variation in $^{187}Re/^{188}Os$ to produce a meaningful isochron (Fig. 3), the mechanism behind this variation is not fully understood. As discussed above, variation may be driven by interaction with formation waters[30], or because the asphaltites analysed in this study were collected over the course of three years, and likely represent products of continuous, low intensity seepage. Therefore, the variation could also be attributable to the prolonged duration (>1 Myr) of bitumen generation and expulsion when the chronometer is initially reset[12].

The MSWD of the revised regression (Fig. 3B) is low (<1), owing to the tight clustering of the analysed samples. Although an improvement from the regression of all asphaltite Re-Os data, the revised regression also yields a date that is still relatively imprecise (68 ± 15 Ma, 22%). Such a spread in a Re-Os generation age is not abnormal[11,13,14], and likely the result of prolonged generation over millions of years, combined with variation in the initial $^{187}Os/^{188}Os$ composition of the source unit[11,12,14]. Potential mixing of variable $^{187}Os/^{188}Os$ values across a source rock may be particularly applicable to oils and bitumen derived from OAE2 deposits, given the extent of variability at metre to centimetre scale across the interval (Fig. 6). Progressive generation across the OAE2 interval, potentially augmented by hydrocarbons expelled from thermally mature, pre- or post-OAE2 organic matter, would likely create a spread in the Os_i values of the resulting oil, thereby reducing the precision of the final Re-Os age.

Assessment of Cretaceous potential source rocks in the Bight Basin using a two-dimensional basin model suggests that a Cenomanian-Turonian source interval would have generated and expelled hydrocarbons from the mid-Campanian (~74 Ma) to the present[20]. A previous one-dimensional model also supports generation starting from approximately the mid-Campanian[33]. The age determined by the Re-Os systematics of the asphaltites is consistent with these models, supporting the interpretation that this age represents the timing of generation and that the parent petroleum system incorporates an OAE2 source rock.

Previous studies conclude that the Os_i value of an oil is inherited directly from its source rock and may therefore aid oil-source correlations[9–11,13–15]. The comparison of the asphaltite Os_i with the Os_g profiles of other, well-studied examples of OAE2 may provide preliminary interpretations regarding the nature of the asphaltite source, as the event preserves globally reproducible trends (Fig. 6). In no case do the asphaltites appear likely to be derived exclusively from organic matter deposited during the onset of OAE2, as the Os_i (0.66 ± 0.12) is notably more radiogenic than the calculated Os_g of the A-B interval (~0.2; Fig. 6). However, in most examples, the asphaltite Os_i range is consistent with the Os_g values in the latter section of OAE2 (interval B-C), as well as those of the pre- and post-OAE2 intervals in certain regions (Fig. 6).

Although the asphaltites are thought to originate from an OAE2 source rock[17,20], no exploratory or stratigraphic drilling within the Bight Basin has reached the Cenomanian-Turonian boundary to provide confirmation. A recent attempt to assess the potential for preservation of an OAE2 interval within the Bight Basin by the International Ocean Discovery Program (IODP) Expedition 369 was unable to reach to the necessary depth, due to a hole deviation of ~26° from vertical during coring operations[34]. The fact that organic-rich lithofacies associated with OAE2 are yet to identified and sampled does not preclude the possibility that other source rocks which may have been deposited in the offshore Bight Basin due to local anoxic conditions arising from its palaeogeographic location within a narrow re-entrant of the Tethys Ocean (Fig. 5). This scenario would similarly satisfy the requirements defined by their geochemistry[2,17]. Multiple alternative marine intervals with high source potential are also inferred from the late Aptian to Santonian in the Bight Basin based on the tectonostratigraphic framework defined by data from wells drilled in the proximal regions of the basin[21,33]. However, the existence of these putative basinward source intervals is similarly yet to be confirmed.

While the OAE2 interval is characterised by an abrupt non-radiogenic shift in $^{187}Os/^{188}Os$ values (Fig. 6), the global record also demonstrates regional variability driven by differential inputs of osmium from local continental weathering and submarine volcanism[27,28]. The extent to which such inputs may have impacted the $^{187}Os/^{188}Os$ ratio across the Cenomanian-Turonian boundary interval in the Bight Basin remains unknown until a local record becomes available. Meanwhile, the lack of relevant analytical data on potential source rocks in the distal reaches of the basin precludes definitive asphaltite-source rock correlation. Such gaps in the knowledge of frontier basins are common. The uncertainties inherent in our initial interpretation of the Os isotope signatures of these Australian asphaltites will be reduced as understanding of the geology and geochemistry of the Bight Basin improves with further exploration.

Conclusions

Through the application of Re-Os radiometric dating to heavy asphaltic crude oil released from natural seafloor seepage we have demonstrated that the technique may be applied to constrain the timing of hydrocarbon generation and potential source intervals within offshore sedimentary basins. The Re-Os systematics of crude oils stranding in coastal environments may therefore have widespread application to the identification of their respective offshore hydrocarbon systems. The ability to inform or validate the timing of generation determined from basin models provides a new approach to reducing the uncertainty and risk associated with petroleum exploration in frontier basins, particularly in deepwater settings where the cost of exploratory drilling is extremely high. Our findings also highlight the potential use of Os isotopes in correlating oils to their parent source rocks at high resolution, particularly those deposited during OAE2 which exhibit highly anomalous $^{187}Os/^{188}Os$ values. However, such correlations may be affected by inherent local variability in the marine osmium isotope record and hence wherever possible should use data from the proposed source rock in the basin of origin, rather than the global record.

Materials and Methods

Re-Os isotope data. All Re-Os sample preparation and isotopic analyses were conducted at the Laboratory for Source Rock Geochronology and Geochemistry and Arthur Holmes Laboratory at Durham University (UK). Samples were prepared for Re-Os analysis using published methods[16]. Approximately 200 mg of whole oil sample from each asphaltite was dissolved in a minimum volume of chloroform ($CHCl_3$) and loaded into a Carius tube, with the solvent subsequently evaporated at 65 °C. All samples were then spiked with a mixed tracer solution containing a known amount of ^{185}Re and ^{190}Os. The tracer solution was homogenised with the sample in the Carius tube using inverse *aqua regia* (3 mL of ~12 N HCl, 6 mL of 16 N HNO_3) and heated at 220 °C for 48 hours. Osmium was subsequently extracted and purified using $CHCl_3$ solvent extraction and microdistillation. The Re-bearing *aqua regia* was dried on a hot plate at 80 °C overnight and then purified by NaOH-acetone solvent extraction and anion chromatography.

The purified Re and Os were loaded onto Ni and Pt wire filaments, respectively, and analysed by Negative Thermal Ionization Mass Spectrometry (NTIMS) on a Thermo Scientific TRITON mass spectrometer. The total procedural blanks were 2.4 ± 1.0 pg/g for Re and 0.15 ± 0.05 pg/g for Os, with a ^{187}Os/^{188}Os of 0.25 ± 0.05 (n = 4). The uncertainty for all Re-Os data was determined using full error propagation of uncertainties. The Re-Os data were regressed using *Isoplot V4.15*[24] and a ^{187}Re decay constant of 1.666×10^{-11} a^{-1} [35].

Re-Os data deviation assessment. Data points responsible for introducing significant uncertainty in the regression of all the available data (Fig. 3A) were identified by determining the percentage of deviation between the observed ^{187}Os/^{188}Os composition in each sample compared to the predicted value defined by the regression described by Equation (1). The calculated value for each sample was obtained using the isochron equation listed as Equation (2), where λ is the decay constant for ^{187}Re and t is the age in years, using values defined by the regression of all of data points (i.e. where $t = 68$ Myr and $^{187}Os/^{188}Os_{Initial} = 0.63$). Samples with a deviation of >2% from the initial regression were excluded for the revised regression (Fig. 3B).

$$\text{Deviation}(\%) = \left(^{187}\text{Os}/^{188}\text{Os}_{\text{measured}} - {}^{187}\text{Os}/^{188}\text{Os}_{\text{calculated from data best-fit initial}}\right) \times 100 \quad (1)$$

$$^{187}\text{Os}/^{188}\text{Os} = {}^{187}\text{Os}/^{188}\text{Os}_{\text{initial}} + {}^{187}\text{Re}/^{188}\text{Os} \times (e^{\lambda t} - 1) \quad (2)$$

Calculation of OAE2 osmium composition during the asphaltite generation window. The ^{187}Os/^{188}Os composition of each OAE2 section during the asphaltite generation window of 68 ± 15 Ma was calculated using Equation (2) and the composition of each individual data point is listed in Table S6.

Whole-oil gas chromatography-mass spectrometry. All sample preparation and analyses were conducted in the Biogeochemistry Laboratory at the University of Adelaide. A sub-sample (≤200 mg) was removed from each bitumen specimen and dissolved in 10 mL of dichloromethane/methanol (93:7, v:v). An aliquot of this solution was used for whole-oil GC-MS. Analyses of the samples collected in 2014 and 2015 were performed on an Agilent 6890 gas chromatograph interfaced with a 5973 N MSD (electron energy 70 eV) and tuned using automatic setup parameters for each sequence. Chromatography was carried out on an Agilent HP-5MS fused silica column (30 m × 0.25 mm i.d. × 0.25 µm film thickness), using either a split (50 mL/min) or splitless injection mode, the latter employed if split injection data showed low responses. The oven was held at an initial temperature of 50 °C for 1 min, followed by heating at 8 °C/min to 300 °C. The carrier gas was helium at a flow rate of 1 mL/minute. GC-MS analyses of the samples collected in 2016 were performed on an Agilent 7890B gas chromatograph interfaced with a 5977B MSD (electron energy 70 eV) and tuned using automatic setup parameters for each sequence. Chromatography was undertaken on a J&W DB-5MS fused silica column (30 m × 0.25 mm i.d. × 0.25 µm film thickness), using the same operating conditions as employed for the 2014 and 2015 samples. In both cases, whole-oil GC-MS was conducted in the scan mode (scan interval 45–500 AMU at approx. 3 scans/sec). All data were processed using *MSD ChemStation* (Agilent Technologies, Inc.).

Isolation of saturated, aromatic and asphaltene fractions. The saturated and aromatic hydrocarbon fractions were separated from 20 mg aliquots of whole bitumen using silica gel liquid chromatography[36]. The recovered saturated hydrocarbons were stored in 2 mL chromatography vials and the aromatics in 2 mL amber glass vials to ensure minimal degradation by ultraviolet light. The asphaltene fraction of each sample was separated by adding an excess of *n*-pentane to bulk bitumen sub-samples (0.3–0.7 g) dissolved in a mixture of dichloromethane and methanol (93:7). The dissolved maltene fraction was then removed using a Pasteur pipette, allowing the precipitated asphaltene fraction to be dried and weighed.

Selected ion monitoring gas chromatography-mass spectrometry (SIM GC-MS). GC-MS analysis of the saturated hydrocarbon fractions for sterane and hopane degradation assessment was performed on an Agilent 7890 A gas chromatograph interfaced with a 5975 C MSD (electron energy 70 eV) tuned using automatic setup parameters on the day of the analysis. Chromatography was carried out on a J&W DB-5MS fused silica column (60 m × 0.25 mm i.d. × 0.25 µm film thickness). A 1 µL aliquot of the saturates fraction was injected into the split/splitless injector at 300 °C operating in splitless mode. After being held at an initial temperature of 40 °C for 2 minutes, the oven was heated at 20 °C/minute to 200 °C and then ramped to 310 °C at 2 °C/minute. The carrier gas was helium at a flow rate of 1.5 mL/min.

GC-MS analyses of the aromatic fractions to determine alteration to water-soluble compounds was performed on a Perkin Elmer SQ8T/680 Clarus gas chromatograph. Chromatography was carried out on a Perkin Elmer PE-5MS fused silica column (30 m × 0.25 mm i.d. × 0.25 µm film thickness). A 1 µL aliquot of the aromatics fraction was injected into the split/splitless injector at 300 °C operating in splitless mode. The oven temperature was held at 50 °C for 1 min., followed by heating at 8 °C/min to 300 °C. Helium was the carrier gas at a flow rate of 1 ml/min. Data were acquired in the scan mode (Scan 45:500AMU at approx. 3 scans/sec).

Data Availability

All data needed to assess the conclusions of this paper are included in the paper and/or Supplementary Materials. Any additional information regarding samples is available on request.

References

1. National Research Council. *Oil in the Sea III: Inputs, Fates and Effects*. https://doi.org/10.17226/10388, (The National Academies Press, Washington DC, 2003).
2. Edwards, D., McKirdy, D. M. & Summons, R. E. Enigmatic asphaltites from the southern Australian margin: molecular and carbon isotopic composition. *Pet. Explor. Soc. Aust. J.* **26**, 397–420 (1998).
3. Edwards, D. S., McKirdy, D. M., Rowland, S. J., Heath, D. J. & Gray, P. S. Waxy bitumen stranding in southern Australia: A geochemical study of multiple oil families and their likely origins. *Org. Geochem.* **118**, 132–151 (2018).
4. Warnock, A. M., Hagen, S. C. & Passeri, D. L. Marine Tar Residues: a Review. *Water, Air, Soil Pollut.* **226**, 24 (2015).
5. Lorenson, T. D. *et al*. Natural Offshore Oil Seepage and Related Tarball Accumulation on the California Coastline; Santa Barbara Channel and the Southern Santa Maria Basin; source identification and inventory. *U.S. Geological Survey Open-File Report 2009–1225 and MMS report 2009-030* (2009).
6. Kvenvolden, K. A. & Cooper, C. K. Natural seepage of crude oil into the marine environment. *Geo-Marine Lett.* **23**, 140–146 (2003).
7. Peters, K. E., Walters, C. C. & Moldowan, J. M. *The Biomarker Guide Volume 2: Biomarkers and Isotopes in Petroleum Exploration and Earth History*. (Cambridge University Press, 2005).
8. Olaru, R. *et al*. 3D Basin modelling of Oligocene - Miocene Maikop source rocks offshore Romania and in the Western Black Sea. *J. Pet. Geol.* **41**, 351–365 (2018).
9. Selby, D. & Creaser, R. A. Direct radiometric dating of hydrocarbon deposits using rhenium-osmium isotopes. *Science* **308**, 1293–1295 (2005).
10. Selby, D., Creaser, R., Dewing, K. & Fowler, M. Evaluation of bitumen as a Re–Os geochronometer for hydrocarbon maturation and migration: A test case from the Polaris MVT deposit, Canada. *Earth Planet. Sci. Lett.* **235**, 1–15 (2005).
11. Finlay, A. J., Selby, D. & Osborne, M. J. Re-Os geochronology and fingerprinting of United Kingdom Atlantic margin oil: Temporal implications for regional petroleum systems. *Geology* **39**, 475–478 (2011).
12. Lillis, P. G. & Selby, D. Evaluation of the rhenium–osmium geochronometer in the Phosphoria petroleum system, Bighorn Basin of Wyoming and Montana, USA. *Geochim. Cosmochim. Acta* **118**, 312–330 (2013).
13. Cumming, V. M., Selby, D., Lillis, P. G. & Lewan, M. D. Re–Os geochronology and Os isotope fingerprinting of petroleum sourced from a Type I lacustrine kerogen: Insights from the natural Green River petroleum system in the Uinta Basin and hydrous pyrolysis experiments. *Geochim. Cosmochim. Acta* **138**, 32–56 (2014).
14. Liu, J., Selby, D., Obermajer, M. & Mort, A. Re-Os geochronology and oil-source correlation of Duvernay Petroleum System, Western Canada Sedimentary Basin: Implications for the application of the Re-Os geochronometer to petroleum systems. *Am. Assoc. Pet. Geol. Bull.* **102**, 1627–1656 (2017).
15. Rooney, A. D., Selby, D., Lewan, M. D., Lillis, P. G. & Houzay, J.-P. Evaluating Re–Os systematics in organic-rich sedimentary rocks in response to petroleum generation using hydrous pyrolysis experiments. *Geochim. Cosmochim. Acta* **77**, 275–291 (2012).
16. Selby, D., Creaser, R. A. & Fowler, M. G. Re–Os elemental and isotopic systematics in crude oils. *Geochim. Cosmochim. Acta* **71**, 378–386 (2007).
17. Hall, P. A., McKirdy, D. M., Grice, K. & Edwards, D. S. Australasian asphaltite strandings: Their origin reviewed in light of the effects of weathering and biodegradation on their biomarker and isotopic profiles. *Mar. Pet. Geol.* **57**, 572–593 (2014).
18. Ross, A. *et al*. *Asphaltite and tarball surveys. Final Report GABRP Project 5.2. Research Report Series Number 25a* (2017).
19. Summons, R. E. *et al*. Geochemical Analogs for Australian Coastal Asphaltites - Search for the Source Rock. In *AAPG Annual Convention, Denver, Colorado*. (AAPG Search and Discovery Article #90906, 2001).
20. Totterdell, J. M. *et al*. Mid-Late Cretaceous organic-rich rocks from the eastern Bight Basin: implications for prospectivity. In *PESA Eastern Australasian Basins Symposium III Special Publication*. (eds Blevin, J. E., Bradshaw, B. E. & Uruski, E.) 137–158 (2008).
21. Totterdell, J. M. *et al*. A new sequence framework for the Great Australian Bight: Starting with a clean slate. *APPEA J.* **40**, 95–118 (2000).
22. Totterdell, J. M. & Bradshaw, B. E. The structural framework and tectonic evolution of the Bight Basin. In *PESA Eastern Australasian Basins Symposium II* (eds Boult, P. J., Johns, D. R. & Lang, S. C.) 41–61 (2004).
23. Baghurst, B. *et al*. Findings from the Great Australian Bight Research Program – an integrated study of environmental, economic and social values. *APPEA J.* **57**, 388–392 (2017).
24. Ludwig, K. *User's manual for Isoplot version 3.75–4.15: a geochronological toolkit for Microsoft Excel*. (Berkley Geochronological Center Special Publication No. 5, 2012).
25. Selby, D. & Creaser, R. A. Re–Os geochronology of organic rich sediments: an evaluation of organic matter analysis methods. *Chem. Geol.* **200**, 225–240 (2003).
26. Turgeon, S. C. & Creaser, R. A. Cretaceous oceanic anoxic event 2 triggered by a massive magmatic episode. *Nature* **454**, 323–326 (2008).
27. Du Vivier, A. D. C. *et al*. Marine 187Os/188Os isotope stratigraphy reveals the interaction of volcanism and ocean circulation during Oceanic Anoxic Event 2. *Earth Planet. Sci. Lett.* **389**, 23–33 (2014).
28. Du Vivier, A. D. C., Selby, D., Condon, D. J., Takashima, R. & Nishi, H. Pacific 187Os/188Os isotope chemistry and U–Pb geochronology: Synchroneity of global Os isotope change across OAE 2. *Earth Planet. Sci. Lett.* **428**, 204–216 (2015).
29. Cohen, A. S., Coe, A. L., Bartlett, J. M. & Hawkesworth, C. J. Precise Re–Os ages of organic-rich mudrocks and the Os isotope composition of Jurassic seawater. *Earth Planet. Sci. Lett.* **167**, 159–173 (1999).
30. Mahdaoui, F., Michels, R., Reisberg, L., Pujol, M. & Poirier, Y. Behavior of Re and Os during contact between an aqueous solution and oil: Consequences for the application of the Re–Os geochronometer to petroleum. *Geochim. Cosmochim. Acta* **158**, 1–21 (2015).
31. Reisberg, L., Michels, R. & Mahdaoui, F. Reply to the comment by Wu *et al*. (2016) on "Behavior of Re and Os during contact between an aqueous solution and oil: Consequences for the application of the Re–Os geochronometer to petroleum" [Geochim. Cosmochim. Acta 158 (2015) 1–21]. *Geochim. Cosmochim. Acta* **186**, 348–350 (2016).
32. Peucker-Ehrenbrink, B. & Ravizza, G. The marine osmium isotope record. *Terra Nov.* **12**, 205–219 (2000).
33. Struckmeyer, H. I. M. *et al*. In *Eastern Australian Basin Symposium, A Refocused Energy Perspective for the Future. Petroleum Exploration Society of Australia, Special Publication*. (eds Hill, K. C. & Bernecker, T.) 543–552 (2001).

34. Huber, B. T., Hobbs, R. W., Bogus, K. A. & Scientists, E. 369. *Expedition 369 Preliminary Report: Australia Cretaceous Climate and Tectonics*, https://doi.org/10.14379/iodp.pr.369.2018 (2018).
35. Smoliar, M. I., Walker, R. J. & Morgan, J. W. Re-Os Ages of Group IIA, IIIA, IVA, and IVB Iron Meteorites. *Science (80-.).* **271**, 1099–1102 (1996).
36. Bastow, T. P., van Aarssen, B. G. K. & Lang, D. Rapid small-scale separation of saturate, aromatic and polar components in petroleum. *Org. Geochem.* **38**, 1235–1250 (2007).
37. Sageman, B. B., Meyers, S. R. & Arthur, M. A. Orbital time scale and new C-isotope record for Cenomanian-Turonian boundary stratotype. *Geology* **34**, 125–128 (2006).
38. Jenkyns, H. C., Matthews, A., Tsikos, H. & Erel, Y. Nitrate reduction, sulfate reduction, and sedimentary iron isotope evolution during the Cenomanian-Turonian oceanic anoxic event. *Paleoceanography* **22**, 1–17 (2007).
39. Forster, A., Schouten, S., Moriya, K., Wilson, P. A. & Sinninghe Damsté, J. S. Tropical warming and intermittent cooling during the Cenomanian/Turonian oceanic anoxic event 2: Sea surface temperature records from the equatorial Atlantic. *Paleoceanography* **22**, 1–14 (2007).
40. Forster, A. *et al.* The Cenomanian/Turonian oceanic anoxic event in the SouthAtlantic: New insights from a geochemical study of DSDP Site 530A. *Palaeogeogr. Palaeoclimatol. Palaeoecol.* **267**, 256–283 (2008).
41. Jarvis, I., Lignum, J. S., Gröcke, D. R., Jenkyns, H. C. & Pearce, M. A. Black shale deposition, atmospheric CO_2 drawdown, and cooling during the Cenomanian-Turonian Oceanic Anoxic Event. *Paleoceanography* **26**, 1–17 (2011).
42. Meyers, S. R. *et al.* Intercalibration of radioisotopic and astrochronologic time scales for the Cenomanian-Turonian boundary interval, western interior Basin, USA. *Geology* **40**, 7–10 (2012).

Acknowledgements

We thank C. Dyt, Z. Angelini, R. Kempton, C. White, A. Pickard, S. Maslin, S. Armand, L. Tucker and S. Margot for assistance in completing the 2014–2016 beach surveys. We also thank S. Valladares for the donation of asphaltites from his private collection for this research and A. Hofmann and G. Nowell for assistance with the Re-Os determinations. A.J.C. acknowledges the support of a University of Adelaide postgraduate scholarship. D.S. acknowledges the Total Endowment Fund and the CUG Wuhan Dida Scholarship. This research was funded by the Bernold M. "Bruno" Hanson Memorial Environmental Grant awarded by the AAPG Grants-In-Aid Program and the D R Stranks Travelling Fellowship awarded by the University of Adelaide to A.J.C. Fieldwork and further travel financial support was provided by the Great Australian Bight Research Program. The Great Australian Bight Research Program is a collaboration between BP, CSIRO, the South Australian Research and Development Institute (SARDI), the University of Adelaide, and Flinders University. The program aims to provide a whole-of-system understanding of the environmental and social values of the region; providing an information source for all to use.

Author Contributions

A.J.C., D.S., D.M.McK., P.A.H. and A.S.R. designed the research project. A.J.C., C.T., S.G., D.M.McK. and A.S.R. collected the samples. A.J.C. and D.S. collected and interpreted the Re-Os data. A.J.C., P.A.H., S.G. and D.M.McK. collected and interpreted the gas chromatography data. A.J.C. wrote the manuscript with discussion and input from all co-authors.

Additional Information

Supplementary information accompanies this paper at https://doi.org/10.1038/s41598-018-37884-x.

Competing Interests: The authors declare no competing interests.

Publisher's note: Springer Nature remains neutral with regard to jurisdictional claims in published maps and institutional affiliations.

Open Access This article is licensed under a Creative Commons Attribution 4.0 International License, which permits use, sharing, adaptation, distribution and reproduction in any medium or format, as long as you give appropriate credit to the original author(s) and the source, provide a link to the Creative Commons license, and indicate if changes were made. The images or other third party material in this article are included in the article's Creative Commons license, unless indicated otherwise in a credit line to the material. If material is not included in the article's Creative Commons license and your intended use is not permitted by statutory regulation or exceeds the permitted use, you will need to obtain permission directly from the copyright holder. To view a copy of this license, visit http://creativecommons.org/licenses/by/4.0/.

© The Author(s) 2019

Marine and Petroleum Geology 112 (2020) 104062

Contents lists available at ScienceDirect

Marine and Petroleum Geology

journal homepage: www.elsevier.com/locate/marpetgeo

Research paper

A second type of highly asphaltic crude oil seepage stranded on the South Australian coastline

Alexander J. Corrick[a,*], Philip A. Hall[a], Se Gong[b], David M. McKirdy[a], David Selby[c,d], Christine Trefry[e], Andrew S. Ross[e]

[a] Department of Earth Sciences, School of Physical Sciences, University of Adelaide, SA 5005, Australia
[b] Energy, CSIRO, North Ryde, NSW 2113, Australia
[c] Department of Earth Sciences, Durham University, Durham, DH1 3LE, UK
[d] State Key Laboratory of Geological Processes and Mineral Resources, School of Earth Resources, China University of Geosciences, Wuhan, 430074 Hubei, China
[e] Energy, CSIRO, Kensington, WA 6151, Australia

ARTICLE INFO

Keywords:
Bight Basin
Asphaltite
Asphaltic tar
Oil-oil correlation
CSIA
Sulphur isotopes
Re-Os
Thermochemical sulphate reduction

ABSTRACT

Strandings of semi-solid to solid asphaltic bitumen along the coastline of South Australia have been reported as far back as the late 1800s. Hitherto only a single variety, now referred to as asphaltite, has been attributed to seepage from the nearby Bight Basin. The geochemistry of the asphaltites suggest they were derived from a marine source rock deposited under anoxic or euxinic conditions, most likely a Cretaceous ocean anoxic event, and were generated within the early/main oil window. Here we identify a new type of semi-solid asphaltic bitumen collected following a severe storm event in 2016. Termed asphaltic tars, these viscous oils bear a strong geochemical resemblance to the asphaltites. Both oil types have high asphaltene contents, identical *n*-alkane carbon isotopic profiles and near identical source-specific sterane distributions. However, several notable geochemical variations can distinguish these new strandings from the asphaltites. The most notable of these differences include heavier bulk sulphur isotopic composition, extremely high abundances of Re and Os with distinct $^{187}Re/^{188}Os$ and $^{187}Os/^{188}Os$ values and thermal maturity parameters consistent with generation in the late oil window. The differences in sulphur isotopic composition and Re-Os systematics could be considered evidence that despite their other source-specific similarities, the asphaltic tars originated from a different source rock. However, alteration of these two parameters can occur due to thermochemical sulphate reduction. Conclusive identification of this alteration process typically relies on further diagnostic parameters which are unfortunately not available in the case of coastal oil strandings. This introduces uncertainty to the correlation of these two types of asphaltic oil. In either scenario, the similarities between these two types of oil suggest their source rock(s) contained highly comparable organic matter inputs. We therefore attribute the origin of these new asphaltic tar strandings to natural seepage from the offshore Bight Basin.

1. Introduction

Ocean beaches along Australia's southern margin are known to collect bitumen emitted from seafloor seeps associated with a variety of different petroleum systems (e.g. McKirdy et al., 1986, 1994; Padley, 1995; Edwards et al., 1998, 2016, 2018). Reports of asphaltene-rich coastal bitumen strandings (asphaltum, now referred to as asphaltite) in the region date back to the early 1800s and continue to the present (Trewartha, 1850; Tolmer, 1882; Sprigg and Woolley, 1963; Volkman et al., 1992; Edwards et al., 1998; Hall et al., 2014; Ross et al., 2017). Historical reports of these asphaltite strandings predate anthropogenic inputs of hydrocarbons to the region, suggesting that they are the product of natural offshore seepage. Although asphaltite is the least common variety of coastal bitumen recognised along the Australian coastline, it contributes the largest specimens, with individual pieces weighing up to 7 kg (Edwards et al., 1998, 2016).

Source and maturity-specific biomarkers indicate that these asphaltites are derived from a Mesozoic marine shale, deposited under sub-oxic to euxinic conditions, which expelled petroleum within the early oil window (Edwards et al., 1998; Hall et al., 2014; Scarlett et al., 2019). The source rock is presently thought to have been deposited during an oceanic anoxic event (OAE). However, interpretations vary from the Cenomanian-Turonian OAE2 (Totterdell et al., 2008; Boreham, 2009; Hall et al., 2014; Corrick et al., 2019), the Albian

* Corresponding author.
E-mail address: alexander.corrick@adelaide.edu.au (A.J. Corrick).

https://doi.org/10.1016/j.marpetgeo.2019.104062
Received 12 April 2019; Received in revised form 23 September 2019; Accepted 24 September 2019
Available online 27 September 2019
0264-8172/ Crown Copyright © 2019 Published by Elsevier Ltd. All rights reserved.

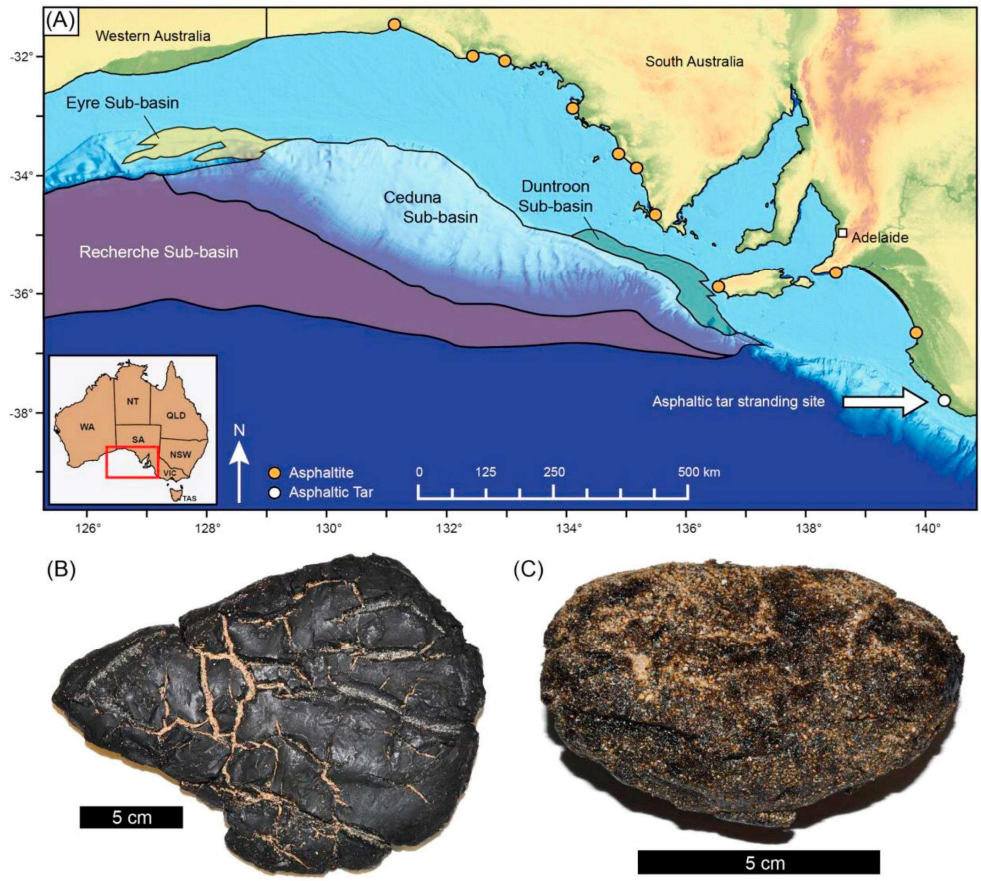


Fig. 1. (A) Locations of analysed asphaltite and asphaltic tar samples and the Jurassic-Cretaceous sub-basins of the offshore Bight Basin. (B) Photograph of asphaltite sample W13/007507 collected from Waitpinga Beach in 2014, exhibiting characteristic shrinkage cracks. (C) Photograph of asphaltic tar sample/001059 collected from Number 1 and 2 Rocks in 2016.

OAE1d (Boult et al., 2005; Hall et al., 2014), the Aptian OAE1a and Albian OAE1b events (Scarlett et al., 2019). Inspection of the GeoMark™ global petroleum database suggests that the asphaltites are not products of any documented petroleum system (Summons et al., 2001). Unlike the majority of the tar balls found along the South Australian coastline (viz. 'waxy bitumens') which have been geochemically linked to Cenozoic petroleum systems in southeast Asia (Padley, 1995; Edwards et al., 2016, 2018), the asphaltites are currently thought to originate from an undiscovered petroleum system in the offshore Bight Basin (Fig. 1A) located on Australia's southern margin (Boreham et al., 2001; Totterdell et al., 2008; Hall et al., 2014). This interpretation is supported by analysis of organic-rich samples with similar geochemistry dredged from the basin (Totterdell et al., 2008; Boreham, 2009) and rhenium-osmium (Re-Os) geochronology of the asphaltites (Corrick et al., 2019), which demonstrated their timing of generation is consistent with existing petroleum systems models for the basin (Struckmeyer et al., 2001; Totterdell et al., 2008). Previous studies have also proposed seepage from other nearby basins, such as the Otway Basin (Boult et al., 2005; Hall et al., 2014). However, recent modelling of the metaocean conditions of the Great Australian Bight suggests that offshore seepage from the Otway Basin is unlikely to migrate west, a requirement given the observed spatial distribution of asphaltite strandings along the coastline (Ross et al., 2017). Seepage from the Ceduna or Duntroon sub-basins of the Bight Basin, however, is consistent with the documented regions of asphaltite stranding (Ross et al., 2017).

The Bight Basin comprises an approximately 15 km-thick succession of Late Jurassic to Cretaceous sediments (Fig. S1) deposited in response to the separation of Australia and Antarctica during the break-up of the supercontinent Gondwana (Fraser and Tilbury, 1979; Totterdell et al., 2000; Totterdell and Bradshaw, 2004). These Mesozoic deposits are unconformably overlain by Palaeogene sediments with no source potential (Totterdell et al., 2008). Proposed petroleum systems in the basin are primarily associated with thick mid-to late Cretaceous deltaic

and marine sediments, namely the Blue Whale, White Pointer, Tiger and Hammerhead supersequences (Blevin et al., 2000; Struckmeyer et al., 2001; Totterdell et al., 2000, 2008). However, no working petroleum systems have yet been proven within the basin.

Aside from the asphaltite strandings, no other seeped hydrocarbons that have been found on the South Australian coastline are considered products of the Bight Basin. In this study we report a new variety of asphaltene-rich crude oil stranded on the southeastern coastline of South Australia in October 2016. Referred to herein as asphaltic tar, these new strandings display strong geochemical similarities to the asphaltites, suggesting that the two oil types may originate from lateral equivalents of the same source rock.

2. Materials and methods

2.1. Sample suite

The stranding locations of the specimens analysed in this study are shown in Fig. 1A and their collection details are summarised in Table S1. Details of the four representative waxy bitumen samples also included in this study to illustrate their contrasting *n*-alkane $\delta^{13}C$ profiles may be found in Ross et al. (2017). The asphaltites are visually distinctive, jet black, semi-solid to solid bitumens with a petroliferous odour and commonly exhibit deep shrinkage cracks (Fig. 1B). Fresh specimens with a soft and slightly pliable interior are rare, as most asphaltites collected on the coastline have become brittle, breaking apart with a diagnostic conchoidal fracture. The asphaltic tars are similarly jet black in colour but emit a stronger petroliferous odour and have remained viscous and sticky with a surficial sand coating (Fig. 1C).

The specimens compared in this study were recovered during three systematic annual surveys of 30 ocean beaches spanning the South Australian coastline in the period 2014 to 2016, as part of the Great Australian Bight Research Program (Ross et al., 2017). The sample suite was further supplemented with additional samples donated from private collections. Representative asphaltites were selected from each of the three surveys while ensuring a spatial distribution that encompassed the entire survey area (Fig. 1A). Asphaltic tar samples were only encountered in the final survey conducted in October of 2016, at the Number 1 and 2 Rocks beach in the Canunda National Park, located on the Bonney Coast approximately 40 km west of Mount Gambier. This survey occurred 24 days after a one-in-fifty-year storm event that affected much of the South Australian coastline (Bureau of Meteorology, 2016; Burns et al., 2017) and found the spatial distribution of coastal bitumen deviated significantly from the previous two surveys (Ross et al., 2017).

2.2. Bulk bitumen analyses

2.2.1. Whole-oil gas chromatography-mass spectrometry

A sub-sample (≤200 mg) was removed from each bitumen specimen and dissolved in 10 mL of dichloromethane/methanol (93:7, v:v). An aliquot of this solution was used for whole-oil GC-MS. Analyses of the samples collected in 2014 and 2015 were performed on an Agilent 6890 gas chromatograph interfaced with a 5973N MSD (electron energy 70 eV) and tuned using automatic setup parameters for each sequence. Chromatography was carried out on an Agilent HP-5MS fused silica column (30 m × 0.25 mm i. d. × 0.25 μm film thickness), using either a split (50 mL/min) or splitless injection mode, the latter employed if split injection data showed low responses. The oven was programmed at an initial temperature of 50 °C for 1 min, followed by heating at 8 °C/min to 300 °C. The carrier gas was helium at a flow rate of 1 mL/min. GC-MS analyses of the samples collected in 2016 were performed on an Agilent 7890B gas chromatograph interfaced with a 5977B MSD (electron energy 70 eV) and tuned using automatic setup parameters for each sequence. Chromatography was carried out on a J&W DB-5MS fused silica column (30 m × 0.25 mm i. d. × 0.25 μm film thickness), using the same operating conditions as employed for the 2014 and 2015 samples. In both cases, whole-oil GC-MS was conducted in scan mode (scan interval 45–500 AMU at approx. 3 scans/sec).

2.2.2. Elemental analysis (EA)

The sulphur content (weight %) of each sample was determined using a Perkin Elmer 2400 series II CHNS/O Elemental Analyzer in CHNS configuration. The combined combustion/reduction tube was packed with Perkin Elmer EA6000 and Perkin Elmer 'Hi-Purity' Copper (reaction temperature of 975 °C). Results were calibrated against a Perkin Elmer Organic Analytical Standard (cystine, 3–4 mg) with a known abundance of sulphur (26.69 ± 0.3%). The maximum uncertainty in sulphur content values was ±0.5%.

2.2.3. Elemental analysis – isotope ratio mass spectrometry (EA-IRMS)

Sulphur isotope data ($\delta^{34}S$) were collected using a Eurovector EuroEA Elemental Analyzer modified with a Valco valve to allow separation of combustion SO_2 from CO_2 and N_2. Results from interior subsamples of each bitumen specimen were calibrated to two in-house standards (S2 and S3) of silver sulphide (Ag_2S) with $\delta^{34}S$ values of +22.7‰ and −32.3‰, respectively. Due to the range in sulphur content between the asphaltites and asphaltic tars, results were calibrated against multiple weights of each standard (in the range 2–4 mg). The maximum uncertainty in $\delta^{34}S$ values was ±0.38‰.

2.2.4. Re-Os isotopic composition

Re-Os analysis of three asphaltic tars was conducted using the same analytical approach as that taken for the asphaltites by Corrick et al. (2019), based on the methods of Selby et al. (2007). The precision for all Re-Os data was determined using full error propagation of all sources of uncertainty.

2.3. Analysis of saturated, aromatic and polar fractions

2.3.1. Oil fractionation

The saturated, aromatic and polar fractions were separated from 20 mg aliquots of whole bitumen using the procedure of Bastow et al. (2007). The recovered saturated hydrocarbons and polar fractions were stored in 2 mL chromatography vials, while the aromatics fraction was stored in 2 mL amber glass vials to ensure minimal degradation by ultraviolet light.

2.3.2. Separation of n-alkanes and branched/cyclic alkanes

Saturates fractions were dissolved in cyclohexane and transferred on to 5 Å molecular sieve (activated at 450 °C) before heating in an oven at 80 °C overnight to ensure complete *n*-alkane absorption. The resulting branched/cyclic alkane fraction was used for biomarker analyses (see Sections 2.3.3 and 2.3.4). For selected samples, the separated *n*-alkanes were then retrieved for compound-specific isotope analysis by digesting the molecular sieve in approximately 8 mL of 40% hydrofluoric acid in a polytetrafluoroethylene test tube and extracting the released *n*-alkanes using *n*-pentane. The resulting *n*-alkane fractions were concentrated under a stream of nitrogen prior to further analysis.

2.3.3. Selected ion monitoring gas chromatography-mass spectrometry (SIM GC-MS)

GC-MS analysis of the branched/cyclic alkanes was performed on an Agilent 7890A gas chromatograph interfaced with a 5975C MSD (electron energy 70 eV) tuned using automatic setup parameters on the day of the analysis. Chromatography was carried out on a J&W DB-5MS fused silica column (60 m × 0.25 mm i. d. × 0.25 μm film thickness). A 1 μL aliquot of the branched/cyclic saturate fraction dissolved in petroleum ether was injected into the split/splitless injector at 300 °C operating in split mode (20 mL/min). After being held at an initial temperature of 40 °C for 2 min, the oven was heated at 20 °C/min to 200 °C and then ramped to 310 °C at 2 °C/min. The carrier gas was helium at a

flow rate of 1.5 mL/min.

2.3.4. Gas chromatography tandem mass spectrometry (GC-MS-MS) with cold electron ionisation

GC-MS-MS analysis of the branched/cyclic alkanes was performed on a Perkin Elmer 680 Clarus gas chromatograph interfaced with a Perkin Elmer iQT Quadrupole Time of Flight (QToF) mass spectrometer fitted with a Cold-EI source and tuned using automatic setup parameters for each sequence. Chromatography was carried out on a J&W DB-5MS fused silica column (60 m × 0.25 mm i. d. × 0.25 μm film thickness). A 1 μL aliquot of saturates fraction dissolved in cyclohexane was injected at 300 °C into the injector operating in splitless mode. The oven was held at an initial temperature of 50 °C for 1 min, followed by heating at 12 °C/min to 180 °C and then at 4 °C/min to 310 °C. IIelium was the carrier gas at a flow rate of 2 mL/min.

2.3.5. Carbon compound-specific isotope analysis (CSIA)

The carbon isotopic composition ($\delta^{13}C$) of individual *n*-alkanes from representative asphaltite, asphaltic tar and waxy bitumen samples was measured by gas chromatography-combustion-isotope ratio mass spectrometry using a 6890N GC connected to a GC-C/TC III combustion device coupled via open split to a Thermo MAT 253 mass spectrometer. The *n*-alkane fractions (1 μL) were injected into the inlet system in splitless mode (1 min). The injector was held at a temperature of 290 °C. The *n*-alkanes were separated on a fused silica capillary column (SGE BP-5, 30 m × 0.25 mm ID, 0.25 mm film thickness). The GC oven was held at 50 °C for 2 min, then heated at 25 °C/min to 120 °C, followed by a second heating ramp of 5 °C/min to 310 °C, and finally held isothermal for 8 min. The analytes of the GC effluent stream were oxidised to CO_2 in the combustion furnace at 950 °C on a CuO/NiO/Pt catalyst. The produced CO_2 was transferred on-line to the mass spectrometer to determine its $\delta^{13}C$ value. All results were calibrated to replicate measurements of individual *n*-alkanes from internal reference standards (IU A6 and B3). The maximum error in analytical precision was ±0.26‰.

2.3.6. GC-MS analyses of aromatic and polar fractions

Analyses of the aromatic and polar fractions were performed on a Perkin Elmer SQ8T/680 Clarus GC-MS fitted with a Perkin Elmer PE-5MS fused silica column (30 m × 0.25 mm i. d. × 0.25 μm film thickness). A 1 μL aliquot was injected at 300 °C into the injector operating in splitless mode. The oven was held at an initial temperature of 50 °C for 1 min, followed by heating at 8 °C/min to 300 °C. Helium was the carrier gas at a flow rate of 1 mL/min. Data acquisition was conducted in scan mode (Scan 45:500AMU at approx. 3 scans/sec).

2.4. Asphaltene separation

The asphaltene content of each specimen was determined by dissolving a bulk sub-sample (0.3–0.7 g) in a minimum volume of dichloromethane/methanol (93:7). The asphaltene fraction was then precipitated by adding an excess of *n*-pentane. After the asphaltene precipitate settled from suspension, the maltene supernatant was removed using a Pasteur pipette and further *n*-pentane added. This process was repeated several times, until the maltene fraction had been entirely removed. The remaining asphaltene fraction was then rinsed with a final wash of *n*-pentane, dried and weighed.

3. Results and discussion

3.1. Comparison of source-specific saturated hydrocarbons

Source-specific biomarker parameters of the asphaltites and asphaltic tars are listed in Table 1. The freshest asphaltite specimen (W13/007976) preserves *n*-alkanes as light as C_8 (note that lighter gasoline-range *n*-alkanes would lie outside the detection range), with a slightly bimodal front-end distribution displaying maxima at C_{10} and C_{13}, thereafter decreasing in abundance towards C_{35} (Fig. 2A). Relative to this specimen, other asphaltites in the sample suite have less low-molecular-weight *n*-alkanes. This mild weathering results in a unimodal *n*-alkane distribution in the range C_{10}–C_{35}, with a maximum between C_{15} and C_{17} (Fig. 2B). Although the majority of samples selected for comparison were not significantly weathered asphaltites, two mildly degraded specimens (W13/007493 and W13/007668) are also included in the sample suite for reference. These samples contain less *n*-alkanes, demonstrated by elevated Pr/C_{17} ratios compared to the other specimens. The asphaltic tar specimens preserve *n*-alkanes from C_9 to C_{35} with a maximum at C_{17} (Fig. 2C). Having been recovered from a single stranding location during one survey and being of highly uniform composition, the asphaltic tars are likely fragments of a single larger piece of tar separated by wave action during or shortly prior to stranding.

The C_{27}: C_{28}: C_{29} and C_{27} Dia/(Dia + Reg) sterane ratios of both families are highly consistent (Fig. 3; Table 1). Some minor grouping of the two oils is based on the relative proportions of the C_{27} and C_{28} ααα 20*R* steranes. The asphaltic tars typically contain a slightly lower proportion of C_{27} steranes and slightly elevated C_{28} steranes. However, there remains some overlap between the two oil types based on variability in these values in specific samples. The C_{31} (22R)/C_{30} αβ hopane ratios of the asphaltites and asphaltic tars are effectively identical, with respective values of 0.30–0.35 and 0.31–0.34, consistent with a marine source (Peters et al., 2005). This is supported in both oil families by the presence of diagnostic marine biomarkers such as dinosterane, a 4-methylsterane derived from marine dinoflagellates (Summons et al., 1987) and 24-*n*-propylcholestanes derived from marine chrysophyte algae (Moldowan et al., 1990). Furthermore, the complete lack of freshwater algal markers such as botryococcane (e.g. Moldowan and Seifert, 1980; McKirdy et al., 1986), and of angiosperm markers such as oleanane or bicadinanes (e.g. Edwards et al., 2018) together with a low abundance of tetracyclic polyprenoids (IIolba et al., 2000) suggests negligible inputs from terrestrial or freshwater biota. Hence, the parent oils of both types of asphaltic bitumen originated from source rocks which contain only marine organic matter, consistent with the previously inferred source affinity of the asphaltites (Edwards et al., 1998; Hall et al., 2014).

The pristane/phytane ratio (Pr/Ph), a commonly used indicator of source redox conditions (Powell and McKirdy, 1973), varies between 1.1 and 1.4 in the asphaltite sample suite, suggesting that their source rock was deposited under sub-oxic conditions. However, their high C_{35} homohopane index values (7–9) and high sulphur content (≈4 wt %) are consistent with more reducing conditions. The Pr/Ph ratios of the asphaltic tars are consistently lower, suggesting anoxia (<1; Table 1). This evidence of anoxia is further supported by a higher abundance of C_{35} homohopanes, expressed by high values of the C_{35} homohopane index (10–12) and C_{35}/C_{34} hopane ratio (1.00–1.05). Despite the evidence of a more oxygen-depleted (anoxic) setting (cf. the conflicting sub-oxic to anoxic parameters of the asphaltites), the sulphur content of the asphaltic tars varies between 2.5 and 3.5%, which is generally lower than that of the asphaltites (viz. 3.6–4.4% in the analysed suite).

The lithofacies of the asphaltite's source rock has previously been interpreted as a shale containing little to no carbonate, based on their C_{29}/C_{30} αβ hopane ratio being <1 (Fig. 4, Table 1), their high relative abundance of diasteranes and the complete absence of 2α-methylhopanes (Edwards et al., 1998). Abundant 2α-methylhopanes are observed in oils derived from carbonate source rocks (Summons et al., 1999), while lower abundances are reported in deeper water facies, a trend attributed to the distribution of their precursor cyanobacteria which predominantly reside in shallow-water ecosystems (Eigenbrode et al., 2008). The unusual absence of 2α-methylhopanes in the asphaltites could therefore support the interpretation that the source rock was deposited in a deepwater setting, consistent with their complete lack of molecular markers indicating terrestrial or freshwater organic matter inputs.

Table 1
Asphaltene content and selected biomarker parameters of asphaltite and asphaltic tar specimens. See Supplementary Information for explanation of compound abbreviations.

Samples	Asphaltene %	Sulphur %	$\delta^{34}S$ (‰)	Pr/Ph	Pr/C_{17}	27 : 28: 29 αααR steranes (*m/z* 217)	27 : 28: 29 αββ (20R + S) steranes (*m/z* 218)	C_{27} Dia/(Dia + Reg) steranes (*m/z* 217)	C_{35} homohopane index (%)	C_{29}/C_{30} αβ hopane (*m/z* 191)	C_{31} (22R)/C_{30} αβ hopane (*m/z* 191)	C_{35} (22S)/C_{34} (22S) hopane (*m/z* 191)	^{Ts}/(Ts + Tm)
Asphaltites													
W13/007472	59	4.0	−5.79	1.3	0.5	40 : 23: 36	37 : 25: 37	0.41	9.3	0.64	0.34	0.95	0.40
W13/007475	58	4.1	−6.53	1.3	0.5	38 : 23: 39	38 : 26: 37	0.45	7.8	0.65	0.33	0.90	0.41
W13/007476	53	4.3	−5.34	1.3	0.5	43 : 20: 38	38 : 25: 37	0.42	7.6	0.60	0.35	0.90	0.41
W13/007488	56	4.4	−5.30	1.2	0.5	43 : 20: 37	38 : 25: 37	0.43	8.6	0.64	0.33	0.92	0.39
W13/007493	52	4.1	−5.97	1.4	0.7	44 : 19: 36	37 : 25: 38	0.34*	8.3	0.69*	0.31	0.91	0.35
W13/007507	54	3.9	−5.66	1.2	0.5	40 : 27: 33	39 : 25: 36	0.43	7.4	0.65	0.32	0.79	0.40
W13/007516	55	4.0	−6.15	1.3	0.5	44 : 19: 37	38 : 25: 37	0.42	8.0	0.66	0.33	0.91	0.38
W13/007668	59	4.1	−7.13	1.1	1.3	37 : 27: 36	37 : 26: 37	0.45	7.7	0.67	0.30	0.90	0.38
W13/007671	54	3.8	−7.59	1.1	0.5	37 : 23: 39	37 : 25: 38	0.42	7.9	0.65	0.32	0.90	0.41
W13/007672	54	3.8	−7.34	1.2	0.4	43 : 20: 37	39 : 25: 36	0.43	8.4	0.65	0.33	0.94	0.38
W13/007845	51	3.7	−8.82	1.2	0.5	39 : 27: 34	39 : 26: 35	0.46	7.2	0.64	0.30	0.82	0.37
W13/007976	51	3.6	−7.80	1.2	0.4	38 : 26: 36	38 : 25: 37	0.45	7.6	0.62	0.30	0.82	0.41
Asphaltic Tars													
/001056	35	2.8	+2.61	0.7	0.6	35 : 29: 36	36 : 26: 38	0.43	11.0	0.82	0.32	1.02	0.22
/001063	22	3.2	+2.88	0.7	0.5	35 : 29: 36	36 : 26: 38	0.43	10.4	0.80	0.32	1.00	0.22
/001067	35	2.7	+4.84	0.7	0.6	34 : 29: 37	35 : 25: 40	0.43	11.3	0.78	0.33	1.03	0.22
/001068	25	3.2	+4.50	0.8	0.6	35 : 29: 36	36 : 25: 39	0.44	10.6	0.75	0.31	1.01	0.22
/001076	25	2.5	+4.27	0.7	0.5	37 : 26: 37	36 : 23: 42	0.43	11.0	0.79	0.34	1.05	0.27
/001079	27	3.0	+4.30	0.7	0.6	33 : 29: 38	35 : 25: 41	0.43	11.8	0.73	0.33	1.02	0.19
/001081	26	3.5	+4.85	0.7	0.5	32 : 29: 38	35 : 25: 40	0.44	11.8	0.76	0.33	1.04	0.19

* = Ratio variation attributed to significant weathering of the specimen.
C_{27} Dia/(Dia + Reg) steranes = (C_{27} βα 20S + 20R)/[(C_{27} βα 20S + 20R) + (C_{27} ααα 20S + 20R)].
C_{35} homohopane index = [C_{35} 17α(H),21β(H)-homohopanes (22S + 22R)/Σ C_{31-35} 17α(H),21β(H)-homohopanes (22S + 22R)] x 10.

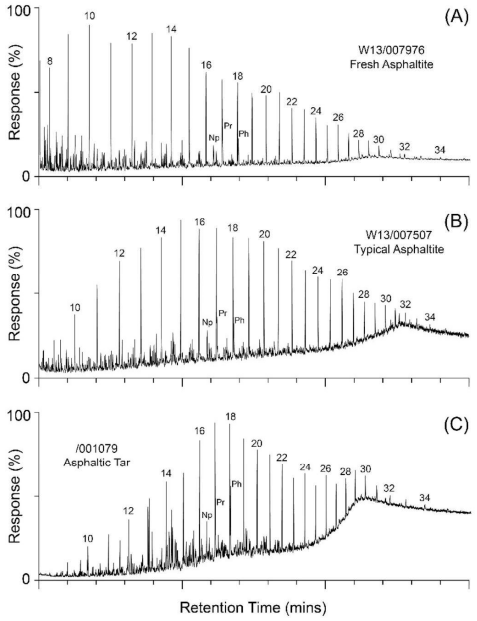


Fig. 2. Whole-oil GC-MS total ion chromatograms for: (A) The freshest identified asphaltite specimen W13/007976; (B) A typical, lightly weathered asphaltite specimen W13/007507; and (C) An asphaltic tar specimen/001079; Np = norpristane, Pr = pristane, Ph = phytane, peak numbers correspond to *n*-alkane chain length.

Unlike the asphaltites, the asphaltic tars contain 2α-methylhopanes in low abundance. However, the significance of their presence is uncertain, as 2α-methylhopanes appear to require cracking from kerogen and are hence strongly affected by burial temperature (Peters et al., 2005). Additionally, the 17α-22,29,30-trisnorhopane (Tm) occurs in much higher abundance relative to the 18α-22,29,30-trisnorneohopane (Ts). These compounds are usually compared in the Ts/(Ts + Tm) ratio, which is commonly employed as a thermal maturity parameter (Seifert and Moldowan, 1978). However, the low values of this ratio obtained from the asphaltic tars (0.19–0.27) are inconsistent with other thermal maturity parameters which indicate that these samples originated from the late oil window (discussed in Section 3.3). In addition to thermal maturity, the relative influence of lithology and redox conditions of the source rock on the Ts/(Ts + Tm) ratio is not fully understood, with several studies reporting systematically lower values in oils derived from carbonate source rocks deposited under anoxic conditions (McKirdy et al., 1983, 1984; Rullkötter et al., 1985; Price et al., 1987). Aside from this anomalous parameter, the composition of the asphaltic tars appears consistent with their derivation from an anoxic shale. To explain their abnormal Ts/(Ts + Tm) values, we tentatively propose that the source rock composition has a relatively high carbonate content, lying between the endmembers of shale and carbonate (i.e. a calcareous shale). In an anoxic setting, this may have been sufficient to account for their unusually low Ts/(Ts + Tm) values, despite the high thermal maturity of the parent oil.

3.2. Comparison of stable isotopic composition

The overall similarity of the asphaltic tars and asphaltites indicated by their near-identical source-specific sterane compositions is further reinforced by their internally consistent *n*-alkane $\delta^{13}C$ profiles, a valuable tool in the geochemical correlation of crude oils (e.g. Murray et al., 1994; Dowling et al., 1995; Blevin et al., 1998). The carbon isotopic composition of individual hydrocarbons in a crude oil is controlled principally by the primary organic matter inputs to its source rock. Hence oils derived from similar sources share comparable compound-specific $\delta^{13}C$ values (Hayes et al., 1990; Murray et al., 1994). The *n*-alkane $\delta^{13}C$ profiles of representative asphaltites and asphaltic tars, and of selected examples of Indonesian-derived waxy bitumens which also strand on the South Australian coastline (Ross et al., 2017) are shown in Fig. 5. The isotopic values for each individual *n*-alkane in these specimens are listed in Table S2. The waxy bitumens, products of distal petroleum systems with source characteristics notably different to those of the asphaltites (cf. Edwards et al., 2018), contain C_{15+} *n*-alkanes with $\delta^{13}C$ values ranging between approximately −25.5 and −32‰.

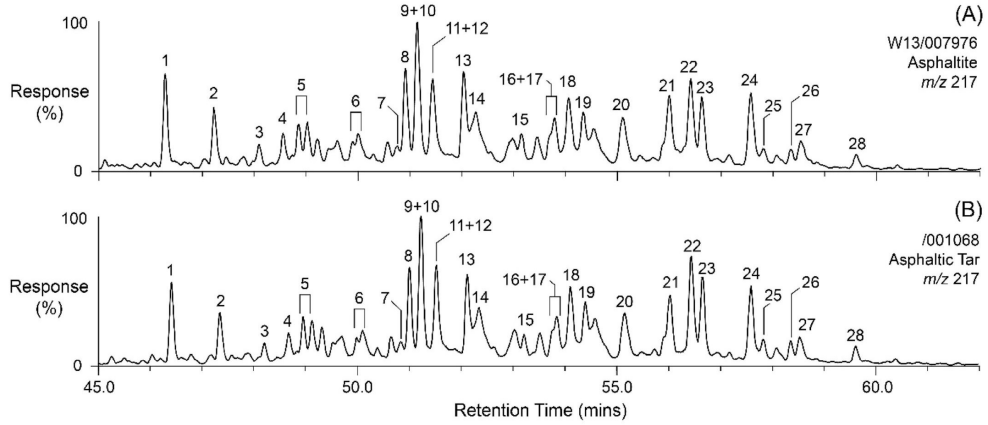


Fig. 3. Partial *m/z* 217 chromatograms of representative asphaltite and asphaltic tar specimens demonstrating the similarity of their sterane and diasterane distributions. For a full list of peak assignments see Supplementary Information.

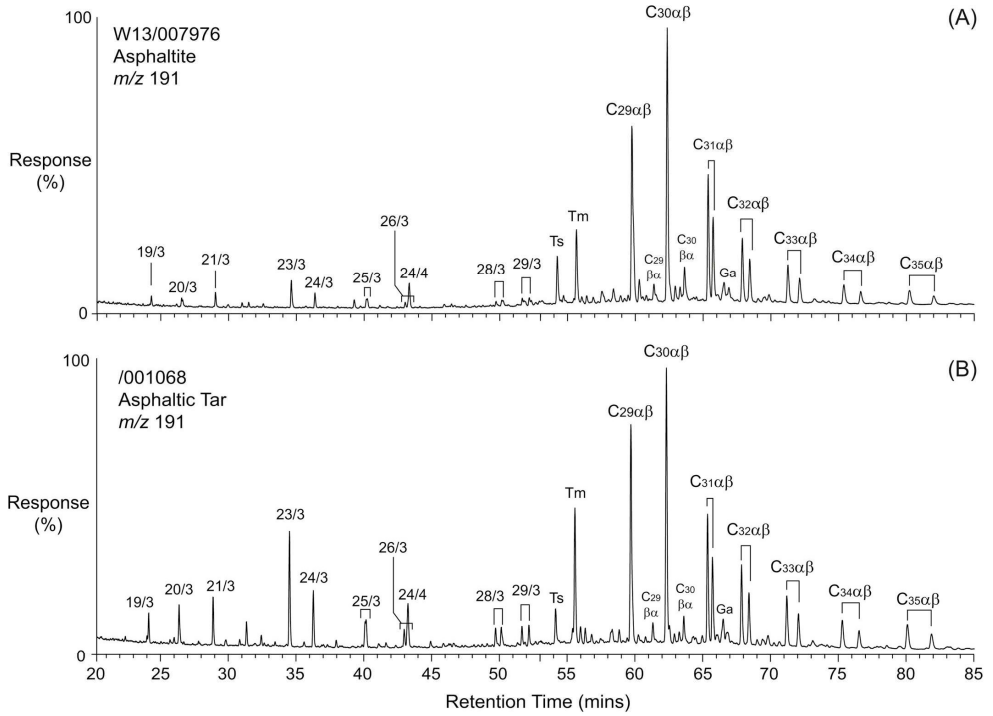


Fig. 4. Partial *m/z* 191 chromatograms of (A) asphaltite sample W13/007976; and (B) asphaltic tar sample/001068. See Supplementary Information for full list of compound abbreviations.

These results align with those of a previous assessment of the waxy bitumens' *n*-alkane isotopic composition, which demonstrated their similarity to the Minas and Duri oils from the Central Sumatra Basin (Dowling et al., 1995). In contrast, the *n*-alkane $\delta^{13}C$ values of the asphaltites and asphaltic tars are more uniform, with values between −30 and −34‰. Similarly, flat *n*-alkane $\delta^{13}C$ profiles are observed in other oils derived from marine source rocks (Murray et al., 1994).

Although the carbon isotopic values of the two oil families are highly consistent, their bulk sulphur isotopic compositions ($\delta^{34}S$) differ considerably. The $\delta^{34}S$ signature of an oil may be used to aid oil-oil and oil-source correlations, as the unaltered value typically reflects that of the source kerogen (Thode et al., 1961; Thode and Monster, 1970; Orr, 1986). Although the primary source of the sulphur in marine organic matter is seawater sulphate, the process of bacterial sulphate reduction in the sediment prior to deeper burial results in organically-bound sulphur becoming depleted in ^{34}S (Jones and Starkey, 1957; Harrison and Thode, 1958; Thode et al., 1960). Hence, the $\delta^{34}S$ values of petroleum generated from this organic matter are typically ca. 15‰ lighter than contemporaneous inorganically precipitated sulphur minerals such as gypsum, which may either accurately preserve the composition of seawater or be enriched in ^{34}S (Thode and Monster, 1965). In asphaltites, bulk $\delta^{34}S$ values range between −3.6 and −4.6‰, while the values for the asphaltic tars are between +2.61 and + 4.85‰, reflecting a much greater enrichment in the heavier isotope (Table 1). Given the variability in the $\delta^{34}S$ composition of seawater sulphate during the Cretaceous, these heavier values remain geologically reasonable (cf. Paytan et al., 2004). However, the sulphur isotopic composition of crude oil may also be altered to heavier values under certain conditions (discussed in Section 4.2).

3.3. Comparison of thermal maturity parameters

The maturity parameters of the asphaltite and asphaltic tar samples are summarised in Table 2. As discussed previously, although the Ts/(Ts + Tm) ratio may often constrain thermal maturity, it is unreliable in this case due to likely source interference. The methylphenanthrene index (MPI-1), arguably the most robust molecular measure of thermal maturity (Radke, 1987), varies between 0.49 and 0.62 across the asphaltite samples. Using the relationship between MPI-1 and vitrinite reflectance defined by Radke and Welte (1983), the calculated vitrinite reflectance (R_c) of the asphaltites' source rock falls between 0.7 and 0.8%, indicating a thermal maturity in the early/main oil window, consistent with previous studies (Volkman et al., 1992; Edwards et al., 1998; Hall et al., 2014; Scarlett et al., 2019). Other aromatic maturity indices, namely the methylnaphthalene ratio (MNR) and dimethylnaphthalene ratio (DNR-1), yield slightly higher maturities in the range 0.9–1.0% R_c. This may be the result of mixing with a more mature oil charge, which will influence the methylnaphthalenes of the oil more than the higher-molecular-weight methylphenanthrenes.

The asphaltites used for comparison in this study were collected from widely separated stranding locations along the coastline (Fig. 1A) and, with few exceptions, preserve phenanthrene, comparable to those

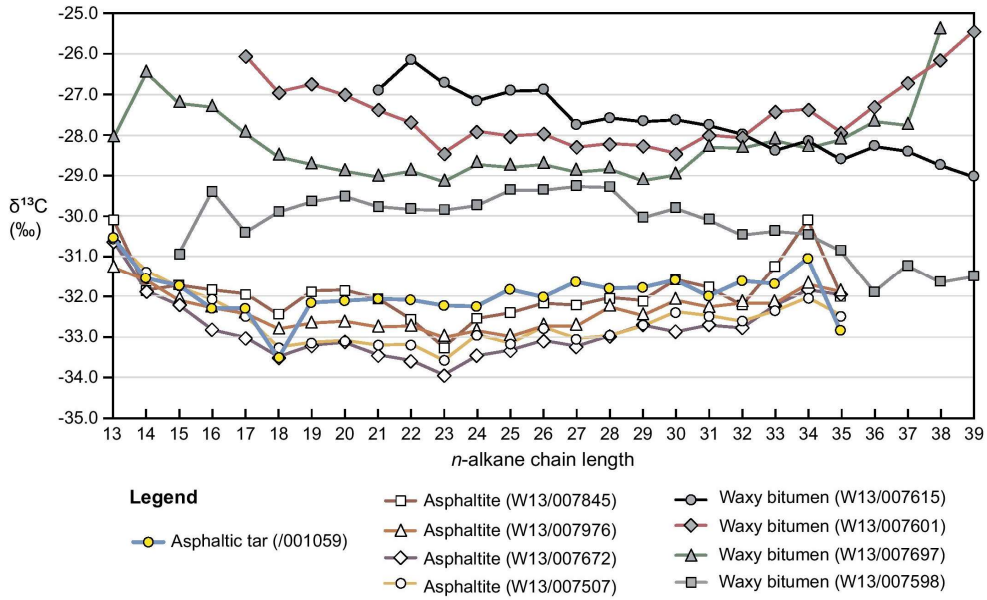


Fig. 5. CSIA data on *n*-alkanes from interior subsamples of different coastal bitumen oil families collected from the South Australian coastline. The carbon isotopic profile of the asphaltic tar specimen plots in the same region as those of numerous asphaltites but differs markedly from those of waxy coastal bitumens derived from petroleum systems in Southeast Asia. Each of the waxy bitumen varieties shown are derived from different oil families identified using the presence/absence and abundance of key biomarker alkanes identifiable using whole-oil GC-MS (Corrick et al., 2016; Ross et al., 2017).

in previous studies (cf. Volkman et al., 1992; Edwards et al., 1998; Hall et al., 2014). Therefore, most asphaltites within the sample suite have undergone minimal alteration due to water-washing, supporting the interpretation that they are the product of a local seafloor seep (Hall et al., 2014). However, degraded asphaltites do occur (e.g. samples W13/007493 and W13/007668). Such mild to moderately degraded examples exhibit significant alteration to the methyl- and dimethylnaphthalenes, while the MPI-1 ratio appears relatively unaffected (Corrick et al., 2019).

The aromatic hydrocarbon fraction of the asphaltic tars differs notably from that of the asphaltites (Fig. S2, Table 2). Their MPI-1 values of 1.23–1.34 are equivalent to R_c values of 1.1–1.2%, indicating a thermal maturity within the late oil window. MNR and DNR-1 likewise yield R_c values of 1.1 and 1.2% respectively. This consistency between aromatic maturity indicators suggests the asphaltic tars are unlikely to represent a mix of earlier and later expulsion products (*c.f.* the higher R_c values from MNR and DNR-1 vs. MPI-1 in the asphaltites). Like the asphaltites, the preservation of somewhat water-soluble naphthalenes, despite exposure to the marine environment, supports the interpretation that the asphaltic tars also originated from a nearby petroleum system.

The abundance of tricyclic terpanes relative to 17α-hopanes has been shown to increase at higher thermal maturities due to the preferential release of tricyclic terpanes from kerogen (Aquino Neto et al., 1983; van Graas, 1990; Farrimond et al., 1999). The tricyclic terpanes/17α-hopanes ratios of the asphaltites are low (0.07–0.15), consistent with their other maturity parameters which suggest generation and expulsion from a source rock in the early oil window. The markedly higher thermal maturity of the asphaltic tars indicated by their aromatic maturity parameters is further supported by their higher tricyclic terpanes/17α-hopanes ratio of 0.24–0.34 (Table 2). However, the abundance and composition of tricyclic and tetracyclic terpanes can also reflect source input (Peters et al., 2005). This makes distinguishing the influence of source and thermal maturity difficult when comparing two oils of markedly different maturities.

3.4. Comparison of Re-Os systematics

The Re-Os geochronology of crude oils has been demonstrated to constrain the timing of oil generation and expulsion from the source rock (Selby et al., 2005; Selby and Creaser, 2005; Finlay et al., 2011; Lillis and Selby, 2013; Liu et al., 2018). Application of the Re-Os geochronometer to asphaltites recently collected from the South Australian coastline provided a generation age of 74 ± 26 Ma (n = 16; Corrick et al., 2019), while analysis of a smaller suite of archival specimens collected in the 1990's yielded a set of data points with lower analytical uncertainty which define an age of 103 ± 22 Ma (n = 5; Scarlett et al., 2019). These generation ages show 19 Myr of potential overlap when considering their respective uncertainties. However, the remaining variation between these two determined ages is unlikely to be soley attributable to the differences in analytical uncertainty between these two studies, as the results obtained from numerous asphaltites analysed by Corrick et al. (2019), despite their higher analytical uncertainty, do not overlap with, or plot along the isochron defined by Scarlett et al. (2019). This suggests that a geologic component to the variation is also likely. The overall high uncertainty present in both of the determined ages may be associated with the mixing of increasingly mature oil, given the variation observed between the aromatic maturity parameters used herein (Table 2).

The asphaltic tars contain 30.1–31.4 parts per billion (ppb) Re and

Table 2
Thermal maturity parameters and calculated vitrinite reflectance (R_c) values of asphaltites and asphaltic tars. MPI-1 ratio after Cassani et al. (1988). Relationship between MPI-1 and R_c after Radke and Welte (1983). MNR, DNR-1 ratios and their respective relationships to R_c after Radke et al. (1984). See Supplementary Information for all compound abbreviations.

Sample	Tricyclics/ 17α-hopanes	MPI-1	R_c (%) from MPI-1	MNR	R_c (%) from MNR	DNR-1	R_c (%) from DNR-1
Asphaltites							
W13/007472	0.08	0.49	0.7	0.63	0.9	2.57	1.0
W13/007475	0.10	0.62	0.8	0.75	0.9	2.20	1.0
W13/007476	0.09	0.51	0.7	0.81	1.0	2.39	1.0
W13/007488	0.09	0.49	0.7	0.81	1.0	2.20	1.0
W13/007493	0.07	0.60	0.8	*	*	*	*
W13/007507	0.12	0.49	0.7	0.98	1.0	2.43	1.0
W13/007516	0.10	0.53	0.7	0.72	0.9	2.46	1.0
W13/007668	0.11	0.61	0.8	*	*	*	*
W13/007671	0.10	0.55	0.7	0.72	0.9	2.31	1.0
W13/007672	0.10	0.53	0.7	0.77	1.0	2.31	1.0
W13/007845	0.15	0.51	0.7	0.83	1.0	2.58	1.0
W13/007976	0.11	0.54	0.7	0.93	1.0	2.98	1.0
Asphaltic Tars							
/001056	0.31	1.28	1.2	1.76	1.1	6.82	1.2
/001063	0.33	1.26	1.2	1.73	1.1	7.22	1.2
/001067	0.31	1.23	1.1	1.66	1.1	7.10	1.2
/001068	0.34	1.25	1.1	1.59	1.1	6.24	1.2
/001076	0.24	1.33	1.2	1.62	1.1	6.07	1.2
/001079	0.26	1.34	1.2	1.71	1.1	7.29	1.2
/001081	0.27	1.31	1.2	1.55	1.1	6.42	1.2

* Ratio altered due to significant water washing and removal of key aromatic compounds.
Tricyclics/17α-hopanes = ΣC_{19-30} tricyclic terpanes/Σ C_{29-35} αβ hopanes.
MPI-1 = [1.89 × (2-MP + 3-MP)]/[P + 1.26 (1-MP + 9-MP)].
R_c (%) from MPI-1 = 0.60 × MPI-1 + 0.40.
MNR = 2-MN/1-MN.
R_c (%) from MNR = 0.17 × MNR + 0.82.
DNR-1 = (2,6-DMN + 2,7-DMN)/1,5-DMN.
R_c (%) from DNR = 0.046 × DNR-1 + 0.89.

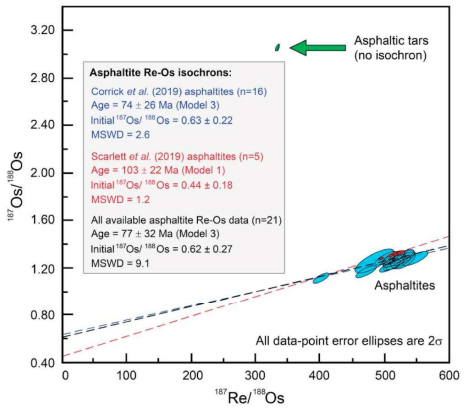


Fig. 6. Comparison of Re-Os ratios of asphaltic tars with those of asphaltites analysed by Corrick et al. (2019) and Scarlett et al. (2019). Results for individual samples are listed in Table S3. MSWD = mean square of weighted deviates.

599.9–627.6 parts per trillion (ppt) Os, concentrations significantly greater than in the asphaltites, which contain between 2.6 and 4.2 ppb Re and 24.6–45.0 ppt Os (Corrick et al., 2019; Scarlett et al., 2019). Such high abundances of Re and Os are unusual, particularly as these elements predominantly reside within the asphaltene fraction of crude oil (Selby et al., 2007; Georgiev et al., 2016; Liu and Selby, 2018; Liu et al., 2019) and the asphaltic tars contain less asphaltenes (22–35% versus 51–59% in the asphaltites; Table 1). The $^{187}Re/^{188}Os$ and $^{187}Os/^{188}Os$ ratios of the analysed asphaltic tars are highly uniform at 332.2–333.9 and 3.057–3.063, respectively (Table S3). These values overlap when considering the range of analytical uncertainty. Thus, insufficient variation exists to apply a linear regression to these data points to determine a meaningful generation age for the asphaltic tars. Their homogenous Re and Os composition is likely due to both the small number of samples analysed (n = 3), and the high probability that the specimens analysed represent individual fragments of a single larger piece of tar, as discussed previously. Whilst internally consistent, these values differ from those obtained from the asphaltites (Fig. 6), which yield $^{187}Re/^{188}Os$ values between 400.5 and 547.8 and $^{187}Os/^{188}Os$ values of 1.122–1.334 (Corrick et al., 2019; Scarlett et al., 2019).

4. Do both oils originate from the same source rock?

The geochemistries of these two varieties of asphaltic crude oil exhibit several source-related similarities, such as their highly comparable sterane distributions and *n*-alkane $\delta^{13}C$ values. However, clear and systematic differences are also evident between these two oil types, most notably in their respective Ts/(Ts + Tm) ratios, bulk $\delta^{34}S$ values and Re-Os systematics. Oil-oil and oil-source correlations can become particularly complex when taking into account possible lateral variations in both the organic facies and thermal maturity of the source rock. Therefore, the relationship between these two oil types must be considered in terms of two competing interpretations: (1) The asphaltic tars and asphaltites were derived from separate source rocks which contained similar organic facies; or (2) both oil types originated from lateral equivalents of the same source rock unit. In the latter interpretation, the observed geochemical variations reflect minor lateral variability in the source rock composition, combined with increased thermal maturity and possible alteration by thermochemical sulphate reduction (TSR; discussed below).

In both scenarios, correlation of the two oil types based on multiple source-specific parameters supports their derivation from organic-rich rocks which contained highly comparable organic matter inputs. Thus, these two asphaltic oils are likely to have originated from within the same basin, presently considered to be the offshore Bight Basin. However, the implications of the two potential interpretations for the quality and location of the parent petroleum system of the asphaltic tars may differ considerably.

4.1. The case for two separate source rocks

Multiple marine intervals with high source potential are proposed to occur throughout the Blue Whale, White Pointer, Tiger and Hammerhead supersequences of the Bight Basin (Blevin et al., 2000; Totterdell et al., 2000, 2008; Struckmeyer et al., 2001); and many of these now lie within different stages of the hydrocarbon generation window, depending on their location. For example, in the depocentre of the Ceduna Sub-basin, the proposed source rocks in the Blue Whale and White Pointer supersequences reside in the gas window or overmature zones, while laterally these intervals pass through both the main and late oil window in both the marginal and basinward areas (Fig. 7). It is reasonable to consider that organic matter inputs to a marine sedimentary basin would be similar, though not necessarily identical through time. An interpretation of two discrete marine source rock intervals with similar organic matter inputs would permit the near-identical compound-specific $\delta^{13}C$ values and sterane distributions of the asphaltites and asphaltic tars. However, the observed differences in $\delta^{34}S$ values and Re-Os systematics may be attributed to variations of

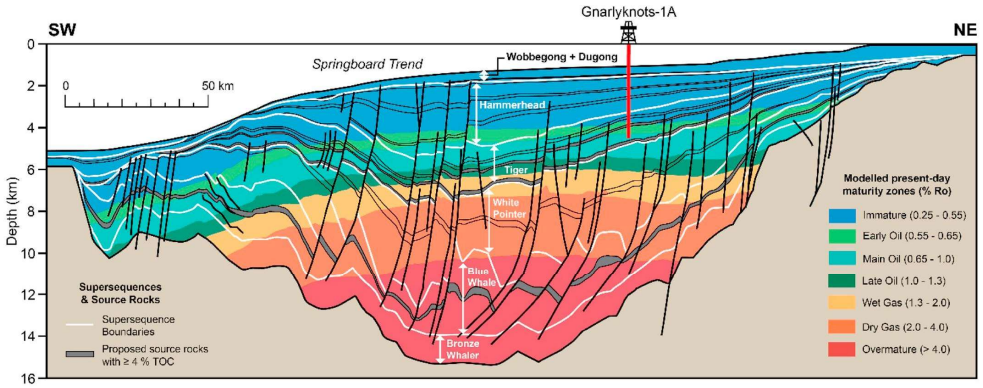


Fig. 7. Cross-section of the Ceduna Sub-basin of the Bight Basin with supersequence boundaries, proposed source intervals (>4% TOC) and modelled present-day maturity (% R_o) zones. Figure modified after Totterdell et al. (2008).

seawater chemistry through time (e.g. Paytan et al., 2004; Du Vivier et al., 2014). Although this may account for different $^{187}Re/^{188}Os$ and $^{187}Os/^{188}Os$ values between the two oils, it does not explain the unusually high abundance of Re and Os present in the asphaltic tars. Whilst the possibility of two separate sources cannot be discounted, this interpretation relies predominantly on attributing all observed variations between these two asphaltic oil strandings to differences in source rock composition, with little to no acknowledgement of the role that lateral facies variation and differing thermal maturity may also have had on the composition of the oil generated throughout the basin.

4.2. The case for a single source rock

The geochemical differences between the asphaltic tars and asphaltites may also be attributed to a combination of minor lateral variation in source rock facies, differences in thermal maturity and alteration of the asphaltic tars by TSR. This latter process occurs when oil comes into contact with a source of dissolved sulphate at temperatures at or above 100–140 °C (Goldhaber and Orr, 1995; Machel, 2001). Potential sources of dissolved sulphate include buried seawater, basin brines (groundwater) or dissolved evaporite deposits of gypsum or anhydride (Machel, 2001). During TSR, low-molecular-weight hydrocarbons are oxidised in order to reduce the dissolved sulphate. Branched and *n*-alkanes are the most reactive, followed by cyclic and monoaromatic compounds (Krouse et al., 1988; Manzano et al., 1997; Machel, 2001). Products of this reaction include hydrogen sulphide (H_2S), carbonate, metal sulphides and pyrobitumen (Machel, 2001). The release of H_2S in particular can also have important technical implications for oil production, as the oxidation reduces the overall hydrocarbon potential and production costs are increased due to the toxicity of H_2S and its associated corrosion of drilling equipment.

Both the sulphur isotopic composition and Re-Os systematics of a crude oil, two parameters typically inherited from seawater at the time of source rock deposition, are severely altered during TSR. Alteration of primary $\delta^{34}S$ values occurs due to the back reaction of the resulting H_2S with the oil. This incorporates sulphur derived from the dissolved sulphate, driving the $\delta^{34}S$ composition towards heavier values (e.g. Orr, 1974; Lillis and Selby, 2013). This is consistent with the observed difference in $\delta^{34}S$ composition between the asphaltic tars and asphaltites (Table 1). TSR has also been observed to reset the Re-Os systematics of crude oils, with the resulting age representing the cessation of this alteration process (Lillis and Selby, 2013). Oils affected by TSR are enriched in both Re and Os relative to the parent oil and possess different $^{187}Re/^{188}Os$ and $^{187}Os/^{188}Os$ ratios (Lillis and Selby, 2013). This suggests that during TSR both Re and Os are also transferred from the dissolved sulphate phase to the oil, though the exact nature of this process remains unclear. The resulting $^{187}Re/^{188}Os$ and $^{187}Os/^{188}Os$ values of the oil will therefore represent mixed signatures of the original oil and the dissolved sulphate. The nature of this alteration is unlikely to be systematic in all cases (i.e. $^{187}Os/^{188}Os$ will not always increase), as the composition of the dissolved sulphate will vary in different settings according to the sources of Re and Os (e.g. balance of Re and Os derived from mantle inputs vs. continental weathering). Disruption of the Re-Os systematics due to TSR is consistent with the differences observed between the asphaltites and asphaltic tars. In particular, the significant enrichment of both Re and Os in the latter, despite their lower asphaltene content. Although the asphaltic tars lacked the necessary variation to produce a meaningful isochron, it is likely that their Re-Os systematics actually constrain the cessation of TSR. Hence, their marked departure from those of the asphaltites, which are considered to record a generation age (Corrick et al., 2019; Scarlett et al., 2019).

A second potential explanation for resetting Re-Os systematics is oil-water interaction without TSR. Laboratory experiments have also shown Re and Os may be rapidly transferred to liquid oil when in contact with a solution enriched in Re and Os (Mahdaoui et al., 2015; Hurtig et al., 2019). Though these studies cannot fully mimic natural oil-water interactions in a geologic setting, their results suggest that interaction of oil with formation waters, which contain much lower abundances of Re and Os, may be capable of altering and resetting the Re-Os composition of an oil, given sufficiently high water/oil ratios (ca. 250). In this case, such formation waters would require highly radiogenic Os in order to alter the $^{187}Os/^{188}Os$ ratios of the asphaltic tars to their observed values (3.057–3.063), which are much higher than those reported for the asphaltites (1.122–1.334: Corrick et al., 2019; Scarlett et al., 2019). However, the influence of basinal water on the Re-Os systematics of crude oils and their application to constraining the timing of generation has been demonstrated to be limited or negligible in the Duvernay petroleum system of the West Canada Sedimentary Basin (Liu et al., 2018) wherein certain oils contain very low concentrations of both Re (0.04–3.78 ppb) and Os (0.6–41.2 ppt). Such examples should be extremely sensitive to any Re-Os contamination, but such alteration is not observed. Therefore, overprinting from typical interaction with formation waters is unlikely, given the evidence supportive of their alteration by TSR.

Definitive identification that a crude oil has been altered by TSR

typically requires identification of thiaadamantanes (Wei et al., 2012), or a combination of evidence from obtained from complementary analyses, notably assessment of the resulting gases (H_2S and CO_2), low-molecular-weight hydrocarbons and precipitated phases including carbonates, pyrobitumens and metal sulphides (e.g. Machel et al., 1995; Machel, 2001; Li et al., 2005; Hao et al., 2008; Liu et al., 2016). Unfortunately, the asphaltic tars do not appear to contain any compounds with mass spectra consistent with thiaadamantane or its various methylated homologues. However, if thiaadamantanes were originally present, they would likely have been lost along with the other low-molecular-weight hydrocarbons due to weathering in the marine environment. Therefore, without fresh examples for comparison, the absence of thiaadamantanes does not definitively preclude TSR in this case. Furthermore, as these oils were collected from the coastline, complementary analyses of the other products of TSR discussed above are not available for comparison as the location of the reservoir is not known. Given this ambiguity, we cannot conclusively determine that TSR has altered the asphaltic tars, although we note it would be consistent with their bulk $\delta^{34}S$ values and Re-Os systematics. Analysis of these oils in a more concentrated form using GC-MS-MS targeting the 2-thiaadamantane and the methlated thiaadamantanes may be able to assess this interpretation further. Alternatively, comparison of the compound-specific sulphur isotopic composition of the benzothiophenes and dibenzothiophenes may also be diagnostic (Amrani et al., 2012).

The other noted differences between the asphaltites and asphaltic tars are consistent with minor lateral variation in organic facies and the expulsion of the latter from the source rock later in the oil generation window. The carbonate content and redox conditions of a source rock formation may vary laterally across a basin due to its proximity to shallow water carbonate systems and variations in seafloor topography beneath a stratified water column, respectively. Such variability would be consistent with the minor variations in redox parameters (e.g. Pr/Ph, C_{35} homohopane index) between the two oil types and a calcareous shale source for the asphaltic tars, as indicated by their unusually low Ts/(Ts + Tm) values for an oil generated in the late oil window. The higher thermal maturity of the asphaltic tars is also consistent with their greater abundance of tricyclic terpanes relative to hopanes when compared to the asphaltites. Finally, both increasing thermal maturity and TSR are known to affect the $\delta^{13}C$ composition of the oil. Mature oils contain individual low-molecular-weight hydrocarbons which are 1–3‰ more enriched in ^{13}C relative to their less mature equivalents, while alteration by TSR results in even greater enrichment (> +15‰: Rooney, 1995). The light hydrocarbons affected by these processes are not preserved in the asphaltic tars, and therefore neither of these diagnostic changes can be assessed based on the isotopic composition of their C_{13}–C_{35} *n*-alkanes (Fig. 5).

In summary, whilst the differences between the asphaltites and asphaltic tars could be attributed to their derivation from separate source rocks, the specific points of variation are also consistent with the latter's higher thermal maturity, alteration by TSR and minor lateral variation in source facies (Table 3).

4.3. Potential mechanisms of heavy petroleum formation

Naturally occurring viscous tars/bitumen may form in response to a variety of different processes. These include: (1) extensive biodegradation of crude oil in a shallow subsurface reservoir; (2) weathering and amalgamation of a sea-surface oil slick, leaving a viscous residue which may be subsequently separated by wave action (Logan et al., 2010; Warnock et al., 2015); (3) *in situ* thermal maturation of a crude oil resulting in the formation of pyrobitumen (Machel, 2001); (4) separation of heavy petroleum to form subsurface tar mats, which may occur in several different ways (Dahl and Speers, 1986; Wilhelms and Larter, 1994a, 1994b); and (5) direct seepage of heavy petroleum onto the seafloor (e.g. Brüning et al., 2010), where it then becomes immobile.

Many of these potential mechanisms are inconsistent with the composition of the asphaltic tars and may therefore be discounted. Firstly, although they have a slightly lower *n*-alkane content than the freshest examples of asphaltite, the asphaltic tars do not appear to be heavily biodegraded, as they still contain C_{10+} *n*-alkanes. The preservation of the somewhat water-soluble naphthalenes in the least altered asphaltites and the entire suite of asphaltic tars also suggests that, despite their interaction with seawater, water washing has not been extensive. This likely precludes their formation from the weathering and amalgamation of an oil slick, whether from a spilled oil or natural seepage. Liquid oil in seawater will disperse into a thin surface slick with an extremely high surface area to volume ratio, making the oil extremely vulnerable to water washing, oxidation and microbial action. Generally, such oil in the marine environment will lose the majority of its low-molecular-weight components in a matter of hours (Head et al., 2006). Additionally, other known examples of marine tars amalgamating from sea surface oil slicks notably required calm oceanic conditions to form (e.g. Lorenson et al., 2009). The high energy environment of the Great Australian Bight, including the intense storm which occurred prior to the collection of the asphaltic tars, is unlikely to be supportive of this process.

In-situ thermal maturation of reservoired crude oil or alteration by TSR are known to form pyrobitumen. These solid residues are only weakly soluble in organic solvents (Wilhelms and Larter, 1994b) and are unlikely to seep. Previous assessment of their origin by Hall et al. (2014) demonstrated that the asphaltites are not pyrobitumen as they readily dissolve in dichloromethane. Although the asphaltic tars were generated and expelled during the late oil window, they are similarly soluble in dichloromethane and therefore they, too, cannot be considered residues of thermal maturation.

Hall et al. (2014) proposed that the asphaltites are transported remnants of subsurface tar mats, also known as viscous oil zones, polar-enriched zones (Larter et al., 1990) or heavy oil tar zones (Haldorsen et al., 1985). These deposits of heavy petroleum are reported in both clastic and carbonate settings and may range in thickness from < 1 m to as much as 6 m (Larter et al., 1990; Wilhelms and Larter, 1994a, 1994b). Well characterised examples demonstrate these emplacements of heavy petroleum share comparable biomarker geochemistry with their parent oils but are more enriched in asphaltenes (20–60 wt %; cf. 1–5 wt % in the oil leg: Wilhelms and Larter, 1994a, 1994b). Tar mats are readily soluble in organic solvents, clearly distinguishing them from weakly soluble pyrobitumen formed during reservoir maturation (Milner et al., 1977; Wilhelms and Larter, 1994a). These deposits may separate from the main oil charge in response to several different processes, including gravity segregation, introduction of gas to the reservoir and decreasing reservoir pressures, or are due to permeability barriers (Milner et al., 1977; Dahl and Speers, 1986; Wilhelms and Larter, 1994a, 1994b). In particular, deasphalting of the oil in response to gas generation from a maturing reservoired oil could account for the formation of the asphaltic tars, given that their thermal maturity (R_c = 1.1–1.2%) lies at the boundary of the wet gas window (R_c = 1.3%). Migration of gas into the reservoir is also possible, given the faulting which may connect to regions of the basin in the gas window (Fig. 7). However, ultimately none of the processes listed above can be discounted, as the resulting heavy petroleum in each case displays no diagnostic changes to its geochemistry. A more detailed knowledge of the geologic context of their parent petroleum system is therefore required to assess these mechanisms further.

Considering the asphaltic tars and asphaltite strandings as pieces of previously emplaced tar mats is also problematic, as it also requires facilitating their migration to the seafloor, despite their tendency to remain in place in the subsurface. Hall et al. (2014) suggested that following their formation as tar mats, the asphaltites escaped the subsurface by way of submarine canyon incision. However, it is more likely that seepage of both the asphaltites and the asphaltic tars is analogous

Table 3
Summary of processes capable of creating the observed geochemical differences between the asphaltic tars and asphaltites under the single source rock interpretation.

Deviation from asphaltite geochemistry	Potential mechanisms
(1) Higher abundance of tricyclic terpanes relative to hopanes	• Preferential expulsion of terpanes from kerogen at higher thermal maturities (Aquino Neto et al., 1983; van Graas, 1990; Farrimond et al., 1999)
(2) Lower sulphur content	• Lateral variability in euxinic conditions across basin • Thermal decomposition of organosulphur compounds in oil to gases (Orr, 1974; Tissot and Welte, 1984)
(3) Heavier $\delta^{34}S$ values	• Uptake of sulphur from dissolved sulphates and/or back reaction of H_2S during TSR (Orr, 1974; Lillis and Selby, 2013)
(4) Enriched Re and Os abundance and highly different Re-Os ratios	• Alteration due to TSR (Lillis and Selby, 2013)
(5) Pr/Ph < 1	• Lateral variability of source rock redox conditions
(6) Minor variation in C_{29}/C_{30} αβ hopane ratio	• Minor lateral variability in source rock carbonate content • Preferential thermal degradation of C_{30} αβ hopane (Peters et al., 2005)
(7) Presence of 2α-methylhopanes	• Minor increase in carbonate content • Increased thermal maturity
(8) Lower Ts/(Ts + Tm)	• Greater relative abundance of Tm attributed to higher carbonate content and anoxic conditions rather than thermal maturity (e.g. McKirdy et al., 1983, 1984; Rullkötter et al., 1985; Price et al., 1987)

to the asphalt flows observed on the seafloor in the Gulf of Mexico (Brüning et al., 2010). In this case, heavy petroleum that has not yet become immobile reaches the seafloor in a viscous state and flows away from the seepage site. The loss of volatile components, oxidation and other processes progressively increases the viscosity of the oil to the point where it becomes immobile and ultimately solidifies. The deposit forms deep fissures and cracks due to the loss of its low-molecular-weight hydrocarbons. The bitumen eventually fragments, releasing material into the overlying water column where it can become entrained in ocean currents. This process is certainly consistent with the shrinkage cracks seen in the larger asphaltites (Fig. 1B). The asphaltic tars, which have not solidified, may be more analogous to the seafloor tar mounds/whips observed off the southern coast of Santa Barbara (Lorenson et al., 2009). In this case, however, the oil has not been extensively biodegraded like that encountered in the Santa Barbara seeps.

4.4. Constraining the location of the asphaltic tar petroleum system

The prior coastal surveys conducted in November 2014 and September 2015 found no examples of this new variety of asphaltic crude oil across the 30 systematically surveyed beaches (Ross et al., 2017). There are similarly no reports of any oil matching their geochemical signature in previous studies of Australian coastal bitumen (McKirdy, 1984a, 1984b; Currie et al., 1992; Volkman et al., 1992; Summons et al., 1993; Alexander et al., 1994; Padley, 1995; Edwards et al., 1998, Hall et al., 2014; Edwards et al., 2016, 2018). The beach where the asphaltic tars were found, Number 1 and 2 Rocks, is also the most prominent collection point for coastal bitumen identified on the South Australian coastline (Padley, 1995; Edwards et al., 2016; Ross et al., 2017). Despite the abundance of coastal bitumen recovered from this site, no asphaltites were found there during the three annual surveys conducted in 2014–2016 (Ross et al., 2017), nor during the systematic bi-monthly surveys conducted in 1990 and 1991 (Padley, 1995; Edwards et al., 2016). However, it is important to acknowledge that the asphaltic tar strandings were collected just 24 days after a one-in-fifty-year storm event which affected much of the South Australian coastline (Bureau of Meteorology, 2016; Burns et al., 2017). The resulting abnormal wind and wave behaviour likely caused a significant departure from their traditional oceanic transport pathway and ultimate stranding location. Therefore, the single stranding location of the asphaltic tars presently provides little constraint on their point of origin.

If the asphaltic tars were derived from an oil affected by TSR then the parent oil must reside within a region of the subsurface which meets the required minimum onset temperature of 100–140° (Goldhaber and Orr, 1995; Machel, 2001). This may permit assessment of potential reservoirs based on the general increase in temperature with depth (e.g. Fig. 7). However, locally increased temperatures will also occur in proximity to volcanism and circulating hydrothermal fluids. The Bight Basin hosts an approximately 50,000 km^2 complex of volcanic intrusions in the Ceduna Sub-basin and the overlying Eucla Basin, with isolated igneous bodies also reported in the adjacent Duntroon Sub-basin (Schofield and Totterdell, 2008). Thus, circulating hydrothermal fluids could also provide the necessary temperatures and dissolved sulphate for TSR to occur within shallower regions of the basin. This is further supported by the recent identification of hydrocarbon-containing fluid inclusion assemblages in the Duntroon Sub-basin which appear to have been altered by hydrothermal fluids (Bourdet et al., 2019). However, no hydrocarbons extracted from fluid inclusions in the Bight Basin have a composition consistent with the asphaltites or asphaltic tars (Kempton et al., 2019; Gong et al., 2019).

Oils altered by TSR are primarily encountered in reservoirs with limited clay content such as clean sandstones or carbonates, as the presence of iron within clay minerals will react with available H_2S to form pyrite, rather than permitting it to accumulate to high concentrations (Worden and Smalley, 2001; Machel, 2001). In order for TSR to occur in clastic sediments containing clays, a larger source of dissolved sulphate is required (e.g. dissolved evaporite deposits) to exhaust all of the available iron before H_2S can accumulate. Presently there are no proposed carbonate reservoirs or evaporite deposits within the Bight Basin. Therefore, if the asphaltic tars have been altered by TSR, the reservoir would likely reside within clean sandstones deposited as part of the Ceduna delta, using sulphate sourced from groundwaters or circulating hydrothermal fluids. However, as the evidence for alteration by TSR is not conclusive, proposing an exact location for the parent petroleum system within this frontier basin remains speculative.

5. Conclusions

A new type of stranded crude oil termed 'asphaltic tar' was encountered during coastal surveys of South Australia in October 2016. These strandings share source-specific features with the well-studied asphaltites, also found on the South Australian coastline. Thermal maturity parameters constrain the asphaltic tar to the late oil window, unlike the asphaltites which were generated within the early oil window. The contrasting thermal maturity of the two oil types renders their correlation uncertain. Despite their source-specific similarities, differences in several geochemical parameters of the two oil types suggest that each may have originated from separate source rocks with comparable marine organic matter inputs. However, the most prominent differences accord with the higher thermal maturity of the asphaltic tar and its alteration by thermochemical sulphate reduction.

Both interpretations are consistent with these two oil types originating from within the same basin. As the asphaltites are presently attributed to an undiscovered petroleum system in the nearby Bight Basin, we consider these newly discovered asphaltic tars to have a similar origin.

Funding

Fieldwork and analytical costs for the research were met by the Great Australian Bight Research Program. Further financial support for the acquisition of Re-Os data was provided by the Bernold M. “Bruno” Hanson Memorial Environmental Grant to A.J.C. as part of the AAPG Foundation's Grants-In-Aid Program.

Acknowledgements

CSIA data were collected by the Davis Isotope Laboratory, University of California. Re-Os data were collected at the Laboratory for Source Rock Geochronology and Geochemistry and Arthur Holmes Laboratory at Durham University (UK). A.J.C. acknowledges the financial support of the Bernold M. “Bruno” Hanson Memorial Environmental Grant from the AAPG Foundation's Grants-In-Aid Program, The D R Stranks Travelling Fellowship, a University of Adelaide postgraduate scholarship and additional funding from the Great Australian Bight Research Program. D.S. acknowledges the Total Endowment Fund and the CUG Wuhan Dida Scholarship. We thank Zachary Angelini, Chris Dyt, Richard Kempton, Cameron White, April Pickard, Stacey Maslin, Stephane Armand, Les Tucker and Su Margot for their assistance in completing the 2014–2016 beach surveys. We also thank Mark Rollog and Robyn Williamson for conducting the EA-IRMS analyses; Antonia Hofmann and Geoff Nowell for assistance with the Re-Os determinations; and Stuart Valladares for the donation of asphaltites from his personal collection for this research. Finally, we thank Charlotte Stalvies, Chris Boreham, HIerbert Volk and Jennifer Totterdell for their constructive feedback on our manuscript.

The Great Australian Bight Research Program is a collaboration between BP, CSIRO, the South Australian Research and Development Institute (SARDI), the University of Adelaide, and Flinders University. The program aims to provide a whole-of-system understanding of the environmental and social values of the region; providing an information source for all to use.

Appendix A. Supplementary data

Supplementary data to this article can be found online at https://doi.org/10.1016/j.marpetgeo.2019.104062.

References

Alexander, R., Currie, T.J., Kagi, R.I., 1994. The origins of coastal bitumens from Western Australia. Aust. Pet. Expor. Assoc. J. 34 (1), 787–798.

Amrani, A., Deev, A., Sessions, A.L., Tang, Y., Adkins, J.F., Hill, R.J., Moldowan, J.M., Wei, Z., 2012. The sulfur-isotopic compositions of benzothiophenes and dibenzothiophenes as a proxy for thermochemical sulfate reduction. Geochim. Cosmochim. Acta 84, 152–164. https://doi.org/10.1016/J.GCA.2012.01.023.

Aquino Neto, F.R., Trendel, J.M., Restle, A., Connan, J., Albrecht, P.A., 1983. Occurrence and formation of tricyclic and tetracyclic terpanes in sediments and petroleum. In: Bjoröy, M., Albrecht, P., Cornford, C., de Groot, K., Eglinton, G., Galimov, E., Leythaeuser, D., Pelet, R., Speers, G. (Eds.), Advances in Organic Geochemistry 1981. John Wiley & Sons Limited, Chichester, pp. 659–676.

Bastow, T.P., van Aarssen, B.G.K., Lang, D., 2007. Rapid small-scale separation of saturate, aromatic and polar components in petroleum. Org. Geochem. 38, 1235–1250. https://doi.org/10.1016/j.orggeochem.2007.03.004.

Blevin, J.E., Boreham, C.J., Summons, R.E., Struckmeyer, H.I.M., Loutit, T.S., 1998. An effective lower cretaceous petroleum system on the North west shelf: evidence from the Browse basin. In: Purcell, P.G., Purcell, R.R. (Eds.), The Sedimentary Basins of Western Australia II. Petroleum Exploration Society of Australia, pp. 397–420.

Blevin, J.E., Boreham, C.J., Summons, R.E., Struckmeyer, H.I.M., Loutit, T.S., 2000. Hydrocarbon prospectivity of the Bight Basin - petroleum systems analysis in a frontier basin (compiler) In: In: Wood, G.R. (Ed.), 2nd Sprigg Symposium - Frontier Basins, Frontier Ideas, vol. 60. Geological Society of Australia, pp. 24–26 Abstracts.

Boreham, C., 2009. Organic geochemistry – source rock characterisation. In: Totterdell, J., Mitchell, C. (Eds.), Bight Basin Geological Sampling and Seepage Survey: RV Southern Surveyor SS01/2007, pp. 36–60. Geoscience Australia Record 2009/24. http://pid.geoscience.gov.au/dataset/ga/68689.

Boreham, C.J., Krassay, A.A., Totterdell, J.M., 2001. Geochemical comparisons between asphaltites on the southern Australian margin and Cretaceous source rock analogues. In: Hill, K.C., Bernecker, T. (Eds.), Eastern Australasian Basins Symposium, A Refocused Energy Perspective for the Future. Petroleum Exploration Society of Australia Special Publication, pp. 531–541.

Boult, P.J., McKirdy, D., Blevin, J., Heggeland, R., Lang, S., Vinall, D., 2005. The oil-prone Morum sub-basin petroleum system, Otway Basin, south Australia. MESA J. 38, 28–33.

Bourdet, J., Kempton, R.H., Dvia, V., Pironon, J., Gong, S., Ross, A.S., 2019. Constraining the timing and evolution of hydrocarbon migration in the Bight Basin. Mar. Pet. Geol submitted for publication.

Brüning, M., Sahling, H., MacDonald, I.R., Ding, F., Bohrmann, G., 2010. Origin, distribution, and alteration of asphalts at chapopote Knoll, southern Gulf of Mexico. Mar. Pet. Geol. 27, 1093–1106. https://doi.org/10.1016/j.marpetgeo.2009.09.005.

Bureau of Meteorology, 2016. Severe Thunderstorm and Tornado Outbreak South Australia, 28 September 2016.

Burns, G., Adams, L., Buckley, G., 2017. Independent Review of the Extreme Weather Event South Australia 28 September – 5 October 2016. Report Presented to the Premier of South Australia.

Cassani, F., Gallango, O., Talukdar, S., Vallejos, C., Ehrmann, U., 1988. Methylphenanthrene maturity index of marine source rock extracts and crude oils from the Maracaibo Basin. Org. Geochem. 13, 73–80. https://doi.org/10.1016/0146-6380(88)90027-7.

Corrick, A.J., Hall, P.A., McKirdy, D.M., Gong, S., Trefry, C., Dyt, C., Angelini, Z., Ross, A.S., Kempton, R., Armand, S., White, C., 2016. A revised oil family classification scheme and geochemical weathering proxies for South Australian coastal bitumen strandings. In: 19th Australian Organic Geochemistry Conference, Program and Abstracts. Fremantle, pp. 30–31.

Corrick, A.J., Selby, D., McKirdy, D.M., Hall, P.A., Gong, S., Trefry, C., Ross, A.S., 2019. Remotely constraining the temporal evolution of offshore oil systems. Sci. Rep. 9, 1327. https://doi.org/10.1038/s41598-018-37884-x.

Currie, T.J., Alexander, R., Kagi, R.I., 1992. Coastal bitumens from Western Australia - long distance transport by ocean currents. Org. Geochem. 18, 595–601.

Dahl, B., Speers, G.C., 1986. Geochemical characterization of a tar mat in the Oseberg field Norwegian sector, North Sea. Org. Geochem. 10, 547–558. https://doi.org/10.1016/0146-6380(86)90053-7.

Dowling, L.M., Boreham, C.J., Hope, J.M., Murray, A.P., Summons, R.E., 1995. Carbon isotopic composition of hydrocarbons in ocean-transported bitumens from the coastline of Australia. Org. Geochem. 23, 729–737. https://doi.org/10.1016/0146-6380(95)00061-I.

Du Vivier, A.D.C., Selby, D., Sageman, B.B., Jarvis, I., Gröcke, D.R., Voigt, S., 2014. Marine $^{187}Os/^{188}Os$ isotope stratigraphy reveals the interaction of volcanism and ocean circulation during oceanic anoxic event 2. Earth Planet. Sci. Lett. 389, 23–33. https://doi.org/10.1016/j.epsl.2013.12.024.

Edwards, D., McKirdy, D.M., Summons, R.E., 1998. Enigmatic asphaltites from the southern Australian margin: molecular and carbon isotopic composition. PESA J. 26, 397–420.

Edwards, D.S., Vinall, D.R., Corrick, A.J., McKirdy, D.M., 2016. Natural bitumen stranding on the ocean beaches of Southern Australia: a historical and geospatial review. Trans. R. Soc. S. Aust. 140, 152–185. https://doi.org/10.1080/03721426.2016.1203532.

Edwards, D.S., McKirdy, D.M., Rowland, S.J., Heath, D.J., Gray, P.S., 2018. Waxy bitumen stranding in southern Australia: a geochemical study of multiple oil families and their likely origins. Org. Geochem. 118, 132–151. https://doi.org/10.1016/j.orggeochem.2017.12.010.

Eigenbrode, J.L., Freeman, K.H., Summons, R.E., 2008. Methylhopane biomarker hydrocarbons in Hamersley Province sediments provide evidence for Neoarchean aerobiosis. Earth Planet. Sci. Lett. 273, 323–331. https://doi.org/10.1016/J.EPSL.2008.06.037.

Farrimond, P., Bevan, J.C., Bishop, A.N., 1999. Tricyclic terpane maturity parameters: response to heating by an igneous intrusion. Org. Geochem. 30, 1011–1019. https://doi.org/10.1016/S0146-6380(99)00091-1.

Finlay, A.J., Selby, D., Osborne, M.J., 2011. Re-Os geochronology and fingerprinting of United Kingdom Atlantic margin oil: temporal implications for regional petroleum systems. Geology 39, 475–478. https://doi.org/10.1130/G31781.1.

Fraser, A.R., Tilbury, L.A., 1979. Structure and stratigraphy of the Ceduna Terrace region, Great Australian Bight Basin. Aust. Pet. Explor. Assoc. J. 19 (1), 53–65. https://doi.org/10.1071/AJ78007.

Georgiev, S.V., Stein, H.J., Hannah, J.L., Galimberti, R., Nali, M., Yang, G., Zimmerman, A., 2016. Re-Os dating of maltenes and asphaltenes within single samples of crude oil. Geochim. Cosmochim. Acta. https://doi.org/10.1016/j.gca.2016.01.016.

Goldhaber, M.B., Orr, W.L., 1995. Kinetic controls on thermochemical sulfate reduction as a source of sedimentary H_2S. In: Vairavamurthy, M.A., Schoonen, M.A.A., Eglinton, T.I., Luther, G.W., Manowitz, B. (Eds.), Geochemical Transformations of Sedimentary Sulfur. American Chemical Society, pp. 412–425. https://doi.org/10.1021/bk-1995-0612.ch023.

Gong, S., Kempton, R.H., Ross, A.S., Bourdet, J., 2019. Characterisation of migrated hydrocarbons reveal insights into the source rocks of the Bight Basin. Mar. Pet. Geol submitted for publication.

Haldorsen, H.H., Mayson, H.J., Howarth, S.M., 1985. The heavy oil/tar mat in the Prudhoe Bay Field, Alaska - characterization and impacts on reservoir performance. In: 3rd International UNITAR/UNDP Heavy Crude and Tar Sands Conference, Preprints, vol. 2. Information Centre, New York, pp. 481–503.

Hall, P.A., McKirdy, D.M., Grice, K., Edwards, D.S., 2014. Australasian asphaltite strandings: their origin reviewed in light of the effects of weathering and biodegradation on their biomarker and isotopic profiles. Mar. Pet. Geol. 57, 572–593. https://doi.org/10.1016/j.marpetgeo.2014.06.013.

Hao, F., Guo, T., Zhu, Y., Cai, X., Zou, H., Li, P., 2008. Evidence for multiple stages of oil cracking and thermochemical sulfate reduction in the Puguang gas field, Sichuan Basin, China. Am. Assoc. Pet. Geol. Bull. 92, 611–637. https://doi.org/10.1306/01210807090.

Harrison, A.G., Thode, H.G., 1958. Mechanism of the bacterial reduction of sulphate from isotope fractionation studies. Trans. Faraday Soc. 54, 84–92.

Hayes, J.M., Freeman, K.H., Popp, B.N., Hoham, C.H., 1990. Compound-specific isotopic analyses: a novel tool for reconstruction of ancient biogeochemical processes. Org. Geochem. 16, 1115–1128. https://doi.org/10.1016/0146-6380(90)90147-R.

Head, I.M., Jones, D.M., Röling, W.F.M., 2006. Marine microorganisms make a meal of oil. Nat. Rev. Microbiol. 4, 173–182. https://doi.org/10.1038/nrmicro1348.

Holba, A.G., Tegelaar, E., Ellis, L., Singletary, M.S., Albrecht, P., 2000. Tetracyclic polyprenoids: indicators of freshwater (lacustrine) algal input. Geology 28, 251–254. https://doi.org/10.1130/0091-7613(2000)28<251:TPIOFL>2.0.CO;2.

Hurtig, N.C., Georgiev, S.V., Stein, H.J., Hannah, J.L., 2019. Re-Os systematics in petroleum during water-oil interaction: the effects of oil chemistry. Geochim. Cosmochim. Acta 247, 142–161. https://doi.org/10.1016/J.GCA.2018.12.021.

Jones, G.E., Starkey, R.L., 1957. Fractionation of stable isotopes of sulfur by microorganisms and their role in deposition of native sulfur. Appl. Microbiol. 5, 111–118.

Kempton, R.H., Bourdet, J., Gong, S., Ross, A.S., 2019. Revealing hidden oil migration in the frontier Bight Basin, Australia. Mar. Pet. Geol submitted for publication.

Krouse, H.R., Viau, C.A., Eliuk, L.S., Ueda, A., Halas, S., 1988. Chemical and isotopic evidence of thermochemical sulphate reduction by light hydrocarbon gases in deep carbonate reservoirs. Nature 333, 415–419. https://doi.org/10.1038/333415a0.

Larter, S.R., Bjørlykke, K.O., Karlsen, D.A., Nedkvitne, T., Eglinton, T., Johansen, P.E., Leythaeuser, D., Mason, P.C., Mitchell, A.W., Newcombe, G.A., 1990. Determination of petroleum accumulation histories: examples from the Ula field, central graben, Norwegian North sea. In: Buller, A.T., Berg, E., Hjelmeland, O., Kleppe, J., Torsæter, O., Aasen, J.O. (Eds.), North Sea Oil and Gas Reservoirs—II. Graham and Trotman, London, Dordrecht, pp. 319–330. https://doi.org/10.1007/978-94-009-0791-1_27.

Li, J., Xie, Z., Dai, J., Zhang, S., Zhu, G., Liu, Z., 2005. Geochemistry and origin of sour gas accumulations in the northeastern Sichuan Basin, SW China. Org. Geochem. 36, 1703–1716. https://doi.org/10.1016/J.ORGGEOCHEM.2005.08.006.

Lillis, P.G., Selby, D., 2013. Evaluation of the rhenium–osmium geochronometer in the Phosphoria petroleum system, Bighorn Basin of Wyoming and Montana, USA. Geochim. Cosmochim. Acta 118, 312–330. https://doi.org/10.1016/j.gca.2013.04.021.

Liu, J., Selby, D., 2018. A matrix-matched reference material for validating petroleum Re-Os measurements. Geostand. Geoanal. Res. 42, 97–113. https://doi.org/10.1111/ggr.12193.

Liu, Q., Zhu, D., Jin, Z., Liu, C., Zhang, D., He, Z., 2016. Coupled alteration of hydrothermal fluids and thermal sulfate reduction (TSR) in ancient dolomite reservoirs – an example from Sinian Dengying Formation in Sichuan Basin, southern China. Precambrian Res. 285, 39–57. https://doi.org/10.1016/J.PRECAMRES.2016.09.006.

Liu, J., Selby, D., Obermajer, M., Mort, A., 2018. Re-Os geochronology and oil-source correlation of Duvernay Petroleum System, Western Canada Sedimentary Basin: implications for the application of the Re-Os geochronometer to petroleum systems. Am. Assoc. Pet. Geol. Bull. 102, 1627–1656. https://doi.org/10.1306/12081717105.

Liu, J., Selby, D., Zhou, H., Pujol, M., 2019. Further evaluation of the Re-Os systematics of crude oil: implications for Re-Os geochronology of petroleum systems. Chem. Geol. 513, 1–22. https://doi.org/10.1016/J.CHEMGEO.2019.03.004.

Logan, G.A., Jones, A.T., Kennard, J.M., Ryan, G.J., Rollet, N., 2010. Australian offshore natural hydrocarbon seepage studies, a review and re-evaluation. Mar. Pet. Geol. 27, 26–45. https://doi.org/10.1016/j.marpetgeo.2009.07.002.

Lorenson, T.D., Hostettler, F.D., Rosenbauer, R.J., Peters, K.E., Dougherty, J.A., Kvenvolden, K.A., Gutmacher, C.E., Wong, F.L., Normark, W.R., 2009. Natural Offshore Oil Seepage and Related Tarball Accumulation on the California Coastline; Santa Barbara Channel and the Southern Santa Maria Basin; Source Identification and Inventory. U.S. Geological Survey Open-File Report 2009-1225 and MMS report 2009-030.

Machel, H.G., 2001. Bacterial and thermochemical sulfate reduction in diagenetic settings — old and new insights. Sediment. Geol. 140, 143–175. https://doi.org/10.1016/S0037-0738(00)00176-7.

Machel, H.G., Krouse, H.R., Sassen, R., 1995. Products and distinguishing criteria of bacterial and thermochemical sulfate reduction. Appl. Geochem. 10, 373–389. https://doi.org/10.1016/0883-2927(95)00008-8.

Mahdaoui, F., Michels, R., Reisberg, L., Pujol, M., Poirier, Y., 2015. Behavior of Re and Os during contact between an aqueous solution and oil: consequences for the application of the Re–Os geochronometer to petroleum. Geochim. Cosmochim. Acta 158, 1–21. https://doi.org/10.1016/j.gca.2015.02.009.

Manzano, B.K., Fowler, M.G., Machel, H.G., 1997. The influence of thermochemical sulphate reduction on hydrocarbon composition in Nisku reservoirs, Brazeau river area, Alberta, Canada. Org. Geochem. 27, 507–521. https://doi.org/10.1016/S0146-6380(97)00070-3.

McKirdy, D.M., 1984a. Coastal Bitumens and Potential Source Rocks, Duntroon Basin, South Australia (AMDEL Report F 5769/84 for Getty Oil Development Company Ltd., South Australian Department of Mines and Energy Open File Envelope No. 5876.

McKirdy, D.M., 1984b. Coastal Bitumens and Potential Source Rocks in the Western Otway Basin, South Australia and Victoria (AMDEL Report F 5840/84 for Australian Aquitaine Petroleum Pty Ltd. and Ultramar Australia Inc., South Australian Department of Mines and Energy Open File.

McKirdy, D.M., Aldridge, A.K., Ypma, P.J.M., 1983. A geochemical comparison of some crude oils from pre-Ordovician carbonate rocks. In: Bjoröy, M., Albrecht, P., Cornford, C., de Groot, K., Eglinton, G., Galimov, E., Leythaeuser, D., Pelet, R., Speers, G. (Eds.), Advances in Organic Geochemistry 1981. John Wiley & Sons Limited, Chichester, pp. 99–107.

McKirdy, D.M., Kantsler, A.J., Emmett, J.K., Aldridge, A.K., 1984. Hydrocarbon genesis and organic facies in cambrian carbonates of the eastern officer basin, south Australia. In: In: Palacas, J.G. (Ed.), Petroleum Geochemistry and Source Rock Potential of Carbonate Rocks. AAPG Studies in Geology, vol. 18. pp. 13–31. https://doi.org/10.1306/St18443C2.

McKirdy, D.M., Cox, R.E., Volkman, J.K., Howell, V.J., 1986. Botryococcane in a new class of Australian non-marine crude oils. Nature 320, 57–59. https://doi.org/10.1038/320057a0.

McKirdy, D., Summons, R., Padley, D., Serafini, K., Boreham, C., Struckmeyer, H., 1994. Molecular fossils in coastal bitumens from southern Australia: signatures of precursor biota and source rock environments. Org. Geochem. 21, 265–286.

Milner, C.W.D., Rogers, M.A., Evans, C.R., 1977. Petroleum transformations in reservoirs. J. Geochem. Explor. 7, 101–153. https://doi.org/10.1016/0375-6742(77)90079-6.

Moldowan, J.M., Seifert, W.K., 1980. First discovery of botryococcane in petroleum. J. Chem. Soc., Chem. Commun. 19, 912–914.

Moldowan, J.M., Fago, F.J., Lee, C.Y., Jacobson, S.R., Watt, D.S., Slougui, N.-E., Jeganathan, A., Young, D.C., 1990. Sedimentary 24-*n*-propylcholestanes, molecular fossils diagnostic of marine algae. Science 247, 309–312. https://doi.org/10.2307/2873627.

Murray, A.P., Summons, R.E., Boreham, C.J., Dowling, L.M., 1994. Biomarker and *n*-alkane isotope profiles for Tertiary oils: relationship to source rock depositional setting. Org. Geochem. 22, 521–542. https://doi.org/10.1016/0146-6380(94)90124-4.

Orr, W.L., 1974. Changes in sulfur content and isotopic ratios of sulfur during petroleum maturation - study of Big Horn Basin Paleozoic oils. Am. Assoc. Pet. Geol. Bull. 58, 2295–2318.

Orr, W.L., 1986. Kerogen/asphaltene/sulfur relationships in sulfur-rich Monterey oils. Org. Geochem. 10, 499–516. https://doi.org/10.1016/0146-6380(86)90049-5.

Padley, D., 1995. Petroleum Geochemistry of the Otway Basin and the Significance of Coastal Bitumen Strandings on Adjacent Southern Australian Beaches (PhD thesis). University of Adelaide.

Paytan, A., Kastner, M., Campbell, D., Thiemens, M.H., 2004. Seawater sulfur isotope fluctuations in the Cretaceous. Science 304, 1663–1665. https://doi.org/10.1126/science.1095258.

Peters, K.E., Walters, C.C., Moldowan, J.M., 2005. The Biomarker Guide, second ed. Biomarkers and Isotopes in Petroleum Exploration and Earth History, vol. 2 Cambridge University Press.

Powell, T.G., McKirdy, D.M., 1973. Relationship between ratio of pristane to phytane, crude oil composition and geological environment in Australia. Nat. Phys. Sci. 243, 37–39.

Price, P.L., O'Sullivan, T., Alexander, R., 1987. The nature and occurrence of oil in Seram, Indonesia. In: Proceedings of the Indonesian Petroleum Association, 16th Annual Convention. Indonesian Petroleum Association, Jakarta, Indonesia, pp. 141–173.

Radke, M., 1987. Organic geochemistry of aromatic hydrocarbons. In: In: Brooks, J., Welte, D.H. (Eds.), Advances in Petroleum Geochemistry, vol. 2. Academic Press, London, pp. 141–207.

Radke, M., Welte, D.H., 1983. The methylphenanthrene index (MPI). A maturity parameter based on aromatic hydrocarbons. In: Bjoröy, M., Albrecht, P., Cornford, C., de Groot, K., Eglinton, G., Galimov, E., Leythaeuser, D., Pelet, R., Speers, G. (Eds.), Advances in Organic Geochemistry 1981. John Wiley & Sons Limited, Chichester, pp. 504–512.

Radke, M., Leythaeuser, D., Teichmüller, M., 1984. Relationship between rank and composition of aromatic hydrocarbons for coals of different origins. Org. Geochem. 6, 423–430. https://doi.org/10.1016/0146-6380(84)90065-2.

Rooney, M.A., 1995. Carbon isotopic data of light hydrocarbons as indicators of thermochemical sulfate reduction. In: Grimalt, J.O., Dorronsoro, C. (Eds.), Organic Geochemistry: Development and Applications to Energy, Climate, Environment and Human History 1995. A.I.G.O.A. Donostia-San Sebastian, pp. 523–525.

Ross, A., Corrick, A., Trefry, C., Gong, S., McKirdy, D., Hall, T., Dyt, C., Angelini, Z., Kempton, R., Pickard, A., White, C., Maslin, S., Griffin, D., Middleton, J., Luick, J., Armand, S., Vergara, T., Schinteie, R., 2017. Asphaltite and Tarball Surveys. Final Report GABRP Project 5.2. Research Report Series Number 25a.

Rullkötter, J., Spiro, B., Nissenbaum, A., 1985. Biological marker characteristics of oils and asphalts from carbonate source rocks in a rapidly subsiding graben, Dead Sea, Israel. Geochim. Cosmochim. Acta 49, 1357–1370. https://doi.org/10.1016/0016-7037(85)90286-8.

Scarlett, A.G., Holman, A.I., Georgiev, S.V., Stein, H.J., Summons, R.E., Grice, K., 2019. Multi-spectroscopic and elemental characterization of southern Australian asphaltites. Org. Geochem. https://doi.org/10.1016/J.ORGGEOCHEM.2019.04.006.

Schofield, A., Totterdell, J.M., 2008. Distribution, Timing and Origin of Magmatism in the Bight and Eucla Basins. Geoscience Australia Record 2008/24.

Seifert, W.K., Moldowan, J.M., 1978. Applications of steranes, terpanes and monoaromatics to the maturation, migration and source of crude oils. Geochim. Cosmochim. Acta 42, 77–95. https://doi.org/10.1016/0016-7037(78)90219-3.

Selby, D., Creaser, R.A., 2005. Direct radiometric dating of hydrocarbon deposits using rhenium-osmium isotopes. Science 308, 1293–1295. https://doi.org/10.1126/science.1111081.

Selby, D., Creaser, R., Dewing, K., Fowler, M., 2005. Evaluation of bitumen as a Re–Os geochronometer for hydrocarbon maturation and migration: a test case from the Polaris MVT deposit, Canada. Earth Planet. Sci. Lett. 235, 1–15. https://doi.org/10.1016/j.epsl.2005.02.018.

Selby, D., Creaser, R.A., Fowler, M.G., 2007. Re–Os elemental and isotopic systematics in

crude oils. Geochim. Cosmochim. Acta 71, 378–386. https://doi.org/10.1016/j.gca.2006.09.005.
Sprigg, R.C., Woolley, J.B., 1963. Coastal bitumen in southern Australia with special reference to observations at Geltwood Beach, south-east South Australia. Trans. R. Soc. S. Aust. 86, 67–103.
Struckmeyer, H.I.M., Totterdell, J.M., Blevin, J.E., Logan, G.A., Boreham, C.J., Deighton, I., Krassay, A.A., Bradshaw, M.T., 2001. Character, maturity and distribution of potential cretaceous oil source rocks in the Ceduna sub-basin, Bight Basin, Great Australian Bight. In: Hill, K.C., Bernecker, T. (Eds.), Eastern Australian Basins Symposium: a Refocused Energy Perspective for the Future. Petroleum Exploration Society of Australia, Special Publication, pp. 543–552.
Summons, R.E., Volkman, J.K., Boreham, C.J., 1987. Dinosterane and other steroidal hydrocarbons of dinoflagellate origin in sediments and petroleum. Geochim. Cosmochim. Acta 51, 3075–3082. https://doi.org/10.1016/0016-7037(87)90381-4.
Summons, R.E., Bradshaw, J., Brooks, D.M., Goody, A.K., Murray, A.P., Foster, C.B., 1993. Hydrocarbon composition and origins of coastal bitumens from the Northern Territory, Australia. PESA J. 21, 31–42.
Summons, R.E., Jahnke, L.L., Hope, J.M., Logan, G.A., 1999. 2-Methylhopanoids as biomarkers for cyanobacterial oxygenic photosynthesis. Nature 400, 554–557. https://doi.org/10.1038/23005.
Summons, R.E., Logan, G.A., Edwards, D.S., Boreham, C.J., Bradshaw, M.T., Blevin, J.E., Totterdell, J.M., Zumberge, J.E., 2001. Geochemical analogs for Australian coastal asphaltites - search for the source rock. In: Abstracts, AAPG Annual Convention, Denver, Colorado. Am. Assoc. Pet. Geol. Bull., vol. 85 (Suppl.).
Thode, H.G., Monster, J., 1965. Sulfur-isotope geochemistry of petroleum, evaporites, and ancient seas. In: In: Young, A., Galley, J.E. (Eds.), Fluids in Subsurface Environments, vol. 4. Am. Assoc. Pet. Geol. Mem., pp. 367–3677. https://doi.org/10.1306/M4360.
Thode, H.G., Monster, J., 1970. Sulfur isotope abundances and genetic relations of oil accumulations in Middle East Basin. Am. Assoc. Pet. Geol. Bull. 54, 627–637.
Thode, H.G., Harrison, A.G., Monster, J., 1960. Sulphur isotope fractionation in early diagenesis of Recent sediments of Northeast Venezuela. Am. Assoc. Pet. Geol. Bull. 44, 1809–1817.
Thode, H., Monster, J., Dunford, H., 1961. Sulphur isotope geochemistry. Geochim. Cosmochim. Acta 25, 159–174. https://doi.org/10.1016/0016-7037(61)90074-6.
Tissot, B.P., Welte, D.H., 1984. Petroleum Formation and Occurrence, second ed. Springer-Verlag, Berlin.
Tolmer, A., 1882. Reminiscences of an Adventurous and Chequered Career at Home and in the Antipodes. Sampson Low, Marston. Searle & Rivington, London.
Totterdell, J.M., Bradshaw, B.E., 2004. The structural framework and tectonic evolution of the Bight Basin. In: Boult, P.J., Johns, D.R., Lang, S.C. (Eds.), Eastern Australasian Basins Symposium II. Petroleum Exploration Society of Australia Special Publication, pp. 41–61.
Totterdell, J.M., Blevin, J.E., Struckmeyer, H.I.M., Bradshaw, B.E., Colwell, J.B., Kennard, J.M., 2000. A new sequence framework for the Great Australian Bight: starting with a clean slate. Aust. Pet. Prod. Explor. J. 40, 95–118. https://doi.org/10.1071/AJ99007.
Totterdell, J.M., Struckmeyer, H.I.M., Boreham, C.J., Mitchell, C.H., Monteil, E., Bradshaw, B.E., 2008. Mid-Late Cretaceous organic-rich rocks from the eastern Bight Basin : implications for prospectivity. In: Blevin, J.E., Bradshaw, B.E., Uruski, E. (Eds.), Eastern Australasian Basins Symposium III. Petroleum Exploration Society of Australia Special Publication, pp. 137–158.
Trewartha, J., 1850. South Australian Government Gazette. pp. 25 April 282.
van Graas, G.W., 1990. Biomarker maturity parameters for high maturities: calibration of the working range up to the oil/condensate threshold. Org. Geochem. 16, 1025–1032. https://doi.org/10.1016/0146-6380(90)90139-Q.
Volkman, J.K., O'Leary, T., Summons, R.E., Bendall, M.R., 1992. Biomarker composition of some asphaltic coastal bitumens from Tasmania, Australia. Org. Geochem. 18, 669–682. https://doi.org/10.1016/0146-6380(92)90092-C.
Warnock, A.M., Hagen, S.C., Passeri, D.L., 2015. Marine tar residues: a review. Water Air Soil Pollut. 226, 24. https://doi.org/10.1007/s11270-015-2298-5.
Wei, Z., Walters, C.C., Moldowan, M.J., Mankiewicz, P.J., Pottorf, R.J., Xiao, Y., Maze, W., Nguyen, P.T.H., Madincea, M.E., Phan, N.T., Peters, K.E., 2012. Thiadiamondoids as proxies for the extent of thermochemical sulfate reduction. Org. Geochem. 44, 53–70. https://doi.org/10.1016/J.ORGGEOCHEM.2011.11.008.
Wilhelms, A., Larter, S.R., 1994a. Origin of tar mats in petroleum reservoirs. Part I: introduction and case studies. Mar. Pet. Geol. 11, 418–441. https://doi.org/10.1016/0264-8172(94)90077-9.
Wilhelms, A., Larter, S.R., 1994b. Origin of tar mats in petroleum reservoirs. Part II: formation mechanisms for tar mats. Mar. Pet. Geol. 11, 442–456. https://doi.org/10.1016/0264-8172(94)90078-7.
Worden, R.H., Smalley, P.C., 2001. H_2S in North Sea oil fields: importance of thermochemical sulphate reduction in clastic reservoirs. In: Cidu, R. (Ed.), Water-Rock Interaction: Proceedings of the Tenth International Symposium on Water-Rock Interaction, WRI-10, Villasimius, Italy, 10-15 July 2001. Swets & Zeitlinger, Lisse, pp. 659–662.